Vol. 64 September, 1960 No. 9

THE JOURNAL OF PHYSICAL CHEMISTRY

(Registered in U. S. Patent Office)

CONTENTS

34th NATIONAL COLLOID SYMPOSIUM, Lehigh University, Bethlehem, Pa., June 16–17, 1960

NOTES

THE JOURNAL OF PHYSICAL CHEMISTRY

(Registered in U. S. Patent Office)

W. ALBERT NOYES, JR., EDITOR

ALLEN D. BLISS — ASSISTANT EDITORS — A. B. F. DUNCAN

Published monthly by the American Chemical Society at 20th and Northampton Sts., Easton, Pa.

Second-class mail privileges authorized at Easton, Pa. This publication is authorized to be mailed at the special rates of postage prescribed by Section 131.122.

The *Journal of Physical Chemistry* is devoted to the publication of selected symposia in the broad field of physical chemistry and to other contributed papers.

Manuscripts originating in the British Isles, Europe and Africa should be sent to F. C. Tompkins, The Faraday Society, 6 Gray's Inn Square, London W. C. 1, England.

Manuscripts originating elsewhere should be sent to W. Albert Noyes, Jr., Department of Chemistry, University of Rochester, Rochester 20, N. Y.

Correspondence regarding accepted copy, proofs and reprints should be directed to Assistant Editor, Allen D. Bliss, Department of Chemistry, Simmons College, 300 The Fenway, Boston 15, Mass.

Business Office: Alden H. Emery, Executive Secretary, American Chemical Society, 1155 Sixteenth St., N. W., Washington 6, D. C.

Advertising Office: Reinhold Publishing Corporation, 430 Park Avenue, New York 22, N. Y.

Articles must be submitted in duplicate, typed and double spaced. They should have at the beginning a brief Abstract, in no case exceeding 300 words. Original drawings should accompany the manuscript. Lettering at the sides of graphs (black on white or blue) may be pencilled in and will be typeset. Figures and tables should be held to a minimum consistent with adequate presentation of information. Photographs will not be printed on glossy paper except by special arrangement. All footnotes and references to the literature should be numbered consecutively and placed in the manuscript at the proper places. Initials of authors referred to in citations should be given. Nomenclature should conform to that used in *Chemical Abstracts*, mathematical characters be marked for italic, Greek letters carefully made or annotated, and subscripts and superscripts clearly shown. Articles should be written as briefly as possible consistent with clarity and should avoid historical background unnecessary for specialists.

Notes describe fragmentary or incomplete studies but do not otherwise differ fundamentally from articles and are subjected to the same editorial appraisal as are articles. In their preparation particular attention should be paid to brevity and conciseness. Material included in Notes must be definitive and may not be republished subsequently.

Communications to the Editor are designed to afford prompt preliminary publication of observations or discoveries whose value to science is so great that immediate publication is imperative. The appearance of related work from other laboratories is in itself not considered sufficient justification for the publication of a Communication, which must in addition meet special requirements of timeliness and significance. Their total length may in no case exceed 500 words or their equivalent. They differ from Articles and Notes in that their subject matter may be republished.

Symposium papers should be sent in all cases to Secretaries of Divisions sponsoring the symposium, who will be responsible for their transmittal to the Editor. The Secretary of the Division by agreement with the Editor will specify a time after which symposium papers cannot be accepted. The Editor reserves the right to refuse to publish symposium articles, for valid scientific reasons. Each symposium paper may not exceed four printed pages (about sixteen double spaced typewritten pages) in length except by prior arrangement with the Editor.

Remittances and orders for subscriptions and for single copies, notices of changes of address and new professional connections, and claims for missing numbers should be sent to the American Chemical Society, 1155 Sixteenth St., N. W., Washington 6, D. C. Changes of address for the *Journal of Physical Chemistry* must be received on or before the 30th of the preceding month.

Claims for missing numbers will not be allowed (1) if received more than sixty days from date of issue (because of delivery hazards, no claims can be honored from subscribers in Central Europe, Asia, or Pacific Islands other than Hawaii), (2) if loss was due to failure of notice of change of address to be received before the date specified in the preceding paragraph, or (3) if the reason for the claim is "missing from files."

Subscription Rates (1960): members of American Chemical Society, $12.00 for 1 year; to non-members, $24.00 for 1 year. Postage to countries in the Pan American Union $0.80; Canada, $0.40; all other countries, $1.20. Single copies, current volume, $2.50; foreign postage, $0.15; Canadian postage $0.05; Pan-American Union, $0.05. Back volumes (Vol. 56–59) $25.00 per volume; (starting with Vol. 60) $30.00 per volume; foreign postage, per volume $1.20, Canadian, $0.15; Pan-American Union, $0.25. Single copies: back issues, $3.00; for current year, $2.50; postage, single copies: foreign, $0.15; Canadian, $0.05; Pan American Union, $0.05.

COMMUNICATIONS TO THE EDITOR

THE JOURNAL OF
PHYSICAL CHEMISTRY

(Registered in U. S. Patent Office)

VOLUME 64 SEPTEMBER 23, 1960 NUMBER 9

THE FAILURE OF DISPERSION ENERGY CALCULATIONS TO REPRODUCE HEATS OF ADSORPTION ON GRAPHITIC CARBON

BY DONALD GRAHAM

Organic Chemicals Department, Research Contribution No. 291, Jackson Laboratory, E. I. du Pont de Nemours and Company Inc., Wilmington, Delaware

Received March 7, 1960

Isosteric heats of adsorption of nitrogen on diamond, amorphous carbon, and thermally graphitized P-33 differ but little at the coverage approaching completion of the first monolayer. The effect of the much greater density of diamond is thus balanced by a correspondingly greater contribution (per atom) from the electrons of the graphitic carbons. Calculated dispersion energies fail to reproduce this result, indicating the possible importance of other forms of electronic interaction.

Introduction

Heats of physical adsorption are calculated with some success as sums of dispersion energies of interaction between the units involved. The formal treatment of dispersion interaction between an adsorbed molecule and the adsorbent involves three factors.

(1) The dispersion constant, a measure of the energy of interaction between an adsorbent atom and an adsorbed molecule at the equilibrium distance or the depth of the potential well. The currently favored approximation for the dispersion constant is that of Kirkwood and Muller,[1] in which

$$c = 6mc^2 \left(\frac{\alpha_1 \alpha_2}{\frac{\alpha_1}{\chi_1} + \frac{\alpha_2}{\chi_2}} \right)$$

m represents the mass of the electron, c the speed of light and the α's and χ's, respectively, the polarizabilities and diamagnetic susceptibilities of the interacting units.

(2) A force law relating energy of interaction with distance of separation between any two interacting units. For dispersion energies, the Lennard-Jones (6–12) potential is commonly employed, assuming a decay of attraction with the 6th power of the separation distance and decay of repulsion with the 12th power of the separation distance.

(3) A summation of the interactions of the adsorbed molecule with all of the atoms of the solid. To a first approximation, this is proportional to the number of atoms per unit volume of the solid or to its density. (This summation does not include the lateral interaction between adsorbed molecules.)

This treatment, particularly the approximation for the dispersion constant assumes an isotropic non-polar, non-conducting solid adsorbent and spherical adsorbate molecules having no permanent dipole moment.

Although graphite is an anisotropic semiconductor, such a treatment of the adsorption of argon on Graphon (a graphitized carbon black) gave results in good agreement with experiment.[2] Fair success also was reported in the application of this theory to the adsorption of krypton on graphitized carbon black and, surprisingly, also on copper and iron.[3]

Investigators have realized for some time, however, that although treatment of graphitized carbon as a non-conducting adsorbent may give reasonable calculated heat values, a correct approach must include recognition of its electronic properties. An early consideration of this question, in relation to the heats of adsorption of nitrogen and argon on graphite, gave somewhat low values when covalent bonding (diamond structure) was assumed and quite high values when the model was an isotropic metal.[4]

The results of a more recent study have indicated that heats of adsorption on carbon can be explained in large part as an interaction between an electric field outside the carbon surface (caused by protrud-

---

[1] A. Muller, *Proc. Roy. Soc.* (*London*), **A154**, 624 (1936).

[2] E. L. Pace, *J. Chem. Phys.*, **27**, No. 6, 1341 (1957).

[3] R. A. Pierotti and G. D. Halsey, Jr., THIS JOURNAL, **63**, 680 (1959).

[4] R. M. Barrer, *Proc. Roy. Soc.* (*London*), **161A**, 476 (1937).

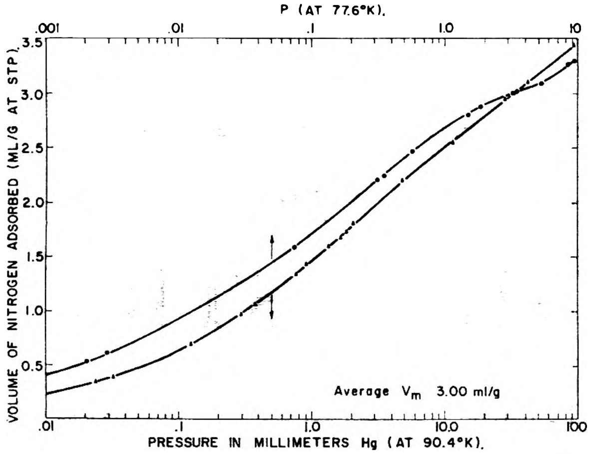

Fig. 1.—Adsorption of nitrogen on diamond at 90.4 and 77.6°K.

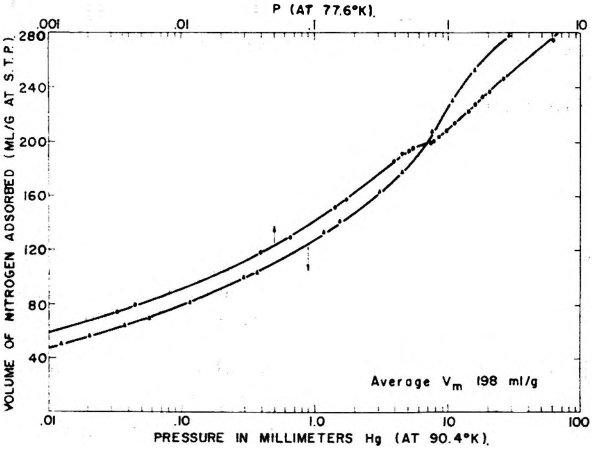

Fig. 2.—Adsorption of nitrogen on amorphous carbon at 90.4 and 77.6°K.

ing conduction electrons) with a dipole induced by that field in an adsorbate molecule.[5]

Disregard of the structural anisotropy of graphitic carbon adsorbents finds some support in the repeatedly observed high degree of energetic surface uniformity of certain graphitized carbon blacks.[6,7] However any success in ascribing heats of adsorption on graphitic carbon to dispersion energies alone may have involved the possible wide latitude in selection of values for the variables which make up the dispersion constant or the parameters of the force law. It is therefore useful to compare measured heats of adsorption of a non-polar gas on carbon adsorbents of different crystal structure with those predicted from dispersion energy calculations using the most self-consistent values available. This has been done using, as adsorbents, diamond, an amorphous carbon, and a thermally graphitized carbon black (P-33).

Experimental

Materials.—Diamond dust was obtained from Kay and Warren Co. (33 Box Street, Brooklyn 22, N. Y.) as gem grade, No. 1 size (largest dimension $<2\ \mu$). It was extracted with aqueous hydrofluoric acid followed by aqueous hydrochloric acid and distilled water. It then was dried, heated under vacuum at 150° and purged repeatedly with nitrogen.

The amorphous carbon was prepared by the reaction of hexachlorobenzene with sodium amalgam.[8] The product, after extraction, steaming, and finally sweeping with nitrogen at a temperature above 500°, contained less than 0.5% chlorine. It showed no graphite lines in the X-ray powder pattern but was jet black in color, indicating a high degree of conjugation and, to this extent, may be considered graphitic.

The sample of P-33 carbon black (heat treated at 2700°) was obtained from Mr. W. D. Schaeffer, then of the Research and Development Department of Godfrey L. Cabot, Inc.

The nitrogen was obtained from the Linde Air Products Co. as 99.99% high-purity dry nitrogen. The oxygen used in the gas thermometer (for measurements at 90.4°K.) was Linde's spectroscopic grade.

The equipment and methods used in obtaining the adsorption isotherms have been described in an earlier paper.[7] Liquid nitrogen and liquid oxygen baths were employed to maintain adsorbent temperatures of 77.6 ± 0.1°K. and 90.4 ± 0.1°K., respectively. Isosteric heats were calculated by conventional application of the Clausius–Clapeyron equation to the isotherms.

Results

The adsorption isotherms are plotted in Figs. 1, 2 and 3 with logarithmic pressure scales to show the low coverage values more clearly. The isosteric heats of adsorption as functions of coverage are shown in Fig. 4.

The adsorption data from the diamond sample failed to give a satisfactory BET plot but the coverage representing the first monolayer was quite clearly defined by the characteristic sharp drop in the heat curve. A second diamond sample of larger particle size was studied with similar results. A very high degree of heterogeneity may be responsible for this behavior.

The adsorption data from the amorphous carbon sample, like that from diamond, showed a very high degree of heterogeneity and gave curved BET lines. Again it was necessary to determine the content of the first monolayer from the heat curve. This point is less well defined than in the case of diamond, possibly due to condensation in small capillaries.

The P-33 data are an extension of those previously reported.[7]

Discussion

Measurement of the effects of differences in crystal structure upon the net energy with which carbon holds an adsorbed nitrogen molecule requires comparison of the isosteric heats at a coverage favorable to separation of that part of the heat of adsorption due to lateral adsorbate interaction. The extensive heterogeneity of the diamond and amorphous carbon samples precludes comparison at low coverage because the minority strong sites are occupied first. The coverage selected is therefore that just preceding the sharp drop in heat due to approaching completion of the first monolayer and onset of appreciable second layer deposition ($\theta \sim 0.85$). Since the isosteric heat is a differential quantity and since the minority strong sites have been occupied below this coverage, there is little residual effect of heterogeneity. It may also be assumed that the contribution of lateral interaction has reached its maximum at $\theta \sim 0.85$ and is approximately the same for the three systems. Its

---

(5) J. H. de Boer and S. Kruyer, *Trans. Faraday Soc.*, **54**, 540 (1958).

(6) M. H. Polley, W. D. Schaeffer and W. R. Smith, THIS JOURNAL, **57**, 469 (1953).

(7) D. Graham, *ibid.*, **61**, 1310 (1957).

(8) J. Gibson, M. Holohan and H. L. Riley, *J. Chem. Soc.*, 456 (1946).

value is obtained from the heat-coverage plot for nitrogen on P-33 as the difference between the heat at coverage near zero and that at the maximum ($\theta \sim 0.85$). The very few strong sites in the surface of this particular adsorbent influence only a minute first portion of the curve and the resulting rise near zero coverage (Fig. 7, ref. 7) is not shown here. The contribution of lateral interaction at $\theta \sim 0.85$ is thus approximately 400 cal./mole. Its subtraction from the isosteric heats at $\theta \sim 0.85$ leaves the net heat of interaction between the carbon and the adsorbed nitrogen as shown in Table I.

TABLE I

HEATS OF ADSORPTION (IN CAL./MOLE) OF NITROGEN ON CARBON ADSORBENTS OF DIFFERENT CRYSTAL STRUCTURE

	Adsorbent		
	Diamond	Amorphous carbon	Graphitized P-33
Isosteric heat of adsorption	−2960	−2920	−2820
Heat of lateral interaction	− 400	− 400	− 400
Net heat of adsorbent–adsorbate interaction	−2560	−2520	−2420
Ratio of net heat to that on diamond	1.00	0.98	0.95

These net heats are, like the isosteric heats, closely similar although the adsorbents vary widely in density (Table III). The greater density of diamond is balanced by correspondingly greater contributions from each atom of the lighter graphitic carbons which means that the energy with which an atom in an adsorbent attracts an adsorbed molecule varies markedly with the nature of its bonds to other atoms within the solid. The next step is to determine the extent to which these compensations are reflected in the results of dispersion energy calculations.

The physical constants employed in calculation of the dispersion constants are listed (with source references) in Table II.

TABLE II

DATA FOR DISPERSION CONSTANTS REPRESENTING INTERACTION OF NITROGEN WITH CARBON ADSORBENTS

Substance	Diamagnetic susceptibility (emu./molecule or atom) Value	Ref.	Polarizability, $cm.^3$ Value	Ref.
Nitrogen	-2.0×10^{-29}	9	1.76×10^{-24}	12
Diamond	-0.90×10^{-29}	10	0.93×10^{-24}	13
Amorphous carbon	-1.00×10^{-29}	11	1.07×10^{-24}	14
Graphitized P-33	-13.5×10^{-29}	11	1.07×10^{-24}	14

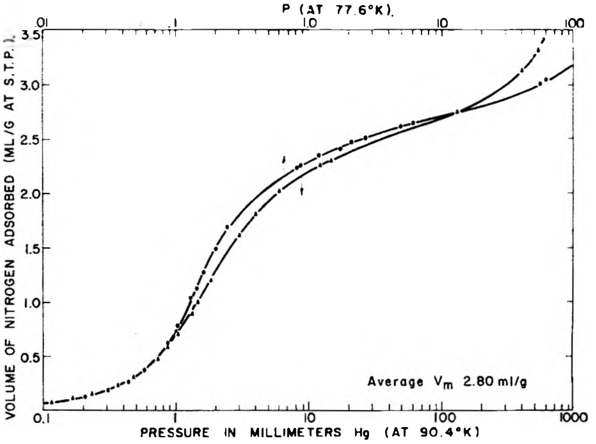

Fig. 3.—Adsorption of nitrogen on P-33 at 90.4 and 77.6°K.

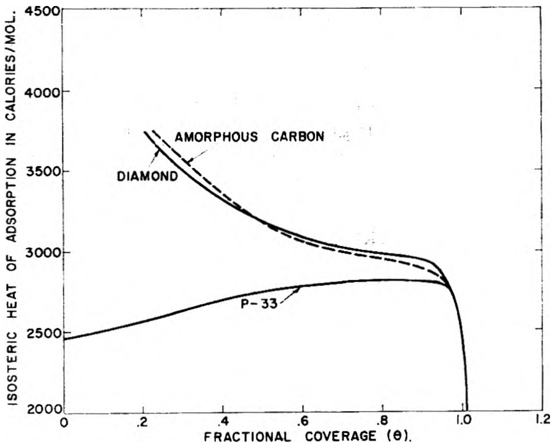

Fig. 4.—Isosteric heats of adsorption for nitrogen on diamond, amorphous carbon and P-33.

The diamagnetic susceptibility and polarizability values for nitrogen and for diamond differ but little from those employed by earlier investigators. Since the effects of anisotropy upon the diamagnetic susceptibility of graphite are reduced with crystallite size,[11,15] the value for amorphous carbon differs but little from that of diamond. The value selected for the polarizability of amorphous carbon and of graphite is that given by Landolt-Börnstein for aromatic carbon. It is only about 15% greater than that of diamond. The greatest variation from earlier usage is in the diamagnetic susceptibility of graphitized P-33. Fortunately, there are considerable data indicating the approximate level and one measurement on a similarly graphitized sample of P-33.

For interpreting these results, the diamond–nitrogen system is the selected standard of reference because its physical constants are best known and because, being isotropic, covalently bonded and non-conducting, it most nearly fulfills the requirements for pure dispersion interaction. Since we are interested only in the ratios of the adsorption energies of the other systems to this standard, and since the assumption of dispersion energies implies a common force law, we may assume that the dispersion energies are, to a first approximation, proportional to the product of the adsorbent density times the dispersion constant. These values are

---

(9) E. C. Stoner, "Magnetism," Methuen and Co., Ltd., London, 1948, p. 36.

(10) A. Sigamony, *Proc. Indian Acad. Sci.*, **19A**, 310 (1944).

(11) H. T. Pinnick, *Phys. Rev.*, **94**, 319 (1954).

(12) J. O. Hirschfelder, C. F. Curtis and R. B. Bird, "Molecular Theory of Gases and Liquids," John Wiley and Sons, Inc., New York, N. Y., 1954, p. 950.

(13) J. A. Ketelaar, "Chemical Constitution," Elsevier Pub. Co., New York, N. Y., 1953, p. 90.

(14) Landolt-Börnstein, "Zahlenwerte und Funktionen," Springer, 1951, 6 Aufl. Bd. I/3, p. 513.

(15) N. Gangul:, *Phil. Mag.*, **21**, 355 (1936).

given in Table III in comparison with the corresponding measured net heat ratios.

TABLE III

A COMPARISON OF CALCULATED DISPERSION ENERGIES WITH MEASURED NET HEATS OF INTERACTION

	Adsorbent		
	Diamond	Amorphous carbon	Graphitized P-33
Density (D)	3.5	1.9	2.2
Dispersion constant (C) $\times 10^{59}$	−4.22	−4.74	−9.62
CD Product ($\times 10^{59}$)	−14.7	−9.0	−21.1
Ratio $\frac{CD}{CD_{(\text{Diamond})}}$	1.00	0.61	1.44
Ratio $\frac{(\text{Net heat of intern.})}{(\text{Net heat of intern.})_{\text{Diamond}}}$	1.00	0.98	0.95

The ratios compared in Table III indicate failure of the dispersion energy calculation to reproduce measured net heats of adsorption. It may be significant, in relation to the results of earlier calculations, that an average of the calculated values from amorphous carbon and from graphitized P-33 would be an acceptable result. It is possible that this failure lies in one or more of the values selected for the variables making up the dispersion constants. It seems more probable, however, that interaction energies, other than those of dispersion, may arise from the peculiar electronic properties of graphitic carbon. For example, nuclear magnetic resonance measurements have demonstrated an interaction of unpaired electrons in the surfaces of graphitic carbon with adsorbed molecules.[16]

In the three systems considered here, the effects of variation in adsorbent density (up to a factor of almost 2) are compensated by some combination of electronic effects to the extent that the over-all variation in adsorption energy is small. This conclusion makes it easier to accept the observed (and repeatedly confirmed) high energetic uniformity of the adsorbent surfaces of certain graphitic carbon blacks which may involve an analogous electronic compensation for the effects of structural anisotropy.

Finally, the results of this study emphasize the importance of differences in electronic properties of solid adsorbents in general and the necessity for their consideration in any realistic theoretical treatment.

DISCUSSION

R. A. PASTERNAK (Stanford Research Institute).—To what extent could the carbon surfaces have been covered by contamination such as chlorine or oxygen?

DONALD GRAHAM.—The surfaces of all of the carbon samples studied were essentially clean. The least pure was the amorphous carbon, which contained less than 0.5% chlorine. Since the value of V_m (content of the first monolayer) for nitrogen on this sample was 198 ml./g., only a very small fraction of the total surface could have been covered by chlorine, even if all of it was on the surface.

PHILIP L. WALKER, JR. (Pennsylvania State University).—Why is the diamond surface so heterogeneous? Is it possible that the carbon arrangement at the surface is not that of diamond?

DONALD GRAHAM.—Electron micrographs show the diamond particles to be rough and irregular with little evidence of clean fracture along normal cleavage planes. Also, since diamonds are valence crystals, bonds are broken at cleavage leaving free valences which are probably quickly satisfied by random interaction with each other. The bonds between the surface atoms are therefore no longer tetrahedral and possibly not even symmetrically distributed. Care was taken to avoid temperatures, in conditioning the sample, which might permit surface graphitization. Although it seems improbable that the distortion of bonds between the diamond surface atoms would materially alter the energy of interaction between the particle and an adsorbed molecule, the observed surface roughness may, at least in part, explain the observed heterogeneity.

GEORGE R. LESTER (Universal Oil Products).—What is the nature of the BET plot for nitrogen on the amorphous carbon? Did the form of the equation for low values of n yield a better plot?

DONALD GRAHAM.—The normal BET plot was not linear but a better line was obtained by use of lower coverage data as suggested by MacIver and Emmett (*J. Phys. Chem.*, 60, 824 (1956)). This gave a V_m of 217 ml./g. compared with the 198 ml./g. indicated by the heat curve.

GEORGE R. LESTER.—Is it proper to consider the dispersion constant-density product as representing interaction energy for such high area materials as the amorphous carbon, especially in view of the suggested cage-like structure proposed by Gibson, *et al.* I realize the product is only relative, but question the comparison of these products for materials so different in area as amorphous carbon and diamond dust or P-33.

DONALD GRAHAM.—The dispersion constant-density product is, of course, only proportional as a first approximation to interaction energy and does indeed suffer from the extreme porosity of amorphous carbon. The effects of wall thinness and pore condensation oppose each other with the resulting over-all error probably tending to make the calculated value high. The observed discrepancy, however, is quite large and in the opposite direction, so any improvement in the approximation would be expected to show the dispersion energy calculation to be still less satisfactory.

D. J. C. YATES (Columbia University).—Would you care to comment on the rather surprising similarity of the heat curves for diamond and amorphous carbon? It might seem that the heat curves are rather insensitive to changes in the crystallographic nature of carbon.

DONALD GRAHAM.—The similarity of the heat curves for the adsorption of nitrogen on diamond dust and on amorphous carbon is particularly significant because of the roughly two-fold difference between their densities. The effect of difference in crystal structure, or more, explicitly, electronic character, is thus opposite and approximately equal to the effect of the difference in density.

The heterogeneity of the amorphous carbon surface was expected. That of the diamond dust was consistent with the surface roughness indicated by electron microscopy.

---

[16] D. Graham and W. D. Phillips, *Proc. Second Internatl. Congr Surface Activity*, **2**, 22 (1957).

HYDROGEN SORPTION ON GRAPHITE AT ELEVATED TEMPERATURES[1,2]

BY J. P. REDMOND AND P. L. WALKER, JR.

Department of Fuel Technology, The Pennsylvania State University, University Park, Pennsylvania

Received March 7, 1960

The sorption of hydrogen on selected types of nuclear and spectroscopic graphite has been studied. On nuclear graphite, the desorption of hydrogen over the temperature range 1035 to 1375° follows the Elovich equation. The activation energy of desorption over the coverage range (θ), 0.32 to 0.68, can be approximated as $E' = 137 - 42(\theta)$ kcal./mole. On the basis of limited results, it is found that the adsorption of hydrogen at 1335° on nuclear graphite can also be expressed by the Elovich equation. Isotherms for sorption of hydrogen on both nuclear and spectroscopic graphites over the temperature range 920 to 1495° are of the Temkin-type. However, at temperatures of 1085° and above, the isotherms consist of two straight-line regions of markedly different slopes. From the isotherms at 1335 and 1495° for the nuclear graphite, the heat of adsorption over the coverage range, 0.50 to 0.80, can be approximated as $Q = 58 - 56(\theta)$ kcal./mole. It is concluded that the adsorption of hydrogen occurs on carbon atoms at the edge of crystallites and that significant intracrystalline sorption does not occur.

Introduction

Artificial graphite of use in graphite-moderated nuclear reactors, as anodes for mercury vapor rectifiers, and crucibles for vacuum fusion work should contain little gas. Otherwise, when the graphite is heated to operating temperatures, the gas desorbs from the graphite resulting in adverse effects. For example, in the graphite-moderated nuclear reactor, hydrogen and carbon monoxide released from the graphite can interact with the fuel cladding material (usually zirconium or stainless steel) resulting in hardening and embrittlement of the metal. Released carbon monoxide can disproportionate on the cooler metal heat exchanger surfaces depositing carbon,[3] resulting in an adverse effect on the heat transfer and flow properties of the system.

A number of workers[4-8] have determined the amount and analysis of gases which are desorbed from graphite and amorphous carbons upon heating *in vacuo*. In general, they report that hydrogen and carbon monoxide are the major constituents of the released gas (especially at the higher temperatures), with significant amounts of carbon dioxide and water vapor released at the lower temperatures. In some cases, hydrocarbons also are released.

Little definitive work is available on the rates of sorption (adsorption and/or desorption) of gases from graphite. Eltzin and Jewlew[9] conclude from rate measurements that the evolution of gas from graphite consists of two first-order processes—desorption from the external surface and diffusion from the interior of the graphite structure to the surface. Barrer,[10] whose work will be discussed later, studied the rate of hydrogen adsorption on graphite and diamond.

In recent years, many workers have found the equation

$$\frac{dq}{dt} = ae^{-\phi q} \qquad (1)$$

to be applicable to their adsorption data for a wide variety of systems, where dq/dt is the rate of adsorption and a and ϕ are constants. Equation 1, which is now commonly called either the Elovich or Roginsky-Zeldovich equation can be derived theoretically on the basis of a linear increase in activation energy of adsorption with increase in surface coverage.[11] As will be seen, equation 1 will be applicable in the present studies.

In the present studies, the rate of hydrogen adsorption and desorption from graphite has been investigated. Also adsorption isotherms for hydrogen on graphite have been obtained. Hydrogen has been chosen for the initial study since it is the major constituent released from nuclear and spectroscopic graphites at elevated temperatures. Additional work is in progress studying the sorption of carbon monoxide and mixtures of hydrogen and carbon monoxide on graphite.

Experimental

Apparatus.—The graphite samples used in this study were cylindrically shaped, 1 in. long by 1/2 in. in diameter. A 0.035 in. diameter hole, 3/8 in. deep, was drilled into one end of each sample. The sample was supported by a tungsten wire (0.028 in. in diameter and 2.5 in. long) which was inserted into the hole in the graphite sample and in turn cemented to a 7/8 in. diameter mullite base. The base supporting the sample sat in the bottom of a 1 in. diameter quartz tube which served as the sorption chamber. A quartz window was sealed to the bottom of the quartz tube and a standard taper connected to the top. A Pyrex section containing a mating standard taper and an optical window connected the quartz tube to the pumping and measuring system.

The pumping system consisted of a liquid nitrogen cold trap and a two stage Van Hespen mercury diffusion pump. The evolved gases were removed continually from the desorption chamber during a run, with the pump capable of operating against a back pressure of *ca.* 10 mm. The evolved gases not condensed in the liquid nitrogen trap (including all of the hydrogen) were pumped into a reservoir consisting of two 2 liter bulbs and 1.22 liters of connecting tubing. At intervals, a small fraction of the accumulated gas was bled through a Knudsen leak into a mass spectrom-

---

[1] Based on a Ph.D. thesis submitted by J. P. Redmond to the Graduate School of The Pennsylvania State University, June, 1959.

[2] This paper presents the results of one phase of research carried out under Contract No. AT(30-1)-1710, sponsored by the Atomic Energy Commission.

[3] P. L. Walker, Jr., J. F. Rakszawski and G. R. Imperial, THIS JOURNAL, **63**, 133 (1959).

[4] P. Lebeau and M. Picon, *Compt. rend.*, **179**, 264 (1924).

[5] E. J. Norton and A. L. Marshall, *Trans. Am. Inst. Mining Met. Engrs.*, **156**, 351 (1944).

[6] R. L. Carter and R. R. Eggleston, Proceedings of the First and Second Carbon Conference, U. of Buffalo, N. Y., pp. 149–153, 1956.

[7] R. B. Anderson and P. H. Emmett, THIS JOURNAL, **51**, 1308 (1947).

[8] R. B. Anderson and P. H. Emmett, *ibid.*, **56**, 753 (1952).

[9] I. A. Eltzin and A. P. Jewlew, *Physik. Z. Sowjetunion*, **6**, 687 (1934).

[10] R. M. Barrer, *J. Chem. Soc.*, 1256 (1936).

[11] B. M. W. Trapnell, "Chemisorption," Butterworth Scientific Publications, London, 1955, pp. 103–106.

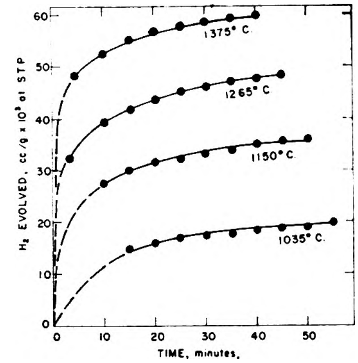

Fig. 1.—Rate of hydrogen desorption from virgin nuclear graphite (TSP) at different temperatures.

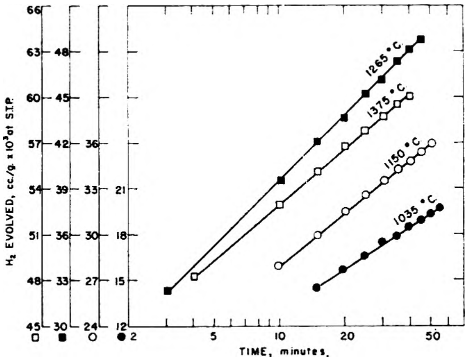

FIGURE 2

Fig. 2.—Elovich plots for hydrogen desorption from virgin nuclear graphite (TSP) at different temperatures.

eter to determine the hydrogen pressure. With the leak used, the maximum pressure which could be measured by the mass spectrometer was *ca.* 200 μ.

Power to heat the graphite sample was supplied by a 5 Kw. high-frequency induction generator. A "radiamatic" pyrometer located above the optical window in the sorption chamber sighted on the graphite sample, with its signal being fed into a recorder-controller. The output from the controller was fed in turn to a saturable reactor which gave a two-position control action for the induction generator. This regulation system controlled the temperature to ±10°.

The "radiamatic" pyrometer did not indicate the "true" temperature of the graphite sample because the target was too small to be focused properly on the thermopile. Therefore, this temperature was read by a disappearing filament optical pyrometer. In turn, this temperature was corrected for the emissivity of the graphite and absorptivity of the optical window to yield the true temperature.

Procedure for Measuring the Rate of Desorption of Hydrogen from Graphite.—After placing the graphite sample in the sorption chamber, the apparatus was outgassed at room temperature for at least 12 hours. A run was initiated when the induction generator was turned on and the graphite heated to a predetermined temperature. At regular intervals, a sample of the accumulated gas was bled into the mass spectrometer for hydrogen analysis. The lag time between the release of the hydrogen from the graphite sample and the recording of desorbed hydrogen by the mass spectrometer was *ca.* 10 seconds.

Procedure for Measuring the Rate of Adsorption of Hydrogen on Graphite.—The graphite was cleaned by degassing it at 2000° for about 30 minutes, prior to cooling the sample to room temperature under vacuum. A known pressure of prepurified hydrogen (less than 200 μ) was admitted to the system at room temperature and the graphite sample rapidly heated to the adsorption temperature. The decrease in pressure of hydrogen with time was followed by introducing some gas into the mass spectrometer at known time intervals. A correction for the decrease in pressure caused by loss of hydrogen to the mass spectrometer was made. With a reservoir volume of 5.2 liters, there was not a large pressure change during a typical run. At the conclusion of a run, the sample was cooled quickly to room temperature (by turning off the induction power supply) and the hydrogen remaining in the gas phase was evacuated. The sample was then reheated to 2000°, the quantity of desorbed hydrogen measured and compared with the amount calculated to have been adsorbed. The agreement, for the run reported, was within 5%.

Procedure for Measuring Adsorption Isotherms.—The graphite was cleaned by degassing at 2000°, prior to cooling to room temperature. A known pressure of hydrogen was admitted, the sample heated quickly to a predetermined temperature, and the sample held at this temperature for at least one hour. The sample was quickly cooled to room temperature and the hydrogen remaining in the gas phase removed. The sample was again heated to 2000° and the amount of hydrogen desorbed determined. Isotherms were obtained by repeating this procedure for various pressures of hydrogen at a constant temperature.

Description of Graphites Used.—One grade of nuclear graphite (TSP) and one grade of spectroscopic graphite (AGKSP) manufactured by the National Carbon Company were used in this study. The raw materials used for the production of the graphites were petroleum coke and coal tar pitch. A detailed description of the manufacture and general properties of these graphites can be found elsewhere.[12-14] Table I lists some selected properties for the graphites.

Table I

Selected Properties of the Graphites

Property	Graphite TSP	Graphite AGKSP
BET surface area, m.²/g.	0.30	0.40
Apparent density, g./cc.	1.70	1.56
True density, g./cc.	2.26	2.26
Porosity, %	25.2	31.2
Total ash content, %	0.004	<0.001

Results

Rate of Desorption of Hydrogen from Graphite.—Figure 1 shows typical curves for hydrogen evolution from a nuclear graphite (TSP) at a series of temperatures. A new sample of graphite was used for each temperature run. Figure 2 shows linear plots for these data, when the volume of hydrogen evolved is plotted against the log of time (called Elovich plots).

If the energy of activation for desorption, E', decreases linearly with increasing surface coverage (θ)

$$E' = E_0' - \beta\theta \tag{2}$$

and θ is not close to zero, Trapnell[11] shows that

$$\theta = \frac{RT}{\beta}\ln\frac{RT}{\beta b} - \frac{RT}{\beta}\ln t \tag{3}$$

where b is a constant. Since $\theta = 1 - q/v_m$, where q is the volume of hydrogen desorbed at time t and v_m is the total amount of hydrogen desorbed, equation 3 can be expressed as

$$q = \frac{RTv_m}{\beta}\ln t - \frac{RTv_m}{\beta}\ln\frac{RT}{\beta b} - v_m \tag{4}$$

where RTv_m/β, $RT/\beta b$ and v_m are constants at constant temperature (T) for a given graphite. Thus, plots of q *vs.* $\ln t$ will be linear, as is found in Fig. 2.

---

(12) H. W. Abbott, "Encyclopedia of Chemical Technology," Vol. 3, The Interscience Encyclopedia, Inc., New York, N. Y., 1949, pp. 1–23.

(13) L. M. Currie, V. C. Hamister and H. G. MacPherson, "The Production and Properties of Graphite for Reactors," International Conference on the Peaceful Uses of Atomic Energy, 1955.

(14) P. L. Walker, Jr., and Emile Raats, This Journal, **60**, 364 (1956).

In these desorption studies, v_m was taken as the total amount of hydrogen evolved when the graphite was heated to a maximum temperature of 2000°, under experimental conditions previously described. For the TSP samples on which degassing rates were determined at temperatures of 1035, 1150, 1265 and 1375° (Fig. 1), v_m values were 0.071, 0.075, 0.076 and 0.069 cc./g. (S.T.P.), respectively.

It is possible to determine the activation energy for desorption from data on the rate of desorption at various temperatures at constant θ. In order to obtain these data, it was necessary to extrapolate, in some cases, q *vs.* ln t plots to overlapping regions of θ. Figure 3 presents Arrhenius plots for the desorption of hydrogen from TSP graphite (data shown in Fig. 1) for various coverages. From Fig. 3, the activation energy is calculated to vary from 108 ± 3 kcal./mole at $\theta = 0.68$ to 124 ± 3 kcal./mole at $\theta = 0.32$.

In Fig. 4, the variation in activation energy for desorption with coverage is shown for the TSP graphite. The linear decrease in activation energy over the limited range of coverage studied can be expressed by the equation $E' = 137 - 42(\theta)$ kcal./mole.

Values of β also can be calculated by two additional methods. For each adsorption temperature in Fig. 3, the different rates for different coverages can be attributed to a variation in $e^{-E'/RT}$ with coverage. Thus, $\Delta E'$ can be calculated for a change in coverage. From values of $\Delta E'$ calculated at each desorption temperature studied, as coverage goes from 0.68 to 0.32, β is found to equal 37.5 ± 0.5 kcal./mole. It is recalled, according to equation 4, that the slope of an Elovich plot equals RTv_m/β. The plots in Fig. 2 at different temperatures yield a value of 42.0 ± 2.3 kcal./mole for β. Thus, the three methods of determining β yield values in reasonable agreement.

Limited desorption studies (at 925°) were conducted on spectroscopic graphite (AGKSP). For this graphite, desorption of hydrogen was measured over a period of 300 minutes, in contrast to the shorter desorption periods studied for hydrogen release from TSP graphite. The objective of the longer desorption run for the spectroscopic graphite was to put the Elovich equation to a more severe test. Keier and Roginsky[15] studied the kinetics of hydrogen desorption from sugar charcoal over periods of time of up to 700 minutes. Their plots of volume desorbed *vs.* log of time were not linear after approximately 100 minutes, but became convex to the abscissa for longer times. Figure 5 shows that the evolution of hydrogen as a function of time for the spectroscopic graphite can be expressed by the Elovich equation, at least for desorption times up to 300 minutes at 925°.

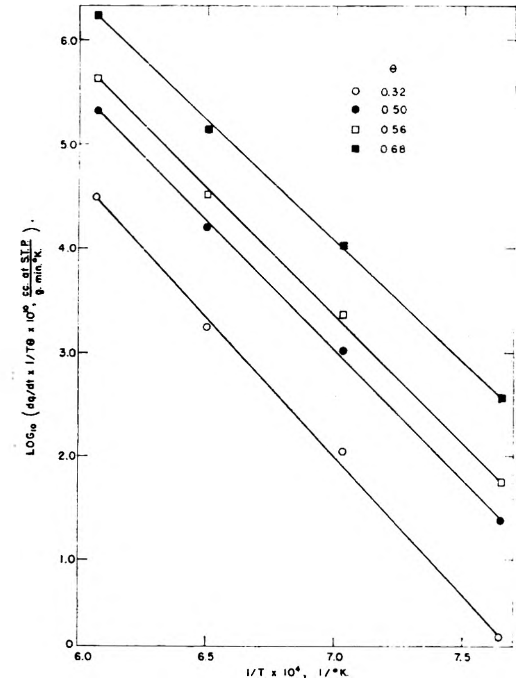

Fig. 3.—Arrhenius plots for hydrogen desorption from virgin nuclear graphite (TSP) at different coverages.

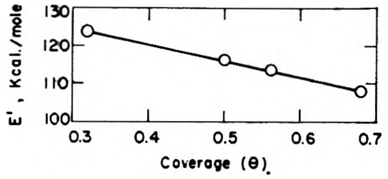

Fig. 4.—Variation in activation energy with coverage for desorption of hydrogen from virgin nuclear graphite (TSP).

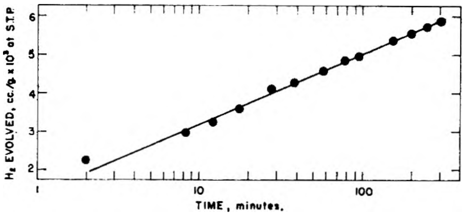

Fig. 5.—Elovich plot for hydrogen desorption from virgin spectroscopic graphite (AGKSP) at 925°.

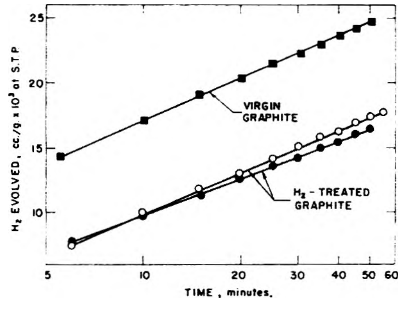

Fig. 6.—Elovich plots for hydrogen desorption from virgin and hydrogen-treated nuclear graphite (TSP) at 1085°.

To this point, the rate of hydrogen desorption from virgin graphite has been discussed. It is of interest to consider the rate of hydrogen evolution from graphite to which hydrogen has been added under controlled conditions. Results of such an experiment are shown in Fig. 6 for a sample of TSP graphite. The rate of hydrogen evolution from the virgin sample was first measured at 1085°, as shown, prior to its being heated to 2000° to remove the remaining hydrogen. The sample was then exposed to an arbitrary hydrogen pressure of 100 mm.

---

[15] N. P. Keier and S. Z. Roginsky, *Zhur. fiz. Khim.*, **23**, 897 (1949).

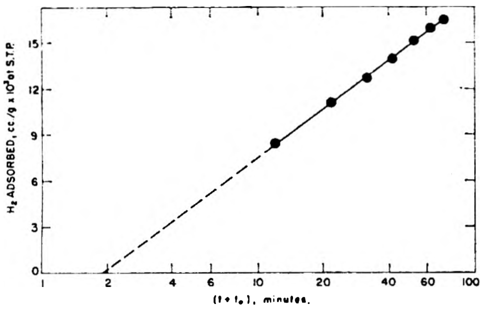

Fig. 7.—Elovich plot for hydrogen adsorption on nuclear graphite (TSP) at 1335° and 50 μ pressure (t_0 = 2 minutes).

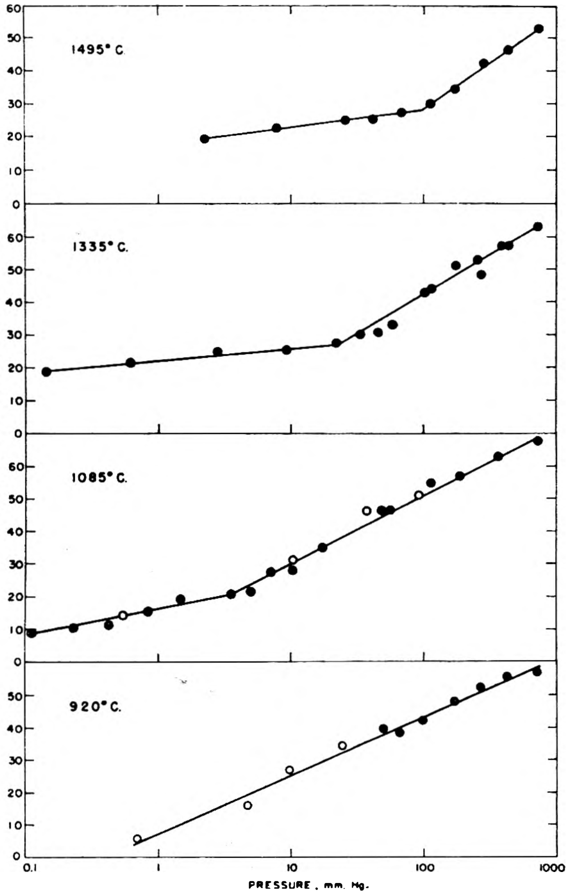

Fig. 8.—Temkin isotherms for the adsorption of hydrogen on nuclear graphite (TSP). (● and ○ represent equilibration times of 75 and 240 minutes, respectively.)

at 1085° for 30 minutes, followed by rapidly cooling the sample to room temperature and evacuating the remaining gaseous hydrogen. The sample was reheated to 1085° and the rate of hydrogen evolution measured. Following this run, the identical procedure was again repeated on the same sample of graphite and another desorption run performed at 1085°. The three runs can be expressed by the Elovich equation, with the slope of the curves the same within experimental error. From the slope of the Elovich plots for the two samples treated in hydrogen, β equals 43.3 ± 0.4 kcal./mole, in close agreement with the value previously found for hydrogen released from virgin TSP graphite over a range of temperatures.

Rate of Adsorption of Hydrogen on Graphite.—Only limited work was done studying the rate of hydrogen adsorption on graphite, since the main interest was desorption kinetics. If the energy of activation for adsorption, E, increases linearly with increasing surface coverage

$$E = E_0 + \alpha\theta \qquad (5)$$

and θ is not close to unity, Trapnell[11] shows that

$$q = \frac{RTv_m}{\alpha}\ln\,[t + t_0] - \frac{RTv_m}{\alpha}\ln t_0 \qquad (6)$$

where $t_0 = RT/\alpha a$ and a is a constant. Thus, at constant temperature, plots of q *vs.* log $(t + t_0)$ will be linear. Such a plot is shown in Fig. 7 for the adsorption of hydrogen on TSP graphite at 1335°. The adjustable constant, t_0, has a value of 2 minutes for this run. It is noted that with $t_0 = 2$, $q \rightarrow 0$ when $(t + t_0) = 2$ or $t \rightarrow 0$. Thus, there is no indication, under these conditions, of a very rapid, massive initial adsorption of hydrogen (which does not obey the Elovich equation) on TSP graphite. Rapid, initial chemisorption of hydrogen on some oxide systems has been reported by Taylor and Thon.[16]

Adsorption Isotherms of Hydrogen on Graphite.—Since $E' = E + Q$, where Q is the heat of adsorption, it follows that the variation in Q with coverage can be given as

$$Q = Q_0 - \sigma\theta \qquad (7)$$

if equations 2 and 5 hold. Trapnell[17] shows that over the middle range of coverage, for either a uniform or non-uniform surface

$$v = \frac{v_mRT}{\sigma}\ln A_0 + \frac{v_mRT}{\sigma}\ln p \qquad (8)$$

where A_0 is a constant. At constant temperature, if equation 8 is obeyed, a plot of v *vs.* ln p will be linear. Such a plot is usually called a Temkin isotherm.[17]

Adsorption isotherms of hydrogen on TSP graphite have been determined over the temperature range 920 to 1495° and plotted according to equation (8) as shown in Fig. 8.[18] At an adsorption temperature of 920°, the Temkin isotherm is linear over the entire pressure range studied. For the higher adsorption temperatures, the isotherms consist of two straight-line regions of markedly different slopes. The pressure at which the slope changes increases with increasing temperature. Possibly, such breaks in the isotherms are caused by surface heterogeneity or the advent of substantial surface mobility[19]; however, no one explanation is proposed at this time.

Figure 9 presents a Temkin isotherm for hydrogen adsorption on spectroscopic graphite (AGKSP) at 1085°. Again, the isotherm consists of two straightline regions of markedly different slopes. The change in slope occurs as close to the same ad-

---

(16) H. A. Taylor and N. Thon, *J. Am. Chem. Soc.*, **74**, 4169 (1952).

(17) Ref. 11, p. 124.

(18) At a temperature of 1180°, the volume of hydrogen adsorbed on samples of TSP graphite varying in weight from 0.7 to 5.3 g. was measured. The results could be extrapolated to essentially zero volume of hydrogen adsorbed at zero weight of graphite, indicating that hydrogen adsorption on the tungsten support-wire was negligible.

(19) A. R. Miller, *Disc. Faraday Soc.*, **8**, 68 (1950).

sorption pressure as that found for TSP graphite at 1085°.

From the adsorption isotherms of hydrogen on TSP graphite, adsorption isobars can be plotted. Five isobars are shown in Fig. 10, over the pressure range 1 to 760 mm. As originally discussed by Taylor,[20] for an adsorption process having a substantial activation energy, isobars are expected to go through a maximum with increasing temperature. The greater the activation energy, the higher the temperature at which the maximum should occur. From Fig. 10, it is seen also that the adsorption pressure can shift the temperature at which the maximum occurs in the isobars.

Numerous other workers have confirmed Taylor's hypothesis (regarding a maximum in the isobar for a chemisorption process) experimentally for diverse adsorption systems. Specifically, in the case of carbon, Barrer[21] found that for hydrogen adsorption on charcoal, the isobar (1000 mm.) went through a maximum at *ca.* 680°. Barrer's finding the maximum in the isobar at a lower temperature than that found in the present work is consistent with the lower activation energy for adsorption of hydrogen on charcoal,[21] as will be discussed shortly.

Using the Clausius–Clapeyron equation and isotherm data for temperatures of 1335 and 1495°, heats of adsorption have been calculated for different amounts of hydrogen adsorbed. The results are shown in Fig. 11. To obtain coverages, v_m values of 0.066 and 0.056 cc./g. were taken at 1335 and 1495°, respectively. The volume of hydrogen adsorbed was estimated to approach asymptotically these v_m values when volume *vs.* pressure plots were extrapolated to a pressure of *ca.* 1000 mm. Over the range of coverage studied, the change in heat of adsorption with coverage can be approximated by $Q = 58 - 56(\theta)$ kcal./mole. Since $E = E' - Q$, it follows that over the range of coverage for which Q and E' are both known (that is, $0.50 < \theta < 0.68$) the activation energy for adsorption of hydrogen on TSP graphite is approximated by $E = 79 + 14(\theta)$ kcal./mole.

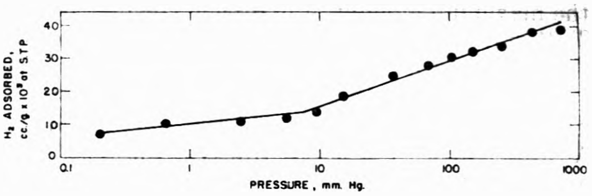

Fig. 9.—Temkin isotherm for the adsorption of hydrogen on spectroscopic graphite (AGKSP) at 1085° (● represents an equilibration time of 75 minutes).

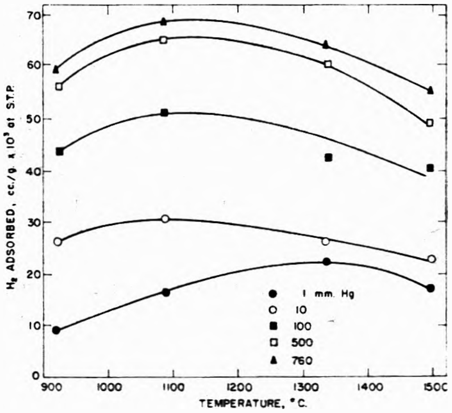

Fig. 10.—Isobars for the adsorption of hydrogen on nuclear graphite (TSP) over the temperature range 920 to 1495°.

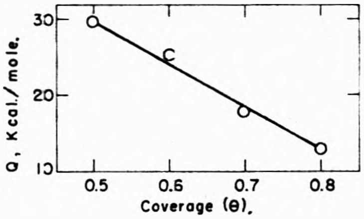

Fig. 11.—Variation in heat of adsorption of hydrogen on nuclear graphite (TSP) with coverage determined from isotherm data at 1335 and 1495°.

Discussion

It is of interest to consider the possibilities of where hydrogen chemisorption on graphite is occurring. In particular, is there sufficient carbon surface to accommodate all the chemisorbed hydrogen or is it necessary to postulate significant intracrystalline sorption of hydrogen?

Necessary for these considerations is an understanding of the structure of graphite bodies—including so-called nuclear and spectroscopic graphites. As discussed previously,[14] the raw materials used for the production of graphite bodies consist of about 25% coal tar pitch and 75% calcined petroleum coke flour. Upon mixing and either extruding or molding of the "green mix" of pitch and coke, the coke particles are coated with a layer of pitch to a thickness amounting to about 7% of the particle diameter.[22] Subsequent baking and graphitizing of the green bodies produce "graphite," which consists of graphitized filler particles bound together by a graphitized binder phase. Properties of the graphite bodies of significance in the present discussion are: (1) the carbon in both the filler and binder phases is multi-crystalline, and (2) the bodies have a significant amount of porosity which is closed to helium at room temperature.[23] As shown by Walker and co-workers,[23] the closed porosity is produced by the stacking of crystallites, the more random the stacking the larger the closed-pore volume.

In agreement with Savage[24] and others, it appears reasonable to assume the hydrogen is chemisorbed as atoms; and so far as surface sorption is concerned, the chemical bonding between hydrogen and carbon atoms occurs only at edges of carbon crystallites and not on the basal plane surfaces. Since for a graphite crystallite the distance between edge carbon atoms is 2.46 Å. and the distance between basal planes is 3.35 Å., an edge carbon atom occupies an area of 8.3 Å.². If one hydrogen atom is assumed to chemisorb on an edge carbon atom,[25]

---

[20] H. S. Taylor, *J. Am. Chem. Soc.*, **53**, 578 (1931).

[21] R. M. Barrer, *Proc. Roy. Soc.* (*London*), **149A**, 253 (1935).

[22] S. Mrozowski, "Proceedings of the First and Second Conference on Carbon," U. of Buffalo, Buffalo, N. Y., 1956, pp. 195–216.

[23] P. L. Walker, Jr., F. Rusinko, Jr., J. F. Rakszawski and L. M. Liggett, "Proceedings of the Third Conference on Carbon," Pergamon Press, New York, N. Y., 1959, pp. 643–658.

[24] R. H. Savage, *Ann. N. Y. Acad. Sci.*, **53**, 862 (1951).

the maximum amount of hydrogen chemisorbed on TSP graphite ($v_{m(\max.)}$ = 0.071 cc./g.) would occupy a surface area of 0.31 m.^{2}/g.

Now, consider the average crystallite size in TSP graphite as being 1000 Å. in diameter and 400 Å. in height.[27] For a crystallite of this size, 44% of the crystallite surface area is edge area and 56% is basal plane area. If on this basis it is postulated that 44% of the BET surface area is composed of crystallite edges, it is estimated that the BET area available for adsorption of hydrogen on TSP graphite is 0.13 m.^{2}/g. This is considerably less than the 0.31 m.^{2}/g. of surface which the chemisorbed hydrogen is thought to occupy. Actually, the discrepancy can be still greater if crystallite alignment is considered. That is, it is known[23] that the filler particles in graphite are more or less "flake-like," the amount of flake-like character depending upon the degree of crystallite orientation within the particle. Since the orientation of the crystallites occurs with their long side (basal-plane side) parallel to the particle surface, the percentage of edge surface contributing to the BET area, in the above case, would be expected to be less than 44%.

The discrepancy between the area calculated to be occupied by chemisorbed hydrogen and that available from BET measurements, could be explained in at least two ways: (1) Hydrogen, in part, is penetrating between the basal planes of the carbon crystallites; and (2) at chemisorption temperatures, there is more area available for hydrogen adsorption than indicated by low temperature (78°K.) nitrogen adsorption. The second reason appears the more likely. Considering the first possibility, Hennig[28] has shown that compounds or elements entering interstitially into spectroscopic graphite markedly affect the electrical properties of the graphite, including its electrical resistivity. In the present work, no detectable change in electrical resistivity of the graphite samples was observed after essentially complete hydrogen removal by degassing at 2000°. The entrance of compounds or elements between the basal planes of graphite also has been found to increase significantly the spacing between basal planes.[29] In the present work, X-ray diffraction measurements showed no change in interlayer spacing upon degassing of graphite. Considering the second possible explanation for the discrepancy between the amount of hydrogen chemisorbed and the BET surface area, two points are considered significant: (1) On the basis of the crystallite size assumed for TSP graphite, 17.6 m.^{2}/g. of edge area is theoretically available for hydrogen chemisorption. (2) Most of this area is thought to be located in the closed pore volume previously discussed. It is suggested that hydrogen at elevated temperatures has access to a fraction of the closed surface area (volume) which was unavailable to both nitrogen at 77°K. and helium at room temperature. This is consistent with at least three facts: (1) The hydrogen molecule is smaller than nitrogen or helium. (2) Diffusion into molecular sized openings is activated and would be considerably more rapid at elevated temperatures. (3) With increasing temperature, the effective size of molecular pore openings is increased because of a greater magnitude of oscillation of the atoms around the opening.[30] To have sufficient area to accommodate the chemisorbed hydrogen, it is necessary that only about 2% of the total crystallite edge area be available at the elevated temperatures where adsorption measurements were made. Barrer[21] also concludes that hydrogen adsorption on "charcoal" at elevated temperatures does not occur by a process of hydrogen penetration between basal planes.

Briefly, the activation energy and heat of adsorption data can be considered. As discussed by Boudart,[31] the change in heat of adsorption with coverage can be the result of the superposition of three distinct phenomena: (1) *a priori* heterogeneity of the surface, (2) induced heterogeneity (induction), and (3) lateral interaction between adsorbed species. In the present study, it would appear that the third phenomenon should be of little importance except at $\theta \rightarrow 1$, because of the small size of the hydrogen atom compared to the spacing between neighboring edge carbon sites and the low polarizability of adsorbed hydrogen.[31] Boudart shows that when induced heterogeneity (produced by the formation of an electric double layer at the surface) is of importance the heat of adsorption should fall linearly with coverage. On the other hand, even though *a priori* heterogeneity also will cause the heat of adsorption to fall with increasing coverage, the nature of this fall-off is uncertain. It is dependent upon the distribution of site energies on the surface of the solid. Therefore, the present results suggest that the linear decrease in heat of adsorption (and activation energy of desorption) with increasing coverage, over the middle range of coverage, probably is caused by induced heterogeneity.

Barrer[10] reports a value of 45 kcal./mole for the heat of adsorption of hydrogen on "Acheson" graphite at a coverage of 0.5 at 790°. He also reports[21] a value of 50 kcal./mole for the heat of adsorption of hydrogen on "charcoal" at a coverage of about 1% over the temperature range 898 to 950°. These values, in addition to the heats of adsorption found in the present work, are considerably less than the calculated value of 108 kcal./mole[26] based on the energies of the C–H and H–H bonds. Upon comparing this calculated value with the experimental value of 50 kcal./mole found by Barrer on charcoal, Long and Sykes[26] suggest that the difference in energies is caused by the loss of resonance energy in the carbon upon chemisorption. In the case of Barrer's result on "Acheson" graphite and the present results, the large difference in heats of adsorption between theory and experiment could also be due, in part, to induced hetero-

---

(25) Actually, some edge carbon atoms are thought to be able to accommodate two chemisorbed hydrogen atoms,[26] but the percentage which do is considered small.

(26) F. J. Long and K. W. Sykes, *Proc. Roy. Soc.* (*London*), **193A**, 377 (1948).

(27) P. L. Walker, Jr., H. A. McKinstry and J. V. Pustinger, *Ind. Eng. Chem.*, **46**, 1651 (1954).

(28) G. Hennig, *J. Chem. Phys.*, **20**, 1443 (1952).

(29) W. Rudorff, *Z. anorg. allgem. Chem.*, **245**, 383 (1941).

(30) D. W. Breck and J. V. Smith, *Sci. Amer.*, **200**, No. 1, 85 (1959).

(31) M. Boudart, *J. Am. Chem. Soc.*, **74**, 3556 (1952).

geneity lowering the experimental values at the high coverage studied.

In conclusion, the close agreement between v_m values for TSP graphite as determined from desorption of hydrogen up to 2000°, and $v_{m(max.)}$ estimated from adsorption isotherm data is, perhaps, surprising. That is, the virgin nuclear graphite used for the desorption studies had on its surface a substantial amount of oxygen, in addition to hydrogen.[32] Upon outgassing up to 2000°, roughly 35% of the total gas desorbed was oxides of carbon. It might be thought that this oxygen would compete with hydrogen for adsorption sites and that the v_m value from outgassing experiments would be lower than $v_{m(max.)}$ from adsorption of hydrogen on previously degassed samples of graphite. The picture can be complicated, however, by the possibility that oxygen chemisorbed on carbon can act as a promoter for hydrogen chemisorption, as has been suggested to be the case on copper.[31] Also it is possible that hydrogen chemisorption was completed in the graphitizer before the graphite came in contact with, and chemisorbed, oxygen. Savage[24] shows that at low temperatures more oxygen than hydrogen is adsorbed on graphite "wear dust," suggesting that some chemisorption of oxygen is possible even when the carbon surface already has reached saturation with regard to hydrogen.

Acknowledgments.—The authors wish to thank Jean Worrall, L. G. Austin and E. T. Nelson for their helpful discussions during the progress of this work.

(32) J. P. Redmond, Ph.D. Thesis, The Pennsylvania State Univ., 1959.

ADSORPTION STUDIES ON METALS. IX. THE NATURE OF THE THERMAL REGENERATION OF OXIDE-COATED NICKEL, COBALT AND COPPER

By A. C. Zettlemoyer, Yung-Fang Yu and J. J. Chessick

Surface Chemistry Laboratory, Lehigh University, Bethlehem, Penna.

Received March 7, 1960

It is well known that oxidation of nickel, cobalt and copper at 25° proceeds by two steps, a fast followed by a slow process. Upon heating these oxide-coated metals at modest temperatures such as 300° *in vacuo*, oxidation will again proceed multimolecularly by a rapid step at 25° even though no oxygen was evolved during thermal treatment. The regeneration could be due to (a) migration of metal ions to the metal-oxide interface; (b) dissolution of the oxide film in the bulk metal; or (c) crystallization of the oxide film to reveal bare metal. In this work, organic vapors were used as a probe for any bare metal surface uncovered during regeneration. The heats of adsorption of *n*-propylamine and acetic acid on the bare, oxide-coated and regenerated metal surfaces support the contention of Dell[3] that recrystallization occurs. That is to say, initial heats of adsorption were much higher on the regenerated surfaces, in accord with the values for the freshly reduced metals, and were much lower on the oxide-coated surfaces. The extents of irreversible adsorption followed the pattern to be expected from the heat measurements.

Introduction

Russell and Bacon[1] first observed that reduced nickel saturated with oxygen near 0° and then heated at 300° *in vacuo*, was able to adsorb oxygen again at 0° even though no oxygen was evolved during thermal treatment. Low temperature oxidation and thermal regeneration of nickel, cobalt and copper has been the subject of a number of papers[2] from this Laboratory. It was found that the oxidation of reduced nickel, cobalt and copper powders at 25° (or below) proceeds in two steps: an initial fast process followed by a slow, exponential decay process. During the fast process, three apparently non-activated processes probably take place: chemisorption of oxygen on bare metal, oxide formation from one to several layers and oxygen chemisorption on the underlying oxide as O^- ions. The slow process can be explained semiquantitatively by the Mott and Cabrera theory for very thin oxide film growth. Accordingly, the electric field created across the thin oxide film, *i.e.*, between the adsorbed oxygen anions on the surface and the metal cations at the metal–oxide interface, aids the cations to diffuse through the oxide outward to the surface where they react with oxygen to form oxide. Oxidation stops, or at least proceeds at a very low rate, at some limiting film thickness.

These film-covered surfaces took up oxygen again after heating to a high temperature *in vacuo*. This process could be accomplished if during thermal treatment: (a) the limiting film thickness is reduced by migration of metal atoms to the metal–oxide interface; (b) the oxide film dissolves into the bulk of the metal; or (c) the oxide crystallizes into discrete crystallites covering a part of the surface. Dell[3] recently reviewed pertinent work in the literature and concluded that recrystallization occurs during the regeneration process. This hypothesis of Dell's was based on deductive reasoning and needs quantitative data for support. The object of this work is to obtain such data. Organic vapors were used as a probe for any bare metal surface uncovered during regeneration.

(1) W. W. Russell and O. C. Bacon, *J. Am. Chem. Soc.*, **54**, 54 (1932).

(2) (a) Y.-F. Yu, J. J. Chessick and A. C. Zettlemoyer, *Advances in Catalysis*, **9**, 415 (1957); (b) J. J. Chessick, Y.-F. Yu and A. C. Zettlemoyer, "Proceedings of the Second World Congress on Surface Activity," Vol. II, Academic Press, New York, N. Y., 1957, p. 269; (c) A. C. Zettlemoyer, Y.-F. Yu, J. J. Chessick and F. H. Healey, This Journal, **61**, 1319 (1957).

(3) R. M. Dell, *ibid.*, **62**, 1139 (1958).

Experimental

Materials.—The nickel, copper and cobalt powders were prepared by thermal decomposition of C.P. nickel carbonate, basic copper carbonate and hydrated cobalt nitrate, respectively, under reduced pressure at 400°. The outgassing was continued for 12 hours beyond the point of no apparent gas evolution. These nickel, copper and cobalt samples were then reduced with dry hydrogen at 400, 300 and 350°, respectively. After reduction the metal powders were degassed at 10^{-6} mm. at 450, 350 and 400°, respectively, just prior to adsorption studies. These temperatures are the lowest permissible so that sintering could be minimized.

The organic liquids used to provide the adsorption vapors were reagent grade. They were dried with anhydrous magnesium sulfate and then frozen and pumped through several cycles. Only the middle portions were taken for the adsorption measurements.

Adsorption Apparatus.—The basic feature of the adsorption apparatus is the Teflon stopcocks. Besides the simplification these stopcocks made possible, they eliminated possible contamination of the metal samples with mercury from the cut-offs usually employed. These stopcocks would not hold a good vacuum at the outset, but they steadily improved when operated frequently during the first ten days of use. A liquid nitrogen trap was employed between the adsorption system and the pumps.

The adsorption system includes a sample tube, glass break-seal, organic vapor reservoir and a calibrated doser, and it is terminated with a glass Bourdon spoon gage. The gage is balanced with helium pressure which is measured by an Apiezon B oil manometer; small deflections of the gage from zero are determined by a microscope eyepiece. The equilibrium pressures can be determined to ±0.02 mm. and the range of the oil manometer is from 0–10 cm. A side arm is attached to the gage and immersed in silicone oil to dampen vibrations.

The reduced samples were sealed off and transferred to the adsorption apparatus. The seal was broken by a magnetically operated plunger just prior to each run. For studies on oxide-coated surfaces, the reduced powders were first exposed to dry oxygen at 25° and 1 cm. for 10 minutes so that the oxide films resulting were from 10 to 15 Å. thick.

After each initial isotherm on a given surface, the system was outgassed at 25° employing a liquid nitrogen trap and high vacuum system for 24 hours to a vacuum of better than 10^{-6} mm. A good vacuum was obtained in about 4 hours. The isotherms were then repeated to give new BET V_m's. These and the initial V_m value were used to estimate the amount irreversibly adsorbed.

Nickel, copper and cobalt were activated *in vacuo* after oxidations at 350, 250 and 375°, respectively. These temperatures are 0.37 times the melting points of the metals in each case. Since the degree of regeneration is dependent on the temperature and time of activation, these variables were controlled to within 5° and 5 minutes, respectively.

Calorimeter.—The basic calorimeter design was that used previously for heats of chemisorption of oxygen on these same metals.[2] Modification included a glass break-seal so the sample could be transferred from the apparatus on which it was reduced and a 25 junction copper–constantan thermocouples with the reference junctions held within 0.1° of the adsorption temperature to minimize heat loss through the thermocouple wires. The e.m.f. was amplified then recorded on a Brown Recorder. The sensitivity of the calorimeter is 0.001° or about 0.01 cal.; the heat capacity of the filled calorimeter ranged from 10 to 15 cal. per degree.

It was estimated for the calorimetric heats recorded here that over 90% of the heat evolution occurred within the first two minutes after the introduction of each portion of organic vapor.

Results

Heat curves for the adsorption of *n*-propylamine on reduced, oxidized and regenerated samples of nickel and cobalt are plotted in Figs. 1 and 2 as a function of surface coverage, θ. The high initial heats for the amine on nickel suggest chemisorption, probably through electron transfer to the unfilled d-band of the metal. In contrast to the high initial heats obtained on the base metal surface, those for the oxidized nickel surface are much lower. There seems to be little doubt that physical adsorption predominates now. The heats of adsorption on the regenerated sample are the same as those found for adsorption on the reduced metal in the range of θ from 0 to ~ 0.7; thereafter they fall abruptly to values slightly less than those for the oxidized surface. The initial values suggest that metal atoms exist on the regenerated nickel surface and comprise about 70% of the available area.

The heat curve for propylamine adsorption on reduced cobalt is similar in shape to the one obtained with nickel; initial heat values, however, on reduced cobalt are considerably smaller. Again, initial heats of adsorption on the regenerated cobalt sample are in agreement with initial heats on the reduced sample. The data indicate that metallic areas comprising 60 to 70% of the external surfaces are re-exposed on both nickel and cobalt samples during regeneration. This agreement is not unexpected since equivalent members of oxide layers were deposited on both metals prior to regeneration. On the other hand, the total saturation amounts of oxygen taken up by reduced cobalt and nickel in numbers of layers are 10.2 and 4.4, respectively.

Heats of adsorption of *n*-propylamine on regenerated copper samples were not measured with sufficient precision to present here, but were of the same order of magnitude as on the oxide-coated surface. However, the lack of significant oxygen uptake on regenerated copper samples suggests little alteration in the state of the oxidized surface during regeneration. In another study, similar heats of adsorption were successfully measured for water on the bare, oxidized and regenerated copper surface. The similarity in the heat data for the adsorption of water on oxidized and regenerated copper samples plotted in Fig. 3 supports the belief that regeneration at 250° has little effect on the structure of the oxidized surface.

Heat values extrapolated to zero coverages, per cent. irreversibly adsorbed at 25° and 10^{-6} mm. and cross-sectional areas for the adsorption of *n*-propylamine on nickel, cobalt and copper samples are listed in Table I. Heat values and per cent. irreversibly adsorbed increase in the order

$$\mathrm{Cu} < \mathrm{Co} < \mathrm{Ni}$$

TABLE I

HEAT AND ADSORPTION DATA FOR *n*-PROPYLAMINE ADSORPTION ON METALLIC SAMPLES

	Cu	Co	Ni
Reduced			
$\Delta H_{(\theta=0)}$ (kcal./mole)	28	38	62
% Irreversibly adsorbed	19	27	58
C.S.A. (Å.^{2})	22	22	20
Oxide-coated			
$\Delta H_{(\theta=0)}$ (kcal./mole)	[a]	21	21
% Irreversibly adsorbed		7	0
C.S.A. (Å.^{2})		36	33

[a] Heat values at sufficiently low θ values were not measured.

Sharing of electrons of the amine grouping with unfilled d-levels in nickel and to a lesser extent in cobalt seems likely. The electron-rich copper cannot participate in such transfer. Cross-sectional area values of 20 to 23 Å.[2] suggest oriented, close-packing on all base metal surfaces. The low heats of adsorption at zero coverage and high per cent. reversibilities for propylamine on oxide-coated samples are indicative of physical adsorption and the cross-sectional areas suggest flat-wise orientation.

The heat curves for acetic acid adsorption on nickel and copper are plotted in Figs. 4 and 5. The high heat on reduced nickel suggests chemical reaction between the acid and nickel. In contrast, the acid is only physically adsorbed on reduced copper surface. Since the acid group is generally considered to be an electrophilic group, it is rather difficult to explain the chemisorption on the basis of the donation of electrons from acid to Ni. On the other hand, the fact that nickel is more electropositive than the copper in the electromotive series may explain the different behavior of the two metals.

The heats of adsorption on both oxidized nickel and copper surfaces indicate some type of strong interaction. Whether this is due to electrostatic interaction between the dipole of the acid and the isolated O^- of the oxide or actual chemical reaction cannot be decided on the basis of the present results alone. The absence of any water probably precludes the ordinary type of substitution reaction. Further study of these systems by other techniques such as infrared spectroscopy should be helpful.

Discussion

The similarities in the heat curves for propylamine adsorbed on reduced and regenerated surfaces of nickel and cobalt suggest similar processes. The excellent agreement between the heat values in the region of θ from 0 to about 0.7 for both the reduced and regenerated surface offers strong evidence for the presence of predominant available metal surface after the regeneration of the oxidized surfaces. Recrystallization of surface oxide into discrete crystallites which then migrate and localize at specific crystal faces, boundaries between different faces or heterogeneities, and existence of which leads to a reduction of surface free energy is the most logical explanation. This concept was first proposed by Dell[3] in an excellent review of the existing but not completely definitive data. Obviously, the degree of recrystallization depends on numerous factors such as the heterogeneity of the surface, metal type and surface free energies. The lack of observable recrystallization in the case of copper after regeneration at equivalent temperatures appears to be related in part to the homogeneity of its surface suggested by the linear acetic acid heat curves and its small available area which was generally one-fifth to one-tenth that for nickel and cobalt, respectively.

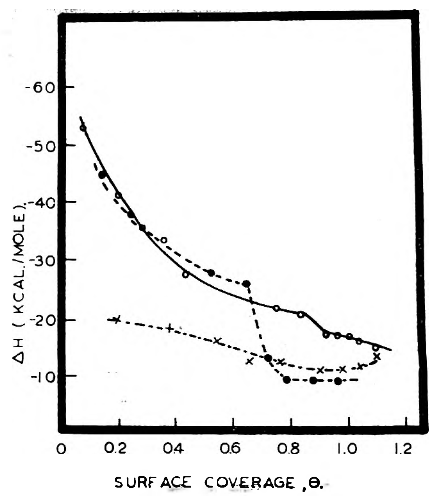

Fig. 1.—Heats of adsorption of n-propylamine on nickel at 21°: ○, reduced; ●, regenerated; X, oxidized samples.

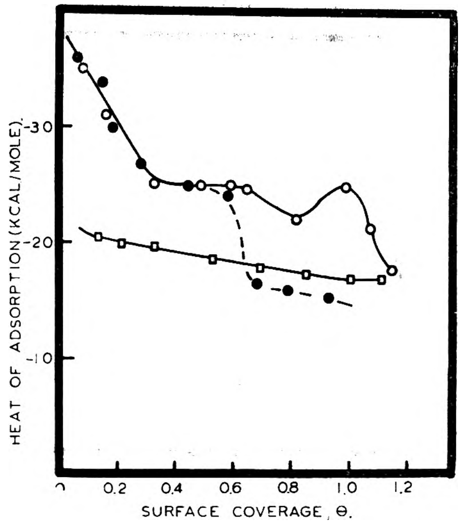

Fig. 2.—Heats of adsorption of n-propylamine on cobalt at 25°: ○, reduced; ●, regenerated; ☐, oxidized samples.

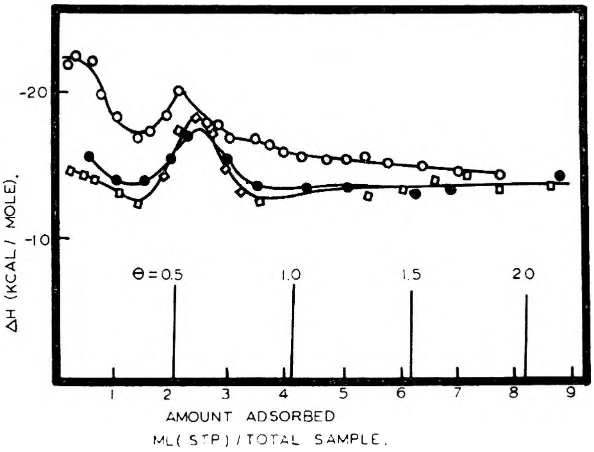

Fig. 3.—Heats of adsorption of water on copper at 23°: ○, reduced; ●, regenerated; ☐, oxidized samples.

The abrupt decrease in the heat values for amine adsorption on the regenerated surfaces after $\theta = \sim 0.7$ suggests the beginning of a radically different process. Then, adsorption occurs on true, oxide crystallites of limited area and is predominantly physical in nature as shown by complete reversibilities for adsorption in this region.

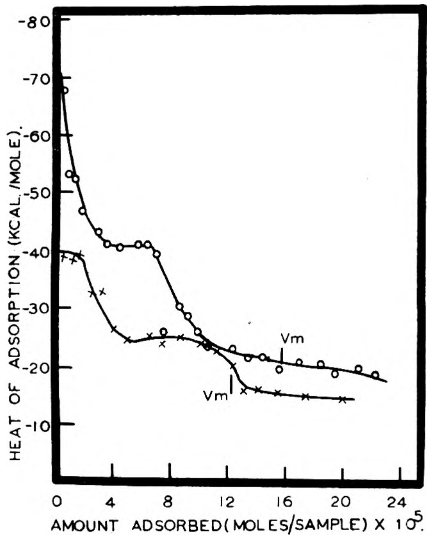

Fig. 4.—Heats of adsorption of acetic acid on nickel; O, reduced; X, oxidized surfaces.

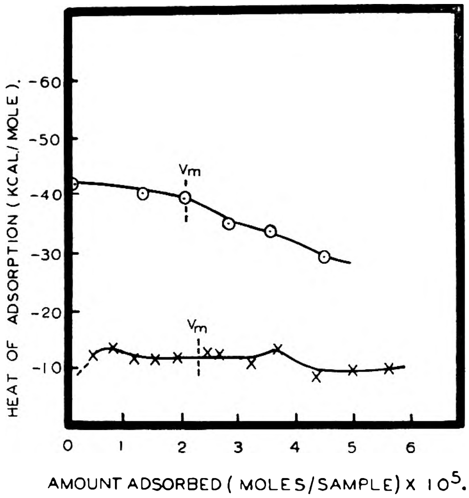

Fig. 5.—Heats of adsorption of acetic acid on copper: O, oxidized; X, reduced surfaces.

The fractions of surface exposed on regeneration were of the same magnitude for nickel and cobalt. In this work, controlled amounts of oxygen were admitted to give an original oxide thickness between 10 to 15 Å. Cobalt on the other hand takes up more than twice the amount of oxygen expressed in equivalent oxide layers compared to nickel when saturated near 25°. Obviously, on regeneration of completely oxidized cobalt the oxide would be expected to occupy more area on the surface because of its presence in larger quantities.

The magnitude of the heat values, irreversibilities for amine adsorption and C.S.A.'s on reduced nickel suggest significant chemisorption. Intermediate heat values for adsorption on reduced cobalt cannot be taken, however, as irrefutable evidence for (or lack of) chemisorption. Adsorption of the amine on copper is predominantly physical in nature although scanty data suggest a rapid rise of heat values at low surface coverages. Similar low heat values and large cross-sectional areas suggest predominantly physical adsorption on the oxidized nickel and cobalt surfaces; the reversibilities on the freshly oxidized surfaces are also almost complete.

Acknowledgment.—The authors wish to express their appreciation for the financial support provided by the Signal Corps, United States Army and to the Office of Ordnance Research for loan of specific items of equipment used in this work.

DISCUSSION

GEORGE R. LESTER (Universal Oil Products).—The heats of adsorption for *n*-propylamine on the oxide surfaces (Ni and Co) seem rather high for physical adsorption. Are there any additional indications, such as entropy values, to support the physical adsorption model?

J. J. CHESSICK.—The use of heat values as criteria for physical adsorption is, obviously, speculative. Nevertheless, corrollary evidence such as cross-sectional areas and reversibilities tends to support the concept of physical adsorption. The oxide surfaces are not true oxides but contain oxygen anions, perhaps O^-. This may contribute to heats greater than the heats of liquefaction.

THE EFFECTS OF OXYGEN ADSORPTION ON THE K X-RAY ABSORPTION EDGE OF ALUMINA SUPPORTED NICKEL

BY P. H. LEWIS

Texaco Research Center, Beacon, New York

Received March 7, 1960

A new analytical technique is applied to show differences in the nickel K X-ray absorption edge due to oxygen chemisorption on small (30 Å.) nickel crystals in an alumina support catalyst. These changes show that the nickel–oxygen bond formed on the nickel surface is similar to that in bulk nickel oxide. The experimental data are interpreted as showing that the chemisorbed oxygen reduces the p character of the nickel's 4s band and increases that of the 4p band. It can further be suggested that the oxygen creates a gap between the almost filled 3d band and the empty 4p band. The alumina support does not affect the small nickel crystals; the absorption edge for the "bare" nickel is the same as that for bulk nickel metal, within the experimental error. The X-ray absorption results are useful in measuring the extent of reduction to the metal of the supported nickel oxide and measuring the nickel content of the catalyst.

Introduction

The infrared technique[1] has been used to show in great detail the chemisorbed state of molecules of hydrocarbons, carbon monoxide and aliphatic acids on small metal catalyst particles. There is a converse problem of how gas chemisorption affects the metal particles. This is a problem that has been attacked by making measurements of ferromagnetism,[2] electrical conductivity and work function[3] for the metal. Of these, only the magnetic measurements can be made on practical, supported metal catalysts. The metal must be, however, ferromagnetic. The results for all three of these techniques are interpretable essentially only in terms of whether electron addition to or extraction from the metal occurs during chemisorption. The ultimate in description of how chemisorption affects a metal would be in terms of the band structure of the metal. The methods of X-ray emission (for studying bands filled with electrons) and absorption spectrometry (for studying unfilled bands) are theoretically well suited for this.

The observed X-ray absorption and emission effects are due to all the atoms of the metal crystals forming the sample. To use the X-ray methods to study the effects of gas chemisorption on surface atoms, the number of surface atoms must be a large fraction of the total number of metal atoms forming the sample. Otherwise, only the absorption characteristics of unaffected, subsurface atoms would be observed. The fraction of surface atoms increases as the crystal size diminishes. For 30 Å. nickel crystals chemisorption effects on the X-ray absorption curve can be observed. For these crystals about 30% of the atoms are on the surface. There is no artificiality about a study of such small crystals because such small metal crystals form the main constituent of many catalysts.

It is the object of this paper to describe the use of K X-ray absorption measurements to study the changes in the unfilled energy bands of these nickel metal crystallites (supported on γ-alumina) caused by oxygen chemisorption. Besides elucidating the effect of the chemisorption of oxygen on nickel, the X-ray absorption technique can be used to study whether or not the smallness of size of nickel crystals affects the band structure and whether or not contact with the alumina affects the nickel crystals. The technique is useful in estimating the extent of reduction of the metal and in determining the per cent. metal present in the catalyst. A somewhat novel method for analyzing the X-ray absorption results is described.

There have been several X-ray absorption studies of bulk and supported catalysts to determine the valence state of the metal ion.[4,5] This paper presents the application of the X-ray technique to the study of the effect of chemisorption on supported catalyst metal.

Experimental

A. The X-Ray System.—Polychromatic radiation was obtained from a copper X-ray tube operated at 20 kilovolts, about 4 kilovolts above the threshold potential for exciting radiation of half the wave length of the nickel edge. The tube output was controlled by Philips Electronics voltage and current stabilizers. To avoid the tungsten $L\alpha_2$ emission line that is superposed on the white radiation used for studying the nickel X-ray absorption edge, a fresh X-ray tube was employed. Some 200 hours of running time can be obtained before the tungsten contamination of the tube anode becomes severe.

Monochromatic X-rays were obtained from the X-ray tube's continuous spectrum by means of a monochromator system based on the Norelco diffractometer. The X-rays were collimated by passing through a 1/12° divergence slit and then through a Soller slit system. These X-rays were monochromatized by a lithium fluoride crystal cleaved from a Harshaw crystal along the (100) plane. This crystal was chosen for the high intensity of its diffracted X-rays and for its dispersive power. The diffracted X-rays were collimated by a 0.003 inch receiving slit, a Soller slit system and a 1/12° scatter slit.

This single crystal apparatus does not have the resolution of a double crystal unit, the half width of the Cu $K\alpha_1$ line being 5 volts instead of the 3 volts obtained by means of a double crystal instrument.[6] For a sacrifice in resolution, however, higher X-ray intensity (roughly 4 times as much) was obtained so that X-ray absorption curves can be obtained in a few hours. A rapid accumulation of data is desirable so as to minimize the time that the sample is exposed to contamination effects.

The success of an X-ray absorption spectrum study using the Norelco diffractometer depends upon accurate maintenance of alignment of the monochromator crystal and the detector. If the former is at an angle θ with respect to the main X-ray beam, the latter must always be at an angle 2θ over the angular range of the absorption edge. To do this the diffractometer was adjusted by the manufacturer to remove excessive gear play and equipped with

---

[1] R. P. Eischens and W. A. Pliskin, *Advances in Catalysis*, **10**, 1 (1958), Academic Press, Inc., New York, N. Y.

[2] P. W. Selwood, *ibid.*, **9**, 93 (1957).

[3] Reviewed by R. Suhrmann, *ibid.*, **7**, 303 (1955).

[4] H. P. Hanson and W. O. Milligan, THIS JOURNAL, **60**, 1144 (1956).

[5] R. P. Keeling, Jr., *J. Chem. Phys.*, **31**, 279 (1959).

[6] A. H. Compton and S. K. Allison, "X-Rays in Theory and Experiment," D. Van Nostrand Co., New York, N. Y., 1935, p. 745.

the new micro-adjuster for maintenance of the 2:1 relationship. The rotation of the monochromator crystal was always made from low to high angles.

The absolute angular settings of the monochromator (these determine the wave length of the radiation detected) cannot be trusted to better than several hundredths of a degree. The absorption measurements on the catalyst sample were therefore calibrated by also measuring the absorption of a nickel foil at each angular setting.[7]

The incident and transmitted X-ray intensities, I_0 and I, were measured with a Norelco pure xenon proportional counter, 62032, operated at 1675 volts, below the voltage that caused afterpulsing. The counter output was preamplified by means of a Hamner feedback stabilized unit SX-3 and then fed to an Atomic Model 204B linear amplifier. The signal pulses were screened from noise and the residual half wave length radiation by means of an Atomic pulse height analyzer, model 510. The noise content of the measured signal was but 0.2 count/second or less. The measured signal was virtually free of half wave length radiation, the test being the identity of absorption coefficients measured for a nickel foil with X-ray tube voltages of 15 and 20 kilovolts.

B. **Vacuum System.**—The sample was placed in a Vycor glass cell located on the X-ray tube side of the monochromator crystal. The cell was mounted with its long axis vertical. For this position the X-ray path is unchanged as the monochromator crystal is rotated. The X-rays pass through mylar-covered slits in the glass walls of this cell. The mylar was fastened to the glass with a thin coat of a polymer cement.[8]

A conventional vacuum system (mechanical pump, oil diffusion pump and liquid nitrogen trap) was attached to the cell. High gas pressures in this cell were measured by means of a calibrated thermocouple gage, RCA 1946, and low pressures by means of a Miller cold cathode gage. Known volumes of oxygen were admitted to the sample cell by means of a mercury-calibrated 0.1 cc. dosing stopcock. The pressure of this gas in the reservoir system was measured by means of a mercury manometer. With the exception of the mechanical pump (connected to the diffusion pump by means of a rubber hose) the entire system was mounted on a flat, wooden base (fitted with height adjusting screws) so as to facilitate the movement of the sample in and out of the X-ray beam. The board was cut so as to just fit the angle formed by the diffractometer base and the X-ray tube housing. This permits reproducible positioning of the sample to the X-ray beam.

The vacuum system was sufficiently good that pressures of the order of 10^{-5}-10^{-6} mm. can be maintained for 5–6 hours without pumping. This was the time required to accumulate the X-ray absorption data.

The sample was heated by means of focussed radiation from a 1000 watt projection lamp positioned at the focus of an ellipsoidal reflector.[9] Its rays were directed perpendicular to the X-ray beam, in the horizontal plane. The sample plane was turned about its vertical axis so as to be 30° to the X-ray beam. In this position the sample can intercept both the X-rays and the heat rays.

While the Vycor tube transmits a high percentage of the infrared radiation, enough is absorbed to overheat the Mylar windows. These were cooled, therefore, with air jets.

The temperature of the sample was measured by means of an iron–constantan thermocouple mounted on the shade side of the sample. The temperature of the sample was not uniform; the temperature measurement was good enough to ensure that sufficient heat was furnished to the sample to reduce the nickel.

C. **Materials.**—The nickel–alumina catalysts were prepared by impregnating Alcoa F-10 alumina with a water solution of Baker's reagent grade nickel nitrate. This powder, after drying, was compressed into sheets about 0.02 cm. in thickness. The sample sheets weigh about 0.3 g. Additional sample was mounted in a cavity below the sample sheet, outside the X-ray beam, to bring the total weight of the sample exposed to gas to about a gram. The additional sample reduces somewhat the effect of contamination and increases the precision with which gas adsorptions can be measured. Electrolytic hydrogen, purified by passage over hot copper and through a liquid nitrogen trap, was used. Commercial oxygen was used without further purification.

D. **Experimental Procedure.**—The "bare" nickel sample was made in the following manner. The nickel nitrate impregnated alumina sample was dehydrated by slowly raising its temperature to 350° while maintaining it under vacuum. The sample was then reduced under flowing hydrogen for 15 hours at 350°. The reduction step was followed by evacuation at 350° to a residual pressure of 10^{-4} mm. Following this procedure the pressure in the cell ranged from 10^{-5} to 10^{-6} mm. at room temperature. The entire process was then repeated before obtaining X-ray absorption data. The sample was regarded as having "clean" nickel crystals. No change in the X-ray absorption data was observed upon repeating this procedure 6 more times. Known amounts of oxygen were added to this sample to study the effects of oxygen chemisorption.

The X-ray intensity measurements at each angular setting (changed in steps of 0.01 degree, 2θ) were made in the following sequence: (1) incident beam, (2) beam transmitted through a nickel foil, (3) beam transmitted through catalyst sample and (4) another measurement of the incident beam. Each incident beam intensity measurement was made in terms of the time required to accumulate 12,800 counts. The time to accumulate 6400 counts was measured for the transmitted beams. The maximum difference between the two measurements of incident beam intensity tolerated was 3%. The error, estimated using 2σ statistics, included both the statistical error and an error due to variation in the background counting rate of 0.1 count/second. The larger statistical error was selected to allow for X-ray tube output variations. Each logarithm (base 10) of the ratio of incident to transmitted beam intensity has an absolute error of ±0.014. This logarithmic ratio is equal to the product of the absorption coefficient μ and the sample thickness t divided by 2.303.

Method for Analysis of X-Ray Absorption Edge Data

Rather poor experiences with the two conventional techniques (fitting X-ray absorption results to an arc tangent function[10] and measurement of the wave length at which the change in absorption is half the maximum[11]) for analyzing X-ray absorption results initiated a search for a better technique. Both of these conventional techniques utilize a rather small percentage of the total absorption data accumulated and indicate changes in but one part of the absorption edge. The analytical technique actually used avoids these difficulties. The method depends upon the additivity of absorption for the components of a multicomponent sample. For the two components of a nickel–alumina catalyst, s

$$(\mu t)_s = (\mu t)_1 + (\mu t)_2$$

where component 1 is the nickel and component 2 is the alumina. This equation is rigorous for any measurement made at any single wave length. The application of this equation to the analysis of X-ray absorption data obtained over the range of wave lengths of the edge can be done in the following way. For the narrow wave length region of the nickel edge, $(\mu t)_2$ is a constant, $2.303B$. Only a statistical fluctuation in pure alumina absorption data was noted in measurements made by varying the double Bragg angle (2θ) from 43.15 to 43.45° (the nickel edge is measured between these angles).

---

(7) This was suggested to the author by H. Cole of the IBM Research Laboratories, Poughkeepsie, New York.

(8) Bonding agent R-313, made by Carl H. Biggs Company of Los Angeles.

(9) E. H. Nicollian, G. R. Gunther-Mohr and L. R. Weisberg, *IBM J. Research and Development*, **1**, 349 (1957). Dr. Gunther-Mohr was most helpful in getting us started in using these heaters.

(10) R. K. Richtmyer, S. W. Barnes and E. Ramberg, *Phys. Rev.*, **46**, 843 (1934).

(11) H. W. B. Skinner and J. E. Johnson, *Proc. Roy. Soc.* (*London*), **A161**, 420 (1937).

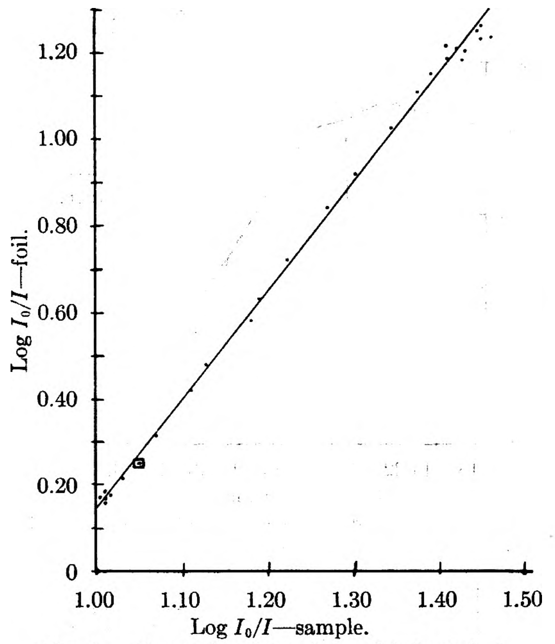

Fig. 1.—Absorption data; bare nickel catalyst

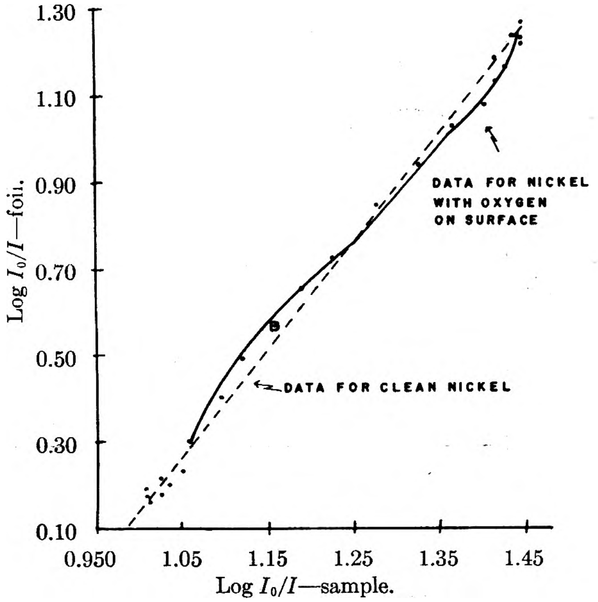

Fig. 2.—Absorption data—nickel catalyst with oxygen chemisorbed on it.

If the nickel dispersed on the alumina has bulk metal properties, the ratio $(\mu t)_1/(\mu t)_f$ is also a constant, A, over the entire wave length range of the absorption edge. Here $(\mu t)_f$ is the absorption of the bulk nickel foil used for calibration. Hence

$$(\mu t)_s = A(\mu t)_f + 2.303B$$

or

$$\log (I_0/I)_s = A \log (I_0/I)_f + B \qquad (1)$$

In consequence, a logarithmic plot of the absorption of the sample *vs.* the absorption of the nickel foil for all the X-ray edge data should be linear if no perturbation of the catalyst nickel has occurred.

If A is constant, the weight percentage of nickel, X_1, may be calculated from A and B using

$$X_1 = \frac{A(\rho t)_f}{A(\rho t)_f + (2.303B/(\mu/\rho)_2)}$$

where ρ is density. The (ρt) for the calibrating nickel foil, determined by making weight and area measurements, was found to be 8.99×10^{-3} g./cm.². The mass absorption coefficient for alumina, 28.5 cm.²/g., was obtained by interpolating between reported[6] absorption data measured at 1.39 and 1.54 A., using the cube dependence of absorption coefficient on X-ray wave length to get the coefficient at the wave length 1.49 Å. The per cent. nickel was compared with that determined by a gravimetric analysis involving the determination of both Al_2O_3 and Ni in the sample. The determination of both of the catalyst constituents prevents a systematic error due to water present in the alumina. The X-ray result was (4.52 ± 0.03) %; the gravimetric (4.42 ± 0.03) %. The reason for this discrepancy is not yet known.

Results

The comparison of bare nickel-alumina catalyst absorption characteristics at the nickel K edge with that of nickel foil is shown in Fig. 1. The plot is not made in terms of absolute absorption coefficients because of the difficulty of making an accurate estimate of the density and thickness of the sample wafer. The experimental data were taken every 1.83 volts (0.01 degree, 2θ). The plotted data adequately cover the energy region of X-ray edge associated with atomic characteristics in contrast to the high energy edge region, the so-called Kronig region. Absorption characteristics in this last energy region are to be associated with energy bands controlled by crystal structure. The straight line was derived from the data by the least squares method. Within the experimental error (indicated by the small box) the data are adequately represented by the straight line. The slope of this straight line can be reproduced with a 1% error, the intercept with but a 0.5% error.

Data for the interaction of oxygen with the nickel were taken at three oxygen/nickel ratios: $^1/_{3.4}$, $^1/_{5.5}$ and $^1/_{6.2}$. The gas adsorption measurements showed that a monolayer coverage of oxygen occurred at the largest of these ratios. The evidence that the coverage of oxygen was a monolayer at the oxygen/nickel ratio $^1/_{3.4}$ was based on the marked rise in pressure within the cell upon further addition of oxygen. A real change in the absorption curve could just be observed when one oxygen was adsorbed per 6.2 nickel atoms.

Figure 2 shows the comparison of a nickel-alumina catalyst with a nickel foil when the catalyst nickel has one oxygen adsorbed for every 5.5 nickel atoms in the sample. It is clear that a straight line relationship does not exist for these data. The straight line that is drawn (dashed) was determined using the bare nickel catalyst data shown in Fig. 1. For discussion purposes the data of Fig. 1 and Fig. 2 were converted into the more usual form for showing X-ray absorption edges. The smoothed curves are shown in Fig. 3. The curve for bare nickel is, within the experimental error, the same as for bulk nickel metal.[12] The effect of the oxygen is to cause changes in the A and B regions of the absorption edge. The absorption edge data for the other two oxygen-nickel samples were of the same type as shown in Figs. 2 and 3, the magnitudes of the distortions being appropriately bigger or smaller, depending on the oxygen/nickel ratio.

In order to understand the changes in X-ray

---

(12) W. W. Beeman and H. Friedman, *Phys. Rev.*, **56**, 392 (1939).

absorption edge characteristics caused by the chemisorption of oxygen, the catalyst nickel was completely oxidized by heating the sample to 350° in oxygen at a pressure of 10.9 cm. The absorption data for this sample were analyzed by the log–log plot for comparison with nickel foil. The more conventional representation of the oxidized catalyst absorption data along with the absorption curve for the sample clean of chemisorbed gas is shown in Fig. 4. It is clear that the effect of bulk oxidation on the nickel is similar in kind to that observed after oxygen chemisorption, but, of course, greater in magnitude.

Useful information may be derived from the maximum differences in X-ray absorption between bare and oxygen treated nickel catalysts. Plots of these differences in the A and B regions are shown in Figs. 5 and 6 for the A and B regions, respectively. The oxygen/nickel ratios were calculated using the total weight of nickel in the X-ray absorption cell and the amounts of oxygen admitted to the cell by means of the calibrated doser. Figure 5 shows that in the A region all the differences are linearly related to the oxygen/nickel ratios.

Figure 5 also shows that at an oxygen/nickel ratio of about 0.1 the experimental error is the same size as the difference between oxidized and unoxidized nickel X-ray absorption. If the X-ray absorption data for the "bare" nickel catalyst in a log–log plot (shown in Fig. 4) obeys a linear relationship, one can conclude that the nickel must have been at least 90% reduced. Using the crystal size derived from the oxygen adsorption data, 30 Å., (assumption: each surface atom adsorbs one oxygen atom) this corresponds to a surface at least 67 % clean of oxygen. These analyses do not preclude the possibility that the extent of the reduction of the nickel is greater.

The plot shown in Fig. 6 for the B region of the X-ray adsorption edge contrasts with that shown for the A region. It is clear that the changes caused by small additions of oxygen (low O/Ni ratios) fall on a straight line. The experimental point for the sample containing nickel completely oxidized to NiO falls off the straight line by a good deal more than the experimental error. For the B region the amount of the effect on the X-ray absorption of the nickel is different for the first oxygen atoms adsorbed than for those that complete the conversion of the metal crystal to NiO.

Discussion

The interpretation of the effect of the chemisorption of oxygen on the nickel X-ray absorption edge is to be made in terms of the band theory of solids. A brief review of the fundamentals of band theory is in order. First, a band: in a crystal the valence electrons of a constituent atom no longer occupy the discrete, sharp energy levels that are associated with a free atom. Instead the electrons occupy broadened energy levels called bands. Each band is formed by closely spaced (so closely that the levels merge into a continuum) atom levels, the number of levels forming each band being equal to the number of atoms forming the crystal. Each band is named according to the atom levels used to form it. The bands to be discussed subsequently are the 3d, 4s and 4p bands of nickel.

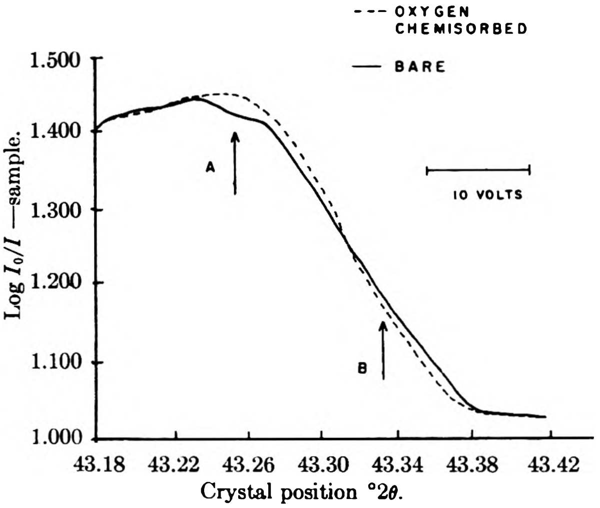

Fig. 3.—Absorption data—nickel catalyst, oxygen chemisorbed.

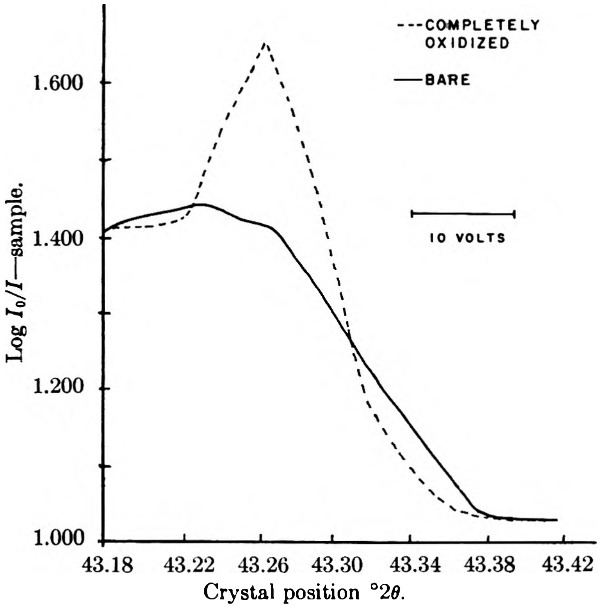

Fig. 4.—Absorption data—nickel catalyst, completely oxidized.

Each band is characterized by the number density of energy levels forming it. The number density as a function of energy has been calculated by Rudberg and Slater[13] for nickel and is shown in Fig. 7. The figure shows that the 3d band extends over an energy range from −13 to −5.5 volts. The density of 3d energy levels is high. However, much of this band is filled with electrons. The Fermi level (F. L.) marks the boundary between the energy levels that are filled and those that are empty (to be more rigorous it is the energy position at which the probability of finding an electron has fallen to $^1/_2$). The 4s band occupies an energy range roughly coincident with the 3d band, extending from −13 to −0.5 volts. The density of energy levels is small. At point M the 4s and 4p bands almost meet. The failure to make perfect contact

---

(13) E. Rudberg and J. C. Slater, *Phys. Rev.*, **50**, 150 (1936).

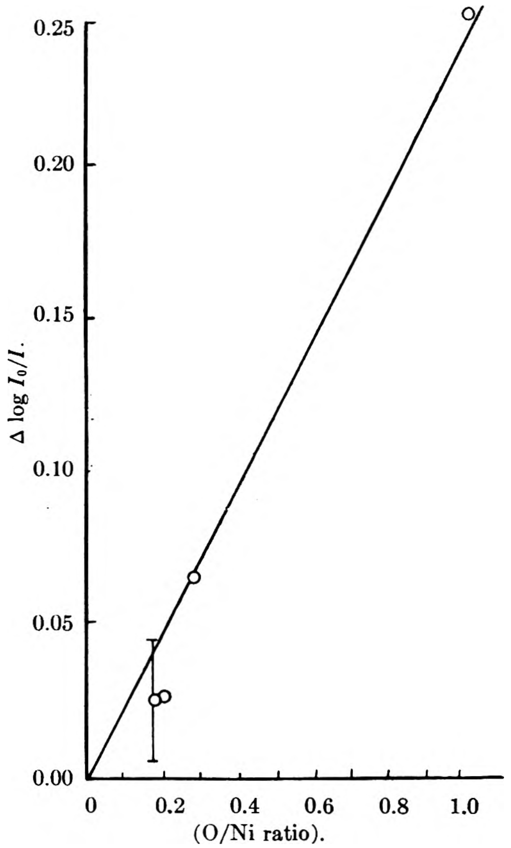

Fig. 5.—X-Ray absorption edge changes; A region.

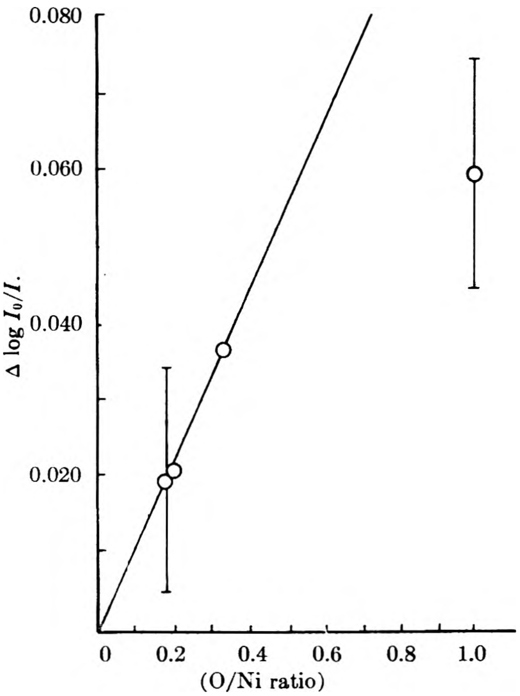

Fig. 6.—X-Ray absorption edge changes; B region.

results in a dip in the density curve. The 4p region extends from about 0 to 20 volts. The accuracy of this band picture cannot be substantiated to the last detail. However, it is regarded as being reasonably reliable.[12]

The bands are further characterized by their symmetry properties. The symmetry properties of each band are related to the angular momentum quantum number *l* that characterizes the discrete atom levels. Thus the 4p band is mostly p in its symmetry characteristics. The symmetry characteristics of the bands of solids is complicated by the fact that the bands do not exhibit pure symmetry. Thus the 3d and 4s bands will have considerable amounts of p character.[14] This is called state mixing. State mixing is a quantum-mechanical description of the breakdown of the conservation of angular momentum about an atomic center which occurs when atoms are joined to form a solid.

The concept of state mixing is useful in studying catalysts in that the extent of state mixing is affected by the neighbors of the metal atom.[15] State mixing is extensive in a metal; in a non-metal, ionic substance the state mixing is severely reduced and the bands become purer in their symmetry characteristics.

The object of the X-ray absorption work is to follow changes in band symmetry properties and energy level density for small nickel crystals due to the chemisorption of oxygen. The work is confined to the 4s and 4p bands since these are not filled with electrons. Changes in the electron-filled 3d band are the proper study of an X-ray emission experiment.

The fundamentals of K-absorption spectrum are these. X-Rays of wave length λ and energy E excite a K electron to a band level at an energy E above the K level. The absorption coefficient for these X-rays is proportional to the product of the number density of levels, $N(E)$ and the probability of exciting a K electron to an empty band level, $P(E)$.[16] The probability of excitation is governed in part by the symmetry characteristics of the band. Since the selection rule holds (that the change in angular momentum quantum number must be 1 for an electric dipole transition to take place) for the X-ray transitions in the absorption edge[17] the excitation of a K electron must be to a state with p characteristics. The nickel–oxygen X-ray absorption results are thus related to the number density of energy levels in the 4s and 4p bands and to the relative amounts of p character of these bands.

The first conclusion from the X-ray absorption results is based on the close resemblance between the X-ray absorption curves of nickel crystals that have oxygen chemisorbed on them (Fig. 3) and nickel crystals completely converted to the oxide (Fig. 4). In both cases the oxygen enhances the X-ray absorption in the *A* region, decreases it in the *B* region. The close resemblance shows that the bond that is formed between the nickel and the chemisorbed oxygen atom is similar to that in the bulk oxide and hence is ionic. The nickel, therefore, has electrons extracted from it by the chemisorbed oxygen. This result is entirely consistent with results obtained using measurements of magnetic susceptibility,[18] conductivity[3] and work function.[3]

---

(14) H. Krutter, *Phys. Rev.*, **48**, 664 (1935).

(15) N. F. Mott, "Applications of X-ray Spectroscopy to Solid State Problems," NAVEXOS P-1033, page 1 (1950).

(16) H. Jones and N. F. Mott, *Proc. Roy. Soc. (London)*, **162**, 49 (1937).

The close resemblance between the absorption curves for the nickel with chemisorbed oxygen on it and for nickel completely converted to the oxide is somewhat surprising because of the importance placed on the effect of the crystal field in which the metal atom lies.[19] It would have been expected that the asymmetrical field produced at the nickel-oxygen interface would have caused a much different X-ray absorption curve from that for the bulk oxide in which the nickel exists in a symmetrical, octahedral field. That this is not so would indicate that the absorption curve is most affected by the electron transfer from metal atom to oxygen atom rather than by the metal atom's charged neighbors.

The close resemblance between the X-ray absorption curves for nickel with chemisorbed oxygen on it and nickel oxide was not fully expected. An alternate mechanism assumes that the metal's band structure is unaffected by the oxygen chemisorption, electrons being simply removed from the filled 3d band. This would entail a lowering of the Fermi level. If this had occurred, the X-ray absorption curve would have retained its shape, but would have been shifted toward lower energy (or longer wave length). The effect on the log-log plots used to analyze the X-ray absorption data would be that seen in Fig. 8, where the absorption data for the bare nickel catalyst were artificially displaced 2 volts with respect to those of the nickel foil. These data cannot be represented by a straight line. The shape is that of a reversed C, instead of the sinusoidal curve actually observed in Fig. 2.

The A region of Fig. 3 is commonly associated with the X-ray absorption properties of the 4p band.[4] The increased X-ray absorption in this region correlates well with what is to be expected. The chemisorption of oxygen in forming the nickel ions decreases the surface nickel atoms' 4p band state mixing, increases its p character. This increase is accompanied by an increased probability of K absorption and hence a larger X-ray absorption coefficient is observed.

Figure 5 shows that the change in absorption coefficient per added oxygen atom is linear over the range 0 to 1 in oxygen/nickel ratio. The nickel 4p band is thus affected to the same extent whether an oxygen is added to a surface nickel atom or whether it is completing the transformation of the nickel crystal to nickel oxide.

The interpretation of the *B* region is less easily made. Figure 3 shows that the region covers approximately 13 volts. Knowing (because of the relatively poor resolution) that this is somewhat larger than it should be, the *B* absorption region must still extend over the 4s band and the dip in density of energy levels at M shown in Fig. 7. It is therefore not clear whether the decreased absorption in the *B* region during oxygen chemisorption is due to decreased p character of the 4s band or to a widening of the separation of the 4s and 4p bands to form a gap. The reduction in density of energy levels would reduce the absorption coefficient. The formation of a gap would be expected[20] since a monolayer of oxygen on the nickel produces a two dimensional periodic field. The gap produced (if this is the correct explanation for the B region) by the two dimensional nickel-oxygen periodic field appears to occur at about the same position as that for the three dimensional bulk nickel oxide.

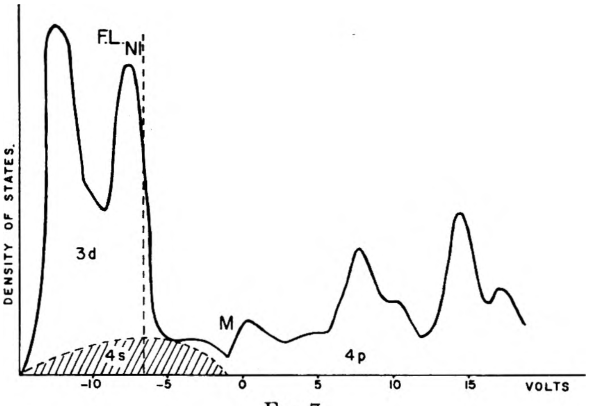

Fig. 7.

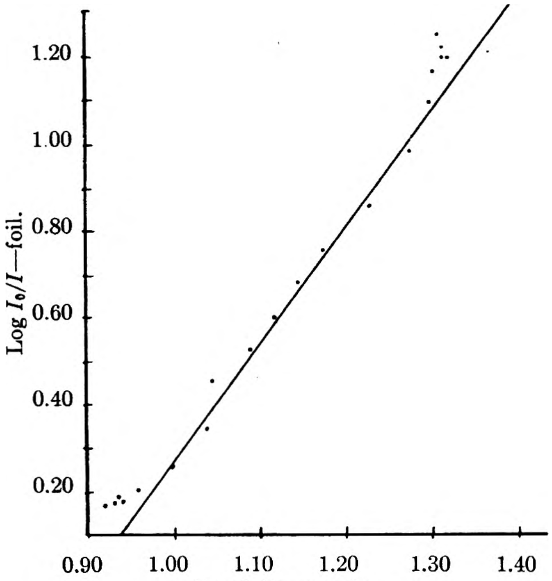

Fig. 8.—Effect of absorption edge shift.

The change in X-ray absorption per nickel atom in the *B* region is apparently greater when oxygen is adsorbed on the surface than when the oxygen is completing the transformation to the bulk oxide. Any interpretation of this must take into account that this change is proportional to the number of atoms affected by each chemisorption act and to the effect per nickel atom. For several reasons the tendency is to assume that the oxygen chemisorption affects more than one nickel atom. This hypothesis fits Brewer's[21] original concept of the mechanism by which a small number of impurity atoms can poison a catalyst surface. Second, the

---

(17) H. W. B. Skinner, *Reports Prog. Phys.*, **5**, 257 (1938).

(18) L. E. Moore and P. W. Selwood, *J. Am. Chem. Soc.*, **78**, 697 (1956).

(19) W. W. Beeman, J. Forss and J. N. Humphrey, *Phys. Rev.*, **67**, 217 (1945).

(20) Slater discusses the single dimension periodic field. The reasoning can be extended to two dimensions; J. C. Slater, *Encyclopedia of Physics*, **19**, 24 (1956).

(21) A. K. Brewer, This Journal, **32**, 1006 (1928).

formation of the periodic field on the surface would be expected to affect at least the layer of nickel metal atoms just beneath the affected layer.

It is noteworthy that the clean, supported metal crystals seem to exhibit the same X-ray absorption edge properties as that of bulk nickel metal. This was shown by the straight line relationship for the log-log plot of absorption data for catalyst and foil (Fig. 1). Seemingly, small crystal size and the contact with alumina do not affect the nickel X-ray absorption edge spectrum. It must be recognized that the instrumentation used and counting error inherent in intensity measurements prevent the observation of small changes in X-ray absorption edge structure. It is therefore possible that a small crystal effect and interaction with the alumina could occur without actually being observed by the present X-ray technique. At least it can be said that the contact of the nickel crystals with the oxide ions of the alumina does not affect the nickel as much as chemisorbed oxygen.

Acknowledgment.—A number of people have been most helpful in bringing this work to fruition. I would like to thank Drs. L. C. Roess, S. A. Francis, R. P. Eischens and members of the Physical Research Department of the Texaco Research Center for their helpful criticism. Dr. G. R. Gunther-Mohr of IBM helped me greatly in getting started in the use of heat lamps. The suggestion of Dr. H. Cole of IBM that nickel foil be used in calibration of the X-ray absorption data was of enormous help.

DISCUSSION

A. C. ZETTLEMOYER (Lehigh University).—I am surprised at your conclusion that the sorption of an oxygen affects only the nickel atom to which it is attached. Many other pieces of evidence, such as the change in work function with coverage, suggests a farther reaching effect. Another experimental approach might be the measurement of low temperature heat capacities.

PAUL H. LEWIS.—The conclusion rests on the experimental evidence shown in Fig. 2. This distortion of the linear relationship is different from that expected if the oxygen adsorption had merely caused a change in the Fermi level (see Fig. 8). It is to be further pointed out that the X-ray evidence leads to the conclusion that the *primary* atom affected by the chemisorption act is the one on which chemisorption takes place. Atoms near to this atom are secondarily affected (see the discussion of Fig. 6). I agree that low temperature heat capacity measurements would be useful in studying small crystals; see the work of J. A. Morrison and D. Patterson, *Trans. Faraday Soc.* **52**, 764 (1956); *Can. J. Chem.*, **33**, 240 (1955).

R. A. PASTERNAK (Stanford Research Institute).—This symposium has emphasized phenomena involving chemisorption on bare metals. The "bareness" of the metal surface in the investigation under discussion, and in other studies presented here, might be open to question. Flash filament studies have shown that at 10^{-8} mm. smooth tungsten (J. A. Becker. "Advances in Catalysis," (Academic Press, New York, N. Y., 1955) Vol. VII, p. 136) and molybdenum (R. A. Pasternak and H. U. D. Wiesendanger, to be published) surfaces are saturated with oxygen, nitrogen, hydrogen, and other active gases in about 10 minutes and proportionatley faster at higher pressures. For hydrogen adsorption the situation is particularly bad because adsorbed hydrogen is rapidly and irreversibly replaced by nitrogen and oxygen even at exceedingly low partial pressures. I would expect that under the customary vacuum conditions of 10^{-6} mm. the large internal surfaces of supported catalysts or of evaporated metal films also become covered quite rapidly with adsorbed gas. Moreover, I wonder whether the usual degassing procedures are sufficient to generate truly clean surfaces.

In order to obtain and maintain truly clean surfaces, ultrahigh vacuum is highly desirable. New techniques now make it relatively simple to attain such conditions. Biondi (*Rev. Sci. Inst.*, **30**, 831 (1959)) recently has described a non-refrigerated high-conductance isolation trap, charged with alumina or zerolite pellets, which is a substitute for the liquid nitrogen trap in a vacuum system based on an oil diffusion pump. At Stanford Research Institute we have used such a vacuum system successfully (H. U. D. Wiesendanger and R. A. Pasternak, *Experientia*, in press (1960)) in our extensive flash filament study of gas–molybdenum interactions. Base pressures of below 5×10^{-10} mm. were obtained routinely. During the study we were able to maintain pressures below 10^{-8} to 10^{-6} mm. while passing hydrogen or nitrogen through our unit at high flow rates. No traces of oil vapors were discovered in the unit even after continuous operation of the pumping system for about three months.

PAUL H. LEWIS.—The experimental fact that the X-ray absorption properties of the atoms in catalyst nickel are the same as those in the interior of bulk nickel metal shows that the surface of the catalyst nickel cannot be covered with more than a third of a monolayer of oxygen. The answer lies in the large surface area of the sample. The sample weighing about a gram contains 7×10^{-4} g. atoms of nickel and has roughly 10 square meters of surface area. About a third of the nickel atoms are on the surface. The sample cell contains gas at 10^{-6} mm. pressure with a volume of 1 liter so it contains 1×10^{-9} g. atom of gas at any given instant. Suppose all this gas is "gettered" by the catalyst nickel every second, and a leak admits gas into the cell at the same rate. It would take about an hour to cover the surface to the extent of 1%. A 5 or 6% coverage would not be observed in the X-ray experiment. It must be remembered that the experiments cited by you involve the use of metal samples of low surface area (of the order of square centimeters).

SURFACE CHEMISTRY FROM SPECTRAL ANALYSIS OF TOTALLY INTERNALLY REFLECTED RADIATION*

BY N. J. HARRICK

Philips Laboratories, Irvington-on-Hudson, New York

Received March 7, 1960

A study has been made of the phenomenon of total internal reflection with the possibility in mind of applying it to the study of the spectra of surfaces of optically transparent materials, particularly semiconductors. It is found that the radiation penetrates the surfaces into the rarer medium to a depth predicted by Maxwell's theory and that this radiation is sensitive to molecular absorption on the surface. The degree of interaction on each reflection is comparable to that observed for a single transmission if the film thickness is equal to or less than the penetration depth. Since many total internal reflections can be used without power loss, this technique should be a sensitive one in the study of the chemistry of surfaces of optically transparent materials and of thin films which can be deposited on optically more dense and transparent dielectrics.

Introduction

One of the most direct approaches to the study of chemisorbed molecules on solid state surfaces is to analyze the infrared spectrum of the surface.[1a] Not only does the spectrum tell us what molecule is on the surface but it also tells us something about the nature of the bonding to the surface. This technique has worked successfully for metals.[1a] Here the sample was powdered in order to gain surface area. The beam was transmitted through the sample and spectrally analyzed. Thin samples have been spectrally analyzed by placing them on polished metal surfaces and, to gain sensitivity, multiply reflecting the infrared beam between two such mirrors.[1b] Even though the reflectivity of the metal may be high, the beam is rapidly attenuated for many reflections which may be required to gain sensitivity as the power in the beam is finally R^n where R is the reflectivity and n the number of reflections.

It is particularly important to apply similar techniques to the study of semiconductor surfaces in order to correlate the chemistry of the surface with our present knowledge of the physics of the surface. Powdering of the semiconductor has the disadvantage that the characteristics of the semiconductor may change drastically, when the sample is powdered, especially if the powder size is comparable to or less than a Debye length. A beam transmitted through a sample consisting of several separated layers has the disadvantage that reflectivity losses are high. The same disadvantage applies to a greater degree to a beam multiply reflected between two parallel plates. It has been suggested[2] that total internal reflection using radiation above the lattice absorption edge might work because on reflection the beam actually penetrates the surface and is pumped into and out of the rarer medium. This beam, if it is sensitive to molecular resonances, should give information regarding the type of impurity on the surface and the nature of the bonding to the surface. Since total internal reflection means that the reflection is 100%, many internal reflections can be used and thus the sensitivity of this technique can be much greater than that of transmission or external reflection.

To determine whether application of total internal reflection to the study of the surfaces of optically transparent materials is possible the following questions must be answered: (a) Is this reflected radiation sensitive to molecular absorption? (b) How great is any interaction compared to that in a transmission measurement?

Before giving the experimental results we will review briefly some aspects of the phenomenon of reflection. When a beam strikes at normal incidence an interface of a non-conducting medium it is reflected to a degree given by $R = (n_{12} - 1)^2/(n_{12} + 1)^2$, where n_{12} is the relative index of refraction of the two media. As the angle of incidence is increased, the reflectivity remains constant until the principal angle, $\theta_p = \tan^{-1} n_{21}$, is reached. For further increase in incident angle, the reflectivity increases rapidly to unity at grazing incidence when the second medium is more dense than the first. If, however, the second medium is less dense than the first, the reflectivity becomes unity for an angle only slightly larger than the principal angle which may be much less than 90°. This is called the critical angle and is given by $\theta_c = \sin^{-1} n_{21}$. For angles greater than the critical angle many reflections may take place with losses occurring only due to absorption in the bulk and reflectivity losses at the entrance and exit surfaces of the sample. The dense medium thus acts as a wave guide or light pipe. These features of the reflection phenomenon are shown in Fig. 1 for the Ge–air interface.

Maxwell's theory predicts that the totally reflected beam actually penetrates into the rarer medium (see insert of Fig. 2a) where the electric field intensity falls off exponentially. The depth of penetration, defined as the distance where the

---

* This work has been reported in *Phys. Rev. Letters*, **4**, 224 (1960).

(1) (a) R. P. Eischens and W. A. Pliskin, "Advances in Catalysis," Vol. 10, Academic Press, Inc., New York, N. Y., 1958; (b) S. A. Francis and A. H. Ellison, *J. Opt. Soc. Am.*, **49**, 131 (1959).

(2) Discussion by N. J. Harrick following paper by R. P. Eischens in session on New Techniques at Second Conference on Semiconductor Surface, Naval Ordnance Laboratories, White Oak, Md., Dec. 2–4, 1959. *J. Phys. Chem. Solids*, to be published (1960). It was brought to the author's attention after the work described here was completed that Dr. J. Fahrenfort of the Royal Dutch Shell Laboratories, Amsterdam, has described what appears to be a similar technique to observe the spectra of organic materials on silver chloride, at the Fourth International Congress on Molecular Spectroscopy, Bologna, Sept. 7–12, 1959.

ADDED NOTE: Dr. J. Fahrenfort shows that total internal reflection gives spectra of much higher contrast than conventional reflection. He suggests that total internal, rather than conventional, reflection might thus be utilized to obtain spectra when it is inconvenient or impossible to obtain the spectra from transmission measurements. He is concerned with a single reflection. Our approach is to utilize total internal reflection in order to gain sensitivity through many reflections and thus ultimately examine films of the order of a monolayer thick. The author wishes to thank Dr. Fahrenfort for a preprint of his paper to be published in the proceedings of the Bologna conference.

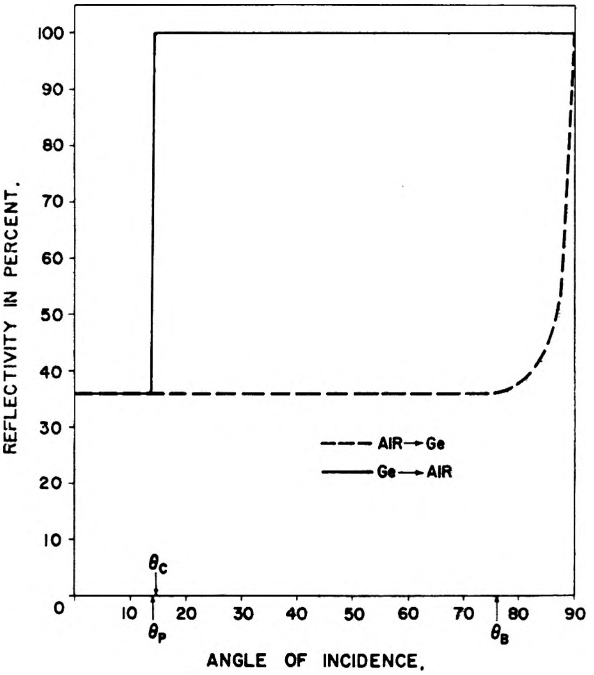

Fig. 1.—The reflectivity of the germanium–air interface as a function of angle of incidence.

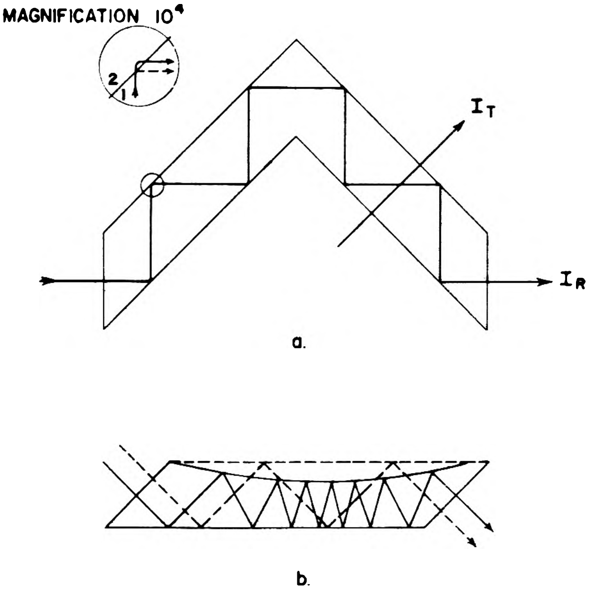

Fig. 2.—Sample shapes for total internal reflection measurements.

electric intensity has fallen to one-half of its value at the surface, is given by[3]

$$x_{1/2} = \frac{0.693\ \lambda_1}{2\pi(\sin^2\theta - n_{21}{}^2)^{1/2}}$$

Here λ_1 is the wave length in the denser medium, θ the angle of incidence and n_{21}, which is less than unity, the relative index of refraction of medium 2 to medium 1. The penetration depth at a wave length of 3.4 μ as a function of angle of incidence and calculated from this formula is shown in Fig. 3 for germanium, dielectric constant 16, in contact with polyethylene, dielectric constant 2.3. Except near the critical angle when $\sin\theta \simeq n_{21}$, the penetration depth is about one-tenth of a wave length. It should be noted the penetration is proportional to the wave length in the denser medium and becomes less as the dielectric constant of the rarer medium decreases. This penetration into the rarer medium has been demonstrated in numerous experiments. Penetration with displacement as shown in the insert of Fig. 2a was demonstrated in a remarkable experiment by Goos and Hänchen[4] who compared total internal reflection with metallic reflection (dotted line in the insert of Fig. 2a) and found after many reflections a displacement of the two beams relative to each other. They found for the displacement distance for a single reflection the expression

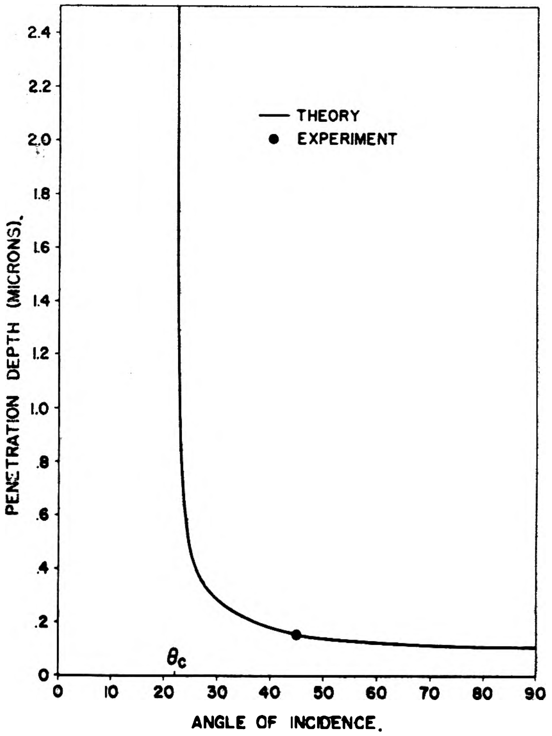

Fig. 3.—The penetration depth *vs.* angle of incidence for total internal reflection at the germanium–polyethylene interface. The experimental point is obtained from the experimental data of Fig. 6.

$$D = Kn_2 \frac{\lambda_1}{(\sin^2\theta - n_{21}{}^2)^{1/2}}$$

where $K = 0.52$ and $n_2 = \lambda_0/\lambda_2$. The displacement is thus directly proportional to the depth of penetration and thus follows a curve as a function of angle of incidence similar to that shown in Fig. 3. The phenomenon of the penetration into the rarer medium of totally internally reflected radiation has been demonstrated in other experiments. Here we list a few such experiments demonstrating this fascinating effect.

1. Schaefer and Gross[5] have measured the penetration in the rarer medium for total internal reflection at the glass–air interface using radiation of 15 cm. wave length.

---

[3] J. A. Stratton, "Electromagnetic Theory," McGraw-Hill Book Co., Inc., New York, N. Y., 1941. This penetration depth is that for a non-absorbing medium.

[4] F. Goos and H. Hänchen, *Ann. Phys.*, [6] **1**, 333 (1947).

[5] Cl. Schaefer and G. Gross, *Ann. Physik*, **32**, 648 (1910).

2. If phosphor is placed on an optical surface where total reflection is taking place, the phosphor will light up indicating a penetration into the rarer medium.[6] The objection that the condition of total reflection has been disturbed when the phosphor makes contact is ruled out if this experiment is done properly.

3. If a convex lens makes contact to a surface where total reflection is taking place, a spot larger than the point of contact and without fringes appears.[7] The size of the spot indicates that transmission of light through the lens is not limited to the point of contact. If the spot is viewed through the lens, it appears white with a reddish border; whereas if it is viewed through the prism, it appears black with a bluish border. This color separation is an indication of the wave length dependence of the penetration into the rarer medium.

4. If a razor blade is brought down to a surface of a light pipe, the edge of the blade will become illuminated just before contact.[7]

5. The frustrated total internal reflection filter takes advantage of the penetration of the radiation into the rarer medium.[8]

6. If metal strips forming a grating are evaporated on the reflecting surface of a prism an interference pattern can be observed at grazing incidence outside and behind the reflecting surface even though the incident angle is greater than the critical angle so that condition for total internal reflection is met.[9]

7. When total internal reflection is occurring and a metal is brought into contact with the reflecting surface, the reflectivity of the interface becomes less than total. Measurements of the reflectivity in this case can provide a measure of the conductivity of the material making contact to the dielectric. Such measurements have been made for the Ge–Hg interface.[10]

The object of the present experiment is to place known molecules on the surface of the optical wave guide and to attempt to detect their presence through analysis of the spectrum of the reflected radiation.

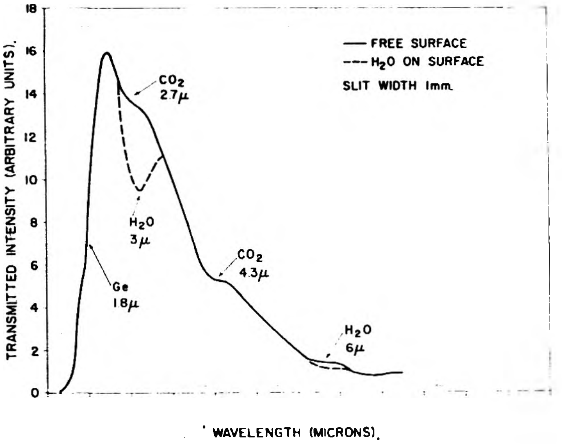

Fig. 4.—Spectra of beam I_R of Fig. 2a. The lines attributed to CO_2 indicate its presence in the atmosphere.

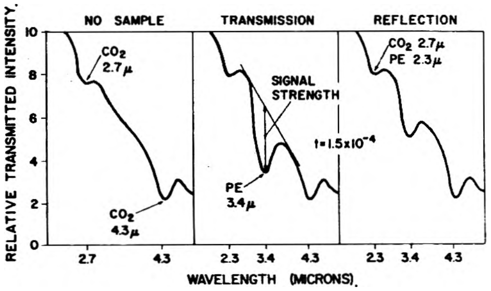

Fig. 5.—The spectrum of a 1.5×10^{-4} cm. polyethylene film from reflection and transmission measurements.

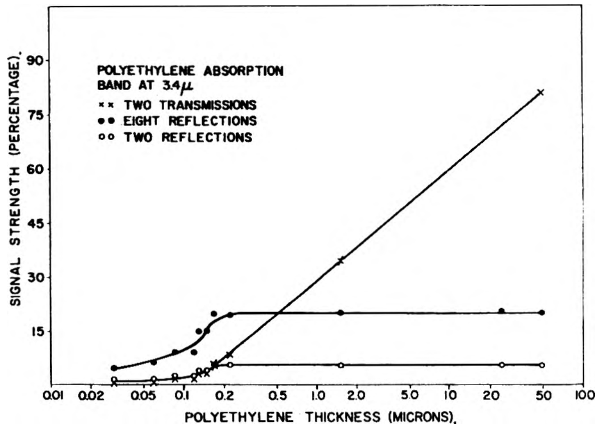

Fig. 6.—Comparison of the signal strength for transmission and reflection beams, I_T and I_R of Fig. 2a, for the polyethylene absorption line at 3.4 μ. The spectrometer slit width was 0.5 mm. for these measurements.

Experimental

The sample was cut, lapped and diamond polished in one piece from 30 ohm-cm., p-type germanium having the shape shown in Fig. 2a. This particular sample shape has the advantage that the exit beam is axial with the entrance beam. This leads to fewer complications in the optics of the spectrometer. The dimensions were such as to give eight reflections with the entrance face having dimensions of $^1/_4'' \times {}^3/_4''$. The angle of incidence was made 45° because this results in the largest usable aperture for the sample and makes machining of the angles involved easier. The sample was placed in a cell so that all of the surfaces except the entrance and exit faces could be surrounded by a liquid or a gas. If narrow spectrometer slits are used, the sample can be made thinner and the number of reflections can thus be increased. Figure 2b shows how the surface might be curved to increase the number of reflections and thus increase the sensitivity. For the example shown, the number of reflections has been increased from four to fourteen by curving the surface. Care must be taken in such a sample that the angle of incidence does not decrease to a value less than the critical angle otherwise the beam will be lost. The exit infrared beam was analyzed with the aid of a Perkin-Elmer Model 12C Spectrometer. Because of the lack of sensitivity of the present infrared set-up, we chose to work with absorption bands in the two to four micron range where the radiation intensity of the globar is high. The polyethylene was placed on the sample surface by first dissolving it in xylene to a dilution of 0.04% by weight and spraying it on the surface of the sample. It was thus possible to control the thickness of the polyethylene film. The signal intensity for transmission and reflection were compared by analyzing the beams I_T and I_R of Fig. 2a.

---

(6) R. W. Wood, "Physical Optics," The Macmillan Co., New York, N. Y., 1956.

(7) Jenkins and White, "Fundamentals of Optics," McGraw-Hill Book Co., Inc., New York, N. Y., 1957.

(8) P. J. Leurgans and A. F. Turner, *J. Opt. Soc. Am.*, **37**, 983(A) (1947). The term "frustrated reflections" was coined here.

(9) P. J. Leurgans, private communication.

(10) N. J. Harrick, *J. Opt. Soc. Am.*, **49**, 376 (1959).

Results

1. **Water.**—The experimental results for water are shown in Fig. 4. The solid line represents the transmission of the sample after eight reflections. The CO_2 absorption bands, due to the surrounding atmosphere, are detectable. The dotted lines show the deviation from the solid curve when the sample is surrounded by water. The water absorption bands at 3 and 6 μ are clearly visible. A rough check of the depth of penetration of the 3 μ radiation into the water was made by comparing the signal strength in Fig. 4 to that observed from a film of water of known thickness. The signal in Fig. 4, assuming a comparable strength of interaction in the transmission and reflection experiments, was calculated to correspond to a penetration depth of about 0.15 μ, in agreement with theory.

2. **Polyethylene.**—The experimental results for the polyethylene absorption band at 3.4 μ are shown in Figs. 5 and 6. Figure 5 compares the spectra observed for reflection and transmission for a film thickness of 1.5 μ. Figure 6 shows how the signal strengths behave as the film thickness is changed. For a film thickness less than 0.5 μ, the signal from two transmissions is less than that due to eight reflections. The reflection signal is independent of film thickness except for films less than 0.16 μ thick. This thickness is thus a measure of the depth of the penetration of the radiation in the polyethylene. This experimental point falls right on the theoretical curve given in Fig. 3 and calculated from the formula given in the text for the germanium–polyethylene interface. When two reflections are compared to two transmissions it is evident that the signal strengths are about the same for film thicknesses less than a penetration depth.

Discussion

This experiment has provided another demonstration and test of Maxwell's theory on the penetration of radiation into the rarer medium on total internal reflection. It has been shown that this radiation is sensitive to molecular absorption to about the same degree that is observed in transmitted radiation for film thicknesses less than a penetration depth. The measured depth of penetration agrees with that calculated from theory. The results show that the technique outlined here can be used to investigate surface impurities on optically transparent materials. A particularly important application of the technique should be found in the study of semiconductor surfaces. Another useful application can be found in the study of thin films. The latter application is important as it is known that thin films often have properties different from the bulk.

From the present results we would estimate that through the use of more reflections and a more sensitive spectrometer one to ten molecular layers can be detected using this technique. We reach this conclusion from the observation that an absorption band in a film 0.03 μ thick was readily detected (see Fig. 6) through the use of only eight reflections and a rather insensitive spectrometer set-up.

In applying this technique one should be aware of the following possible difficulties.

The index of refraction may change rapidly in the vicinity of molecular resonances if the damping effects are small. When this is the case, the condition of total reflection at the interface may be no longer met and the radiation can then escape the light pipe. It would return to the light pipe if total reflection occurs at the outside boundary of the film[11] on the light pipe and if the radiation is not completely absorbed by the film. That the radiation does not escape the light pipe in our experiment is immediately evident from the observation in Fig. 6 that the signal strength is independent of film thickness beyond a thickness of 0.16 μ. Hence, any change of index of refraction is not great enough to violate the condition of total internal reflection at 45° angle of incidence used in the present experiment. Such an effect could undoubtedly be observed by adjusting the angle of incidence. Furthermore, such measurements could be used to provide a sensitive determination of the index of refraction in the vicinity of molecular resonance.

In analyzing the spectrum of the impurities on the surface it is necessary to take into account any absorptions in the bulk: *e.g.*, oxygen in silicon,[12] and the spectrum of the free carriers, *e.g.*, holes.[13]

Although the absorption coefficient of the free carriers in a semiconductor is low ($\sim 10^{-16}$ cm.^{2} per free carrier), it is advisable to keep their density low especially if the sample is traversed many times when many reflections are used to increase the sensitivity. The density of free carriers can be kept at a low value by using either wide band gap or near intrinsic semiconductors and by working at low temperatures if necessary. High surface barriers, when the number of free carriers may not be negligible, should also be avoided since the carriers in the space charge region also contribute to the absorption of the infrared radiation.[14]

The author is indebted to Mr. R. C. Hughes for the germanium crystals and to Mr. H. W. Keese for technical assistance.

DISCUSSION

DIETRICH SCHULTZE (Mellon Institute).—How is it possible to distinguish between actual extinction due to absorbed molecules and interference extinction of the light beam?

N. J. HARRICK.—Firstly, the dimension of the sample and the angle of incidence are such that it is unlikely that any interference will occur; secondly, it is generally a simple matter to recognize an interference pattern because of its symmetrical feature.

J. A. RASHKIN (E. I. du Pont de Nemours Co.).—In the calculation of the penetration depth for a monolayer adsorbed on the surface, where you use the refractive index of the rarer medium, which refractive index do you use? The "refractive index" of the adsorbed molecules? The re-refractive index?

---

(11) It should be realized that if the constants of the media 1 and 2 are such as to give total reflection it makes no difference whether the constants change gradually or abruptly.

(12) W. Kaiser, P. H. Keck and C. F. Lange, *Phys. Rev.*, **101**, 1264 (1956).

(13) W. Kaiser, R. C. Collins and H. Y. Fan, *ibid.*, **91**, 1380 (1953).

(14) N. J. Harrick, *J. Phys. Chem. Solids*, **8**, 106 (1959).

N. J. HARRICK.—Firstly, the penetration depth is considerably larger than one monolayer and thus it does not make much difference whether the reflection is considered to take place on the inside or the outside of the monolayer. Secondly, the index of refraction is a macroscopic quantity and is thus really undefined for a monolayer or a single molecule. In dealing with such thin layers, Maxwell's theory cannot be used and it is necessary to go to an atomic model. The condition of total reflection can be unsatisfied at the surface of the light pipe yet this technique should work since the radiation is not necessarily lost from the system—see footnote (11).

DONALD GRAHAM (E. I. du Pont de Nemours & Co.).—To what extent would this technique be applicable to silica or alumina as represented by fused quartz or sapphire?

N. J. HARRICK.—This technique should work for any transparent material. It is convenient to have a high index of refraction so that the angle of incidence can be made small and thus increase the number of reflections per unit sample length.

DONALD GRAHAM.—Is it not possible that grinding, lapping, and diamond polishing of hard surfaces could introduce surface defects making the surface comparable to that of small particles?

N. J. HARRICK.—Yes. To avoid this effect the surface should be etched, cleaved, or annealed. The sample may also be initially grown to the shape desired, *e.g.*, dendrites.

THE CHEMISORPTION OF OXYGEN ON NICKEL[1]

BY ROBERT J. LEAK AND P. W. SELWOOD

Chemical Laboratory of Northwestern University, Evanston, Illinois

Received March 7, 1960

The chemisorption of oxygen on nickel–silica catalyst systems has been investigated by the low frequency a.c. permeameter method and volumetric gas adsorption techniques. The nickel particles were in the superparamagnetic range or slightly larger. A method has been developed for distinguishing between true chemisorption of oxygen on nickel as contrasted with surface oxide formation. The method makes use of what appears to be a change of magnetic anisotropy energy in particles of nickel in the 100 Å. diameter range. A possible explanation is discussed for the so-called "hydride anomaly" in the chemisorption of hydrogen on nickel at low temperatures.

Introduction

There have been many studies of the interaction of oxygen with nickel surfaces, but there are two basic points which have not been elucidated. First, there is no clear distinction as to where surface chemisorption ends and where bulk oxidation begins. And secondly, there has been some confusion as to the effect of chemisorbed oxygen on the magnetization of nickel.

The first point has been further confused by loose terminology. "Chemisorption" is sometimes used when actually bulk oxidation probably occurred. Chemisorption of oxygen and oxidation are easily confused because of the ease with which the former can be converted into the latter.

Oda[2] showed that penetration of oxygen into the nickel lattice occurred even at −183°. His work on evaporated films showed that the oxygen "sorption" proceeded until three molecules of oxygen were taken up per surface nickel atom. Further slow "sorption" also occurred. Scheuble[3] reported similar studies at room temperature on evaporated films. He found a "sorption" of oxygen equivalent to 9.5 times that needed for a monolayer if the surface were smooth.

Beeck and co-workers[4] found that oxygen was taken up at 23° to the extent of two molecules per lattice site. Moreover the oxygen adsorption layer will diffuse into the interior even if no additional oxygen is available from the gas phase. Although not so stated, this amounts to oxidation, not simply chemisorption. Stone and co-workers[5] showed the limit of oxygen uptake by nickel powders depends not only on temperature, but also on pressure and porosity. These two factors are important because they determine the efficiency of the dissipation of the heat of reaction. Further evidence concerning this matter is given by Higuchi, Ree and Eyring[6] who show a wide discrepancy between the calculated and observed heat of adsorption of oxygen on nickel.

The complexity of the situation has been shown by Zettlemoyer and co-workers[7] who found four layers of oxygen, namely, oxide, chemisorbed O^-, strongly physically adsorbed O_2, and weakly physically adsorbed O_2. The reaction was not stopped between the transition of the chemisorbed layer into the oxide, but at least the existence of two chemically bound layers was demonstrated.

There has been some experimental evidence showing a distinction between chemisorption of oxygen and oxidation. Farnsworth and Schlier[8] showed by electron diffraction experiments on single nickel crystals that a monolayer of oxygen is chemisorbed at room temperature after a pressure–time exposure of 2×10^{-6} mm.-min. Above 10^{-5} mm.-min. a nickel oxide layer is formed.

Shurmovskaya and Burshtein[9] have shown by contact potential measurements that at 35° oxygen

---

[1] Taken in part from the thesis of Robert J. Leak submitted to the Graduate School of Northwestern University in partial fulfillment of the requirements for the degree of Doctor of Philosophy.

[2] Z. Oda, *Bull. Chem. Soc. Japan*, **27**, 465 (1954).

[3] W. Scheuble, *Z. Physik*, **135**, 125 (1953).

[4] O. Beeck, A. E. Smith and A. Wheeler, *Proc. Roy. Soc. (London)*, **A177**, 62 (1940).

[5] R. M. Dell, D. F. Klemperer and F. S. Stone, THIS JOURNAL, **60**, 1586 (1956).

[6] I. Higuchi, T. Ree and H. Eyring, *J. Am. Chem. Soc.*, **79**, 1330 (1957).

[7] A. C. Zettlemoyer, Y. F. Yu, J. J. Chessick and F. H. Healey, THIS JOURNAL, **61**, 1319 (1957).

[8] R. E. Schlier and H. E. Farnsworth, "Advances in Catalysis," Vol. IX, Edited by D. D. Eley, W. G. Frankenburg and V. I. Komarewsky, Academic Press, Inc., New York, N. Y., 1957, p. 434.

[9] N. A. Shurmovskaya and R. Kh. Burshtein, *Zhur. Fiz. Khim.*, **31**, 1150 (1957).

increases the work function of nickel and at 100° decreases the work function even at a surface coverage of one tenth. This may be interpreted as chemisorption at the lower temperature and oxidation at the higher temperature. Apparently a real difference exists between nickel with oxygen chemisorbed on the surface and bulk nickel oxide.

Some question as to the effect of relatively electronegative adsorbates on the magnetization of nickel arose when a paper from this Laboratory reported that hydrogen and water decrease the magnetization of nickel while oxygen and nitrous oxide increase the magnetization.[10,11] These results were found with an apparatus that did not permit thorough evacuation of the sample. Later experiments with the AC permeameter showed that all gases thus far studied produce the same effect on the sign of the magnetization change provided that they are measured at the same temperature and on the same catalyst.

The purpose of this work was to extend further the study of the interaction of oxygen with nickel.

Experimental

All measurements were made with the AC permeameter and volumetric adsorption apparatus that has already been described.[12,13] A nickel-kieselguhr catalyst produced by Universal Oil Products Co. was used in an unsintered and sintered form. The nickel content was 52.8%. The unsintered catalyst was used by reducing the catalyst *in situ* for 12 hours at 350° with flowing hydrogen and evacuating for two hours at the same temperature. The sintered catalyst was reduced with hydrogen as before and then sintered in helium for one hour at 500° and one hour at 600° before weighing and sealing in the permeameter for reduction and evacuation.

Hydrogen and nitrous oxide were obtained from commercial cylinders. Hydrogen was purified by passage through a Deoxo unit and silica gel at −78°. Nitrous oxide was purified by fractional freezing at −196° to remove nitrogen. Oxygen was obtained by decomposing dried potassium permanganate and passage of the gas through a silica gel trap at −78°.

Gas analyses were made with a vapor phase chromatograph with silica gel as the column packing according to the results of Janak.[14]

Results

Preliminary Investigations.—Initial experiments on unsintered catalysts showed that oxygen produces the same effect as hydrogen on nickel, namely, a decrease of magnetization. The magnetization–volume isotherms for hydrogen and oxygen in Fig. 1 show how the two gases alter the relative magnetization in the same direction for measurements up to one atmosphere pressure at room temperature. The oxygen takeup of 59.9 cc./g., which lowered the magnetization to 43% of the original value, was 3.3 times that of hydrogen chemisorption under the same conditions. Evacuation did not remove any of the oxygen nor did it restore any of the loss in magnetization.

An attempt was made to use the decomposition of nitrous oxide as a source of oxygen to prevent oxidation and thus to study the chemisorptive process alone. Analyses of the gases in the system were made by removing samples and transferring to the vapor phase chromatograph. The results showed that nitrous oxide is decomposed instantaneously on unsintered nickel catalysts even at temperatures as low as −78°, only 11° above the boiling point of nitrous oxide.

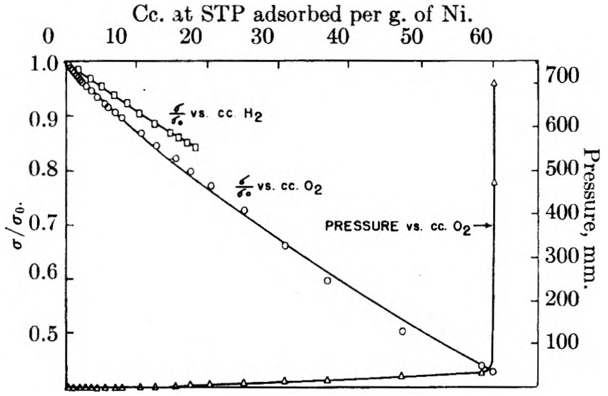

Fig. 1.—Magnetization–volume isotherms for oxygen and hydrogen (and pressure–volume isotherm for oxygen) on nickel at 25°.

The decrease of magnetization accompanying the decomposition of nitrous oxide could have been due to either chemisorption or oxidation. The catalyst then was sintered as described above and used in an attempt to slow down the decomposition of nitrous oxide and the reaction of the oxygen product with the nickel. This sample was found to show an *increase* of magnetization upon chemisorption of hydrogen or of nitrous oxide at low temperatures.

Previous work in this Laboratory[15] has shown that hydrogen adsorbed on nickel at room temperature sometimes causes a positive change of magnetization as measured at low temperatures. It has been surmised (incorrectly) that this indicated some change of nickel–hydrogen bond type as a function of nickel particle size. In view of these results it was felt necessary to make a more detailed study of hydrogen adsorption on nickel. These new results are reported here together with new results on oxygen and nitrous oxide.

Chemisorption on Sintered Catalysts.—A sample of UOP catalyst reduced for 12 hours at 350° was heated for 1 hour at 500° and 1 hour at 600° in helium. Adsorption of hydrogen on this sample gave the results summarized in Fig. 2. In each case the temperature of admission was the same as the temperature of measurement as indicated. It will be noted that on this sample hydrogen at 22° gave a negative change of magnetization although the isotherm deviated from the straight line found with the use of smaller nickel particles.

At −20° the magnetization isotherm had a positive slope at low coverages, followed by a negative slope as coverage increased, while at −78° the hydrogen had a strong positive effect on the magnetization for all but the highest coverages.

For all three temperatures evacuation removed a

---

[10] L. E. Moore and P. W. Selwood, *J. Am. Chem. Soc.*, **78**, 697 (1956).

[11] J. J. Broeder, L. L. van Reijen and A. R. Korswagen, *J. chim. phys.*, **54**, 37 (1957).

[12] P. W. Selwood, *J. Am. Chem. Soc.*, **78**, 3893 (1956).

[13] P. W. Selwood, *ibid.*, **79**, 4637 (1957).

[14] J. Janak, *Collection Czechoslov. Chem. Commun.*, **20**, 343 (1955).

[15] E. L. Lee, J. A. Sabatka and P. W. Selwood, *J. Am. Chem. Soc.*, **79**, 5391 (1957).

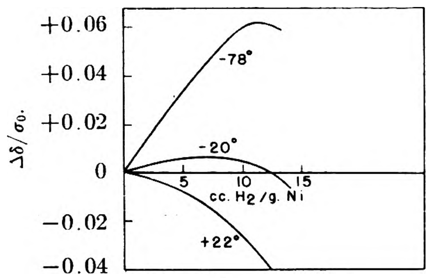

Fig. 2.—Magnetization–volume isotherms for hydrogen on sintered nickel-on-kieselguhr at −78, −20 and 22°.

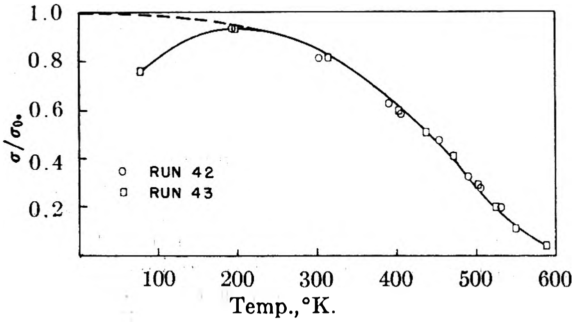

Fig. 3.—Thermomagnetic curve for sintered nickel-on-kieselguhr obtained with AC permeameter. Dotted line indicates usual shape for unsintered catalysts.

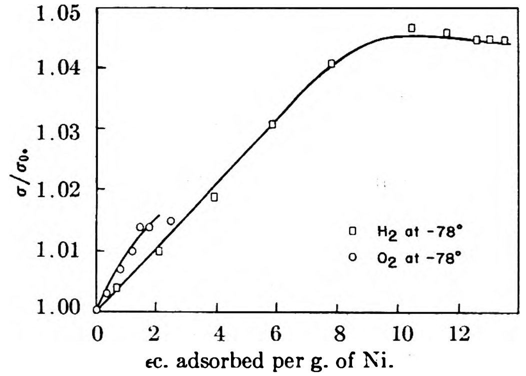

Fig. 4.—Magnetization–volume isotherms for hydrogen and oxygen (as derived from nitrous oxide decomposition) on sintered nickel-on-kieselguhr at −78°.

moderate part of the hydrogen and in each case the change of magnetization so produced was positive in sign and reversible on readmission of hydrogen. In each case the pressure–volume isotherms were normal for the temperature and thus gave no indication of the anomalous magnetic changes occurring in the nickel.

Further investigation of these effects produced the following information.

A sintered sample was treated with 9.9 cc. of hydrogen per g. of nickel at −78°. The sample was then evacuated to remove the trace of hydrogen in the dead-space and some of the more loosely bound chemisorbed hydrogen. This treatment caused a 2.2% increase of magnetization. The sample was warmed to 22° with no further adsorption or desorption and was found to have suffered a 2.4% decrease of magnetization as compared with the sample prior to hydrogen admission at 22°. Recooling showed the change at −78° to be reproducible.

Several additional samples of sintered catalyst gave results in agreement with those shown in Fig. 2. The highest temperature at which hydrogen produced a positive magnetic change was found to depend on the nickel particle size. Thus for particles in the 35 Å. diameter range no positive effect was found above −253°, for 60 Å. particles the corresponding temperature was −78°, while for 85 Å. particles a positive effect was found at 20°, (these diameters are based on X-ray line width broadening, and are approximate only).

A sintered sample gave a small positive magnetization change on physical adsorption of nitrogen at −78°, in contrast to the small negative change observed on smaller nickel particles.[16]

The negative thermal transients which occur when hydrogen is flushed onto smaller nickel particles were found with the sintered samples, but the sign of the effect was reversed when the hydrogen was admitted at low temperatures.

A plot of magnetization *versus* temperature for a sintered sample was obtained on the AC permeameter for comparison with a thermomagnetic curve obtained by the Faraday method at above 8000 oersteds. This is shown in Fig. 3. It will be noted that the AC method shows an apparent maximum of magnetization in the neighborhood of 200°K., whereas the high field magnetization approaches the normal for stable single-domain behavior.

A magnetization–volume isotherm for oxygen on a sintered catalyst was obtained as follows. Nitrous oxide was admitted in small doses to a reduced catalyst at −78°. Evacuation and fractionation with a Toepler pump and buret showed only nitrogen in the gas phase. The volume of oxygen (as O_2) chemisorbed was half the volume of nitrous oxide admitted. Figure 4 shows the oxygen isotherm obtained in this manner and compared with a hydrogen isotherm at the same temperature on the same catalyst. The slope of the oxygen isotherm could not be investigated to any great extent because of the competing nitrous oxide chemisorption and physical adsorption at higher coverages. Admission of a large dose of air to the same system produced a loss of magnetization.

Results were also obtained for the chemisorption of molecular oxygen on sintered catalysts. Oxygen was admitted in small doses to the sintered catalyst as above at −78° after the usual reduction and evacuation. Figure 5 shows that molecular oxygen initially increased the magnetization but, after about 4 cc. per g. of nickel was adsorbed, further addition of oxygen decreased the magnetization. The total takeup of oxygen was corrected for physical adsorption by evacuation and readmission to atmospheric pressure. No significant change of magnetization occurred upon evacuation and readmission, thus showing that no chemically bound oxygen was affected by the evacuation. After correcting for physical adsorption the total takeup of oxygen was 23.90 cc./g. of nickel, or 1.8 times the hydrogen chemisorption at the same temperature on the same catalyst.

The oxygen-covered nickel was evacuated and

---

[16] P. W. Selwood, *J. Am. Chem. Soc.*, **80**, 4198 (1958).

hydrogen was then admitted. This, as shown in Fig. 5, increased the magnetization to near the original value for an uncovered surface.

Similar measurements were made at −130°. Oxygen initially increased the magnetization of the nickel, but further addition beyond 14 cc./g. produced a decrease similar to that shown in Fig. 5. The total takeup of oxygen was 1.9 times that of hydrogen at the same temperature. Evacuation and admission of hydrogen to the oxygen-covered surface caused an increase of magnetization.

Measurements at −183 to −196° were complicated by physical adsorption. The initial portion of several isotherms obtained show a lack of quantitative reproducibility, but clearly show an increase of magnetization caused by oxygen chemisorption. After small doses of oxygen had been admitted to produce a total gain in magnetization of 1.6% in one run at −196° a large dose of oxygen was admitted and decreased the magnetization to 94.6% of the original magnetization for a bare surface. A similar effect was found by warming the catalyst to near room temperature and re-cooling to −196°.

Discussion

A dispersed catalytic system such as nickel-on-kieselguhr is well known to be pyrophoric. The admission of large quantities of oxygen, or even diluted oxygen as air, can produce a complete oxidation of the nickel. It was hoped that the admission of small doses of oxygen such as used in obtaining magnetization–volume or pressure–volume isotherms would produce a true chemisorption instead of bulk oxidation. The decrease of magnetization shown in Fig. 1 could be caused by chemisorbed oxygen decreasing the magnetic moment of metallic nickel due to covalent bonds formed on the surface or to the total conversion of some of the superparamagnetic nickel to paramagnetic nickel oxide. (Nickel oxide is ordinarily antiferromagnetic, but in a dispersed system it could be paramagnetic.) The second explanation seems more plausible since the total oxygen uptake was three times that of the hydrogen chemisorption, but other explanations related to the magnetic anisotropy are not excluded.

Penetration of the nickel lattice below the surface may have occurred. An alternative interpretation is then that chemisorption occurred during the initial portion with conversion to the oxide in later stages. But since the magnetization–volume isotherm is a straight line with no breaks or change of slope, it is more likely that the same process was being measured in both the initial and later stages of the isotherm, that is, oxidation. Local hot spots probably occurred which took up more than a monolayer of oxygen before all of the surface was covered. The total oxygen takeup at one atm. pressure corresponded to the production of $NiO_{0.3}$.

The chromatographic analyses during measurements with nitrous oxide on unsintered catalysts showed that the dispersed nickel system is such a powerful catalyst that molecular nitrous oxide cannot be stably chemisorbed. Immediate decomposition to form an oxide layer and liberation of molecular nitrogen to the gas phase occurred even at −78°. Any previous work on the nickel–nitrous oxide system may need to be re-evaluated if gas analyses were not made during chemisorption measurements.

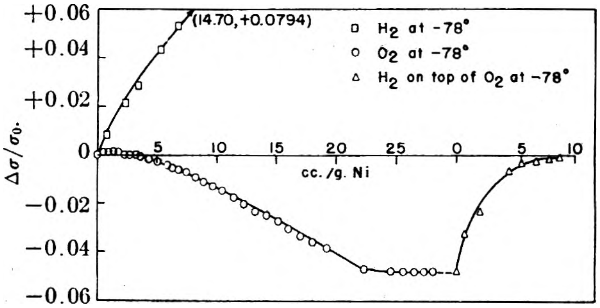

Fig. 5.—Magnetization–volume for hydrogen and oxygen on sintered nickel-on-kieselguhr and for hydrogen on an oxygen covered surface of the same sintered nickel at −78°.

The high reactivity of dispersed nickel necessitated sintering the catalyst in order to diminish oxidation and this led to the observation that sintered catalysts give, under certain conditions, a positive magnetization change on chemisorption of hydrogen or of oxygen.

In summary the conditions tending to produce a positive magnetic change rather than a negative one are the following: (1) nickel particles rather larger than those normally produced in nickel–silica catalyst and averaging in the neighborhood of 100 Å. in diameter; (2) low temperatures; (3) low fields; (4) the use of AC rather than DC fields. But these conditions are not sharply defined and positive magnetic changes may be produced with DC fields at room temperature on certain samples.

Four theories were considered during the course of this work to explain the anomalous results. These were (1) a temperature dependent equilibrium between adsorption on two types of sites; (2) competing chemical and physical phenomena; (3) competition between large metallic particles and small atomic particles; (4) the effect of magnetic anisotropy.

An equilibrium between protonic and hydridic sites of adsorption on nickel already has been proposed to explain positive magnetic effects at liquid hydrogen temperature.[10] The positive effects were thought to occur for small particles which became ferromagnetic only at low temperatures. This coupled with the relatively low uptake of hydrogen for extremely finely divided catalysts led to the conclusion that the direction of electron transfer depended on the particle size. Hydrogen donated electrons to the nickel if the particles were large. Nickel donated electrons to the hydrogen if the particles were small. The present work at first supported the notion that there was an equilibrium between two sites. However since the positive effect became more positive with sintering, the positive effect could not be due to negative hydride ions on small particles. The positive magnetic effect seemed more closely associated with large particles than small particles. Since the sign of magnetic change depended on the temperature of measurement, it appeared that there might be some temperature dependent equilibrium involving desorption and migration between sites. But any mechanism proposing two sites, and an equilibrium between them was ruled out by the experiment in which both positive and negative effects were found for the same adsorbed hydrogen when the magnetization was measured at two different temperatures, the higher of which was by no means high enough to cause appreciable desorption.

The idea of a competition between a chemical and a physical phenomenon was based on the observation that measurements at low fractions of magnetic saturation showed a negative magnetic effect, whereas measurements at higher fractions of magnetic saturation showed a positive effect. High field studies were considered to be measuring directly the donation of electrons from the d-band of nickel to covalent chemical bonds with the adsorbate. It was postulated that each electron being donated had a compensated spin so the loss would produce an increase in the observed magnetization. Low field studies were considered to be measuring the suppression of the already low Curie temperature of nickel particles with less than an average coördination number of 12 by diminishing the exchange forces of the metal. Although Crittenden and Hoffman's[17] work on thin film supports the notion of a variation of the Curie temperature with number of nearest neighbors, any alteration of the number of unpaired electrons would affect the exchange forces in the same manner as it does the magnetic moment. Secondly, the lack of a defined Curie point in the thermomagnetic curve for these particles is not due to a variation of the Curie temperature with coördination number, but is due rather to the superparamagnetism of these small particles.

Since there is a range of particle sizes for the nickel in these catalysts, it was considered that the larger particles could be behaving as normal metallic nickel, where the smaller particles could be acting atomically. The two size ranges could be considered responsible for the two different effects on the magnetization for hydrogen chemisorption. However no variation in the bond character with particle size was observed.

The best explanation at the present time for the phenomena found here lies in a consideration and application of the magnetic anisotropy of ferromagnetic substances.

If the applied magnetic field is strong enough it can orient the great majority of the domains and so saturate the sample magnetically. The application of any thermal energy will tend to disarray the alignment. Therefore the magnetization will drop with increasing temperature. However, consider what will occur if the applied field is so weak that it will not be energetic enough to turn all of the domains. If the process is begun near −273° and then the sample is warmed, the thermal energy will help to turn some of the domains that are not parallel to the field to become aligned with the field. If the sample is further warmed the thermal energy will become sufficient so there will be a disturbance of the alignment and the magnetization will decrease. Therefore warming a ferromagnetic sample from near absolute zero to its Curie temperature in the presence of a weak magnetic field will produce first an increase of apparent magnetization followed by a decrease at higher temperatures. Thermomagnetic curves obtained at different field strengths will then appear as shown by Bozorth.[18] They are similar to the thermomagnetic curves obtained for sintered nickel catalysts at low fields.

The magnetic anisotropy phenomenon is important for the AC measurements that were made here, because there is a continual turning of the domains back and forth, through 180°, 60 times a second as the current alternates. The unsintered catalysts have particles of nickel so small that they behave as true superparamagnetics. As the particles grow with sintering the magnetic anisotropy becomes prominent enough to produce a maximum at the thermomagnetic curve.

The effect of anisotropy can also explain the increase of magnetization found when gases are chemisorbed on sintered catalysts at low temperatures. The magnetic anisotropy is believed due to a spin-orbit coupling of the outer electrons with the electrostatic field of the lattice. If the number of free spins is altered then there should be a drop in the anisotropy energy. Brooks[19] has shown by using a band model for ferromagnetics the relation of the anisotropy constants to the number of free spins. He has also predicted correctly the decrease in anisotropy when alloying occurs. The chemisorption of gases also produces a decrease in the number of free spins. Therefore the anisotropy energy is lowered to allow the resultant moments to align more readily with the field to show an increase of magnetization, which is found experimentally. This assumes that the anisotropy is more sensitive to a change in the number of free spins than is the magnetic moment. The motion of domains over the energy barrier is not by the addition of more thermal energy, instead the transfer is facilitated by a decrease in the depth of the potential well for the domains which are not aligned. There is also a decrease in the depth of the potential well for the configuration with the domains aligned, but this is a smaller fraction of the total well depth.

Figure 2 shows how the effect which we have attributed to magnetic anisotropy predominates in measurements of hydrogen chemisorption at −78°. At higher coverages the anisotropy effect is eventually overcome and a slight decrease of magnetization results from further chemisorption of hydrogen. This can be explained in terms of a simple decrease in the magnetic moment of superparamagnetic particles. At a higher temperature, −22°, the anisotropy effect is still present, but is smaller in magnitude and is overcome at lower surface coverages than at −78°. At a still higher temperature, +22°, the thermal disordering is large enough so there is little evidence for any magnetic anisotropy except for the gentle curvature of the magnetization-volume isotherm instead of the linear isotherm found for unsintered catalysts.

These observations on sintered catalysts make

---

[17] E. C. Crittenden and R. W. Hoffman, *J. phys. radium*, **17**, 270 (1956)

[18] R. M. Bozorth, "Ferromagnetism," D. Van Nostrand Co., Inc., New York, N. Y., 1951, p. 714.

[19] H. Brooks, *Phys. Rev.*, **58**, 909 (1940).

available a technique for distinguishing surface chemisorption of oxygen and bulk oxidation at low temperatures. The former may produce an increase of magnetization as does hydrogen. The latter produces a decrease because of the conversion of a superparamagnetic to a paramagnetic substance. The increase of magnetization produced by oxygen, as derived from nitrous oxide, and hydrogen at −78° was shown in Fig. 4. It is of interest to note that the relative magnetic increase per unit volume of oxygen is twice that of hydrogen. This suggests that twice as many nickel atoms are being altered per oxygen atom on the surface as per hydrogen atom. If one electron is donated by the nickel to form a covalent bond with each hydrogen atom, then apparently two electrons are donated to form a coördinate covalent linkage to each oxygen atom or alternatively, two nickel atoms are involved per oxygen atom taken up. But it must be stated that the relation of positive magnetization changes to saturation moments is speculative.

The results with molecular oxygen on sintered catalysts at −78° in Fig. 5 show that surface chemisorption occurs at low coverages, but the oxygen penetrates the nickel lattice at higher coverages in what may best be called an oxidation process. The initial rise in magnetization with oxygen at −78° appears to be similar to that found for hydrogen and nitrous oxide at the same temperature and may be interpreted as due to surface chemisorption. The leveling off and eventual drop in magnetization to less than the initial magnetization, after 4 cc./g., has been interpreted as due to penetration of the nickel lattice. If hydrogen is chemisorbed to form a monolayer, and since the oxygen takeup is 1.8 times that of hydrogen, then the oxygen penetrates the nickel to a depth of almost two layers. It is possible that some of the nickel, which chemisorbs hydrogen, is inaccessible to oxygen because of the pore size of the support.[20,21] If there were equal accessibility of nickel to hydrogen and oxygen, the oxygen-hydrogen ratio might have been closer to 2.0.

The recovery of magnetization upon admission of hydrogen to the oxygen covered surface shows that the oxidation process does not simply produce stable nickel oxide. The oxygen which is taken up by the nickel is left in a highly reactive state and is readily hydrogenated to form water at −78°. An alternate explanation for the rise in magnetization for hydrogen on top of oxygen on nickel is that it could be due to hydrogen being chemisorbed on nickel particles which are inaccessible to oxygen.

The results at −130° confirm those at −78°. The only difference is the further extent of chemisorption and the delay in transition to oxidation. The chemisorbed oxygen is apparently more stable at −130° than at −78° and more oxygen has to be admitted to produce oxidation. This is in contrast with the electron diffraction work of Farnsworth and Tuul[22] who found chemisorbed oxygen more stable at a higher temperature (150°) than a lower (25°).

The small amount of chemisorption and the large amount of physical adsorption at the boiling point of oxygen, −187°, and below, −196°, make quantitative comparisons of the effect of oxygen and hydrogen impossible. Qualitative conclusions are evident. Small doses of oxygen produce chemisorption as shown by the increase of magnetization. Large doses or warming produce oxidation.

The low temperature results for hydrogen and oxygen show that both gases have the same effect on the magnetization of nickel, provided oxidation is prevented. The simplest way to explain how an electronegative adsorbate such as oxygen can have the same effect as hydrogen is to consider that both are covalently bonded to the surface, as has already been suggested.[23] It appears that unpaired electrons of the d-band of nickel are donated to form covalent bonds in chemisorption as postulated by Broeder, *et al.*,[24] to decrease the magnetic moment. Some workers[25,26] have considered that oxygen should be bound to nickel through the s-band of the metal whereas the magnetic results indicate the d-band participates. The two views are not mutually exclusive. The s-band electron may be directly involved in bonding the oxygen to the surface, while a secondary redistribution of electrons in the d-band may cause the magnetic moment to be altered. This is possible because of the overlap of the two bands.

An alternate model for explaining the magnetic results of chemisorption may possibly be based on the quantum mechanical calculation of Grimley[27] and Koutecky,[28] provided that these can be extended to d-band interactions.

Acknowledgment.—The authors are indebted to Robert E. Dietz for his interest in these problems and for drawing attention to the possible role of magnetic anisotropy in explaining the positive magnetization change sometimes observed when hydrogen is chemisorbed on nickel. They are indebted to Remola Ciola for assistance with the gas chromatography of nitrous oxide.

This work was performed under contract DA-11-022-ORD-2285 with the Office of Ordnance Research.

DISCUSSION

DIETRICH SCHULZE (Mellon Institute).—An alternative explanation of the magnetic changes occurring during chemisorption may be that the heat of reaction sinters the small nickel particles to larger particles which have a different Curie temperature.

R. J. LEAK.—If any such sintering occurs I assume it would be irreversible. Therefore, evacuation and readsorp-

---

[20] G. C. A. Schuit and L. L. van Reijen, "Advances in Catalysis," Edited by D. D. Eley, W. G. Frankenburg and V. I. Komarewsky, Academic Press, Inc., New York, N. Y., 1958, p. 242.

[21] J. A. Sabatka, Doctoral Dissertation, Northwestern University, 1956.

[22] H. E. Farnsworth and J. Tuul, *Phys. and Chem. of Solids*, **9**, 48 (1959).

[23] P. W. Selwood, "Advances in Catalysis," Vol. IX, Ed. by D. D. Eley, W. G. Frankenburg and V. I. Komarewsky, Academic Press, Inc., New York, N. Y., 1957, p. 93.

[24] J. J. Broeder, L. L. van Reijen, W. M. H. Sachtler and G. C. A. Schuit, *Z. Elektrochem.*, **60**, 838 (1956).

[25] B. M. W. Trapnell, *Proc. Roy. Soc.* (*London*), **A218**, 566 (1953).

[26] O. D. Gonzalez and G. Parravano, *J. Am. Chem. Soc.*, **78**, 4533 (1956).

[27] T. B. Grimley, *Proc. Phys. Soc.*, **72**, 103 (1958).

[28] J. Koutecky, *Trans. Faraday Soc.*, **54**, 1038 (1958).

tion should show changes in the isotherm. However the isotherm for the $Ni-H_2$ system is reproducible over successive measurements.

Paul H. Lewis (Texaco, Inc.).—Why does the susceptibility curve increase with the addition of hydrogen and increasingly so at lower temperatures? Would this be due to sintering?

R. J. Leak.—The increase is produced by altering the spin-orbit coupling of the electrons with the lattice which is responsible for the magnetic anisotropy. The activation energy barrier between aligned and non-aligned orientation apparently is lowered so as to make it easier for the domains to be oriented with the magnetic field. The effect becomes more pronounced at lower temperatures because there is less thermal energy available to cause transition over the barrier.

A. C. Zettlemoyer (Lehigh University).—When Ni is oxidized, O^- ions form on the NiO. Do these influence the magnetization measurements?

R. J. Leak.—The O^- ions that are proposed by Chessick, Yu and Zettlemoyer in the latter stages of oxidation are not in contact with the metal and would be unlikely to have any effect through an insulating barrier of NiO.

J. A. Rashkin (E. I. du Pont de Nemours & Co.).—Can you say anything about bond localization in the adsorption of oxygen and hydrogen? You say that the hydrogen atom donates an electron to form a covalent bond with the nickel. Can you reconcile this with work done by Handler and others who have shown that adsorbed hydrogen atoms increase the p-type surface conductivity of the sputtered germanium surface, indicating that hydrogen is acting electronegatively?

R. J. Leak.—From the work presented here I cannot. However, from high field-low temperature saturation measurements it has been concluded that the hydrogen-nickel bond is localized (R. E. Dietz and P. W. Selwood, *J. Appl. Phys.*, **30**, 1015 (1959)). The formation of a covalent bond by the hydrogen and nickel each donating an electron tells nothing *a priori* about the polarization of the bond. Other workers have shown that hydrogen forms the negative end of the polarized nickel hydrogen covalent bond (J. J. Broeder, L. L. van Reijen, W. M. H. Sachtler and G. C. A. Schuit, *Z Elektrochem.*, **60**, 838 (1956)).

Paul H. Lewis.—The authors comment that the magnetization-volume isotherm *versus* O_2 adsorbed (Fig. 1) is a straight line. They deduce from this that the nickel is undergoing the same process at the start of the admission of oxygen as at the end. From the fact that the O_2/H_2 adsorption ratio is 3.3 they conclude that the process is bulk oxidation. Is this a valid conclusion? Why wouldn't the formation of a $Ni^{++}-O^-$ bond at the surface have the same effect as one in the bulk?

R. J. Leak.—Nothing definite can be stated from Fig. 1 about the bonding of oxygen to nickel except that it is the same throughout the isotherm. Proof of a difference between chemisorption of oxygen and oxidation at −78° is given in Figs. 4 and 5 with confirmatory evidence quoted at −130, −183 and −196°.

A PREDICTION OF HETEROGENEOUS CATALYTIC REACTIONS

By R. A. Gardner[1]

Contribution from the Chemical and Physical Research Laboratory, The Standard Oil Company (Ohio), Cleveland, Ohio

Received March 7, 1960

A "kinetic isotope effect" was predicted for the catalytic oxidation of hydrogen-deuterium mixtures. With copper oxide as the catalyst H_2O would be formed at a faster rate than D_2O while with nickel oxide as a catalyst the two reactions were predicted to occur at the same rate. This paper presents the methods used to arrive at these predictions and the results of the experimental investigation of these reactions. Reaction mechanisms are proposed and additional predictions are made which will be investigated experimentally.

Infrared spectra have been obtained of carbon monoxide chemisorbed on copper, nickel and cobalt and several compounds of these metals.[2] An infrared technique similar to that developed by Eischens[3] was used to obtain the spectra. Several infrared absorption bands were observed to result from the adsorption of carbon monoxide on a single adsorbent. For example, the chemisorption of carbon monoxide on copper oxide produced infrared absorption bands at 2173, 2127 and 2000 cm.$^{-1}$. The vibration frequencies of the neutral carbon monoxide molecule and the carbon monoxide positive ion are reported by Herzberg[4] as 2143 and 2184 cm.$^{-1}$, respectively. The neutral carbon monoxide molecule has 10 valence electrons. The carbon monoxide positive ion has 9 valence electrons. It was hypothesized[2] therefore that an infrared absorption band for chemisorbed carbon monoxide at 2173 cm.$^{-1}$ corresponds to a carbon monoxide species which has a non-integral number of valence electrons between 9 and 10. The experimental data of this study were interpreted using the Wolkenstein[5] hypothesis of the mechanism of chemisorption. This led to the formulation of a relationship between the vibration frequencies of adsorbed carbon monoxide species and the number of valence electrons associated with these species. From this relationship the vibration frequencies of the adsorbed carbon monoxide species on copper oxide were found to correspond to 9.30, 10.30 and 11.30 valence electrons for the species producing the absorption bands at 2173, 2127 and 2000 cm.$^{-1}$, respectively. The concept of fractional numbers of electrons associated with adsorbed species has suggested a method for the qualitative prediction of rates, mechanisms and catalysts for certain heterogeneous catalytic reactions.

The hypothesis which has been used in the prediction of heterogeneous catalytic reactions was proposed by Myers.[6] He advanced the concept that for certain reactions a coincidence between the vibration frequencies of the reactants is necessary.

---

(1) Chemical and Physical Research Department, Standard Oil Company (Ohio), Cleveland, Ohio.

(2) R. A. Gardner and R. H. Petrucci, "The Chemisorption of Carbon Monoxide on Metals" (1959) a thesis, submitted for publication.

(3) R. P. Eischens, W. A. Pliskin and S. A. Francis, *J. Chem. Phys.*, **22**, 1786 (1954).

(4) G. Herzberg, "Spectra of Diatomic Molecules," D. Van Nostrand Co., Princeton, N. J., 1955, pp. 522.

(5) Th. Wolkenstein, "Advances in Catalysis," Vol. IX, Academic Press, Inc., New York, N. Y., 1957, pp. 807–817.

(6) R. R. Myers, *Ann. N. Y. Acad. Sci.*, **72**, 341 (1958).

When the electrons of two potential reactants are in the same or harmonic energy levels, these electrons can be exchanged and combined to form a product. The examples which he presents of the oxidation, hydrogenation, halogenation and alkylation reactions of ethylene strongly support his fundamental hypothesis that a coincidence of vibration between reacting species is a necessary condition for certain reactions.

The concept of a "fractional electron population" is also used in the prediction of catalysts and reactions. This refers to the non-integral or fractional portion of the number of valence electrons associated with adsorbed species on a particular metal or metal compound. The fractional electron population is hypothesized to be a property of the metal. Since the carbon monoxide species on copper oxide possessed 9.30, 10.30 and 11.30 valence electrons, the fractional electron population of copper(II) is designated as 0.30. Therefore hydrogen species on Cu(II) will possess 0.30 and 1.30 valence electrons, and oxygen species on Cu(II) may possess 4.30, 5.30, 6.30 and 7.30 valence electrons.

On the basis of the above hypothesis and concepts, the prediction of heterogeneous catalytic systems requires a knowledge of: (1) the vibration frequencies or energy levels of the gaseous species which may enter into the reaction; (2) the fractional electron population of the surface atoms of possible catalysts; (3) the vibration frequencies or energy levels of the chemisorbed species which may enter into the reaction; (4) a reaction mechanism.

The particular reaction to be considered is the oxidation of hydrogen–deuterium mixtures catalyzed by copper oxide and nickel oxide. The fundamental vibration frequencies of the gaseous reactants were obtained from data presented by Herzberg.[7] The vibration frequencies of these gases are: H_2, 4159.2 cm.$^{-1}$; D_2, 2990.2; and O_2, 1556.2.

The fractional electron populations of the two metals are 0.30 for copper as copper oxide and 0.00, 0.95 and approximately 0.90 for nickel as nickel oxide. These values for nickel were determined in a manner similar to that used for copper(II) from our infrared studies of the vibration frequencies of carbon monoxide chemisorbed on nickel and several nickel compounds.[2] The greater number of fractional electron populations for nickel results from the possibility of one and two partially filled 3d orbitals.

The proposed energy levels of the chemisorbed species of oxygen, hydrogen and deuterium can be derived on the basis of dissociative chemisorption of the molecular gases forming atomic species. The energy levels of the chemisorbed atoms can be determined from the following equations which relate the energy levels to the number of valence electrons associated with the particular adsorbed species. The number of electrons is in turn determined by the fractional electron population of the particular catalyst. The equations are

$$\nu_H = 4159.2e_H \qquad (1)$$

$$\nu_D = 2990.2e_D \qquad (2)$$

$$\nu_O = 778.1(8 - e_O) \qquad (3)$$

where ν = energy level of the adsorbate in cm.$^{-1}$, e = number of valence electrons associated with the particular adsorbate species.

Finally, the low temperature catalytic reaction of H_2 or D_2 with O_2 to form H_2O or D_2O suggests two types of reaction mechanisms: (1) the reaction of a gaseous hydrogen molecule with an adsorbed oxygen atom, or (2) the surface reaction of two adsorbed hydrogen atoms with one adsorbed oxygen atom.

The prediction of the catalyst and mechanism of a reaction involves a matching of the fundamental vibration frequencies or energy levels of gaseous and chemisorbed reactants. As has been proposed by Myers[6] the first overtone frequencies may also be used. The following equations show the reactants with the closest matching frequencies, the energy levels in cm.$^{-1}$ as subscripts, the numbers of electrons associated with the various species as superscripts, and the percentage difference of the frequencies from their average.

$$\begin{array}{llll}
\mathrm{Ni(O)}^{8.00} + 2\mathrm{Ni(H)}^{0.00} \longrightarrow & & & \\
\quad 0.0 \qquad\qquad\quad 0.0 & \mathrm{Ni(H_2O)}^{8.00} \longrightarrow \mathrm{Ni} + (\mathrm{H_2O})^{8.00} & & (4) \\
 & \quad \%\ \text{diff. } 0 & &
\end{array}$$

$$\begin{array}{llll}
\mathrm{Ni(O)}^{8.00} + 2\mathrm{Ni(D)}^{0.00} \longrightarrow & & & \\
\quad 0.0 \qquad\qquad\quad 0.0 & \mathrm{Ni(D_2O)}^{8.00} \longrightarrow \mathrm{Ni} + (\mathrm{D_2O})^{8.00} & & (5) \\
 & \quad 0\%\ \text{diff.} & &
\end{array}$$

$$\begin{array}{llll}
\mathrm{Cu(O)}^{6.30} + \mathrm{H_2}^{2.00} \longrightarrow & \mathrm{Cu(H_2O)}^{7.30} \longrightarrow & & \\
\quad 2100 \qquad\quad 4159 & \quad 0.48\%\ \text{diff.} & & \\
\quad (4200) & \mathrm{Cu(H_2O)}^{8.30} \longrightarrow \mathrm{Cu} + (\mathrm{H_2O})^{8.00} & & (6)
\end{array}$$

$$\begin{array}{llll}
\mathrm{Cu(O)}^{4.30} + \mathrm{D_2}^{2.00} \longrightarrow & \mathrm{Cu(D_2O)}^{6.30} \longrightarrow & & \\
\quad 2879 \qquad\quad 2990 & \quad 1.88\%\ \text{diff.} & & \\
 & \mathrm{Cu(D_2O)}^{8.30} \longrightarrow \mathrm{Cu} + (\mathrm{D_2O})^{8.00} & & (7)
\end{array}$$

The harmonic frequency is shown in parentheses. The electrons in equations 6 and 7 used in the transition from $\mathrm{Cu(H_2O)}^{7.30} \rightarrow \mathrm{Cu(H_2O)}^{8.30}$ and $\mathrm{Cu(D_2O)}^{6.30} \rightarrow \mathrm{Cu(D_2O)}^{8.30}$ are available from the catalyst and fractions of electrons remaining after desorption of the product return to the catalyst. In accordance with the Wolkenstein[5] hypothesis of the mechanism of chemisorption, the various adsorbed species exist in equilibrium. Desorption from the surface is hypothesized to occur through the adsorbed species that is closest in electronic configuration to the neutral gaseous molecule. For H_2O and D_2O on Cu(II), this is the adsorbed species possessing 8.30 valence electrons. The metals in the above equations are in the form of oxides.

According to the detailed reaction mechanisms presented in the above equations, hydrogen and deuterium react with oxygen over nickel oxide by the surface combination of hydrogen or deuterium ions (H^+ or D^+) with oxide ions (O^{-2}). These are protons or deuterons having no valence electrons and oxygen species having 8 valence electrons. The reactions of hydrogen and deuterium with oxygen catalyzed according to the above equations by copper oxide proceed by the attack of gaseous hydrogen and deuterium molecules onto chemisorbed oxygen species which are in a positive electronic configuration. The numbers of valence electrons associated with these oxygen species chemisorbed on

---

(7) G. Herzberg, ref. 4, pp. 532, 533 and 560.

copper oxide in equations 6 and 7 are 5.30 and 4.30. The energy levels of the electrons of these species can be calculated from equation 3. The oxygen species on copper oxide which reacts with a hydrogen molecule has 5.30 valence electrons with an energy level of 2100 cm.$^{-1}$. The chemisorbed oxygen species on copper oxide which reacts with a deuterium molecule is more electron deficient having 4.30 valence electrons and an energy level of 2879 cm.$^{-1}$.

Reactions 4, 5 and 6 show a matching of frequencies within less than 0.5%. These reactions are predicted to proceed readily. Reaction 4 however, with a percentage difference of 1.88, is predicted to proceed at a slower rate. Therefore, the reaction of a mixture of hydrogen, deuterium and oxygen containing equal molar amounts of H_2 and D_2 over copper oxide is predicted to produce H_2O more rapidly than D_2O at conditions where the reactants and chemisorbed species are those noted above. The reaction of hydrogen, deuterium and oxygen over nickel oxide is predicted to produce H_2O and D_2O at the same rate. These predicted reactions should predominate at the minimum reaction temperature, since they show the closest matching of frequencies of gaseous and chemisorbed reactants.

Experimental Method and Results

On the basis of the above considerations, mixtures of hydrogen, deuterium and oxygen were passed over copper oxide and nickel oxide. A large excess of oxygen was used to ensure maintenance of the metal oxides. The products were condensed in traps cooled by Dry Ice–acetone mixtures and analyzed by infrared spectroscopy for OD and OH absorption frequencies. The composition of the entering gaseous mixture was determined by mass spectrometry. The data are presented in Table I in terms of the OD/OH ratio in the product divided by the D_2/H_2 ratio in the feed (the isotope effect) as a function of the temperature of the reaction.

As was predicted, the preferential oxidation of H_2 in H_2–D_2 mixtures over copper oxide increases as the reaction temperature approaches a minimum. The prediction also stated that H_2O and D_2O would be formed at essentially the same rate over nickel oxide at the minimum reaction temperature. This is also substantiated by the data in Table I. The necessity for specifying the minimum reaction temperature arises as a result of the existence of alternative reaction mechanisms which can make increasing contributions to the product formation as the temperature is raised. The following equation illustrates an alternative reaction for D_2O formation over copper oxide.

$$\begin{array}{llll} 2\mathrm{Cu(D)}^{1.30} + & \mathrm{Cu(O)}^{5.30} & \longrightarrow \mathrm{Cu(D_2O)}^{7.30} \longrightarrow & \\ 3888 & 2100 & 3.86\%\ \text{diff.} & \\ & (4200) & & \\ & & \mathrm{Cu(D_2O)}^{8.30} \longrightarrow \mathrm{Cu} + \mathrm{D_2O} & (8) \end{array}$$

Discussion

During work on this system, several interesting observations have been made. For example, the effluent gas after contact with nickel oxide contained HD as well as H_2 and D_2. The reaction mechanisms for the formation of H_2O and D_2O over nickel oxide presented in equations 4 and 5 show the combination of adsorbed oxide ions (oxygen species possessing eight electrons) with protons and deuterons (hydrogen species possessing no electrons) to produce H_2O and D_2O. Since nickel oxide is hypothesized[2] to adsorb gases as ions and atoms (or molecules), the existence of H^+, H, H^-, D^+, D, D^-, O^{+2}, O^+, O, O^- and O^{-2} on the surface of nickel oxide permits the formation of HD, H_2O, D_2O and HDO as possible desorbed products.

TABLE I

THE OXIDATION OF HYDROGEN–DEUTERIUM MIXTURES CATALYZED BY COPPER OXIDE AND NICKEL OXIDE

	CuO		Catalyst		NiO		
Temp., °C.	D_2/H_2 Feed	OD/OH Product	Isotope effect	Temp., °C.	D_2/H_2 Feed	OD/OH Product	Isotope effect
252	1.00	0.111	0.111	174	15.8	15.6	0.986
266	1.00	.113	.113	179	1.19	1.13	.950
274	1.00	.150	.150	204	15.8	13.6	.861
282	1.00	.150	.150				
310	1.00	.185	.185				
349	1.00	.210	.210				

In contrast to nickel oxide, no HD was observed after the gas had contacted copper oxide. As shown in equations 6 and 7 the gases adsorbed on copper(II) exist in electronic configurations that are intermediate between ions and atoms (or molecules). The following reactions compare the formation of HD over copper oxide and nickel oxide.

$$\begin{array}{llll} \mathrm{Cu(H)}^{0.30} + & \mathrm{Cu(D)}^{0.30} & \longrightarrow \mathrm{Cu(HD)}^{1.30} \longrightarrow & \\ 1247 & 897 & 16.3\%\ \text{diff.} & \\ & & \mathrm{Cu} + (\mathrm{HD})^{2.00} & (9) \end{array}$$

$$\begin{array}{llll} \mathrm{Ni(H)}^{0.00} + & \mathrm{Ni(D)}^{0.00} & \longrightarrow \mathrm{Ni(HD)}^{0.00} \longrightarrow & \\ 0 & 0 & 0\%\ \text{diff.} & \\ & & \mathrm{Ni(HD)}^{2.00} \longrightarrow \mathrm{Ni} + (\mathrm{HD})^{2.00} & (10) \end{array}$$

As can be seen from the percentage differences of the vibration frequencies of adsorbed H and D on each catalyst, the formation of HD over nickel oxide is greatly favored over the formation of HD over copper oxide.

The presence of the above mentioned ions on the surface of nickel oxide also leads to the formation of HDO from H_2, D_2 and O_2 by surface reactions. Since the prediction concerned the oxidation of hydrogen and deuterium and the product analyses were made by the infrared absorbances of the OH and the OD bands, there was no determination of the concentration of HDO. The reaction mechanisms shown in equations 6, 7 and 9 preclude the formation of HDO from H_2, D_2 and O_2 over copper oxide at the minimum reaction temperature.

A consideration of the vibration frequency of the HD molecule indicates that it should be even less reactive to oxidation over copper oxide than D_2. The three reactions with the electronic configurations of the adsorbed species, their energy levels, and the percentage difference of the matched frequencies are presented

$$\begin{array}{llll} \mathrm{Cu(O)}^{5.30} + & \mathrm{H_2}^{2.00} & \longrightarrow \mathrm{Cu(H_2O)}^{7.30} \longrightarrow & \\ 2100 & 4160 & 0.48\%\ \text{diff.} & \\ (4200) & & \mathrm{Cu(H_2O)}^{8.30} \longrightarrow \mathrm{Cu} + \mathrm{H_2O} & (11) \end{array}$$

$$\begin{array}{lllll}
\mathrm{Cu(O)}^{4.30} & + & \mathrm{D}_2^{2.00} & \longrightarrow & \mathrm{Cu(D_2O)}^{6.30} \longrightarrow \\
2879 & & 2990 & & 1.88\%\ \text{diff.} \\
 & & & & \mathrm{Cu(D_2O)}^{8.30} \longrightarrow \mathrm{Cu} + \mathrm{D_2O} \quad (12)
\end{array}$$

$$\begin{array}{lllll}
\mathrm{Cu(O)}^{5.30} & + & \mathrm{HD}^{2.00} & \longrightarrow & \mathrm{Cu(HDO)}^{7.30} \longrightarrow \\
2100 & & 3628 & & 7.3\%\ \text{diff.} \\
(4200) & & & & \mathrm{Cu(HDO)}^{8.30} \longrightarrow \mathrm{Cu} + \mathrm{HDO} \quad (13)
\end{array}$$

At 660° F. percentage differences of 0.48 and 1.88 correspond to a 5 to 1 reaction rate difference. Therefore it can be predicted that a mixture of H_2, D_2 and HD containing an equal number of moles of these gases with excess oxygen when contacted with copper oxide at the minimum reaction temperature will form the oxidized products at the following relative rates: $H_2O > D_2O$ or HDO. The experimental investigation of this prediction will be a part of the continuing examination of these concepts and hypotheses.

Conclusion

The foregoing has described a tentative method for the prediction of heterogeneous catalytic reactions. This has been applied to the prediction of a preferential oxidation of H_2 in H_2-D_2 mixtures catalyzed by copper oxide—a "kinetic isotope effect"—and the absence of this effect in the reactions catalyzed by nickel oxide at the minimum reaction temperatures. On this basis details of the reaction mechanisms have been advanced. The experimental investigation of these predictions has produced data which support these hypotheses. In addition it has been shown that predictions can be made concerning the reactivity of HD toward oxidation over copper oxide and nickel oxide. The applicability of these concepts will be probed by future experiments.

Acknowledgment.—The author wishes to acknowledge the advice and assistance of Dr. H. A. Strecker and Mrs. R. Krizan in this study, and to thank the Standard Oil Company (Ohio) for permission to publish this work.

DISCUSSION

D. J. C. YATES (Columbia University).—The gas phase spectrum of nickel carbonyl under resolution normally used in this type of work gives a very strong and very sharp symmetrical band at about 2060 cm.$^{-1}$. Small quantities of this gas could have given the band shown on adding CO to evaporated nickel films.

R. A. GARDNER.—Attempts were made to condense gaseous nickel carbonyl when carbon monoxide was contacted with a vacuum evaporated nickel film. No indication of gaseous nickel carbonyl was observed; however, this point was not pursued exhaustively since the 2060 cm.$^{-1}$ band was not used to establish the relationship between the vibration frequency of CO units and the number of valence electrons associated with the CO units (Ref. 2 and R. A. Gardner and R. H. Petrucci, *J. Am. Chem. Soc.*, **82**, in press (1960).

A. C. ZETTLEMOYER (Lehigh University).—How do you take care of heterogeneity of surface states and their alteration with increasing coverage?

R. A. GARDNER.—According to the Wolkenshtein hypothesis there are discrete donor sites and acceptor sites. The ratio of those being occupied depends on the surface coverage.

P. A. LEWIS (Texaco Research Center).—How do you divorce the frequency shifts observed from bond length rather than numbers of valence electrons?

R. A. GARDNER.—Bond length, bond order and stretching vibration frequency depend on the number of electrons associated with the molecule. For carbon monoxide the bond length decreases and the vibration frequency increases as electrons are removed from the molecule.

SITES FOR HYDROGEN CHEMISORPTION ON ZINC OXIDE[1]

BY V. KESAVULU AMD H. AUSTIN TAYLOR

Wm. H. Nichols Laboratory, New York University, New York 53, N. Y.

Received March 7, 1960

The adsorption of hydrogen on zinc oxide shows maxima around 60 and 300. Repeated adsorptions at 300° enhance the adsorption at 60°. This is attributed to a reduction of ZnO producing highly polarized zinc atoms located in the negative potential wells between three oxide ions. These highly polarized atoms are considered Type A sites responsible for the 60° maximum. Oxidation of the surface is shown to eliminate these sites, which can be regenerated by reduction. Water produced during the reduction has been proved by mass-spectrometric analysis. By a series of heating and cooling experiments it has been shown that the Type A sites are independent of the Type B sites responsible for the high temperature maximum. Type A sites can be degassed effectively at 150°. A study of the kinetics on Type A sites alone becomes possible. The energy of activation on Type A is zero. An accounting is offered for the H_2-D_2 exchange on Type A sites. A mechanism for Type B chemisorption is proposed and the effect of free electron density in the crystal on both types A and B is considered. The over-all picture is a synthesis of the geometric and electronic views of the catalyst surface.

H. S. Taylor's[2] original concept of "active centers" in chemisorption and catalysis has undergone considerable change. The geometrical interpretation, of faces, edges and corners with varying degrees of saturation, has given way to an electronic interpretation. Sites are viewed as centers on the surface where the exchange of electrons with the interior is energetically favorable. As applied to the chemisorption of a gas on a semiconductor, this electronic interpretation implies the migration of mobile quasi-free electrons or of positive holes to the surface and then a binding of the reactant in a charged or polarized state. This presupposes the presence of electrons in the conduction band or of holes in the valence band. The chemisorptive property of a solid should be closely related to its electrical conductivity, which is determined by the density of free electrons and holes in the crystal. Efforts to establish such a relationship have not always been successful. The realization that a site which is active for the adsorption of one gas need not necessarily be active for all gases implies a specificity in such a relationship. The problem reduces to a recognition of the sites on a particular surface which are active for the adsorption of a particular gas. The study of chemisorption developed here presents itself as a powerful tool for such recognition and leads to a synthesis of the geometric and electronic points of view so far as zinc oxide and hydrogen are concerned.

Preliminary Experiments.—An adsorption study, involving a continuous variation of the catalyst temperature, was devised as a rapid means of scanning the characteristics of a catalyst over a wide range of temperature. The use of this technique for determining the behavior of ZnO toward hydrogen chemisorption revealed that an irreversible change was taking place in the characteristics of the catalyst around 60°. Examination showed that this change was brought about by a chemical reduction of the catalyst surface. At the same time, scarcely any change in the surface behavior for hydrogen adsorption around 300° was observable.

The apparatus was a conventional constant volume system in which pressure changes were measured on a dibutyl phthalate manometer. Hydrogen was purified by passage through a heated palladium thimble. The zinc oxide powder, ZnO-I, 15.41 g., was made by heating zinc oxalate at 450° in a current of air. The catalyst chamber was first cooled by a stream of nitrogen cooled by liquid nitrogen. After the temperature fell below −80° a known volume of hydrogen was admitted to the reaction vessel. By controlling the flow of nitrogen around the catalyst chamber and by adjusting the furnace current, the temperature of the reaction system could be raised slowly. The heating rate was approximately one degree per minute. Starting at −60°, pressure and temperature readings were taken at 20° intervals until the catalyst temperature reached 320°. A blank experiment was made using helium, instead of hydrogen, in the catalyst chamber. Prior to each run, the catalyst was degassed by evacuation at 375° for 17 hours and by flushing three times with helium at this temperature.

In Fig. 1 are plotted the values of q, the volume of hydrogen in ml. S.T.P. adsorbed as a function of the catalyst temperature for two runs in the order in which they were performed. These curves are not isobars since the pressure is continuously changing. The difference in the two q-T curves is striking. The first shows a slight maximum around 80°; the second, a marked maximum at 60° with only slight change around 300°. The apparent cause of this remarkable change must have been the prior treatment with hydrogen around 300°.

Taylor and Strother[3] were the first to discover two maxima in the isobars of hydrogen adsorption on ZnO. Their isobars were constructed from kinetic studies made at different temperatures. Their first maximum occurs around 80°; the second, at 218°. That the maxima occurring in the present work are similar to those found by Taylor and Strother rather than resulting from the steady temperature increase is demonstrated by the data in Table I. Two successive rate measurements, 1 and 2, made at 60° are given. The catalyst was degassed overnight at 350° before each run. The initial hydrogen pressure was about 76 cm. DBP (dibutyl phthalate) in each case. The runs duplicate each other quite closely. Obviously, overnight evacuation at 350° has very little effect on the kinetics or the extent of adsorption at 60°.

These runs were followed by eleven runs in which the rates of adsorption at 300° were measured. Succeeding these, another run at 60° was made. Table I, 3 shows the data obtained. The increase in the rate and extent of adsorption is unmistakable. The inference drawn from the q-T plots is confirmed, namely, that the hydrogen treatment at 300° causes an increase in chemisorption around 60°.

Type A Sites.—It is to be noted that ZnO-I, after its formation from oxalate at 420°, never had been heated above 400°. The degassing had been carried out at 350 to 375°. The maximum temperature at which it had been in contact with hydrogen was 320°. The only change that could have occurred during these treatments is the removal of oxygen from the surface either as oxygen gas or as water. It seems inevitable that the steady improvement in the capacity of zinc oxide for hydrogen chemisorption in the low temperature region must be associated with the removal of oxygen and consequent production of free zinc atoms on the surface. Had the catalyst been heated to a higher temperature, the zinc atoms could have diffused into the crystal to occupy interstitial positions. The mild treatment has left most of them at the surface.

An examination of the structure of the zinc oxide crystal shows that not all positions on the surface are suitable for the location of a zinc atom. There are only a few positions

---

[1] Abstracted from a dissertation in the Department of Chemistry submitted by V. Kesavulu to the faculty of the Graduate School of Arts and Science in partial fulfillment of the requirements for the degree of Doctor of Philosophy at New York University, June, 1960.

[2] H. S. Taylor, *Proc. Roy. Soc. (London)*, **A108**, 105 (1925).

[3] H. S. Taylor and C. O. Strother, *J. Am. Chem. Soc.*, **56**, 589 (1934).

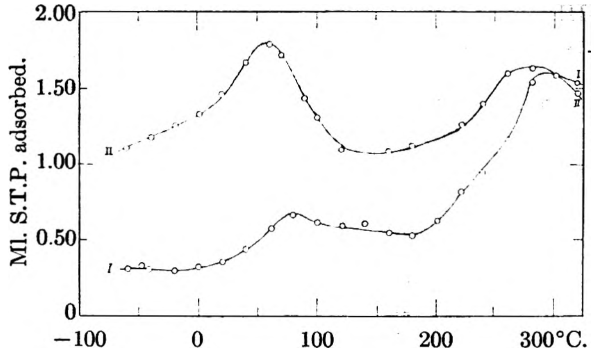

Fig. 1.—q–T heating curves, H_2 on ZnO-1: successive runs separated only by evacuation at 350°, P_0 is 75 cm. DBP.

TABLE I

Irreversible Change for H_2 on ZnO-I at 60°

	1. P_0 = 76.10	2. P_0 = 76.32	3. P_0 = 77.99 cm. DBP
t, min.	q	q	q, ml. STP
0.5	0.85	0.86	0.99
1	1.05	1.07	1.20
2	1.31	1.30	1.41
3	1.48	1.46	1.58
5	1.67	1.64	1.80
7	1.79	1.75	1.95
10	1.92	1.88	2.10
15	2.07	2.01	2.28
20	2.15	2.15	2.40
40	2.34	2.45	2.68
50	2.43	2.53	2.78
85	2.66	2.58	(80) 2.94
100	2.66	..	(105) 3.03

on and around the faces perpendicular to the hexagonal axis which are suited for this purpose. The zinc atoms may be pictured as located in the negative potential wells created by three neighboring, negatively charged, bulky oxygen ions. A zinc atom so situated would be highly polarized, with the valence electrons being pushed away from the ZnO surface. Forland[4] has observed that if ions such as Ag^+, Pb^{++} and Hg^{++} are adsorbed on a heteropolar substrate, they act like a catalytic metal surface. If they are adsorbed on a metal surface they poison it and are catalytically indifferent like an ionic surface. The explanation is given in terms of the behavior of the valence electrons. These are repelled in the first case and turned away from the substrate; in the second case they are attracted and drawn into the metal.

It is postulated that these highly polarized zinc atoms located in suitable positions on the zinc oxide surface are the sites for chemisorption of hydrogen at low temperatures. They will be referred to as Type A sites. Their concentration on the surface will be determined by the previous history of the sample and depend on the total number of zinc atoms produced in the activating processes and on the number of available positions for them on the surface. If more atoms are produced than positions available for them, the atoms will cluster, forming crystallites and so will be thrown out of action. If the temperature is sufficiently high, diffusion of the atoms into the lattice may occur. Since diffusion is an activated process, its effect at low temperatures could be negligible.

If this picture is correct, it is to be expected that very little relation will exist between the catalytic properties, including chemisorptive capacity, of ZnO at low temperature and the bulk properties such as conductivity. Indirect effects may exist. For example, increasing or decreasing the electron density in the crystal could alter the degree of polarization of these atoms, and therefore increase or decrease their reactivity, that is, the rate of adsorption. Since their number will be a constant for a given preparation the extent of chemisorption is nevertheless fixed.

The second peak in the q–T curves, around 300°, was assumed by Taylor and Strother[3] to be due to a second type of active center. They may be referred to as Type B sites.

Effect of Oxidation.—If the postulate for Type A sites is correct, it is to be expected that a reoxidation of the ZnO should eliminate or suppress the low temperature chemisorption. The effect on the high temperature process could also give information on Type B sites.

To this end the catalyst chamber was evacuated for fifteen hours at 350°, then filled with dry oxygen (70 cm.) and maintained at about 500° for twenty-four hours. The temperature was lowered to 300° and the catalyst chamber evacuated. Further evacuation at 350° was carried out for eight hours. The volume of hydrogen adsorbed in 100 min. then was measured at 60° and at 300°. Table II presents the data.

TABLE II

EFFECT OF OXIDATION

	Type A, 60° q	Type B, 300° q, ml. STP
Before	3.03	2.52
After	1.19	3.09
Δq	−1.84	+0.57

There is obviously a marked decrease in the amount adsorbed at 60° whereas there is only a slight increase at 300°. The result is confirmatory of the postulate and also indicates a marked difference in the behavior of the two types of site.

After a second oxidation treatment similar to that previously described a series of hydrogen adsorption runs was performed alternately at 60° and at 300°. After a run at 60° the reaction vessel was evacuated, flushed twice with helium and then the temperature raised to 350° and the vessel evacuated overnight. It is assumed that no marked change in the catalyst is brought about as a result of such treatment. However, after a run at 300°, the temperature was raised to 350°, the catalyst maintained at this temperature for half an hour in contact with hydrogen and then subjected to overnight evacuation. It was anticipated that this treatment would bring about some reduction of the surface. Table III presents the data in the order of performance. The temperature regulation during these runs was poor and variations of as much as ±7° occurred. The purpose of the experiments nevertheless was well served.

The rate and extent of adsorption at 60° are progressively increasing from run to run. This is a direct result of the reducing treatment to which the catalyst is subjected prior to each run. The marked increase in type A adsorption is not paralleled in the type B adsorption. Initially the type B reactivity falls but soon levels off. The type B sites must be radically different from type A sites.

Independence of Type A and B Sites.—This difference in the two types of site is shown by the experiments plotted in Fig. 2 showing (1) an adsorption run at 300°; (2) an adsorption run at 60° and (3) an adsorption at 300° followed by gradual cooling to room temperature with the catalyst in contact with hydrogen. After runs (1) and (2) the catalyst was degassed at 350°.

The amounts of hydrogen adsorbed in 100 min at 300° and at 60° are 1.67 and 1.64 ml., respectively. In (3) hydrogen is adsorbed at 300° for 65 min. and then the catalyst is cooled to room temperature in a period of 535 min. More hydrogen is picked up during the cooling period. The total amount of hydrogen taken up at 60° during this cooling is 3.74 ml., which is close to the sum of the amounts, 1.67 + 1.64 = 3.31 ml., in the individual runs at 300° and 60°.

These considerations will show that this result is not just accidental: at 300° type B sites are filled to an extent depending on the time allowed and the saturation value. As the catalyst is cooled, more sites are filled as desorption, an activated process, becomes less significant. This progression will continue to occur until the sites are completely filled or until the temperature at which the rate of type B adsorption becomes negligibly small. Further cooling will not produce any change until type A reaction begins to occur. If the two types were well separated in terms of temperature, the cooling curve should show a flat region between the cessation of one type and the onset of the second. The absence of a flat region indicates that the two types are not separated

---

[4] K. S. Forland, *Tidskr. f. Kjemi, Bergv. O.Mell.*, **7**, 260 (1950). See H. Seifert, "Structure and Properties of Solid Surfaces," University of Chicago Press, Chicago, Ill., p. 356.

Table III

Hydrogen Adsorption on ZnO-I after Oxidation

Run →	1	2	3	4	5	6	7	8	9
T, °C. →	70	60	300	60	300	60	300	60	300
P_0, cm. DBP→	75.60	76.10	76.74	75.60	76.10	76.74	76.93	77.08	76.82
t, min.					q, ml. STP				
0.5	0.14	0.25	0.61	0.32	0.55	0.46	0.59	0.50	0.55
1	.20	.29	.80	.42	.70	.55	.74	.62	.71
2	.25	.33	1.02	.51	.86	.70	.91	.75	.86
3	.29	.38	1.13	.57	1.03	.76	1.03	.83	.98
5	.32	.42	1.32	.64	1.12	.86	1.18	.95	1.12
7	.37	.44	1.39	.70	..	.94	1.26	1.03	1.23
10	.41	.46	1.47	.75	1.32	1.00	1.34	1.10	1.34
15	.48	.50	1.56	.83	1.42	1.07	1.43	1.19	1.45
20	.53	.53	1.62	.87	1.46	1.14	1.49	1.26	1.54
30	.61	.56	1.74	.94	1.55	1.23	1.53	1.34	1.64
40	.64	..	1.81	1.00	1.57	1.29	1.57	1.42	1.68
50	.65	.66	1.83	1.03	1.57	1.34	1.59	1.49	1.69
65	.69	..	1.89	1.07	1.62	1.42	1.67	1.53	1.73
80	.74	..	1.93	1.11	1.69	1.45	1.74	1.60	1.75
100	.70	.75	2.00	1.14	1.77	1.52	1.80	1.66	1.73

with respect to temperature. The three experiments in the above set involve degassing procedures between runs which produce slight variations in the catalyst. It is possible, however, to eliminate this difficulty by combining all three into a single experiment. Prior to this run the catalyst was oxidized by heating to 420° in oxygen. Figure 3 shows the data. Adsorption at 60° for 120 min. is followed by heating to 300° in 210 min., cooling to −20° in 1000 min. and finally heating to 350° in 300 min. In the range 25 to 150° the cooling and subsequent heating curves almost coincide. The cooling rate is very slow while the heating is relatively rapid. In view of this difference, the coincidence of the curves must denote equilibrium. The separation of the curves above 150° indicates that the points on the cooling curve had not reached the equilibrium values under the experimental conditions. In the range −20 to 20°, the points are horizontal, showing that the type A reaction has reached a saturation value and also is well separated from other reactions both chemical and physical.

The Position of the Maxima.—The maxima in q-T curves such as Fig. 1 result from a combination of adsorption and desorption processes. The ascending curve will be a function of the rate of adsorption and the rate of heating. The descending curve represents a near-equilibrium condition of desorption. Although a change in the rate of heating could thus slightly modify the position of a maximum, the main factor affecting the position must be the nature of the site and its interaction with the gas. The maxima at 80 and 300° must involve two different types of site, with Type B adsorption around 300° having a higher energy of activation than for Type A around 60°.

Referring again to Fig. 1, a change in the position of the first maximum from 80 to 60° is apparent. The heating rate was the same in both cases. The shift is therefore not mechanical. In later experiments this Type A maximum was found around 30°. Taylor and Strother[3] and Cimino, *et al.*,[5] have observed the first maximum in their isobars at different temperatures, the former at 80°, the latter at 50°. Such a wide variation is not easily attributable to varied experimental conditions. Rather would it seem to indicate differences in the catalyst samples. Since the observed progressive shift of the maximum to lower temperature accompanies an increase in adsorption attributable to an increase in concentration of zinc atoms, a surprising conclusion results, namely, that an increase in concentration of sites is accompanied by an increase in reactivity.

The chemical reduction of ZnO which produces zinc atoms will be accompanied by some diffusion of zinc into interstitial positions in the crystal. Because of the high dielectric constant these interstitial atoms are ionized easily by thermal energy and give rise to conduction electrons. An increase in concentration of Type A sites will therefore be accompanied by an increase in the density of free electrons in the bulk. This, in turn, will increase the degree of polarization of the zinc atoms in the surface, resulting in an increased reactivity and lower apparent energy of activation. Other methods of changing the electron density in the crystal, such as the introduction of indium, gallium or lithium atoms in substitutional positions is discussed later.

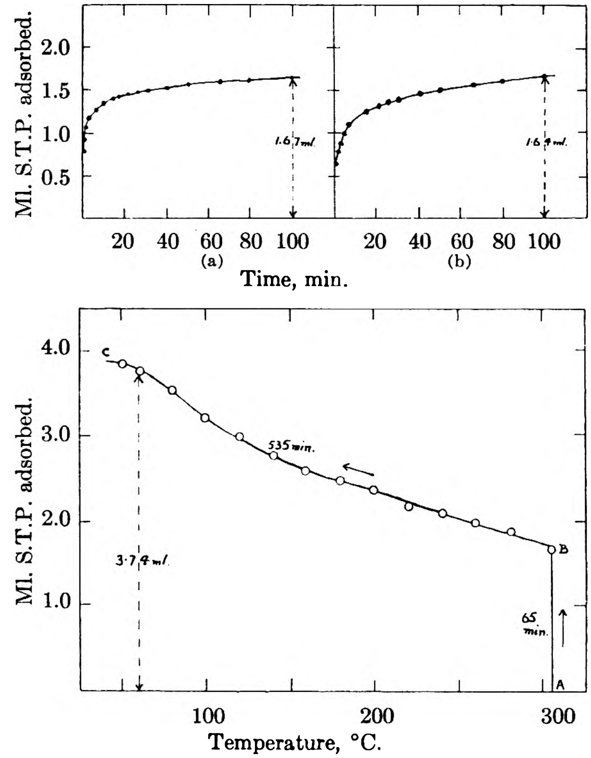

Fig. 2.—a, Rate of adsorption, H_2 on ZnO-I at 300° and P_0 is 75 cm. DBP; b, same at 60°; c, adsorption at 300° followed by cooling in H_2 to room temperature.

Effect of Reduction of ZnO.—Another sample, ZnO-5, (19.39 g.) was prepared by heating the oxalate in a current of oxygen at about 450°. By a BET measurement using nitrogen it had a total area of 153.34 meter². After thorough evacuation at 360°, a known volume of hydrogen was introduced into the catalyst chamber at room temperature and adsorption as a function of time followed for 30 min. The temperature then was raised gradually and adsorption as a function of temperature was studied. These measurements were extended to 500°. The gas now was pumped off through a receiver in liquid nitrogen and analyzed by the mass spectrometer. Large amounts of water were found. The water must be taken as proof of a chemical reduction of the ZnO by hydrogen since the hydrogen used in the experiment showed only a trace of water by separate mass spectro-

---

(5) A. Cimino, E. Cipolini and E. Molinari, *Naturwiss.*, **43**, 58 (1956).

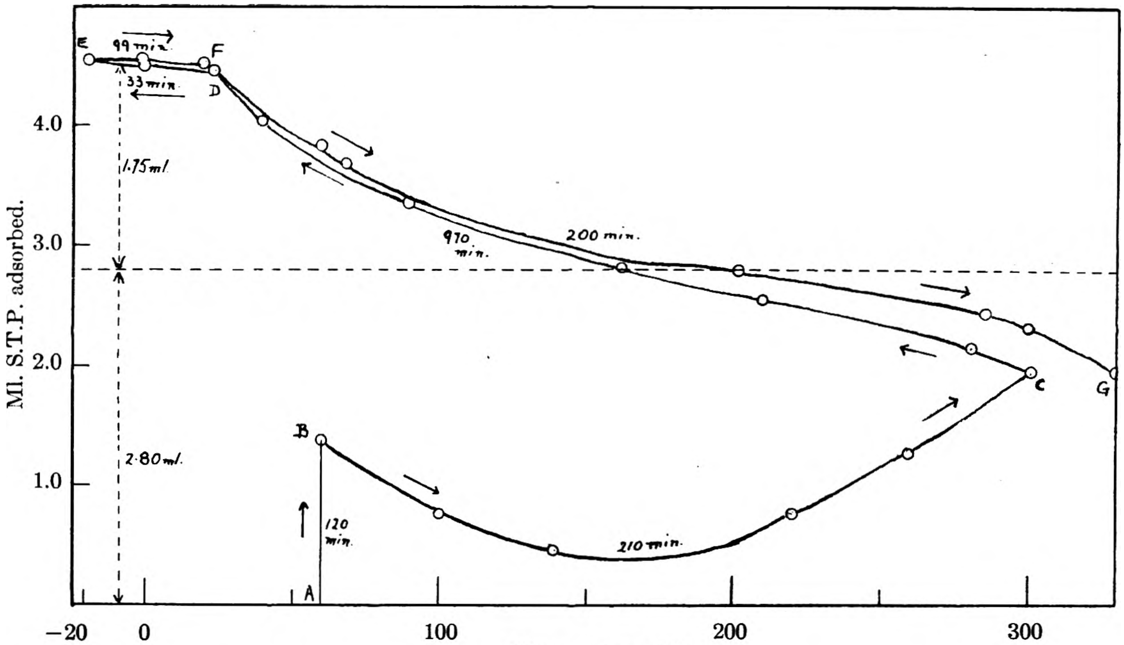

Fig. 3.—Heating–cooling–heating curves, H_2 on ZnO-I, P_0 is 75 cm. DBP.

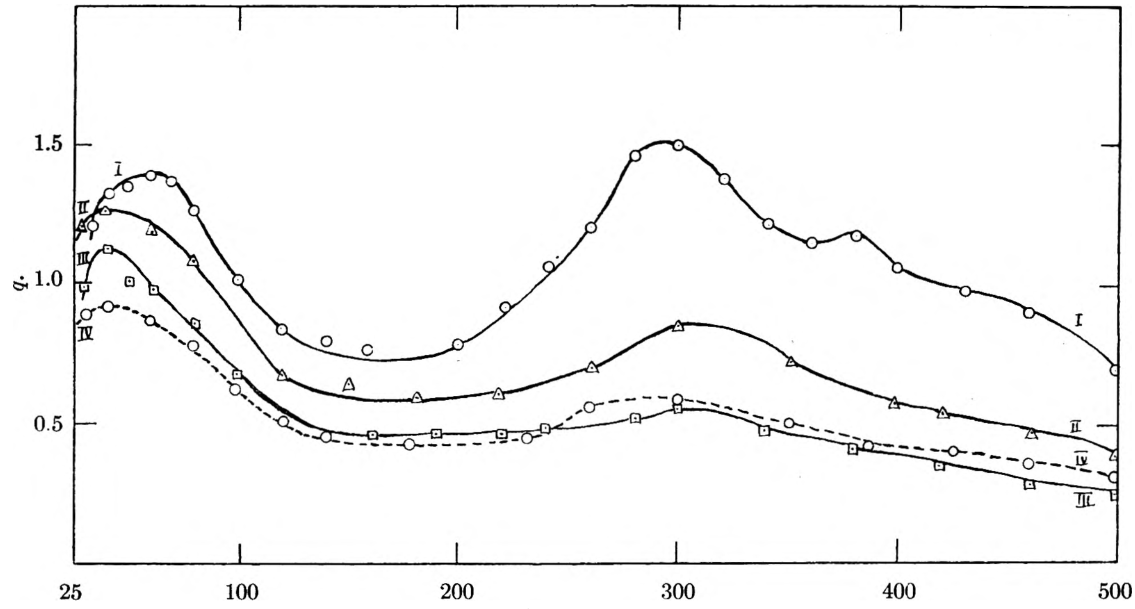

Fig. 4.—q–T curves for H_2 on ZnO-5: successive runs each followed by overnight evacuation at 375°; P_0 is 75 cm. DBP.

metric analysis and the degassing at 360° could leave only traces of water on the catalyst.

The catalyst was evacuated overnight at 375°, cooled to room temperature and a calibration run with helium performed. A surface area measurement showed that the heating to 500°, once in hydrogen and again in helium, had decreased the area to 111.24 meter². Figure 4 shows four successive q-T plots each preceded by a BET measurement. It is to be noted that the extension of the heating range to 500° has resulted in a general decrease in the amounts adsorbed throughout the whole temperature range. There is, nevertheless, a smaller change in the amount adsorbed around 60° compared with the large change around 300°. Furthermore, the similarity of curves III and IV indicates that the concentrations of sites of both type A and type B have reached saturation values.

Table IV presents the maximum amounts adsorbed per unit area for Types A and B for the four runs in Fig. 4. The progressive increase in the maximum amount of hydrogen adsorbed in the low temperature region demonstrates the increase in free zinc atom concentration brought about by the progressive reduction. The opposite trend in the Type B values demonstrates a suppression of Type B sites accompanying the reduction. The increased value for the last run clearly shows that a limit exists to this type B site suppression, however drastic the reduction may be, so that a diminution in surface area leads to an increase in the amount adsorbed per unit area. It is furthermore obvious that the total surface area is not the sole factor for Type B activity.

Attention is again drawn to the shift in the position of the maximum from above 60° in I to less than 40° in IV accompanying the increase in the amount adsorbed per unit area. The reduction at 500° is accompanied by diffusion of zinc atoms into the lattice increasing the electron density and thereby increasing the reactivity of the surface zinc atoms. Once the crystal becomes saturated with interstitial atoms no further enhancement in reactivity can be expected.

Temperature Dependence of Adsorption.—From the pre-

TABLE IV

AMOUNTS ADSORBED PER UNIT AREA

Run	Area S meter²	Type A q, ml. STP	Type A 100 /S	Type B at 300° q, ml. STP	Type B at 300° 100q/S
I	153.34	1.39 (60°C.)	0.91	1.49	0.97
II	111.24	1.26 (40°C.)	1.14	0.85	0.77
III	83.33	1.13 (40°C.)	1.36	0.56	0.67
IV	66.09	0.93 (40°C.)	1.41	0.58	0.88

vious results it appears that the type A site density has reached its maximum value. If a method were available of degassing these sites without changing their number, the effect of temperature on the rate of adsorption should give the energy of activation of adsorption. From Fig. 4 it is clear that at low temperatures the type A reaction is well separated from the type B reaction. The difficulty of degassing without changing the type A site density was solved by evacuation at 150°. Table V gives data for the kinetics of adsorption of hydrogen on ZnO-5 from −196 to 300° in the order in which the experiments were performed. After a run at 0°, the reaction vessel was evacuated at this temperature for about 10 min. and then the temperature was raised to 150°. Evacuation was continued at 150° for one hour, the vessel flushed three times with helium and then cooled to 0°. A second adsorption run was made at 0° at approximately the same initial pressure of hydrogen. From the data in Table V it is clear that reproducibility of the surface has been achieved. In the subsequent low temperature studies degassing at 150° for two hours was employed. For the three higher temperature runs the catalyst was degassed at 360 to 370°. For −196° liquid nitrogen was used; for −78°, Dry Ice–acetone; for 0°, ice water. For −116° and −23° partially frozen ether and carbon tetrachloride, respectively, were used but it was difficult to maintain constant temperature. The surface area before the runs was 66.1 meter². After completion of the series the value was 62.4 meter².

The rapid adsorption, complete within three minutes at −196°, is undoubtedly largely physisorption. The most remarkable feature of Table V is the almost identical kinetics at temperatures from −116 to 31.5°, throughout the whole course of the runs. Even a strict application of the Arrhenius equation, that is, to specific rates rather than momentary rates, since the site density and the gas pressure are constant, must mean that the energy of activation is zero in this range which involves only type A sites. For the range 0 to 56°, Taylor and Strother found a value of 3 to 6 kcal. depending on the coverage. Their catalyst was prepared from oxalate as was that used here but was not subjected to any drastic reduction treatment. It obviously contained few interstitial zinc atoms and the surface zinc atoms were consequently less polarized and thus less reactive.

The data fall into three groups: (1) −78° to 32°; (2) 32° to 200°; (3) 200° to 300°. Group (1) is the zero activation energy group already referred to. Group (3) corresponds to an apparent energy of activation of 8 kcal./mole and is the region where type B is predominant. Group (2) would yield an apparent negative energy of activation. It is possible that in the region 135 to 200° both types of reaction are occurring but it is unmistakable that a large part of the region from 32 to 135° is predominantly type A. Any type B reaction in this region would make the temperature coefficient more positive. It follows, therefore, that the rate measured by the amount adsorbed in the first minute does not represent the true initial rate but rather a net rate of approach to equilibrium in this region. This is seen from the isobars plotted in Fig. 5, A after one minute; B after 100 min. Since the 100 min. values represent the near-equilibrium state, the identity of the curves shows that in one minute the reverse reaction of desorption is already significant. Curve C in Fig. 5 is a q-T curve obtained immediately after the kinetic studies. The low temperature maximum appears to be at about 30°. As expected, it lies above the 1 min. curve but below the 100 min. curve.

Type A Sites and Bulk Properties.—That type A chemisorption can occur with zero energy of activation might suggest a weak interaction only of hydrogen with the surface. Smith and Taylor[6] and others, however, have demonstrated H_2–D_2 exchange on ZnO even at −78°. The interaction, consequently, cannot be weak but must involve strong electronic changes. If such strong electronic changes were to include part of the bulk, say, one or two atomic layers below the surface, it is difficult to see how the reaction could proceed with such ease. Such interaction with the bulk, should it occur, would produce changes in the electrical and other associated properties of the solid. But Kubokawa and Toyama[7] have shown that, below 110°, hydrogen adsorption on a sample of sintered ZnO has no effect on the conductivity of the solid. This also rules out the possibility that the active center may be Zn^{++} ions of the lattice or Zn^+ ions occupying interstitial positions. The independence by type A chemisorption of bulk properties agrees with the view that type A sites are zinc atoms located in the negative potential wells created by three adjacent O^- ions on the ZnO surface.

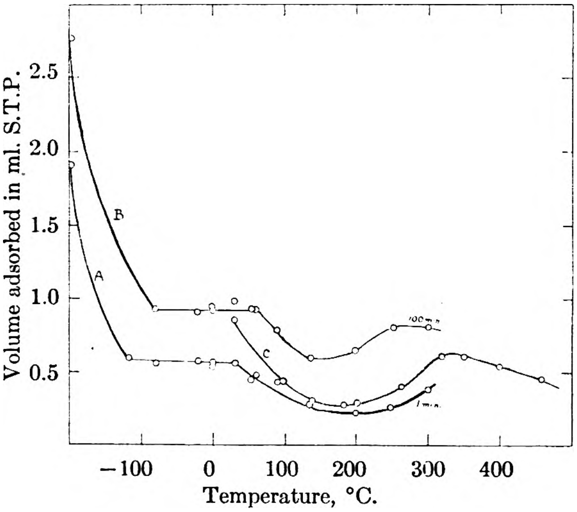

Fig. 5.—A and B, 1 and 100 min. "isobars," P_0 is 75 cm. DBP; C, q-T heating curve immediately following the kinetic runs.

Effect of Type B on Type A.—The catalyst ZnO-5 having become exposed to air, was again oxidized in oxygen for several hours at 600 and at 400°. It then was evacuated for three days at 500° and for one day at room temperature. The subsequent data show that sintering was extensive. The rate of adsorption at 0° was measured first. Then, with hydrogen still in the catalyst chamber, the temperature was raised to 280°. After two hours at this temperature, the catalyst had adsorbed a further 0.97 ml. of hydrogen and was cooled to 140° and degassed for 48 hours. The treatment was expected to produce a catalyst in which the type B sites are covered but the type A sites empty. The catalyst now was cooled to 0° and the rate of hydrogen adsorption again measured. It is assumed that this relatively mild treatment, following the treatment at 500°, did not alter the surface characteristics other than that of the type B chemisorption. Table VI gives the data for the two rates, without and with type B sites filled.

It is clear that hydrogen chemisorbed on type B sites has an inhibitory effect on type A chemisorption. It would seem that the effect is purely a steric one, a blocking of type A sites, rather than an electronic one, which, if predominant, should lead to an enhancement of the reactivity of the type A sites. Similar results were found with ZnO-6.

Desorption from ZnO-5.—After the second adsorption at 0° on ZnO-5, both types of site presumably being occupied, the catalyst was cooled in liquid nitrogen and evacuated for five minutes. A known volume of helium was introduced and the temperature gradually raised. At definite temperature intervals, the volume of gas present in the system was determined. The increase in volume measures the hydrogen desorbed. Figure 6 shows the data obtained. Two distinct stages of desorption are discernible. Up to 110° the desorption must be from type A sites; from 200° onward, from type B. Of the 0.97 ml. adsorbed at 280°, over 0.8 ml. is desorbed at 400°, showing that most, if not all, of it stayed on the surface. Again, evacuation at −196° has not removed any Type A adsorption; 0.47 ml. was adsorbed at 0° while 0.49 ml. is desorbed at 110°.

---

(6) C. A. Smith and H. S. Taylor, *J. Am. Chem. Soc.*, **60**, 362 (1938).

(7) Y. Kubokawa and O. Toyama, *J. Phys. Chem.*, **60**, 833 (1956).

TABLE V

EFFECT OF TEMPERATURE ON ADSORPTION RATE

Run	1	2	3	4	5	6	7	8	9	10	11	12	13	14
°C.	0	0	−78	−196	31.5	−23	−116	60	88	135	55	300	200	250
P_0, mm. DBP	74.50	75.07	74.14	73.98	73.65	74.15	73.70	75.04	74.30	74.94	73.60	73.15	73.57	75.25
t, min.	q, ml. STP													
1	0.56	0.54	0.55	1.92	0.54	0.56	0.58	0.48	0.43	0.27	0.45	0.37	0.22	0.26
3	.64	.64	.65	2.76	0.62	.64	.66	.57	.52	.30	.55	.47	.28	.34
5	.69	.66	.70	2.77	.066	.68	.70	.60	.55	.32	.58	.54	.33	.38
10	.72	.71	.75	..	0.73	.70	.77	.69	.61	.37	.66	.61	.38	.46
20	.77	.76	.81	2.77	0.80	.76	.78	.81	.68	.43	.76	.69	.44	.55
30	.81	.80	.87	2.77	0.83	.79	.82[b]	.82	.69	.45	.81	.71	.50	.60
45	.84	.83	..	..	0.89	.81	..	.82	.73	.50	.84	.73	.54	.67
60	.87[a]	.86	.89	..	0.91	.92	.84[c]	.91	.75	.52	.86	.76	.57	.70
100	.93	.91	.92	..	0.98	.98	..	.93	.79	.59	.92	.78	.65	.80

[a] 65 min. [b] 35 min. [c] 50 min.

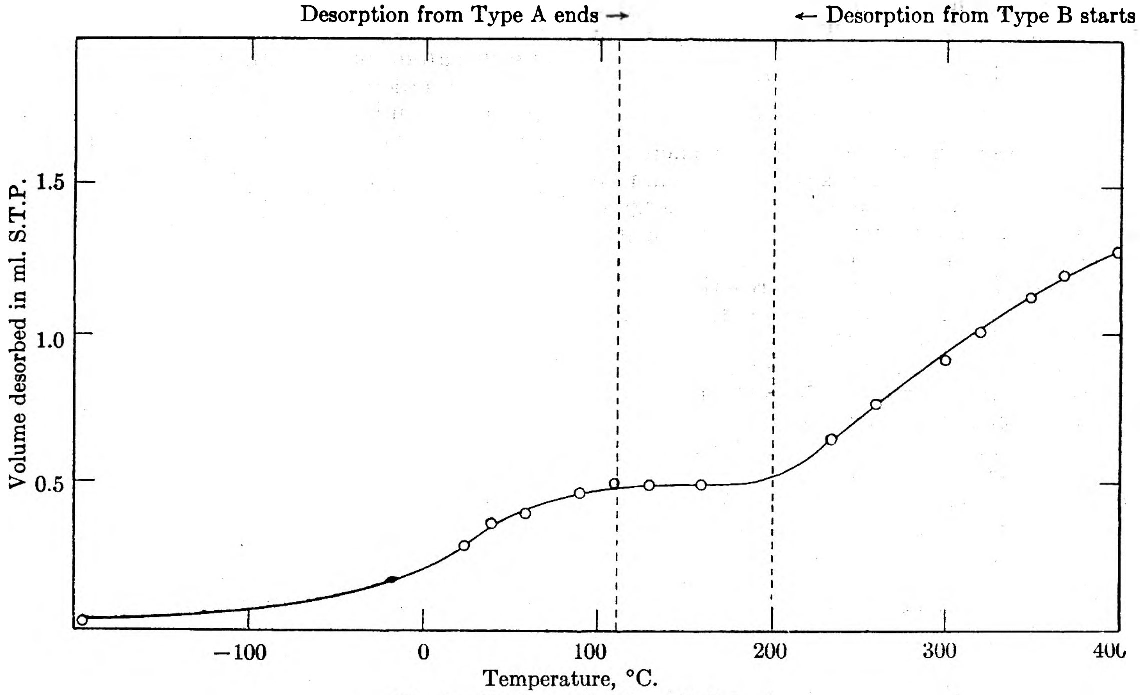

Fig. 6.—H_2 desorption from ZnO-5.

TABLE VI

EFFECT OF TYPE B ON TYPE A CHEMISORPTION, ZnO-5, TYPE A RATES AT 0°

Time, min.	Without Type B	With Type B
	q, ml. STP	
1	0.40	0.3
3	.46	.34
5	.47	.37
10	.49	.40
20	.55	.45
30	.60	.47

Readings were not taken in the interval −196 to 0° and the shape of the desorption curve in this range is uncertain. It does not seem likely, however, that the temperature at which appreciable amounts of hydrogen are desorbed can be far below 0°. In this run the surface is almost fully covered at the start and desorption is quite appreciable. In an adsorption run, desorption will not become significant until sufficient adsorption has taken place. This, therefore, justifies taking the amount adsorbed in the first minute as the initial rate, unaffected by desorption at the lower temperatures. Finally, the slowness of desorption from Type B sites between 110 and 200° corroborates the observed reproducibility of Type A chemisorption by evacuation at 150°.

Nature of the Zinc–Hydrogen Complex.—On the basis of the foregoing, it is possible to reinterpret earlier experiments on the hydrogen–deuterium exchange on zinc oxide. Smith and Taylor[6] appealed to surface heterogeneity to explain their findings. Molinari and Parravano[8] used pure and modified ZnO. Their interest lay in a connection between catalytic activity and semiconductivity.[9]

Molinari and Parravano demonstrated that ZnO catalytic activity can be achieved by treatment with hydrogen at 350° or by extended heating in vacuum at 450°. These are the conditions found here as necessary for developing type A activity. Further, they find that activated samples can be deactivated by air or oxygen. Thus the H_2–D_2 exchange on ZnO is intimately connected with the formation of free zinc atoms on the surface. That diffusion of some of these atoms into the lattice makes the solid

---

[8] E. Molinari and G. Parravano, *J. Am. Chem. Soc.*, **75**, 5233 (1953).

[9] G. Parravano and M. Boudart, *Advances in Catalysis*, Vol. VII, pp. 47–68 (1955).

an extrinsic semiconductor is only incidental and not the cause of catalytic activity.

Smith and Taylor[6] show exchange occurring as low as 140°K. at a rate increasing with rise in temperature corresponding to an energy of activation of 7–8 kcal./mole between −78 and 100°. Since it has been proved in this work that no chemisorption of type B occurs at −78°, it is obvious that the exchange must occur on type A sites. It is inevitable that type A chemisorption of hydrogen must involve complete, or almost complete, dissociation of the H_2 molecule producing a surface complex, $Zn^{++} \cdot 2H^-$. Since in ZnO there is some covalent character along the crystal axis, a similar situation may occur in the Zn–2H bond with an incomplete electron transfer.

On this view, the exchange mechanism can be that of Thon and Taylor.[10] The chemisorption by

$$ZnH + D_2 \longrightarrow ZnD + HD$$

$$ZnD + H_2 \longrightarrow ZnH + HD$$

type A has been shown to have zero energy of activation. The value 7–8 kcal./mole found by Smith and Taylor must therefore be the energy of activation of the above steps. This is reasonable, since these reactions are almost equivalent to the homogeneous $H + D_2$ or $D + H_2$ reactions. The only difference is the localization of the H or D atom on the surface and, by the reaction, there is no great change in the surface since D replaces H and *vice versa*. That exchange is 50–800 times faster than adsorption is to be expected. The value of 7.2 ± 0.5 found by Molinari and Parravano for the exchange between 25 and 230° on a freshly prepared ZnO activated by hydrogen at 350° is similar to that of Smith and Taylor and subject to the same explanation. Addition of alumina will increase the free electron density while Li_2O will decrease it. The energies of activation found, 5 and 25 kcal./mole, are qualitatively in agreement with this. What is more significant, the relative exchanges at 160° per unit surface are 5% for Li_2O and 40% for Al_2O_3,[9] a striking confirmation of the relative reactivity of the zinc atom center.

Nature of Type B Sites.—In contrast to their observation that below 110° hydrogen chemisorption has no effect on the conductivity of ZnO, Kubokawa and Toyama[7] find that above this temperature there is a marked increase in conductivity with both sintered and unsintered samples. This must point to an electronic nature of Type B chemisorption.

Heiland[11] has shown that a well-conducting surface layer can be produced on a zinc oxide single crystal by treatment with atomic hydrogen in the temperature range −187 to 227°, whereas molecular hydrogen has no effect. The conductivity is completely eliminated by heating in vacuum to 327°. The increase in conductivity with time follows a logarithmic law as does chemisorption. Since single crystals have no surface zinc atoms and molecular hydrogen is without effect, although atomic hydrogen is effective, while sintered ZnO containing surface zinc atoms will react to molecular hydrogen, it appears that atomic hydrogen is necessary for type B reaction. In the reaction

$$H + O^- \rightleftarrows OH^- + e^-$$

the transfer of the electron from the surface to the low-lying levels of the conduction band will determine the efficiency of the reaction and its over-all energy of activation. With increasing electron density in the crystal, the reaction will become slower and its apparent energy of activation increase. The reaction is presented as a truly reversible adsorption-desorption equilibrium on type B sites. At higher temperatures, apparently around 350°, an irreversible reaction becomes possible

$$H + OH^- \longrightarrow H_2O + e^-$$

which provides a mechanism for the production of free zinc atoms on the surface.

The interdependence of type A and type B chemisorption is apparent. Type A sites, free surface zinc atoms, result from a reduction which occurs via type B chemisorption. For type B chemisorption, atomic hydrogen from type A sites is necessary. The necessity for and difficulty of the "activating" process for zinc oxide becomes obvious. It was found in the present work with samples ZnO-3 and ZnO-4 that evacuation at 350° for 26 hours was insufficient to produce any activity for hydrogen chemisorption in the entire temperature range from 30 to 360°. These samples, Kadox-15 and S.P. ZnO-500, from the New Jersey Zinc Company, are formed by burning zinc vapor in air. They contain large amounts of adsorbed H_2O and CO_2. Repeated mass-spectrometric analyses of the gas from the catalyst chamber have shown that it is very difficult to remove carbon dioxide even by heating at 500°. Possibly this introduces some complication in the interpretation of the results. However, from the mode of preparation, these samples may be expected to be nearly stoichiometric compounds with no free zinc atoms either at the surface or in the interior. A systematic investigation of the "activating" process could be informative. It does not seem likely that, after the activating treatment currently used, such species as O^- or O_2^-, postulated by Parravano, Friedrich and Boudart,[12] following Morrison,[13] if ever present could remain on the surface through the pretreatment and subsequent repeated use of the catalyst. They have shown that air or oxygen which would yield adsorbed oxygen actually deactivates ZnO. The absence of an isotope effect found by Parravano, *et al.*,[12] in the rate of adsorption of hydrogen is to be expected on the basis of the mechanism proposed here. The temperature region studied was that where type B chemisorption occurs and its over-all rate is determined not by H_2 or D_2 but by the rate of transfer of electrons from the surface to the conduction band. To discern a type A chemisorption isotope effect, this work suggests that measurements should be made at low temperatures, for example, −78°.

Considerable work remains to be done especially

---

[10] N. Thon and H. A. Taylor, *J. Am. Chem. Soc.*, **75**, 2747 (1953).

[11] G. Heiland, *Z. Physik*, **138**, 459 (1954).

[12] G. Parravano, H. G. Friedrich and M. Boudart, THIS JOURNAL, **63**, 1144 (1959).

[13] R. S. Morrison, *Advances in Catalysis*, Vol. VII, 290–294 (1955).

relative to type B sites. The picture presented offers a synthesis of the geometric and electronic views of catalyst surfaces which frequently have appeared irreconcilable. The procedure used in the investigation offers a means of analysis of other similar oxide surfaces.

DISCUSSION

Donald Graham (E. I. du Pont de Nemours & Co.).—To what extent might the proposed mechanism of the formation of type B sites lead to catalyst deactivation through formation of clusters of zinc atoms and, in turn, zinc crystallites.

V. Kesavulu.—Progressive reduction of the surface certainly would produce large numbers of zinc atoms which would cluster together to form zinc crystallites which would be catalytically inactive. This would explain the gradual loss of catalytic activity by the catalyst on repeated use.

H. Austin Taylor.—Initially, however, zinc atoms, once formed, will migrate to the negative potential wells of the oxide ions and thus become stabilized temporarily.

STUDIES OF SILICATE MINERALS. VI. ACID SITES ON KAOLIN AND SILICA–ALUMINA CRACKING CATALYSTS

By A. C. Zettlemoyer and J. J. Chessick

Surface Chemistry Laboratory, Lehigh University, Bethlehem, Penna.

Received March 10, 1960

The determination of the strength of acid sites on a variety of synthetic silica–alumina and kaolin-based cracking catalysts was carried out. Samples first activated at 400° under vacuum were exposed to saturated *n*-butylamine vapor at 25°. The total amount chemisorbed and amounts desorbed at incremental temperatures between 25 and 400° under vacuum were not determined. These desorption curves, themselves, are indicative of the spectrum of acid sites on the catalyst surfaces studied. More quantitatively, desorption data can be combined with heats of immersional wetting measured as a function of surface concentration to furnish differential heat and site energy distribution curves. In addition, the number of sites for amine adsorption which developed as activation temperature increased was followed. Adsorption of amines of varying size was utilized to provide information concerning the spatial distribution of acid sites.

Introduction

From heat of immersion measurements, it was demonstrated[1] recently that the energy distribution of the acid sites on attapulgite clay could be developed. In these initial studies, *n*-butylamine was found to be a convenient adsorbate and immersional liquid. Portions of a sample completely saturated with *n*-butylamine vapor were outgassed at increasing temperatures. The heats of immersion of these gradually desorbed portions provided a curve of heats of immersion *vs.* coverage. From the inverse of the slopes of this curve, an approximate site energy distribution curve was constructed. For attapulgite activated at 400°, no sites retained amine after outgassing at 25° if the interaction energies were less than about 15 kcal. per mole; a peak in the distribution curve occurred at about 17.5 kcal. per mole. These studies were prompted by the suspicion that the acid sites promoted deterioration of certain organic adsorbates when the attapulgite was used as a carrier.

The present work was directed toward similar studies of cracking catalysts; both typical silica–alumina and kaolin types were included. In petroleum cracking, it is well established that a carbonium ion mechanism is developed by the acid sites. A preponderant current view is that the alumina in a silica–alumina catalyst is there primarily as γ-alumina or as incipient γ-alumina[2]; such six-coördination aluminum is drawn into four-coördination and so provides a Lewis acid site at alumina–silica junctions when a hydrocarbon or other basic molecule approaches. Yet it is well known that cracking catalysts carry water on their surfaces under reaction condition and thus Brönsted sites must certainly be present.[3] The question of which type of sites is effective or most effective in cracking has not been resolved.[4]

The structure of kaolin clays has been shown to be virtually destroyed in catalyst preparation.[2] It is believed that essentially the same type of structure and characteristics as in silica–alumina catalysts are developed on acid treatment and calcination.

Based on ammonium ion-exchange studies, the conclusion has been reached that acid sites of varying strength do not exist on the catalyst.[2] On the other hand, aqueous titrations,[5] non-aqueous titrations,[6] gas titrations,[7] the indicator method,[8] and differential thermal analysis[9] all have shown acid sites in a variety of strengths. None of these methods has the advantage of providing a topographical site energy distribution, as can be obtained by the heat of immersion method.

Experimental

Two American Cyanamid Company Aerocat silica–alumina catalysts were investigated; one contained 13% alumina (SA-13), the other 25% alumina (SA-25). Their characteristic properties are given in Table I.

A minor amount of work was also performed on another familiar commercial silica–alumina catalyst, a Davison

---

[1] J. J. Chessick and A. C. Zettlemoyer, This Journal, **62**, 1217 (1958).

[2] T. H. Milliken, A. G. Oblad and G. A. Mills, "Proceedings of the National Clay Conference," Berkeley, Calif., 1952.

[3] D. S. MacIver and P. H. Emmett, This Journal, **62**, 935 (1958).

[4] A. G. Oblad, T. H. Milliken and G. A. Mills, "Advances in Catalysis," Vol. III, Academic Press, New York, N. Y., 1951, p. 199.

[5] C. L. Thomas, *Ind. Eng. Chem.*, **41**, 2573 (1949).

[6] O. Johnson, This Journal, **59**, 827 (1955).

[7] G. A. Mills, E. R. Boedeker and H. G. Oblad, *J. Am. Chem. Soc.*, **72**, 1559 (1950).

[8] C. Walling, *ibid.*, **72**, 1164 (1950).

[9] R. L. Stone and H. F. Rase, *Anal. Chem.*, **29**, 1273 (1957).

Table I

Silica–Alumina Cracking Catalysts[a]

Type	Aerocat fluid SA-13	Aerocat triple A SA-25
Av. particle size, μ	42	53
Loss on ignition, wt. %	13	13
Apparent bulk density, g./cc.	0.48	0.43
Pore volume, cc./g.	0.75	0.89
Activity (1 hr., 940°F.)		
1.4 (VHSV) weight	105	110
Chemical anal. (wt. % of dry catalyst)		
Al_2O_3	13.3	25.0
SiO_2, by difference	86.6	74.4
Na_2O	0.01	0.01
Fe	0.04	0.04
Surface area, m.²/g.	450–600	450–600

[a] Data supplied by manufacturer.

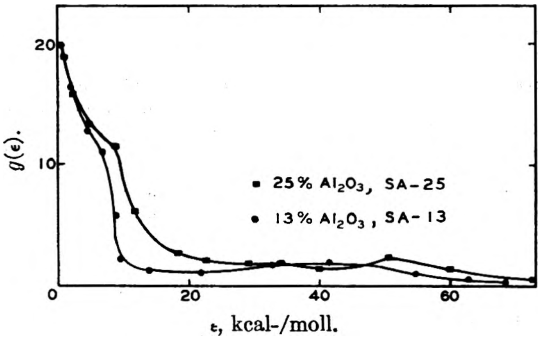

Fig. 1.—Distribution of adsorption site energies for Aerocat, silica-alumina catalysts initially activated at 400° *in vacuo*.

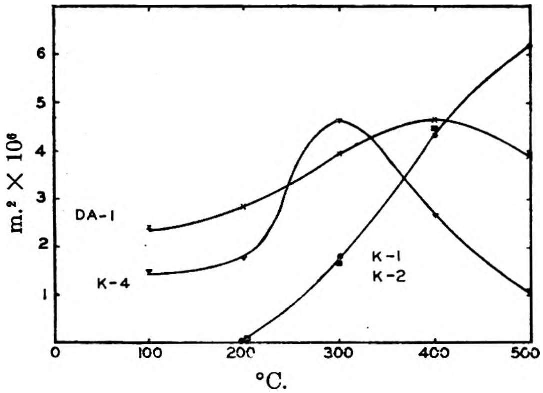

Fig. 2.—Total amine adsorption at 25° and 10^{-5} mm. on catalysts as a function of initial activation temp.

Synthetic Catalyst DA-1 (Davison Chemical Co.). This catalyst also contains about 13% alumina.

The kaolin cracking catalysts were all based on Georgia kaolin. K-1 was a pelletized sample which had not been steam deactivated. K-2 was a pelletized sample which had been steam treated at 1400°F. for 24 hours. K-3 was obtained by dry-grinding K-1 to fluid catalyst size: 25% 100/200 mesh, 50% 200/325 mesh and 25% T/325 mesh. K-4 was a fluid-type kaolin catalyst. The K-catalysts were prepared by the Minerals and Chemicals Corporation of America.

The BET nitrogen surface areas after outgassing at 400° and water surface areas after outgassing at 100° are listed in Table II.

Table II

Surface Areas of Catalysts as a Function of Activation Temperature

Catalyst	N_2 area m.²/g. 100°	N_2 area m.²/g. 400°	Water area 100°
Syn. silica alumina, DA-1	560	424	373
Kaolin			
K-1 (pelletized)	97	97	64
K-2 (pelletized, steam treated)	87	86	41
K-3 (ground K-2)	80	80	74
K-4 (fluidized, *ca.* 60)	135	110	124

Samples were first evacuated at the stated activation temperature and at 1 × 10^{-5} mm. or better and then weighed. They were then exposed to saturated *n*-butylamine vapor at 25° overnight. In this way, all the acid sites whatever their strength were exposed and presumably coated with the adsorbate. (It is not possible to adsorb throughout the catalyst sample sequentially on first the most active sites, next the most active sites, and so on.) The samples were then evacuated at 25° and 1 × 10^{-5} mm. to constant weight. The net gain in weight was attributed to chemisorbed butylamine. Desorption curves were then followed as the temperature was raised in steps. These desorption curves are themselves characteristic of the distribution of site energies. They suffice to establish important differences between samples. While the results reported here were obtained with five to ten gram samples and an analytical balance, the use of spring balances would make it possible to follow the weight loss of several samples simultaneously. In the case of K-2, it became of interest to extend the desorption studies to diethylamine and to pyridine.

For the heats of immersion studies, which were only performed for *n*-butylamine on SA-13 and SA-25, the amine was dried and distilled directly into the thermistor calorimeter. Twenty-six determinations of the heats of immersion of the evacuated and partly amine coated samples were made. Details of the calorimetric and purification techniques were given previously.[1] The slopes of the expanded plots of heats of immersion *versus* coverage yielded curves of the differential heats of adsorption *versus* coverage. The inverse slopes of the latter curves *versus* the adsorption energies provided a first approximation to site energy distribution curves. Because of the double differentiation and because the adsorption energies were not obtained at absolute zero,[10] the distribution curves must be considered only rough approximations.

Results and Discussion

On SA-13, 0.193 g. of *n*-butylamine per gram of catalyst was chemisorbed at 25° after 400° activation; on SA-25, 0.203 g. per g. catalyst. The additional number of sites on SA-25 is reflected in the distribution curves in Fig. 1. Since the uncertainty in these curves is considerable, no difference in the number of high energy sites is apparent. SA-25 did display a larger number of sites of energy between 10 and 25 kcal./mole. These additional low energy sites might be expected to yield higher activity; the high energy sites would likely be permanently contaminated under reaction conditions. From Table I it can be seen that the rated activity of SA-25 is also larger than that of SA-13 and in the same proportion as is the amount of chemisorbed amine at 25°.

The significant variations in the moles of amine adsorbed per unit area at 25° for several catalysts as a function of activation temperature are illustrated in Fig. 2. The kaolin fluid catalyst, K-4, takes up significant amounts after mild activation at 100°. Indeed, over 75% of this amount adsorbed is retained after thermal treatment at 100° *in vacuo*. Condensation of surface hydroxyl groups does not occur during such mild thermal

---

[10] L. E. Drain and J. A. Morrison, *Trans. Faraday Soc.*, **48**, 316 (1952).

treatment; therefore adsorption apparently occurs over Brönsted or Lewis[1] sites made active or produced by water desorption during thermal activation.

An abrupt increase in amine uptake was observed for K-4 after activation at 300°. The area occupied by butylamine adsorbed at 25° after 300° initial activation was calculated to be 67 m.²/g. based on a cross-sectional area of 20 Å.² per molecule. This area amounts to about 56% of that available as measured by nitrogen adsorption and is far in excess of that expected on the basis of adsorption on catalytically active acid sites. Rather it appears that water loss by condensation of adjacent hydroxyl groups leads to the formation of surface sites of the type

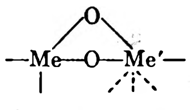

$$\overset{\displaystyle O}{\mathrm{-Me{-}O{-}Me'-}}$$

where Me and Me′ represent silicon and aluminum ions, respectively. Siloxane groups begin to form on a hydrated silica surface by this mechanism during thermal evacuation at about 170°[11]; much less is known about the condensation of hydroxyls on alumina or on mixed oxides.

The decreases in amine uptake after 400 and 500° activations, evident in Fig. 2, are not paralleled by decreases in the total surface area of K-4; that is, the nitrogen area decreases only by 5%. On the other hand, amine adsorption after 500° activation is only about one-quarter that found after activation at 300°. This comparison precludes loss of a significant number of surface sites as a result of sintering. Furthermore, the conversion of Brönsted to Lewis sites by water loss at increasing temperature of activation cannot account for decreased amine adsorption since n-butylamine adsorbs on both types of sites. The possible formation of stable 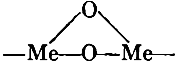 $\overset{\displaystyle O}{\mathrm{-Me{-}O{-}Me-}}$ type surface groups through strain relief at elevated, activation temperatures seems likely. This decreased amine adsorption in the range of activation temperatures employed was restricted to the kaolin fluid catalyst, and appears to be related to the amorphous nature of this higher area solid. Hackerman[12] has demonstrated that the heat of wetting of silicas in water decreases as surface area increases, a finding which could be accounted for if stable siloxane groups form more readily on the high area and more amorphous samples.

The total number of sites for amine adsorption at 25° on the Kaolin pellet catalysts K-1 and K-2 (steam treated) increased with activation temperature beyond 200° and up to 500°. In addition, the number of sites is very nearly the same for both these solids.

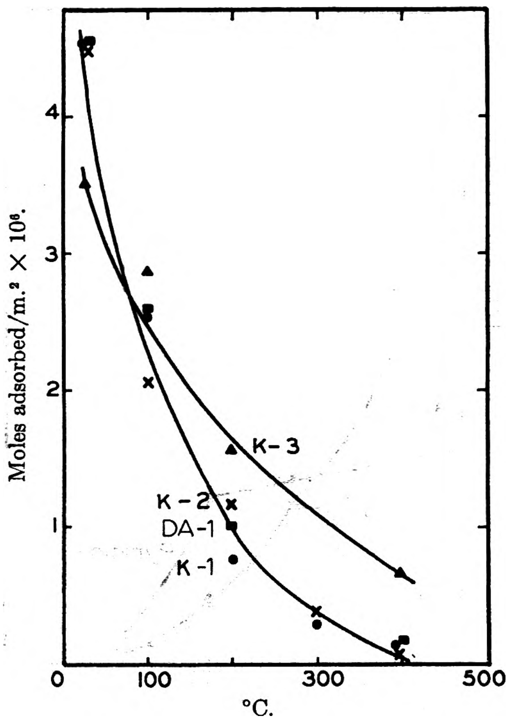

Fig. 3.—The desorption of n-butylamine from catalyst samples as a function of evacuation temperature (initial activation temperature 400°).

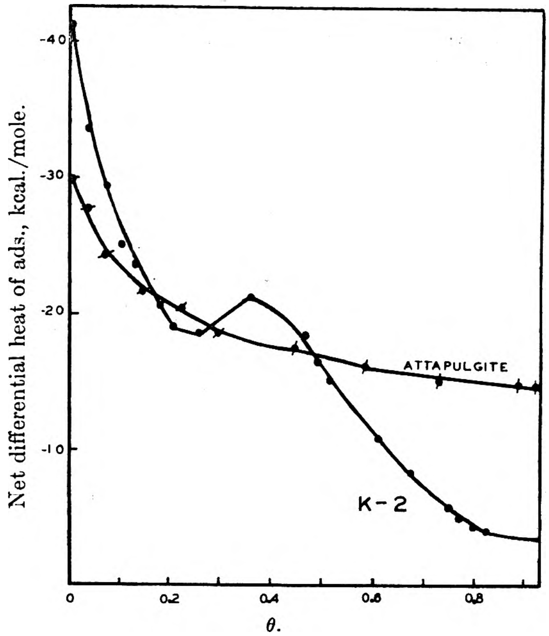

Fig. 4.—Differential heat of adsorption at 25° for n-butylamine adsorbed on a kaolin pelletized catalyst K-2 and on attapulgite clay.

Desorption curves for K-1, K-2, K-3 and DA-1 catalysts activated at 400° *in vacuo* before adsorption studies are compared in Fig. 3. The desorption curve for K-1 may not be completely meaningful because some reaction of the amine was observed during evacuation at 300°; the catalyst remained slightly colored even after outgassing at 400°. On a unit area basis, the chemisorbed butylamine capacities of K-1, K-2 and DA-1 are approximately 4.5 × 10^{-6} mole per square meter. Of course, on a per gram basis the capacity of DA-1 was about five times larger. More surprising was the finding that the desorption curves for K-1, K-2 and DA-1 agreed fairly well. This close concord-

---

(11) G. J. Young, *J. Colloid Sci.*, **13**, 67 (1958).

(12) A. C. Makrides and N. Hackerman, THIS JOURNAL, **63**, 594 (1959).

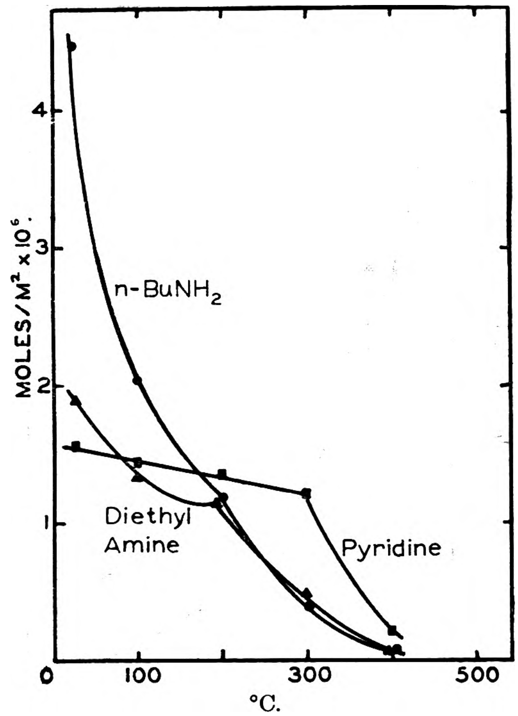

Fig. 5.—Desorption of various amines from kaolin catalyst K-2 as a function of evacuation temperature (sample initially activated at 400°).

ance may be fortuitous in view of the dissimilarities between the curves of Fig. 2 for the fluid DA-1 catalyst compared to those for the Kaolin pellet catalysts.

Catalyst K-3, prepared by grinding K-2 after catalytic evaluation, has the lowest total amine uptake presumably as a consequence of the evaluation study. The larger number of sites stable at higher evacuation temperatures apparently were developed by the grinding process.

In Fig. 4, the differential heat curve, obtained by taking slopes of the heat of immersion curve, is plotted against coverage for K-2 in comparison with the curve for attapulgite.[1] These θ values represent fractions of the monolayer values considering the chemisorbed amount after 25° evacuation to represent a monolayer. The maximum at 0.4 θ made it unrealistic to attempt to determine a site energy distribution curve; the slope of the curve reverses sign through the maximum. It was suspected that this maximum was due to lateral interactions, that is, that on the surface of K-2 acid sites were situated quite near to each other. The lack of neighbor–neighbor interaction is implicit in the approximate method of establishing a distribution curve from heats of immersion.

To verify this conjecture about neighbor sites, diethylamine was chosen as an adsorbate. The base strength of this amine, $K_B = 1.26 \times 10^{-3}$, is not much different from that of the butylamine, 4.6×10^{-4}. Due to steric hindrance, however, near neighbor sites might be expected to be inoperative. In Fig. 5, the desorption curve for diethylamine is compared to that for *n*-butylamine. The total number of sites upon which diethylamine was chemisorbed is slightly less than half of those which chemisorb *n*-butylamine. The extra sites which take up the *n*-butylamine were low energy sites because the desorption curves coincide at elevated temperatures.

To contrast these results with those for a base with considerably lower strength, pyridine with a K_B of 2.3×10^{-9} was used as an adsorbate. The amount chemisorbed at 25°, 1.6×10^{-6} mole per square meter, was lower than the amount of diethylamine chemisorbed, 1.9×10^{-6} mole per square meter. The amounts remaining at higher temperatures were somewhat higher apparently due to a higher escaping tendency for the larger molecule.

Summary

Saturation amounts of *n*-butylamine adsorbed on several cracking catalysts have been determined as a function of initial activation temperature. In addition, the amounts of total amine retained at successively higher temperatures of evacuation were measured. These data coupled with heat of immersional wetting values were used to calculate acid site energy distribution curves for amine adsorption on several cracking catalysts. Extensive chemisorption of amine on activated samples was associated with loss of surface hydroxyls as water. Supplementary information was obtained through use of amines of different basicities and molecular size and shape.

Further work is required for a more intimate characterization of such catalyst surfaces. Adsorption and desorption studies, as well as heat of wetting measurements, would be included for various amounts of water pre-adsorbed on the cracking catalysts. These same comprehensive studies with amines and water adsorbed on both silica and alumina surfaces separately would aid further in explaining the nature of the acid sites.

DISCUSSION

Alfred E. Hirschler (Sun Oil Company).—Mills and co-workers have interpreted the rather low chemisorption of quinoline at 300°, as compared to other measures of catalyst acidity at room temperature, as an indication that the number of potential acid sites on a catalyst is strongly temperature dependent. Could you comment on whether your data on the desorption of amines as a function of temperature are in accord with this interpretation, or are the adsorption energies such that only the strongest sites would be able to retain amines at 300°?

A. C. Zettlemoyer.—From our measurements we conclude that only the strongest sites would be able to retain simple amines at 300°. There is a need to study this question as a function of adsorbed water.

A. L. McClellan (California Research Corporation).—Do you attach any significance to the breaks in the curves of Fig. 5? Similar breaks have been reported in ammonia titration curves.

A. C. Zettlemoyer.—No, we do not. The data are uncertain enough so that smooth curves could just as well be drawn through the points. It does appear, however, that the pyridine remains mostly adsorbed above 300°.

THE OXIDATION OF INTERMETALLIC COMPOUNDS. I. HIGH TEMPERATURE OXIDATION OF InSb[1]

BY ARTHUR J. ROSENBERG* AND MARY C. LAVINE

Lincoln Laboratory, Massachusetts Institute of Technology, Lexington 73, Massachusetts

Received March 7, 1960

The oxidation of single-crystal InSb was studied in the range 212–494°. Initially antimony is preferentially attacked and evaporates from the surface as $(Sb_2O_3)_2$. In_2O_3 is simultaneously formed and produces a compact crystalline film. Further reaction is then confined to the formation of In_2O_3 and elemental antimony. The latter accumulates at the In_2O_3–InSb interface, as demonstrated both by electron diffraction and dissolution of the film. Associated with the crystallization of the In_2O_3 film, there is a singularity in the kinetics; the rate drops precipitously and comes under diffusion control. The rates increase slightly with oxygen pressure and vary with crystallographic orientation. Small lattice substitutions of Te (for Sb) or Cd (for In) in InSb increase the rate. The maximum oxide film thickness which is attainable in reasonable times is less than one micron. The rate constant for diffusion-limited oxide growth is four orders of magnitude less than that for antimony alone, but only a factor of two less than that for indium alone. The ratio of the rate constants for the oxidation of InSb and of In is quantitatively predicted on the premise that both reactions are controlled by the diffusion of In^{+3} through interstitial positions in In_2O_3.

I. Introduction

In recent years, considerable effort has been directed to the preparation of binary compounds of metals with elements in Groups IVB, VB, and VIB of the periodic table.[2] Aside from their semiconducting properties, the compounds have unique characteristics which may strongly influence their surface behavior. Their largely covalent character[3] concentrates the chemical energy of the system in directed bonds between each atom and its nearest neighbors alone, constraining the crystal to a high degree of chemical and structural perfection. This is reflected in the low solubility of excesses of either element in the compound, *i.e.*, restricted homogeneity ranges,[4] small diffusion and self-diffusion coefficients,[5] and resistance to cold work and plastic flow.[6] Contaminations of less than one part per million[2a] and dislocation densities of less than 10^3/cm.^{2} [7] are thus commonplace.

It is to be expected that each of these factors may affect significant departures from the normal surface behavior of metals and their alloys. Directed bonding will affect the mechanism of ion detachment and of adsorption of foreign atoms.[8] The space charge associated with the surface of semiconductors can profoundly influence electron transfer reactions,[9] and the relative absence of chemical and lattice defects will be reflected in the rates of nucleated reactions.[10] The detachment of one element from the compound forces the detachment of the other, since the latter cannot be accommodated by the remaining compound. It must either react itself or accumulate at the interface between the compound and the reacting medium.

The reactions of the semiconducting intermetallic compounds offer, accordingly, an excellent means for studying some of these factors in detail. The present paper is concerned with a typical surface reaction—high temperature oxidation—of a typical compound of this class—InSb. InSb (m.p. 525°) crystallizes in the zinc-blende structure where each atom is tetrahedrally coördinated through covalent sp^3 hybrid bonds to atoms of the opposite kind.[11] In the temperature range under consideration InSb is intrinsic,[12] and its semiconducting properties should not strongly influence its chemical behavior. It exhibits, however, the typical properties pointed out above, including low solubility of excess In or Sb,[13] high energy of defect formation,[5] negligible self-diffusion,[5] and a low normal dislocation density.[7]

II. Experimental Procedure

A. **Sample Preparation.**—Single crystals of InSb were grown by the Czochralski technique[14] from a stoichiometric melt of In and Sb. The components had been purified to 99.999+% purity by zone-refining in all quartz vessels. The conventional use of graphite or carbon-blacked linings for the melt-containing vessels was avoided since carbon apparently dissolves to about 1 part in 10^5 in molten InSb.[15] When crystals so contaminated are oxidized at elevated temperatures, the carbon is oxidized preferentially giving spurious kinetic results. Several crystals were used during the course of the experiments without observable differences in oxidation behavior. Unless otherwise noted the crystals were n-type containing an uncompensated impurity concentration of $<10^{16}$ atoms per cc.

The crystals were grown along a $<111>$ axis. Samples were cut and ground so that only a single crystallographic face was exposed. Thus, the all {100} samples were rec-

---

* Materials Research Lab., TYCO, Inc., Waltham, Mass.

(1) The work reported was performed by Lincoln Laboratory, a center for research operated by Massachusetts Institute of Technology with the joint support of the U. S. Army, Navy and Air Force.

(2) See for instance (a) J. M. Whelan, "Semiconductors," ed. by N. B. Hannay, Reinhold Publ. Corp., New York, N. Y., 1959, chapt. 9. (b) H. Welker and H. Weiss, *Advances in Solid State Phys.*, **3**, 1 (1956).

(3) See for instance (a) G. A. Wolff and J. D. Broder, *Acta Cryst.*, **12**, 313 (1959); (b) L. C. Pauling, "The Nature of the Chemical Bond," Cornell University Press, Ithaca, N. Y., 1949; (c) H. Welker, *Z. Naturforschg.*, **7a**, 744 (1952); **8a**, 248 (1953); (d) E. Mooser and W. B. Pearson, *J. Electronics*, **1**, 629 (1956).

(4) M. Hansen, "Constitution of Binary Alloys," McGraw-Hill Book Co., Inc., New York, N. Y., 1958.

(5) F. H. Eisen and C. E. Birchenall, *Acta Met.*, **5**, 265 (1957).

(6) C. Kolm, E. P. Warekois and S. A. Kulin, *Trans. Met. Soc. of AIME*, **212**, 827 (1958).

(7) R. L. Bell, *J. Elec. Cont.*, **3**, 487 (1957).

(8) G. A. Wolff and W. B. Pearson, *Disc. Faraday Soc.*, Kingston, Ont. (1959), to be published.

(9) See for instance (a) K. Hauffe and H. J. Engell, *J. Elektrochem.*, **56**, 366 (1952); **57**, 762 (1953); (b) P. Aigrain and A. Dugas, *ibid.*, **56**, 363 (1952).

(10) For a general discussion see: *Discussions Faraday Soc.*, 28 (1959).

(11) T. S. Liu and E. A. Peretti, *Trans. ASM*, **44**, 539 (1952).

(12) H. J. Hrostowski, F. J. Morin, T. H. Geballe and E.-H. Wheatley, *Phys. Rev.*, **100**, 1672 (1955).

(13) K. K. Hulme, *J. Elec. Control*, **6**, 397 (1959).

(14) For a general discussion of crystal growing techniques see: M. Tanenbaum, "Semiconductors," ed. by N. B. Hannay, Reinhold Publishing Co., New York, N. Y., 1959, chapt. 3.

(15) A. J. Rosenberg, unpublished.

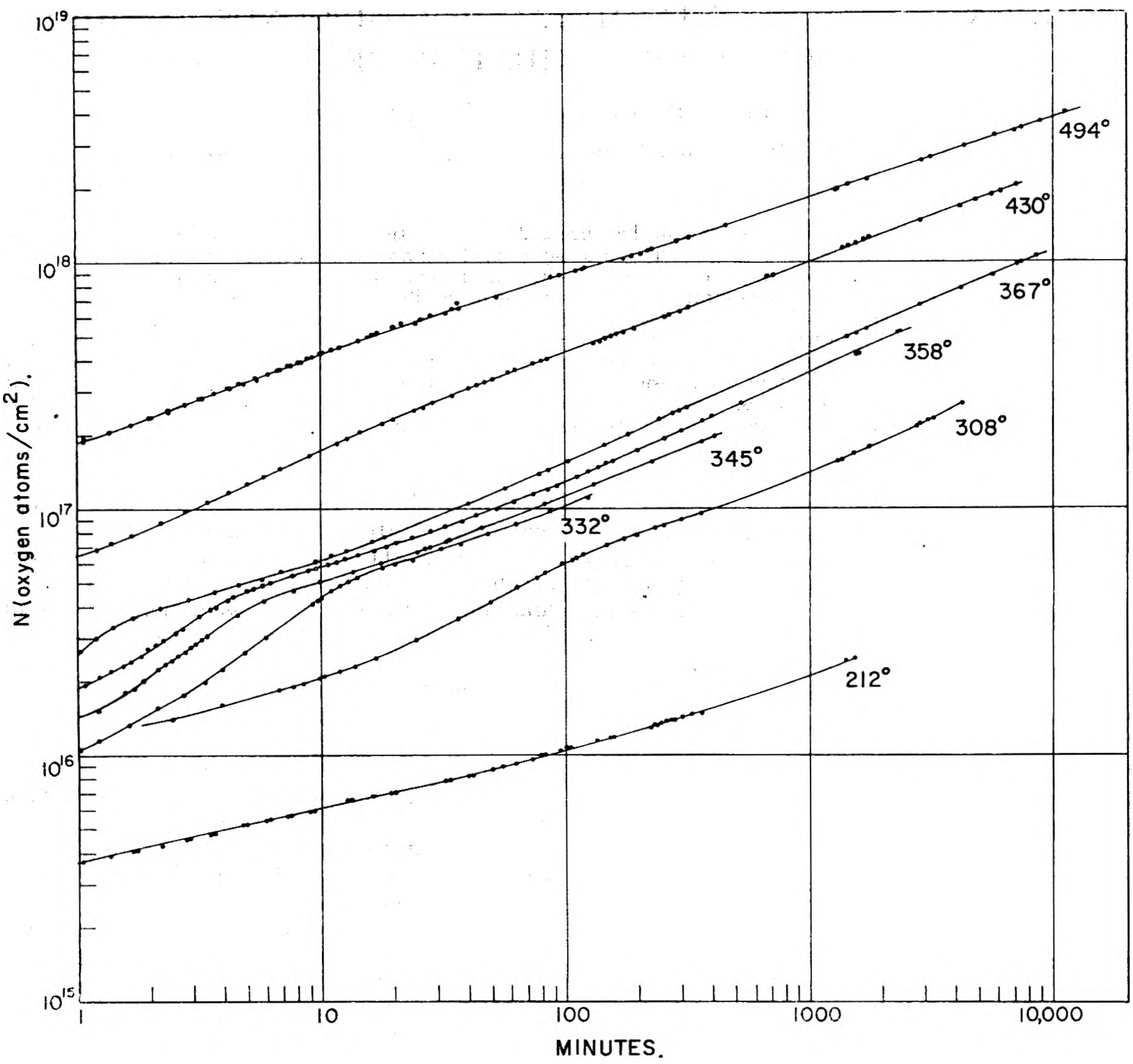

Fig. 1.—Oxidation of {110} InSb surfaces, 212–494°. Oxygen pressure = 0.3–0.4 mm. Data normalized to unit geometric surface area.

tangular parallelepipeds, the all {111} samples were tetrahedrons, and the all {110} samples were trapezoidal parallelepipeds.

The following technique of chemically polishing the surfaces of a sample and transferring it to the adsorption system was found to ensure the development of uniform oxides as judged by the interference colors which were produced on oxidation. A sample chamber consisting of 10 cm. of 10 to 15 mm. Pyrex tubing was joined to a short length of 1 mm. capillary tubing which was capped with a polyethylene plug. The sample, ground previously with 1600 grit garnet powder was polished by a 5-second immersion in a mixture of 70% HNO_3, 48% HF and glacial acetic acid in the ratio, 2:1:1 by volume, and rinsed successively in distilled water and 95% ethyl alcohol. The sample was transferred without drying to the sample chamber, which was filled within an inch of the top with water, and a 6-inch section of 2 mm. capillary was sealed to the top. The bottom was uncapped and 250 cc. of water followed by 150 cc. of alcohol was drawn through the tube by aspiration. The sample was then dried under a stream of pure nitrogen. The capillary at the bottom was sealed, and the chamber was jointed to a gas adsorption apparatus.[16]

B. **Adsorption Measurements.**—All measurements of oxidation were made by observing pressure changes at constant volume. The principal feature of the adsorption apparatus is the use of a thermistor manometer which permits essentially instantaneous measurements (time constant <0.1 second) of pressures up to 500 μ with a sensitivity of 0.01 μ.[16] The accuracy of the measurements of oxygen uptake kinetics is limited, however, to about ±0.5% because of non-equilibrium of pressure in the apparatus, fluctuations in room temperature and their effect upon the parts of the adsorption system which are not thermostated, fluctuations in the level of liquid nitrogen in the trap isolating the sample chamber from the remainder of the system, and fluctuations of ±1° in the temperature of the sample which was maintained with a simple furnace. One advantage of the precise manometer is that the total drop in pressure during a run can be conveniently restricted to 10% without loss of accuracy. As will be shown below the variation of reaction rate under a 10% change of pressure is virtually nil.

The volumes employed were such that the maximum sensitivity of the uptake measurements was 0.3 μcc./hr. (1 μcc. ≈ 3.24×10^{13} molecules at 25°).

Prior to each experiment the system was outgassed and the sample baked under vacuum ($<10^{-6}$ mm.) overnight at the reaction temperature before admitting oxygen.

Spectroscopically pure oxygen was used in all experiments

III. Results

A. **Kinetic Data.**—Figure 1 summarizes the oxidation kinetics of {110} InSb surfaces at elevated temperatures. The oxygen uptake (N) of samples maintained at a fixed temperature (T) in the range 212–494°, and at oxygen pressures

---

[16] A. J. Rosenberg, *J. Am. Chem. Soc.*, **78**, 2929 (1956).

(P) in the range, 300–400 μ, is plotted *vs.* reaction time (t). All data are normalized to unit geometric surface area. The over-all range of N is $3 \times 10^{15} - 4 \times 10^{18}$ oxygen atoms/cm.². Taking the roughness factor as 1.3,[17] and taking into account the film composition to be discussed below, the maximum value of the film thickness, which was obtained by an 11,000 minute exposure at 494° (m.p. InSb = 525°) is still somewhat under one μ.

The internal precision of the curves in Fig. 1 is better than 0.2%. The reproducibility of separate runs at 367 and 494° was checked repeatedly. Maximum deviations in $N(t)$ were less than 10%, and these are accountable for the most part by a scaling error due to uncertainties in the real surface area.

The curves appear related, particularly in the occurrence of an inflection at $N \sim 5 \times 10^{16}$ atoms/cm.². To obtain a more functional expression of the data, one can eliminate time as a variable and consider the dependence of the rate, $V = \mathrm{d}N/\mathrm{d}t$, upon N, T and P.

1. Dependence of Rate upon Film Thickness.—The data of Fig. 1 may be used to obtain the derivative

$$-\left(\frac{\partial \log V}{\partial \log N}\right)_{T,p} \equiv \epsilon \qquad (1)$$

which is plotted *vs.* log N in Fig. 2 for each of the various temperatures. Three results are immediately evident.

(i) The value of ϵ is *always* larger than zero. This means that, at a given temperature, the rate of oxidation continually diminishes with increasing N. The film is thus ever more protective, but it is not possible to classify the oxidation as a "parabolic" ($\epsilon = 1$), cubic ($\epsilon = 2$) or higher order ($\epsilon > 2$) protective reaction.

(ii) The composition and structure of the film are not uniquely determined by thickness. If they were, the curves of Fig. 2 would be strictly superimposable.

(iii) Certain similarities are evident, particularly the singularities occurring in the neighborhood of 5×10^{16} atoms/cm.². Beyond the maximum ϵ decreases to a value between 1 and 2, then almost imperceptibly rises again. This quasi-stationary value of ϵ lies between 1.0 and 1.4 between 308 and 367°. At 430 and 494° the curves appear to show additional singularities but ϵ eventually tends to a constant value of 2.0.

2. Dependence of Rate upon Temperature.—The experimental activation energies must, of course, be evaluated by comparison of rates at constant N. It is also necessary to distinguish between the temperature at which a measurement of V is made, and the temperature at which the oxide film is formed. The former is designated T, the latter, T_f. In the data of Fig. 1, $T = T_f$ and the experimental activation energies obtained are given by

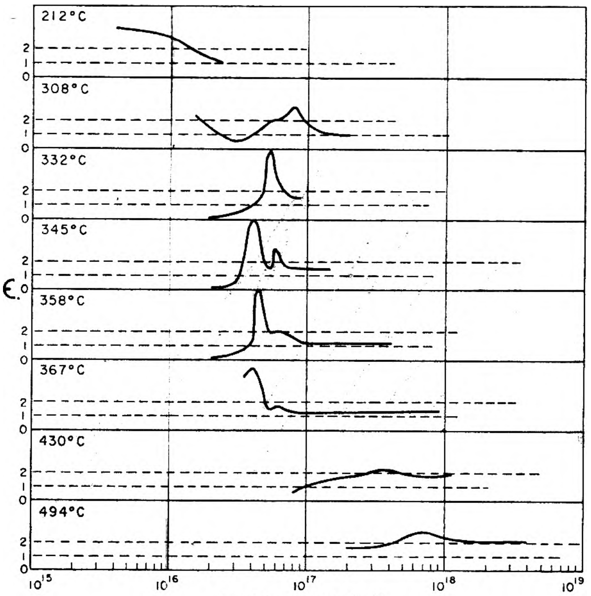

Fig. 2.—Variation of $\epsilon \equiv -(\partial \log V/\partial \log N)$ with N.

$$R\left(\frac{\partial \log V}{\partial 1/T}\right)_{N,T_f=T} = -\Delta E_1^* \qquad (2)$$

Plots of log V *vs.* $1/T$, derived from the data in Fig. 1, are given in Fig. 3. The linear representation observed between 308 and 494° does not extrapolate properly to the data at 212°. ΔE_1^* goes through a maximum at $N \sim 4 \times 10^{16}$ atoms/cm.² and declines with further growth of the film (Fig. 4).

Another activation energy, ΔE_2^*, may be defined as

$$R\left(\frac{\partial \log V}{\partial 1/T}\right)_{N,T_f=\text{const}} = -\Delta E_2^* \qquad (3)$$

This refers to an experiment in which the film is grown to a given thickness at a fixed temperature; the temperature is then varied, without a significant increase in N, and the rates are measured at several values of T. The results of three such experiments, performed under similar conditions, are given in Fig. 3b. The internal precision of ΔE_2^* is greater than that of ΔE_1^*, since the uncertainty in the area of the samples is not encountered. For the value of N and P at which the activation energies may be compared, $\Delta E_2^* > \Delta E_1^*$ (Fig. 4).

3. Dependence of Rate upon the Oxygen Pressure.—Samples oxidized to various thicknesses were subjected to changes in the oxygen pressure with the results shown in Fig. 5. The rate is seen to rise slightly with increasing P. For various experiments $n \equiv [\partial \log V/\partial \log P]_{N,T}$ was found to lie between 0.10 and 0.17. No systematic variation of n with N and T was observed.

4. Dependence of Rate upon Crystallographic Orientation.—The rates of oxidation of various low index crystallographic surfaces are compared in Fig. 6. At 212° the initial rates decrease in the order $\{100\} \approx \{111\} > \{\overline{111}\} > \{110\}$, but, beyond $N = 1.5 \times 10^{16}$, the $\{111\}$ surfaces are most slowly oxidized. At 367°, the initial rates decrease in the order $\{100\} > \{111\} > \{\overline{111}\} \approx \{110\}$, but beyond $N = 2.0 \times 10^{17}$, the order

---

[17] Chemically polished InSb surfaces microscopically resemble those of chemically polished germanium which have been shown to have a roughness factor of 1.3. (a) J. T. Law, THIS JOURNAL, **59**, 543 (1955); (b) S. P. Wolsky, Proceedings of 1958 International Conference on Semiconductors, *J. Phys. Chem. Solids*, **8**, 114 (1959).

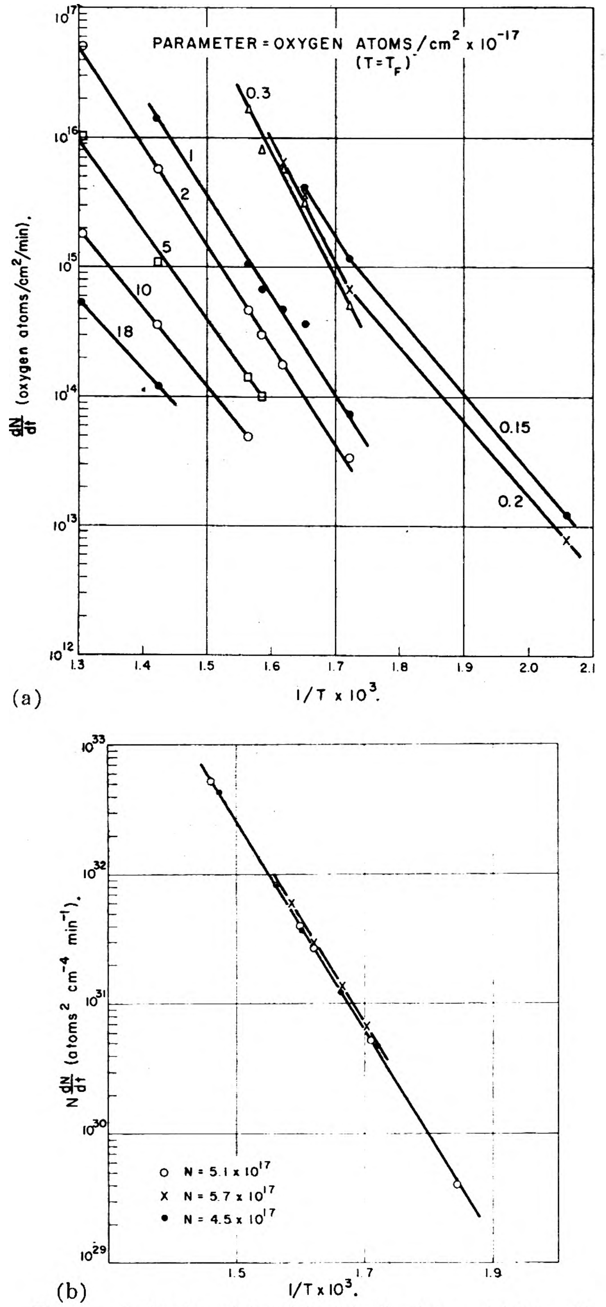

Fig. 3.—Arrhenius plots of the kinetic data. (a) $T = T_f$. Parameter = oxygen atoms/cm.². (b) The data were obtained on three samples oxidized previously to the indicated value of N at 358°. The total increase in N during the subsequent temperature variations was less than 0.3×10^{17} atoms per cm.² in each case. For normalization purposes, the product $N(dN/dt)$ rather than dN/dt is plotted. Ideally, the data would coincide if ϵ were equal to one.

changes to {111} > {110} > {$\overline{111}$} ≈ {100}. At 494°, the initial rates on the {100} surfaces are much larger than on the {110} surfaces, but the rates converge after 200 min. when $N > 1 \times 10^{19}$. A comparison of the absolute rates is sensitive to differences in roughness factor[18] which may be as high as 10%. A more accurate, though less precise, comparison was achieved by oxidizing a single specimen which exposed a number of crystallographic faces, and examining the interference colors which appeared. The sequence of colors produced as the film thickened were determined independently by using {110} samples. By this technique it was established that the relative rates decrease in the order {111} > {211} > {$\overline{111}$} > {110} > {100} for N up to 3×10^{17} at 367° at which point further growth of the {100} becomes slower than that of the {110}.

It should be noted that the rate anisotropy, while distinct, is of a smaller magnitude than that observed in the low temperature oxidation of metals and of Ge.[19]

5. Dependence of Rate upon Doping.—One InSb crystal was grown containing 2×10^{18} tellurium atoms/cc.; Te occupies lattice positions normally held by Sb, and dopes InSb more n-type.[20] Another crystal was grown containing 6×10^{18} cadmium atoms/cc.; Cd occupies lattice positions normally held by In and dopes InSb *p*-type.[20] The oxidation rates of both doped crystals were higher than that of undoped material at 400°. The Te-doped sample oxidized about five times faster and the Cd-doped sample about two times faster.

B. Nature of the Oxide Film.—The preceding kinetic results are naturally resolved into two regions separated by a singularity in $\epsilon(N)$ which occurs in the neighborhood of $N \sim 5 \times 10^{16}$ atoms/cm.², which is the equivalent of approximately 50 monolayer equivalents of oxygen. At this point the rate drops precipitously to a new magnitude, and then declines more or less uniformly with increasing N. Simultaneously the activation energy changes abruptly. The data suggest a change of mechanism, which is most plausibly accounted for in terms of a sudden change in the composition of the oxide film.

The following independent experimental results strengthen this conclusion and indicate that beyond $N \sim 10^{17}$ atoms/cm.² the film consists of In_2O_3 containing dissolved Sb, separated from the surface of the substrate by a layer of elemental Sb.

1. Dissolution of the Film.—Dewald[21] observed that anodically formed oxide films on InSb dissolved readily upon immersion in tartaric acid at 25°. The films produced by high temperature oxidation are not perceptibly attacked by this solvent. However, slow, relatively uniform dissolution does take place in 0.004 N H_2SO_4 + 0.08 M tartaric acid at 40° at a rate which is still considerably faster than that of InSb itself. By progressively dissolving the oxide films and microanalyzing the solutions for In and Sb, it was established that the films contained essentially equal

---

[18] The zinc blende structure shows polarity in the <111> direction so that parallel {111} surfaces are not chemically identical. On one set of {111} surfaces Sb atoms, triply bonded to the lattice, are exposed, while on the parallel set of {111} surfaces the In atoms are triply bonded. The former set have arbitrarily been designated {$\overline{111}$} while the latter have been designated {111}. See, for instance, M. C. Lavine, A. J. Rosenberg and H. C. Gatos, *J. Appl. Phys.*, **29**, 1131 (1958).

[19] A. Gwathmey and K. Lawless in "The Surface Chemistry of Metals and Semiconductors," ed. by H. C. Gatos, to be published by John Wiley and Sons.

[20] The extent of doping was determined by measuring the Hall coefficient, R_H, at 78°K. and using the relation $n = 6.25 \times 10^{18}/R_H$ cm.$^{-3}$.

[21] J. F. Dewald, *J. Electrochem. Soc.*, **104**, 244 (1957).

total quantities of In and Sb. The distributions were not uniform, however; the outer surface of the films contained a large excess of In, while the inner surface contained a large excess of Sb. It was observed, furthermore, that the total In and Sb content of the film was much larger than one would predict by assuming that the oxygen consumption is divided between the oxidation of In (to In_2O_3) and Sb (to Sb_2O_3 or Sb_2O_5). It would appear, accordingly, that while one component is fully oxidized, the other is not. Even so, the latter, which will be shown to be Sb, is rendered soluble.

2. **Electron Diffraction.**—The oxide films are too thin to permit either optical or electron micrographs of sections, and attempts to separate the film for transmission electron diffraction were unsuccessful. Suitable reflection patterns were obtained, however. The outer portion of the film gives a "spotty ring" pattern[22] ascribable in all details to microcrystalline In_2O_3.[23] By cracking an oxidized sample and scanning the exposed section (Fig. 7), a pattern characteristic of elemental Sb was also obtained, arising from a layer between the InSb and the In_2O_3. The Sb pattern consists primarily of spots, indicating preferential orientation.[22] The experiment was repeated for various film thicknesses with the same results. In no case was a pattern ascribable to any of the known antimony oxides observed.

C. **Comparison of Rates of Oxidation of In, Sb and InSb.**—The rates of oxidation of In, Sb and InSb at 360° are compared in Fig. 8. The data on antimony are taken from an earlier communication from this Laboratory.[24] The data on indium (m.p. 124°) were obtained by decanting the pure liquid under vacuum into a 10 mm. Pyrex tube which was then connected to the gas-handling apparatus. After a brief initial reaction, lasting 2.9, 0.6 and 1.5 minutes for InSb, Sb and In, respectively, each rate becomes essentially parabolic ($\epsilon \approx 1$) for an extended interval. If the pre-parabolic uptake is designated as α, then

$$N = \alpha + Ct^{1/2}$$

for the parabolic region and plots of log $(N - \alpha)$ *vs.* log t will be linear with a slope of $^1/_2$ as in Fig. 8. In this region the growth of the film probably is diffusion-controlled ($\epsilon \sim 1$), in which case $C = (2k)^{1/2}$, where k is the specific rate constant for film growth. The parameters α, C and k are summarized in Fig. 8.

The parabolic rates of In and InSb differ by a factor of two. The parabolic rate constant for Sb is a factor of 10^2 and the specific rate constant, a factor of 10^4, higher than those of In or InSb.

The large pre-parabolic uptake, α, for In is probably attributable in large part to the instability of a clean molten surface of indium. Indium does not wet Pyrex and the meniscus is convex. Upon adsorption of oxygen, the surface tension drops drastically and the glass is wetted. The shape of the surface changes rapidly and stabilizes to a configuration which is quite flat. Before it is stabilized the oxide cannot protect the metal surface.

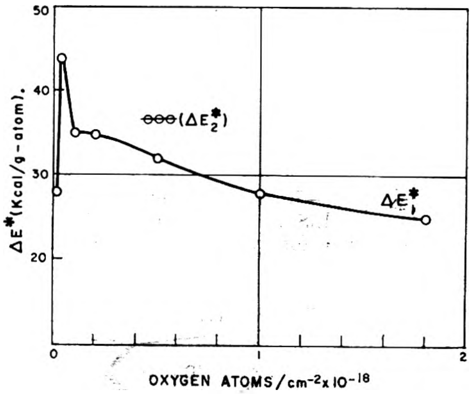

Fig. 4.—Variation of the activation energies with film thickness.

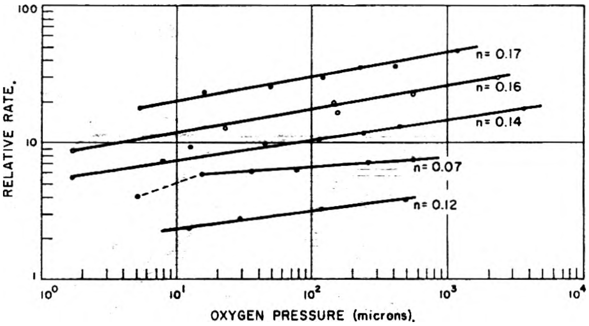

Fig. 5.—Dependence of the oxidation rate upon oxygen pressure. Each curve represents the relative change of the rate with pressure at fixed values of T and N in the range T = 300–400°, and $N = 10^{17}$–10^{18} oxygen atoms/cm.^{2}. No systematic dependence of n on either T or N was observed.

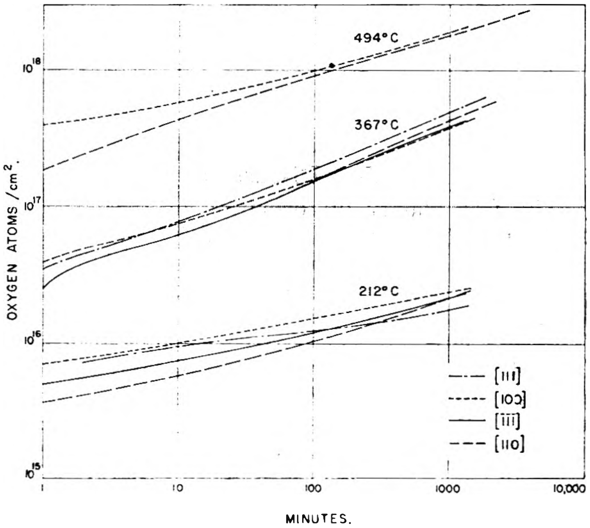

Fig. 6.—Dependence of the oxidation kinetics upon crystallographic orientation.

Despite the uncertainties in the mechanism of preparabolic growth, it is obvious that in this phase of reaction, as well as in the later parabolic stage, the rate of oxidation of Sb must greatly exceed that of InSb.

---

[22] R. Hocart and A. Oberlin, *Mem. services chim. etat Par.*, **39**, 119 (1954).

[23] H. E. Swanson, N. T. Gilfrich and G. M. Ugrinic, *NBS Circular 539*, **5**, 27 (1955).

[24] A. J. Rosenberg, A. A. Menna and T. P. Turnbull, *J. Electrochem. Soc.*, **107**, 196 (1960).

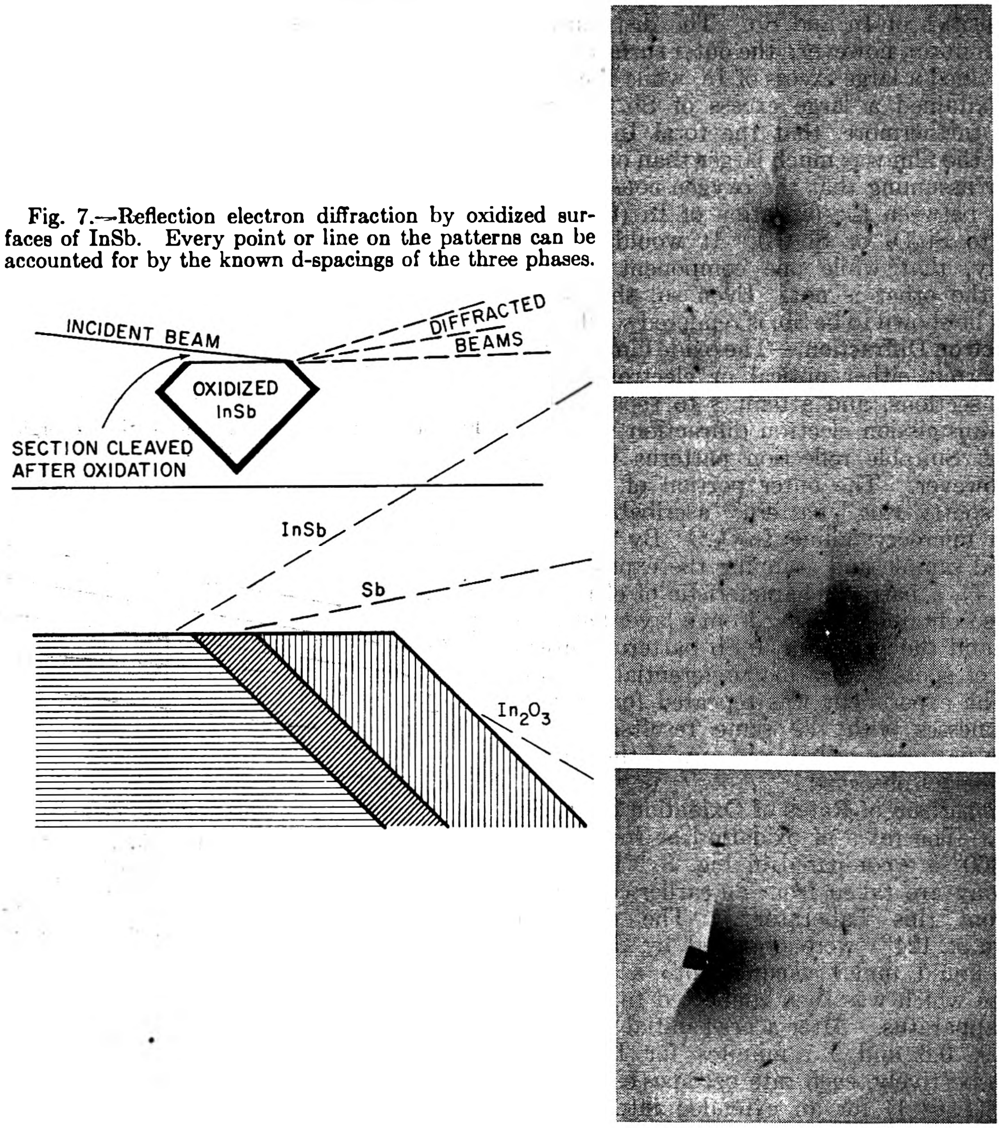

Fig. 7.—Reflection electron diffraction by oxidized surfaces of InSb. Every point or line on the patterns can be accounted for by the known d-spacings of the three phases.

IV. Discussion

The free energy of formation of InSb is quite small by chemical standards (Table I). From a thermochemical standpoint it is thus difficult to distinguish the compound from a physical mixture or an hypothetical solid solution of the elements. The distinctive physical and electronic properties of InSb arise, therefore, not from the binding energy of the system but from the distribution of this energy. It is a coincidence that the energies of vaporization of elemental indium and elemental antimony are nearly the same (Table I). The structure of indium is such that each atom is surrounded almost equally by 12 other atoms[25]; the average bond energy is thus about 58/6 = 9.6 kcal. In crystalline antimony each atom is surrounded by three nearest neighbors at a distance of 2.87 Å., and three next-nearest atoms at a distance of 3.37 Å., compared to the van der Waals diameter of 4.4 Å.[26]; the average bond energy is thus 61/3 = 20.3 kcal. InSb is characterized, on the other hand, by the concentration of the energy in localized bonds between each atom and its four nearest neighbors. (It can be argued, indeed, that the zinc blende structure provides the most distinct chemical arrangement for a binary compound.[27]) The bond energy is approximately 61/2 = 30.5 kcal.

The redistribution of the binding energy not only changes the physical properties of the In–Sb system but can markedly influence the chemical reactivity as well. It should in particular raise the activation energy for atom detachment. This is reflected in the early stages of the individual reactions of indium, antimony and InSb with oxygen, the rates of which are given indirectly through the parameter, α, in Fig. 8. Although the free energy of formation of In_2O_3 exceeds that of Sb_2O_3 (Table I), the latter is formed more readily from the elements (Fig. 8), and evaporates as $(Sb_2O_3)_2$.[28]

---

[25] W. B. Pearson, "A Handbook of Lattice Spacings and Structures of Metals and Alloys," Pergamon Press, 1958.

[26] E. Mooser and W. B. Pearson, *J. Phys. Chem. Solids*, **7**, 65 (1958).

[27] A. J. Rosenberg and T. C. Harman, *J. Appl. Phys.*, **30**, 1621 (Oct. 1959).

[28] The high temperature oxidation of antimony is ultimately limited by the vapor phase diffusion of $(Sb_2O_3)_2$ from a vapor region immediately surrounding the sample to a cold point outside the sample

TABLE I

THERMOCHEMICAL PARAMETERS FOR THE REACTIONS OF In, Sb AND O_2

Standard Oxygen Pressure = 0.3 mm.

Reaction	T, °K.	ΔH, kcal./mole	ΔS°, e.u.	ΔF°, kcal./mole	Ref.
$Sb + {}^3/_4O_2 = {}^1/_2Sb_2O_3(s)$	600	− 85	−45	−58	29
$Sb + O_2 = {}^1/_2Sb_2O_4(s)$	600	−104	−58	−69	29
$Sb + {}^5/_4O_2 = {}^1/_2Sb_2O_5(s)$	600	−114	−75	−69	29
$Sb + {}^3/_4O_2 = {}^1/_4(Sb_2O_3)_2$ (g)	600	− 73	−33	−53	29
$In + {}^3/_4O_2 = {}^1/_2In_2O_3(s)$	600	−112	−52	−81	29
In(s) + Sb(s) = InSb(s)	298	− 6.94	− 3.98	− 5.76	30
In(l) + Sb(s) = InSb(s)	600			− 3.6	30
Sb(s) = Sb(g)	298	+ 60.8	+ 3.25	+51.1	31
In(s) = In(g)	298	+ 58.2	+ 2.88	+49.6	31

It is to be expected, therefore, that a physical mixture of In + Sb should be oxidized at a rate nearly equivalent to that of antimony alone. While Sb_2O_3 is one of the initial products of the reaction of InSb with oxygen, as evidenced by the appearance of minute crystallites of Sb_2O_3 at the entry to the sample furnace, the rate of the reaction is orders of magnitude less than that of antimony alone.

As $(Sb_2O_3)_2$ vaporizes from the surface the indium which remains is oxidized to In_2O_3. As the latter accumulates about crystalline nuclei, access of oxygen to the substrate surface is progressively hindered and finally is prevented entirely. This progressive restriction is reflected kinetically in the rise of ϵ (Fig. 2). Once the In_2O_3 film is completed, reaction can continue only if oxygen, indium, and/or antimony can diffuse through the film. ϵ then approaches a value between 1 and 2 which is characteristic of diffusion control. For reasons to be discussed in the succeeding paper of this series, it is believed that the interstitial diffusion of cations controls the rate. It is to be expected that indium will move more readily than antimony through its own oxide lattice. The In_2O_3 film grows and although some antimony enters the film, a large fraction will remain behind. It cannot redistribute itself in the substrate since the infinitesimal solubility and diffusion coefficient of excess Sb in InSb prevent it. It is constrained, therefore, to accumulate at the $In–In_2O_3$ interface, as confirmed by electron diffraction.

Wagner[32] has shown that, in a composite film of the type observed in the present study, the interface between the more noble metal (Sb) and the oxide of the less noble metal (In) is predisposed to pronounced topographical irregularities. It is to be expected, therefore, the promontories of antimony will project into the oxide film. This may account in part for the large concentrations of antimony which, judging from the dissolution experiment, are associated with In_2O_3. It seems certain, however, that antimony partially replaces indium in the In_2O_3 lattice,[33] and under appropriate conditions[34] can migrate to the oxide–gas interface to be discharged as $(Sb_2O_3)_2$.

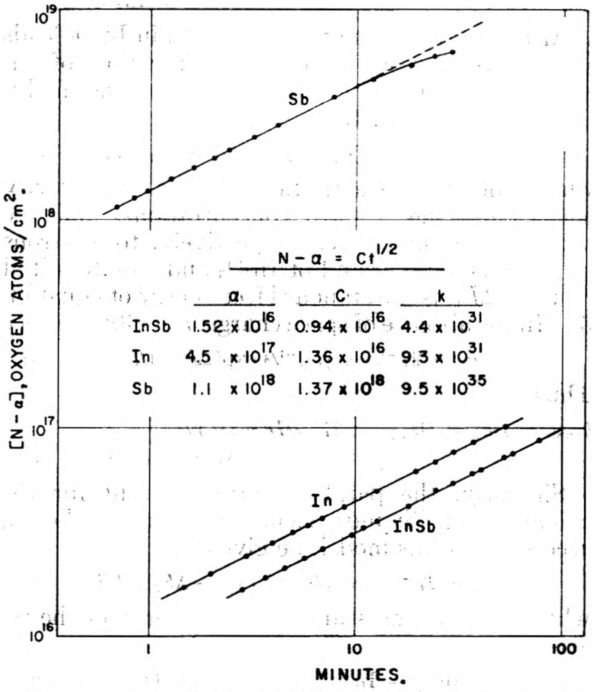

Fig. 8.—Comparison of oxidation rates of In, Sb and InSb at 367°. The data are normalized to unit surface area using a roughness factor of 1.3 for InSb, and the cross-sectional area of the sample tube for In. Unit roughness factor is assumed for Sb which was obtained by cleavage.

Comparison of the Oxidation Rates of InSb and Indium.—Although the composition of the oxide film is complicated by the presence of antimony, it will be shown in the following article that the principal features of protective oxide growth upon InSb are determined by the diffusion of interstitial indium ions through In_2O_3. Within this context one can predict the comparative rates of oxidation of InSb and of elemental indium.

Consider an ideal model in which the rate of oxidation is controlled by the diffusion of interstitial indium ions through a pure monocrystalline film of In_2O_3 in contact with InSb. The parabolic rate constant, k, will be given by Da_i, where D is the diffusion coefficient of the interstitials and a_i is their activity in the oxide when the latter is at equilibrium with InSb. It is assumed that the oxygen pressure is high enough so that the activity of interstitials at the oxide/oxygen interface is negligible compared to a_i. D is a fundamental property of the oxide, although it may be affected by a_i. a_i depends upon the free energy expended in the transfer of an indium ion from the InSb into an interstitial position in In_2O_3 through the reaction

---

furnace, and an Sb_2O_3 layer of stationary thickness is established on the surface of the sample (A. J. Rosenberg, A. A. Menna and T. P. Turnbull, *J. Electrochem. Soc.*, **107**, 196 (1960)). The transition from a rate controlled by the formation of the Sb_2O_3 film to a rate controlled by gaseous diffusion is indicated in Fig. 8 by the negative deviation of the experimental points after ten minutes' reaction.

(29) J. P. Coughlin, Bull. 542, U. S. Bur. Mines (1954).

(30) W. E. Schottky and M. B. Bever, *Acta Met.*, **6**, 320 (1958).

(31) F. D. Rossini, *et al.*, "Selected Values of Chemical Thermodynamic Properties," Circ. Natl. Bur. Standards 500, U. S. Govt. Printing Office, Wash., D. C., 1952.

(32) C. Wagner, *J. Electrochem. Soc.*, **103**, 571, 628 (1956).

(33) In this connection it is of interest that indium can replace up to 50% of the antimony in the C33 rhombohedral structure of Sb_2Te_3 with a negligible change in the lattice parameter (A. J. Rosenberg, to be published).

(34) To be described in the following article, THIS JOURNAL, **64**, 1143 (1960).

$$\mathrm{InSb(s)} = \mathrm{Sb(s)} + \mathrm{In}^{+3}(\mathrm{In_2O_3}) + 3\mathrm{e}(\mathrm{In_2O_3}) \quad (4)$$

Although the dissolution of indium in In_2O_3 leads to an extraordinarily high concentration of interstitial cations, one may, on formal thermodynamic grounds,[35] write

$$a_i a_e^3 = (n_i n_e^3)(\gamma_i \gamma_e^3) = \exp(-\Delta F_1^0/RT) \quad (5)$$

where the a's are activities, the γ's are activity coefficients, the n's are concentrations, and the subscripts e and i refer, respectively, to electrons in the conduction band of In_2O_3 and to interstitial cations. ΔF_1^0 is the standard free energy of equation 5. In the absence of space charge, $n_e = 3n_i$, whence

$$n_i = 27^{-1/4}(\gamma_i \gamma_e^3)^{-1/4} \exp(\Delta F_1^0/4RT) \quad (6)$$

Thus

$$k_{\mathrm{InSb}} = Da_i = Dn_i\gamma_i = 27^{-1/4}D(\gamma_i/\gamma_e)^{3/4} \exp(-\Delta F_1^0/4RT) \quad (7)$$

Similarly, the parabolic rate constant for the oxidation of (liquid) elemental indium should, according to this model, be given by

$$k_{\mathrm{In}} = 27^{-1/4} D(\gamma_i/\gamma_c)^{3/4} \exp(-\Delta F_2^0/4RT) \quad (8)$$

where ΔF_2^0 is the standard free energy of the reaction

$$\mathrm{In(l)} = \mathrm{In}^{+3}(\mathrm{In_2O_3}) + 3\mathrm{e}(\mathrm{In_2O_3}) \quad (9)$$

The major factor contributing to the difference between k_{In} and k_{InSb} is the change of ΔF^0 which is reflected exponentially in its effect upon n_i. The latter can, in turn, influence the γ's and D, with a consequent second order effect upon n_i. As long as the change in ΔF^0 is small, however, the second-order effect can be neglected, *i.e.*, the γ's and D will be essentially the same during reaction 4 as during reaction 9 at the same temperature. Under these conditions

$$\frac{k_{\mathrm{InSb}}}{k_{\mathrm{In}}} = \exp[(\Delta F_1^0 - \Delta F_2^0)/4RT] \quad (10)$$

By subtracting eq. 4 from eq. 9 one has the net reaction

$$\mathrm{In(l)} + \mathrm{Sb(s)} = \mathrm{InSb} \quad (11)$$

Thus $\Delta F_1^0 - \Delta F_2^0$ corresponds exactly to $\Delta F^0_{\mathrm{InSb}}$, the standard free energy of formation of InSb at the temperature of the experiment. According to the results of Schottky and Bever,[30] $\Delta F^0_{\mathrm{InSb}} \approx -3600$ cal. per mole in the vicinity of 600°K. (Table I). At 640°K., therefore

$$\frac{k_{\mathrm{InSb}}}{k_{\mathrm{In}}} \approx \exp(\Delta F^0_{\mathrm{InSb}}/4RT) = \exp[-3600/(4 \times 2 \times 640)] = 0.49 \quad (12)$$

The experimental value is 0.47 (Fig. 8). The close agreement may be partially fortuitous since the normalization of the data of Fig. 8 involves an inexact estimate of the surface areas. Nevertheless, the result provides fundamental support for a mechanism in which the rate is dominated by the thermal diffusion of indium ions through an In_2O_3 lattice.

Oxidation of Other $A^{III}B^{V}$ Compounds.—The course of the oxidation of InSb may well be repeated in the reactions of the eight other $A^{III}B^{V}$ compounds where A^{III} = Al, Ga or Sb and B^{V} = P, As or Sb. In each case, the free energy of formation of A_2O_3 exceeds that of the B oxides[27] while the latter are more readily formed and are volatile. A protective film of A_2O_3 should be formed provided that (1) the formation of A_2O_3 is controlled by the diffusion of A^{+3} ions; (2) the diffusion coefficient of B in A_2O_3 is much smaller than that of A; (3) the vapor pressure of neither B nor of its oxides is high enough to disrupt the film mechanically. By analogy with eq. 10, the parabolic rate constants will be given, approximately, by

$$k_{\mathrm{AB}} = k_{\mathrm{A}} \exp(\Delta F^0_{\mathrm{AB}}/4RT) \quad (13)$$

where ΔF^0_{AB} is the standard free energy of formation of the $A^{III}B^{V}$ compound. If the mechanism does apply generally to the $A^{III}B^{V}$ compounds, eq. 13 provides a method for obtaining ΔF^0_{AB}.

It is of interest to speculate on the relative rates of oxidation of the $A^{III}B^{V}$ compounds. k_{A} (eq. 13) depends linearly on several physical characteristics of A_2O_3 which should not differ substantially for Al_2O_3, Ga_2O_3 and In_2O_3.[36] It depends exponentially, however, on ΔF_i^0, the free energy of a reaction equivalent to eq. 9 and ΔF_d^*, the free activation energy of their diffusion through A_2O_3. Thus

$$k_{\mathrm{AB}} \propto e^{-\Delta F_d^*/RT}\, e^{-(\Delta F_i^0 - \Delta F^0_{\mathrm{AB}})/4RT} \quad (14)$$

ΔF_1^0 is related to the energy of formation of A_2O_3 and should increase with decreasing atomic number. This is borne out by the ease with which the electronic conductivity, hence the concentration of interstitial atoms, is increased by heating In_2O_3 under vacuum,[37] while Al_2O_3 remains an insulator. It is to be expected that the effect on ΔF_d^* will be in the same direction. Thus the net effect of decreasing atomic number should be to lower k_{A} substantially. This is confirmed by the fact that the rate of oxidation of Al at 600°[38] is orders of magnitude less than that of In [obtained by extrapolating the present data at 360° using an activation energy of 36,000 cal./mole (Fig. 3b.)]. From existing data on the energies of formation of the $A^{III}B^{V}$ compounds[29,39,40] it is clear that ΔF^0_{AB} increases with decreasing atomic number, the effect being more pronounced for a change in B^{V} compared to a change in A^{III}. Since A^{III} also affects the rate strongly through ΔF_i and ΔF_d^*, changes in A^{III} should, nevertheless, have a greater net effect than changes in B^{V}.

Therefore, the relative rates of the high temperature oxidation of the $A^{III}B^{V}$ compounds should, subject to the conditions set out above, decrease in the order

InSb > InAs > InP; GaSb > GaAs > GaP;
AlSb > AlAs > AlP

Acknowledgments.—The authors wish to express their thanks to Dr. H. C. Gatos for suggesting the problem and for many helpful discussions, to Mr. T. P. Turnbull for the electron diffraction analysis of the oxide films, and to Mr. C. S. Martel, Jr., for his skillful technical assistance.

---

(35) The statistical justification for this is discussed in the following article.

(36) E. A. Gulbransen, *Ann. N. Y. Acad. Sci.*, **58**, 830 (1954).

(37) G. Rupprecht, *Z. Physik*, **139**, 504 (1954).

(38) I. A. Makolkin, *Z. angew. Chem. USSR*, **24**, 460 (1951).

(39) K. Weiser, THIS JOURNAL, **61**, 513 (1957).

(40) J. V. D. Boomgaard and K. Schol, *Philips Res. Rep.*, **12**, 12 (1957).

OXIDATION OF INTERMETALLIC COMPOUNDS. II. INTERRUPTED OXIDATION OF InSb[1]

BY ARTHUR J. ROSENBERG *

Lincoln Laboratory, Massachusetts Institute of Technology, Lexington 73, Massachusetts

Received March 7, 1960

The later stages of the oxidation of InSb above 300° are limited by the migration of atomic defects through the growing film of In_2O_3. By utilizing a new kinetic procedure it has been shown that the concentration of defects is sufficient to confine any space charge to negligibly thin regions at the boundaries of the oxide film. The motion of defects is, accordingly, a field-free diffusion process. The experimental method is based on rate measurements following interruptions of the reaction, and permits the simultaneous determination of D, the diffusion coefficient, and C_0, the solubility, of the mobile defect in In_2O_3. The necessary mathematical formulation has a simple analytical form and contains a rigorous internal check. In the temperature range 308–407°, the quantities D and C_0 are given by $D = 0.0078 \exp(-31200/RT)$ cm.^{2}/sec., and $C_0 = 9.4 \times 10^{22} \exp(-5400/RT)$ defects/cm.^{3}. The results find a consistent statistical interpretation when it is assumed that the defects are interstitial indium cations, and that a heavy mass approximation applies to conduction electrons in In_2O_3. The values of D and C_0 decrease gradually with increasing film thickness in the range 600–1500 Å.; the effect is not related, however, to thermal aging of the oxide. Evidence is also presented that antimony can penetrate In_2O_3 during the interruptions.

I. Introduction

In the preceding article of this series,[2] the oxidation of InSb in the temperature range 212–494° was described. After a brief initial reaction during which Sb_2O_3 vaporizes from the surface, a protective oxide film consisting largely of In_2O_3 forms and restricts further reaction to the simultaneous formation of In_2O_3 and of elemental antimony which accumulates at the In_2O_3–InSb interface. The present article is concerned with the mechanism of the latter phase of the oxidation.

The driving force of the reaction is the free energy of oxidation of InSb which resolves itself kinetically into a gradient of electrochemical potential under which a diffusible species is driven through the growing oxide film, whence[3]

$$j_{\mathrm{i}}(x) = -\frac{D_{\mathrm{i}}}{RT}\, n_{\mathrm{i}}(x)\, \{\mathrm{grad}\ \mu_{\mathrm{i}}(x) + N_{\mathrm{i}} z_{\mathrm{i}} e E(x)\} \quad (1)$$

where $j_{\mathrm{i}}(x)$ is the flux of the ith species across a boundary at a distance, x, measured from the inner surface of the oxide, D_{i} is its diffusion coefficient, $n_{\mathrm{i}}(x)$ is its concentration, $\mu_{\mathrm{i}}(x)$ is its chemical potential, and z_{i} is its charge. N_{L} is the Loschmidt number, e is the electronic charge, E is the electrostatic field and R and T have their usual meaning. For uncharged species, $z_{\mathrm{i}} = 0$ and eq. 1 can be solved to give the rate of increase of the film thickness, X

$$\frac{\mathrm{d}X}{\mathrm{d}t} = k_1 X^{-1} \quad (2)$$

where k_1 is a constant for given experimental conditions. Generally, however, the diffusing species are ionized and can move independently of their countercharges. The ionization of adsorbed oxygen atoms and the differing tendency of ions and electrons to enter the oxide creates local charge imbalances at the boundaries of the oxide.[4] These charge imbalances, called space charges, are confined to layers whose thicknesses are similar at each interface and are given to an order of magnitude by

$$\lambda \sim \left(\frac{\kappa k T}{8\pi e^2 n}\right)^{1/2} \quad (3)$$

where κ is the dielectric constant of the oxide; n is the average mobile charge density, and the other quantities have their usual meaning. As long as X is much larger than λ, the more mobile charge carriers are constrained to move with the slower ones in the bulk of the film, which then remains neutral. The reaction is then under thermal diffusion control, and eq. 1 yields

$$\frac{\mathrm{d}X}{\mathrm{d}t} = k_2 X^{-1};\ k_2 = \Omega D\,|C_0 - C_1| \quad (4)$$

where Ω is the volume increase associated with the oxidation of one substrate atom, and C_0 and C_1 are the diffusing ion concentrations at the inner and outer interfaces, respectively.[4]

When X is comparable to λ, however, field-induced migration in the boundary layers can influence the rate. A general analytical solution of eq. 1 is not possible, but for the case where X is much smaller than the λ's, several special solutions have been developed.[3-5] Each assumes electronic equilibrium at the oxide–O_2 interface. While this assumption has been questioned,[6] since it requires that the electrons move easily over a considerable energy barrier, it does lead to practical solutions which give a qualitative picture of thin film oxidation kinetics. For this condition Grimley[5a] writes eq. 1 as

$$\frac{\mathrm{d}X}{\mathrm{d}t} = kX^{-\epsilon} \quad (5)$$

where ϵ depends on X and the defect character of the oxide film. For p-type oxides, in which the predominant defects are cation vacancies and electron holes, $\epsilon = 1$ at very low X and increases to 2, 3, or even higher values depending upon the valence on the vacancy. For n-type oxides in

---

*Materials Research Lab., TYCO, Inc., Waltham, Mass.

[1] The work reported was performed at Lincoln Laboratory, a center for research operated by Massachusetts Institute of Technology with the joint support of the U. S. Army, Navy and Air Force.

[2] A. J. Rosenberg and M. C. Lavine, THIS JOURNAL, **64**, 1135 (1960).

[3] See K. Hauffe, "Oxydation von Metallen und Metallegierungen," Springer, Berlin, 1956, p. 73 ff.

[4] N. Cabrera and N. F. Mott, *Rep. Progr. Phys.*, **12**, 163 (1948).

[5] (a) See T. B. Grimley in "Chemistry of the Solid State," ed. W. E. Garner, Butterworths, London, 1955, p. 336 ff. (b) T. B. Grimley and B. M. W. Trapnell, *Proc. Roy. Soc.* (*London*), **A234**, 405 (1956).

[6] N. Cabrera in "Semiconductor Surface Physics," ed. R. H. Kingston, U. of Penn. Press, Philadelphia, Penna., 1957, p. 333.

which interstitial cations and electrons are involved, ϵ starts at 1, drops to $^1/_2$, and reverts to 1 as X increases. ϵ changes very slowly with X, however, so that it is virtually constant for the measurable range of X at any given temperature.

The oxide phase in the oxidation of InSb is structurally that of In_2O_3, which has been established to be normally n-type, containing an excess of indium.[7] Substitution of antimony for indium within this structure can only tend to make it more n-type. If a thin film mechanism of the type underlying eq. 5 applies, therefore, ϵ should not exceed unity. In point of fact, however, ϵ always exceeds unity once the In_2O_3 film is established, and approaches 2.0 at higher temperatures and film thicknesses.[2]

Ordinarily one would expect a "thin film" mechanism to apply to the oxidation of InSb, which gives film thicknesses of less than one micron. Such a mechanism can account in principle for a dependence of rate on crystal orientation and on pressure[3] while a simple diffusion mechanism cannot. Because of the observed ϵ values, one is led, nevertheless, to re-examine the possibility that field-free diffusion provides a better interpretation of the data, with the discrepancies being attributable to the complex chemistry of the film.

A necessary condition for simple diffusion control is that the film thickness, X, be much larger than λ, defined in eq. 3. In the present case, this requires that λ be less than $\sim 10^{-6}$ cm. Substituting $\kappa = 10$ and $T = 600°$, one finds[8] that

$$n >> 10^{17} \text{ cm.}^{-3} \qquad (6)$$

If eq. 6 is satisfied, there exists a practical kinetic procedure for measuring the diffusion coefficient and the concentration of the particles whose diffusion controls the growth of the oxide layer. This procedure is based on the controlled interruption of the oxidation.

II. Theory of Interrupted Oxidation Kinetics

Consider the generalized oxidation of a metal, taking place at a flat surface

$$y\text{M} + \frac{z}{2}\text{O}_2 = \text{M}_y\text{O}_z \qquad (7)$$

The reaction is assumed to be controlled by the field-free diffusion of M^{+z} ions or M atoms through interstitial positions in the growing monocrystalline oxide lattice. M atoms enter the oxide at $x = 0$, migrate through the film under the influence of their concentration gradient, and complete the reaction with oxygen at the oxide/oxygen interface ($x = X$). The concentration of interstitials at $x = 0$ is C_0 while that at $x = X$ is C_1. These values correspond to those which would be observed if isolated M_yO_z were at equilibrium with oxygen at a pressure (Po_2) equalling, respectively, the dissociation pressure of the oxide (P_{diss}) and the ambient pressure of the experiment (P_1). At any moment

(a) DURING FILM GROWTH

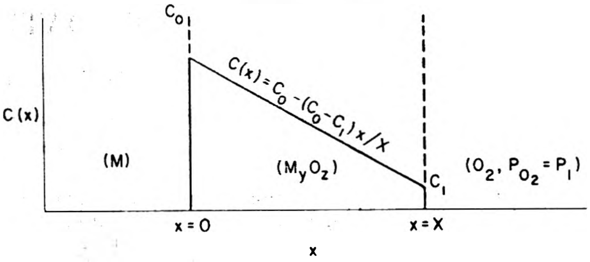

(b) DURING INTERRUPTION

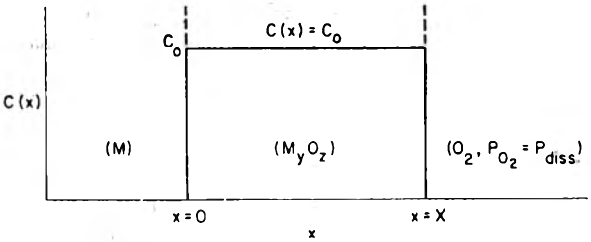

Fig. 1.—Concentration of interstitial cations in a film of M_yO_z growing upon a metal substrate: (a) during growth; (b) during interruption.

$D(\partial^2C/\partial x^2) = \partial C/\partial t = 0$ throughout the film so that C varies linearly with x as shown in Fig. 1a. The diffusion coefficient, D, is taken to be independent of C.

Assume now that the ambient O_2 pressure is dropped from P_1 to P_{diss}. Experimentally, this is easily accomplished by removing excess gaseous O_2 from the apparatus and sealing off the sample enclosure. The sample then acts as a source or a sink, and the oxygen pressure in the enclosure automatically adjusts itself to P_{diss}. M atoms continue to enter the film at $x = 0$, but are no longer removed at $x = X$. The M concentration approaches the equilibrium value, C_0, throughout the film, and reaction ceases (Fig. 1b). If the pressure is then raised to P_1, $C(X)$ is again reduced to C_1. The cations resume their outward flow and the concentration distribution of Fig. 1a is re-established.

If C_0X is large enough, this "restoration" of the steady-state concentration gradient should resolve itself as a relatively fast initial uptake of oxygen followed by a gradual return to the rate given by eq. 4. Mathematically, the problem may be approximated as follows. It is assumed that cations may be created or destroyed only at $x = 0$ and $x = X$, and that their diffusion coefficient in the oxide is independent of C. Then, at a given temperature

$$\frac{\partial C(x)}{\partial t} = D\frac{\partial^2 C(x)}{\partial x^2} \qquad (8)$$

As boundary conditions, one takes

$$\begin{aligned} \text{at } t = 0: &\quad C(x) = C_0 \text{ for all } x \\ \text{at } t > 0: &\quad C(0) = C_0 \\ &\quad C(X) = C_1 \end{aligned} \qquad (9)$$

where t is measured from re-admission of O_2. The equation is readily solved by standard techniques,[9] giving

---

(7) G. Rupprecht, *Z. Physik*, **139**, 504 (1954).

(8) n can be determined in principle by measuring the electrical conductivity σ of the film and assuming carrier mobilities for use in the expression, $\sigma = nze\mu$. By partially immersing an oxidized sample in mercury, σ can be measured, but the method is insensitive, and, in the present case, led only to a lower limit of 10^{16}/cc. for n.

(9) J. Crank, "The Mathematics of Diffusion," Oxford, 1956, p. 12 ff.

$$C(x) = C_0 - \frac{(C_0 - C_1)x}{X} + \frac{2}{\pi}\sum_1^\infty \frac{C_1 \cos n\pi - C_0}{n} \sin\frac{n\pi x}{X}\, e^{-D'n^2t} + \frac{4C_0}{\pi}\sum_0^\infty \frac{1}{2m+1} \sin\,(2m+1)\,\pi\frac{x}{X}\, e^{-D'(2m+1)^2t} \quad (10)$$

where $D' = D\pi^2/X^2$.

By taking the derivative of $C(x)$ with respect to x, evaluating it at $x = X$, and integrating from $t = 0$ to $t = t$, one obtains an expression for Δ, the number of M atoms crossing unit area of the outer interface in time t.

$$\Delta = D\int_0^t \left(\frac{\partial C}{\partial x}\right)_{x=X} dt = \frac{D(C_1 - C_0)t}{X} - \frac{2X}{\pi^2}\sum_1^\infty [C_1 - C_0(-1)^n]\left[\frac{1}{n^2}\right][e^{-D'n^2t} - 1] + \frac{4C_0X}{\pi^2}\sum_0^\infty \frac{1}{(2m+1)^2}[e^{-D'(2m+1)^2} - 1] \quad (11)$$

For most practical purposes $C_1 << C_0$, and eq. 11 reduces to the equation

$$\frac{\pi^2\Delta}{XC_0} = 2\sum_1^\infty \frac{(-1)^n}{n^2} - 4\sum_0^\infty \frac{1}{(2m+1)^2} - D't + 2\sum_1^\infty \frac{(-1)^n}{n^2} e^{-n^2D't} + 4\sum_0^\infty \frac{1}{(2m+1)^2} e^{-(2m+1)^2D't} \quad (12)$$

The numerical solution of eq. 12 is given in Table I. *Although eq. 12 was derived for a model in which the diffusion of interstitial metal ions or atoms controls the oxidation rate, it is equally applicable to reactions in which the diffusion of interstitial anions, of cation vacancies of anion vacancies or of the corresponding neutral species are rate-controlling.* Only the interpretation of the concentrations, C_0 and C_1, differs from case to case.

Experimentally, one measures Δ by following the oxygen uptake (Δ_N) upon re-admission of oxygen. The relation of Δ_N to Δ depends on the nature of the defect and will be discussed below. It should perhaps be pointed out that the treatment assumes the film thickness does not change appreciably during the experiment. In practice, this means that eq. 12 applies only if $\Delta << X/\Omega$ where Ω is the volume of oxide per metal ion.

When $t << X^2/D$, eq. 12 reduces to a simple linear equation in $t^{1/2}$, *i.e.*

$$\Delta = Bt^{1/2}\ (t << X^2/D) \quad (13)$$

where

$$B = 1.12D^{1/2}C_0 \quad (13a)$$

As t becomes large, eq. 12 reduces to a linear equation in t

$$\Delta = Q + Rt\ (t > X^2/2D) \quad (14)$$

where

$$Q = \frac{XC_0}{3} \quad (14a)$$

and

$$R = \frac{DC_0}{X} \quad (14b)$$

TABLE I

NUMERICAL SOLUTION FOR THE DIFFUSION EQUATION OF INTERRUPTED KINETICS, EQ. 12

$$\frac{\Delta}{XC_0} = \frac{2}{\pi^2}\sum_1^\infty \frac{(-1)^n}{n^2} + \frac{4}{\pi^2}\sum_0^\infty \frac{1}{(2m+1)^2} + \frac{Dt}{X^2} - \frac{2}{\pi^2}\sum_1^\infty \frac{(-1)^n}{n^2} e^{-n^2D\pi^2t/X^2} - \frac{4}{\pi^2}\sum_0^\infty \frac{1}{(2m+1)^2} e^{-(2m+1)^2D\pi^2t/X^2}$$

Dt/X^2	$(Dt/X^2)^{1/2}$	Δ/XC_0
0.02026	0.1422	0.159
.03040	.1744	.195
.04053	.2011	.226
.05066	.2250	.253
.06079	.2466	.276
.07092	.2664	.299
.08115	.2845	.320
.09118	.3020	.339
.1013	.3183	.357
.1114	.3338	.375
.1216	.3485	.392
.1317	.3629	.408
.1418	.3765	.423
.1621	.4026	.453
.1824	.4272	.480
.2026	.4501	.507
.2229	.4720	.532
.2432	.4930	.556
.2837	.5325	.603
.3242	.5694	.647
.3647	.6038	.691
.4053	.6366	.733
.5066	.7117	.837
.6079	.7795	.939
.7092	.8422	1.041
.8105	.9002	1.142
.9118	.9549	1.243
1.0132	1.0065	1.344

Therefore, while direct oxidation rate measurements can at best give the product, DC_0, eq. 4 or eq. 14b, the interrupted rate measurements give additional expressions for C_0 and $D^{1/2}C_0$. A separation of D and C_0 is thus effected; in terms of the parameters of eq. 13 and 14 one obtains

$$C_0 = \frac{0.8}{X}\frac{B^2}{R} \quad (15)$$

$$C_0 = \frac{3Q}{X} \quad (16)$$

$$D = 1.25\left[\frac{RX}{B}\right]^2 \quad (17)$$

One can combine eqs. 15 and 16 to obtain a necessary condition for the mechanism under consideration

$$0.267B^2/QR = 1 \quad (18)$$

III. Experimental Procedure

The procedures of the preceding article were employed. {110} samples were used exclusively, although experiments on {100} and {111} samples were shown to give qualitatively similar results. The reactions were interrupted by evacuating the excess gaseous O_2 and closing off the system for times varying from 1 hour to 3 days, depending on the estimate for X^2/D. This value of time must be exceeded if the concentration distribution of Fig. 1b is to be established.

IV. Results

A. General Form of the Interrupted Kinetics.—A sample was oxidized at 342° and $P_{O_2} = 0.3$ mm. until the total oxygen uptake (N) was 5.76×10^{17} oxygen atoms cm.$^{-2}$. The sample chamber was evacuated and closed off for 15 hours without changing the temperature. Oxygen was then readmitted with the results shown in Fig. 2. The expectations of the diffusion model are qualitatively fulfilled. A rapid uptake of oxygen, proportional to $t^{1/2}$, is observed at the outset, but the rate gradually diminishes and becomes equal to the value observed just before the interruption. Contrary to expectation, however, the intercept of Fig. 2b, which will be designated Z, is not zero.

The experiment was again interrupted under identical conditions with identical results. For control purposes, the reaction was interrupted for less than three minutes. When O_2 was readmitted, the rate prior to the interruption was immediately resumed. The quantity Z will for reasons to be discussed below, be treated as a characteristic constant for each experiment, which must be added to the value of Δ_N in the theoretical equations. In the present experiment, $Z = 2.84 \times 10^{15}$ oxygen atoms cm.$^{-2}$. Utilizing the parameters defined in eq. 13 and 14, one obtains from Fig. 2: $R = 4.92 \times 10^{13}$ oxygen atoms cm.$^{-2}$ min.$^{-1}$, $B = 8.60 \times 10^{14}$ oxygen atoms cm.$^{-2}$ min.$^{-1/2}$, and $Q = 4.04 \times 10^{15}$ oxygen atoms cm.$^{-2}$ (obtained by subtracting Z from the intercept of Fig. 2a). The necessary condition expressed by eq. 18 is satisfied since $0.267B^2/QR = 0.994$.

A complete quantitative test of eq. 12 was made by substituting B, Q and R into eq. 15–17. The values of C_0X and D/X^2 so obtained were substituted directly into the parameters of eq. 12 which form the headings in the numerical solution in Table I. This gives the values of Δ_N corresponding to the entire range of t. Adding Z to Δ_N and plotting the results in Figs. 2a and 2b generates the solid curves drawn in these figures.

The excellent description of the data by eq. 12 is particularly noteworthy since it requires that three independent experimental parameters—B, Q and R—be given by eq. 15–17 which contain only two adjustable theoretical parameters—XC_0 and D/X^2.

In order to obtain D and C_0, one must know the thickness X. In the present case X is estimated from the total oxygen uptake, $N = 5.8 \times 10^{17}$ oxygen atoms/cm.^{2} through the relation $X = \Omega N$. The quantity $\Omega = (M/zN_0Y)$, where M and ρ are the molecular weight and density of the oxide film; z comes from the formula of the oxide, M_yO_z; and N_0 is Avogadro's number. Thus for In_2O_3, Ω is calculated to be 2.14×10^{-23} cm.^{3}/oxygen atom. It must be noted that the gross geometric surface of the sample has been used to normalize all of the oxygen uptake measurements in this paper. Since the true area is larger by a factor, F (the roughness factor), the values of both N and Δ_N must be suitably corrected if true values of X, D and C_0 are to be obtained. Furthermore, the value of C_0 which is obtained when Δ_N is substituted for Δ in eq. 11–14 is actually C_0^N (oxygen atoms per cm.^{3}). To convert C_0^N to C_0, one must use the factor, β, where $\beta = y/z$ (from the formula M_yO_z) if the defect is an M atom or vacancy, while $\beta = 1$ if the defect is an oxygen atom or vacancy. In summary, therefore, if $\{D/X^2\}$ and $\{XC_0\}$ are the values obtained from eq. 15–17 using B, Q and R in units of oxygen atoms per unit geometric surface area, then

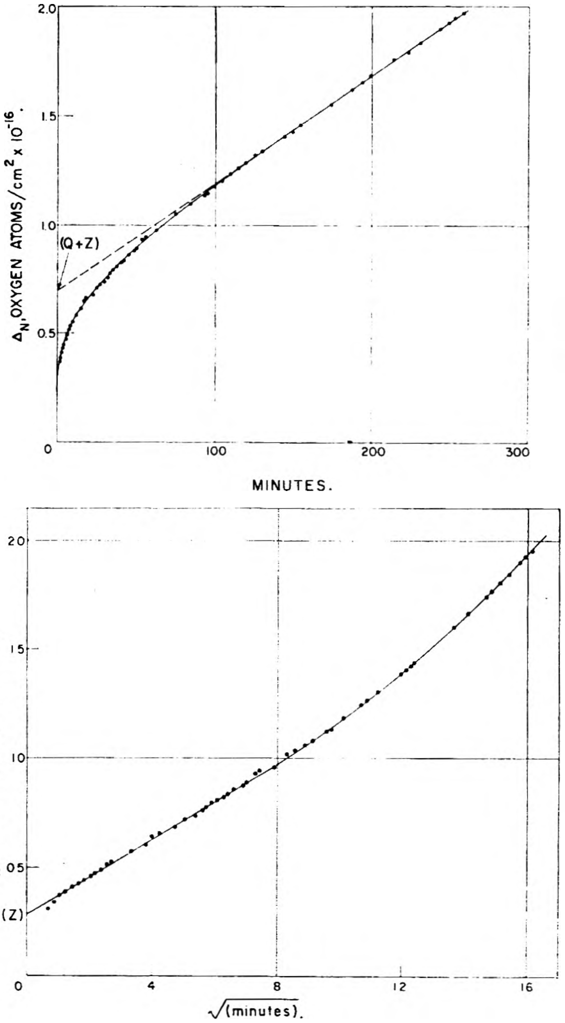

Fig. 2.—Kinetics of oxygen sorption by InSb after interruption of oxide growth. Previous oxygen uptake = 5.76×10^{17} atoms/cm.^{2}, corresponding to *ca.* 950 Å. $T = 342°$, $P_{O_2} \sim 0.3$ mm. (a) Data plotted *vs.* t. (b) Data plotted *vs.* $t^{1/2}$. The solid lines are calculated from eq. 12 using $XC_0 = 1.202 \times 10^{11}$ and $D/X^2 = 4.09 \times 10^{-3}$ (see eq. 19 for conventional units).

$$X = (\Omega/F)N$$
$$D = \{D/X^2\} \times \left(\frac{\Omega N}{F}\right)^2 \qquad (19)$$
$$C_0 = \{XC \times \left(\frac{\beta F}{\Omega N}\right)$$

For chemically polished surfaces of InSb, $F \sim 1.3$, and if the mobile defects in In_2O_3 are indium atoms, ions, or vacancies, $\beta = 2/3$.

One thus obtains for the experiments in Fig. 2

$X \approx 9.5 \times 10^{-6}$ cm.
$D \approx 6.15 \times 10^{-16}$ cm.^{2}/sec.
$C_0 \approx 1.05 \times 10^{21}$ indium defects per cm.^{3}

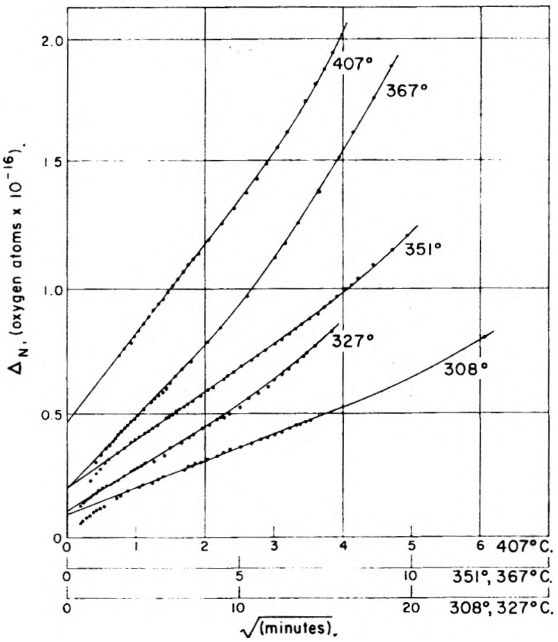

Fig. 3.—Influence of temperature upon kinetics of interrupted oxidation. Experiments performed on a single sample, previously oxidized to $N = 5.3 \times 10^{17}$ oxygen atom/cm.^{2} Sequence followed: 367, 327, 351, 308, 407°. Solid lines calculated from eq. 12.

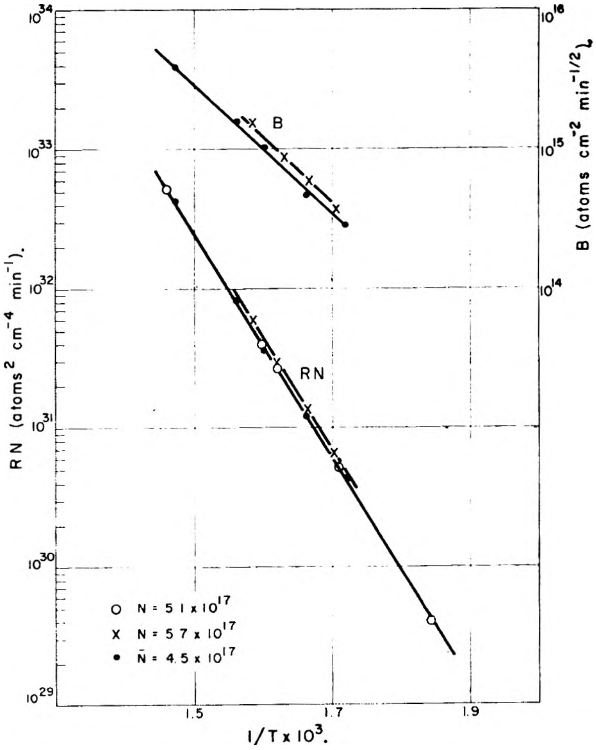

Fig. 4.—Variation of RN and B with temperature. The results on three separate samples are included. Oxides were formed in each case at 352–358°. $\bar{N}$ is the average value of N for the interrupted experiments.

The high value of C_0 eliminates space charge as a significant factor in the reaction. If the indium atoms are not ionized, $z_i = 0$ in eq. 1 and an electrostatic field in the film cannot influence the diffusion. If the atoms are ionized, the electron concentration greatly exceeds the value necessary to confine the space-charge to negligibly thin boundary layers (eq. 6).

B. Variation of Interrupted Rate Parameters with Temperature.—Interrupted rates were measured between 309 and 407° for a film formed at 367° to $N = 5.3 \times 10^{17}$ oxygen atoms/cm.^{2}. The experimental data are shown in Fig. 3. The solid lines are, again, theoretical curves drawn to eq. 12, so that the mechanism under discussion applies to the entire range of data.

The variations of RN and B with temperature are illustrated in Fig. 4. The results of experiments on three different samples are shown. The exponential dependence of RN and B upon $1/T$ is unequivocal. In appropriate units, one obtains

$$B = 2.61 \times 10^{22} \exp(-21{,}000/RT) \text{ oxygen atoms/min.}^{1/2}\text{/cm.}^2 \quad (20)$$

$$RN = 2.96 \times 10^{10} \exp(-36{,}000/RT) \text{ (oxygen atoms)}^2\text{/min./cm.}^4 \quad (21)$$

From eq. 15 and 17 one obtains, in keeping with the discussion of Section IVA

$$C_0 = 9.4 \times 10^{22} \exp(-5400/RT) \text{ indium defects cm.}^{-3} \quad (22)$$

$$D = 0.0078 \exp(-31{,}200/RT) \text{ cm.}^2\text{/sec.} \quad (23)$$

C. Variation of Interrupted Rate Parameters with Film Thickness.—While the thermal diffusion mechanism successfully describes the form of the interrupted rates over a broad temperature range for a given film thickness, it cannot account for the variation of the rate parameters as the film becomes thicker. The model predicts that R, the diffusion-limited rate, should vary as $1/X$ ($\epsilon = 1$); it has been established however that the rate drops more rapidly than this ($\epsilon > 1$). The model predicts, furthermore, that B should be independent of X; the following results establish, however, that B diminishes steadily with increasing X.

An oxidation was interrupted at several stages of film growth. The data obtained upon resumption of reaction at each stage are shown in Fig. 5. The formal predictions of the thermal diffusion model are separately satisfied in all but the first stage, the solid lines being drawn to eq. 12.

The interrupted rate parameters are summarized in Table II. $0.267B^2/QR$ is close to unity in each case. B and RN diminish systematically with increasing X. The decline cannot be attributed to D or C_0 alone, since both decline.

D. The Effect of the Interruption Conditions upon the Rate Parameters.—Provided that the time of interruption, t_i, is long enough to permit equilibrium of the interstitial atoms throughout the film, *i.e.*, $t_i > X^2/D$, the basic diffusion parameters should be unaffected by further increases in t_i. An experiment was performed in which t_i was increased successively from 4.5 hours to 16 hours for a sample in which X^2/D was estimated to be 3.0 hours. The results, shown in Fig. 6, confirm the invariance of the diffusion parameters. The parameter Z, however, shows a definite time-dependence.

Another experiment was designed to examine the effect of the temperature of interruption, T_i, upon the kinetics. During the interruption of a reaction being conducted at 342°, the temperature was

TABLE II

VARIATION OF INTERRUPTED RATE PARAMETERS WITH FILM THICKNESS, 367°

N		× 10^{17} oxygen atoms/cm.^{2}	1.70	3.73	5.02	7.11	9.43
Z		× 10^{15} oxygen atoms/cm.^{2}	2.62	2.46	2.73	3.18	2.46
B		× 10^{15} oxygen atoms/cm.^{2}/min.$^{1/2}$	1.53	1.34	1.14	0.97	0.89
Q		× 10^{15} oxygen atoms/cm.^{2}	3.40	3.38	4.10	5.13	6.77
R		× 10^{14} oxygen atoms/cm.^{2}/min.	3.18	1.43	0.87	0.502	0.318
RN		× 10^{31} oxygen atoms^2/cm.^{4}/min.	5.39	5.33	4.36	3.57	2.99
$0.267B^2/QR$			0.59	0.99	0.96	0.97	0.99
$\{XC_0\}$	eq. 15	× 10^{16} oxygen atoms/cm.		1.01	1.20	1.49	1.99
$\{D/X^2\}$	eq. 17	× 10^{-3} min.$^{-1}$		14.2	7.25	3.35	1.59
X	eq. 19	× 10^{-6} cm.	2.80	6.15	8.28	11.73	15.56
D		× 10^{-15} cm.^{2}/sec.		8.90	8.25	6.56	6.41
C_0		× 10^{20} indium defects/cm.^{3}		11.1	9.65	8.45	8.50

raised to 494° for two hours before equilibrating for 16 hours at 342°. The results are shown in Fig. 7. Ideally the diffusion kinetics should have been independent of this treatment, but its severity apparently introduces irreversible changes in the oxide structure, and small changes in B and R were noted. The principal effect is again associated, however, with the parameter, Z.

These results demonstrate that the apparent decreases in D and C_0 which are observed with increasing extent of reaction, are not related to aging of the oxide, but are truly dependent upon the oxide thickness.

E. The Parameter Z.—It was assumed at the outset that the parameter Z given by the intercept of the Δ_N *vs.* $t^{1/2}$ curves, reflects a reaction of the oxide which proceeds parallel with, but independent of, the slower diffusion reaction described by eq. 12. A striking confirmation of this view lies in the results of the preceding section: substantial increases in Z were observed when the time and temperature of the interruptions were increased, while the parameters of eq. 12 were virtually unaffected.

The noteworthy features of Z which are evident from all of the foregoing results are: (i) the observed values of Z lie in the range 1–5 × 10^{15} oxygen atoms/cm.^{2}, corresponding to 1.3–8 oxygen atoms/surface atom. It is thus evident that the reaction which underlies Z cannot be a simple chemisorption of oxygen on the surface atoms of the oxide; (ii) the reaction occurring during the interruption which sets the stage for Z is time- and temperature-dependent; (iii) the reaction in which Z is actually measured is complete within one minute at the higher temperatures and on the thinner films, while it is measurably slower at the lower temperatures and on the thicker films.

V. Discussion

The excellent description of the experimental data given by eq. 12 over a broad range of temperature and film thickness leaves little doubt that the oxidation of InSb above 300° is controlled by the diffusion of defects through the growing oxide film. The diffusion equation itself cannot be used to identify the defect, since the equation applies equally to metal or oxygen ions, atoms, or vacancies.

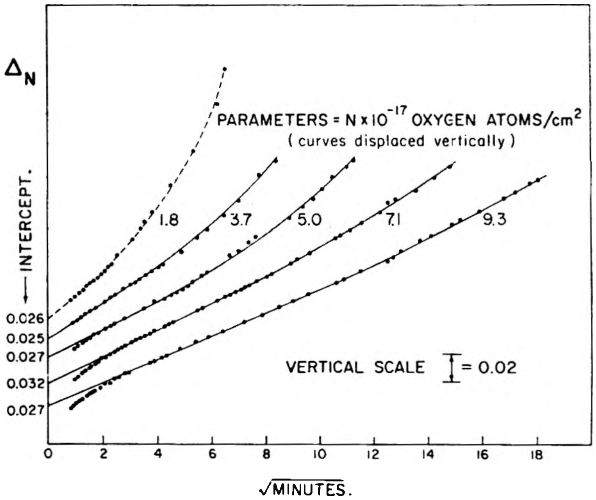

Fig. 5.—Variation of interrupted rate parameters with film thickness. Key = N × 10^{-17} oxygen atoms/cm.^{2}. For all but N = 1.8 × 10^{17}, the solid lines are calculated from eq. 12. T = 367°. The oxide thickness is obtained by multiplying N by Ω/F = 1.64 × 10^{-23} (section IVA). Thus the measurements cover the range 300–1500 Å.

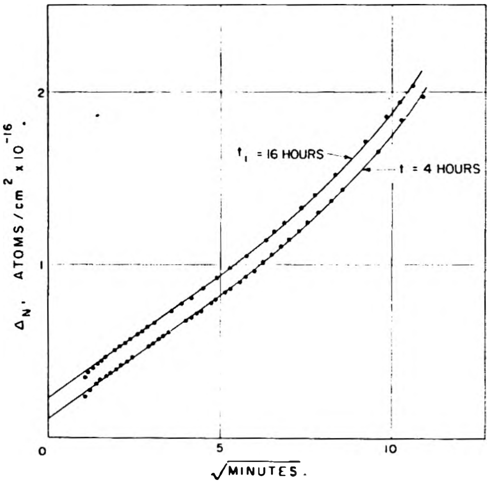

Fig. 6.—The effect of the interruption time: lower curve, oxidation at 342° resumed after 4.5 hours interruption; upper curve, after 16 hours interruption.

It was shown by Rupprecht[7] that the conductivity of In_2O_3 decreases with increasing oxygen pressure, and increases upon heating a sample under vacuum. This can only be true if In_2O_3 is a metal-excess semiconductor, and the mobile defect must, accordingly, be either oxygen ion (or atom) vacancies or interstitial indium ions (or atoms). For

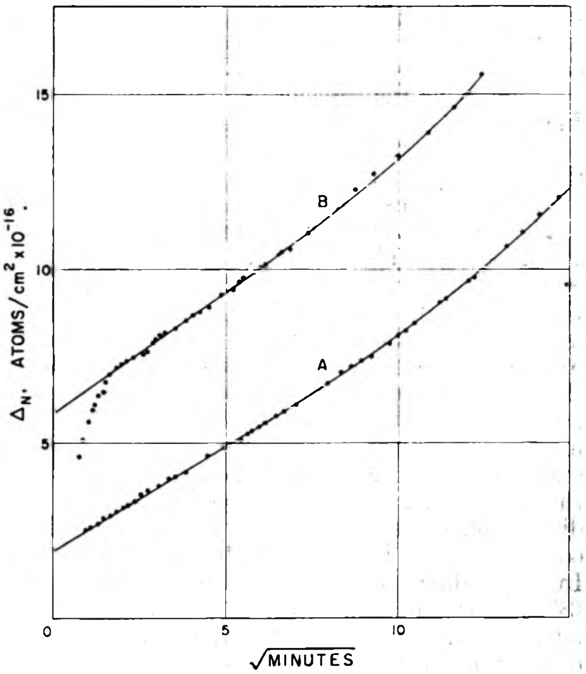

Fig. 7.—The effect of the interruption temperature: (a) oxidation at 342° was resumed after interrupting the reaction for 16 hours at 342°; (b) oxidation at 342° was resumed after interrupting the reaction for 2 hours at 494° followed by 16 hours at 342°.

reasons which will become clear, it has been assumed that the latter are the predominant defects in In_2O_3.

The Diffusion Coefficient D.—The fundamental parameters of the diffusion equation—the diffusion coefficient D and the equilibrium concentration C_0 of the diffusing species—are given by eq. 22 and 23. The physical plausibility of these equations provides additional support for the model. Thus, the expression for D is

$$D = 0.0078 \exp(-31{,}200/RT)\text{cm.}^2/\text{sec.} \qquad (23)$$

This may be interpreted through the use of the absolute rate theory[10] which gives

$$D = \frac{kT}{h}\frac{d^2}{\beta}e^{\Delta S^*/R}\,e^{-\Delta H^*/RT} \qquad (24)$$

where d is the jump distance of an interstitial particle from one position into one of the β equivalent positions surrounding it, while ΔS^* and ΔH^* are the entropy and enthalpy of activation for the jump, and the other symbols have their usual meaning. It has been shown theoretically that ΔS^* must have a small positive value.[11] This requirement is met since, by taking d = 2–3 Å. and β = 2–6, one obtains $0 < \Delta S^* < 4$ e.u. upon comparing eq. 23 and 24. The activation enthalpy is difficult to access theoretically but the value, $\Delta H^* = 31{,}000$ cal., is certainly not unreasonable.

The Concentration C_0.—The experimental expression for C_0 is

$$C_0 = 9.4 \times 10^{22} \exp(-5400/RT) \text{ indium defects cm.}^{-3} \qquad (22)$$

which gives $C_0 \sim 10^{21}$ in the temperature range of this study. This high value, which corresponds to 5% occupation of the available interstitial sites, complicates the interpretation of eq. 22. By examining certain limiting models, however, it can be shown that the preexponential factor in eq. 22 is of the proper magnitude. Some light is also shed on the interpretation of the exponential term, which is the key to understanding the relative rates of oxidation of In and InSb presented in the preceding article.

Consider the transfer of an indium atom from InSb to an interstitial position in In_2O_3 by the reaction

$$\text{InSb(s)} = \text{In}(\text{In}_2\text{O}_3) + \text{Sb(s)} \qquad (25)$$

This can be followed by the ionization of $In(In_2O_3)$

$$\text{In}(\text{In}_2\text{O}_3) = \text{In}^{+z}(\text{In}_2\text{O}_3) + z \text{ electrons} \qquad (26)$$

If n_0, n_+, and n_e are the equilibrium concentration of $In(In_2O_3)$, In^{+z} (In_2O_3) and conduction electrons, respectively, and N is the total concentration of interstitial positions in In_2O_3, one has

$$n_0 \approx f_0 N \exp(-w_0/kt) \qquad (27)$$

$$n_+ \approx f_+ n_0 \left[\frac{\Gamma}{n_e\gamma_e}\right]^z \exp(-w_+/kt) \qquad (28)$$

$$n_e = zn_+ \qquad (29)$$

where f_0 and f_+ are factors which relate to the change of the vibrational entropy in the intermediate vicinity of an interstitial. γ_e is the activity coefficient and Γ is the partition function of conduction electrons in In_2O_3. γ_e increases with n_e and can be written[12]

$$\gamma_e = n_e^y \qquad (30)$$

When $n_e/\Gamma < 1$, $y \sim 0$ and $\gamma \sim 1$; but when $n_e/\Gamma \gtrsim 1$, $y > 0$ and $\gamma_e > 1$. Substituting (27), (29) and (30) into (28) one obtains

$$n_+ \approx \left[\frac{f_0 f_+ N\Gamma^z}{z^{z(1+y)}} \exp(-(w_0 + w_+)/kt)\right] \frac{1}{1 + z(1+y)} \qquad (31)$$

The quantities w_0 and w_+ are the energies of reactions 25 and 26, respectively. As a general rule w_0 is positive, but w_+ will have either a much smaller positive value or can be negative, *i.e.*

$$w_0 > w_+ \qquad (32)$$

The relative magnitudes of n_0 and n_+ depend upon Γ, which in turn depends on the band structure of In_2O_3 and the energy levels associated with the interstitial atoms. These are not known, but the consequences of three limiting cases are of interest. In each case a simple band model is assumed, *i.e.*, the energy bands are spherical and the (kinetic) energy of electrons is proportional to the square of the wave vector.[13]

Case I.—The interstitial atoms depress z eigenstates from the top of the conduction band to a discrete level just below the conduction band. In this case[13]

$$\Gamma = 2\left[\frac{2\pi m^* kt}{h^2}\right]^{3/2} = 5.5 \times 10^{19}\left(\frac{m^*}{m_0}\right)^{3/2} \text{ cm.}^{-3} \text{ at } 600°\text{K.} \qquad (33)$$

---

[10] S. Glasstone, K. J. Laidler and H. Eyring, "Theory of Rate Processes," McGraw-Hill Book Co., New York, N. Y.

[11] C. Zener, "Imperfections in Nearly Perfect Crystals," ed. W. Schockley, *et al.*, John Wiley and Sons, Inc., New York, N. Y., 1952, p. 289.

[12] A. J. Rosenberg, *J. Chem. Phys.*, to be published.

[13] F. Seitz, "Modern Theory of Solids," McGraw-Hill Book Co., New York, N. Y., 1940, p. 271 ff.

where m^* is the effective mass of electrons in the conduction band of In_2O_3, m_0 is the free electron mass, and the other symbols have their usual meaning. If $(m^*/m_0) < 1$, then $\Gamma < 5 \times 10^{19}$; by using eq. 27 through 31, it can be shown that n_0 would then be impossibly high if n_+ were identified with the experimental values of C_0. Thus the diffusing particles in this case would necessarily be indium atoms and eq. 22 would be identified with eq. 27.

Case II.—This is identical to Case I except that (m^*/m_0) is taken to exceed 10, giving $\Gamma > 10^{21}$ cm.$^{-3}$, $\gamma_e \sim 1$, and $y = 0$. The predominant defect is In^{+z} and eq. 22 must be compared with eq. 31 using $y = 0$.[12]

Case III.—It is assumed here that the energy levels associated with the interstitials broaden at high concentrations and form a band which overlaps the conduction band. In this model Γ becomes proportional to n_e and the term in the brackets of eq. 28 becomes nearly constant. All of the interstitials may be regarded as ionized and their concentrations will be given by eq. 28 with $\gamma_e \simeq 1$.[14]

Assuming that $N \sim 3 \times 10^{22}$ cm.$^{-3}$ and that f_0 and f_+ are near unity, the pre-exponential factors in the expressions for C_0 which is predicted in each of the above cases, lies within an order of magnitude of 10^{22} cm.$^{-3}$. In view of the uncertainties involved, the agreement with the experimental value, 9×10^{22} cm.$^{-3}$ (eq. 22) is not unsatisfactory.

Identity of the Mobile Defect.—Cases II and III predict that the predominant defect is an atom while Case I predicts that it is an ion. In the preceding paper,[2] it was shown that the relative rates of oxidation of In and of InSb can be interpreted quantitatively if it is assumed (1) that the diffusing species is In^{+3} (ref. 15) and (2) that the electron concentration can be used in mass action formalism. These assumptions also appear necessary to explain Rupprecht's observation that the conductivity of thin films of In_2O_3 is related to the $-^3/_{16}$ power of oxygen pressure at high temperatures.[7] The two conditions are satisfied simultaneously only in Case II. The evidence thus favors a mechanism in which the interstitial diffusion of trivalent indium ions controls the rate of growth of an In_2O_3 film characterized by a large effective mass for electrons.

The validity of Case II and the consequent applicability of eq. 31 also tend to explain what appears to be an unreasonably small value—+5400 cal./mole according to eq. 22—for the enthalpy accompanying the transfer of an indium atom from InSb to In_2O_3. According to eq. 31 the value appearing in eq. 22 corresponds to only one-fourth of the real value. The latter then is ∼22,000 cal./mole which seems more reasonable.

The Role of Antimony in the Reaction and the Parameter *Z*.—The model also provides a plausible explanation for the time- and temperature-dependent quantity, Z. While the simple model does not allow for the dissolution of antimony in the oxide film, it is clear from the dissolution studies in the preceding article that some antimony does enter the film. During the reaction the diffusion of indium is preferred, and little antimony reaches the steadily advancing oxide–oxygen interface. When the reaction is interrupted, however, the flow of indium soon stops, and antimony can diffuse to the outer surface. There it can displace oxygen from In_2O_3 yielding elemental indium and the volatile $(Sb_2O_3)_2$ which distils to the cold walls near the entry to the furnace.[16] When oxygen is readmitted to the system the accumulated indium will react rapidly. This accounts in a quantitative way for the phenomena associated with the parameter Z.

The other kinetic aspects of the oxidation of InSb which cannot be accounted for by the diffusion of indium through pure In_2O_3 are the apparent decrease of both D and C_0 with film thickness, the anisotropy and the very slight pressure dependence of the rate, and the fact that doping the substrate with either Cd or Te increases the rate. These effects are small compared, for instance, with the 10,000-fold variation of rate between 308 and 494° which can be adequately described by a single activation energy in the ideal model, but they are, nevertheless, significant. While no really convincing treatment is forthcoming, it is not unreasonable to suppose that the presence of antimony, both in the In_2O_3 film and in the underlying crystalline layer, can influence the kinetics. It is probable, for instance, that the rate anisotropy is related in some manner to epitaxial growth of antimony patches on the InSb surfaces. The final proof lies, however, in a comparison with precise results on the oxidation of elemental indium, and further speculation will be postponed until these data become available.

---

(14) γ_e really has no meaning here since the Fermi level becomes independent of n_e (*cf.* ref. 12).

(15) The choice of In^{+2} would have given results within experimental error.

(16) A. J. Rosenberg, A. A. Menna and T. P. Turnbull, *J. Electrochem. Soc.*, **107**, 196 (1960).

INVESTIGATION OF COLLOIDAL HYDRATED CALCIUM SILICATES. I. SOLUBILITY PRODUCTS

By S. A. Greenberg, T. N. Chang and Elaine Anderson

Contribution from Portland Cement Association Research and Development Laboratories, Skokie, Ill.

Received March 10, 1960

The solubility products of these colloidal substances were evaluated by determining the calcium ion and silicic acid concentrations and pH values of the solutions and applying these data to the activity product equations: (1) $K_{sp_1} = a_{Ca^{++}}a_{H_2SiO_4^{--}}$ and (2) $K_{sp_2} = a_{Ca^{++}}a^2_{H_3SiO_4^-}$. Hydrated calcium silicates with mole ratios CaO:SiO$_2$ between 0.8 and 1.5:1 were prepared at 85°. The data for the 1.0, 1.2 and 1.5:1 mole ratio hydrates show that the pK_{sp_1} is 7.0 ± 0.1 at 25°. Equation 2 agrees with data for the 0.8:1 hydrate and the pK_{sp_2} value is 8.5 ± 0.1. As expected, a 1:1 hydrate prepared hydrothermally at 186° exhibits a higher pK_{sp_1} value of 7.3 ± 0.1. The K_{sp_1} values are assigned to the equilibrium between solid CaH_2SiO_4 and water. Hydrates with CaO:SiO$_2$ mole ratios greater than one are assumed to contain calcium hydroxide in solid solution and an equilibrium exists between the calcium hydroxide in aqueous solution and the portion dissolved in the solid CaH_2SiO_4.

Introduction

The solubilities of hydrated calcium silicates have been examined extensively,[1] but only Roller and Erwin[2] estimated a solubility product for hydrated calcium silicates. Because of the increase in available information on hydrated calcium silicates[3,4,5] and on silicic acid,[6] it has become possible to characterize the structures better and to use more accurate dissociation constants for silicic acid for the evaluation of the solubility products of the various calcium silicates.

Knowledge of the solubility products of hydrated calcium silicates is essential to an understanding of the reaction between solid tricalcium silicate and water. This reaction usually is assumed to be the most important one proceeding in fresh concrete mixtures.

Hydrated calcium silicates synthesized below 100° are colloidal and exhibit only a few X-ray diffraction lines. The variety of concentrations of calcium oxide, silica and water in these hydrates is broad. Only the hydrates with mole ratios CaO:SiO$_2$ between 0.8:1 and 1.5:1 were examined in this study. No effort was made to establish the upper or lower limits of the CaO:SiO$_2$ mole ratios. Evidence will be provided in this paper to support the view that hydrated calcium silicates with CaO:SiO$_2$ mole ratios above unity contain calcium hydroxide in solid solution in CaH_2SiO_4. Therefore, on the basis of the evidence obtained in the present study two equilibria appear to be involved in the calcium silicate hydrate–water system. One is that of the solubility of solid CaH_2SiO_4 and the other involves the distribution of calcium hydroxide between solid CaH_2SiO_4 and aqueous solution.

In the present study the hydrated silicates were synthesized from calcium oxide, silica and water mixtures at 85°. Products with mole ratios of CaO:SiO$_2$ of 0.8:1, 1:1, 1.2:1 and 1.5:1 were prepared. The solubilities of the products in calcium hydroxide solutions of various concentrations were determined by analyzing the solutions for calcium and soluble silicic acid concentrations and measuring the pH values. From these data the solubility products were derived. For comparison a well crystallized 1:1 hydrate[3,7] and β-wollastonite CaSiO$_3$[3,7,8] were synthesized and the solubility products of these substances were determined.

Experimental

A. **Materials.**—Mallinckrodt special bulky and standard luminescent silicas, Baker AR grade calcium hydroxide and calcium carbonate, and distilled water were used for the preparation of the hydrated calcium silicates.

B. **Preparation of Silicates.**—Weighed calcium carbonate samples were calcined at 1050° for two hours. The calcium oxide formed on ignition was slaked and then vigorously agitated for ten minutes with 400 ml. of distilled water in a Waring Blendor. The amount of special bulky silica to produce the desired mole ratio of calcium oxide to silica was added to 400 ml. of distilled water in a stainless steel beaker. While the CaO was mixed with water, the silica suspension was heated (>85°) in a water-bath held at 100°. The slaked calcium oxide suspension was added, with stirring, to the hot silica suspension and the resulting mixture was stirred again after 20 minutes. The mixture was allowed to react at a temperature greater than 85° for a total of three hours. The products then were filtered through a medium sintered glass filter and washed first with methanol and then with acetone. Finally, the products were dried in a vacuum oven under reduced pressure at 60°.

In the case of an additional equimolar hydrate (1:1A) the above procedure was followed, but Baker AR grade calcium hydroxide was used directly.

A well crystallized equimolar hydrate was prepared by autoclaving the wet, unwashed 85° hydrate at 186° for 24 hours. The material was washed and dried as previously described. The β-wollastonite was prepared from the pressure hydrated material by calcining the dried product at 1050° for two hours.

Table I is a summary of the experimental conditions used in the preparations of the hydrates and of the temperatures at which the solubility measurements were made (Column 4).

C. **Solubility Study Procedure.**—Gram samples of each of the hydrates were mixed with 100 ml. of calcium hydroxide solution varying in concentration from zero to saturation (0.02 molar) and brought to equilibrium in a constant temperature bath. The samples were shaken in polyethylene bottles for at least seven days at solution temperatures from 25 to 40° (listed in Table I, Column 4). Roller and Erwin[2] have reported that after three days no appreciable change in concentration occurs. It is presumed that after the hydrates were agitated for several days the reaction was essentially complete and no changes in the compositions of the solutions would occur. After equilibrium had been established the solutions were drawn through a fine sintered glass filter in a

---

[1] For review see H. H. Steinour, *Chem. Revs.*, **40**, 391 (1947).

[2] P. S. Roller and G. Erwin, *J. Am. Chem. Soc.*, **62**, 461 (1940).

[3] L. Heller and H. F. W. Taylor, "Crystallographic Data for the Calcium Silicates," Her Majesty's Stationery Office, London, 1956.

[4] K. G. Krasilnikov, "Reports of Symposium on the Chemistry of Cements," edited by P. P. Budnikov, *et al.*, State Publication of Literature on Structural Materials, Moscow, 1956.

[5] Stephan Brunauer and S. A. Greenberg, "Proceedings of the Fourth International Symposium on the Chemistry of Cement," Washington, D. C., 1960.

[6] S. A. Greenberg, *J. Am. Chem. Soc.*, **80**, 6508 (1958).

[7] S. A. Greenberg, This Journal, **58**, 362 (1954).

[8] H. F. W. Taylor *Acta Cryst.*, **10**, 767 (1957).

Table I

Experimental Conditions

1 Sample no.	2 $CaO:SiO_2$	3 Preparation temp., °C.	4 Solution temp., °C.	5 Remarks
1	0.8:1	85	25	...
2	1:1	85	25, 40	...
3	1:1A	85	30	$Ca(OH)_2$ used directly
4	1.2:1	85	25	...
5	1.5:1	85	25	...
6	1:1	186	30	Prepared by autoclaving sample No. 3
7	1:1	1050	30	Prepared by ignition of sample No. 6

system open to the atmosphere only through a tube containing a mixture of sodium hydroxide on asbestos (Ascarite) and anhydrous $Mg(ClO_4)_2$ (Anhydrone) to remove carbon dioxide. The *p*H values of the filtrates were measured immediately. The filtrates were examined also for calcium ion and silicic acid concentrations. Filtrates were stored in polyethylene bottles at all times.

D. **Analytical.**—Calcium was determined by titration with Versene.[9] Analysis for silicic acid was made colorimetrically on the blue reduced form of the silico-molybdate complex by the method of Bunting.[10]

E. **Equipment.**—The *p*H measurements were performed with a calomel reference electrode, a glass measuring electrode, and a Leeds and Northrup No. 7664 *p*H meter. A Beckman DU spectrophotometer was available for transmission measurements. The solutions were equilibrated in a constant temperature water bath held to ±0.02°.

The X-ray diffraction patterns were made with a Norelco Diffraction unit using copper Kα radiation at 40 kilovolts and 20 milliamps. Patterns were recorded on a Brown instrument through a goniometer circuit.

Results

Nature of the Silicates.—The structure and properties of the colloidal products were examined in the present study by X-ray diffraction methods and water adsorption techniques.

The X-ray patterns for samples I through 5 (Table I) exhibited relatively strong 3.06 Å. spacings and weak 2.81 and 1.83 Å. spacings characteristic of these poorly crystallized hydrated calcium silicates. For samples 6 and 7 the patterns of well crystallized tobermorite and β-wollastonite,[3] respectively, were found.

The surface areas of samples 1, 2, 4 and 5 (Table I) were measured by water adsorption. The BET areas[11] were determined at 25° by gravimetric methods.[12] The surface areas of the samples with mole ratios of $CaO:SiO_2$ of 0.8:1, 1:1, 1.2:1 and 1.5:1 were 330, 280, 260, and 275 sq. m. per gram ignited weight of sample. In a previous paper[13] it was reported that the nitrogen adsorption surface area of a 1:1 mole ratio hydrate like sample 2 was 54 sq. m./g. Thus nitrogen and water adsorption results differ markedly. These differences have been attributed by Kalousek[14] to the penetration of the layers of the crystals by water, but not by nitrogen. However, Brunauer, Kantro and Copeland[15] have reported evidence that water does not penetrate the layers and they ascribe the difference to the fact that the hydrated calcium silicate sheets may be aggregated or rolled into fibers which may cause the formation of regions on the surface which are not available to nitrogen.[5] It is apparent that the surface areas of samples 2, 4 and 5 do not vary markedly from the average of 270 sq. m./g. On the other hand sample 1 with a $CaO:SiO_2$ mole ratio of 0.8:1, which is the lowest in this group, shows a surface area of 330 sq. m./g. The free energy states and consequently the solubilities of the samples would be expected to be a function of the surface areas.

A sample of well-crystallized hydrate like sample 6 has been reported[7] to exhibit a nitrogen adsorption surface area of less than 90 sq. m./g.

It is obvious that the presence of such impurities as silica, calcium hydroxide or calcium carbonate would impose additional restrictions on the composition of the solutions, but the equilibrium constants for the hydrated calcium silicates should not be affected since each equilibrium constant is independent of the constants for the other substances.

Compositions of the Solutions.—In Fig. 1 and 2 the calcium ion concentrations at equilibrium are compared with the silicic acid concentrations and *p*H values of the solutions. It is apparent (Fig. 1) that in general the silica concentration decreases with calcium ion concentration. The *p*H *versus* calcium ion concentration curves (Fig. 2) show an increase of *p*H with calcium concentration. It may be noted in Fig. 1 that the ratios of calcium $(Ca)_F$ and silicic acid $(SiO_2)_T$ in solution are not equal to the ratios in the solids, and that the ratios of $(Ca)_F$ to $(SiO)_{2T}$ increase with $CaO:SiO_2$ mole ratio in the solids and concentrations of calcium in the solutions. Solutions in which the ratios of components are not equal to the ratios of components in the solids are sometimes referred to as incongruent.

The removal of calcium from solution by the hydrated calcium silicates is demonstrated in Fig. 3 to increase, in general, with the ratio of SiO_2 to CaO in the hydrate. It is clear that the 186° and β-wollastonite samples do not absorb as much calcium as do the other samples. The maximum amount of calcium absorbed by the hydrates increased the $CaO:SiO_2$ ratios of the solid samples by approximately 0.02, 0.01, 0.2, and 0.1 for the samples 1, 2, 4, and 5, respectively.

Kinetics Study.—An examination was made of the composition of the solution in a reaction mixture of solid silica and calcium hydroxide solution. This study was made to determine whether or not the composition of the solutions was controlled primarily by the solid hydrated calcium silicate product.

A 1:1 $CaO:SiO_2$ mole ratio mixture of 950 ml. of 0.0127 molar calcium hydroxide and 0.887 g. of S. L. silica (81.5% SiO_2) was placed in a three-necked flask and stirred at a moderate speed. The flask itself was inserted into a constant temperature bath

---

(9) H. H. Willard, N. H. Furman and C. E. Bricker, "Elements of Quantitative Analysis," 4th Ed., D. Van Nostrand Co., Inc., Princeton, N. J., 1956.

(10) W. E. Bunting, *Ind. Eng. Chem., Anal. Ed.*, **16**, 612 (1944).

(11) S. Brunauer, P. H. Emmett and E. Teller, *J. Am. Chem. Soc.*, **60**, 309 (1938).

(12) Stephen Brunauer, D. L. Kantro and C. H. Weise, *Can. J. Chem.*, **37**, 714 (1959).

(13) S. A. Greenberg, This Journal, **61**, 373 (1957).

(14) G. L. Kalousek, *J. Am. Concrete Inst.*, **26**, 233 (1954).

(15) Stephen Brunauer, D. L. Kantro and L. E. Copeland, *J. Am. Chem. Soc.*, **80**, 761 (1958).

held at 50 ± 0.02°. Samples were removed periodically and the calcium ion concentrations, silicic acid concentrations and pH were determined on the filtered solutions. The results are listed in Table II.

TABLE II

RESULTS OF KINETICS STUDY AT 50°

1 Reaction time, (min.)	2 $(Ca)_F$, m./l. × 10^{-3}	3 $(SiO_2)_T$, m./l. × 10^{-4}	4 pH	5 K_{sp_1} $a_{Ca^{++}}a_{H_2SiO_4^{--}}$ × 10^{-7}	6 pK_{sp_1} ($-\log K_{sp_1}$)
3	8.35	2.22	11.60	2.73	6.56
10	8.27	2.21	11.50	2.26	7.58
18	7.61	2.57	11.45	2.65	7.19
25	7.03	2.81	11.33	2.73	7.13
50	7.13	2.83	11.40	2.83	7.08
75	6.98	2.96	11.38	3.01	6.52
100	6.42	1.19	11.40	1.13	6.95
125	6.34	2.02	11.40	1.90	6.72
150	6.06	1.42	11.39	1.30	6.89
200	5.96	2.38	11.35	2.07	6.68

Discussion: Equilibria

A. Solutions.—When hydrated calcium silicates are brought to equilibrium with aqueous solutions it is necessary to consider several relationships in the solution phases and between the solids and aqueous solutions in order to derive the solubility products.[16,17] First, let us consider the solutions. Two equations must be satisfied in solutions of hydrated calcium silicates. One is that of electroneutrality

$$2(Ca^{++}) + (H^+) = (OH^-) + (H_3SiO_4^-) + 2(H_2SiO_4^{--}) \quad (1)$$

where the quantities in parentheses are in moles/l. Since the pH values of the solutions are high, the hydrogen ion concentrations may be neglected. The second equation is

$$(SiO_2) = (H_4SiO_4) + (H_3SiO_4^-) + (H_2SiO_4^{--}) \quad (2)$$

which merely states that the soluble silicic acid (SiO_2) is monomeric[6] and is composed of three species, the undissociated form H_4SiO_4 and the two ions $H_3SiO_4^-$ and $H_2SiO_4^{--}$. It is assumed in this study that the dissolved species are monomeric. By the analytical procedure used, only the concentrations of monomeric species were determined. No polymeric species were noted.

B. Solids–Aqueous Solutions.—One of the equilibria between the solids and solutions will be expressed by the equations

$$Ca(H_2SiO_4)(s) = Ca^{++}aq + H_2SiO_4^{--}aq \quad (3)$$

$$Ca(H_3SiO_4)_2(s) = Ca^{++}aq + 2H_3SiO_4^{-}aq \quad (4)$$

The other equilibrium involved will be discussed in a later section. For Eq. 3 and 4 the solubility products K_{sp_1} and K_{sp_2} may be written as

$$\begin{aligned} K_{sp_1} &= a_{Ca^{++}}a_{H_2SiO_4^{--}} \\ &= (Ca^{++})(H_2SiO_4^{--})f_{\pm}^2 \end{aligned} \quad (5)$$

$$\begin{aligned} K_{sp_2} &= a_{Ca^{++}}a^2_{H_3SiO_4^-} \text{ or} \\ &= (Ca^{++})(H_3SiO_4^-)^2 f_{\pm}^3 \end{aligned} \quad (6)$$

where a refers to activity and $f^{\pm}$ is the mean activity coefficient in each equation. The first and second dissociation constants, K_1 and K_2, for silicic acid, H_4SiO_4, may be expressed by the equations[6]

$$K_1 = \frac{a_{H^+}(H_3SiO_4^-)f_{H_3SiO_4^-}}{(H_4SiO_4)f_{H_4SiO_4}} \quad (7)$$

$$K_2 = \frac{a_{H^+}(H_2SiO_4^{--})f_{H_2SiO_4^{--}}}{(H_3SiO_4^-)f_{H_3SiO_4^-}} \quad (8)$$

where $f_{H_4SiO_4}(f_{H_4})$, $f_{H_3SiO_4^-}(f_{H_3^-})$ and $f_{H_2SiO_4^{--}}$ $(f_{H_2^-})$ are the activity coefficients; $f_{H_4SiO_4}$ is assumed to be unity and the quantities in parentheses are in moles/l.

The usual procedures for deriving (OH^-), the ionic strength, f_{OH^-}, $f_{H_2^-}$, $f_{H_3^-}$, (H_4SiO_4), ($H_3SiO_4^-$), ($H_2SiO_4^=$) were used.[18] The OH^- concentration may be obtained from the pH values by the relationships: $k_w = a_{H^+}a_{OH^-}$; $pH = -\log a_{H^+}$; $(OH^-) = a_{OH^-}/f_{OH^-}$ and the Debye-Hückel expression,[19] $-\log f_i = AZ_i^2\mu^{1/2}$. In these equations K_w is the ionization constant of water, a is the activity of each species, f_i is the activity coefficient of species i, A is a constant, μ is the ionic strength, and Z is the va-

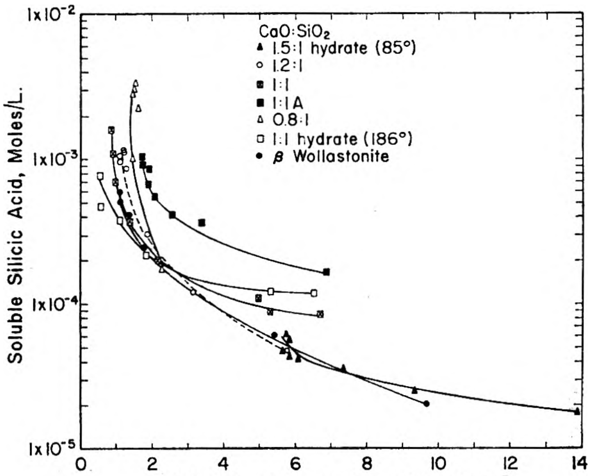

Fig. 1.—Soluble silicic acid vs. calcium concentration.

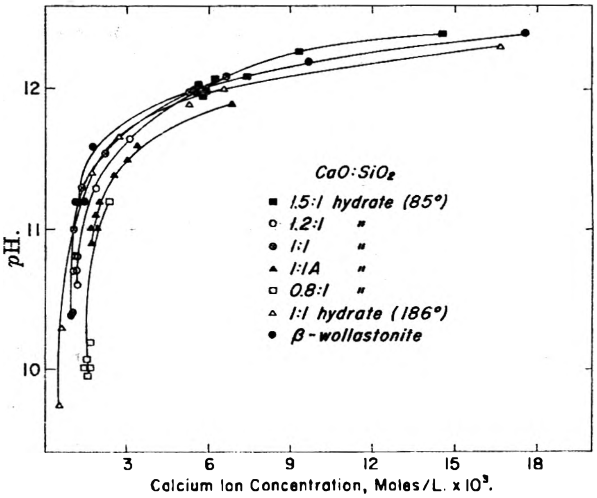

Fig. 2.—The pH of the solutions as a function of Ca^{++} concentration.

---

(16) T. B. Smith, "Analytical Processes," 2nd Ed., Edward Arnold and Co., London, 1940.

(17) H. S. Harned and B. B. Owen, "The Physical Chemistry of Electrolytic Solutions," Reinhold Publishing Corp., New York, N. Y., 1958.

(18) R. A. Robinson and R. H. Stokes, "Electrolytic Solutions" Butterworth Scientific Publications, London, 1955.

(19) P. Debye and E. Hückel, *Physik Z.*, **24**, 185, 305 (1923).

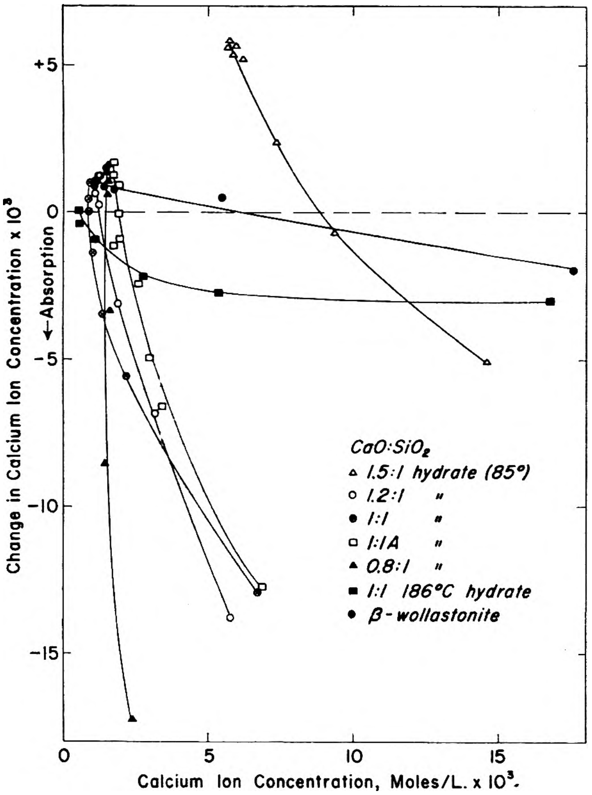

Fig. 3.—Change in Ca^{++} concentration (ΔCa^{++}) of the solutions as a function of the calcium ion concentration.

lence of the ionic species. The values of pK_w are 14.0 at 25° and 13.83 at 30°. The ionic strengths were estimated from a knowledge of the concentrations of calcium$(Ca)_F$ and silicic acid $(SiO_2)_T$, and the pH values in each solution. The activity coefficients f_{OH^-}, $f_{H_2^-}$ and $f_{H_3^-}$ may be evaluated by means of the Debye-Hückel expression.

The negative of the logarithms of the constants K_1 and K_2 (Eq. 7 and 8) for silicic acid, pK_1 and pK_2, are[6]

	25°	30°	40°	50°
pK_1	9.8	9.7	9.6(6)	9.6
pK_2	11.8	11.7	11.6	11.5

The values at 40 and 50° were estimated from those at 25 and 30°. It is apparent that when the pH, $(Ca^{++})_F$ and $(SiO_2)_T$ values are obtained experimentally, it is then possible to estimate the values of the ionic strength μ and with this information the coefficients $f_{H_2^-}$ and $f_{H_3^-}$ may be evaluated. It is possible then to calculate (Eq. 2, 7, 8) the concentrations of $H_4SiO_4^-$, $H_3SiO_4^-$ and $H_2SiO_4^{--}$.

The experimental data were tested by means of Eq. 1. Very good correlation was found. This was not the case with the data of Roller and Erwin.[2] Because small changes in pH values correspond to relatively large changes in OH^- concentrations, the latter values are difficult to derive accurately from pH measurements. Also at high and low concentrations of calcium ions it was difficult to determine accurately the silicic acid concentrations.

By incorporating the empirical relationship[20]

$$-\log f^{\pm} = Z_+Z_-A\mu^{1/2} - B'\mu \tag{9}$$

where Z_+ and Z_- are the absolute values of the valences of the ions and B' is an empirical constant, into Eq. 5 and 6, it is possible to obtain Eq. 10 and 11.

$$\log K_{sp_1}^* - 8A\mu^{1/2} = \log K_{sp_1} - 2B'\mu \tag{10}$$

$$\log K_{sp_2}^* - 6A\mu^{1/2} = \log K_{sp_2} - 3B'\mu \tag{11}$$

In Eq. 10 and 11, $K_{sp_1}^*$ is the concentration constant (Ca^{++}) $(H_2SiO_4^{--})$ and K_{sp_1} is the activity constant; $K_{sp_2}^*$ is the concentration constant $(Ca^{++})(H_3SiO_4^-)^2$ and K_{sp_2} is the activity constant. These equations are convenient for obtaining $K_{sp_1}^*$ and $K_{sp_2}^*$ at infinite dilution where $\mu = 0$ and these constants are equal to the activity constants.

A quick examination of the $K_{sp_1}^*$ and $K_{sp_2}^*$ values for the various hydrates shows that $K_{sp_1}^*$ over most of the calcium ion concentration ranges is approximately 10^{-7}, whereas, except for sample 1, the values for $K_{sp_2}^*$ vary between 10^{-9} (sample 3) and 10^{-12} (sample 5) and that relatively large variations in the values of $K_{sp_2}^*$ are exhibited for each sample over the whole calcium ion concentration range. Also it may be noted that the $K_{sp_1}^*$ value for each sample, in general, decreases with a decrease in ionic strength as expected (Eq. 5) since K_{sp_1} is constant and $f_{\pm}$ increases with a decrease in concentration of ions. However, in the case of sample 1, $K_{sp_1}^*$ values increase with a decrease in ionic strength and $K_{sp_2}^*$ remains relatively constant over most of the concentration range between 4.27 and 5.89×10^{-9}. It was therefore concluded that K_{sp_1} held, at least for samples 2 through 8 with $CaO:SiO_2$ mole ratios of one or more, and K_{sp_2} held for sample 1 which was synthesized from a 0.8:1 $CaO:SiO_2$ mole ratio reaction mixture.

It was found that the concentration of calcium in solution $(Ca)_F$ begins to increase rapidly with the 1.5 $CaO:SiO_2$ ratio sample and that the highest concentration of 0.0146 molar is beginning to approach the 0.02 molar concentration of a saturated calcium hydroxide solution.

The $K_{sp_1}^*$ data (except for the erratic values at low and high calcium ion concentration) were inserted with the corresponding ionic strength values in Eq. 10 and the left-hand side of the Eq. 10, $\log K_{sp_1}^* - 8A\mu^{1/2}$, was plotted as a function of μ (Fig. 4). The intercepts of the curves on the ordinates give $K_{sp_1}^*$ values at zero μ where $K_{sp_1}^* = K_{sp_1}$. The results are summarized in Table III.

TABLE III

SUMMARY OF pK_{sp_1} VALUES

Sample no.	Hydrate	Soln. temp., °C.	pK_{sp_1} ($-\log K_{sp_1}$)
1	0.8:1 (85°)	25	8.5 ± 0.1 (pK_{sp_2})
2	1:1	25	6.9 ± 0.1
		40	7.0 ± .1
3	1:1A	30	7.0 ± .1
4	1.2:1	25	6.9 ± .1
5	1.5:1	25	7.0 ± .1
6	1:1 (186°)	30	7.3 ± .1
7	1:1 β-$CaSiO_3$	30	7.0 ± .1

The pK_{sp_1} values are reasonably close to 7.0 for the 1.5:1, 1.2:1 and 1:1 hydrates as well as β-wollastonite. The well crystallized hydrate (sam-

---

(20) D. I. Hitchcock and A. C. Taylor, *J. Am. Chem. Soc.*, **59**, 1812 (1937).

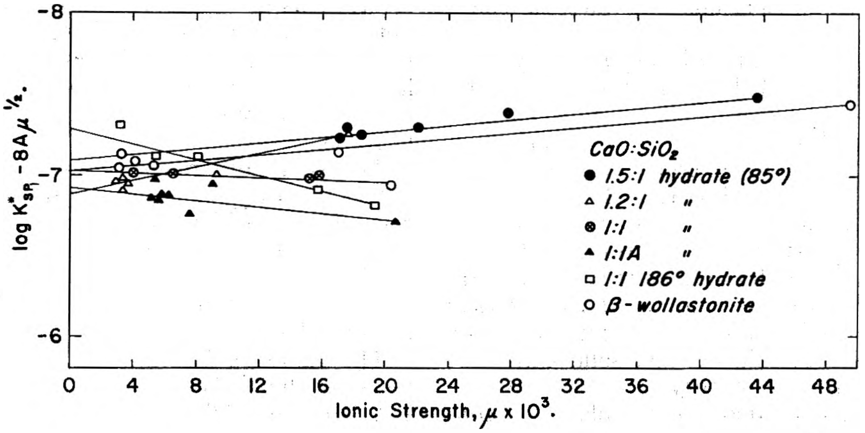

Fig. 4.—Application of Eq. 9 to data (plot of log $K^*_{\mathrm{sp}_1} - 8A\mu^{1/2}$ vs. μ).

ple 6) showed a pK_{sp_1} of 7.3. The pK_{sp_1} of a 1:1 hydrate was found to be 7.0 at 40° which indicates a small dependence of K_{sp_1} on temperature.

From the plot of log $K_{\mathrm{sp}_2} - 6A\mu^{1/2}$ *versus* μ according to Eq. 11 for the 0.8:1 hydrate data, a pK_{sp_2} value of 8.5 ± 0.1 was derived from the intercept of the curve on the ordinate.

Definite evidence for a K_{sp_2} equilibrium (Eq. 4) apparently exists only for the 0.8:1 hydrate at lower concentrations of calcium ions. Krasilnikov[4] has reported a higher solubility for the 0.8:1 hydrate than that for the 1:1 mole ratio hydrate. It would seem reasonable to conclude from the results that the other hydrates, in general, obey Eq. 5.

It is interesting to note that two 1:1 hydrate preparations (samples 2 and 3) prepared under somewhat different conditions (Table I) show similar pK_{sp_1} values of 6.9 and 7.0, respectively; a difference which seems to be within the range of experimental error. It may be reasonable to assume from these results that small differences in preparation and such impurities as calcium carbonate do not *markedly* affect the solubility product values.

The similarity of the pK_{sp_1} value for β-wollastonite and that for the calcium silicate hydrates indicates that at least the surface of the β-wollastonite must be hydrated. The X-ray pattern shows almost no change on hydration of the $CaSiO_3$. Kantro[21] has found also that β-wollastonite hydrates under certain conditions at room temperature. Evidence in this case was derived from ignition loss and X-ray data.

It is necessary to explain why the ratios of components of the solutions are not the same as the ratios of components in the solid phases. It is obvious also that Eq. 5 and 6 cannot apply to hydrates with mole ratios 0.8:1 to 1.5:1 without considering additional factors.

Many investigators[1,22] have shown that the concentration of calcium ions in solution is a function of the $CaO:SiO_2$ mole ratio in the solid. In the range of calcium concentration from zero to 0.003 Taylor[23] has reported that the mole ratio of $CaO:SiO_2$ in the solid increases sharply from zero to 1:1. However, in the solid mole ratio range of 1:1 to 1.5:1 the concentrations of calcium in solutions increases sharply with the $CaO:SiO_2$ mole ratio in the solids. Solutions in equilibrium with *both* solid hydrated calcium silicate and solid calcium hydroxide would be expected to exhibit concentrations of calcium hydroxide about 0.02 molar, which is the equilibrium solubility of calcium hydroxide. It is evident that this concentration will be present in contact with the two solids because the solubility product of calcium hydroxide at 25° is 9.04×10^{-6}, which is larger by about a factor of 100 than the 1.0×10^{-7} solubility product exhibited by hydrated calcium silicate.

Let us first consider the equilibria between the aqueous solutions and solids with mole ratios of $CaO:SiO_2$ greater than 1:1 and equal to or less than 1.5:1. Steinour[22] has pointed out that with fixed temperature and pressure the equilibria between these solids and solutions are not invariant. Therefore, we must assume that there are three components and two phases. Thus with one solution phase there is only one solid. How the calcium hydroxide in excess of the 1:1 $CaO:SiO_2$ ratio is involved in the CaH_2SiO_4 solid is not completely clear.[15,22] There are two probable possibilities. Either the calcium hydroxide is adsorbed on the large surface area or is dissolved in the CaH_2SiO_4. Brunauer, Kantro and Weise[12] explored the first possibility and concluded that the calcium hydroxide is not adsorbed. They found no correlation between the surface areas and $CaO:SiO_2$ mole ratios. Also extraction of calcium hydroxide with organic solvents[24] demonstrates that the excess calcium hydrate is not adsorbed on the silicate surface. Therefore, it must be concluded that the excess calcium hydroxide is in solid solution in the CaH_2SiO_4 crystals.

Therefore, we propose that in the equilibria between aqueous solutions and hydrates with $CaO:SiO_2$ mole ratios 1:1 and 1.5:1 two equations describe the system

$$CaH_2SiO_4(s) = Ca^{++}aq + H_2SiO_4{}^{=}aq \qquad (3)$$

$$Ca(OH)_2(s)(\text{absorbed}) = Ca^{++}aq + 2OH^{-}aq \qquad (12)$$

In addition to these reactions $H_2SiO_4{}^{--}aq$ may hydrolyze to $H_3SiO_4{}^{-}aq$ and then to H_4SiO_4aq species

---

[21] D. Kantro, private communication.

[22] H. H. Steinour in "Proceedings of the Third International Symposium on the Chemistry of Cement," London, 1952.

[23] H. F. W. Taylor, *J. Chem. Soc.*, 3682 (1950).

[24] E. E. Pressler, Stephen Brunauer, and D. L. Kantro, *Anal. Chem.*, **28**, 896 (1956).

according to the dissociation constants of silicic acid.

In this system the data may be explained by these equations. Equation 3 describes the dissociation of solid CaH_2SiO_4 which may contain calcium hydroxide in solid solution. The distribution of calcium hydroxide between aqueous solution and in solid solution is described by Eq. 12.

Qualitatively at least, Eq. 12 holds. The data of Taylor[23] show that the mole ratio of $CaO:SiO_2$ in the solid increases with the calcium ion concentration in solution. An experimental and theoretical study of the distribution of calcium hydroxide between the aqueous solution and solid CaH_2SiO_4 is in progress in this laboratory.

Equations 3 and 5 adequately explain the constancy of the activity product $a_{Ca^{++}}a_{H_2SiO_4^{--}}$. In addition the incongruity of the solutions may be understood when the reactions described by Eq. 3 and 12 are considered.

The equilibria that exist for hydrates with $CaO:SiO_2$ mole ratios less than 1:1 are not well understood. In the system of $CaO-SiO_2-H_2O$ at low CaO contents we are apparently dealing with silica dissolved in calcium hydroxide solutions. The increase in solubility of silica with *p*H has been explained[25] by the relationship and the equations

$$SiO_2(s) + nH_2O = H_4SiO_4aq \qquad (13)$$

for the dissociation of $H_4SiO_4^-$ and $H_3SiO_4^-$. Equation 13 describes the equilibrium between silica and a saturated solution of monosilicic acid. This solubility is fixed at a *p*H 7. However, as the *p*H of the solution is increased by addition of $Ca(OH)_2$, $H_3SiO_4^-$ and $H_2SiO_4^=$ form to increase the solubility of the silica. It has been shown[25] how the solubility data for silica may be explained by these equilibria.

Flint and Wells[26] have shown that although the soluble silicic acid contents of the solutions increase initially with the calcium ion concentrations in solution, when the solid precipitates show mole ratios of $CaO:SiO_2$ greater than 0.103, the concentration of silicic acid begins to decrease. Presumably silica reacts first on the surface with calcium hydroxide, and then at higher calcium hydroxide contents, hydrated calcium silicates apparently form with calcium hydroxide diffused throughout the polymeric silica structure. In the present study the 0.8:1 $CaO:SiO_2$ hydrate-water equilibrium seems to show the presence of $Ca(H_3SiO_4)_2$. Further investigation of this portion of the system is in progress.

Thermodynamics.—It is difficult to justify the assumption that the systems discussed here are in equilibrium. Steinour[22] has discussed the problems involved in treating these systems as thermodynamically stable. However, let us presume that the equilibria refer to systems which do not change over long periods of time.

The constancy of the activity product $a_{Ca^{++}}\cdot a_{H_2SiO_4^{--}}$ for the 1:1, 1.2:1 and 1.5:1 hydrates at about 7.0 ± 0.1, which is within experimental error, leads us to the conclusion that the chemical potential of the solid phase CaH_2SiO_4 is not markedly affected by the absorption of calcium hydroxide. Similar results were reported by Fock[27] for the solubility of solid solutions of $TlNO_3$ in KNO_3.

The small difference between the 6.9 and 7.0 values for pK_{sp_1} for the 1:1 hydrate at 25 and 40°, respectively, which is within experimental error, indicates that the heat of solution of CaH_2SiO_4 is small. From this one can conclude that the free energy of solution is a function mainly of the entropy change.

The standard free energy changes for the solutions of the CaH_2SiO_4 in the 1:1 hydrate (85°), 1:1 hydrate (186°) and β-wollastonite evaluated from $\Delta F^0 = -RT \ln K_{sp_1}$ are

Sample number		ΔF^0, kcal./mole
2	1:1 Hydrate (85°)	9.6 ± 0.2 (25°)
6	1:1 Hydrate (186°)	10.1 ± 0.2 (30°)
7	1:1 β-Wollastonite	9.55 ± 0.2 (25°)

This illustrates the higher ΔF^0 change on solution (10.1 kcal./mole) for the well crystallized hydrate (186°) compared to the poorly-crystallized 85° hydrate (9.6 kcal./mole) and therefore a lower free energy state exists for the hydrate prepared at 186°.

Kinetics Study.—The K_{sp_1} and pK_{sp_1} values are listed in Table II (columns 5 and 6) for the reacting system composed of calcium hydroxide, silica and water. It is immediately apparent that for the period of reaction between 3 and 200 minutes the K_{sp_1} is approximately 10^{-7}, which is reasonably close to the value exhibited by hydrated calcium silicates with ratios greater than 0.8 $CaO:SiO_2$ (Table III). The pK_{sp_1} values may be seen to vary around a value somewhat less than 7 which is reasonable for the K_{sp_1} at 50°. It may be concluded, therefore, that the solution composition is almost immediately (after 20 minutes) controlled by the hydrated calcium silicate which forms on reaction of silica and calcium hydroxide solutions, since the silica–calcium hydroxide solution system for dilute solutions would show a much different solubility for silica.[25]

Surface Areas.—It is apparent from the results that samples 2, 4 and 5 which exhibit similar water adsorption surface areas of about 270 sq. m./g. were found to show pK_{sp_1} values of 7.0 ± 0.1. Therefore it is reasonable to conclude that the differences in full energies of the samples because of the differences in surface areas were not sufficient to cause marked changes in solubility.

Sample 1 with a mole ratio of 0.8:1 $CaO:SiO_2$ and a surface area of 330 sq. m./g. exhibits a different solubility product K_{sp_2}.

Sample 6 which is a well crystallized form of sample 2 shows a higher nitrogen adsorption surface area than sample 2. Nevertheless the pK_{sp_1} value of sample 6 is 7.3 compared to the 6.9 of sample 2, which indicates that sample 6 is

---

(25) S. A. Greenberg and E. W. Price, This Journal, **61**, 1539 (1957).

(26) E. P. Flint and L. S. Wells, *J. Research Natl. Bur. Standards*, **12**, 751 (1934).

(27) H. Fock, *Ber.*, **28**, 408, 2734 (1891); *Z. Kryst.*, **28**, 337 (1891); *Chem. Zentr.*, **68**, I, 710 (1891); W. C. Lewis, "A System of Physical Chemistry," Vol. I, Longmans, Green and Co., New York, N. Y., 1916, p. 344.

less soluble. Therefore, it is possible to conclude that the lower solubility of sample 6 is due to the lower free energy state of the well crystallized sample and that the larger surface area does not cause a substantial increase in solubility.

Yates[28] has recently pointed out that colloidal silicate–water systems may be thermodynamically stable because of adsorption of ions which materially lowers the surface free energy.

Acknowledgments.—The authors wish to thank Drs. H. H. Steinour and S. Brunauer for their many helpful discussions and suggestions. Thanks are also due to Dr. D. L. Kantro who kindly provided the water adsorption surface area measurements.

(28) P. C. Yates, paper presented in symposium "Colloidal Silica and Silicates" at 137th National Meeting of the American Chemical Society, Cleveland, April 13, 14, 1960.

DETECTION OF METAL ION HYDROLYSIS BY COAGULATION: II. THORIUM[1,2]

BY E. MATIJEVIĆ, M. B. ABRAMSON,[3] K. F. SCHULZ[4] AND M. KERKER

Clarkson College of Technology, Potsdam, New York

Received March 7, 1960

Coagulation and stabilization concentrations for aqueous thorium nitrate solutions were obtained as a function of *p*H using silver iodide, silver bromide and silver chloride sols *in statu nascendi*. At $p\mathrm{H} < 4$ the coagulation concentration shows a constant value corresponding to a four-valent species, Th^{4+} or $Th(H_2O)_x^{4+}$. With increasing *p*H the coagulation concentration increases and levels off at a value characteristic for trivalent counterions. It is believed, therefore, that the initial hydrolysis step of Th^{4+} consists in formation of $[Th(H_2O)_{x-1}OH]^{3+}$ species. At still higher *p*H's the coagulation concentrations again become much lower indicating high valent species, possibly a dimer $[Th(H_2O)_{x-1}OH]_2^{6+}$. Reversal of charge is produced by the hydrolyzed Th-species, whereas the four-valent Th-ion does not reverse the charge. The problem of reversal of charge has been discussed and it is concluded that this effect is caused by OH-bridging of counterions.

Introduction

Hydrolysis of thorium ion already has been a subject of extensive investigations. However, owing to the complexity of the problem, unambiguous conclusions are difficult to make and therefore different authors have decided on different complex species as products of the hydrolysis process. Thus, Kraus and Holmberg[5] believe that the main species in perchlorate medium are $Th(OH)_2^{2+}$ and $Th_2(OH)_2^{6+}$ whereas Hietanen[6,7] using the "inert medium method" found evidence for polynuclear complexes of the type $Th[(OH)_3Th]_n^{(4+n)+}$ and Hietanen and Sillén[8] using the "self-medium method" claim the complexes are of $Th_2(OH)_2^{6+}$ and Th_2OH^{7+} type. From Lefevbre's calculations[9] it appears that the predominant complex species is $Th_5(OH)_{12}^{8+}$ in addition to $Th_7(OH)_x$, $Th_2(OH)_2^{6+}$ and $Th(OH)_2^{2+}$. Faucherre and Schaal[10,11] concluded that during the hydrolysis process a tetramer $[Th_4O_4]^{8+}$ is formed. In an older work Chauvenet and Tonnet[12] and Chauvenet and Souteyrand-Franck[13] proposed the species $Th(OH)_2^{2+}$ and ThO^{2+}. Finally, Kasper's[14] conclusion is that the main hydrolysis product is $Th(OH)^{3+}$.

Obviously, more work is required in order to clarify the problem of the hydrolysis of Th^{4+}. Especially desirable should be the introduction of new techniques that would give an independent clue as to the hydrolysis products.

In an earlier paper[1] we have shown that the coagulation technique can be successfully employed in investigating metal ion hydrolysis. It is well known that the electrolytic coagulation of lyophobic colloids is influenced in a very sensitive way by the charge of the counterion in solution. Thus, any change in counterion caused by its hydrolysis that gives rise to species of different charge will be reflected in the change of the critical coagulation concentration of the solution in question. From this change, the charge of predominant new species can be determined which in turn can lead to conclusions as to the hydrolytic processes taking place in such a solution. If data, obtained using the coagulation method, are combined or compared with results obtained employing other techniques, such as potentiometric titration, conductivity, freezing point depression, etc., more conclusive answers regarding the hydrolysis products can be expected. The coagulation technique has another great advantage when compared with other common methods since it utilizes solutions of extremely low concentrations, ranging from 10^{-4} to 10^{-7} mole/l. This eliminates the usual complications connected with the activity changes which appear at higher concentrations. Furthermore, since no addition of neutral salts are necessary in order to keep the activity coefficient constant, the hydrolysis products can-

(1) Part I, E. Matijević and B. Težak, THIS JOURNAL, **57**, 951 (1953).

(2) Supported by the U. S. Atomic Energy Commission Contract No. AT(30-1)-1801.

(3) Participant in the NSF Summer Research Project, 1959.

(4) On leave of absence from Institute for Medical Research, Zagreb, Yugoslavia.

(5) K. A. Kraus and R. W. Holmberg, THIS JOURNAL, **58**, 325 (1954).

(6) S. Hietanen, *Acta Chem. Scand.*, **8**, 1626 (1954).

(7) S. Hietanen, *Rec. trav. chim.*, **75**, 711 (1956).

(8) S. Hietanen and L. G. Sillén, *Acta Chem. Scand.*, **13**, 533 (1959).

(9) J. Lefevbre, *J. chim. phys.*, **55**, 227 (1958).

(10) J. Faucherre and R. Schaal, *Compt. rend.*, **226**, 118 (1947).

(11) R. Schaal and J. Faucherre, *Bull. soc. chim. France*, **15**, 143 (1948).

(12) E. Chauvenet and J. Tonnet, *ibid.*, [4] **47**, 701 (1930).

(13) E. Chauvenet and Mme. Souteyrand-Franck, *ibid.*, [4] **47**, 1128 (1930).

(14) J. Kasper, Dissertation, The John Hopkins University, Baltimore, Maryland, 1941.

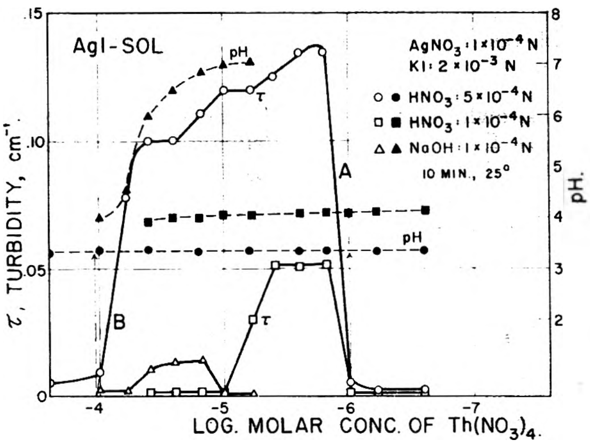

Fig. 1.—Coagulation curves of thorium nitrate for silver iodide sol *in statu nascendi*, 10 minutes after mixing the reacting components. Concentrations: $AgNO_3$, 1×10^{-4} *N;* KI, 2×10^{-3} *N;* $Th(NO_3)_4$, varied; (○) HNO_3, 5×10^{-4} *N*, (□) HNO_3, 1×10^{-4} *N*, (△) NaOH, 1×10^{-4} *N*. Full lines and open points represent turbidity measurements. A denotes the coagulation limit and B the stabilization limit. Dashed curves and blackened points give corresponding *p*H's.

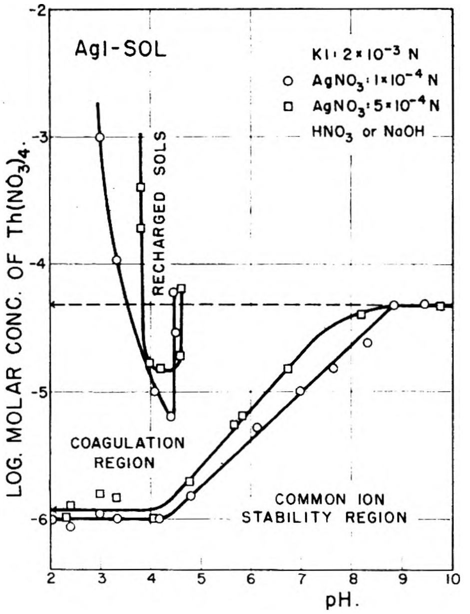

Fig. 2.—The plot of coagulation concentrations (lower curves) and stabilization concentrations due to the reversal of charge (upper curves) against *p*H for thorium nitrate on silver iodide sol. Two different sol concentrations were employed: ○, 1×10^{-4} mole/l. and □, 5×10^{-4} mole/l. AgI.

not be influenced by possible complexing with foreign ions.

We have used silver iodide, silver bromide and silver chloride sols *in statu nascendi* and coagulated them with solutions of thorium nitrate adding different amounts of nitric acid or caustic soda. The *p*H of these solutions was also measured. The plots of coagulation concentrations against *p*H revealed the changes in charges in ionic species in solutions.

Another aspect of this work is the general study of coagulation effects of thorium salt solutions on silver halide sols. Of particular interest was the determination of the correct coagulation concentration for the four-valent counterion, Th^{4+}, and the effect of *p*H on the reversal of charge of the sol particles. The very diversified coagulation phenomena caused by thorium ions on silver halide sols have been studied before.[15-21] However, no systematic work on *p*H dependence of the coagulation and the reversal of charge has been done. Kruyt and Troelstra[21] have investigated the influence of addition of HNO_3 and NaOH on coagulation effects of thorium nitrate solutions on silver iodide sols, but only presented the data in a schematic way and did not follow the appreciable *p*H changes which accompany the hydrolysis of the thorium ions. Our present work at low *p*H gives a precise coagulation concentration for Th^{4+} species for silver iodide, silver bromide and silver chloride sols *in statu nascendi* and, in addition, shows the correlation between the stability limit caused by the reversal of charge and *p*H in investigated sols. This has resulted in a better understanding of the reversal of charge phenomena.

Experimental

We have followed the coagulation of silver iodide, silver bromide and silver chloride *in statu nascendi* by mixing equal volumes (5 ml.) of silver nitrate solutions of constant concentration with solutions containing constant amounts of potassium halide component and varying amounts of thorium nitrate. The turbidity changes were measured by observing the light scattering at 45° in an Aminco light scattering microphotometer using the 546 mμ line. Nitric acid, when required, was added to the solution of halide and thorium components. However, when measurements were performed in the presence of NaOH, the silver nitrate and thorium nitrate solutions were mixed first, and the NaOH added to the halide solutions. This was done in order to prevent the formation of silver or thorium hydroxide due to the local supersaturations when the more concentrated stock solutions of NaOH were added. All measurements were performed at 25°. For a detailed description of the experimental technique and the method of analyzing the data in order to obtain the critical coagulation concentration we refer to our previous papers.[22,23]

Half of the total amount of the prepared sol solution was used for turbidity measurements whereas the rest was utilized for *p*H measurements. A Beckman Model G *p*H meter was employed, the scale of which was calibrated with appropriate buffer solutions prior to taking *p*H readings.

All chemicals were of the highest purity grades further purified when necessary. Water was doubly distilled, the second time from an all-Pyrex still and regularly tested for *p*H and conductivity. All glassware was thoroughly cleaned and steamed before use.

Results

Three typical curves for coagulation of silver iodide sols by thorium nitrate solutions are given as an example in Fig. 1. The turbidities are taken from "time-turbidity" plots of each individual system 10 minutes after mixing the reacting components. This time has been found to be critical for

---

(15) G. N. Gorochowski and J. R. Protass, *Z. physik. Chem.*, **A174**, 122 (1935).

(16) F. Bosch and H. Haemers, *Natuurw. Tijdschr. Belg.*, **18**, 90 (1936).

(17) J. Gillis and J. Eeckhout, *ibid.*, **19**, 49 (1937).

(18) E. Matijević and B. Težak, *Arhiv kem.*, **22**, 62 (1950).

(19) B. Težak, E. Matijević and K. Schulz, *J. Am. Chem. Soc.*, **73**, 1602, 1605 (1951).

(20) K. F. Schulz and E. Matijević, *Kolloid-Z.*, **168**, 143 (1960).

(21) H. R. Kruyt and S. A. Troelstra, *Kolloid-Beih.*, **54**, 262 (1943).

(22) B. Težak, E. Matijević and K. Schulz, This Journal, **55**, 1557 (1951).

(23) E. Matijević and M. Kerker, *ibid.*, **62**, 1400 (1958).

the coagulation of silver iodide sols.[22] Two of the given curves represent systems to which HNO_3 (1×10^{-4} and 5×10^{-4} mole/l.) was added, whereas the third one was obtained in the presence of NaOH (1×10^{-4} mole/l.). In all cases the concentrations of $AgNO_3$ (1×10^{-4} mole/l.) and KI (2×10^{-3} mole/l.) were kept constant. In all curves two limits, the coagulation limit (A) and stabilization limit (B), appear, the latter being caused by the reversal of charge on the sol particles. The critical coagulation and stabilization concentrations are obtained by extrapolating the steepest part of limits A and B to zero turbidity. Corresponding *p*H's are then read from *p*H curves at relevant concentrations, as indicated by arrows (for one curve) in Fig. 1. We have obtained such coagulation curves over a wide range of *p*H and plotted the coagulation and stabilization concentrations of $Th(NO_3)_4$ (expressed in moles/l.) against corresponding *p*H values.

Figure 2 gives such a plot for AgI-sol at two different sol concentrations. The lower curves represent the *p*H dependence of the coagulation limits and the upper curves that of the stabilization limits. The coagulation concentration of thorium ion increases from a lower limiting value at low *p*H's to an upper limiting value at higher *p*H's. Experiments could not be extended to even higher *p*H's since the simultaneous formation of metal hydroxides would interfere with the coagulation of silver iodide. The reversal of charge effect is restricted to a rather narrow *p*H range for both sol concentrations being somewhat narrower for the sol of higher concentration.

The effects obtained with the silver bromide sol are represented in Fig. 3. The general picture is similar to that of silver iodide. The only significant difference is in the trend of the coagulation concentration *vs.* *p*H curve at higher *p*H's, where, after leveling off between *p*H 7 and 8, the curve drops again to values even lower than those obtained at low *p*H. Also, the reversal of charge region appears to be wider than in the case of AgI sols.

Finally, Fig. 4 gives the same plot for the silver chloride sol. The trend of the coagulation concentration *vs.* *p*H curve is similar to that of silver bromide, and the reversal of charge region is even wider than for both the silver iodide and the silver bromide sols.

Discussion

A. On Hydrolyzed Species of Thorium from Coagulation Effects.—It is apparent from Figs. 2, 3 and 4 that for all three silver halide sols, the coagulation concentration of thorium nitrate solutions decreases to a constant value below *p*H 4. This concentration is 1×10^{-6} mole/l. for AgI, 6×10^{-7} mole/l. for AgBr and 3×10^{-7} mole/l. for AgCl sol. The quantitative expressions for the Schulze–Hardy rule give precisely this range of values for four-valent counterions.[24-26] Thus, we conclude that at low *p*H's the four-valent thorium ion (Th^{4+}, or $Th(H_2O)_x{}^{4+}$) is the predominant species in solution. This is in agreement with results obtained by Kraus and Holmberg.[5] When *p*H becomes higher than 4 the coagulation concentration increases until at *p*H ~7, it levels off again at a much higher concentration of $Th(NO_3)_4$. This concentration is 5×10^{-5} mole/l. for AgI sol and 2×10^{-5} mole/l. for AgBr sol (for AgCl sol the value could not be determined unambiguously from Fig. 4). Again, calculations carried out before[24-26] reveal that these concentrations correspond very well with critical coagulation concentrations of trivalent counterions. As a matter of fact, the experimentally obtained coagulation concentrations for La^{3+} and Al^{3+} under comparable conditions[24,25,27] for AgBr and AgI sols are in a very good agreement with the above cited values. We should keep in mind that for comparison purposes the molarities of thorium nitrate solution have to be multiplied by 3 in this case, since coagulation concentrations are always expressed in normalities of counterions in

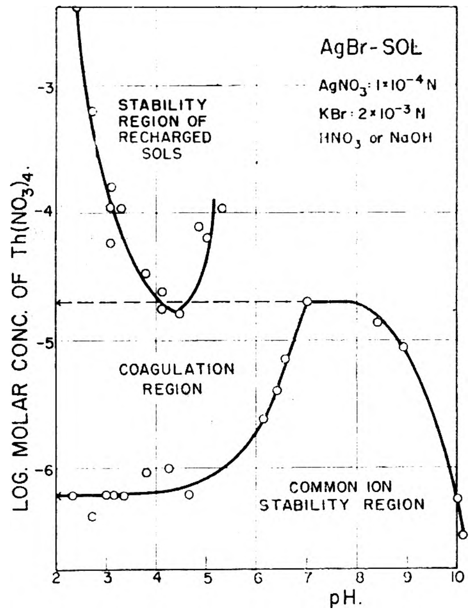

Fig. 3.—The same plot as in Fig. 2 for silver bromide sol: AgBr, 1×10^{-4} mole/l.

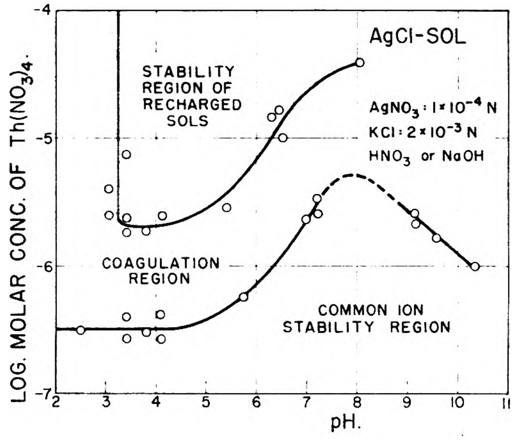

Fig. 4.—The same plot as in Fig. 2 for silver chloride sol: AgCl, 1×10^{-4} mole/l.

---

(24) B. Težak, E. Matijević and K. F. Schulz, *ibid.*, **59** 769 (1955).

(25) E. Matijević, K. F. Schulz and B. Težak, *Croat. Chem. Acta*, **28**, 81 (1956).

(26) E. Matijević, D. Broadhurst and M. Kerker, THIS JOURNAL, **63**, 1552 (1959).

(27) B. Težak, E. Matijević and K. Schulz, *ibid.*, **55**, 1567 (1951).

solution. It is, therefore, fair to assume that the thorium ion exists at $p\mathrm{H} > 7$ in the form of trivalent hydrolyzed species. The simplest mechanism for such hydrolysis is given by the equilibrium equation

$$\mathrm{Th(H_2O)_x}^{4+} + \mathrm{H_2O} \rightleftharpoons [\mathrm{Th(H_2O)_{x-1}OH}]^{3+} + \mathrm{H_3O^+} \quad (1)$$

It appears, thus, that in *dilute* thorium salt solutions the initial major step in hydrolysis is the formation of the trivalent monohydroxy ion. This is very similar to what has been established for the hydrolysis of uranium(IV)[28,29,32] and plutonium(IV) ions.[28,30-32] Our findings are in agreement with conclusions drawn by Kasper.[14] Kraus and Holmberg[6] calculated a rather low equilibrium constant for reaction 1. Even so, they found that they had to take it into account at their *lower* concentrations of Th salt solutions in order to reconcile their experimental and calculated data. Since our working concentrations are still lower by 2 orders of magnitude it is reasonable that equilibrium 1 becomes predominant. In addition, we should also keep in mind that our results are obtained in aqueous solution in the presence of very small quantities of foreign ions, whereas Kraus and Holmberg worked in highly concentrated perchlorate solutions. The latter remark also refers to work by Hietanen[6,7] as well as to that by Hietanen and Sillén[8] which was performed at very high concentration of thorium ions (0.5 and 0.7 mole/l.).

Our results on silver bromide and silver chloride sol indicate that at our highest $p\mathrm{H}$ range a rather sharp drop in coagulation concentrations of thorium nitrate again takes place. Especially in the case of AgBr sol, the coagulation concentrations were even lower than those obtained for four-valent Th-ion, indicating an existence of species of charge higher than four. We could not pursue our investigations to still higher $p\mathrm{H}$ in order to obtain the lower limit of the coagulation curve which would give a definite answer as to the charge of counterions. However, the most probable next step in the hydrolysis equilibrium would be a dimerization of the trivalent species as

$$2[\mathrm{Th(H_2O)_{x-1}OH}]^{3+} \rightleftharpoons [\mathrm{Th(H_2O)_{x-1}OH}]_2^{6+} \quad (2)$$

As a matter of fact, the existence of species $\mathrm{Th_2(OH)_2}^{6+}$ has been claimed by several investigators.[5,8,9,12]

B. The Problem of Reversal of Charge.—From the colloid chemical point of view this work represents a contribution to two problems. Firstly, it gives the coagulation concentration of a four-valent counterion for three silver halide sols, which can be utilized for theoretical calculations.[26]

In addition we have investigated systematically the dependence of the reversal of charge limit on several factors. It appears from Figs. 2, 3 and 4 that the higher the charge density of sol particles the smaller is the region of reversal of charge. Thus, the AgI-sol, which is known to be the strongest charged sol among three silver halides, shows a very narrow range where particles are of reversed charge. AgCl-sol, which shows the weakest charge has the widest range of reversed charged particles.

Another feature of our results is, that at lowest $p\mathrm{H}$'s, where the counterion appears to have the highest charge, its ability to reverse the charge of sol particles completely disappears. Thus, the charge or valency of the counterion itself cannot be considered as solely responsible for the reversal of charge effect. This has been pointed out before by Kruyt and Troelstra,[21] but they assumed that this effect was caused essentially by *insoluble* hydroxides. A similar conclusion was reached by Bosch and Haemers[16] for coagulation of silver iodide by thorium nitrate. From our present experiments, it follows that *soluble* hydrolyzed thorium species cause the reversal of charge. Thus, the hydroxyl group in a counterion complex seems to be the main factor causing this effect. This is substantiated by adsorption experiments by Schulz and Herak,[33] who have shown that thorium species are strongly adsorbed on positive rather than on negative silver halide sols. There is more evidence available that the hydroxyl group is responsible for the reversal of charge. We have made a survey of ions that have been found experimentally to cause this phenomenon, and they all contain in their ionic structure hydroxyl groups, *e.g.*, all heteropoly ions,[34,35] citrate ion,[36] hydrolyzed aluminum ion,[1] etc. It is especially interesting to note that the hexavalent hexol ion reverses the charge when incompletely dissociated but loses this ability when its hydroxyl groups become protonated.[26] Thus, we believe that hydroxyl groups in soluble counterion species are responsible for their adsorption on sol particles, which in turn causes the reversal of charge. This naturally does not apply to detergents and similar ions that reverse the charge,[37] but where the adsorption is not due to hydroxy bridges.

Acknowledgment.—We wish to record our thanks to Mr. Charles Rapp for his assistance in a part of the experimental work.

DISCUSSION

R. H. OTTEWILL (University of Cambridge).—Is it possible that the decrease in coagulation concentrations found at high $p\mathrm{H}$ values for silver chloride and silver bromide can be explained by the formation of silver oxide on the surface of the particles? Silver oxide appears very prone to form on silver bromide and it would be expected to be more so for silver chloride and less so for silver iodide. It is interesting that no decrease is found for silver iodide. It could be very useful to have some complementary measurements by another technique, *e.g.*, microelectrophoresis, to prove that the surface of the sol particles is not appreciably charged in this region.

E. MATIJEVIĆ.—Dr. Ottewill's suggestion is a possibility. However, we believe that it is more likely that with

---

(28) K. A. Kraus and F. Nelson, *J. Am. Chem. Soc.*, **72**, 3901 (1950).

(29) R. H. Betts and R. M. Leigh, *Can. J. Research*, **28B**, 514 (1950).

(30) K. A. Kraus in "National Nuclear Energy Series," Div. IV, Vol. 14B, No. 3.16, Edited by G. T. Seaborg, J. J. Katz and W. M. Manning, McGraw-Hill Book Co., Inc., New York, N. Y., 1949.

(31) J. C. Hindman, ref. 30, No. 4.4.

(32) J. J. Katz and G. T. Seaborg, "The Chemistry of Actinide Elements," Methuen & Co., Ltd., London, 1957.

(33) K. F. Schulz and M. J. Herak, *Croat. Chem. Acta*, **30**, 127 (1958).

(34) E. Matijević and M. Kerker, THIS JOURNAL, **62**, 1271 (1958).

(35) E. Matijević and M. Kerker, *J. Am. Chem. Soc.*, **81**, 5560 (1959).

(36) B. Težak, *et al.*, THIS JOURNAL, **57**, 301 (1953).

(37) E. Matijević and R. H. Ottewill, *J. Colloid Sci.*, **13**, 242 (1958).

the AgI sol the decrease in coagulation concentration at higher pH's does not occur because of an interaction of the iodide ion and the complex thorium ion with a corresponding change in charge. The iodide ion might act as a "penetrator." At the present moment there is no proof for either assumption.

J. TH. G. OVERBEEK (University of Utrecht).—With reference to Dr. Ottewill's remark, I want to report that in our measurements and those of P. L. de Bruyn at M.I.T. on the adsorption of I^- and Ag^+ ions on AgI difficulties were encountered at high pH (9 or 10) but very definitely before the normal solubility product of silver oxide is reached. The silver iodide became darkly colored and adsorption was poorly reproducible.

E. MATIJEVIĆ.—In our experiments no changes in colors were observed. In the pH range investigated the silver halide sols retained the same appearance.

J. TH. G. OVERBEEK.—If the transition of the flocculation value in going from valence 4 to valence 3 is exclusively due to the reaction $Th^{4+} + OH^- \rightarrow ThOH^{3+}$, one might expect the transition to be very similar for the three silver halides. However, according to Figs. 2, 3 and 4, the transition increases in steepness in the order AgI, AgCl, and AgBr.

E. MATIJEVIĆ.—Some differences in the transition range probably are caused by specific properties of the three silver halide sols. It is known that these sols show slightly different effects when coagulated with mixtures of ions.

J. TH. G. OVERBEEK.—How is it possible that the reversal of charge concentration in Fig. 2 is lower than the flocculation concentration for the trivalent $ThOH^{3+}$ if the reversal is due exclusively to this trivalent ion?

E. MATIJEVIĆ.—As shown in Fig. 1, the pH in neutral and basic solutions depends strongly on the concentration of the thorium salt in solution. Thus, for the same coagulation curve the concentration limits for coagulation and stabilization appear at different pH's. Since the stability limit is always at high Th-salt concentrations, the corresponding pH is lower, giving the stability range of recharged sols as presented in Fig. 2.

S. LEVINE (University of Manchester).—What is the evidence for the dimerization described by your Eq. (2)?

E. MATIJEVIĆ.—The dimer is only given as a possible explanation for the drop in coagulation concentrations at high pH's. It was, however, detected by a number of investigators cited in the introduction of this paper.

R. R. IRANI (Monsanto Chemical Company).—Do you feel that your technique is applicable to the hydroxyl complexes of ferric ion, particularly since several species have been reported to coexist and their relative concentrations change with pH, *e.g.*, $Fe(OH)^{+2}$, $Fe_2(OH)_2{}^{+4}$, $Fe(OH)^+$, etc.

E. MATIJEVIĆ.—In principle, there is no reason why the method could not be employed for hydrolysis of ferric ion. The coexistence of several species could imperil the deductions. However, if one of the species becomes predominant its charge will be indicated by the coagulation behavior.

NON-STEADY-STATE FLUID FLOW AND DIFFUSION IN POROUS MEDIA CONTAINING DEAD-END PORE VOLUME[1]

BY RICHARD C. GOODKNIGHT, WALDEMAR A. KLIKOFF, JR., AND IRVING FATT[2]

Department of Mineral Technology, University of California, Berkeley, California

Received March 10, 1960

A system of equations is derived that describes pressure transients during non-steady-state flow of a fluid through a linear porous medium which contains dead-end pore volume. Analogous equations are shown to describe non-steady-state diffusion through fluid contained in such porous media. The equations are solved for a set of boundary conditions which are identical to those for which laboratory data were obtained. The theoretical and experimental results are in excellent agreement thereby establishing the validity of the equations.

Introduction

The conventional treatment of non-steady-state fluid flow or diffusion through porous media uses only two pore structure parameters. For fluid flow these are the porosity and permeability; for diffusion they are the porosity and tortuosity. Recently the adequacy of the two-parameter treatment has been questioned by Fatt[3] for fluid flow through porous media and by Klute[4] for diffusion in polymer films. These authors point out that dead-end pore volume (defined as volume which contains the flowing or diffusing species but through which there is no flux during steady-state fluid flow or diffusion) may alter transient fluid flow or diffusion behavior.

In this paper we derive equations for non-steady-state flow and diffusion in a general form which includes the dead-end volume. The resulting system of equations is solved for appropriate boundary conditions and the solutions compared with experimental data.

Nomenclature

A	cross-sectional area of porous flow channel
A_o	cross-sectional area of orifice
c	compressibility
C_1	boundary concentration
C_0	initial concentration
C	variable concentration
C'	dimensionless concentration, $C' = (C - C_0)/(C_1 - C_0)$
D	diffusion coefficient
D_e	effective diffusion coefficient, $D_e = D/\theta^2$
G	a function
G'	a function
k	permeability of porous flow channel
k_o	permeability of orifice
h	a constant
H	a constant
l_o	length of orifice
L	length of porous medium
M	diffusion flow of solute in flow channel
M'	diffusion flow of solute to sink
N	number of dead-end pores
P'	dimensionless pressure in flow channel $P' = \dfrac{P - P_0}{P_b - P_0}$
P'_2	dimensionless pressure in sink $P_1' = \dfrac{P_2 - P_0}{P_b - P_0}$
P	pressure (variable) ($P_1 \equiv P$)
P_0	initial pressure (constant)
P_b	boundary pressure (constant)
P_2	pressure in sink (variable)
$\bar{P}$	Laplace transform of P'
$\bar{P}_2$	Laplace transform of P'_2
Q	volumetric flow rate in porous flow channel
Q'	volumetric flow rate toward sink
R	gas constant
S	parameter of the Laplace transform
t	time
T	temperature
V_1	pore vol. of porous flow channel (not including dead-end vol.)
V_2	total volume of all sinks (chambers)
V_o	volume of individual sinks (chambers)
v_1	gas velocity (flux) cm./sec. in flow channel
x	distance coördinate
Y	a constant
α	diffusivity coefficient for liquid $\alpha = k/\phi_1\mu c$
α'	diffusivity coefficient for gas $\alpha' = k/2\phi_1\mu$
β	a constant
γ	specific weight of gas
∇^2	the operator $\dfrac{\partial^2}{\partial x^2} + \dfrac{\partial^2}{\partial y^2} + \dfrac{\partial^2}{\partial z^2}$
θ	tortuosity = diffusion path length/L
ϕ_1	porosity of porous flow channel (not including sinks) ($\phi_1 = V_1/AL$)
ϕ_2	V_2/AL
μ	viscosity

During single-phase, non-steady-state fluid flow through porous materials, pressure transients are usually said to obey differential equations of the form

$$\frac{\partial P}{\partial t} = \alpha \nabla^2 P \qquad (1)$$

if liquid is flowing, or

$$\frac{\partial P}{\partial t} = \alpha' \nabla^2 P^2 \qquad (2)$$

if gas is flowing. Non-steady-state diffusion through the fluid contained in the pores of a porous medium is said to be described by an equation equivalent to equation 1, namely

$$\frac{\partial C}{\partial t} = D_e \nabla^2 C \qquad (3)$$

In the body of this paper the equations for pressure transients in a liquid-filled porous medium will be solved and the solution compared with experimental data. An identical but abbreviated treatment for diffusion, equation 3, is given in Appendix I.

Equations 1, 2, and 3 are derived with the assumption that there are no sources of flux within the system. The more general equations that describe pressure transients contain a function that accounts for any sources of flux and have the form

$$\frac{\partial P}{\partial t} = \alpha \nabla^2 P + G(x, y, z, t) \qquad (4)$$

if liquid is flowing, or

$$\frac{\partial P}{\partial t} = \alpha' \nabla^2 P^2 + G'(x, y, z, t) \qquad (5)$$

---

(1) Taken in part from the M.S. theses of R. C. Goodknight, January 1960, and W. A. Klikoff, Jr., June 1960, University of California, Berkeley.

(2) Send requests for reprints to I. Fatt.

(3) I. Fatt, *Trans. Am. Inst. Mining, Met. Engrs.*, **216**, 449 (1959).

(4) C. H. Klute, *J. Polymer Sci.*, **41**, 307 (1959).

if gas is flowing, where $G(x, y, z, t)$ and $G'(x, t, z, t)$ are the source functions. The source whose strength is described by the G function may be a dead-end pore which contains compressed liquid or gas. If flow is into a dead-end pore, the pore is a sink and the G function has a negative sign. An accurate prediction of pressure transients in porous media which contain such dead-end pore volume requires that the source function be known explicitly and that equations 4 or 5 be solved for the appropriate boundary conditions.

Fatt[5] has shown previously that sintered glass probably does not have dead-end pores. He did not show, however, how much effect a given amount of dead-end pore volume would have nor what amount his method of measurement could detect. Klikoff[6] has demonstrated experimentally that under certain conditions observable changes in the form of the pressure transient results when one-third of the total pore volume is dead-end volume.

Theory

We assume that in a porous medium there are uniformly distributed pores which have only one opening to the main pore structure. Furthermore we assume that the opening is in the form of a neck or construction whose cross-sectional area is much less than that of a pore. We assume steady-state flow in the neck between the dead-end pore and the main flow channel. This is a good assumption, if the volume of the neck is small compared to the volume of the dead-end pore. We also assume that the flow rate into the dead-end pore is so small compared to the rate in the x direction in the main channel that the average velocity remains in the x direction.

The continuity equation for this system is

$$\operatorname{div}(v_1\gamma_1) = -\frac{\partial}{\partial t}(\phi_1\gamma_1 + \phi_2\gamma_2) \qquad (6)$$

where

$$\gamma_i = \gamma_0 \exp(cP_i),\ (i = 1, 2) \qquad (7)$$

if the fluid is a liquid, and

$$\gamma_i = \frac{P_i}{RT},\ (i = 1, 2) \qquad (8)$$

if the fluid is a perfect gas. In equation 6 and all following equations $i = 1$ refers to the main flow channel and $i = 2$ refers to dead-end volume.

From Darcy's law we have

$$v_1 = -\frac{k}{\mu}\frac{\partial P_1}{\partial x} \qquad (9)$$

By definition

$$\phi_i = \frac{V_i}{AL},\ (i = 1, 2) \qquad (10)$$

Assuming isothermal flow, equations 6, 7, 9 and 10 can be combined to give for liquid flow (assuming that liquid compressibility is small and independent of pressure)

$$\frac{\partial P}{\partial t} = \frac{k}{\phi_1\mu c}\frac{\partial^2 P}{\partial x^2} - \frac{\phi_2}{\phi_1}\frac{\partial P_2}{\partial t} \qquad (11)$$

For isothermal gas flow, equations 6, 8, 9 and 10 are combined to give

$$\frac{\partial P}{\partial t} = \frac{k}{2\phi_1\mu}\frac{\partial^2 P^2}{\partial x^2} - \frac{\phi_2}{\phi_1}\frac{\partial P_2}{\partial t} \qquad (12)$$

For laboratory analysis of the above equations the sinks are replaced by chambers connected to the flow channel by sandstone orifices of cross-sectional area A_0, length l_0, and permeability k_0. Assuming a continuous sink distribution the flow rate into an elemental sink is given by Darcy's law as

$$Q' = \frac{A_0 N k_0}{\mu l_0}(P - P_2)\,dx \qquad (13)$$

The amount of fluid stored per unit time in the elemental sink is for liquids

$$Q' = \frac{V_2 c}{L}\frac{\partial P_2}{\partial t}\,dx \qquad (14)$$

and for perfect gases

$$Q' = \frac{V_2}{P_2 L}\frac{\partial P_2}{\partial t}\,dx \qquad (15)$$

When the flowing fluid is liquid, we equate 13 and 14 and substitute into 11 to give

$$\frac{\partial P}{\partial t} = \frac{k}{\phi_1\mu c}\frac{\partial^2 P}{\partial x^2} - \frac{V_2}{V_1}\frac{\partial P_2}{\partial t} \qquad (16)$$

and

$$\frac{\partial P_2}{\partial t} = \frac{k_0 A_0(P - P_2)}{\mu l_0 c V_c} \qquad (17)$$

For gas as the flowing fluid we equate 13 and 15 and substitute into 12 to give

$$\frac{\partial P}{\partial t} = \frac{k}{2\phi_1\mu}\frac{\partial^2 P^2}{\partial x^2} - \frac{V_2}{V_1}\frac{\partial P_2}{\partial t} \qquad (18)$$

and

$$\frac{\partial P_2}{\partial t} = \frac{k_0 A_0 P_2(P - P_2)}{\mu l_0 V_c} \qquad (19)$$

For brevity in the following discussion we let

$$\frac{k_0 A_0}{\mu l_0 c V_c} = H \qquad (20)$$

The method of solution of the system of equations given by equations 16 and 17 is given in Appendix II for the boundary conditions

$$P'(0, T) = 1,\ \frac{\partial P'}{\partial x}(L, T) = 0,\ P'(x, 0) = P_2'(x, 0) = 0$$

The solution is

$$P'(x, t) = 1 - \sum_{n=1}^{\infty}\frac{\left[\sin(2n - 1)\frac{\pi x}{2L}\right]\exp(S_n t)}{S_n L\left(\frac{\partial\beta}{\partial s}\right)_n} \qquad (21)$$

where

$$\left(\frac{\partial\beta}{\partial S}\right)_n = -\left\{1 + \frac{V_2}{V_1}\left(\frac{H}{S_n + H}\right)^2\right\}\frac{1}{2\alpha\beta_n} \qquad (22)$$

$$S_n = \frac{-H\left(1 + \frac{V_2}{V_1}\right) - \alpha\beta_n^2 \pm \sqrt{\left\{H\left(1 + \frac{V_2}{V_1}\right) + \alpha\beta_n^2\right\}^2 - 4H\alpha\beta_n^2}}{2} \qquad (23)$$

$$\beta_n = (2n - 1)\frac{\pi}{2L} \qquad (24)$$

Equations 18 and 19 probably can be solved by finite difference methods using an extension of the

---

(5) I. Fatt, THIS JOURNAL, 63, 751 (1959).

(6) W. A. Klikoff, Jr., M.S. thesis, University of California, Berkeley, June 1960.

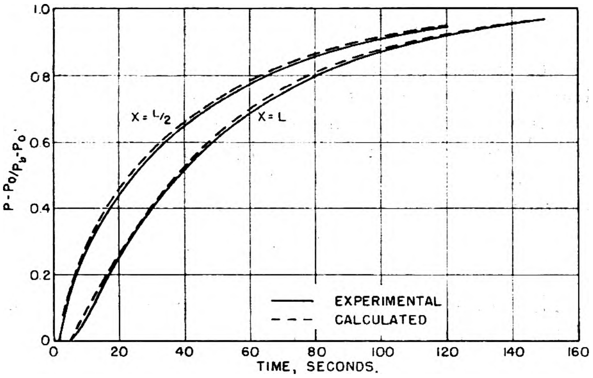

Fig. 1.—Dimensionless pressure *versus* time for laboratory model with $V_2/V_1 = 0.4859$ (50 ccm. side chambers) and $H = 0.1347$ sec.$^{-1}$ (0.122 Darcy-cm. orifices).

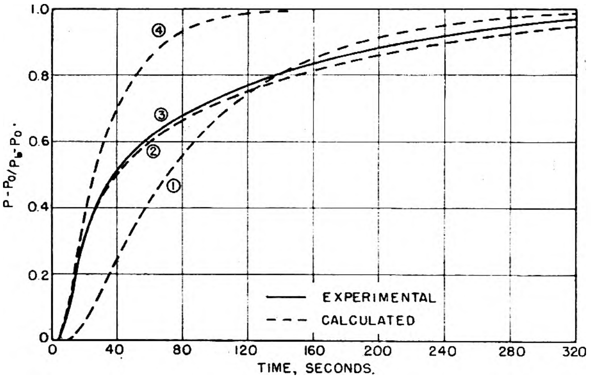

Fig. 2.—Dimensionless pressure *versus* time for laboratory model. Curves 2 and 3 for model with $V_2/V_1 = 1.6911$ (174 cm.^{3} side chambers), and $H = 0.0130$ sec.$^{-1}$ (0.0411 Darcy-cm. orifices). Curve 1 is for model with side chambers but no orifices in series. Curve 4 is for model with no side chambers.

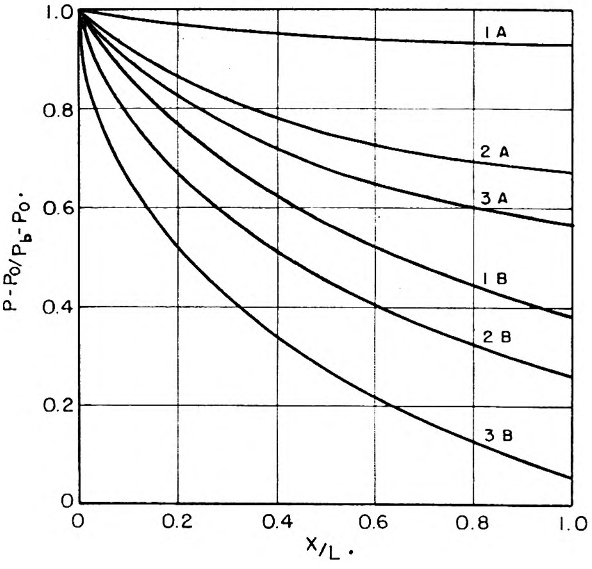

Fig. 3.—Pressure along the main flow channel as a function of time. Curves marked A are at 80 sec.; curves marked B are at 20 sec. Curves 1A and 1B for main flow channel only. Curves 2A and 2B for main flow channel with 174 cm.^{3} side chambers connected through 0.0411 Darcy-cm. orifices. Curves 3A and 3B for main flow channel with 174 cm.^{3} side chambers connected directly to channel (no orifices in series).

method given by Aronovsky and Jenkins.[7] Such solution has not been attempted here. However, the excellent results of the analysis of the case of a liquid lends weight to the validity of equations 18 and 19.

The series in equation 21 was evaluated by Goodknight[8] by use of a FORTRAN program on an IBM 704 digital computer.

Experimental

The laboratory model was similar to that used by Fatt.[3] The model consisted of a main flow channel and nine sinks connected to it. Each sink was an empty chamber connected to the main flow channel through an orifice. The fluid used was air at pressures very close to atmospheric. The pressure drop across the system was never greater than 0.02 atm. The change in compressibility from beginning to end of a run was never greater than 2% and therefore the air is acting as a slightly compressible fluid.

The main flow channel was a 2″ × 2″ × 60″ piece of sandstone quarried near Boise, Idaho. After coating with an epoxy resin, the permeability and porosity were measured and found to be 1.46 Darcys and 23.6%, respectively. The pore volume was 926 ccm.

To obtain access to the sandstone, holes were drilled into the plastic coating at each end and at nine equally-spaced points along one side. A quick-opening valve was installed at one end and needle valves in the nine holes along the side. An orifice and chamber were connected to each valve along the side of the main flow channel. The orifices were $^1/_4$″ × $^1/_4$″ pieces of Boise sandstone mounted in plastic and then cut to 2″ or 4″ lengths. The average permeance of the nine 2″-long orifices was 0.122 Darcy-cm.; the nine 4″-long orifices had an average permeance of 0.0615 Darcy-cm. The 2″ and 4″ orifices could be connected in series to give nine sets of orifices with an average permeance of 0.0411 Darcy-cm. The individual orifices deviated only a few per cent. from these averages.

Three sizes of chambers were used as sinks: namely, 50, 125 and 174 cm.^{3} The 50 cm.^{3} chambers were of plastic tubing; the others were glass bottles.

Air at constant pressure, for application to the end of the flow channel, was obtained from two precision pressure regulators connected in series to a 90 p.s.i.g. compressed air line. A continuous record of pressure *versus* time at any desired point on the flow channel was made by use of a Wiancko pressure transducer feeding a Foxboro Dynalog chart recorder.

Discussion

Figure 1 shows a set of experimental and theoretical pressure transient curves which are typical of the nine combinations of chamber volume and orifice resistance. The agreement between the experimental results and the solution of equation 21 is within the probable experimental error. Figure 2 compares the pressure transients, both experimental and theoretical, for a system containing dead-end pore volume with the predicted transient behavior, if the dead-end volume or orifice resistance is neglected. Curve 1 was calculated from equation 1 by including all the pore volume, dead-end plus main flow channel, in the α term and neglecting the resistance to flow between the dead-end pores and the main flow channel. Curve 4 was calculated from equation 1 by including only the main flow channel pore volume in α. Fatt[3] and Klikoff[6] have shown experimentally that curves 1 and 4 obtained from the laboratory model of Fig. 1 are in exact agreement with the theoretical curve obtained from the conventional solution of

---

(7) J. S. Aronovsky and R. Jenkins, Proc. 1st Natl. Congress Appl. Mech., Am. Soc. Mech. Engrs., New York, 1952.

(8) R. C. Goodknight, M.S. thesis, University of California, Berkeley, January 1960.

equation 1. It is apparent from Fig. 2 that dead-end pore volume connected through a resistance changes the form of the pressure transient. Curves 1 and 4 cannot be brought into agreement with the experimental curve by any simple modification of the α term. Agreement is brought about only by adding a source function to the basic differential equation.

Figure 3 shows the effect of dead-end pore volume on the pressure transient curve when this curve is plotted as pressure *vs.* distance. Curves 2A and 2B are the pressure profiles, measured in the main flow channel, for a system with dead-end pore volume connected through an orifice. Curves 1A and 1B are for a system with pore volume equal to the main flow channel pore volume; curves 3A and 3B are for a system in which there is no dead-end pore volume but in which the pore volume is equal to the total pore volume of the system of curves 2A and 2B; in other words, for a system in which there is no resistance to flow through the orifices.

Fatt[3] and Klikoff[6] have demonstrated experimentally that the dead-end pore volume should be added to the main channel volume when using equation 1 if there is no resistance to flow between the dead-end volume and the main channel. The theoretical reason for the simple addition of volumes in this case can now be explained. As H approaches infinity then P_2 approaches P and γ_2 approaches γ_1. When $\gamma_1 = \gamma_2$ then equation 6 becomes

$$\operatorname{div}(v_1\gamma_1) = \frac{\partial \gamma_1}{\partial t}(\phi_1 + \phi_2) \qquad (25)$$

Then, from the definition of ϕ, we have

$$\operatorname{div}(v_1\gamma_1) = \frac{\partial \gamma_1}{\partial t}\frac{(V_1 + V_2)}{AL} \qquad (26)$$

Equation 26 shows that if there is no resistance to flow between the dead-end volume and the main flow channel, then the total volume is used to calculate α which in turn is used in equation 1.

If $H = 0$ then ϕ_2 does not exist as far as any flow in the system is concerned. ϕ_2 is then zero in equation 25, and equation 26 becomes

$$\operatorname{div}(v_1\gamma_1) = -\frac{\partial \gamma_1}{\partial t}\frac{V_1}{AL} \qquad (27)$$

Thus far nothing has been said about how one may measure the various parameters that appear in equations 16 and 17. In the laboratory model these parameters were built into the system. However, in the case of a porous medium containing dead-end pore space, neither V_2/V_1 nor H can be measured by any currently available laboratory procedure. A possible approach to this problem may be through a comparison of the measured pressure (or concentration) transients with those predicted from equations 1, 2 or 3. The presence of dead-end pore space connected through a flow resistance will cause disagreement. If there is disagreement, then estimates of V_2/V_1 and H are made and equations 16 and 17, or 18 and 19 or 7A and 8A, are solved and numerically evaluated. If the proper choice of V_2/V_1 and H was made, then equations 16 and 17, or their equivalent, will give a curve in agreement with the experimental data. However, several pore structure parameters are combined in the terms V_2/V_1 and H; and, therefore, it is difficult to obtain a unique set of parameters by this method.

It is of interest to calculate the characteristics of a porous medium containing microscopic dead-end pores that would give pressure transients identical to those obtained on our laboratory model. If we consider the porous medium identical to the model used in the laboratory, then the resistance to flow into the dead-end pores is concentrated in the necks of these pores. Assuming these necks to be cylindrical capillaries, we may determine the dimensions of a system that will give the pressure transients shown in Fig. 1. By Poiseuille's law, the flow rate into the sink is

$$Q = \frac{\pi r^4}{8\mu l}(P - P_2) - cV_c\frac{\partial P_2}{\partial t} \qquad (28)$$

and for the laboratory model

$$Q = \frac{k_oA_o}{\mu l_o}(P - P_2) = cV_c\frac{\partial P_2}{\partial t} \qquad (29)$$

Equating $\partial P_2/\partial t$ in equations 28 and 29 we get

$$\pi r^4/8lV_c = k_oA_o/l_oV_c$$

Therefore, if we assume that all the other parameters are those of the system of Fig. 1 and also assume that $l_o = 10^{-2}$ cm. and $v_c = 10^{-10}$ cm.^{3}, we find that $r = 0.268 \times 10^{-5}$ cm. In other words, a porous medium with the following characteristics would give the transients shown in Fig. 1: porosity 23.6%; permeability 1.46 Darcys; 1.15×10^9 dead-end pores per cm.^{3} of porous material; dead-end volume 10^{-10} cm.^{3} per pore; connecting capillaries of length 10^{-2} cm., and radius 0.268×10^{-5} cm. This is not a unique set of parameters. Any set that gives $v_2/v_1 = 0.4859$ and $H = 0.1347$ sec.$^{-1}$ would describe a system with the pressure transients of Fig. 1.

Conclusions

When a slightly compressible fluid is flowing in a linear porous medium which has dead-end pore volume separated from the main flow channel by a resistance to flow, the pressure transients are described by equations 16 and 17. A similar set of equations is available when the flowing fluid is a gas or for diffusion through the fluid contained in a porous medium.

Acknowledgment.—Acknowledgment is made to the donors of the Petroleum Research Fund, administered by the American Chemical Society, for support of this research.

Appendix I

We consider a porous medium with porosity ϕ_1. The porous material is considered to have N "dead-end" pores of volume V_c. The system has cross-sectional area A, length L, and tortuosity θ. We isolate an element of the system of length dx. The porous medium is assumed to be saturated with solvent. At x there is an amount of solute diffusing in the positive x direction equal to M_x g./sec. At $x + dx$ the diffusion flow out of the element is approximately $M_x + (\partial M_x/\partial x)dx$ g./sec. If the concentration of the solute is denoted by $C(x, t)$, then from Fick's first law we have

$$M_x = -\frac{DA\phi_1}{\theta^2}\frac{\partial C}{\partial x} \qquad (1A)$$

where D (D is assumed to be independent of C) is the diffusivity of the solute in the solvent. Now the difference between the diffusion flow into and out of the system is

$$\frac{DA\phi_1}{\theta^2}\frac{\partial^2 C}{\partial x^2}\,dx \qquad (2A)$$

and this difference must be equal to the amount of solute stored in the element per unit time plus the amount of solute lost to the "sinks" per unit time. Letting the diffusion flow toward the sinks be M' g./sec., we may write

$$\frac{DA\phi_1}{\theta^2}\frac{\partial^2 C}{\partial x^2}\,dx = \phi_1 A\frac{\partial C}{\partial t}\,dx + M' \qquad (3A)$$

where

$$\phi_1 A\frac{\partial C}{\partial t}\,dx \qquad (4A)$$

is the amount of solute stored in the element per unit time.

We now make some assumptions concerning the sinks and M': (i) To each element of volume $A\,dx$ of the porous system there is assigned an elemental "dead-end" volume or "sink" of volume equal to $(dx/L)V_2$ ($V_2 = NV_0$); (ii) there is no communication between these elemental sinks; (iii) each of these sinks is connected to the elemental volume ($A\,dx$) by a "neck" or capillary of cross-section A_0 and length l_0. The average cross-section of the sink is much greater than A_0; (iv) there is steady-state diffusion flow through the neck.

Letting $C_2(x, t)$ be the concentration of solute in the sink at x and t, we may write

$$M' = \frac{V_2}{L}\frac{\partial C_2}{\partial t}\,dx \qquad (5A)$$

and from assumption (iv)

$$M' = \frac{DA_0}{l_0}(C - C_2) \qquad (6A)$$

Replacing M' in equation 3A by equation 5A we get

$$\frac{\partial C}{\partial t} = \frac{D}{\theta^2}\frac{\partial^2 C}{\partial x^2} - \frac{V_2}{V_1}\frac{\partial C_2}{\partial t} \qquad (7A)$$

If 5A is to equal 6A, $(V_2/L)dx = V_c$ or $(dx/L = 1/N)$ Making this substitution and equating 5A and 6A

$$\frac{\partial C_2}{\partial t} = Y(C - C_2) \qquad (8A)$$

where

$$Y = \frac{DA_0}{l_0 V_c}$$

Note the similarity between equations 7A and 8A and equations 16 and 17.

If the following boundary and initial conditions are used when solving equations 7A and 8A

$$C(x, 0) = C_2(x, 0) = C_0$$
$$C(0, T) = C_1$$
$$\frac{\partial C}{\partial x}(L, t) = 0$$

we get by analogy to the solution to the boundary value problem given by equation 21

$$C' = \frac{C - C_0}{C_1 - C_0} = 1 - \sum_{n=1}^{\infty}\frac{\left[\sin(2n-1)\frac{\pi x}{2L}\right]\exp(S_n t)}{S_n L\left(\frac{\partial\beta}{\partial s}\right)_n} \qquad (9A)$$

where

$$S_n = \frac{-Y\left(1 + \frac{V_2}{V_1}\right) - \frac{D\beta^2}{\theta^2} \pm \sqrt{\left\{Y\left(1 + \frac{V_2}{V_1}\right) + \frac{D\beta^2}{\theta^2}\right\}^2 - \frac{4DY\beta^2}{\theta^2}}}{2}$$

$$\beta = (2n-1)\frac{\pi}{2L}, \quad \left(\frac{\partial\beta}{\partial S}\right)_n = -\left\{1 + \frac{V_2}{V_1}\left(\frac{Y}{S_n + Y}\right)^2\right\}\frac{\theta^2}{D\beta_n}$$

Appendix II

We wish to solve

$$\frac{\partial P'}{\partial t} = \alpha\frac{\partial^2 P'}{\partial x^2} - \frac{V_2}{V_1}\frac{\partial P'_2}{\partial t} \qquad (1B)$$

and

$$\frac{\partial P'_2}{\partial t} = H(P' - P'_2) \qquad (2B)$$

simultaneously, subject to the boundary conditions

$$P'(0, t) = 1 \qquad (3B)$$

$$\frac{\partial P'}{\partial x}(L, t) = 0 \qquad (4B)$$

and the initial conditions

$$P'(x, 0) = 0 \qquad (5B)$$

$$P'_2(x, 0) = 0 \qquad (6B)$$

Let $\bar{P}$ be the Laplace transform of P'

$$\bar{P} = \int_0^\infty P'\exp(-St)dt$$

and $\bar{P}_2$ be the Laplace transform of P'_2

$$\bar{P}_2 = \int_0^\infty P'_2\exp(-St)dt$$

We take the Laplace transform of equations 1B, 2B, 3B and 4B and make use of the initial conditions, equations 5B and 6B.

$$S\bar{P} = \alpha\frac{\partial^2\bar{P}}{\partial x^2} - \frac{V_2}{V_1}S\bar{P}_2 \qquad (7B)$$

$$S\bar{P}_2 = H(\bar{P} - \bar{P}_2) \qquad (8B)$$

$$\bar{P}(0, S) = \frac{1}{S} \qquad (9B)$$

$$\frac{\partial\bar{P}}{\partial x}(L, S) = 0 \qquad (10B)$$

Solving equation 8B for $\bar{P}_2$ and substituting into equation 7B, we get

$$\frac{\partial^2\bar{P}}{\partial x^2} - \frac{1}{\alpha}\left\{S + \frac{V_2}{V_1}\frac{SH}{(S + H)}\right\}\bar{P} = 0 \qquad (11B)$$

We let

$$\beta^2 = -\frac{1}{\alpha}\left\{S + \frac{V_2}{V_1}\frac{SH}{(S + H)}\right\} \qquad (12B)$$

then we solve

$$\frac{\partial^2\bar{P}}{\partial x^2} + \beta^2\bar{P} = 0 \qquad (13B)$$

subject to the boundary conditions equations 9B and 10B. This solution is

$$\bar{p} = \frac{\cos \beta(x - L)}{S \cos \beta L} \qquad (14B)$$

We may invert, using the inversion integral

$$P'(x, t) = \frac{1}{2\pi i} \int_{\gamma - i\infty}^{\gamma + i\infty} \frac{\cos \beta(x - L) \exp(St)}{S \cos \beta L} \, \mathrm{d}S \qquad (15B)$$

Equation 14B is analytic except for isolated singularities and one essential singularity and is single-valued. There is a simple pole at $S = 0$ and there are simple poles at those values of S for which $\beta = (2n - 1)(\pi/2L)$; $n = 1, 2, \ldots$. The essential singularity occurs at $S = -H$. Without regard to the conditions under which the inversion integral 15B represents $P'(x,t)$ and the integral over the infinite semicircle in the left plane tends to zero, we use a series representation for $P'(x,t)$ by summing the residues of 14B. Neglecting the contribution (if any) of the essential singularity at $S = -H$

$$P'(x, t) = 1 - \sum_{n=1}^{\infty} \frac{\left[\sin (2n - 1) \frac{\pi x}{2L}\right] \exp(S_n t)}{S_n L \left(\frac{\partial \beta}{\partial S}\right)_n} \qquad (16B)$$

where

$$\left(\frac{\partial \beta}{\partial S}\right)_n = -\frac{1}{2\alpha\beta_n} \left\{1 + \frac{V_2}{V_1} \left(\frac{H}{S_n + H}\right)^2\right\}$$

and S_n is obtained by solving equation 12B with $\beta = (2n - 1)(\pi/2L)$. Where the symbol S_n appears in a series without a superscript it is inferred that there are two series

$$2S_n^+ = -\left\{H\left(1 + \frac{V_2}{V_1}\right) + \alpha\beta^2\right\} + \sqrt{\left\{H\left(1 + \frac{V_2}{V_1}\right) + \alpha\beta^2\right\}^2 - 4\alpha\beta_n^2 H} \qquad (17B)$$

and

$$2S_n^- = -\left\{H\left(1 + \frac{V_2}{V_1}\right) + \alpha\beta^2\right\} - \sqrt{\left\{H\left(1 + \frac{V_2}{V_1}\right) + \alpha\beta^2\right\}^2 - 4\alpha\beta_n^2 H}$$

We now show that equation 16B is the complete solution (*i.e.*, that there is no contribution from the essential singularity at $s = -H$) by demonstrating that $P'(x,t)$ from equation 16B satisfies equation 1B to 6B.

The investigation of the convergence of equation 16B proceeds in two steps. We first consider the case in which the radical of equation 17B is taken with the negative sign. For this case each term of the series of equation 16B is in absolute value equal to or less than

$$\frac{4}{\pi} \frac{\exp(-\alpha\beta_n^2 t)}{(2n - 1)} \qquad (18B)$$

Since

$$\frac{\pi}{4} \sum_{n=1}^{\infty} \frac{\exp(-\alpha\beta_n^2 t_1)}{(2n - 1)} \qquad (19B)$$

converges, by the ratio test, for $t_1 > 0$, we have by the Weierstrass M-test that for this case ($S_n = S_n^-$) the series of equation 16B converges uniformly with respect to x and t for $0 \leqslant x \leqslant L$ and $t \geqslant t_1 > 0$.

We next consider the case when the radical of equation 17B has the positive sign. Here we notice that as $n \rightarrow \infty$, $\beta \rightarrow \infty$ and $S_n^- \rightarrow -H$. For this case each term of the series in equation 16B is in absolute value equal to or less than

$$\frac{1}{S_n^- L \left(\frac{\partial \beta}{\partial S^-}\right)_n} \qquad (20B)$$

But the following integrals (with monotonic integrands) exist

$$\int_1^{\infty} \frac{\mathrm{d}n}{S(\mathrm{n}) L \frac{\partial \beta(\mathrm{n})}{\partial S}} = \int_{S_0}^{-H} \frac{\mathrm{d}S}{S(\mathrm{n}) L \frac{\partial \beta}{\partial n}} = \frac{1}{\pi} \int_{S_0}^{-H} \frac{\mathrm{d}S}{S}$$

$$(21B)$$

where S_0^+ is evaluated from equation 17B taking $\beta = \beta_n = \pi/2L$ and n is a continuous variable, $1 \leqslant n \leqslant \infty$. By the integral test

$$\sum_{n=1}^{\infty} \frac{1}{S_n^+ L \left(\frac{\partial \beta}{\partial S}\right)_n} \qquad (22B)$$

converges. The Weierstrass M-test shows that for this case, ($S_n = S_n^+$), the series in equation 16B converges absolutely and uniformly with respect to x and t for $0 \leqslant x \leqslant L$ and $t \geqslant 0$. Furthermore, for $t = 0$ the two series of equation 16B combine to form the Fourier series for 1, which is uniformly convergent for $0 < x_1 \leqslant x \leqslant L$. Therefore we are assured of the uniform convergence of $P'(x,t)$ in the range $0 \leqslant x \leqslant L$ for $0 < t_1 \leqslant t$ and $0 < x_1 \leqslant x \leqslant L$ for $t = 0$.

We are justified then in integrating $P'(x,t)$ term by term and we may therefore evaluate $P_2'(x,t)$ using the convolution integral. From equation 8B we have

$$\bar{P}_2 = \frac{H}{S + H} \bar{P} \qquad (23B)$$

Therefore, since the inverse transform of $1/(S + H)$ is e^{-Ht} we get, using the convolution integral

$$P'_2(x, t) = H \int_0^t e^{-H(t-\tau)} P'(x, \tau) \mathrm{d}\tau \qquad (24B)$$

and replacing $P(x, t)$ in 24B by 16B and performing the termwise integration, we get

$$P'_2(x, t) = 1 - H \sum_{n=1}^{\infty} \frac{\left[\sin(2n - 1) \frac{\pi x}{2L}\right] e^{S_n t}}{S_n L \left(\frac{\partial \beta}{\partial S}\right)_n (S_n + H)} + e^{-Ht} \left\{H \sum_{n=1}^{\infty} \frac{\sin (2n - 1) \frac{\pi x}{2L}}{S_n L (S_n + H) \left(\frac{\partial \beta}{\partial S}\right)_n} - 1\right\} \qquad (25B)$$

But by substituting the values of S_n^- and S_n^+ from 17B into the second series above, we find that

$$\sum_{n=1}^{\infty} \frac{H \left[\sin(2n - 1) \frac{\pi x}{2L}\right]}{S_n L \left(\frac{\partial \beta}{\partial S}\right) (S_n + H)} = \frac{4}{\pi} \sum_{n=1}^{\infty} \frac{\left[\sin (2n - 1) \frac{\pi x}{2L}\right]}{2n - 1} = 1$$

$$(26B)$$

Therefore

$$P_2'(x, t) = 1 - \sum_{n=1}^{\infty} \frac{H}{S_n + H} \frac{\left[\sin(2n - 1) \frac{\pi x}{2L}\right] e^{S_n t}}{S_n L \left(\frac{\partial \beta}{\partial S}\right)_n}$$

$$(27B)$$

and furthermore, the uniform convergence of this series with respect to x and t in the same region specified for $P'(x,t)$ is ensured by the uniform convergence of $P'(x,t)$ since each term of the series representing $P_2(x,t)$ is in absolute value equal to or less than the corresponding terms of the series representing $P'(x,t)$.

It is a simple matter now to show that the series representations of $\partial P'_2/\partial t$. $\partial P'/\partial t$ and $\partial^2 P'/\partial x^2$ are all uniformly convergent. The series representation of $\partial P_2/\partial t$ is equal to the sum of the two uniformly convergent series representing HP and $-HP_2$. The terms of the series representing $\partial P'/\partial t$ are in absolute value less than the terms of the uniformly convergent series representing $\partial P_2/\partial t$, hence the series representing $\partial P'/\partial t$ is uniformly convergent by the M-test. Finally, the series representing $\partial^2 P'/\partial x^2$ is equal to the sum of the two uniformly convergent series representing $(1/\alpha)\cdot(\partial P'/\partial t)$ and $(1/\alpha)(V_2/V_1)(\partial P_2/\partial t)$. We have shown then that the term-by-term differentiation of the series representing P' and P'_2, both with respect to x and t (twice with respect to x) is justified; furthermore, we have shown that the solutions $P'(x,t)$ and $P_2(x,t)$ satisfy the partial differential equations—equations 1B and 2B.

That the solutions satisfy the boundary conditions—equations 3B and 4B—may be verified by inspection. The authors have verified that the solutions also satisfy the initial conditions—equations 5B and 6B—by substitution; consequently, the validity of the series of residues is established. Furthermore, the solution is unique.

VISCOSITY-CONCENTRATION AND FLUIDITY-CONCENTRATION RELATIONSHIPS FOR SUSPENSIONS OF SPHERICAL PARTICLES IN NEWTONIAN LIQUIDS

By T. F. Ford[1]

Dairy Products Laboratory, Eastern Utilization Research and Development Division, Agricultural Research Service, United States Department of Agriculture, Washington, D. C.

Received March 7, 1960

It was established by Bingham[2] that plots of fluidity against concentration tend to be linear over considerable concentration ranges, whereas viscosity plots are always curved. Many illustrations, for proteins, have been given by Treffers.[3] DeBruijn[4] and Vand[5b] have made use of such plots. In general, however, the fluidity function has received little attention, despite the first order reciprocal relationship between the linear equation $\phi/\phi_0 = 1 - 2.5C_v$ (I) and the Einstein equation as usually written $\eta/\eta_0 = 1 + 2.5C_v$ (II). It is the purpose of this paper to show that the consensus of present theoretical and empirical equations for the flow of suspensions of rigid spherical particles alone makes I a closer approximation than II, and by re-examination of available data to support this conclusion to the extent it may even be suggested that equation I and its exact reciprocal, $\eta/\eta_0 = 1 + 2.5C_v + 6.25C_v^2 + \ldots$ (III) may describe accurately the flow of suspensions of rigid spheres in Newtonian liquids at low and moderate concentrations.

Collected Viscosity Equations and Their Reciprocal or Fluidity Forms

Various equations relating viscosity to concentration for suspensions of spheres are listed in Table I together with the reciprocal or fluidity forms of each. For ready comparison all equations are given in Table I as power series, $Y = 1 + aC_v + bC_v^2 + cC_v^3 + \ldots$,[6] where Y designates either relative viscosity, η/η_0, or relative fluidity, ϕ/ϕ_0, and C_v is the volume fraction of the dispersed phase. The several pairs of equations are exactly equivalent and are obtained, the one from the other, by long division. The over-all purpose of the table is to show that without regard to theoretical or experimental background all of these equations are more nearly linear in the fluidity form.

It is seldom noted that Einstein's derivation[7] really led to the equation $\eta/\eta_0 = (1 + 0.5C_v)/(1 - C_v)^2$, from which the series given in Table I are derived. This equation takes no account of interactions between particles. It applies, therefore, over concentration ranges in which interactions can be disregarded; but these ranges may be considerably wider than those to which the simplified form, II, applies.

Interactions between particles have been considered by various authors, in particular Simha and co-workers (*cf.* ref. 8), DeBruijn,[4] and Vand.[5a] DeBruijn,[4] with Burgers,[9] give a derivation which is unique in utilizing the fluidity function and is semi-independent of Einstein's. DeBruijn obtains $\phi/\phi_0 = 1 - 2.5C_v + 2.5kC_v^2$. He evaluates the constant k in an empirical way by making $\phi/\phi_0 = 0$ at $C_v = 0.74$, the volume fraction occupied by

(1) Naval Research Laboratory, Washington, D. C.

(2) E. C. Bingham, "Fluidity and Plasticity," McGraw-Hill Book Co., Inc., New York, N. Y., 1922.

(3) H. P. Treffers, *J. Am. Chem. Soc.*, **62**, 1405 (1940).

(4) H. DeBruijn, *Rec. trav. chim.*, **61**, 863 (1942); Proceedings of the International Congress of Rheology, Amsterdam, 1949, p. II-95.

(5) V. Vand, (a) THIS JOURNAL, **52**, 277 (1948); (b) **52**, 300 (1948).

(6) A catalog of viscosity equations converted to power series is also given by Bredée and de Booys. Their list includes several earlier forms omitted here. H. L. Bredee and J. deBooys, *Kolloid Z.*, **79**, 31 (1937).

(7) A. Einstein, (a) *Ann. Physik*, **19**, 286 (1906); (b) **34**, 591 (1911).

(8) R. Simha, (a) THIS JOURNAL, **44**, 25 (1940); (b) *J. Applied Physics*, **23**, 1020 (1952).

(9) J. M. Burgers, "First and Second Report on Viscosity and Plasticity," N. V. Noord-Hollandsche Uetgeversmaatschappij, Amsterdam, Holland, 1938.

TABLE I

EXPRESSIONS RELATING RELATIVE VISCOSITY AND RELATIVE FLUIDITY TO VOLUME CONCENTRATION FOR SUSPENSIONS OF RIGID SPHERICAL PARTICLES

Author	Year	Ref.	Viscosity form	Fluidity form
			Theoretical equations	
Einstein	1906–11	(7)	$\eta/\eta_0 = 1 + 2.5C_v + 4C_v^2 + 5.5C_v^3 \ldots$	$\phi/\phi_0 = 1 - 2.5C_v + 2.25C_v^2 - 1.25C_v^3 ..$
DeBruijn	1942	(4)	$1 + 2.5C_v + 4.7C_v^2 + 7.77C_v^3 \ldots$	$1 - 2.5C_v + 1.552C_v^2 \ldots$
Vand	1948	(5a)	$1 + 2.5C_v + 7.349C_v^2 \ldots$	$1 - 2.5C_v - 1.099C_v^2 \ldots$
Simha[a]	1952	(8b)	$1 + 2.5C_v + 3.73C_v^2 + 6.94C_v^{7/3} ..$	$1 - 2.5C_v + 2.52C_v^2 - 6.94C_v^{7/3} ..$
Kynch[a]	1956	(10)	$1 + 2.5C_v + (7.5 \text{ to } 6.75)C_v^2 \ldots$	$1 - 2.5C_v - (1.25 \text{ to } 0.50)C_v^2 \ldots$
			Empirical equations	
Arrhenius	1887	(11)	$1 + 2.5C_v + 3.125C_v^2 + 2.60C_v^3 ..$	$1 - 2.5C_v + 3.125C_v^2 - 2.60C_v^3 \ldots$
Vand	1948	(5b)	$1 + 2.5C_v + 7.17C_v^2 + 16.2C_v^3 \ldots$	$1 - 2.5C_v - 0.92C_v^2 + 4.0C_v^3 \ldots$
Robinson	1949	(16)	$1 + 2.5C_v + 4.6C_v^2 + 8.4C_v^3$	$1 - 2.5C_v + 1.65C_v^2 - 1.0C_v^3 \ldots$

[a] Both Simha's and Kynch's second and higher order coefficients change with concentration. The equations given are for dilute solutions. See text.

close-packed uniform spheres. This makes $k = 0.6209$ and gives the equations attributed to DeBruijn in the table. It will be seen in the discussion of experimental results, however, that for rigid particles it is more probable that $\phi/\phi_0 = 0$ at $C_v = 0.5236$, the volume fraction in cubical packing. Imposing this condition makes $k = 0.222$ and the two equations become $\eta/\eta_0 = 1 + 2.5C_v + 5.123C_v^2 + 9.99C_v^3$ and $\phi/\phi_0 = 1 - 2.5C_v + 1.127C_v^2$, respectively.

DeBruijn's and Vand's equations both represent attempts to fit the complete concentration range. Recently Simha[8b] and more recently Kynch[10] have deduced that the constants of the higher power terms must change with concentration. The equations attributed to Simha in the table are expansions of one of his theoretical equations (7a) applicable at low concentrations, up to $C_v = 0.065$. This equation contains a parameter defined by the relationship $f^3 = 8C_{\text{max.}}$ where $C_{\text{max.}}$ may be either that corresponding to cubical packing, $C_v = 0.5236$ ($f = 1.61$), or to close packing, $C_v = 0.74$ ($f = 1.81$). In evaluating the constants for Table I cubical packing has been assumed. In his discussion Simha notes that to fit experimental data over the whole concentration range, f must actually change from a value around 1.3 to less than 2. His final evaluation thus becomes semi-empirical.

Kynch's derivative differs from Simha's but the net result is about the same. Kynch states that a popular value for the second order constant in the viscosity equation is 6.25. This makes the second order constant zero in the fluidity form. According to Simha's treatment the second order constant 6.25 is possible, requiring only that f be given the value $\sqrt[3]{2.5}$ or 1.357. Kynch's observation is of interest in the light of statistical analyses to be presented in the next section of this paper.

The empirical equation due to Arrhenius[11] is usually written in $\eta/\eta_0 = kC_v$. For inclusion in the table it has been rewritten as $\eta/\eta_0 = e^{kC_v}$, expanded as the series $\eta/\eta_0 = 1 + kC_v + \overline{kC_v}^2/2! + \overline{kC_v}^3/3! + \ldots$, and the constant k arbitrarily assigned the value 2.5.

The second and third order constants in the empirical equation assigned to Robinson in Table I are averages based on three extrapolated experimental values of sediment volumes for glass spheres, 1.77, 1.81 and 1.88, given by him. The reciprocals of these numbers, 0.565, 0.553 and 0.532, compare well with the volume fraction of uniform spheres in cubical packing, $(4/3\ r^3)/(8r^3)$ or 0.5236.

Review of Experimental Results

Viscosity measurements which are sufficiently extensive and rigorous for mathematical analysis and on systems acceptable as models of suspensions of spherical particles are scanty. No data yet reported are adequate in all respects. This arises in part from uncertainties as to concentration and shape in molecular and colloidal solutions, and in part from uncertainties in correcting results on visible particles for effects due to size alone. The experiments here considered were selected for various reasons, some merely because prominence previously given them demands their inclusion. In every case the original data were carefully scrutinized and recalculated. Insofar as justified, statistical methods were applied since the purpose was refinement of precision in establishing the constants in the type equation $Y = 1 + aC_v + bC_v^2 + cC_v^3 + \ldots$.

Bancelin's Experiments on Gamboge Sols.— Bancelin's experiments[12] are the first in point of time and apparently were performed very carefully. He prepared monodisperse suspensions of gamboge by centrifugation (the method of Jean Perrin), and for each fraction determined viscosities at various concentrations. Bancelin's object was to test the Einstein equation which as then published was $\eta/\eta_0 = 1 + C_v$. He obtained as his average result $\eta/\eta_0 = 1 + 2.9C_v$. He therefore wrote to Einstein who informed him that the equation should have been $\eta/\eta_0 = 1 + 2.5C_v$. Bancelin's paper gives values for a suspension containing particles 0.30 μ in diameter, at six concentrations between 0.0024 and 0.0211 ml. per ml. Least squares analysis of these data, using the type equation $Y = k + aC_v$, gives

$$\eta/\eta_0 = 0.9994 + 2.715C_v \qquad \text{(S.E.E., 0.00069)}$$

and

$$\phi/\phi_0 = 1.0000 - 2.549C_v \qquad \text{(S.E.E., 0.00052)}$$

Here, the numbers in parentheses are the standard errors of estimate of Y, a convenient measure of the

---

(10) G. J. Kynch, *Proc. Roy. Soc.* (*London*), **A237**, 90 (1956).

(11) S. Arrhenius, *Z. physik. Chem.*, **1**, 285 (1887).

(12) M. Bancelin, *Compt. rend.*, **152**, 1382 (1911).

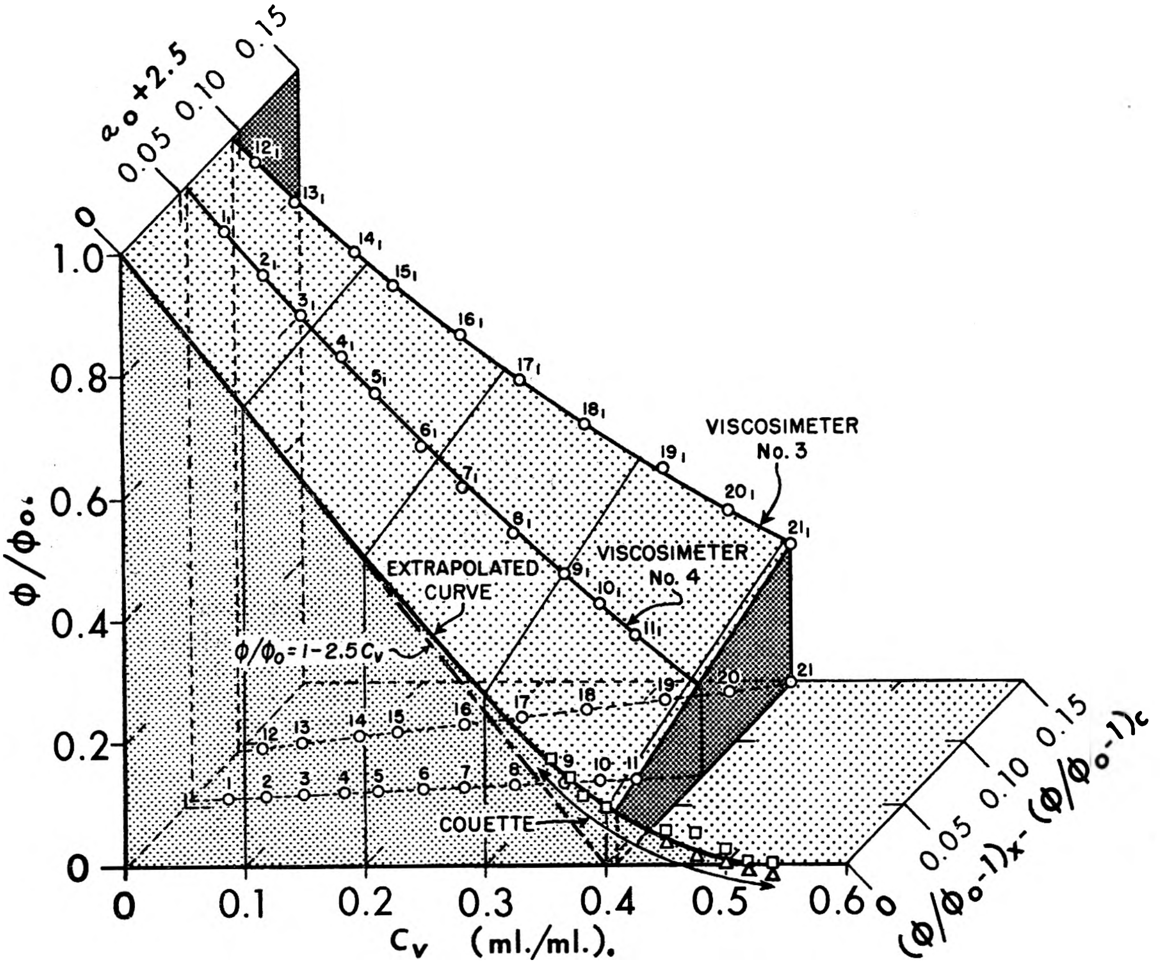

Fig. 1.—Fluidity–concentration plots for suspensions of 125–205μ diameter glass beads, data by Vand.[5b] Points for stirred suspensions (Couette) indicated by open triangles, for non-stirred suspensions by open squares. The method of extrapolation is described in the text.

fit.[13] These results show that to a close approximation, for these data $k = 1$, a necessary check, and that the experimental first order constant is much closer to 2.5 than to 2.9 as reported by Bancelin and repeatedly quoted since.

The data cover a low concentration range. Nevertheless, the measures of deviation given above indicate that over this concentration range the fluidity function is the more linear.

It is possible that for Bancelin's gamboge the experimental first order constant was actually about 2.55, considering that errors in effective volume concentration, due to slight departure from the spherical shape, for example, would be positive. If the concentrations be corrected accordingly by the factor 2.55/2.5, the data are now fit by

$$\eta/\eta_0 = 1 + 2.5C_v + 6.75C_v^2 \qquad \text{(S.E.E., 0.00053)}$$

and

$$\phi/\phi_0 = 1 - 2.5C_v - 0.1C_v^2 \qquad \text{(S.E.E., 0.00052)}$$

Experiments on Suspensions of Glass Spheres.—Suspensions of glass spheres have been used as model systems by Eirich, Bunzl and Margaretha,[14] Eirich and Goldschmidt,[15] Vand,[5b] Robinson,[16] and Eveson and Whitmore (ref. 10).

The experiments by Eirich, *et al.*, which were on yeast cells and mushroom spores as well as glass beads, are generally credited with establishing the first order constant within limits of ±0.3 by use of capillary viscosimeters, and within limits of ±0.2 by use of the Couette viscosimeter. The glass spheres used by Eirich, *et al.*, were from 0.0125 to 0.0205 cm. in diameter. Subsequent to their experiments it has been pointed out by Vand (*vide infra*) that use of particles of this size requires appreciable corrections of both C_v and $\phi/\phi_0 - 1$, by factors which are related to the dimensions of the viscosimeters. Such corrections cannot be applied with assurance to Eirich's capillary data, but they can be applied to the Couette data, and the Couette data are for a low concentration range, $C_v = 0.01$ to 0.08, not adequately covered by other workers with glass beads. A large scale plot of these data discloses that they do not extrapolate to $\phi/\phi_0 = 1$ at $C = 0$; and least squares analysis indicates that the C_v values are too low by the constant amount $\Delta C_v =$

---

[13] The standard error of estimate is the square root of the mean of the squared deviations, $S_y = \sqrt{\Sigma d^2/N}$. Other measures of the fit, mean deviations, standard deviations, and coefficients of correlation, agreed with the standard errors of estimate.

[14] F. Eirich, M. Bunzl and H. Margaretha, *Kolloid. Z.*, **74**, 276 (1936).

[15] F. Eirich and O. Goldschmidt, *ibid.*, **81**, 7 (1937).

[16] J. V. Robinson, (a) This Journal, **53**, 1042 (1949); (b) **55**, 455 (1951).

0.0010, approximately. The C_v values adjusted by this amount and the observed $\phi/\phi_0 - 1$ values were corrected by the use of formulas later developed by Vand.[5b] Thus corrected the data are fit by the equation $\phi/\phi_0 = 1 - 2.50C_v + 0.95C_v^2$, S.E.E., 0.0015. The data as given are fit by the equation $\phi/\phi_0 = 1 - 2.39C_v + 3.29C_v^2$ S.E.E., 0.0018. These experiments by Eirich, *et al.*, provide a second close check of the first order constant, 2.5.

Vand[5b] used the same glass beads as Eirich, *et al.*, loaned to him by Prof. Eirich, but he suspended them in a more viscous liquid, made other refinements in technique, and extended the concentration range almost to saturation. Vand gives an average diameter of 0.013 cm. for these beads. Like Eirich, *et al.*, he used two Ostwald viscosimeters, of different bore diameters, and a Couette viscosimeter, the Couette machine only at concentrations of 35% and higher.

Vand multiplied all of this C_v and $\phi/\phi_0 - 1$ values by specific correction factors for each instrument, and finally combined his corrected data as a composite plot. His final equation is designed to fit a smooth curve through these points. Inclusion of the Couette results has been criticized by Kynch[10] on theoretical grounds. The data themselves, however, provide sufficient reason for their reexamination. With both the Couette and Ostwald instruments, at concentrations beginning immediately above $C_v = 0.35$, different viscosities were obtained depending on whether the suspensions were stirred or not. These known deviations are greater than the total deviations at lower concentrations. This fact is itself sufficient to exclude most of the Couette data, and some of the Ostwald data, or at least to diminish the weight to be given these data. It is noted also that Vand's corrected values for his two Ostwald viscosimeters fall more nearly on smooth curves if plotted separately than if combined. This was confirmed by comparison of the fit of second order equations obtained by least squares analysis. The deviation of the two curves indicates a more empirical analysis than used by Vand.

A method of blind extrapolation in the direction of zero corrections is illustrated by Fig. 1. Here smooth curves through the original uncorrected Ostwald points are drawn in the two receding vertical planes, and the corrected Couette values and the extrapolated Ostwald curve are shown in the plane of the paper. The positions of the receding vertical planes are determined as follows: at $C_v = 0$ by requiring that the first order constants, 2.445 and 2.405, found in the usual way by plotting $(\phi/\phi_0 - 1)/C_v$ against C_v, shall extrapolate to 2.5 for an infinite capillary; and at $C_v = 0.35$ by placing the experimental Ostwald $\phi/\phi_0 - 1$ values, 0.760 and 0.680, and the corrected Couette value, 0.820, on a straight line. The two Ostwald curves thus placed in space and extrapolated into the plane of the paper give a third curve for which the corrections are certainly reduced.

The assumptions involved are: (1) That the first order constant is in fact 2.5. This is supported experimentally by Bancelin's and Eirich's results. (2) That the Couette fluidity used at $C_v = 0.35$ is approximately correct. This seems justified within limits by the apparent absence of stirring errors at this concentration, and by the fact the Couette corrections are in any case small (roughly one-fifth to one-tenth of the Ostwald corrections). (3) That the effective or total corrections vary not only with bore diameter, but also with concentration. This is supported by the observations that Vand's $\phi/\phi_0 = 1$ corrections, for wall effects, are in fact averages of values which apparently vary, approximately linearly, by as much as 12% over the range $C_v = 0.05$ to 0.35.

The extrapolations actually were performed analytically. Interpolated fluidities for the two Ostwald viscosimeters at concentrations increasing by 5% were taken from large scale plots, and also calculated from the second order equations fit to the original data by least squares. Using the analytically interpolated Ostwald values and referring the extrapolation at $C_v = 0.35$ to the corrected Couette values (Fig. 1), the extrapolated curve is fit over the range $C_v = 0.05$ to 0.35 by the equation

$$\phi/\phi_0 = 1 - 2.5C_v - 0.11C_v^2 + 1.6C_v^3$$

Referring the extrapolations to the uncorrected Couette values the equation is

$$\phi/\phi_0 = 1 - 2.5C_v - 0.08C_v^2 + 1.9C_v^3$$

The graphically interpolated values give essentially the same constants. The uncertainty in the second order constant is ±0.10, approximately. Although the type equation $Y = 1 \pm 2.5C_v + bC_v^2 + cC_v^3$ is used here, the extrapolated curves are fit equally well, over most or all of the range $C_v = 0.05$ to 0.35, by equations of the form $\phi/\phi_0 = 1 - 2.5C_v + dC_v^4$.

While the above described extrapolations, based on the uncorrected data, seem to avoid many assumptions, they also include a certain error. This is because in the polynomial equations used the concentration and all multipliers of it are involved as powers higher than the first. It is noted, however, that the C_v corrections (multipliers) as calculated by Vand are less than half his $\phi/\phi_0 - 1$ corrections for wall effects; and it is noted also that it is only in the latter and not in the concentration corrections that any reason for variation with concentration is apparent. Accordingly, Vand's corrected C_v values were combined with his uncorrected $\theta/\theta_0 - 1$ values, and the various manipulations repeated. Referring the extrapolations to the corrected C_v and corrected $\theta/\theta_0 - 1$ Couette values at $C_v = 0.35$, for the range $C_v - 0.05$ to 0.35 the equation obtained is

$$\phi/\phi_0 = 1 - 2.5C_v + 0.00C_v^2 + 1.4C_v^3$$

Referring the extrapolations to the corrected C_v and uncorrected $\phi/\phi_0 - 1$ Couette values the equation is

$$\phi/\phi_0 = 1 - 2.5C_v + 0.11C_v^2 + 1.5C_v^3$$

The uncertainty in the second order constant is 0.10, approximately.

The foregoing calculations all indicate that within the apparent accuracy of the data, in an equation of the form $\phi/\phi_0 = 1 - 2.5C_v + bC_v^2 + cC_v^3 + \ldots$, the second order constant "b" is numerically small, and may be zero.

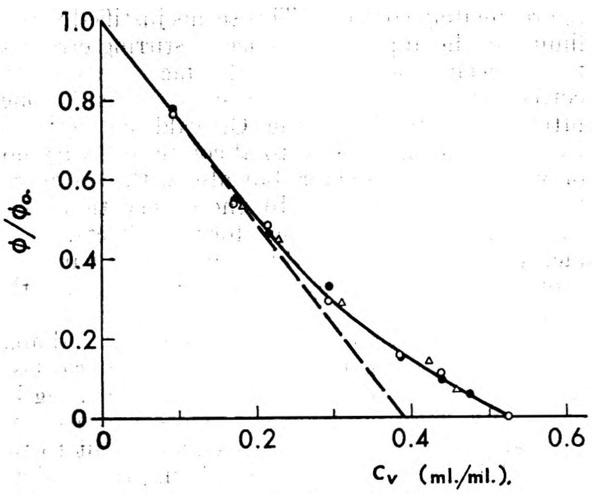

Fig. 2.—Fluidity–concentration plot for suspensions of glass beads, 10–30μ diameter, in no. 30 motor oil (open circles), no. 50 motor oil (closed circles), and castor oil (open triangles). Data are by Robinson.[17a]

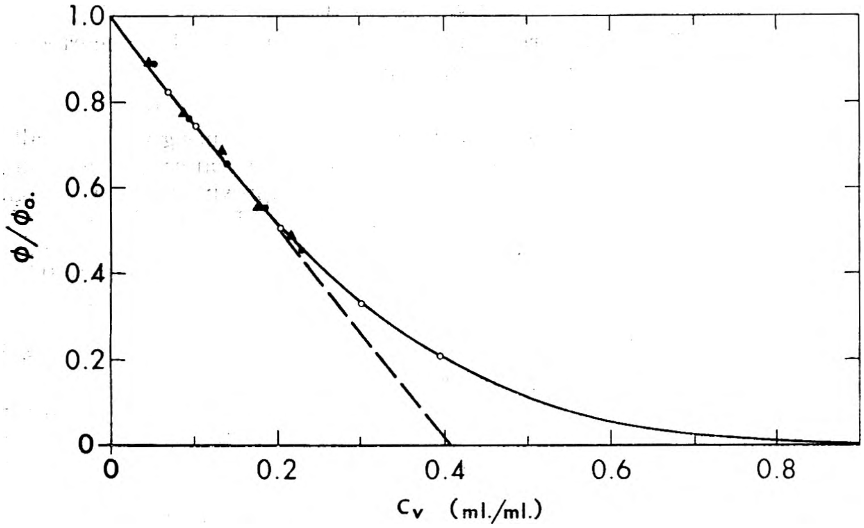

Fig. 3.—Fluidity–concentration plot for milk fat suspensions in fat-free milk serum. Three sets of data are by Leviton and Leighton.[20] The solid curve drawn through the points is that determined by the theoretical equation developed by these authors. Compare the experimental points with those for rubber latex, Fig. 4.

Robinson used beads 3 to 30 μ in diameter, an order of magnitude smaller than Eirich's and Vand's beads, suspended both in oils[16a] and in water-glucose solutions.[16b] He used a Couette viscosimeter. The fluidity plot for his oil suspensions is shown in Fig. 2. Corrections according to Vand's formulas have been applied, but practically the identical curve is given by the uncorrected data. Both this plot and the similar plot for the water-glucose suspensions confirm the general shape of the Vand extrapolated and Couette curve of Fig. 1, and particularly the final intercept in the neighborhood of $C_v = 0.5236$. It will be recalled that Robinson's sediment volumes, obtained by centrifugal packing, also indicate approximately this value.

Sven Odén's Experiments on Sulfur Sols.—Sven Odén's viscosity measurements on sulfur sols[17] do not support statistical analysis. The first order constants obtained graphically vary from 2.95 to 4.29, depending on particle size and temperature. Odén used two size fractions, containing particles about 10 mμ and 100 mμ in diameter, and temperatures from 5 to 40°. It is found that plots of the first order constants against temperature extrapolate to 2.5 at 95°, approximately, for both sizes of particles. Except in this indirect way Odén's results contribute little as a check of the Einstein equation.

The temperature extrapolations are of interest in connection with shells of bound water, postulated by Hatschek[18] to explain the deviations noted. The implication above is that the shells disappear at 95°. It seems plausible, however, that shape factors are involved, the particles becoming more spherical as they approach the melting point.

Milk Fat, Latex, and Asphalt Emulsions.—Data on suspensions of milk fat (cream) variously diluted with fat-free milk serum, by Leviton and Leighton,[19] are plotted in Fig. 3. One of their four sets of data has been omitted because the viscosity of the serum was made much higher than for the other three by addition of cane sugar. The curve drawn through the points (Fig. 3) is that determined by a theoretical equation[20] derived by the authors. This equation takes account of the fact that milk fat is liquid,[21] by making use of Taylor's correction of Einstein's constant 2.5 for sympathetic flow inside liquid particles. This correction lowers the theoretical first order constants to 2.44, 2.45 and 2.39, respectively, for the three sets of data; the average experimental value is 2.44, corresponding to a linear intercept at $C_v = 0.41$ as drawn. Although the dimensions of the viscosimeters are not given, and therefore correction by Vand's formulas is not attempted, the particles are so small these corrections would be negligible in any case. This is confirmed by Leviton and Leighton's comparison of two emulsions containing particles 3 μ and 0.7 μ in diameter, for which exactly the same viscosities were obtained.

These data again confirm the Einstein first order constant, as well as Taylor's correction, but they indicate a final intercept well beyond $C_v = 0.5236$. Since milk fat particles are liquid as well as spherical they should be sufficiently deformable to roll, one over the other, and therefore flow past the concentration corresponding to cubical packing is to be

---

(17) S. Odén, *Z. physik. Chem.*, **80**, 709 (1912); "Der Kolloide Schwefel," *Nova Acta Regiae Soc. Sci. Upsaliensis*, (4) 3 (1913).

(18) E. Hatschek, *Kolloid Z.*, **7**, 301 (1910); **11**, 280 (1912).

(19) A. Leviton and A. Leighton, This Journal, **40**, 71 (1936).

(20) Expanded as a polynominal this equation is $\phi/\phi_0 = 1 - 2.44W + 2.98W^2 - 2.4W^3 + \ldots$, where $W = C_v + C_v{}^{5/3} + C_v{}^{11/3}$.

(21) Viscosity 14 centipoises.

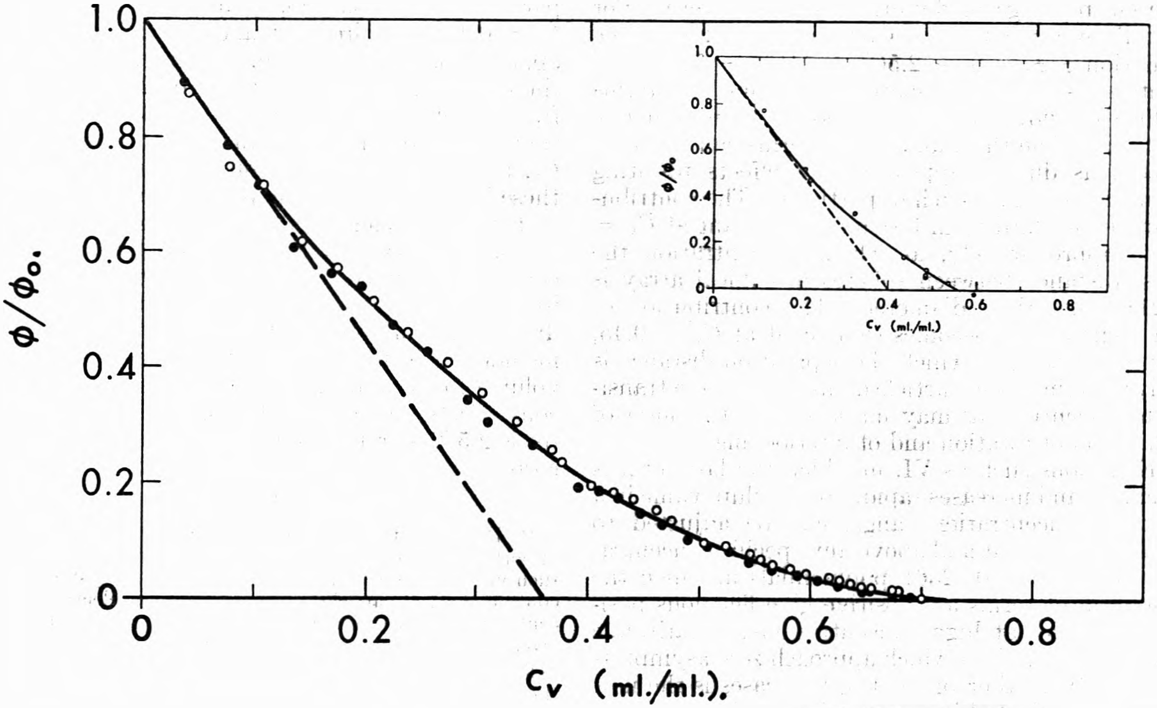

Fig. 4.—Fluidity–concentration plots for rubber latex (main plot) and asphalt emulsions (inserted box). Latex data are by Rhodes and Smith[23]; asphalt data by Eilers.[24] Independent sets of data are indicated by different types of points.

expected. Cream can be concentrated to 72 to 74% by centrifuging at room temperature, and an actual intercept in this neighborhood seems possible.

Fluidity plots for two natural rubber latexes and for two asphalt emulsions, derived from data by Rhodes and Smith,[22] and Eilers,[23] respectively, are shown in Fig. 4. Both of these sets of data have been used in connection with derivations of viscosity equations. In Fig. 4 the latex data are plotted as given by the authors, since a Hoeppler viscosimeter was used and Vand's corrections therefore do not apply. The first order constant calculated for the latex curve is about 2.8, and the final intercept is in the neighborhood $C_v = 0.74$. Both results are reasonable. Latex particles are often not spherical, may be pear shaped, and may even have tails: therefore, the first order constant could well include a shape factor. Latex particles also are plastic and deformable. These experiments are, therefore, of little value as a check of the Einstein equation.

The asphalt data, inserted box of Fig. 4, were first corrected by use of Vand's formulas. The corrections are necessarily approximate. Eilers' particle sizes range from less than 1.6 μ to 9.7 μ in diameter: a diameter of 5.6 μ based on the average particle volume was used. Eilers gives three capillary diameters and apparently reports average viscosities obtained with the three instruments: therefore, average C_v and $\phi/\phi_0 - 1$ corrections were appplied. Thus corrected a first order constant of 2.3, approximately, is indicated. This is impossible since the viscosity of the asphalt used is so high that Taylor's correction for sympathetic flow, as applied by Leviton and Leighton, is insignificant. Remembering the errors involved, for the plot shown the $\phi/\phi_0 - 1$ values have been again multiplied by such a factor as to make $a = 2.5$; this makes $C_{\max.} = 0.56$, approximately. No really accurate interpretation of these data can be attempted because of the scarcity of points at low concentrations, which makes it impossible definitely to establish a first order constant.

Discussion

Limiting Equations, Viscosity and Fluidity.—It appears that for dilute suspensions meeting the requirements of Einstein's original derivation, the equation $\phi/\phi_0 = 1 - 2.5C_v$ (I) is a closer approximation than $\eta/\eta_0 = 1 + 2.5C_v$ (II). Within the limits of accuracy of available measurements, at low and even moderate concentrations, low order terms in C_v higher than the first tend to vanish when the fluidity function is used. Thus, the limiting fluidity equation describing the flow of suspensions of rigid spheres appears to be I, as given above. The limiting viscosity equation appears to be not II but the reciprocal of I, $\eta/\eta_0 = 1 + 2.5C_v + 6.25C_v^2 + \ldots$ (III). This last compares with Einstein's original complete equation, $\eta/\eta_0 = 1 + 2.5C_v + 4.0C_v^2 + \ldots$ (IV).

Complete Equations.—The distinction between limiting equations expanded to include hydrodynamic effects not considered by Einstein, and equations expanded merely to cover wide concentration ranges is not always clear. In some derivations the added effects have been imposed on II, not on IV. Such derivations nullify the basic hydrodynamics considered by Einstein, and are inadequate to the extent II is inadequate.

Empirical equations of the form $\phi/\phi_0 = 1 - 2.5C_v + mC_v^p - nC_v^{p+q}$ (VI), where p is at least 5, can be made to fit experimental fluidity plots over

---

(22) E. Rhodes and H. F. Smith, *J. Rubber Research Inst. Malaya*, **9**, 171 (1939).

(23) H. Eilers, *Kolloid. Z.*, **97**, 313 (1941).

the entire range of fluidities from 1 to zero. For Vand's extrapolated and Couette curve (Fig. 1) the equation $\phi/\phi_0 = 1 - 2.5C_v + 11C_v^5 - 11.5C_v^7$ is quite satisfactory. Apparently the first two terms suffice for flow subject to classical hydrodynamic analysis. The third and fourth terms can be interpreted as due to appearance of effects resulting from the near approach of particles. The contribution of the third term becomes significant at $C_v = 0.25$, approximately, at which concentration the least distance between spheres in cubical array is 0.218 times their diameter. The contribution of the fourth term becomes significant at $C_v = 0.45$, approximately, at which the separation distance is only 0.05 times the particle diameter. These transition concentrations may mark in turn the onset of inhibition of rotation and of interlocking.

Equations such as VI, in which the last term is negative and increases rapidly in absolute value in a certain concentration range, can be adjusted to make $\phi/\phi_0 = 0$ at and above any specific concentration, *e.g.*, $C_v = 0.5236$; polynomials in which the last term or terms are positive give fictitious positive fluidities at high concentrations; logarithmic series give fluidities which approach zero asymptotically. In neither of the last two cases is the flow behavior indicated in accord with the facts.

Correction Factors.—The various corrections evaluated and applied directly by Vand for his glass beads, and implicitly involved in the extrapolations of his data described here, are in general numerically unimportant with true colloidal systems, *e.g.*, gamboge, latex, sulfur sols, mushroom spores, fat suspensions, and protein solutions. If for visible particles, such as glass beads, the corrections are to a certain degree inadequate, this certainly may be due in part to the several assumptions and approximations necessary in their evaluation. It also may be due to omission of still other types of corrections. Correction of C_v for real or presumed shells of bound water, for example, would be comparable with the aggregate of the other C_v corrections used by Vand.

Applications.—The tangent to ϕ/ϕ_0 *vs.* C_v plots $C_v = 0$ usually can be determined graphically with considerable accuracy. The slope of this line, the reciprocal of its intercept at $\phi/\phi_0 = 0$, is the first order constant in the equation $\phi/\phi_0 = 1 - aC_v + \ldots$ This constant is identical with the *intrinsic viscosity*. Its evaluation by using fluidity rather than viscosity data is the more accurate to the extent the fluidity-concentration relationship is the more linear.

Since it seems established that for rigid spherical particles the initial slope intercept should fall at $C_v = 0.4$, as required to make $a = 2.5$, and since it appears that the actual final intercept should be in the near neighborhood of $C_v = 0.5263$, the volume fraction of spheres in cubical packing, it follows that if for a given set of data a suitable multiplier of C_v, the dry volume fraction, will give a plot with these intercepts, then the particles must be spheres and the multiplier equal to V, the voluminosity.

Voluminosity, a term proposed by Bredee,[24] is commonly defined as the ratio of the effective or hydrodynamic volume of a dispersed particle to the dry volume of contained colloid. As such it may include shape factors as well as corrections of the volume for hydration, solvation, and for electroviscous effects (*cf.* ref.[25]). For spheres the shape factor is 2.5/2.5 or 1, making V in this case a volume correction only.

DISCUSSION

R. H. Ottewill (Cambridge University).—I think it is important to stress that one has to be careful about applying such viscosity–concentration relationships to systems which contain charged particles in solutions of low electrolyte concentration. For example, in some recent work of Professor Overbeek and myself on very concentrated sols of silver iodide, containing near spherical particles of radius 250Å., the coefficients of C_v^2 and C_v^3 were found to vary considerably with rate of shear and the electrolyte concentration of the suspending medium.

T. F. Ford.—Reference to the electroviscous effect is made in the paper. It is agreed that in many systems large apparent changes in V can be brought about by changes in the ionic environment. Such changes are insignificant for the systems here discussed.

J. G. Brodnyan (Rohm and Haas Co.)—Is there any reason why you ignored Mooney's equation which was derived using a functional method?

T. F. Ford.—Mooney's equation (*J. Coll. Sci.*, 6, 162 (1951)) is only one of many which were omitted. It could be included in Table I between Vand's and Simha's equations. The expanded forms are

$$n/n_0 = 1 + 2.5C_v + (3.125 + 2.5k)C_v + \cdots \text{ and}$$
$$\phi/\phi_0 = 1 - 2.5C_v + (3.125 - 2.5k)C_v^2 + \cdots$$

Mooney sets the value of k, for monodisperse systems, only roughly between the limits 1.35 and 1.91, the reciprocals of the volume fractions of uniform spheres in close packing and cubical packing, respectively. The actual value to be used is left for experimental determination. To fit Vand's data he makes $k = 1.43$, and to fit Eiler's data on (polydisperse) asphalt he makes $k = 0.75$. In any case it will be seen that Mooney's equation also is more nearly linear in the fluidity form. It was omitted in the interest of brevity and because it would contribute little to the basic conclusion.

---

[24] H. L. Bredee and L. A. Van Bergen, *Chem. Weekblad*, **30**, 223 (1933).

[25] J. T. G. Overbeek and H. G. Bungenberg de Jong, in H. G. Kruyt, "Colloid Science," Elsevier Publishing Co., Inc., New York, N. Y., 1949, Vol. II, p. 209.

ULTRACENTRIFUGAL DETERMINATION OF THE MICELLAR CHARACTER OF NON-IONIC DETERGENT SOLUTIONS[1]

BY C. W. DWIGGINS, JR., R. J. BOLEN AND H. N. DUNNING

Petroleum Research Center, Bureau of Mines, U. S. Department of the Interior, Bartlesville, Oklahoma

Received March 10, 1960

An analytical ultracentrifuge has been used to determine the micellar molecular weights of micelles in four aqueous non-ionic detergent solutions at 25°. Transient state methods have been used extensively, and capillary synthetic boundary cells were used to determine relative optical concentrations. Molecular weights were determined for various times and concentrations to ensure accuracy. Three polyoxyethylated phenols formed micelles containing 100 to 300 molecules while Pluronic L-64, a high molecular weight condensate of ethylene and propylene oxides, does not exhibit micelle formation.

Introduction

Several properties of aqueous detergent solutions cease to vary with concentration or change radically at a concentration characteristic of the detergent. This anomalous behavior has been attributed to the formation of micelles. The concentrations at which such changes occur, *critical micelle concentrations*, have been studied extensively and are usually in the parts-per-million range.[2–4]

The structures of detergent and soap solutions have been investigated by several methods, and these studies confirm the formation of micelles. Light-scattering methods have been used to determine the micellar molecular weights of detergents,[5–7] and X-ray diffraction studies have contributed much to the understanding of micelle formation.[8,9] The study of vapor pressure lowering of detergent solutions[10] has also furnished valuable data. The theory of micelle formation has been studied, and a statistical mechanical theory has been described.[11]

The analytical ultracentrifuge provides a convenient method for the determination of the micellar molecular weights of detergent micelles. The problem of micellar molecular weight determination for non-ionic detergents is somewhat simpler than for ionic detergents since ionic materials introduce charge effects that must be suppressed by buffering or treated theoretically.[12]

Transient state ultracentrifuge studies have many of the advantages of true equilibrium methods without the excessive time that equilibrium methods require.[13] In particular, molecular weights may be obtained from transient state methods without independent determinations of diffusion coefficients. Synthetic boundary methods allow the determination of relative optical concentrations and avoid extremely precise determinations of specific refractive increments.[14]

Theoretical

The Spinco analytical ultracentrifuge, fitted with Schlieren optics, presents data as a plot of the relative concentration gradient (dc/dx) *versus* radial distance x in the ultracentrifuge cell. Results of low-speed experiments may be used to calculate apparent weight average molecular weights of sedimentable particles.

The equation required for weight-average molecular-weight determination by transient-state methods at the meniscus[15] is

$$M_{\text{ap}} = \frac{RT}{(1 - \bar{V}\rho)\omega^2} \frac{(\mathrm{d}c/\mathrm{d}x)_{\text{m}}}{x_{\text{m}}c_{\text{m}}} \qquad (1)$$

where

M_{ap} = apparent anhydrous wt. av. mol. wt. for a fixed time and concn.
R = gas constant, ergs/mole/degree
T = absolute temperature, °K.
ω = angular velocity of the centrifuge rotor, radians/sec.
ρ = density of the soln., g./ml.
$\bar{V}$ = partial specific vol. of the solute, ml./g.
c = concn. of the solute, g./100 ml.
x = distance from the axis of rotation to some point in the soln., cm.
m = meniscus of the liquid

The concentration at the meniscus, c_{m}, that is necessary for solution of equation 1 may be calculated from data obtained with the loss-of-plateau transient-state method[16,17] by

$$c_{\text{m}} = c_0 + \frac{1}{(x_{\text{b}}^2 - x_{\text{m}}^2)} \left[\int_{x_{\text{m}}}^{x_{\text{b}}} x^2\,(\mathrm{d}c/\mathrm{d}x)\mathrm{d}x - x_{\text{b}}^2 \int_{x_{\text{m}}}^{x_{\text{b}}} (\mathrm{d}c/\mathrm{d}x)\mathrm{d}x\right] \qquad (2)$$

where

c_0 = initial concentration
b = base of liquid column

The term c_0 in the above equation may be determined from the specific refractive increment of the solute and optical constants for the ultracentrifuge, or synthetic boundary methods may be used. The concentration c_{x} at any point x in the solution may be determined from the equation

$$c_{\text{x}} = c_{\text{m}} + \int_{x_{\text{m}}}^{x} (\mathrm{d}c/\mathrm{d}x)\mathrm{d}x \qquad (3)$$

---

[1] Presented before the 34th National Colloid Symposium, Bethlehem, Pa., June 16–17, 1960.

[2] Lun Hsiao, H. N. Dunning and P. B. Lorenz, THIS JOURNAL, **60**, 657 (1956).

[3] N. Sata and K. Tyuzyo, *Bull. Chem. Soc., Japan*, **26**, 177 (1953).

[4] J. Grindley and C. R. Bury, *J. Chem. Soc.*, 679 (1929).

[5] A. M. Mankowich, THIS JOURNAL, **58**, 1027 (1954).

[6] P. Debye, *J. Appl. Phys.*, **15**, 338 (1944).

[7] P. Debye, THIS JOURNAL, **51**, 18 (1947).

[8] P. A. Winsor, *ibid.*, **56**, 391 (1952).

[9] J. W. McBain and S. Ross, *J. Am. Chem. Soc.*, **68**, 296 (1946).

[10] H. Huff, J. W. McBain and A. P. Brady, THIS JOURNAL, **55**, 311 (1951).

[11] C. A. J. Hoeve and G. C. Benson, *ibid.*, **61**, 1149 (1957).

[12] T. Svedberg and K. O. Pedersen, "The Ultracentrifuge," The Clarendon Press, Oxford, Reprinted by Johnson Reprint Corp., New York, 1959.

[13] H. K. Schachman, "Ultracentrifugation in Biochemistry," Academic Press, New York, 1959, pp. 181–199.

[14] S. M. Klainer and G. Kegeles, THIS JOURNAL, **59**, 952 (1955).

[15] W. J. Archibald, *ibid.*, **51**, 1204 (1947).

[16] A. Ginsburg, P. Appel and H. K. Schachman, *Arch. Biochem. Biophys.*, **65**, 545 (1956).

[17] D. B. Smith, G. C. Wood and P. A. Charlwood, *Can. J. Chem.*, **34**, 364 (1956).

A synthetic boundary experiment[14] may be used to determine relative values of the initial concentration that are directly proportional to the concentration on a weight basis. If the synthetic boundary cell is the same thickness as the cell for the transient-state experiment and if optical constants of the centrifuge are not changed for a given experiment, relative optical concentrations obtained from the following equation may be used to determine molecular weights.

$$c_0, \text{rel.} = \int_{x_m}^{x_b} (\mathrm{d}c/\mathrm{d}x)_s \mathrm{d}x \qquad (4)$$

where

$(\mathrm{d}c/\mathrm{d}x)_s$ = concn. gradient values for a synthetic boundary determination

The same solute concentration should be used for the synthetic boundary and corresponding transient-state experiment.

In practice, initial relative optical concentrations are computed from the synthetic boundary experiment by application of equation 4. The concentration at the meniscus c_m is calculated from equation 2 using data from the transient-state experiments. Concentrations throughout the cell are then calculated by use of equation 3. Thus a plot of $1/xc$ $(\mathrm{d}c/\mathrm{d}x)$ against x may be made from which $1/xc$ $(\mathrm{d}c/\mathrm{d}x)_m$ may be read. This value may then be used in equation 1 to calculate molecular weights.

Experimental

The four non-ionic detergents that were studied are described in Table I. All detergents were used as supplied by the manufacturers. The detergents were over 99% pure surfactant according to the manufacturers. Aqueous solutions of them gave a negative silver nitrate test indicating that halides were absent. The detergent solutions were prepared by weight in freshly redistilled water and stored for only a few days since the solutions sometimes molded after a few weeks storage.

A Spinco Model E ultracentrifuge, equipped with a rotor temperature indicator control (RTIC) and phase plate Schlieren optics, was used.[18] It is possible to sense temperatures to ± 0.02°, and exercise control to ± 0.1° over a range of zero to 40° with the RTIC unit. The temperature-sensing element is a thermistor embedded in the base of the rotor. All ultracentrifuge and density experiments were performed at 25°.

Filled-Epon, 2.5°, double-sector cells of 12-mm. thickness were used for transient-state studies to allow simultaneous recording of the solvent base line and the transient-state Schlieren patterns. Filled-Epon, 2.5°, double sector, capillary-type, synthetic boundary cells of 12-mm. thickness were used for the determination of relative optical concentrations and sedimentation velocity studies. The bottoms of the cells were approximately 7.21 cm. from the center of rotation when the cells were in the rotors.

Eastman Metallographic photographic plates were used for photography of the Schlieren patterns. The coördinates of Schlieren patterns were read directly from the photographic plates with a two-dimensional comparator. Values of the refractive gradient coördinates near the meniscus for transient-state patterns were located reproducible to approximately 1 to 2% for a Schlieren angle of 60°. Values of the refractive gradient adjacent to the meniscus were obtained by extrapolation, since opposing, two-directional divergence of sharply defined fringes occurred. Readings taken within approximately 0.15 cm. (plate distance) of the meniscus from the bisector of the proximal peripheral fringes of the central shadow could lead to an error of 10% in molecular weight.[19] Approximately 0.10 cm. (plate distance) of the image of the bottom of the cell was obscured after careful alignment of optics, so a short extrapolation also was required at the cell bottom.

TABLE I

COMPOSITION OF NON-IONIC DETERGENTS

Detergent	Manufacturer	Approximate[a] mol. wt.	Av. no. oxyethylene groups/molecule
Igepal CO-710, polyoxyethylated nonylphenol	General Aniline and Film Co.	680	10.3
Surfonic N-95, polyoxyethylated nonylphenol	Jefferson Chemical Co.	640	9.5
Triton X-100, polyoxyethylated octylphenol	Rohm and Haas Co.	635	9.7
Pluronic L-64, condensate of ethylene oxide and propylene oxide	Wyandotte Chemical	2850	24

[a] Approximate molecular weights are taken from the manufacturers literature or the best available source.

The usual fluids used for bottom liners of the cells such as silicone oils and Kel-F polymer oil could not be used due to interaction of these substances with the detergents. Since there is some chance for slight convection and other possible disturbances near the bottom of the cells, the refractive gradients at the cell bottoms were not used for transient-state molecular-weight calculations.

A planimeter, capable of measuring areas to four significant figures, was used for integrations required for the synthetic boundary experiments. The numerous integrals required for the transient-state studies were evaluated by numerical integrations.[20]

Partial specific volumes were obtained from pycnometric measurements of solution densities for a series of concentrations.[21] The insulated pycnometer water-bath was maintained at 25 ± 0.01°. The pycnometers had a volume of approximately 5 ml. and were aged for one year. Densities were determined in triplicate for a minimum of six detergent solutions for each detergent, including those to be ultracentrifuged, in the concentration range of 0 to 3% detergent, and densities were then converted to specific volume. Expanded plots of specific volume *vs.* concentration revealed that these plots were linear, within experimental error, to a few per cent. detergent concentration. A least squares fit of a straight line to the specific volume data resulted in an average deviation of ± 0.00003 in specific volume for a typical case, and the deviations were randomly distributed for various concentrations. However the specific volume curves significantly depart from linearity in the range of 30% detergent concentration as might be expected. Thus the slopes of the specific volume *vs.* concentration curves were easily obtained for calculation of partial specific volumes in the concentration range of interest. Partial specific volume of each detergent did not change, within experimental error, up to a few per cent. detergent concentration. Partial specific volumes are listed in Table II, and were reproducible to 3 units in the third significant figure. Partial specific volumes might be expected to change slightly for different batches of the same detergent if the chain-length distributions of the detergent polymers changed.

Results and Conclusions

The results for transient-state molecular-weight determination at various times of centrifugation and initial concentrations are summarized in

---

(18) Technical Bulletin No. TB 6003B, Spinco Division Beckman Instruments, Inc., Palo Alto, California.

(19) R. Trautman and C. F. Crampton, *J. Am. Chem. Soc.*, **81**, 4036 (1959).

(20) H. K. Schachman, "Methods in Enzymology," Vol. IV, Academic Press, New York, N. Y., p. 51.

(21) G. N. Lewis and M. Randall, "Thermodynamics," McGraw-Hill Book Co., New York, N. Y., 1923, p. 38.

TABLE II

PROPERTIES OF NON-IONIC DETERGENT SOLUTIONS AND MICELLES

Detergent	Initial concn., wt. %	Time of run, min.	Density, 25.00°, g./ml.	Micellar mol. wt., $\times 10^{-4}$	Molecules per micelle
Igepal CO-710	0.500	1200	0.9975	8.42	
	.6973	1615	.9977	8.79	
	.9901	1474	.9981	8.24	
	.9901	11179	.9981	8.60	
	2.0245	980	.9993	8.47	
			Av.	8.50 ± 1.8%	125
Surfonic N-95	0.4945	1312	0.9976	16.4	
	.4945	2071	.9976	16.6	
	.7297	1443	.9979	17.2	
	.7297	1915	.9979	16.9	
	1.0161	1571	.9982	17.4	
	1.0161	1933	.9982	17.1	
			Av.	16.9 ± 1.8%	265
Triton X-100	.7049	1506	0.9979	5.96	
	.7049	1761	.9979	5.81	
	1.0073	1020	.9987	6.87	
	1.0073	1858	.9987	6.59	
			Av.	6.31 ± 6.7%	100
Pluronic L-64	1.0737	148	0.9985	0.277	
	1.0737	276	.9985	0.284	
	1.0737	404	.9985	0.290	
	1.4957	246	.9987	0.279	
			Av.	0.282 ± 1.6%	1

Schlieren angle: 60° Camera magnification: 2.146

Temp. 25° Cell thickness: 12.00 mm.

Rotational speeds, r.p.m.

Rotational speeds, r.p.m.

Type of Run	Igepal CO-710	Surfonic N-95	Triton X-100	Pluronic L-64
Transient	9341	9341	9341	47600
Synthetic	9341	9341	9341	47600

Partial specific volume, 25°, ml./g.

Igepal CO-710	Surfonic N-95	Triton X-100	Pluronic L-64
0.914	0.910	0.916	0.890

Table II. The various experimental conditions resulted in a wide range of relative optical concentrations at the meniscus. Polydispersity causes the calculated molecular weights to increase with concentration at the meniscus, while non-ideality effects are in the opposite direction.[13] Thus molecular weight determination at a variety of periods and concentrations should indicate if such effects are significantly influencing the calculated molecular weights. It appears that this is not the case for Igepal CO-710, Surfonic N-95, and Pluronic L-64 within the expected experimental error. It would be desirable to have data for lower concentrations, but error in reading the concentration gradient curves for concentrations lower than those used could introduce much error.

Thus the average values of weight-average molecular weights appear to be reasonable values for the true molecular weights of the detergents at the low concentrations involved. This in no way means that such non-ideality effects may not become important for high concentrations, since experimental conditions were selected so that such effects were suppressed. Concentrations were thus kept as low as practicable to minimize activity effects, and molecular weights were calculated for times of centrifugation as short as practicable consistent with good precision, to reduce any polydispersity effects. It has been shown that polydispersity effects often do not become apparent until after a reasonably long period of centrifugation in comparison to the attainment of equilibrium,[16] even with considerable polydispersity present.

The experimental deviation of the average of molecular weights calculated for Triton X-100 is somewhat higher than for the other detergents. This could mean that there is some dependence of the micellar molecular weight of this detergent on concentration in the concentration range studied. Such a deviation could also result from non-ideality effects or the presence of some unknown contaminant. Hence it is difficult to isolate the contributions of the many possible effects that cause the greater deviation for this detergent.

Pluronic L-64 is a quite interesting exception since the calculated micellar molecular weight shows good agreement with the estimated molecular weight of this detergent. This indicates that little or no micelle formation takes place. Such behavior is not unexpected since light scattering experiments[5] have shown that a homologous detergent does not form micelles. Therefore light scattering,[5] and ultracentrifuge data give the same qualitative results. These studies indicate that the number of molecules per micelle is highly dependent on the composition of the detergent.

Although Igepal CO-710 and Surfonic N-95 are similar detergents, the numbers of molecules per micelle are considerably different for the two detergent solutions. This is not unexpected, since the two detergents have been shown to differ markedly in other respects such as adsorption properties.[22]

DISCUSSION

M. E. GINN (Monsanto Chemical Co.).—Is micellar molecular weight independent of total concentration as a general rule, as the data suggest?

C. W. DWIGGINS, JR.—As a general rule, it would not be expected that micellar molecular weights would be independent of the total concentrations. However, for the low concentrations and experimental conditions involved, the dependence appears to be low for the non-ionic detergents studied. It probably would become quite noticeable as the concentrations necessary for gel formation are approached or at near the critical micelle concentration.

H. B. KLEVENS (Klevens Associates).—Helix formation seems to play a role in ethylene oxide and propylene oxide polymers. With this in mind, it would be easier to accept a value of 2–3 molecules per micelle rather than that of one.

C. W. DWIGGINS, JR.—The Pluronic L-64, detergent was found to contain approximately 1 molecule per micelle, assuming that the molecular weight reported for this detergent is correct. Light scattering experiments of A. M. Mankowich gave an aggregation number of only slightly greater than 1 for a similar detergent.

DONALD G. DOBAY (B. F. Goodrich Company).—Could you comment further on the great difference in number of molecules per micelle between surfactants of approximately the same chemical structure and composition?

C. W. DWIGGINS, JR.—At the present state of knowledge it would be quite difficult to explain this difference since there are many possible explanations. Rather weak forces are involved in micelle formation. Variation in chain length distribution could be partially responsible, or possibly slight contamination of the detergent by some unknown material. As detergents of higher purity and narrower chain length distribution become available, these questions perhaps can be resolved.

IRWIN H. BILLICK (Esso Research and Engineering).—Did you make any measurements of the critical micelle concentration?

C. W. DWIGGINS, Jr.—Not in this work. Surface tension studies by Lun Hsiao, H. N. Dunning and P. B. Lorenz (*J. Phys. Chem.*, *60*, 657 (1956)) indicate that the detergents studied, with the exception of Pluronic L-64, have critical micelle concentrations of the order of $10^{-4}M$. No break in the surface tension *vs.* concentration curve was observed for Pluronic L-64.

---

[22] H. N. Dunning, *Chem. Eng. Data Series*, **2**, No 1, 88 (1957).

BLACK SOAP FILMS[1]

By J. TH. G. OVERBEEK[2]

Department of Chemistry, University of Southern California, Los Angeles 7, California

Received July 18, 1960

During the aging of colored soap films, black spots are formed which are ultrathin parts of the film. They are usually separated from the colored part of the film by a sharp transition and grow spontaneously. The principal forces that govern their thickness are the electrostatic repulsion between the soap ions on the two faces of the film and van der Waals attraction amongst all the molecules of the film. It is essential to take into account the fact that the electrostatic repulsion acts only across the water layer of the film, whereas the water layer and the soap molecules both contribute to the van der Waals forces. The equilibrium thickness of the black films presumably is determined by these forces and by the border suction (surface tension divided by the radius of curvature of the border surface). The rate of formation of black films depends on these forces and on the viscous resistance in the film. An extension of Frankel's theory on the rate of film formation is presented, which takes the influence of electrostatic and van der Waals forces into account. In films formed from solutions of non-ionic detergents both electrostatic repulsion and steric repulsion play a role. Black films do not break spontaneously but breaking may be caused by a number of effects, such as evaporation, dewetting of impurities, local heating, etc.

Introduction

Foams, soap bubbles and soap films are attractive subjects for research, not only from a scientific and technical, but also from an esthetic point of view. It is a pleasure to observe the interesting structures of foams and the beautiful interference colors in not all but most soap lamellae. Freshly formed lamellae may be too thick to show colors, but they all drain under the influence of gravity and when they reach a thickness between a few microns and 0.1 micron the interference colors appear. Given time and enough stability, the films will drain further and become so thin that reflection from the front side and the backside are very nearly in counterphase and the film looks *black*. These black regions are often sharply separated from the colored part of the film or bubble. They seem to be holes, and as early as 1672 Hooke[3] reported "On holes in soap bubbles." Newton[4] also studied these "holes" and observed that black films of different thickness could exist next to each other. Gibbs[5] was quite explicit about black films. He described the sudden thinning from colored to black "very much as if there were an attrac-

---

[1] Invited lecture of the Foreign Guest of Honor, 34th National Colloid Symposium, Lehigh University, June 16, 1960.

[2] Van't Hoff Laboratory, State University of Utrecht, Utrecht, The Netherlands.

[3] R. Hooke, Communication to the Royal Society, March 28, 1672; see T. Birch, History of the Royal Society, A. Millard, London, 1757, Vol. III, p. 29.

[4] I. Newton, "Opticks," Book II, Part I, exp. 17, Dover Publ., New York, N. Y., 1952, based upon the 4th edition, W. Innys, London, 1730.

[5] J. W. Gibbs, "On the Equilibrium of Heterogeneous Substances, see "Collected Works," Yale University Press, New Haven, 1948, p. 311 ff.

tion between the surfaces of the film, insensible at greater distances, but becoming sensible when the thickness of the film is sufficiently reduced." He observed a thicker rim between the black and the colored film and concluded that the black part is not simply formed by extension of the film, but by a spontaneous disproportionation of the thicker colored film into black film plus a thick rim around it. Finally he remarked, "That which is most difficult to account for in the formation of the black spots is the arrest of the process by which the film grows thinner. It seems most natural to account for this, *if possible*, by passive resistance to motion, due to a very viscous or gelatinous condition of the film."

We shall see how these very pertinent remarks by Gibbs remain significant for modern soap film research.

The first question to be answered is, Why should we be so much interested in soap films and particularly in the black ones which are certainly not the most beautiful? The main reason is that foams, and in particular isolated soap films, are very simple "colloidal" systems. The thinning seems to indicate that they are on their way to breaking, but in the formation of the black film the breaking is prevented or at least greatly retarded. In soap films we have a simple model for the behavior of very thin liquid layers between solid particles or emulsion droplets, and we may obtain a better understanding of coagulation of suspensions and of breaking of emulsions by studying soap films. Moreover, there is the practical interest in foams. Some people, such as the manufacturers of shaving cream, or beer, or the users of froth flotation, want to stabilize them. Others, such as distillers, or oil producers, look eagerly for ways to destroy foams.

Formation of Black Films.—A black film can be formed in two different ways. It may form spontaneously somewhere in the middle of a colored, usually rather thin, film and grow in area at the expense of the colored film. It may be formed also at the border (called Plateau border, or Gibbs border) which surrounds a soap film, where it is attached to a frame, to other films (in a foam) or to the horizontal surface of a liquid. Due to the curvature of the surface such a border is always a seat of suction (lower pressure) with respect to adjacent flat film. Mysels, Shinoda and Frankel[6] pointed out that this suction acts more strongly on a thick film than on a thin film, and consequently there is a tendency for thicker film to be sucked in and thinner film to be generated at these borders (see Fig. 1). When the film surface is mobile, this is the main process by which a soap film becomes thinner. This idea can be extended to the welt between black and colored film. The welt can be considered as a kind of border, sucking in the colored film and generating more of the black one, the excess liquid accumulating in the welt and usually breaking away from it in two-dimensional droplets, which flow to the lower parts of the film.[7]

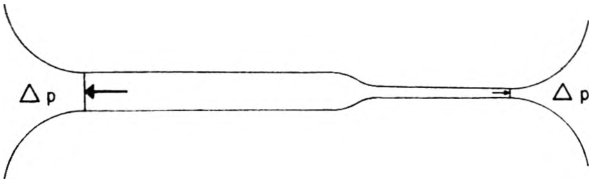

Fig. 1.—Border suction (Δp) acts more strongly on thicker parts of the film, sucks in thick film and generates thinner film.

When the black film is subjected to mild evaporation a second, thinner, black film is formed,[8] but we will limit our discussion nearly exclusively to the first.

Thickness of the Black Film.—The black film is too thin to show interference colors, but it does reflect some light. Light reflected from the front and the back surface has a phase difference slightly exceeding 180°, and thus it is not completely extinguished.

The ratio of reflected and incident light intensities (light beams perpendicular to film) is given by

$$I/I_0 = 4r^2 \sin^2 (2\pi nd/\lambda)$$

where $r^2 = (n - 1)^2/(n + 1)^2$ is the reflection coefficient of one surface, n is the (average) refractive index of the film, d its thickness and λ the wave length in vacuum of the light used. From a measurement of the intensity of the reflected light, the thickness of the film can be determined. It varies between slightly less than 100 Å. and about 500–700 Å. The second black film (the one caused by evaporation) is about 50 Å. thick.

Theoretical Discussion.—We must explain: (a) the great stability of these ultrathin structures, either colored or black; (b) the spontaneous formation of black films, and the fact that they do not thin indefinitely; (c) the multiplicity; (d) the mechanism(s) by which they ultimately break.

The explanation of the fact that soap films can stand a great deal of deformation without rupture has been given by Gibbs.[9] Adsorption of the soap molecules at the water–air interface is accompanied by a lowering of the surface tension. Local extension of the film entails a decrease in the amount of soap adsorbed per unit area and thus leads to an increase in the surface tension, which tends to contract the extended part of the film, thus preventing it from becoming dangerously thin. Variants of Gibbs' theory have been presented by Marangoni,[10] and much more recently by Ewers and Sutherland.[11] The first actual measurement of film elasticity has been made very recently by Mysels, Cox, and Skewis.[12]

As this cause for stability is not a particular property of the black films, we shall not discuss it further.

An attraction between the surfaces of the film as postulated by Gibbs might explain the sudden

---

[6] K. J. Mysels, K. Shinoda and S. Frankel, "Soap Films, Studies of Their Thinning and a Bibliography," Pergamon Press, New York, N. Y., 1959, p. 20 ff.

[7] Ref. 4, plates III and VI, between pp. 62 and 63.

[8] Ref. 6, p. 70 ff.

[9] Ref. 5, p. 300 ff.

[10] C. Marangoni, Fusi. Agosto, Piave, 1865; *cf. Ann. phys.*, (5) **143**, 337 (1871); *Nuovo Cimento*, (3) **3**, 50, 97, 192 (1879).

[11] W. E. Ewers and K. L. Sutherland, *Australian J. Sci. Res.*, **A5**, 697 (1952).

[12] K. J. Mysels, M. C. Cox and J. Skewis, private communication; see also Abstracts of Papers presented at A. C. S. Meeting, Sept., 1959.

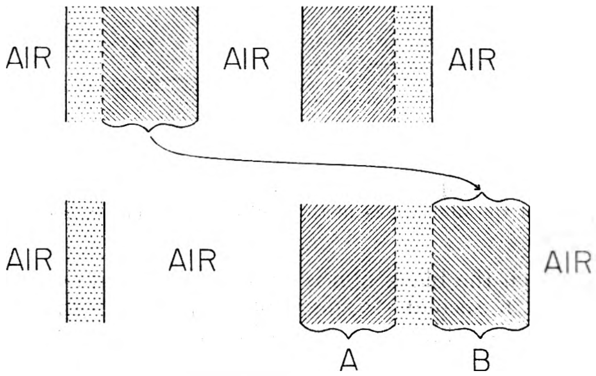

Fig. 2.—Upper part: two thick films far apart; lower part: films rearranged into a thin one and a very thick one. The interaction between the diagonally-marked parts A and B is only present in the lower picture and explains the decrease in potential energy in the rearrangement.

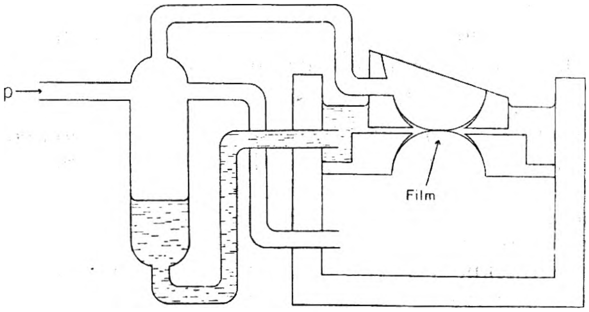

Fig. 3.—Apparatus for studying black films: the pressure p regulates the difference in pressure between the border and the film. The reflection of light projected through the upper window (inclined to avoid undesirable reflections) on the soap film is used to determine its thickness. Apparatus was constructed by Boekelman and Duyvis, and is very similar to that used by Derjaguin and Titijevskaja.

onset of the formation of the black film and the abrupt transition between the black and the colored film. De Vries[13] has proposed that such an attraction may be due to London–van der Waals forces. Indeed, it is well known how the existence of surface tension is explained by the fact that molecules near the surface are attracted toward the interior of the liquid by intermolecular attraction forces. In a very thin film the proximity of the two surfaces makes this inward attraction somewhat weaker or, in other words, lowers the free energy of the film and acts as a factor favoring further thinning of the film. De Vries pointed out that this effect is exactly equivalent to the force between two semi-infinite layers of solution separated by an air gap of the same thickness as the film, and can be treated quantitatively on this basis.

There are different ways in which this effect can be treated. One of them is illustrated in Fig. 2. If a film becomes thinner and the total interface of the system is not changed, the material lost by the film must be added somewhere else in the system, either in the bulk of the liquid or, energetically equivalent, to increase the thickness of an already thick film. The upper part of Fig. 2 depicts two thick films, each divided by an imaginary plane into a thin and a thick layer. The potential energy of each of the thick films is built up from the interactions between all individual pairs of molecules. After the rearrangement shown in the lower part of the figure, the potential energy of the total system is changed by the interaction between the two diagonally hatched parts of the thick film and this makes the lower situation more stable than the upper one. The actual difference ΔV between the energy of the two situations (per cm.^{2} of thin film formed) is given by[14,15]

$$\Delta V = A/12\pi H^2$$

where A is the Hamaker–van der Waals constant, and H is the thickness of the thin film. Consequently the van der Waals attraction is equivalent to a pressure on the film equal to

$$P = A/6\pi H^3$$

It has been shown both experimentally and theoretically that the above equations require modification when H is of the same order or larger than the wave length connected with the London–van der Waals forces. In that case, *retardation* of these forces plays a role. However, the thickness of the black films is usually such that the van der Waals forces are not affected by retardation, and one of the important aspects of black film research is that it may furnish a tool for the determination of non-retarded van der Waals forces.

Van der Waals forces ultimately would lead to bursting of the film unless some opposing force stops the process. This opposing force has been recognized by different authors—Bikerman,[16] Derjaguin,[17] and others—as being due to the electrostatic repulsion between the layers of adsorbed soap ions. If this is correct, the thickness of the black film ought to depend on the thickness of the electric double layer and consequently on the salt content of the soap solution. Derjaguin and Titijevskaja[18] have devised an ingenious experiment, in which they measure the thickness of black films under different levels of border suction. A sketch of the essential parts of the apparatus is shown in Fig. 3. They find a good agreement between calculated and measured film thickness, considered as an equilibrium between border suction and electrostatic repulsion, calculated on the basis of Gouy–Chapman double layers (see Fig. 4). Van der Waals forces were not taken into account. They would not influence the results perceptibly for thick films, obtained at low ionic strength, but one would expect them to make the thin films still thinner. However, the thin films obtained by Derjaguin at high ionic strength are actually even thicker than the calculated value based on repulsion and border suction. Derjaguin ascribes this to a special structure of the solvent, rather in line with Gibbs' suggestion of a "gelatinous behavior."

The exact nature of this gelatinous layer is not

---

[13] A. J. de Vries, *Rec. trav. chim.*, **77**, 383 (1958).

[14] J. H. De Boer, *Trans. Faraday Soc.*, **32**, 21 (1936).

[15] H. C. Hamaker, *Physica*, **4**, 1058 (1937).

[16] B. V. Bikerman, "Foams, Theory and Industrial Applications," Reinhold Publ. Corp., New York, N. Y., 1953, p. 154.

[17] B. V. Derjaguin, *Disc. Faraday Soc.*, **18**, 24 (1954).

[18] B. V. Derjaguin and A. S. Titijevskaja, "Gas–Liquid and Liquid–Liquid Interfaces," *Proc. 2nd Int. Congr. Surf. Activity*, Vol. I, Butterworth, London, 1957, p. 211; see also ref. 17.

clear. There appears to be a contradiction with information derived from electrokinetic phenomena, which, if anything, suggest only a very thin layer of increased viscosity near a phase boundary. Mysels[19] has suggested that the presence of micelles in the film might prevent further collapse. In the author's opinion this question is still unsettled. More experiments, also below the c.m.c., are desirable.

It is, of course, tempting to do similar experiments with soap films between oil layers. They have indeed been done by van den Tempel,[20] although without regulation of the border suction. He found the predicted dependence of the thickness on the ionic strength, but just as in Derjaguin's case, the films at high salt content are thicker than calculated.

If the situation in black soap films can be described as an equilibrium between van der Waals attraction, electrostatic repulsion and some border suction, then this forms an ideal case for the application of the theory of the stability of lyophobic colloids as developed by Derjaguin and Landau[21] and by Verwey and Overbeek,[22] because this theory is based on the same forces. As the van der Waals attraction changes in inverse proportion with some power of the thickness and the electrostatic repulsion varies exponentially with the thickness of the film, a plot of the potential energy of the film against its thickness shows a sharp dip for very small thickness. At intermediate thickness there may be a maximum, which can act as an energy barrier, and there is a shallow minimum at larger thickness (see Fig. 5). The stable black film is supposed to correspond to this shallow minimum.

Experimental information obtained at my laboratory in Utrecht by Duyvis and at the University of Southern California by Skewis is in qualitative agreement with this picture. Recent results obtained by the Bulgarian authors Scheludko and Exerowa[23] even allow the calculation of the Hamaker–van der Waals constant from such experiments. It is found to be equal within a factor 2 or 3 to $A = 5 \times 10^{-13}$ ergs, in good agreement with theoretical predictions.

However, since a hydrophobic colloid usually flocculates at a salt content of about 0.1 molar monovalent electrolyte, one would expect soap films to break at or below that limit. But good soap films do not break, even at 1 molar. This probably should be explained by the fact that electrostatic repulsion acts between the ionic heads of the soap molecules, but van der Waals attraction includes the hydrocarbon tails as well. This is equivalent to a shift between the origins of the attraction and repulsion curves over maybe 10 or 20 Å. In that case the repulsion acts against a less steep part of the attraction as is illustrated in Fig. 6. Calculation shows that a shift of only a few Å. is enough to prevent breaking by even the highest possible concentration of monovalent electrolyte. This would *not* be the case for bivalent ions, but lack of solubility of soaps of bivalent metals makes this a difficult point to check.

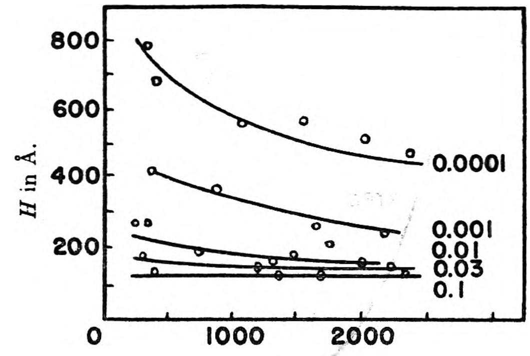

Fig. 4.—Thickness H of sodium oleate films (in Å.) as a function of the border suction (in dynes/cm.²) and sodium chloride content, from Derjaguin and Titijevskaja.[17,18] All solutions contain 10^{-3} M sodium oleate. The molarity of sodium chloride was varied from 0.001–0.1 M, and is indicated in the figure.

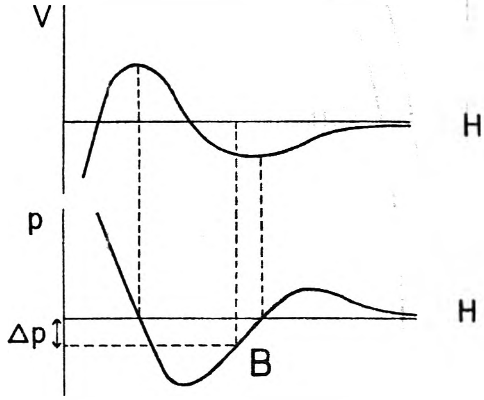

Fig. 5.—General form of potential energy V *vs.* thickness H and pressure p *vs.* H for a combination of electrostatic repulsion with van der Waals compression. In equilibrium with a border suction, Δp, the black film would correspond to point B.

Another point is connected with the formation of the black film. As this takes place spontaneously and at a finite rate, and requires work against viscous resistance, it is by no means certain that the black film, as usually found, is a true equilibrium structure. Frankel[24] has worked out a theoretical treatment of the relation between the thickness of a soap film and the rate at which it is drawn out of a border, considering the whole process as a steady state.

This theory is based on the idea that when the film is drawn it passes from a region of low pressure (the border) to a region of high pressure (the flat film). The pressure gradient squeezes out some of the solution in viscous laminar flow. The slower the film is drawn, the more efficient this squeezing process and the thinner the film becomes. The predicted proportionality between film thickness and the $^2/_3$ power of the rate of drawing was confirmed for film thicknesses between 0.1 and 6μ. The constant of proportionality agreed with prediction.[12,24]

---

(19) K. J. Mysels, private communication.

(20) M. van den Tempel, *J. Colloid Sci.*, **13**, 125 (1958).

(21) B. V. Derjaguin and L. Landau, *Acta physicochim. U.R.S.S.*, **14**, 633 (1941).

(22) E. J. W. Verwey and J. Th. G. Overbeek, "Theory of the Stability of Lyophobic Colloids," Elsevier, Amsterdam, 1948.

(23) A. Scheludko and D. Exerowa, *Kolloid. Z.*, **168**, 24 (1960).

(24) Ref. 6, Chapter V, p. 47 ff.

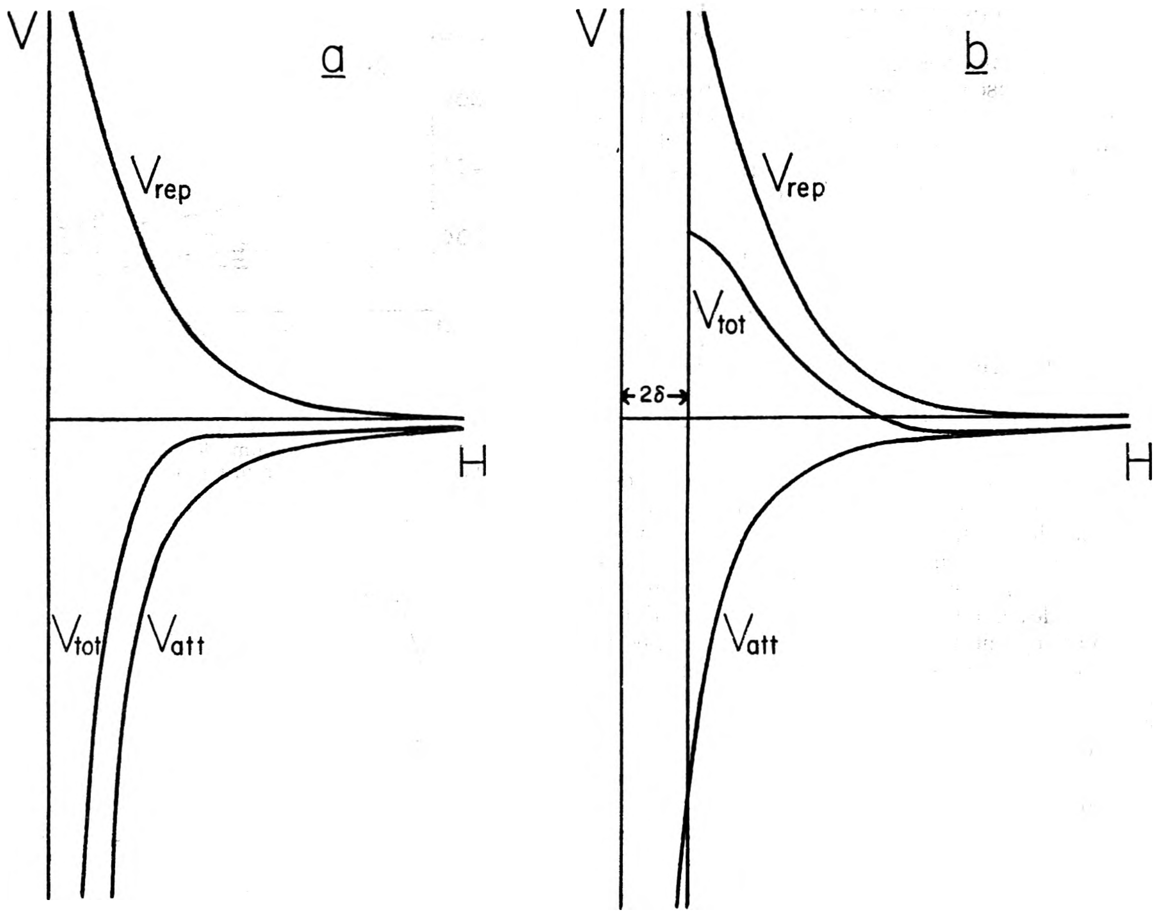

Fig. 6.—Demonstration of stabilizing influence of a small shift in origin between repulsion curve and attraction curve; (6a) repulsion and attraction have the same origin; (6b) repulsion curve is shifted a distance 2δ (twice the thickness of the hydrocarbon part of the soap layer) to the right.

For very thin films van der Waals forces and electrostatic repulsion also contribute to the pressure gradient. This can be expressed quantitatively in an equation for drawing of a film of thickness $T + 2\delta$, at a rate v

$$vT = 2vy + \frac{2\gamma y^3}{3\eta}\frac{d^3y}{dx^3} + \frac{2y^3}{3\eta}\left\{\frac{A}{16\pi(y+\delta)^4} - \frac{16\epsilon T'^2\kappa^2\varphi^3\kappa^2e^{-2\kappa y}}{\pi e^2}\right\}\frac{dy}{dx}$$

where $\varphi = (\exp(ze\psi/2KT) - 1)/(\exp(ze\psi/2KT) + 1)$ and $2y + 2\delta$ is the film thickness in the transition region between the border and the flat film, δ is the thickness of the hydrocarbon part of one soap layer, x is the coördinate perpendicular to the border in the direction of drawing, γ is the surface tension, η the viscosity of the solution, A the van der Waals–Hamaker constant, ϵ the dielectric constant in the double layer, K and T the Boltzmann constant and the temperature, e the elementary charge, z the valence of the counter ions, ψ the electric potential at the ionic heads of the soap molecules and κ the reciprocal of the Debye length.

This equation has been solved using the digital computer facilities at the Western Data Processing Center at the University of California at Los Angeles. Due to the large choice of parameters the data are not yet complete. Preliminary results indicate an easily detectable influence of van der Waals forces and electrostatic repulsion at low rates of drawing and high salt content. They also indicate that the excess tension required to produce black films may be extremely small and in certain cases even negative, pointing to the possibility of spontaneous growth of these films. Moreover, there are regions where the film thickness changes very rapidly with little change in rate or excess tension in agreement with the abrupt transition between black and colored film. It seems also as if the black film formed is not very far from equilibrium, but this conclusion is very definitely a preliminary one. Application of this line of thought to the welt is planned, but will be more difficult, because the welt grows, and thus there is no stationary state. The welt, although qualitatively similar to a double border, is too thin to admit direct quantitative application of the stationary state treatment. This would require that somewhere in the middle of the welt flow is practically loss free, as is the case in a real border far from the film. However, viscous losses cannot be neglected in any part of the welt.

Before finishing this lecture I wish to mention two subjects briefly. The first is that of foams stabilized by non-ionic detergents. My co-worker Duyvis at Utrecht made a number of measurements on films stabilized by polyethylene oxide soaps. He found two "equilibrium thicknesses," one at about 700 Å. probably connected with a weak but long range electrostatic repulsion (low ionic strength) and a second one at about 80 Å. where we assume that the repulsion mechanism is the mechanical interference between the polyethylene oxide chains from both sides of the film.

The second topic is concerned with how and why a film breaks. According to our discussion so far, it should not break at all. Electrostatic repulsion keeps the film above a minimum thickness and it can be shown conclusively that the activation energy for the formation of a hole in such a film is extremely large, so that the process does not occur spontaneously.[25]

In practice, however, small amounts of impurity may accumulate on the frame to which the film is attached and break the film by dewetting. Evaporation, driving the film thickness below the thickness of the maximum in the potential energy curve, is another common mechanism leading to breaking. It may also lead to the thinner second black film if this structure, consisting presumably of only two layers of soap with some water of hydration, is stable. In principle a very tall film or one in a very strong gravitational or centrifugal field could break under its own weight, either because the excess surface tension required to carry the weight becomes too large, or because gravity pushes the film over the energy barrier. Figure 7 shows a combination of van der Waals, electrostatic and gravitational energy which would just lead to film breakage because the V–H line has at best a horizontal slope. The gravitational energy is equal to ρghH, where ρ is the density of the solution, H the film thickness, g the gravitational acceleration and h the height above the surface of the bulk liquid.

Any gradient in the surface tension, caused, *e.g.*, by local heating, local evaporation or local contamination, will lead to an extension of the part of the film with the lower surface tension and lead to rupture.

The study of rupture of the films has as yet not made much progress, but it is obviously important, also for exploiting the parallels between soap films and problems in emulsion and suspension stability.

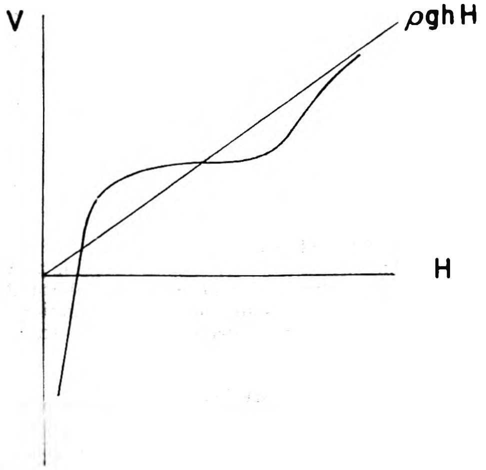

Fig. 7.—Potential energy curve with horizontal point of inflection due to gravity (ρghH) combined with van der Waals and electrostatic forces.

The subject I have chosen for this lecture is one on which research is by no means finished, but I believe that it is a rich source of information, interesting *per se*, and allowing conclusions which are of value to many other fields of colloid science.

To conclude the lecture a movie was shown of a horizontal soap film in which a colored central part was surrounded by a black rim. The movie as shown was accelerated about 60-fold as compared to reality. In the picture the growth of the welt could be seen very clearly, also that the welt detached dropwise and that the "drops" floated downward to the lower and thicker parts of the film. Furthermore it showed some of the complications met with, such as the effect of evaporation.

Acknowledgments.—I wish to express my particular gratitude to Prof. K. J. Mysels, who introduced me to his techniques and considerations on soap film research, loaned me some of the more beautiful slides, and by many discussions increased my understanding of soap films tremendously. I also wish to thank Miss J. Hotchkiss, who prepared the soap films, and Dr. J. Skewis, who made the movie. Mrs. Marjorie J. Vold introduced me to computer programming and helped me in setting up my first programs. To her and to Mr. Wm. Anderson, program consultant at the Western Data Processing Center, I extend my gratitude for their assistance.

Finally, I gratefully acknowledge the support from the Petroleum Research Fund and from the Air Force Office of Scientific Research of the Air Research and Development Command under Contract AF 49(638)-309, who, by their financial support, made my stay at the University of Southern California possible.

---

(25) A. J. de Vries, *Rec. trav. chim.*, **77**, 383, 441 (1958).

THE FRENKEL–HALSEY–HILL ADSORPTION ISOTHERM AND CAPILLARY CONDENSATION

BY CONWAY PIERCE

Department of Chemistry, University of California, Riverside, California

Received March 7, 1960

Previous work has shown that the free surface adsorption of nitrogen, corrected for any capillary condensation, is described by the equation $(V/V_m)^{2.75} = 1.305/(\log p_0/p)$. Investigation of other adsorbates shows that by suitable modification of the constants the equation is of general applicability for adsorption beyond the first layer. A single isotherm for a given adsorbate makes possible accurate prediction of the free surface isotherm of this adsorbate on any sample. Comparison of the computed free surface isotherm with the experimental one is used to detect capillary condensation.

Frenkel,[1] Halsey[2] and Hill[3] have independently suggested that at high relative pressures, where an adsorbed film is several molecular layers in thickness and its properties approach those of bulk liquid, the isotherm may be described by the equation

$$-\ln p/p_0 = \frac{k}{(V/V_m)^s} \qquad (1)$$

where s is an exponent based upon the decay of surface forces with distance. Discussions of this general equation and applications to specific isotherms have been given by Bowers[4] and by Meyer.[5]

Most of the published type II isotherms extending to high relative pressures are for powder samples. If the Frenkel equation is applied to these isotherms widely variant results are obtained. The reason is that the isotherm of a powder sample is the sum of two effects, (1) adsorption in the multilayer film on "free surface" and (2) capillary condensation at contact points between particles. The relative magnitude of the two effects varies from sample to sample because the amount of capillary condensation depends upon the size and shape of the granules and upon the closeness of packing or the average number of contacts per particle.

In a previous study of nitrogen isotherms[6] it was found that the extent of interparticle condensation could be evaluated by comparing the experimental data with a free surface isotherm that gave the multilayer adsorption not due to capillary condensation. It was also observed that the ideal nitrogen isotherm was independent of the solid substrate. At all relative pressures above $0.2p_0$ the number of statistical layers was strictly a function of the relative pressure.

The ideal nitrogen isotherm fits a modification of the multilayer equation, in the form

$$(V/V_m)^{2.75} = \frac{k}{\log p_0/p} = \frac{1.305}{\log p_0/p} \qquad (2)$$

This is in agreement with Halsey,[2] who used data for a single sample, anatase, finding the exponent to have a value of 2.67.

The observation that nitrogen adsorption in the multilayer region is independent of the substrate makes it of interest to investigate the applicability of the Frenkel (or Frenkel-Halsey-Hill) equation to other adsorbates and to see how the constants vary with different molecules and different surfaces. To better control effects of capillary condensation selected samples, previously studied by nitrogen, were used. Ethyl chloride was chosen as adsorbate, as an example of a molecule whose structure is quite unlike that of nitrogen.

Experimental

Three samples were used: Sterling MT (3100), a graphitized carbon black from Cabot.[7] The nitrogen isotherm, reported by Holmes and Beebe,[8] is reproduced in Fig. 1. As previously noted[6] there is no detectable interparticle condensation below $0.95p_0$. Silica, a fluffy SiO_2 powder, was previously studied by Young.[9] The nitrogen isotherm shows no appreciable interparticle condensation below $0.95p_0$. Graphon, Lot 1925, a graphitized carbon black from Cabot.[7] Previous work has shown that at high relative pressure there is extensive condensation between the particles which make up an aggregate.

All samples were evacuated at 300°, to remove preadsorbed vapors. The physical appearance of the silica sample indicated that possibly some water, taken up while sealing it into the adsorption bulb, was not removed by this treatment. The sample showed a tendency to agglomerate, not noted in the original material.

Isotherms were determined gravimetrically at 0° by removing and weighing the bulb after each addition of vapor. After each weighing the adsorbed vapor was pumped off before a new addition was made. This was to avoid any possible adsorption–desorption effects attendant upon the alternate warming and cooling of the bulb as it was removed from the bath for weighing.

The isotherm of graphite MT is shown in Fig. 1, with its nitrogen isotherm for comparison. Isotherms of silica and Graphon are given in Fig. 2. All measurements were carried to $0.95p_0$ or higher.

The applicability of eq. 1 was tested by plotting the amount adsorbed *vs.* $\log p_0/p$, on a log–log scale as was done by Halsey.[2] Log-log plots of the three isotherms are shown in Fig. 3. To facilitate plotting, the amount adsorbed was for all samples reduced to an arbitrary power of 10 so that the initial adsorption falls in the first decade of the plot. This brings all plots to the same decade without altering the slope. A study of the isotherms and these plots yields the conclusions:

1. The slopes of the log-log plots are the same for the silica and carbon samples. That is, the multilayer adsorption is, like that of nitrogen, independent of the substrate surface.
2. The slope of the log-log plot for ethyl chloride is different from that for nitrogen. The isotherm for carbon

---

[1] J. Frenkel, "Kinetic Theory of Liquids," Oxford University Press, 1946.

[2] G. D. Halsey, *J. Chem. Phys.*, **16**, 931 (1948).

[3] T. L. Hill, "Advances in Catalysis," Vol. LV, Academic Press, New York, N. Y., 1952; *J. Chem. Phys.*, **14**, 263, 441 (1946); **15**, 767 (1947); **17**, 580, 668 (1949).

[4] R. Bowers, *Phil. Mag.*, [7] **44**, 467 (1953).

[5] L. Meyer, *Z. physik. Chem.*, **16**, 331 (1958).

[6] C. Pierce, THIS JOURNAL, **63**, 1076 (1959).

[7] Provided through courtesy of W. R. Smith and W. B. Spencer, Godfrey L. Cabot, Inc., Cambridge, Mass.

[8] J. M. Holmes and R. A. Beebe, THIS JOURNAL, **61**, 1684 (1957).

[9] G. J. Young, *J. Colloid Sci.*, **13**, 67 (1958).

MT was used to compute the number of statistical layers, n, as a function of relative pressure. A V_m value of 2.52 mg./g. was chosen by the location of the inflection point, since the shape of the isotherm precludes use of a BET plot. The n values therefore are not absolute but probably good to ±10%. This uncertainty does not affect the relative values, only the absolute. A plot of the n values *vs.* log p_0/p is shown in the lower portion of Fig. 3. It is, of course, parallel to the plots taken directly from the isotherm.

3. The plot of n values for ethyl chloride fits the equation

$$(V/V_m)^{2.18} = n^{2.18} = \frac{0.85}{\log p_0/p} \qquad (3)$$

The values of n for various relative pressures are given in Table I, which has for comparison the previously determined nitrogen values.

TABLE I

NUMBER OF STATISTICAL LAYERS ADSORBED ON A FREE SURFACE

p/p_0	N_2	C_2H_5Cl	CF_2Cl_2
0.30	1.39	1.27	1.17
.40	1.54	1.43	1.36
.50	1.70	1.63	1.60
.60	1.90	1.89	1.95
.70	2.17	2.22	2.35
.80	2.58	2.75	3.05
.90	3.35	3.85	4.70
.95	4.40	5.40	

4. The log-log plot for the Graphon isotherm is linear only up to $0.7p_0$. At higher pressures there is more adsorption than predicted by the straight line, which gives only the contribution of multilayer adsorption on a free surface. Above $0.7p_0$ experimental points fall above the straight line and the divergence increases with rising pressure. This divergence is due to the contribution of capillary condensation at contact points between the particles. The existence of such condensation, not shown by the isotherm itself, is conclusively demonstrated by the divergence of the data from the straight line.

Carman and Raal,[10] Kiselev[11] and others have experimentally compared isotherms for loose powders and porous materials having the same surface as the powder, to detect the effect of pores upon the isotherm. When there are no small pores that fill at low relative pressure the powder data are not needed. The isotherm is determined for the porous sample and the data plotted as in Fig. 3. The linear portion, extrapolated as needed, gives the isotherm that would be obtained from the powder.

5. When the n values for a vapor have been determined from the isotherm of a sample whose adsorption gives a sufficiently long straight line interval in the log-log plot, these values can then be used to determine V_m from the isotherms of other samples. A log-log plot of isotherm data is made as in Fig. 3. Within the linear region the ratio V/n for given relative pressures gives V_m. A computation from the silica isotherm is given in Table II.

TABLE II

COMPUTATION OF V_m FROM SILICA ISOTHERM

p/p_0	Amount adsorbed, V, mg. C_2H_5Cl	n	$V/n = V_m$ (mg. C_2H_5Cl)
0.40	25	1.43	17.5
.50	28	1.63	17.5
.60	33	1.89	17.5
.70	39	2.22	17.6
.80	48	2.75	17.4
.90	68	3.85	17.6

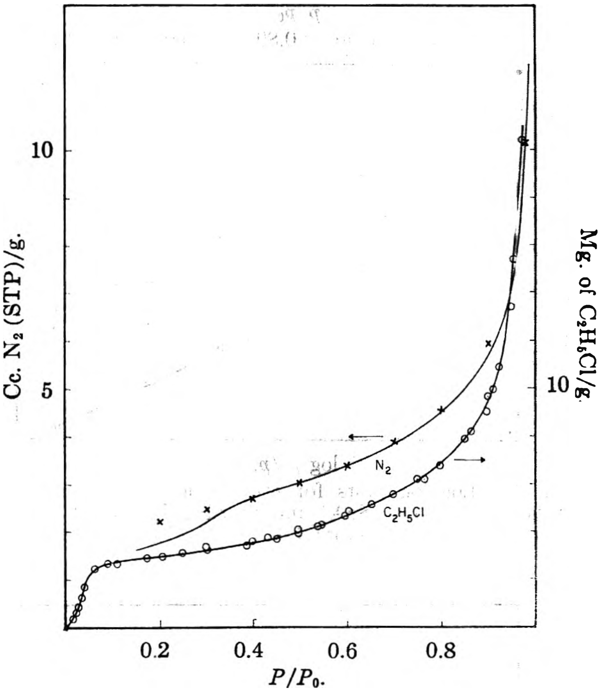

Fig. 1.—Ethyl chloride isotherm of Sterling MT (3100). The nitrogen isotherm of Holmes and Beebe is given for comparison. The crosses on the nitrogen are the adsorption computed from the n values.

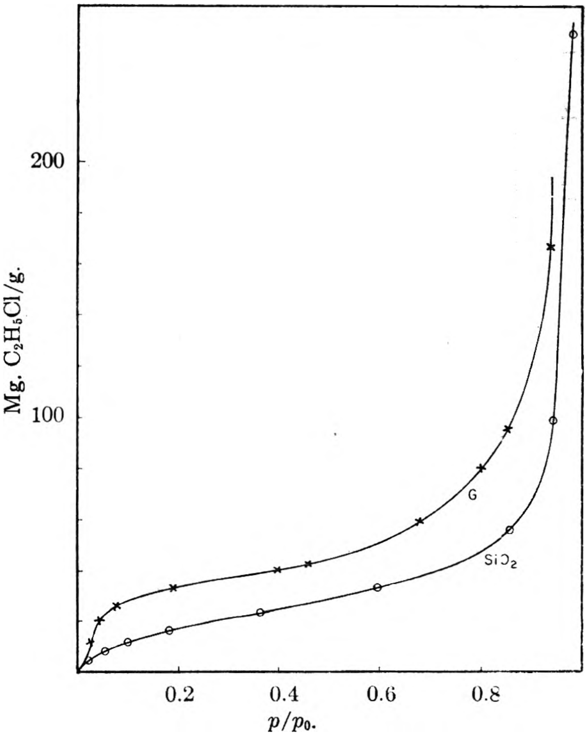

Fig. 2.—Ethyl chloride isotherms of silica and Graphon.

6. The two isotherms of Fig. 2 show a distinct contrast in the primary adsorptions below V_m. Silica adsorbs so weakly that there is no clearly defined inflection in the isotherm when the first layer is completed. Graphon, on the other hand, adsorbs strongly and there is a sharp inflection at the start of the multilayer adsorption. Despite these differences the adsorptions beyond the first layer are identical for the two samples.

7. The nitrogen and ethyl chloride isotherms of MT (Fig. 1) show some interesting effects of adsorption on a

---

[10] P. C. Carman and F. A. Raal, *Proc. Roy. Soc.* (*London*), **A209**, 59 (1951).

[11] A. V. Kiselev, "The Structure and Properties of Porous Materials (Colston Papers)," Butterworth Scientific Publications, London, 1958.

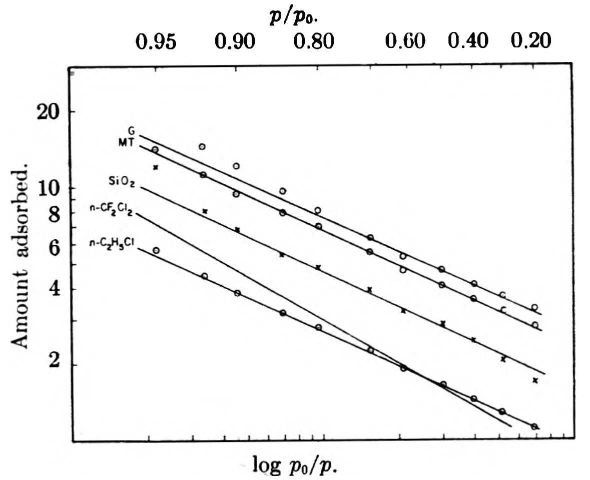

Fig. 3.—Log-log plots for ethyl chloride isotherms of Graphon (G), silica (SiO_2) and Sterling MT 3100 (MT). Lower plots are n values for CF_2Cl_2 and C_2H_5Cl.

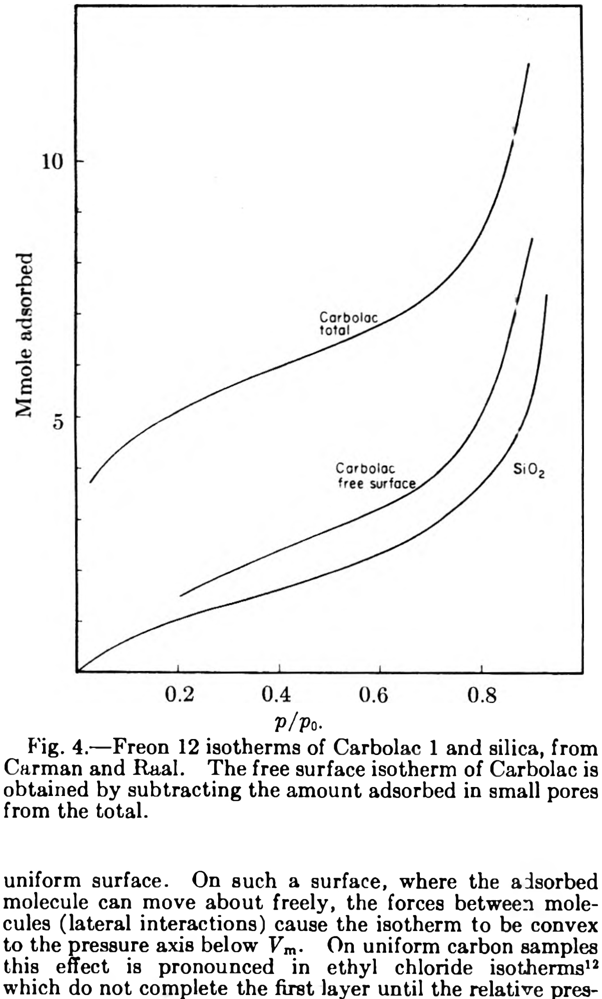

Fig. 4.—Freon 12 isotherms of Carbolac 1 and silica, from Carman and Raal. The free surface isotherm of Carbolac is obtained by subtracting the amount adsorbed in small pores from the total.

uniform surface. On such a surface, where the adsorbed molecule can move about freely, the forces between molecules (lateral interactions) cause the isotherm to be convex to the pressure axis below V_m. On uniform carbon samples this effect is pronounced in ethyl chloride isotherms[12] which do not complete the first layer until the relative pressure is near $0.05p_0$ or higher. Nitrogen isotherms on such samples have a similar shape but V_m is completed at such low pressure that ordinarily the convex shape is overlooked. In extreme cases the lateral interaction effect is so strong that the isotherm becomes practically vertical below V_m. Frequently this is referred to as a "phase transition."

Another effect of a uniform surface is found in the nitrogen isotherm of MT at relative pressures between 0.3 and $0.4p_0$. As previously discussed[6] the isotherm fits eq. 2 above $0.4p_0$ but not below this value. The proposed explanation is that the first layer is not packed to the normal state of 16.2 Å.^{2} per nitrogen atom when the inflection point is reached. Between 0.3 and $0.4p_0$ normal packing is achieved and thereafter the multilayer adsorption is the same as for any other surface. Ethyl chloride does not show this first layer effect; the isotherm is normal throughout the multilayer region.

The similarities and differences in the multilayer adsorptions of nitrogen and ethyl chloride suggest the possibility that the Frenkel equation, with suitable modification of the constants, may be of general applicability to type II isotherms. Halsey[2] showed that it applies to the adsorption of water and nitrogen by anatase and Bowers[4] that it applied to adsorption of nitrogen, oxygen and argon by a metal foil. As a further test the isotherms of Carman and Raal[10] for CF_2Cl_2 on a fluffy silica and on Carbolac 1 were investigated. These isotherms are replotted in Fig. 4. Using Carman and Raal's value of 1.17 mmoles for V_m the n values were computed for the silica sample. A log-log plot of these values is shown in Fig. 3. Its slope differs appreciably from those of nitrogen and ethyl chloride. The plot gives for Freon 12 (CF_2Cl_2) the equation

$$(V/V_m)^{1.76} = \frac{0.685}{\log p_0/p} \qquad (4)$$

Selected n values are given in Table I.

As previously shown[6] from the nitrogen isotherm the adsorption by Carbolac 1 can be broken down into two parts, (1) adsorption in small pores and (2) adsorption on free surface not in these pores. A similar analysis was made of the CF_2Cl_2 isotherm, using the n values of Table I. A computation from the adsorptions at 0.4 and $0.8p_0$ gives

$$\begin{array}{lll} \text{at } 0.8 & 8.60 \text{ mmoles} & = 3.06\, V_m + V_c \\ 0.4 & 5.95 \text{ mmoles} & = 1.35\, V_m + V_c \end{array}$$

Solving, V_c = 3.80 mmoles to fill the small pores and V_m = 1.57 mmoles to cover the surface not in the small pores.

The area of the free surface is computed by use of the silica data. Since 1.17 mmoles forms V_m for a silica area of 300 m.^{2}/g., 1.0 mmole covers 258 m.^{2}. The free surface of Carbolac is therefore 1.57 mmoles/g. × 258 m.^{2}/mmole = 405 m.^{2}/g. A similar computation for nitrogen gave a free surface area of 460 m.^{2}/g., an excellent agreement.

As a further test of the comparison between nitrogen and Freon the volume of the small pores was computed. Using the V_c values gave 0.29 ml. for N_2 and 0.31 ml. for CF_2Cl_2. Here, too, the agreement is excellent.

To test the validity of this analysis a corrected Carbolac isotherm was constructed by subtracting V_c values from the experimental ones. This free surface isotherm is shown as the middle curve of Fig. 4. A log-log plot from this corrected isotherm gave a straight line of proper slope, linear from 0.4 to $0.85p_0$. The uncorrected isotherm does not give any linear region.

Conclusions

In view of the general applicability of a modified Frenkel equation to the various isotherms studied it seems safe to conclude that: (1) The Frenkel equation, with suitable adjustments of the two constants, will fit the multilayer region of most (or perhaps all) type II isotherms provided there is no capillary condensation. (2) A plot of volume adsorbed *vs.* log p_0/p, on a log-log scale, is a convenient test for capillary condensation. If there is no capillary condensation the points fall on a straight line, which represents the free surface isotherm. Condensation causes increased adsorption. (3) For a given adsorbate the slope of the

---

[12] J. Mooi, C. Pierce and R. N. Smith, THIS JOURNAL, **57**, 657 (1953).

log-log plot is independent of the adsorbent. A single isotherm for a non-porous sample permits computation of generally valid n values for the adsorbate used. (4) In the linear region of a log-log plot the monolayer volume, V_m, may be accurately determined from the ratio V/n after the n values have once been experimentally determined. This method can be used for isotherms which are convex to the pressure axis below V_m, where the BET plot is not possible. (5) The free surface adsorption of samples with small pores and the volume in these pores may be separately computed from a single isotherm by use of simultaneous equations for the volume adsorbed at two relative pressures.

DISCUSSION

A. C. ZETTLEMOYER (Lehigh University).—Your log-log plots are for small and rather simple molecules. Would we expect the same slope, for example, for butyl alcohol? Also, are the BET areas for Graphon and for a 350 m.^{2} graphite much in error due to capillary condensation?

CONWAY PIERCE.—As Halsey points out, the slopes vary greatly with different adsorbates. Butyl alcohol undoubtedly will give quite different values. I do not think the BET areas of the samples you mention are affected by the interparticle condensation. This occurs only at high relative pressures, far above the V_m point.

P. L. WALKER, JR. (Pennsylvania State University).—You find a free surface area for Carbolac of 460 m.^{2}/g. using nitrogen. The electron microscope surface area for Carbolac is about 250 m.^{2}/g. Do you interpret the difference as due to surface roughness?

CONWAY PIERCE.—Either to that or to uncertainty in the electron microscope value. Various workers have told me personally that for the very fine Carbolac particles the microscope values are not as reliable as for blacks comprised of larger particles.

THEORY OF A MODIFIED POISSON-BOLTZMANN EQUATION. I. THE VOLUME EFFECT OF HYDRATED IONS

By S. LEVINE* AND G. M. BELL

Department of Mathematics, University of Manchester, England; Department of Mathematics, Manchester College of Science and Technology, England

Received March 21, 1960

By applying Kirkwood's work, which is based on classical statistical mechanics, the general form of the correction to the Poisson–Boltzmann equation due to the short-range forces between the ions is obtained in the case of the diffuse layer of a single, charged colloidal particle immersed in an aqueous electrolyte. The correction can be expanded in powers of the electrolyte concentration and terms up to the square of the concentration are determined. The general expansion is applied to the particular case of a plate-like particle immersed in a 1-1 electrolyte in which it is assumed that the hydration shells of the positive and negative ions are impenetrable and have the same diameter. This is compared with the so-called method of local thermodynamic balance, which has been used by a number of authors. Here, however, the volume fraction statistics of Flory has been assumed, in preference to the various interpretations of molar fraction statistics considered by these authors. It is shown that, provided the distance from the plate is greater than two or three molecular diameters, this method will give the correct form of the term in the above expansion which is linear in the electrolyte concentration. However, it fails to reproduce correctly the next (second-order) term, proportional to the square of the concentration, the principal reason being that no account is taken of the variation of the mean electrostatic potential over a distance of the diameter of the hydration shell. It is also demonstrated that the form of the volume correction to the Poisson–Boltzmann equation changes in the immediate vicinity of the colloidal plate.

1. Introduction

This paper is concerned with a particular problem in the equilibrium of non-homogeneous systems. This is to investigate the effect of the finite volumes occupied by the ion complexes on the equations governing the distribution of ions and the electrostatic potential in the diffuse part of the electric double layers in colloidal solutions. Let the position of a point in such a double layer be denoted by the vector **q** and let $n_i(\mathbf{q})$ be the average number per unit volume at **q** of ions of type i, charge e_i. Then the fundamental equation from which the mean potential $\psi = \psi(\mathbf{q})$ is determined reads

$$\nabla\cdot\mathbf{D} = 4\pi \sum_{i=1}^{m} e_i n_i(\mathbf{q}) = 4\pi \sum_{i=1}^{m} e_i n_i^0 \exp\{-\beta V_i(\mathbf{q})\} \tag{1.1}$$

Here **D** is the dielectric displacement at the point **q**, m is the number of ion types and $\beta = 1/kT$ where k is Boltzmann's constant and T the absolute temperature. $V_i = V_i(\mathbf{q})$ is the potential of the mean force acting on an ion of type i stationed at **q**, the zero of V_i being chosen at a specified reference point where $n_i = n_i^0$ for $i = 1,\cdots,m$. If dielectric saturation is ignored then we may replace the left-hand member of (1.1) by $-\epsilon\nabla^2\psi$ where ϵ is the dielectric constant of the medium (assumed independent of position). If further $e_i\psi$ is substituted for V_i then (1.1) becomes the familiar Poisson–Boltzmann equation.

The latter equation is, of course, also used in discussing the properties of the self-atmospheres of the ions in homogeneous electrolytes. Two quite different approaches have been made to improving its accuracy. The first of these is a rigorous application of classical statistical mechanics to a model representing a homogeneous electrolyte: it was initiated by Fowler[1] and developed further by Onsager[2] and Kirkwood.[3] More recently, the work of Kirkwood has been extended by Hückel and Krafft[4] who were concerned with introducing the volume effect referred to above. The analysis of these authors has been discussed by Bell and Levine[5] in a preliminary report and in the present paper a fuller account of this work will be included. The only objection of any substance to this first approach is that the solvent is treated as a continuum, with a uniform dielectric constant, whereas a completely accurate theory would take the discrete nature of the solvent into account. In view of the great difficulties encountered, however, this approximation seems justified and the main aim of this paper is to apply the method of Kirkwood[3] to the volume effect in diffuse layers.

The second approach to the problem of ion equilibrium can be described as the method of local thermodynamic balance, a term used by Prigogine, Mazur and Defay.[6] It is postulated that the medium can be divided into sub-regions each of which may be treated as containing a statistical assembly at a uniform electric potential ψ. The electrochemical potential of an ion of charge e_i at a given point is thus the sum of a function of the local ion concentrations and $e_i\psi$. The Poisson–Boltzmann equation is derived if ideal mixing is assumed and if, in addition, effects due to ion self-atmospheres, compressibility (electrostriction), polarization of the ion complexes and dielectric saturation of the solvent medium are neglected. Local balance is thus the basis of the Derjaguin–Verwey–Overbeek theory of colloid stability which uses the Poisson–Boltzmann equation. It is also assumed in the theories of the double layer, based on modifications of the Poisson–Boltzmann equation, due to Bikerman,[7] Grimley,[8] Freise,[9] Ohlenbusch,[10] Bell and Levine,[11] and Sparnaay[12]

---

* Visiting Scientist, Division of Applied Chemistry, National Research Council, Ottawa, Canada, on leave of absence from the University of Manchester.

(1) R. H. Fowler, "Statistical Mechanics," Cambridge University Press, 2nd edition, 1936.

(2) L. Onsager, *Chem. Revs.*, **13**, 73 (1933).

(3) J. G. Kirkwood, *J. Chem. Phys.*, **2**, 767 (1934).

(4) E. Huckel and G. Krafft, *Z. physik. Chem.*, **3**, 135 (1955); see also M. J. Sparnaay, *ibid.*, **10**, 156 (1957); *Trans. Faraday Soc.*, **53**, 306 (1957).

(5) G. M. Bell and S. Levine, *Disc. Faraday Soc.*, **24**, 69 (1957).

(6) I. Prigogine, P. Mazur and R. Defay, *J. chim. phys.*, **50**, 146 (1953); see also I. Prigogine, *ibid.*, **49**, 79 (1953).

(7) J. Bikerman, *Phil. Mag.*, **33**, 383 (1942).

(8) T. B. Grimley, *Proc. Roy. Soc.* (*London*), **A201**, 40 (1950).

(9) V. Freise, *Z. Elektrochem.*, **56**, 383 (1952).

(10) H. D. Ohlenbusch, *ibid.*, **60**, 607 (1956).

(11) G. M. Bell and S. Levine, *Trans. Faraday Soc.*, **53**, 143 (1957).

and in the theories of strong electrolytes of Eigen and Wicke,[13] Falkenhagen and Kelbg,[14] and Dutta.[15] The question of how far the local balance assumption is valid is thus of considerable importance. Recently Cahn and Hilliard[16] and Hart[17] have developed a theory of the thermodynamics of non-homogeneous systems in which the local free energy depends on both the local composition and the composition gradients. This is undoubtedly an improvement on local balance theory but it has not been applied so far to the diffuse layers in colloids.

2. Statistical Treatment of Short Range Interactions

It will be supposed that a single charged colloidal particle is immersed in a volume V of electrolyte and that V is very large compared with the part of V in which the electrolyte distribution is influenced by the charge on the particle (*i.e.*, the diffuse layer). If N_i is the total number of ions of type i in V and if the reference point is taken distant from the particle in the "bulk" of the electrolyte then the reference point density n_i^0 can be identified with the average density N_i/V. The total number of ions of all kinds in V is denoted by N. In some of the work below it will be necessary to consider the N separate ions regardless of species and in this case the suffices r, s and t will be used. Where the m ion types are considered, however, the suffixes will be i, j and k. The position of an individual ion r will be denoted by $\mathbf{q}_r$ and the corresponding volume element by $d\mathbf{q}_r$. Thus multiple volume elements are expressed as

$$d\tau = \prod_{s=1}^{N} d\mathbf{q}_s,\quad d\tau^{(r)} = \prod_{s=1,\, s\neq r}^{N} d\mathbf{q}_s,\quad d\tau^{(rt)} = \prod_{s=1,\, s\neq r,\, s\neq t}^{N} d\mathbf{q}_s, \text{ etc.} \tag{2.1}$$

If W_N is the total energy of interaction for a given configuration of the N ions, then the potential V_r of the mean force on ion r is given by

$$\exp\{-\beta V_r(\mathbf{q}_r)\} = Q_N^{-1} V \int \exp(-\beta W_N) d\tau^{(r)} \tag{2.2}$$

where

$$Q_N = \int \exp(-\beta W_N) d\tau \tag{2.3}$$

(It will be understood that in all cases not otherwise specified, integration is over the volume V.) Let W_{N-1} be the total energy of interaction for a given configuration of the N-1 ions, with ion r omitted, and let $U_r(\mathbf{q}_r)$ be the short-range interaction of ion r at $\mathbf{q}_r$ with all the other ions in the solvent medium. It should be noted that both W_{N-1} and $U_r(\mathbf{q}_r)$ include interaction terms with the colloidal surface: for example W_{N-1} will have the familiar electrostatic image terms and the Coulomb interaction with surface ions which constitute the charge on the particle.

It was shown by Kirkwood[3] that

$$\exp\{-\beta V_r(\mathbf{q}_r)\} = \zeta_r(\mathbf{q}_r) \exp\{-\beta V_r^0(\mathbf{q}_r)\} \tag{2.4}$$

where the factor ζ_r is the contribution of the short-range forces, given by

$$\zeta_r(\mathbf{q}_r) = \frac{\int \exp[-\beta\{W_{N-1} + U_r(\mathbf{q}_r)\}] d\tau^{(r)}}{V^{-1}\int \exp[-\beta\{W_{N-1} + U_r(\mathbf{q}_r)\}] d\tau} \tag{2.5}$$

and $V_r^0(\mathbf{q}_r)$ is the part of $V_r(\mathbf{q}_r)$ due to the electrostatic interaction of the ions: the zero of V_r^0 is taken at the specified reference point where $n_i = n_i^0$ and $\zeta_r = 1$. "Ion size" effects depend on the short-range forces so that it is the factor ζ_r which will be considered in this paper. The formalism introduced above was developed by Kirkwood[3] for the self-atmosphere of an ion in a strong electrolyte. But it can be applied, as will be done here, to a diffuse layer. (Our notation differs in some respects from Kirkwood's.)

If $u_{rs}(\mathbf{q}_r-\mathbf{q}_s)$ is the short-range interaction between ion r at $\mathbf{q}_r$ and ion s at $\mathbf{q}_s$ and if $u_r(\mathbf{q}_r)$ is that between ion r at $\mathbf{q}_r$ and the wall of the colloidal particle, then

$$U_r(\mathbf{q}_r) = u_r + \Sigma_s u_{rs} \tag{2.6}$$

Here the sum $\sum_{s=1}^{N}$ with the term $s=r$ omitted is denoted simply by Σ_s and the double sum $\sum_{s=1}^{N}\sum_{t=1}^{N}$ with the terms s = t, s = r, s = r omitted will be similarly denoted by $\Sigma_s\Sigma_t$. It is convenient to introduce

$$f_{rs} = f_{rs}(|\mathbf{q}_r - \mathbf{q}_s|) = \exp(-\beta u_{rs}) - 1 \tag{2.7}$$

$$g_r = g_r(\mathbf{q}_r) = \exp(-\beta u_r) \tag{2.8}$$

so that

$$\exp[-\beta U_r(\mathbf{q}_r)] = g_r \prod_{s=1,\, s\neq r}^{N} (1 + f_{rs}) = g_r[1 + \Sigma_s f_{rs} + \Sigma_s\Sigma_t f_{rs} f_{rt} + \cdots] \tag{2.9}$$

Substituting (2.9) the numerator on the right-hand side of (2.5) is given by

$$Q_{N-1}\, g_r[1 + V^{-1}\Sigma_s \int f_{rs} \exp(-\beta V_s) d\mathbf{q}_s + V^{-2}\Sigma_s\Sigma_t \int f_{rs} f_{rt} \exp(-\beta V_{st}) d\mathbf{q}_s d\mathbf{q}_t + \cdots] \tag{2.10}$$

where

$$Q_{N-1} = \int \exp(-\beta W_{N-1}) d\tau^{(r)} \tag{2.11}$$

$$\exp(-\beta V_s) = Q_{N-1}^{-1}\, V \int \exp(-\beta W_{N-1}) d\tau^{(rs)} \tag{2.12}$$

and

$$\exp(-\beta V_{st}) = Q_{N-1}^{-1} V^2 \int \exp(-\beta W_{N-1}) d\tau^{(rst)} \tag{2.13}$$

so that V_s is the potential of the mean force acting on ion s and V_{st} the potential of the mean forces acting simultaneously on ions s and t in an assembly of $N - 1$ ions. Since N is very large there is a negligible difference betweeen these and the corresponding quantities for the assembly of N ions. It is convenient to define

$$c_{rs}(\mathbf{q}_r) = \int f_{rs} \exp(-\beta V_s) d\mathbf{q}_s = \int f_{rs}\zeta_s \exp(-\beta V_s^0)\, d\mathbf{q}_s \tag{2.14}$$

$$F_{rs}(\mathbf{q}_r, \mathbf{q}_s) = \exp(-\beta V_{rs}) - \exp\{-\beta(V_r + V_s)\} \tag{2.15}$$

$$d_{rst}(\mathbf{q}_r) = \int f_{rs} f_{rt} F_{st}(\mathbf{q}_s, \mathbf{q}_t)\, d\mathbf{q}_s\, d\mathbf{q}_t \tag{2.16}$$

Substituting in (2.10) the numerator in (2.5) is given by

---

[12] M. J. Sparnaay, *Rec. trav. chim. Pays-Bas*, **77**, 872 (1958).

[13] M. Eigen and E. Wicke, *Z. Elektrochem.*, **56**, 551 (1952); THIS JOURNAL, **58**, 702 (1954).

[14] H. Falkenhagen and G. Kelbg, *Ann. Physik*, **11**, 60 (1952).

[15] M. Dutta, *Proc. Natl. Inst. Sci. India*, **19**, 183 (1953); *Naturwiss.*, **40**, 5 (1953): see also M. Dutta and M. Sengupta, *Proc. Natl. Inst. Sci. India*, **20**, 1 (1954); M. Sengupta, *ibid.*, **22**, 13 (1956).

[16] J. W. Cahn and J. E. Hilliard, *J. Chem. Phys.*, **28**, 258 (1958); **30**, 1121 (1959); **31**, 688 (1959).

[17] E. W. Hart, *Phys. Rev.*, **113**, 412 (1959); **114**, 27 (1959).

$$Q_{N-1}\, g_r[1 + V^{-1}\Sigma_s c_{rs} + V^{-2}\Sigma_s\Sigma_t \{c_{rs}c_{rt} + d_{rst}\} + \ldots] \tag{2.17}$$

The denominator on the right-hand side of (2.5) is the average over the volume V of the numerator, *i.e.*, of the expression given by (2.10) or (2.17). Since V is very large compared with the volume occupied by the diffuse layer, this average virtually is equal to the expression given in (2.17) with the terms replaced by their "bulk" values at points distant from the colloid particle. The wall interaction energy $u_r(\mathbf{q}_r)$ is zero except when $\mathbf{q}_r$ is within a distance of molecular order from the colloidal wall and hence the bulk value of g_r is 1. Also V_s is zero outside the diffuse layer and f_{rs} is zero except for small values of $|\mathbf{q}_r - \mathbf{q}_s|$ so that, in the bulk of the electrolyte

$$c_{rs} = \int f_{rs}\, d\mathbf{q}_s = b_{rs} \tag{2.18}$$

which is independent of $\mathbf{q}_r$. If both ions r and s are distant from the colloidal particle V_{rs} and F_{rs} are denoted, respectively, by $V^0{}_{rs}$ and $F^0{}_{rs}$. As V_r and V_s are then both zero, it follows from the definition (2.13) of F_{rs} that

$$F^0{}_{rs} = \exp(-\beta V^0{}_{rs}) - 1 \tag{2.19}$$

The product $f_{rs}f_{rt}$ is non-zero only when ions s and t are both near to ion r. Thus when $\mathbf{q}_r$ is distant from the particle, d_{rst} will assume a constant bulk value to be denoted by $d^0{}_{rst}$. Hence the denominator of (2.6) is

$$Q_{N-1}\,[1 + V^{-1}\Sigma_s b_{rs} + V^{-2}\Sigma_s\Sigma_t \{b_{rs}b_{rt} + d_{rst}{}^0\} + \ldots] \tag{2.20}$$

The value of c_{rs} depends only on $\mathbf{q}_r$ and on the ion types to which ions r and s belong. The c_{rs} may thus be replaced by the set of m^2 position dependent functions c_{ij}. Similarly the d_{rst} can be replaced by the set of m^3 position dependent functions d_{ijk} and the constants b_{rs} and $d^0{}_{rst}$ by b_{ij} and $d^0{}_{ijk}$, respectively. The sums over the individual ions in (2.17) and (2.20) can then be changed to sums over the ion types. If N_iV is replaced by $n_i{}^0$ and the transformed expressions (2.17) and (2.20) are substituted into (2.6), then retaining terms up to the second degree in the ion densities

$$\zeta_i = g_i\left[1 + \sum_{j=1}^{m} n_j{}^0(c_{ij} - b_{ij}) + \right.$$
$$\sum_{i=1}^{m}\sum_{k=1}^{m} n_j{}^0 n_k{}^0\,(c_{ij}c_{ik} - c_{ij}b_{ik} + d_{ijk} - d^0{}_{ijk}) + \ldots \tag{2.21}$$

where ζ_i is the short-range force factor for an ion of type i at a given point in the dispersion medium. However, by the definition (2.14) the c_{ij} depend on the ζ_j, so that to develop ζ_i as a series in the ion concentrations it is necessary to use an iterative process. If we define

$$c^0{}_{ij} = \int f_{ij}g_j \exp(-\beta V_j{}^0) d\mathbf{q}_j \tag{2.22}$$

then, from (2.14) and (2.21) it follows that, to the first degree in the ion densities

$$c_{ij} = c^0{}_{ij} + \sum_{k=1}^{m} n_k{}^0\,\{\int f_{ij}g_j c^0{}_{jk} \times$$
$$\exp(-\beta V_j{}^0) d\mathbf{q}_j - c^0{}_{ij}\, b_{jk}\} + \ldots \tag{2.23}$$

Hence, retaining terms up to the second degree in the ion densities, (2.21) becomes

$$\zeta_i = g_i\, 1 + \sum_{j=1}^{m} n_j{}^0\,(c^0{}_{ij} - b_{ij}) +$$
$$\sum_{j=1}^{m}\sum_{k=1}^{m} n_j{}^0\, n_k{}^0\,\{c^0{}_{ij}(c^0{}_{ik} - b_{ik}) + \int f_{ij}g_j c^0{}_{ik} \times$$
$$\exp(-\beta V_j{}^0) d\mathbf{q}_j - b_{jk}c^0{}_{ij} + d_{ijk} - d^0{}_{ijk}\} + \ldots] \tag{2.24}$$

No approximations have been made in deriving this result other than the assumption that a dilute colloidal solution is being considered. When the ion of type i is beyond two or three molecular diameters from the wall it is possible to simplify (2.24) by putting $g_j = 1$ for $i = 1, \cdots, m$. This point will be further discussed for the particular model used in the next section.

3. Equal Impenetrable Hydration Spheres in a 1-1 Electrolyte

To illustrate the determination of the volume factor ζ_i, a plate-like uniformly charged colloidal particle, in contact with an aqueous electrolyte and large enough for edge effects to be neglected, will be considered. The colloid surface may thus be regarded as a section of an infinite plane and the perpendicular distance from this plane of a point in the diffuse layer will be x. To evaluate the quantity $c^0{}_{ij}$ at the point x it is necessary to consider an ion of type i at x and a second ion of type j in its vicinity at a distance x_j from the plate wall. $V_j{}^0$ will then be a function of x_j in the integral (2.22) for $C^0{}_{ij}$. The case where x is greater than a few molecular diameters, so that we may put $g_i = 1$ for all i, will be considered first. Since f_{ij} will differ significantly from -1 only for small values of the separation between ions i and j, whereas $V_j{}^0(x_j)$ represents a "long-range" electrostatic term, we shall expand $\exp[-\beta V_j{}^0(x_j)]$ in a Taylor series about the point $x_i = x$. It follows from (2.22) that

$$c^0{}_{ij}(x) = \exp[-\beta V_j{}^0(x)]\,[b_{ij} - l_{ij}\beta\,\frac{dV_j{}^0(x)}{dx} +$$
$$\frac{1}{2}\, m_{ij}\left\{\beta^2\left(\frac{dV_j{}^0(x)}{dx}\right)^2 - \beta\,\frac{d^2V_j{}^0(0)}{dx^2}\right\} + \ldots] \tag{3.1}$$

where

$$l_{ij} = \int (x_j - x) f_{ij}\, d\mathbf{q}_j,\ m_{ij} = \int (x_j - x)^2 f_{ij}\, d\mathbf{q}_j \tag{3.2}$$

The simplest application is to a 1–1 valency type of electrolyte in which the hydration shells of anions and cations are regarded as hard spheres of the same diameter. Then $m = 2$, $e_1 = -e_2 = e$, $n_1{}^0 = n_2{}^0 = n$, say, and for all i and j

$$f_{ij} = -1,\ |\mathbf{q}_i - \mathbf{q}_j| < a;\ f_{ij} = 0,\ |\mathbf{q}_i - \mathbf{q}_j| > a \tag{3.3}$$

Using (2.18) and (3.2)

$$b_{ij} = -\frac{4\pi a^3}{3} = b, \text{ say};\ l_{ij} = 0;\ m_{ij} = \frac{1}{5}\, ba^2 \tag{3.4}$$

for all i and j. With this hard-sphere model it is reasonable to assume a "distance of nearest approach" d of an ion center to the wall, such that

$$g_i = 1,\ x > d;\ g_i = 0,\ x < d,\ i = 1,2 \tag{3.5}$$

The electrostatic potentials of the mean force will be written as

$$V_1{}^0 = e\psi + X,\ V_2{}^0 = -e\psi + X \tag{3.6}$$

where ψ is the mean potential at the point x and X is a correction term which will be described below:

the zeros of ψ and X are taken at $x = 0$ and for simplicity it is assumed that X has the same value for the two ion types.

The factor ζ_i can be expressed as a series in powers of the "excluded volume fraction" nb and our object will be to obtain the first and second-order terms proportional to nb and $(nb)^2$, respectively. For first-order terms no error is caused when g_i is put equal to 1 if $x \geqslant d + a$ and for second-order terms if $x \geqslant d + 2a$. If now $\phi = \beta e\psi$, $Y = \beta X$ and dashes denote differentiation with respect to x, then making use of the above formula, the terms of the first degree in the $n_j{}^0$ in (2.24) are given by

$$\sum_{j=1}^{m} n_j{}^0 (c^0{}_{ij} - b_{ij}) = 2bn[\exp(-Y)\cosh\phi - 1] + \frac{1}{5} na^2b \exp(-Y)[\cosh\phi \{(\phi')^2 + (Y')^2 - Y''\} + \sinh\phi\,(\phi'' - 2\phi'Y')] \quad (3.7)$$

The second term on the right is second-order and a first approximation to it is obtained by putting $Y = 0$ and applying the classical Poisson–Boltzmann equation to simplify the resulting expression in ϕ. For a 1–1 electrolyte, the latter equation reads

$$\phi'' = \kappa_0{}^2 \sinh\phi, \quad (3.8)$$

where K_0 is the Debye–Hückel parameter of the electrolyte given

$$\kappa_0{}^2 = 8\pi ne^2\beta/\epsilon$$

A first integral of (3.8) is

$$(\phi')^2 = 2\kappa_0{}^2(\cosh\phi - 1) \quad (3.9)$$

If (3.8), (3.9) and the condition $X = 0$ are substituted into the second term on the right-hand side of (3.7) it becomes

$$-\frac{6}{5} p(nb)^2 (\cosh\phi - 1)(3\cosh\phi + 1) \quad (3.10)$$

where the constant p is defined as $\beta e^2/\epsilon a$

It is well known that the determination of X in electrolyte theory is very difficult and the problem becomes even more involved in the case of electric double layers. We shall suggest here a first approximation to X, applicable when both the electrolyte concentration and the electric field in the diffuse layer are not too large. Let κ be the "local" Debye–Hückel parameter, defined by

$$\kappa^2 = \frac{4\pi e^2\beta}{\epsilon}(n_1 + n_2) \approx \kappa_0{}^2 \cosh\phi \quad (3.11)$$

where n_1 and n_2 are the densities of the two ion types at position x. If, for simplicity, the colloidal wall is assumed to be metallic, then X is given approximately by

$$X = -\frac{e^2}{4\epsilon x}\exp(-2\kappa x) - \frac{e^2}{2\epsilon a}\left(\frac{\tau}{1 + \tau} - \frac{\tau_0}{1 + \tau_0}\right) - \frac{1}{8\pi}\left(\frac{d\psi}{dx}\right)^2 \frac{d\epsilon}{dn} \quad (3.12)$$

where $\tau = \kappa a$ and $\tau_0 = \kappa_0 a$. The first term is the "screened" image term, the second is due to the self-atmosphere of each ion which has been treated by Loeb,[18] Williams[19] and Hill[20] and the third represents the polarization energy of an ion in the electric field of the diffuse layer, which has been considered by Bikerman,[7] Bolt,[21] Prigogine, Mazur and Defay[6] and Sparnaay.[12] Making use of the experimental work of Hasted, Ritson and Collie[22] it may be assumed that

$$d\epsilon/dn = 10^3\delta/\mathbf{N}$$

where **N** is Avogadro's number and δ is a negative constant of the order of 5–10. (The derivative $d\epsilon/dn$ of the dielectric constant of the electrolyte ϵ with respect to the ion density, n, is taken at constant electric field, pressure and temperature.) Making use of (3.9) and (3.11) it is possible to express (3.12) as

$$\beta X = Y = \frac{-\beta\tau_0 e^2}{2\epsilon a}\left[\frac{\exp\{-2\tau_0(x/a)\sqrt{\cosh\phi}\}}{2\tau_0 x/a} + \frac{\sqrt{\cosh\phi} - 1}{(1 + \tau_0)(1 + \tau_0\sqrt{\cosh\phi})} + \frac{10^3\tau_0\epsilon\delta}{2\pi\mathbf{N}e^4\beta^2 a}(\cosh\phi - 1)\right] \quad (3.13)$$

At $T = 25°$, $\kappa_0 = \sqrt{\gamma}/3.04 \times 10^{-8}$ where γ is the electrolyte concentration in mole/l. and in the table the values of Y for $\phi = 1,2,3$ and $\gamma = 0.01$ and 0.1 are given, assuming that $x = 1.5 \times 10^{-7}$ cm. $\delta = -6$ and $a = 5 \times 10^{-8}$ cm. It is seen that $|Y/\phi| << 1$ and it will be assumed therefore that (3.10) is a reasonable estimate of the second-order term in (3.7).

	$\gamma = 0.01$			$\gamma = 0.1$		
ϕ	1	2	3	1	2	3
$-Y$	0.053	0.080	0.122	0.025	0.055	0.028

For second-order accuracy it is possible in the terms with factor $n_j{}^0 n_k{}^0$ of equation (2.24), to neglect the variation of $V_j{}^0$ over the range of integration in $c^0{}_{ij}$ (which is given by (2.22) and to put $V_j{}^0$ equal to $e_j\psi(x)$ so that

$$c_{ij}(x) \approx \int f_{ij} \exp\{-\beta e_j\psi(x)\}\, d\mathbf{q}_j = b\exp\{-\beta e_j\psi(x)\} \quad (3.14)$$

Thus (putting $g_j = g_k = 1$)

$$\int f_{ij}c^0{}_{jk} \exp(-\beta V_j{}^0) d\mathbf{q}_j \approx b\int f_{ij} \exp\{-\beta(e_j + e_k)\psi(x_j)\}\, d\mathbf{q}_j \approx b^2 \exp\{-\beta(e_j + e_k)\psi(x)\}, \quad (3.15)$$

and hence

$$\sum_{j=1}^{m}\sum_{k=1} {}_i{}^0 n_k{}^0 \{(c^0{}_{ij} - b_{ij})c^0{}_{ik} + \int f_{ij}c^0{}_{jk} \exp(-\beta V_j{}^0)\, d\mathbf{q}_j - c^0{}_{ij}b_{jk}\} \approx 8b^2n^2 \cosh\phi\,(\cosh\phi - 1) \quad (3.16)$$

The terms $d_{ijk} - d^0{}_{ijk}$ in (2.24) remain to be considered. Exact evaluation is difficult but we shall be able to estimate the magnitude. Since the ion complexes are hard spheres of radius a, both V_{jk} and $V^0{}_{jk}$ are infinite when the distance $|\mathbf{q}_j - \mathbf{q}_k|$ (which will be denoted by r_{jk} for brevity) is less than a. Hence, from (2.15) and (2.19)

$$F_{jk} - F^0{}_{jk} = 1 - \exp\{-\beta(V_j + V_k)\},\ r_{jk} < a \quad (3.17)$$

---

(18) A. L. Loeb, *J. Colloid Sci.*, **6**, 75 (1951).

(19) W. E. Williams, *Proc. Phys. Soc.* (*London*), **A66**, 372 (1953).

(20) T. L. Hill, THIS JOURNAL, **61**, 548 (1957).

(21) G. H. Bolt, *J. Colloid Sci.*, **10**, 206 (1955).

(22) J. B. Hasted, D. M. Ritson and C. H. Collie, *J. Chem. Phys.*, **16**, 1 (1948).

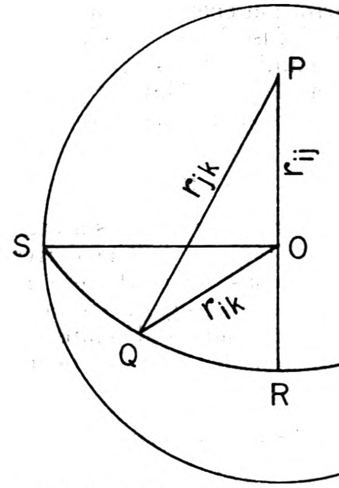

Fig. 1.—[OP = r_{ij}], [PQ = r_{jk}], [OQ = r_{ik}].

When $r_{jk} > 0$, $V_{jk} - V_j - V_k$ is the Coulomb interaction of the ions j and k partially screened by their interpenetrating atmospheres. If V_{jk} is defined as

$$V'_{jk} = V_{jk} - V_j - V_k \tag{3.18}$$

then it follows from (2.15) and (2.19) that

$$F_{jk} - F^0_{jk} = \exp[-\beta(V_j + V_k)][\exp(-\beta V'_{jk}) - 1] - [\exp(-\beta V^0_{jk}) -],\ r_{jk} > a \tag{3.19}$$

which reduces to (3.17) when $r_{jk} < a$ if both V'_{jk} and V^0_{jk} are equated to infinity. According to the Debye–Hückel theory of electrolytes V'_{jk} is given approximately by

$$V'_{jk} \approx \frac{e_j e_k}{\epsilon}\,\frac{e^{\tau}}{1+\tau}\,\frac{e^{-\tau r_{jk}/a}}{r_{jk}} \tag{3.20}$$

and the corresponding approximation to V^0_{jk} is obtained by replacing τ by τ_0 in (3.20).

It is convenient to write

$$d_{ijk} - d^0_{ijk} = \int f_{ij} f_{ik} (F_{jk} - F^0_{jk})\, \mathrm{d}q_j \mathrm{d}q_k = \eta_{ijk} + \xi_{ijk}) \tag{3.21}$$

where η_{ijk} and ξ_{ijk} are the contributions from the regions $r_{jk} < a$ and $r_{jk} > a$, respectively. As in the other second-order terms, the variation of V_j and V_k over the small range of volume in which $f_{ij}f_{ik} \neq 0$ will be neglected and we shall put $V_j = V_j^0 = e_j\psi(x)$. It follows from (3.17) that

$$\eta_{ijk} = [1 - \exp\{-\beta(e_j + e_k)\psi(x)\}] \times \int_{r_{jk}<a} f_{ij} f_{ik}\, \mathrm{d}q_j \mathrm{d}q_k \tag{3.22}$$

For a 1–1 electrolyte the right-hand side of (3.22) will clearly vanish if ions j and k are of opposite sign. Also, since the positive and negative ions are assumed to have equal hydration shells, f_{ij} is independent of the ion types i and j and for hard spheres the integral on the right is equal to $15b^2/32$. This is a familiar result which yields the third virial coefficients in the equation of state of imperfect gases for the hard sphere model.[23] It follows that

$$\sum_{j=1}^{2}\sum_{k=1}^{2} n_j^0 n_k^0 \eta_{ijk} \approx \frac{15}{16}(bn)^2[\cosh 2\phi - 1] \tag{3.23}$$

To determine ξ_{ijk} it is necessary to consider the integral

$$\begin{aligned} I_{jk} &= \int_{r_{jk}>a} f_{ij} f_{ik} G'_{jk} \mathrm{d}q_j \mathrm{d}q_k = \\ &\qquad 8\pi^2 \int_{r_{jk}>a} f_{ij} f_{ik} G'_{jk} r_{ij} r_{ik} r_{jk} \mathrm{d}r_{ij} \mathrm{d}r_{ik} \mathrm{d}r_{jk} \\ &= 8\pi^2 \int_a^{2a} G'_{jk} r_{jk} \mathrm{d}r_{jk} \int_{r_{jk}-a}^{a} r_{ij} \mathrm{d}r_{ij} \int_{r_{jk}-r_{ij}}^{a} r_{ik} \mathrm{d}r_{ik} \\ &= \frac{\pi^2}{3} \int_a^{2a} G'_{jk}(r^5_{jk} - 12a^2 r^3_{jk} + 16a^3 r^2_{jk})\, \mathrm{d}r_{jk} \end{aligned} \tag{3.24}$$

where, for brevity

$$G'_{jk} = \exp(-\beta V'_{jk}) - 1 \tag{3.25}$$

The limits of integration in (3.24) can be obtained from a study of Fig. 1. If O, P and Q define the centres of ions i, j and k, respectively, then P and Q must lie inside a sphere of radius a and center O. If the distances OP = r_{ij} and Pa = r_{jk} are fixed, Q lies on a sphere of radius r_{jk}, center P and therefore r_{ik} varies from OR = $r_{jk} - r_{ij}$ to OS = a. For fixed PR = r_{jk} the distance OP = r_{ij} can now vary from OR = $r_{jk} - a$ to a and finally r_{jk} lies in the range a to $2a$. Inserting the form (3.20) for V'_{jk} and introducing $V = r_{jk}/a$

$$I_{jk}(\tau) = -\frac{15}{32} b^2 H(\mp p,\tau) \tag{3.26}$$

where

$$H(p,\tau) = \frac{2}{5}\int_1^2 (v^5 - 12v^3 + 16v^2) \times \left[1 - \exp\left(\frac{pe^{\tau(1-v)}}{(1+\tau)v}\right)\right] \mathrm{d}v \tag{3.27}$$

and the minus and plus signs refer to like- and unlike-charged ions j and k, respectively. Making the same approximations as in (3.22), it follows from (3.19), (3.21), (3.24) and (3.25) that

$$\xi_{ijk} \approx \exp[-\beta(e_j + e_k)\psi(x)]I_{jk}(\tau) - I_{jk}(\tau_0) \tag{3.28}$$

and it is readily seen that

$$\sum_{i=1}^{2}\sum_{k=1}^{2} n_j^0 n_k^0 \xi_{ijk} \approx \frac{15}{16} b^2 n^2 [(\cosh\phi - 1)H(-p,\tau) + K(p,\tau,\tau_0)] \tag{3.29}$$

where, making use of (3.11), $\tau = \tau_0\sqrt{\cosh\phi}$ and

$$K(p,\tau,\tau_0) = \frac{4}{5}\int_1^2 (v^5 - 12v^3 + 16v^2) \times \left[\cosh\left(\frac{pe^{\tau_0(1-v)}}{(1+\tau_0)v}\right) - \cosh\left(\frac{pe^{\tau(1-v)}}{(1+\tau)v}\right)\right] \mathrm{d}v \tag{3.30}$$

Two limiting cases are the following. If the Coulomb interaction between ions j and k is entirely neglected, then for $r_{jk} > a$, $V'_{jk} = V^0_{jk} = 0$ and $\xi_{ijk} = 0$; therefore (3.29) vanish. At the other extreme if the screening effect due to the self-atmosphere of the ions is ignored

$$V'_{jk} = V^0_{jk} = e_j e_k/\epsilon r_{jk} \tag{3.31}$$

and this will apply in the limit of zero electrolyte concentration when $\tau = \tau_0 = 0$. Then $K(p,0,0) = 0$ and

---

[23] J. O. Hirschfelder, C. F. Curtiss and R. B. Bird, "Molecular Theory of Gases and Liquids," John Wiley and Sons, New York, N. Y., 1954.

$$H(-p,0) = \frac{2}{5}\Big[\frac{17}{6} - \exp(-p)\Big(-\frac{5}{2} + \frac{17}{10}p - \frac{87}{40}p^2 - \frac{179}{360}p^3 - \frac{1}{720}p^4 + \frac{1}{720}p^5\Big) + \exp(-p/2)\Big(-\frac{16}{3} + \frac{56}{15}p - \frac{52}{15}p^2 - \frac{44}{45}p^3 - \frac{1}{180}p^4 + \frac{1}{360}p^5\Big) + \frac{1}{6}p^3\Big(16 + 3p - \frac{1}{120}p^3\Big)\{E_i(p/2) - E_i(p)\}\Big]$$

$$E_i(x) = \int_x^\infty t^{-1}\exp(-t)\mathrm{d}t \quad (3.32)$$

Making use of (3.7), (3.10), (3.16), (3.23) and (3.29) for the particular model considered in this section, the equation (2.24) becomes

$$\zeta = \zeta_1 = \zeta_2 = 1 + 2bn\{\exp(-Y)\cosh\phi - 1\} + 8b^2n^2\Big[(\cosh\phi - 1)\Big\{\cosh\phi - \frac{15}{64}(1 + H(-p,\tau))(\cosh\phi + 1) - \frac{3}{20}p(3\cosh\phi + 1)\Big\} - \frac{15}{128}K(p,\tau,\tau_0)\Big] + \ldots \quad (3.33)$$

Substituting into (2.4), the modified Poisson–Boltzmann equation (1.1) becomes

$$\frac{\mathrm{d}D}{\mathrm{d}x} = -8\pi ne\zeta\exp(-Y)\sinh\phi \quad (3.34)$$

where ζ is given by (3.33). This expression is valid to second-order terms for distances $x > d + 2a$.

To illustrate the values of H and K numerically, we choose $p = 1$ which corresponds to the diameter $a = 7.1 \times 10^{-8}$ cm. at $T = 25°$ and $\epsilon = 78.5$ and at zero electrolyte concentration $K(1,0,0) = 0$ and $H(-1,0) = 0.608$. This is the maximum value that H can attain for the given p. Some values of H and K at two concentrations calculated by numerical integration, are given in the table.

$\tau_0 = 0.7$, $\gamma = 0.089$ mole/l.				$\tau_0 = 0.35$, $\gamma = 0.022$ mole/l.			
τ	ϕ	$H(-1,\tau)$	$K(1,\tau,\tau_0)$	τ	ϕ	$H(-1,\tau)$	$K(1,\tau,\tau_0)$
0.9	1.09	0.306	0.0470	0.7	2.08	0.351	0.155
1.4	2.08	0.224	0.110	0.9	2.58	0.306	0.201

The term in K constitutes a small correction to the second-order term in (3.33), and will be ignored in the discussion which follows. The contribution to the second-order term which is proportional to p is due to the variation of the potential function ψ over a distance of magnitude a. It is true that this effect first makes its appearance in the second-order term, but it does form an important part of this term. Thus, for large ϕ we may replace the expression in the brackets on the right-hand side of (3.33) by $\cosh^2\phi\Big\{1 - \frac{15}{64}(1 + H) - \frac{9}{20}p\Big\} \backsimeq 0.25\cosh^2\phi$ if $p = 1$ and $H = 0.3$. For small ϕ, the expression approaches the value $\frac{1}{2}\phi^2\Big\{1 - \frac{15}{32} \times (1 + H) - \frac{3}{5}p\Big\} \backsimeq -0.21\phi^2$ and here (apart from the contribution from K) the presence of the expression in p results in a change in sign in the second-order term. Comparison of the first and second-order terms in (3.33) for potentials of 50 mv. ($\phi = 2$) which may occur at distances of 1-2 $\times$ 10^{-7} cm. from the wall, indicate that the ratio of these terms can be an appreciable fraction at electrolyte concentrations as low as $\gamma = 0.1$.

Conditions at points too near to the wall to permit the assumption $g_i = 1$ will now be considered. It is seen from (2.22) and (3.3) that in evaluating $c_{ij}(x)$ it is necessary to integrate over a sphere of radius a with center at a point distant x from the wall. From (3.5), if $x < d + a$ this sphere is divided into two parts by a plane parallel to the wall and at a distance d such that in the portion of the sphere nearest to the wall $g_j = 0$ and in the other portion $g_j = 1$. The quantities b_{ij} and l_{ij} defined in (2.18) and (3.2), are now replaced by

$$b^*_{ij} = b\{1 - s(t)\},\ l_{ij}^* = \frac{3}{16}ba(1 - t^2)^2 \quad (3.35)$$

where

$$t = (x - d)/a,\ s(t) = \frac{1}{2}\Big(1 - \frac{3}{2}t + \frac{1}{2}t^3\Big) \quad (3.36)$$

and $-b_{ij}^*$ is the actual volume of the outer portion of the sphere. It is verified readily that if use is made of (3.9) and the term proportional to n^2 is ignored, then for $x < d + a$, (3.33) is replaced by

$$\zeta = 1 + 2bn(L\cosh\phi - 1) + M(|b|n)^{1/2}\sinh\phi(\cosh\phi - 1)^{1/2} + \ldots,\ L = \Big[1 - s(t) - \frac{3}{16}a(1 - t)^2\,\mathrm{d}Y/\mathrm{d}x\Big]\exp(-Y),\ M = \pm\frac{3}{4}\sqrt{3}p^{1/2}(1 - t^2)^2\exp(-Y) \quad (3.37)$$

where the plus or minus sign depends on whether the charge on the wall is positive ($\phi > 0$) or negative ($\phi < 0$). When $x \geq d + a$, $t = 1$, $s(t) = 0$, the last term on the right-hand side of (3.37) vanishes and (3.37) is reduced to the first two terms of (3.33). When $x = 0$, $t = 0$ and $s = {}^1/_2$. It is seen that the "steric hindrance" of the wall alters the form of the linear term in the expansion for ζ and introduces a new term proportional to $n^{1/2}$. It is difficult to estimate the ratio of these two terms, since the function $Y = Y(x)$, which may not be small very close to the wall, has not been determined.

It is not difficult to obtain the term in ζ proportional to n^2 but since the function $Y(x)$ is not known and the model of hard spheres is perhaps too crude at such small distances from the wall, we shall not give the results. The alteration in the expression (3.15), in which we have assumed $g_j = g_k = 1$ is, however, of special interest. From the definition (2.22) of $c_{jk}{}^0$ the condition $g_k = 1$ implies that ion j must be at a distance $x_j > d + a$ from the wall. For this to be true over the whole range of integration with respect to g_j in (3.15), the coördinate x of ion i must be greater than $d + 2a$. Thus, for the model of hard spheres assumed here, the term proportional to n^2 in ζ takes different analytical forms in the three regions $d < x < d + a$, $d + a < n < d + 2a$ and $d + 2a < x < \infty$[24]: the third

---

(24) G. Kelbg (*Disc. Faraday Soc.*, **24**, 72 (1957)) has objected to the Taylor series which the author[5] has originally introduced in the case of the atmosphere surrounding a spherical hydrated ion of diameter a on the grounds that the function $\zeta = \zeta(R)$ is not analytic throughout the range $a < R < \infty$ where R is the radial distance from the ion center. This objection does not apply to the expansion (3.1) since $V_j{}^0(x)$ is an analytic function of x: the spherical case can be treated similarly. Kelbg has also remarked that the form of $\zeta(R)$ in the range $a < R < 2a$ will be different from that in $2a < R < \infty$: the equation 5 obtained by the authors[3] applies to the latter region.

order (n^3) term will assume different forms in four regions and so on. The wall, as it were, affects the distribution in successive boundary layers of ions. It appears therefore that in the immediate vicinity of the colloidal wall the expression for ζ becomes very complicated. Thus theories of volume correction, however accurate in their application to a bulk phase, may be inadequate for the important regions adjacent to the wall. Previous theories of the volume correction have failed to demonstrate this property.

4. The Local Balance Method

If $\chi(n_i)$ denotes the logarithm of the number of arrangements in unit volume available to n_0 solvent molecules and to $n_1, \cdots, n_m$ ions of the various types then, on the assumption of local balance

$$\chi_i - \chi_i^0 = \beta(e_i\psi + X_i),\ i = 1, \ldots, m \qquad (4.1)$$

where $\chi_i = \partial\chi/\partial n_i$ and X_i is the correction term due to image, self-atmosphere and polarization effects. The superscript 0 indicates that the quantity concerned is taken at the reference point where $\psi = 0$ (For the expression on the left-hand side of (4.1) see Bell and Levine (§2) where, however, the approximation $X_i = 0$ was made.) If $e_i\psi + X_i$ is identified with V_i^0 it is clear from (1.1) and (2.4) that the local balance theory gives the short-range interaction or "volume correction" factor ζ_i in the form

$$\ln \zeta_i = \ln n_i/n_i^0 + \chi_i - \chi(n_i) \qquad (4.2)$$

A lattice type theory of solutions can be applied to the particular model of a 1–1 electrolyte described in §3 in the following way. Suppose that v_0 is the partial volume of a solvent molecule and $v_i = hv_0$ the partial volume of an ion of type i with its hydration shell: here $v_1 = v_2$. Then $k\chi(n_j)$ is essentially an entropy of mixing of molecules of different sizes. A zeroth order approximation is given by Flory's formula

$$\chi(n_j) = -\sum_{i=0}^{m} n_i \ln y_i \qquad (4.3)$$

where $y_i = v_in_i$ is the volume fraction of component i, the solvent component being given the index 0. Volume fraction statistics have already been applied to hydrated electrolytes by Glueckauf[25] and Miller.[26] It will be assumed that v_0 and h are uniform throughout the diffuse layer. And so the relation $\sum_{i=0}^{m} n_iv_i = 1$ defines n_0 in terms of $n_1, \cdots, n_m$. Also as in §3 $\zeta_1 = \zeta_2 = \zeta$.

Let the proportion of unit volume occupied by hydrated ions be ξ so that

$$\xi = (n_1 + n_2)v_0h \qquad (4.4)$$

At a point distant from the wall

$$\xi = 2nv_0h = \xi_0 \qquad (4.5)$$

Then, as deduced in Bell and Levine[3] (equation 11), substitution of (4.3) into (4.2) gives

$$\zeta = \zeta_1 = \zeta_2 = (1 - \xi)^h (1 - \xi_0)^{-h} \qquad (4.6)$$

Thus, substituting (4.1) and (4.2) into (4.4)

$$= 2hv_0n\zeta \cosh \phi \exp(-Y) = \xi_0(1 - \xi)^h (1 - \xi_0)^{-h} \times \cosh \phi \exp(-Y) \qquad (4.7)$$

From (4.7) it is possible to express ξ and therefore by (4.6), ζ as a series in powers of ξ_0 giving, finally

$$\zeta = 1 - 2nh^2v_0 \{\exp(-Y) \cosh \phi - 1\} + 2h^3n^2v_0^2 (\cosh \phi - 1)\{(3h - 1) \cosh \phi - (h - 1)\} + \ldots \qquad (4.8)$$

The right-hand sides of (3.33) and (4.8) agree up to the first-order linear terms in the correction factor ζ for the volume effect if we put

$$h^2v_0 = 4\pi a^3/3 = -b \qquad (4.9)$$

Since the most closely packed assembly of rigid spheres cannot occupy the whole volume, the partial volume of a hydrated ion in lattice theory will be rather larger than the volume of this ion in imperfect gas theory, that is we may expect $hv_0 > \pi a^3/6$. It follows from (4.9) that if the first-order terms in the two equations are to agree then it is necessary that $h < 8$. Further, if the terms in p and K are omitted from the second-order term on the right-hand side of (3.33), then it is readily verified that agreement up to second-order terms in n is obtained between (3.33) and (4.8) provided

$$f = (1 + 16/h)/15 \qquad (4.10)$$

and since $h < 8$, this implies $f > 0.2$. This result is unexpected since the theories of Kirkwood and of local thermodynamic balance are based on such different premises. The absence of a term in (4.8) which arises from the variation of the potential ψ over a distance of the order of the diameter demonstrates, however, that from the nature of its basic assumptions a local balance method cannot give the terms depending on the gradients of intensive properties which occur in accurate equilibrium equations of non-homogeneous systems. In this particular case the consequence is that the local balance results, though correct to first-order terms in the volume fraction, overestimate the second-order terms. In these circumstances it does not seem worthwhile to examine the more correct but also far more elaborate methods (Guggenheim[27]) of evaluating the function $\chi(n_j)$, which occurs in the local balance theory.

We shall now briefly consider the local balance method for more general short-range interactions between the ions. If f_{ij} is a function of the distance r_{ij} between the centers of the ions of types i and i then, from (2.18) $b_{ij} = b_{ji}$. If the positions considered are far enough from the wall for all the g_i factors occurring to be equated to 1 then it is easy to show that a χ function can be found which gives ζ_i correctly to the *first order*. From (2.24), if only first degree terms in the ion densities are retained, then

$$\zeta_i \approx 1 + \sum_{j=1}^{m} (n_j - n_j^0)b_{ij}, \qquad \ln \zeta_i \approx \sum_{j=1}^{m} (n_j - n_j^0)b_{ij} \qquad (4.11)$$

By (4.2) a function $\chi(n_j)$ can be found which gives these approximate expressions for $\ln \zeta_i$, since, using (4.11)

---

(25) P. J. Flory, *J. Chem. Phys.*, **10**, 51 (1942).

(26) E. Glueckauf, *Trans. Faraday Soc.*, **51**, 1235 (1955): see also R. A. Stokes and R. H. Robinson, *ibid.*, **53**, 301 (1957).

(27) E. A. Guggenheim, "Mixtures," Oxford University Press, 1952.

$$\partial \ln \zeta_i/\partial n_j = b_{ij} = b_{ji} = \partial \ln \zeta_j/\partial n_i \qquad (4.12)$$

and this is the necessary and sufficient condition that the distribution function χ exists. Expressions like (4.11) for the volume factor have been used by several authors writing on electrolytes (Falkenhagen and Kelbg,[14] Grimley[8] and Schlogl[28]) and on diffuse layers (Freise,[9] Ohlenbusch[10]). One form used by Eigen and Wicke[13] is

$$\zeta = [1 + (n/N)(\cosh \varphi - 1)]^{-1} \qquad (4.13)$$

where their N^{-1} is to be identified with the exclusion volume $-b$. It was pointed out by the authors[5] (see also Robinson and Stokes[26]) that in the lattice model used by Eigen and Wicke their N^{-1} ought rather to be identified with the actual ionic volume which is $^1/_8$ of the exclusion volume, so that the basis of (4.13) is rather doubtful. Also (4.13) overestimates the second-order term at large ϕ.

DISCUSSION

J. TH. G. OVERBEEK (University of Utrecht).—Can you indicate under which conditions the uncorrected Poisson–Boltzmann equation can be applied reasonably well and what would be the first corrections to take into account?

S. LEVINE.—A convenient way of answering Professor Overbeek's question is to compare the work of previous authors with the results obtained in this paper. The approach of all these authors is essentially equivalent to the method of local thermodynamic balance and, as in our paper, they consider a single plate-like particle. M. J. Sparnaay (ref. 12) treats the volume effect of the hydrated ions, the polarization energy of the ions and the dependence of the dielectric constant of the diffuse layer medium on both the electric field (dielectric saturation) and the concentration of ions. By restricting the potential of the colloidal wall and the electrolyte concentration, only small deviations from the Poisson–Boltzmann equation are obtained. The volume and dielectric saturation effects act in the same direction, both tending to deplete the ionic concentration in the diffuse layer. The polarization energy has the same tendency since the hydrated ion complex is less polarizable than a "complex" of water molecules occupying the same volume. Sparnaay finds that the correction due to the dependence of dielectric constant on ionic concentration has the same form as that due the polarization energy but is opposite in sign and three times as large. The volume effect seems to be the main source of deviation from the Poisson–Boltzmann equation. At a surface potential of 100 mv. and a 1–1 electrolyte concentration of 0.01 N, the corrections to the potential distribution amount to 10–20%. Sparnaay retains the linear terms in the ionic densities in all these effects and his treatment breaks down when the concentration is 0.1 N or greater. Our only objection to his analysis is the omission of the image and self-atmosphere terms which counteract and indeed may exceed the polarization energy term. It is unlikely that this will change the conclusion that the volume effect constitutes the main correction at small potentials and small electrolyte concentrations.

H. Brodowsky and H. Strehlow (*Z. Elektrochem.*, **63**, 262 (1959)) introduce the dependence of dielectric constant on electric field and electrolyte concentration and the volume effect. Now in their theory of strong electrolytes at higher concentrations, M. Eigen and E. Wicke (ref. 13) proposed two limiting models to describe the short-range interactions of the ions. The first is precisely that treated in Eq. 3 and 4. On physical grounds it seems possible that the distance of nearest approach may be considerably smaller for oppositely charged ion pairs than for similarly charged pairs. In the second model of Eigen and Wicke, which is adopted by Brodowsky and Strehlow in their treatment of the volume effect, it is assumed that like charged ion pairs have impenetrable hydration shells, whereas the hydration shells of unlike charged pairs are completely penetrable. This model of hydrated ions readily is introduced into the general equations derived in our paper and here again it is found that although the Eigen and Wicke local balance formula, as used by Brodowsky and Strehlow, provides the correct linear term in the ionic densities, it is incorrect in the quadratic term. Also Brodowsky and Strehlow ignore the image and self-atmosphere terms and the polarization energy, *i.e.*, they equate our γ to zero. Their calculations extend to larger values of both the electrolyte concentration (of a 1–1 valency type) and the surface potential than do those of Sparnaay and therefore yield larger departures from the solution of the Poisson–Boltzmann equation. They also find that the volume correction and the dielectric saturation affect this solution in the same direction, producing a larger potential difference across the particle–electrolyte interface for a given surface charge density. This increase is more marked the larger the surface charge density, amounting to 30% or more at charge densities above 16 microcoulombs per cm.^{2}. Their treatment of the dependence of the dielectric constant on ionic concentration is very approximate and they find this correction to be secondary.

There are a number of objections to the work of these authors. At large electrolyte concentrations (> 0.1 N of a 1–1 type) or large surface potentials (> 100 mv., say) the quadratic and higher order terms in the ionic densities in the volume correction become significant and these are not given correctly by the Eigen–Wicke theory. Also, the region of the diffuse layer where the corrections will be largest is precisely that nearest to the colloidal wall and we have shown that next to the wall the form of the volume correction will differ from that in the "interior" of the diffuse layer. Finally, their expression for the dependence of dielectric constant on electric field strength (derived by F. Booth (*J. Chem. Physics*, *19*, 391 (1951)) takes no account of electrostriction, which may be appreciable at large electric field strengths.

G. H. Bolt (*J. Colloid Sci.*, **10**, 206 (1955)) treats the case of a colloidal wall which is so highly charged that only the oppositely charged ions need be assumed to be present in the diffuse layer. He takes into account the polarization energy of the ions, the self-atmosphere effect, the dielectric saturation and the volume effect, using semi-empirical expressions for the latter two. He finds that the self-atmosphere and volume corrections tend to balance each other, although the former is the larger quantity up to ion concentrations of 1 N. The dielectric saturation and polarization energy corrections also offset each other for surface charge densities less than 20 microcoulombs per cm.^{2}. However, Bolt's expression for the polarization energy is incorrect and so he overestimates this term by a factor of almost 2. (The factor $2\epsilon_i + \epsilon_0$ in his Eq. (3), where ϵ_0 is the dielectric constant of the water and ϵ_i that of hydrated ion complex should be $2\epsilon_0 + \epsilon_i$). Bolt follows D. C. Grahame (*J. Chem. Phys.*, **18**, 903 (1950)) in his treatment of dielectric saturation but A. D. Buckingham (*ibid.*, **25**, 428, 1956) shows that Grahame's equations are incorrect, which may account for the difference in sign between the correction for dielectric saturation calculated by Bolt and that by Sparnaay and Brodowsky and Strehlow. Also, he omits the dependence of the dielectric constant on the ion concn. and at least for small wall potentials and electrolyte concns. Sparnaay shows that this effect is three times as large as that from polarization of the ions. Bolt's conclusion, therefore, is in much doubt.

The above three papers appear to be the only ones where an attempt is made to treat the various corrections to the Poisson–Boltzmann equation simultaneously. Others have considered one or two of the effects to the exclusion of the others but this is not justified, particularly at large potentials and electrolyte concentrations. The conditions under which the uncorrected Poisson–Boltzmann equation can be applied is indicated roughly by Sparnaay's results, namely, for moderate potentials (< 100 mv.) and small electrolyte concentrations (< 0.01 N for a 1–1 electrolyte). At higher potentials and concentrations, the work so far is inconclusive because of the omissions and incorrect treatments. Furthermore, our analysis strongly suggests that it will be necessary to divide the immediate vicinity of the colloidal wall into successive layers, each of which requires separate treatment. The Stern theory is in fact a first step in this direction. I would suggest that at large potentials and concns. the volume and dielectric constant effects are the main ones.

---

(28) R. Schlogl, *Z. physik. Chem.*, **202**, 379 (1954).

HEATS OF IMMERSION. IV. THE ALUMINA-WATER SYSTEM—VARIATIONS WITH PARTICLE SIZE AND OUTGASSING TEMPERATURE

By W. H. Wade and Norman Hackerman

Department of Chemistry, The University of Texas, Austin, Texas

Received March 7, 1960

Samples of α-, γ- and amorphous-alumina with surface areas from 0.222 to 221 m.^{2}/g. were studied following vacuum outgassing treatments over the temperature range, 100–450°. In addition, weight loss measurements were made as a function of temperature. Usually a substantial increase was noted for the heats of immersion with decreasing specific area and increasing outgassing temperature. These studies are consistent with the normal alumina surface being covered with a maximum of 19 OH's/100 Å.^{2}.

Introduction

It has been shown in previous communications from this Laboratory[1,2] that there is a large decrease in heat of immersion per cm.^{2}(ΔH_1) with increased specific area of silica samples on immersion in water. Moreover, most silica samples have ΔH_1 variations with outgassing temperature which are interpretable in terms of the normal existence on silica surfaces of both physically (reversibly) adsorbed water molecules and chemically bonded surface hydroxyl goups. Silica surfaces once stripped of their surface -OH groups rehydrate at a rate too low to be observed in most calorimeters.[1,2]

The belief is generally held by others that the coverage of simple oxides with surface hydroxyl groups is probably the rule rather than the exception.[3–5] With specific regard to alumina, the existence of surface hydroxyl groups can be inferred from infrared spectroscopic measurements,[6] dye adsorption studies,[7] high temperature heat of adsorption measurements[3] and from the present heat of immersion measurements.

The present investigation was designed to compare alumina to silica with respect to the variation of the immersional heats with particle size and water content (both physically adsorbed and chemically bonded) of the surface. Furthermore, the effect of crystalline modification (α- or γ-) of the alumina substrate on ΔH_i is raised but unfortunately can be answered only unsatisfactorily.

There is only a single published estimate[8] of the surface energy of alumina—a value of 560 ergs/cm.^{2} obtained from heat capacity measurements on γ-alumina.

Experimental

Samples.—The eight samples of Al_2O_3 studied are listed in Table I along with their purity, specific surface area and crystalline modification. The purities and crystalline modifications are those quoted by the manufacturers. The B.E.T. surface areas were measured by Kr adsorption in a volumetric adsorption apparatus previously described.[9] Above 100° surface areas of all samples were independent of outgassing temperature and, hence, water content of the surface. Samples F and H were furnished with the suppliers N_2 adsorption areas of 64 and 210 m.^{2}/g., respectively. This agreement with the Kr areas is good and for uniformity only the Kr areas were used. The samples had been prepared by high (1000–1300°) temperature calcination of trihydrates and alums with the exception of sample F, prepared by flame hydrolysis, and sample H, prepared by precipitation of the hydroxide followed by calcination at a temperature low enough to prevent collapse of the internal pore structure. Samples D and E had been made from B and C by micronization.

Table I

Sample	Manufacturer's designation	Purity, %	Area (m.^{2}/g.)	Cryst. mod.
A[a]	T-60	99.8	0.222	α-Al_2O_3
B[b]	Alucer MC	99.96	2.72	α-Al_2O_3
C[b]	Alucer HS	99.7	3.04	α-Al_2O_3
D[b]	Alucer MCB	99.96	3.12	α-Al_2O_3
E[b]	Alucer HSB	99.7	4.56	α-Al_2O_3
F[c]	Alon C	99.9	65.2	γ-Al_2O_3
G[b]	Alucer MA	99.96	109	γ-Al_2O_3
H[a]	F-20	99.0	221	Amorph.

[a] Supplied by Aluminum Company of America. [b] Supplied by Gulton Industries, Inc. [c] Special low-chloride Alon C supplied by Mr. Gregor Berstein of Godfrey L. Cabot, Inc.

The samples, before immersion, were outgassed at 10^{-5} mm. Hg for 72 hours in Pyrex bulbs and were sealed off on the outgassing apparatus. The outgassing temperatures listed in Table II are accurate to ±3°.

Table II

Heats of Immersion (Ergs/cm.^{2})

t	Sample m.^{2}/g.								
(°C.)	A 0.222	B 2.72	C 3.04	D 3.12	E 4.56	[a] 7–8	F 65.2	G 109	H 221
100	656	581	370	552	532		412	384	323
150	724	676		590	578	513	436		361
200	821	765	399	673	680			490	401
250	838	856				901	567	561	453
300	847	931	468	875	714	1011		628	514
350	861	1009					728	682	581
400	870	1076	508	1019	712			719	640
450							837	742	682

[a] Data of Good, *et al.*[12]

Calorimeter.—The calorimeter has been described previously.[1] It is of the twin adiabatic type with thermistor temperature sensing elements. All measurements were made at 25 ± 0.1°. Two types of Pyrex sample bulbs were used in these studies: (A), a thin-wall-spherical bulb which was shattered completely during immersion (measured heat of breakage is 0.1 ± 0.05 joule), and (B), a thick-wall-

---

(1) A. C. Makrides and N. Hackerman, This Journal, **63**, 594 (1959).

(2) W. H. Wade, R. L. Every and N. Hackerman, *ibid.*, **64**, 355 (1960).

(3) A. G. Oblad, S. W. Weller and G. A. Mills, *ibid.*, **59**, 809 (1955).

(4) J. H. de Boer, J. J. Steggerda, J. M. H. Fortuin and P. Zwietering, "Second International Congress of Surface Chemistry," Butterworth Scientific Publications, London, 1957.

(5) A. C. Zettlemoyer, *Chem. Revs.*, **59**, 937 (1959).

(6) A. Babushkin and A. V. Uvarov, *Doklady Akad. Nauk S.S.S.R.*, **110**, 587 (1956).

(7) J. H. de Boer, "The Dynamic Character of Adsorption," Chapters VII and VIII, Oxford University Press, New York, N. Y., 1953.

(8) R. Fricke, F. Niermann and C. Fiechtner, *Ber.*, **70B**, 2318 (1937).

(9) M. J. Joncich and N. Hackerman, This Journal, **57**, 674 (1953).

convoluted cylinder only the tip of which was broken[2] (measured heat of tip breakage is less than 0.02 joule). Type (B) bulbs were used for the two samples of lowest area and Type (A) for the remaining samples.

There were four electrical calibrations for each sample immersion. The average deviation for these runs was less than ±1%. All values given in Table II are the averages of a measurement from each calorimeter. Sample weights varied from 10 to 0.1 gram depending on the sample area. Total temperature changes during immersion varied from 1×10^{-3} to 1×10^{-4} degree. Differential baseline temperature variations were less than 2×10^{-6} degree over the 20 minute periods required for a measurement.

Weight Loss Measurements.—The samples, after equilibration with water vapor at 25 ± 1°, were heated in air. Weighings were taken at 50° temperature intervals with intervening 24 hour time intervals. Just prior to weighing, the samples were allowed to cool to room temperature in a desiccator. Weighing operations were performed on a semimicro analytical balance of 0.02 mg. readability.

Results and Discussion

The ΔH_i's measured in the present work are given in Table II and Fig. 1 along with one set of literature values. Two trends are noticeable: first, a general decrease of ΔH_i with increasing specific surface area and second, a generally large increase of ΔH_i with increase in outgassing temperature. The former feature will be discussed first.

Particle Size Effect.—If one considers ΔH_i values for the lower outgassing temperatures, the only exception to the first trend is the 3.04 m.^{2}/g. sample. In addition to this discordant fact, the ΔH_i for the 4.56 m.^{2}/g. material, prepared by micronization of the 3.04 m.^{2}/g. parent, is considerably enhanced. Experience with both the silica-water system and the 2.72-3.12 m.^{2}/g. parent-daughter pair of the present study would dictate a lower ΔH_i for the 4.56 m.^{2}/g. species than for the 3.04 m.^{2}/g. sample. All the following discussion will be presented with no further consideration of the 3.04 m.^{2}/g. sample C.

It is still startling to the authors how regular this particle-size variation is at the lower outgassing temperatures. However, this relationship does appear to be more complex at the higher outgassing temperatures where two types of behavior exist—one being represented by samples A and E and the other by the remaining samples. Apparently this difference in behavior at higher temperatures is substantially masked by several layers of water which remain physically adsorbed at the lowest outgassing temperatures studied.

The only alumina-water immersional data for samples of known surface area to be found in the literature[10-13] are in general agreement with the present work. Stowe's ΔH_i values of 310 and 300 ergs/cm.^{2} for gel samples of specific area 244 and 340 m.^{2}/g., respectively, are slightly lower than those found in the present investigation but due to the differences in sample pretreatment they may be entirely compatible. The work of Puri, *et al.*,[11] is somewhat anomalous since they observe large changes in surface area (determined from water adsorption isotherms) over an outgassing temperature range where pore collapse and sintering does not usually occur for alumina gels. They find a rather random variation of ΔH_i with outgassing temperature with an average value of 278 ergs/cm.^{2}. The data of Good, *et al.*, (see Table II) fit the scheme of ΔH_i *vs.* particle size but it was impossible to reproduce their findings of a long time lag for attainment of thermal equilibrium. On the contrary, all the alumina samples studied were at 95+% thermal equilibrium five minutes after sample breakage. Runs were extended over 30 minute periods in several cases to check this behavior. Since the wetting of as little as 0.5 m.^{2} of surface is measurable to ±2% reproducibility, the phenomena observed by Good, *et al.*, should have been detected easily.

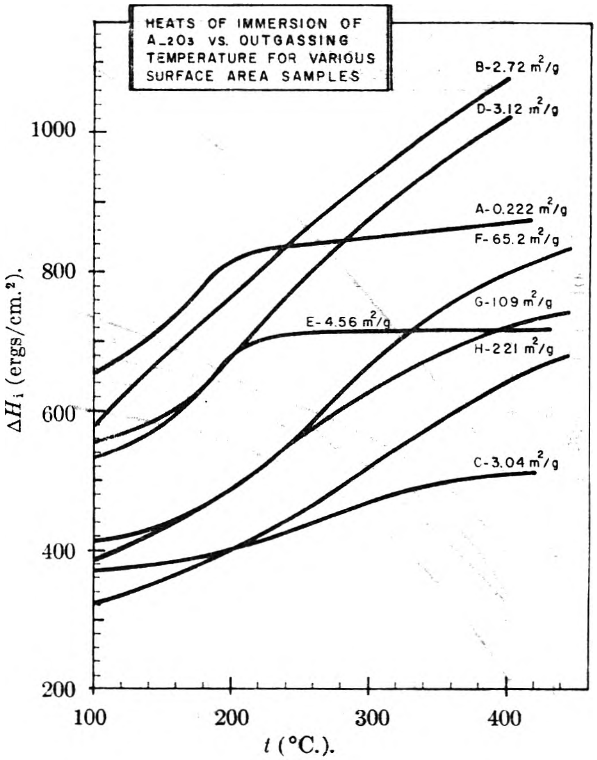

Fig. 1.

In previous studies on the silica-water system,[1,2] the hypothesis was advanced that grinding imparted an amorphous substrate character to the substrate surface layers. That an amorphous substrate should show reduced immersional heats compared to a crystalline surface has been explained qualitatively.[2] This argument cannot be extended bodily to cover the present set of data. Samples A, B, F and G, although of widely varying specific area, all exist as individual single crystals formed during the calcination process. Unless some fundamental but as yet obscure reason exists for the occurrence of an increased amorphous character of the surface with decreased particle size, then some other explanation of the large divergence in ΔH_i for these samples must be found. In fairness to the previous arguments,[2] it should be noted that sample D, prepared by grinding B has a depressed ΔH_i and that the amorphous gel, G, has the lowest ΔH_i measured other than C.

---

(10) V. M. Stowe, *ibid.*, **56**, 484 (1952).

(11) B. R. Puri, S. Mittal and L. R. Sharma, *Res. Bul. Panjab Univ.*, **111**, 309 (1957).

(12) C. A. Guderjahn, D. A. Paynter, P. E. Berghausen and R. J. Good, THIS JOURNAL, **63**, 2066 (1959).

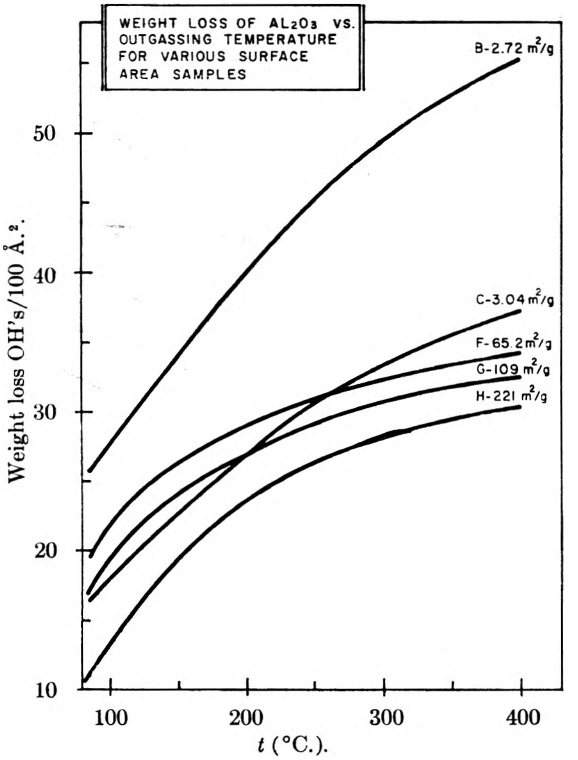

Fig. 2.

An interesting grouping of the data occurs according to α- or γ-crystalline modification. Whether this grouping is accidental or whether the heats of immersion are to this extent sensitive to crystalline form must be left for a more detailed study where both the α- and γ-forms are investigated over a wider range of particle sizes. In view of both the uncertain characterization of the γ-aluminas[13] and their small but still measurable water content at the calcination temperatures used, it is perhaps best to say that the lower heats of immersion of the γ-aluminas simply are the results of immersion of samples of greater surface water content than the corresponding α-aluminas. Better crystallographic classification of the γ-aluminas will be necessary in order to clarify this point.

Outgassing Temperature Effect.—There are two types of outgassing pretreatment behavior of the samples. Samples A and E show an initial increase followed by complete independence of ΔH_i at outgassing temperature above 200° whereas the remaining samples show a continuous increase in immersional heat with outgassing temperature over the entire range (the upper limit of 450° is dictated by collapse of the Pyrex sample bulbs).

Heat of immersion measurements for the silica–water[1,2] and calcite–water[14] systems showed the complete removal of physically adsorbed water between 200–250° and, indeed, this would be expected if adsorption energies are less than a liberal 15–20 kcal./mole. The ΔH_i *vs.* outgassing temperature for samples A and E are indicative of this single mode of existence of water on the surface. The continuous increase of ΔH_i of the remaining samples leads one to postulate the existence of chemically bonded surface hydroxyl groups.

Crystallographic data[15] show that the lattice of α-alumina consists of hexagonal close-packed layers of oxygen ions separated by aluminum ion layers where the Al^{+++} occupy positions in the middle of the $O^=$ triangles. Using the closest O–O spacing of 2.49 Å., one calculates 19 $O^=$/100 A.² in the oxide ion sheet. Since a surface with this oxide sheet exposed represents the most dense possible packing of oxide ions and if one assumes that each of these oxide ions in the surface is normally converted to a surface hydroxyl group, then there is a maximum of 19 OH's/100 Å.² on the α-alumina surface. This can be compared to 8 OH's/100 Å.² on quartz.[16]

For a direct check on the existence of water bonded above 200° (rather arbitrarily chosen as the maximum temperature that H_2O would maintain in chemical identity due to the large bonding forces necessary for its surface localization), weight loss measurements were run on samples B, C, F, G and H. The results of these are shown in Fig. 2. With the exception, once again, of sample C, there is a direct correlation between total weight loss at a given outgassing temperature with the ΔH_i. Over the temperature range of 200–400° the water loss for samples B, F, G and H corresponds to 14, 5, 5 and 6 surface OH's/100 Å.², respectively. All these values are sufficiently less than the theoretical maximum to indicate that it would not be exceeded at still higher temperatures. The correlation between the weight loss and ΔH_i studies is similar to that found in the silica–water system[2] in that it clearly seems that low surface area samples have the higher concentration of surface hydroxyl groups. Infrared studies will be needed for a more direct check on the existence of surface hydroxyl groups on these samples.

As distinct from the silica–water behavior,[1,2] the ΔH_i *vs.* t(°C.) does not pass through a maximum. This indicates a rapid rehydration to the aluminol structure. Recently measured water adsorption isotherms[17] on several of these alumina samples outgassed at temperatures above 200° all show hysteresis at coverages below a monolayer indicating lack of reversibility in the desorption of surface hydroxyl groups at 25°.

At the present time, it is impossible to explain the discrepancies between samples A and E and the remaining samples with regard to the nonexistence of surface hydroxyl groups on just the two samples.

In conclusion, it should be noted that attention has been focused only on relative variations in ΔH_i with a consideration of their absolute magnitude being outside the present scope of attack. It has become increasingly obvious that in this

---

[13] A. S. Russell, Aluminum Res. Lab., Tech. Paper No. 10, Aluminum Co. of America, Pitts., Pennsylvania, 1953.

[14] W. H. Wade and N. Hackerman, This Journal, 63, 1639 (1959).

[15] R. W. G. Wyckoff, "Crystal Structures," Interscience Pub., Inc., New York, N. Y., 1948.

[16] R. K. Iler, "The Colloid Chemistry of Silica and Silicates," Cornell University Press, Ithaca, N. Y., 1955.

[17] R. L. Every, W. H. Wade and N. Hackerman, unpublished data (1960).

regard very little can be inferred from the bulk structural and thermodynamic properties of solids. In other words, the statement that "a solid is in its standard state" has little or no significance with respect to its surface properties. To be specific, "*the* immersional heat of a substance" at the present time is a meaningless assemblage of words unless one can describe *completely* all the parameters of the surface, adsorbent, and adsorbate phases.

Acknowledgments.—This work is a contribution from the American Petroleum Institute, Project 47d and the authors thank them for their continued support and interest. Appreciation is expressed to Mr. R. L. Every and Dr. L. Slutsky and Mr. C. L. Williams, Jr., for their assistance in various phases of the study.

DISCUSSION

L. A. Romo (E. I. du Pont de Nemours & Co.).—Since surface crystallinity appears to be an important factor, I would suggest that electron diffraction be used to determine variations. Do the surface areas stay constant as a function of degassing temperature? What is the evidence you have for the presence of free vibrating hydroxyl groups on anhydrous Al_2O_3 surfaces?

W. H. Wade.—For all samples, the BET areas were found to be independent of outgassing temperature. There are several infrared studies which show discrete surface OH bands.

A. C. Zettlemoyer (Lehigh University).—The question of double layer formation seems not to have been considered. The small amounts of impurities present may possibly produce quite different alumina–water interfaces from sample to sample. In this laboratory such heat effects have been detected easily for the model system of graphite immersed into surfactant solutions; even trace calcium (a few parts per million) gives differences in heats of immersion. Do you believe such effects might be contributing?

W. H. Wade.—I would say that the regularity of the data is very surprising if your hypothesis is correct.

George R. Lester (Universal Oil Products).—You have stated that the calcinations were done by the manufacturer. The outgassing experiments might be very susceptible to time and storage between calcination and outgassing. Secondly, my own calculations, based on a spinel structure for α-alumina, indicate that the average number of O^- ions in the 100, 110, 111 planes is about 11 ions per 100 Å.^{2}. This may explain the lower OH loss for the two samples of α-Al_2O_3. If the "amorphous" sample is really a mixture of true α-Al_2O_3 and amorphous Al_2O_3, as often has been suggested, this explanation may apply also.

D. J. C. Yates (Columbia University).—I wish to congratulate Dr. Wade on his statement that "little can be inferred from the bulk structural and thermodynamic properties of solids." While as to your general statement that the low area materials are more crystalline than high area materials, I agree, but I think that there may be exceptions. For instance, the spectra of the OH groups on Alon C are quite different from those on the higher area alumina gel (Peri, ACS meeting, Sept., 1959). The peaks on Alon C are smeared together, while the better-crystallized alumina gel showed three distinct peaks. This is what one would expect from the flame process used in manufacturing Alon C.

W. H. Wade.—At the present time, I have found no correlation between extent of surface OH coverage and crystallinity.

THE SORPTION OF GASEOUS HYDROGEN CHLORIDE BY DRY LYOPHILIZED β-LACTOGLOBULIN[1]

By Wasyl S. Hnojewyj and Lloyd H. Reyerson

School of Chemistry, University of Minnesota, Minneapolis, Minn.

Received March 7, 1960

The sorption of gaseous HCl by dry lyophilized β-lactoglobulin was studied at 27°. HCl is held so firmly on some of the sorption sites that it cannot be removed by pumping to a high vacuum. The results show that the amount remaining sorbed on the protein is some reciprocal function of the temperature.

Earlier work in this Laboratory[2] showed that gaseous HCl was very strongly sorbed by insulin at −78.9 and 20°. The protein used in that study was the zinc crystalline insulin. In that work it was not possible to determine the total effect of the zinc in the sorption process. However, the amounts of HCl bound more or less permanently depended on the temperature of the sample during the desorption process. As the temperature was lowered, the protein bound more and more HCl. About five times as much was bound at −78.9° as was held at room temperature. It was felt desirable to repeat the sorption studies of HCl by a protein having no metal ions in the structure. Qualitative studies on the sorption of HCl by lyophilized β-lactoglobulin, carried out in the Carlsberg Laboratorium by one of the authors (L.H.R.) indicated that the amounts sorbed were relatively large. This preliminary study also indicated that the protein was quite stable in that the protein containing adsorbed HCl was not appreciably hydrolyzed when put into water. This is in contrast to the marked hydrolysis of the peptide-like bond in nylon when it contained adsorbed HCl. Since a great deal is known about lyophilized β-lactoglobulin, it was decided to determine quantitatively the sorption of HCl by this protein. A complete adsorption isotherm was obtained at 27°. Following desorption the amounts of HCl retained at 10^{-6} mm. pressure were determined at 27, 40 and 60°.

Experimental

The β-lactoglobulin used in this study was a fresh sample of the same protein, obtained from the Carlsberg Labora-

---

(1) Supported by a grant from U.S.P. Health.

(2) L. H. Reyerson and Lowell Peterson, This Journal, **59**, 1117 (1955).

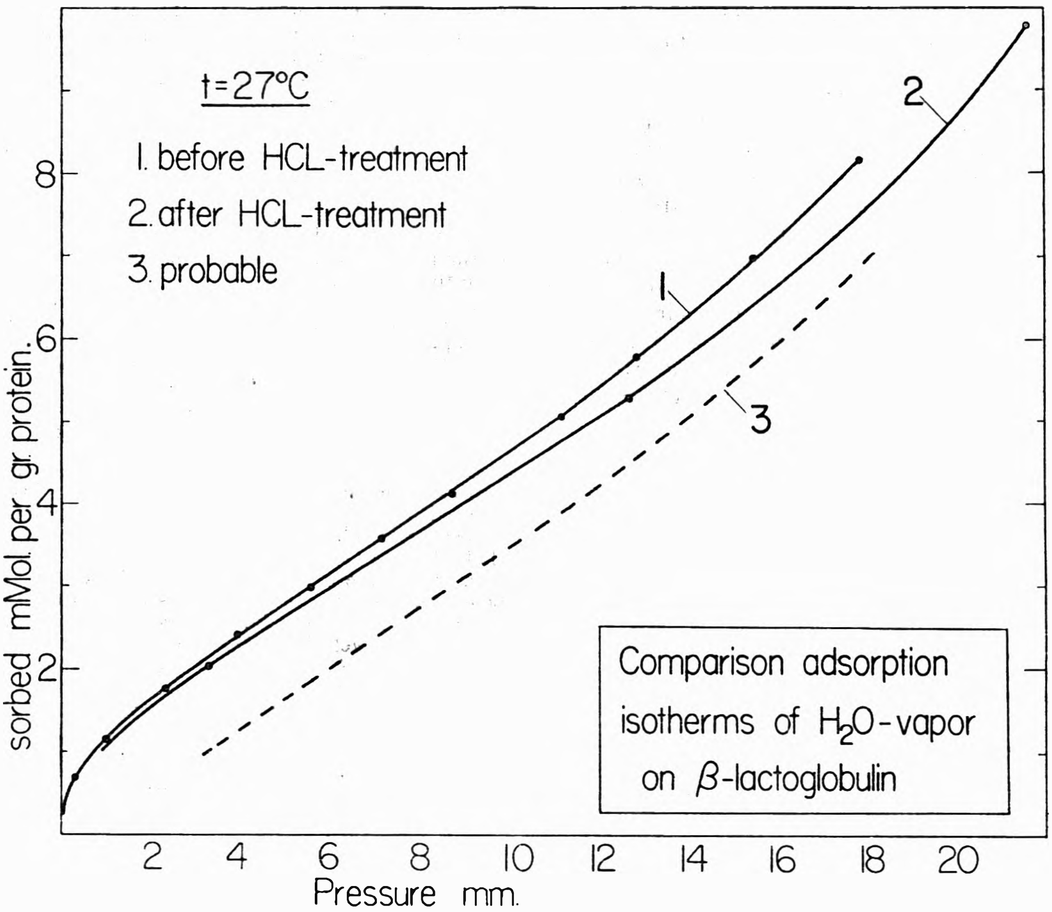

Fig. 1.

torium, on which sorptions of H_2O and D_2O were obtained.[3] 125.8 mg. of this protein was weighed into a glass bucket which was suspended from a McBain quartz spiral balance which had a sensitivity of 2.285 mg./mm. Extension of the spiral was measured with a traveling microscope having a sensitivity of ±0.002 mm. The sample and the quartz spiral were thermostated as previously described.[3] Equilibrium pressures in the system were measured by a mercury manometer using a cathetometer reading to ±0.02 mm. Prior to admitting gaseous HCl to the system, a complete adsorption-desorption isotherm of H_2O vapor was determined for this sample at 27°. The protein weighed exactly the same at the completion of the desorption of H_2O as it did before H_2O vapor was admitted to the sample. The adsorption part of this isotherm is shown as the upper curve in Fig. 1. The results were identical with those reported in the previous study.[3]

Following this, dry gaseous HCl was admitted to the highly evacuated system containing the protein and a complete sorption isotherm was determined in the same manner as previously described.[2] Liquid HCl of 99.87% purity was redistilled several times and the liquid from the last distillation was vaporized to provide the gas used in the sorption. Amounts of HCl adsorbed were determined up to 5.484 mmoles per gram of protein at an equilibrium pressure of 325.3 mm. The adsorption isotherm is given in Fig. 2. The first equilibrium point (1.9 mmoles/g.) was reached in about 3 hours, the equilibrium HCl pressure being 4.515 mm. Following this first rather rapid adsorption, each successive point required from two to three days for equilibrium to be reached. This is from six to ten times longer than was required for the sorption of H_2O. This very slow process of adsorption indicates that a sizable energy of activation is involved.

The HCl was then desorbed as rapidly as possible and the system pumped down to a pressure of 10^{-6} mm. When equilibrium was finally reached, 1.540 mmoles/g. of HCl remained sorbed on the protein. The protein was then heated to 40° again and evacuated to 10^{-6} mm. Some HCl was removed during this process. The protein was then heated to 60° and the evacuation repeated. At this temperature the protein still retained 1.176 mmoles/g. HCl. These three desorptions took about 10 days to complete and the results are given in Table I. With the residue of adsorbed HCl still on the surface of the protein, a second adsorption of water vapor was carried out at 27°. Curve 2 in Fig. 1 gives the isotherm for this second sorption of H_2O, based on the original weight of the protein.

TABLE I

RESIDUAL AMOUNTS OF HCl HELD BY THE PROTEIN AS SOME RECIPROCAL FUNCTION OF THE TEMPERATURE AT A PRESSURE OF 10^{-6} mm.

Temp., °C.	Time of desorption, hr.	Mmoles of HCl bound per g. of protein
27	156	1.5404
40	50	1.4630
60	118	1.1763

Results and Discussion

It is evident from these results that this protein has nowhere near the number of sites available for binding HCl as it has for H_2O and D_2O. Except for the first isotherm point which was reached in a few hours, all other points required days to reach equilibrium, indicating a high energy of activation and some probable form of chemisorption. The isotherm appears to be flattening out as it passed a vapor pressure of more than 300 mm. At the

---

(3) L. H. Reyerson and W. S. Hnojewyj, THIS JOURNAL, 64, 811 (1960).

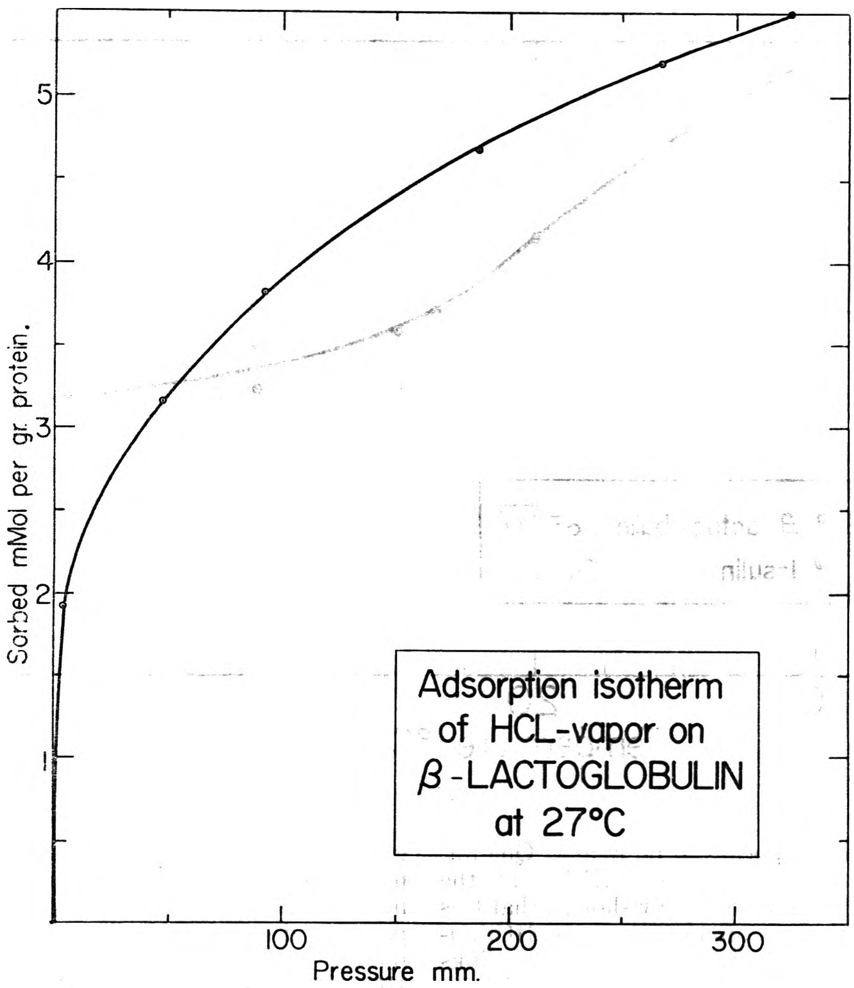

Fig. 2.

highest point reached, 204 molecules of HCl were bound per molecule of protein. This is about half as many as the number of D_2O molecules which had to be adsorbed for the maximum exchange of deuterium observed in our previous study.[3] While all of the H_2O and D_2O molecules are released by the protein during complete desorption at 10^{-6} mm.p., only slightly more than two thirds of the adsorbed HCl molecules can be removed by a high vacuum at 27°. Heating the protein to 40 and then to 60° resulted in slight additional desorptions as shown in Table I. It is interesting to observe that the number of HCl molecules remaining adsorbed at 27° just equals the number of active amino groups in the side chains of this protein. Prolonged heating and evacuation at 40 and 60° only removes one fourth of these molecules, indicating a strong chemical bonding. However, the presence of these strongly bonded HCl molecules has only a minor effect on the adsorption of H_2O as is shown as curve 2 in Fig. 1. If each HCl bonded to an active side-chain amino group prevented an H_2O molecule from being adsorbed, then it was estimated that the isotherm for H_2O on the protein permanently holding HCl molecules ought to be similar to the dotted line 3 in Fig. 1. Isotherm 2 in Fig. 1 lies slightly below isotherm 1, indicating that the residual HCl molecules *do have* some slight effect on the relaxation of the structure of the protein insofar as the adsorption of H_2O is concerned.

Since the numbers and kinds of amino-acid residues are well known for β-lactoglobulin[4] and completely established by Sanger[5] for insulin, it was decided to determine the ratio of the number of HCl molecules bound at zero pressure to the number of active amino groups in the side chains of these two proteins (57 for β-lactoglobulin and 14 for insulin) at the several temperatures studied. The results are shown in Fig. 3. In the case of insulin, where the data at lower temperatures were available,[2] the ratio is greater than 1.5 at 0° but at 27° the ratio for both proteins is nearly unity and it falls slightly thereafter, reaching about 0.75 at 60°, the highest temperature studied. These results seem to be a reasonable proof that the adsorbed HCl molecules are most tightly bound by the amino groups on the side chains of the proteins. This binding may well be of a chemical nature. It seems likely from these results that the adsorption of the HCl on the side chains prevents the opening up of the protein molecule and it does not seem probable that the backbone peptide links get a chance to adsorb many HCl molecules, and if ad-

(4) K. Linderstrøm-Lang, Souvenir, *J. Soc. Biol. Chemists, India*, 191 (1955).

(5) F. Sanger, *Bull. soc. chim. biol.*, **37**, 23 (1955).

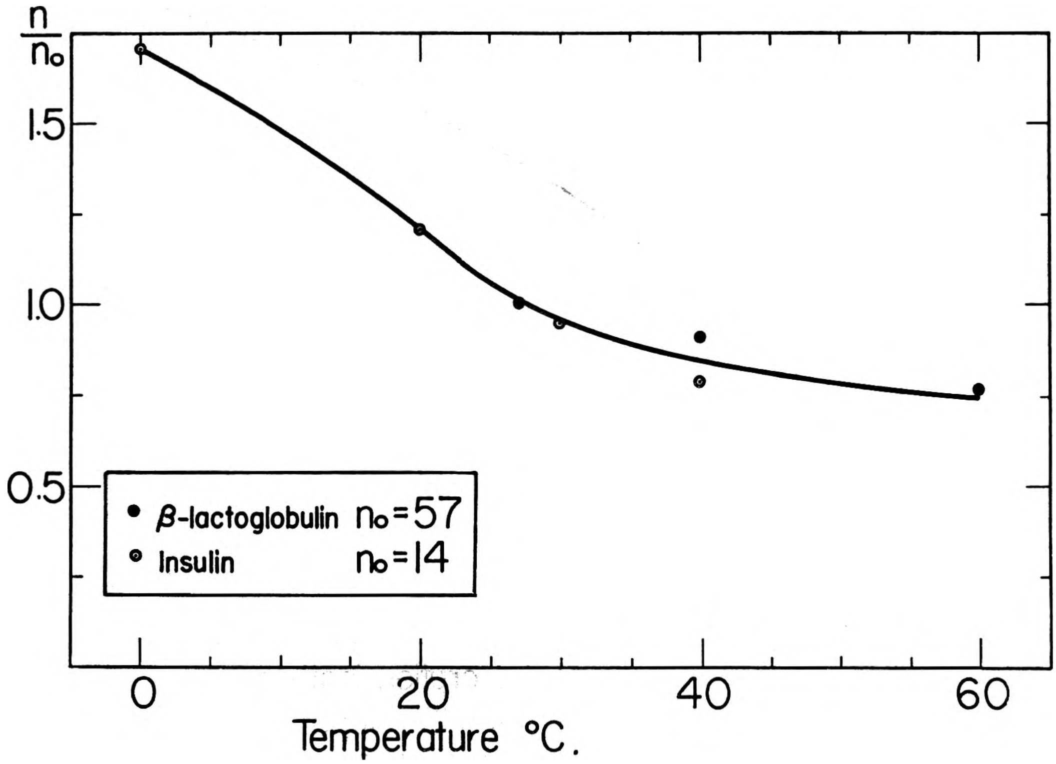

Fig. 3.

sorbed the bonding appears to be weak. Qualitative experiments by one of us (L.H.R.) at the Carlsberg Laboratorium definitely showed that this same protein with a maximum amount of HCl adsorbed was not hydrolyzed at the peptide links when placed in water. The CO-NH bond in nylon does hydrolyze under similar conditions, as is shown in our earlier work in this Laboratory.[6]

Thus there seems to be no question but that the same dry lyophilized protein behaves very differently toward H_2O and D_2O than it does toward dry gaseous HCl, and this seems only reasonable. The number of molecules of D_2O needed for the maximum exchange[3] shows that H_2O and D_2O must, in part, be adsorbed on the peptide bonds in the backbone of the protein. The maximum number of HCl molecules found adsorbed in this study slightly exceeds the number of side chains of the amino-acid residues which have active groups on which adsorption could occur. Certainly the very strong bonding of the HCl, which remains on the protein at essentially zero pressure, can be accounted for by its being bonded to the amino groups on the side chains of the protein.

---

[6] L. H. Reyerson and L. Peterson, THIS JOURNAL, **60**, 1172 (1956).

PHASE SEPARATION IN POLYELECTROLYTE SYSTEMS. I. COMPLEX COACERVATES OF GELATIN

BY ARTHUR VEIS AND CATHERINE ARANYI

Armour and Company, Research Division, Central Research Laboratories, Chicago, Illinois

Received March 7, 1960

The complex coacervation of mixtures of gelatins of different isoionic *p*H ($pI = 5.0, 9.0$) was studied in a test of the applicability of the Voorn–Overbeek thermodynamic analysis of the coacervation process. The compositions of the coexisting phases at equilibrium and the total amounts of gelatin in each phase were determined as functions of the equilibration temperature and initial mixing concentration, C_T. Concentrations ranged from 0 to 1% gelatin and temperatures from 10 to 50°. A parameter, θ, was defined to describe the intensity of the coacervation. In general it was found that θ increased as the temperature was decreased. In isotherms above the gelation temperature ($t \geqslant 40°$) θ decreased as the total gelatin concentration increased. At $t < 40°$ plots of θ *vs.* C_T showed a minimum which shifted to lower values of C_T as t was decreased until, at 10°, the minimum disappeared and θ increased with increasing C_T. These data could not be fitted in with requirements and assumptions of the Voorn–Overbeek theory. A change in the model of the reacting system has been suggested in which electrostatic aggregates are formed in the initial mixture even at $t \geqslant 40°$. The coacervation equilibrium is supposed to exist between dilute solutions of large, nearly neutral polyion aggregates and the concentrated phase of intertwined but not specifically aggregated random coils. Coacervation in the region where gelation is significant ($t < 40°$) is more complicated and must be treated separately.

A binary liquid mixture will form a stable, homogeneous solution if the condition

$$\left(\frac{\partial^2 F_2}{\partial N_2}\right)_{N_1,T,P} > 0 \qquad (1)$$

is satisfied for all values of the mole fraction N_2 of component 2. When this inequality fails, then spontaneous demixing or phase separation occurs. Overbeek and Voorn[1] and Voorn[2,3] have taken this fundamental thermodynamic approach to the problems involved in "complex coacervation," the spontaneous liquid–liquid phase separation that frequently occurs when solutions of oppositely charged polymeric polyelectrolytes are mixed in the same solvent. They reasoned that the critical conditions for phase separation could be determined from analytical expressions for the free energy of mixing of the polyelectrolytes and solvent. When the polyion concentration was greater than the critical demixing concentration, the equilibrium concentrations also could be determined by equating the chemical potentials, derived from F, in both liquid phases.

The crux of the problem became that of formulating F in simple enough terms so that the subsequent calculations could be carried out and still retain the significant experimental parameters. Overbeek and Voorn set

$$F_{\text{total (T)}} = F_{\text{mixing (M)}} + F_{\text{electrostatic (e)}} \qquad (2)$$

and then substituted the Flory–Huggins approximation for F_M. F_e was calculated by treating the polyions as the sum of single charges and approximating the total electrical interaction free energy by the Debye–Hückel theory. Their final result was

$$\frac{F_T}{N_r kT} = \sum_i \frac{\phi_i}{r_i} \ln \phi_i - \alpha \left(\sum_i \sigma_i \phi_i\right)^{3/2} \qquad (3)$$

in which

N_r = total no. of lattice sites in the system
r_i = no. of sites occupied by particle i
σ_i = charge density of particle i
α = electrical interaction constant, $\dfrac{e^2}{3D}\left[\dfrac{4\pi e^2}{DkTv}\right]^{1/2}\left(\dfrac{1}{kT}\right)$
v = site volume
ϕ_i = volume fraction (or site fraction) of particles of type i

The critical conditions for coacervation were derived from equation 3 for the symmetrical two-component case in which each polyion was of the same size ($r_2 = r_3 = r$, subscripts 2 and 3 refer to the polyions, 1 to the solvent) and charge density ($\sigma_2 = \sigma_3 = \sigma$) and both were present in equal initial concentration ($\phi_2 = \phi_3 = \phi$). For the solvent $r_1 = 1$, $\sigma_1 = 0$. The result, equation 4

$$\sigma^3 r = \frac{64}{9\alpha^2}\left[\frac{1}{(1-\phi)^2(1+\phi)}\right] \qquad (4)$$

showed that coacervation would take place at ordinary temperatures in water only when $\sigma^3 r \gtrsim 0.4$ since $\phi << 1$. Similarly, Voorn[2] used equation 3 as the basis for evaluating ϕ^{I} and ϕ^{II}, the polyion volume fractions in equilibrium liquid and coacervate phases, for the symmetrical case. He was unable to obtain solvable equations relating σ and r to ϕ^{I} and ϕ^{II} but by approximations found, equation 5, that at large r ($r > 10^3$) ϕ^{II} was nearly in-

$$\phi^{II}_{(r \to \infty)} \approx \alpha^2 \sigma^3 \qquad (5)$$

dependent of r and depended only on the charge density and, through α, on the temperature and solvent. From equation 5, however, one can see that small changes in σ are reflected by large variations in ϕ^{II}. The polymer size, at large r, is important in regulating ϕ^{I} and ϕ^{II} only when σ is close to its critical value.

Complex coacervation is of special interest because it may be involved in many natural biological phenomena that appear to be influenced by interactions of oppositely charged macromolecules. It seemed appropriate to us to explore the applicability of the thermodynamic analysis described above to biological macromolecules and to proteins in particular.

The model and approximations used in the Voorn–Overbeek treatment place definite limitations on the choice of experimental systems. The major assumptions are: (1) that the heat of mixing

---

(1) J. Th. G. Overbeek and M. J. Voorn, *J. Cellular Comparative Physiol.*, **49**, Suppl. 1, 7 (1957).

(2) M. J. Voorn, *Rec. trav. chim.*, **75**, 317, 405, 427, 925, 1021 (1956).

(3) M. J. Voorn, *Fortschr. Hochpolym.*, Forsch Bd. 1, S192 (1959).

of polyion and solvent be zero; (2) that the charge densities are sufficiently low so that F_e can be given by a Debye–Hückel work term; and (3) that F_M can be expressed in terms of the Flory–Huggins lattice solution theory. These assumptions require: (1) that the polyions have the unperturbed random coil configuration; (2) that the charges be distributed throughout the solution without regard to the fact that they reside on the polymer chains; (3) that there are no specific intermolecular associations between polyions; and (4) that, at the least, the solvent–solute interactions be the same for each partner in the coacervation process.

Gelatin is one of the few proteins that have the random coil configuration, and it is well known that gelatins of different isoionic points can be prepared by proper choice of preconditioning of the gelatin stock. Furthermore, experiments on gelatin mixtures, made for other reasons,[4] had resulted in the formation of two phase coacervate systems. When isoionic solutions of gelatins of different pI are mixed, they titrate each other to equal charge. From titration curves,[5] the net charge on each gelatin (pI = 5 and 9) is ~15 ionized groups per 10^5 grams in the absence of added salt at pH 6.5. Thus the net charge density is relatively low. In view of the similarity in structure and chemical constitution one might also expect that non-electrostatic interactions between gelatin molecules and between gelatin and water would be nearly independent of the gelatin source. Finally, according to the theory given above, once the critical molecular size is exceeded, the actual magnitude of the molecular size does not greatly influence ϕ^{II}. Thus, one would not expect the molecular-weight heterogeneity of the gelatins to be a severe handicap. For all these reasons, we chose to investigate the gelatin–gelatin complex coacervation system in detail.

Experimental Procedure

The basic data required to establish the coacervation phase relationships are simply the compositions of the coexisting phases at equilibrium, the total amounts in each phase, and the equilibrium temperature. Such data were obtained from essentially straightforward measurements but we found that many extreme precautions were required to achieve reproducible behavior. Therefore, these direct experiments must be described in some detail.

I. The Gelatins. Characterization and Analysis.—All measurments were made with two commercial gelatins: gelatin A, an acid-precursor pig-skin gelatin from the Grayslake Gelatin Company, and an alkali-precursor calf-skin gelatin, B, from the Peter Cooper Corp. These gelatins were selected because their light-scattering weight-average molecular weights appeared to be identical.[6] Their sedimentation coefficients were also identical although their intrinsic viscosities were not.[6] The characterization data are given in Table I.

The sedimentation velocity measurements, though yielding the same average apparent S^0 values, showed some differences in boundary spreading indicating that the molecular weight and/or shape distributions were not identical, in accord with the viscosity data.

The pI's were determined by the ion-exchange method of Janus, Kenchington and Ward.[7] Larger batches of each gelatin were deionized by this same technique. Complete desalting was essential. All coacervation experiments were carried out with deionized gelatins.

TABLE I

CHARACTERIZATION OF A AND B GELATINS

Gelatin	Type	$M_w \times 10^{-5}$	S_{40} in 0.1 M KCl	$[\eta]_{40}$ in 0.2 M KCl	pI
A	Acid-precursor	3.3 ± 0.3	5.0	0.42	8.95
B	Alkali-precursor	3.3 ± 0.3	5.0	0.58	5.00

Since the deionized gelatin solutions were free of any other components, refractive index measurements were convenient for concentration determinations. The biuret method[8] was also used. Calibration curves of refractive index *vs.* concentration, and biuret complex optical density *vs.* concentration were identical for both A and B and mixtures of A and B. In practice, refractive index measurements were used to establish most carefully the concentrations of the stock gelatin solutions. The more rapid but less precise biuret method was used to analyze the coacervation mixtures. The basic calibrations were established with gelatin whose moisture was determined by drying at 110° to constant weight.

II. The Coacervation Equilibrium System.—This study has been restricted to the simplest case, that of "symmetrical" mixtures of equal amounts of each gelatin. The total amount of gelatin was varied, however. Each system was set up essentially as follows.

Stock solutions of each deionized gelatin were made up in doubly distilled water. The concentrations of these solutions were determined interferometrically at 40°. Individual solutions of appropriate amount and concentration were then prepared, at 40°, and equal amounts of solutions of A and B at identical concentrations were mixed in an appropriate sized centrifuge tube. The mixing also took place at 40°. The mixtures were then transferred to a bath at the appropriate temperature and were equilibrated at that temperature for 30 ± 1 minutes. The centrifuge tubes were transferred to a Servall centrifuge and spun for 5 minutes at 26,000 × g. As soon as the centrifuge stopped. the tubes were transferred back to the temperature equilibration bath and allowed to stand for about 15 minutes. By this time, the coacervate had formed a liquid layer at the bottom of the tube and a very sharp boundary separated the phases. An aliquot was pipetted from the dilute equilibrium liquid for concentration analysis. The centrifuge tubes were next placed in a Beckman tube slicer and were cut just above the phase boundary. The remainder of the equilibrium liquid was discarded, and the coacervate layer was allowed to gel. The small amount of equilibrium liquid could then be washed off with cold distilled water. At this point, either the coacervate concentration was determined or the total amount of gelatin in the coacervate was measured. Duplicate experiments were analyzed in these alternate ways so that the coacervate volumes could be calculated. When the coacervate volumes were large, they were measured directly in a special device built for this purpose.

The material balance for each coacervation system is given by equation 6 in which

$$V_T C_T = V_C C_C + V_L C_L \qquad (6)$$

V and C refer to volume and concentration, respectively, and the subscripts T, C and L refer, respectively, to the total system, the coacervate phase, and the equilibrium liquid phase. Of these, C_L and $C_C V_C$ can be determined most accurately. However, C_C could also be determined satisfactorily in large scale experiments. An analysis was accepted only when all values checked the over-all material balance.

The complications in this simple procedure are the result of the aggregation and gelation of gelatin at temperatures lower than 40°. We found that, to achieve reproducible results, the time and temperature schedules had to be adhered to strictly. It was particularly important that the thermal history of each gelatin solution was identical and that the A and B solutions be mixed at 40° and then cooled

---

(4) A. Veis, J. Anesey and J. Cohen, "Recent Advances in Gelatine and Glue Research," Pergamon Press, 1957, p. 155.

(5) A. W. Kenchington and A. G. Ward, *Biochem. J.*, **58**, 202 (1954).

(6) A. Veis and J. Cohen, *J. Polymer Sci.*, **26**, 113 (1957).

(7) J. W. Janus, A. W. Kenchington and A. G. Ward, *Research*, **4**, 247 (1951).

(8) A. G. Gornall, C. J. Bardawill and M. M. David, *J. Biol. Chem.*, **177**, 751 (1949).

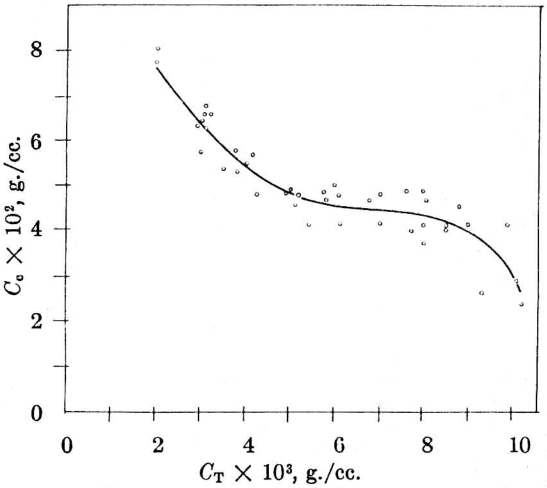

Fig. 1.—The concentration of the coacervate phase at 40° as a function of the initial concentration of gelatin. The smooth curve was calculated from the equation:

$$C_C = 0.1055 - 13.74C_T - 1.229 \times 10^3C_T^2 + 4.992 \times 10^5C_T^3 - 3.137 \times 10^7C_T^4$$

which was computed using all of the experimental points and the least squares method I.B.M. 650 routines No. 6.006 and 6.010. The standard deviation σ was 5.67 × 10^{-3}.

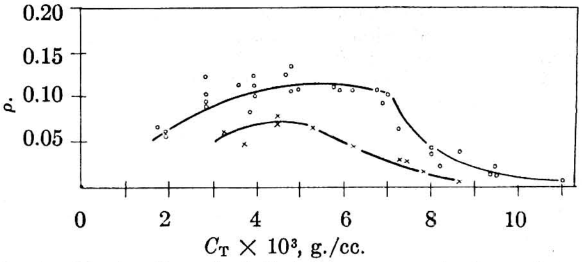

Fig. 2.—The fraction of gelatin in the coacervate phase above the gelation temperature: ○, 40°; ×, 50°.

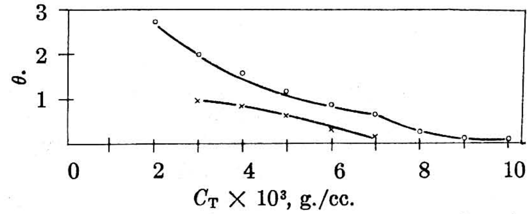

Fig. 3.—The intensity of coacervation as a function of the initial concentration at temperatures above the gelation temperature. The points were calculated from the smooth curve values of C_C, C_L and ρ: ○, 40°; ×, 50°.

to the equilibrium temperature. As an example, for experiments at 10°, each 1.0% gelatin solution would have been gelled, yet when the gelatins were mixed at 40° and then equilibrated at 10°, the system separated into two layers. Each layer was viscous at 10°, but was liquid in character. On the other hand, a mixture of A and B with salt present to prevent coacervation, also would have set to a solid gel.

Although the systems studied are thermodynamically reversible, the dense viscous coacervate droplets form more readily than they disperse without agitation. Thus, it was extremely important to maintain the systems at their chosen equilibrium temperature up to the time of centrifugation. After centrifugation, if the coacervated system were allowed to cool below the equilibration temperature, the supernatant equilibrium liquid became turbid and fresh coacervate began to settle out. As long as a dense coherent second coacervate layer did not form, the low temperature coacervate could be redispersed by heating it to the original equilibrium temperature. If a coherent second layer (usually of high turbidity) did form, it adhered firmly to the first layer and washing the gelled coacervate only served to tear off the surface of the original coacervate. Thus, for measurements above room temperature, it was important to work swiftly after centrifugation and to maintain each system at its equilibrium temperature. The tube-slicing separation of the equilibrium liquid from the coacervate layer reduced this source of error and provided sharply bounded coacervate layers.

Results

I. Coacervation in the Non-gelling Region.—At 40°, intermolecular interactions that lead to gelation[9] do not occur and the thermal history of a gelatin solution is effectively erased. It was, therefore, most important to study the coacervation process at this temperature. A sharply bounded two phase system formed at all concentrations from $C_T = 2 \times 10^{-3}$ to 1×10^{-2} g./cc. The C_C data are shown in Fig. 1. The amounts of coacervate, as the fraction of total protein in the coacervate phase, $C_CV_C/C_TV_T \equiv \rho$, are shown in Fig. 2.

As set up, these symmetrical deionized systems contain only two components, the polymer "salt" P^+Q^- and H_2O. Therefore, in the range where coacervation occurs, one would expect two phases to form with compositions C_C and C_L and that these concentrations would be invariant. Only ρ should change, in a linear fashion, as C_T is varied. In other words, the system represents a single isotherm on a composition-temperature phase diagram and ideally could be represented as a straight line with two points marking C_C and C_L. Inspection of Figs. 1 and 2 shows that these simple phase relationships do not hold and that C_C and ρ depend on C_T.

Neither C_C nor ρ expresses adequately the intensity of the coacervation since ρ may increase when C_C decreases. On empirical grounds it seemed more appropriate to express the coacervation data in terms of some combination of these effects. The two most characteristic parameters are ρ, which describes the fraction of polymer isolated in the concentrated phase, and an enrichment factor, ϵ, the ratio of the coacervate and equilibrium liquid polyion concentrations ($\epsilon \equiv C_C/C_L$). Theoretically, ϵ can be calculated through the thermodynamic formulation described in the Introduction. The intensity of coacervation, θ, is then defined as $\theta \equiv \epsilon\rho$. A plot of θ *vs.* C_T, Fig. 3, shows that the coacervation intensity decreases as C_T increases over the concentration range examined. There is an abrupt drop in θ at $C_T = 7 \times 10^{-3}$ g./cc. These observations will be discussed in detail later.

The data obtained at 50° were similar in all respects to the 40° data except that ρ was smaller. θ is plotted in Fig. 3.

The coacervates at 40 and 50° were very turbid but the equilibrium liquid was clear. The coacervate layer appeared to be uniform over the concentration range examined.

II. Coacervation in the Gelation Region.—When the experiments were carried out at temperatures below 40°, the equilibration mixtures did not set to gels during the 30-minute equilibration period. However, aggregation obviously began immediately. The mixtures became turbid and viscous as they cooled. Centrifugation, however, still separated the system into sharply bounded

---

[9] H. Boedtker and P. Doty, THIS JOURNAL, **58**, 968 (1954).

liquid phases. In every case, even at temperatures as low as 4°, the equilibrium layers were liquid.

Once phase separation had taken place, two different kinds of behavior could be noted on further cooling. Rapid cooling set the entire system to a turbid gel. Slow cooling gelled the coacervate and caused the precipitation of a new coacervate phase from the equilibrium liquid.

Heating a coacervated system to 40°, if carried out without agitation, reduced the turbidity of the layers without causing them to disperse. Indeed, the low-temperature coacervates frequently were water clear at 40°. In such rewarming experiments it became apparent immediately that the coacervates were not of uniform composition but, depending on the temperature at which they were formed, consisted of two or more layers. The initial concentration of the system also affected the number of coacervate layers and their relative amounts. In general, when several coacervate layers were present, they did not have the same turbidity.

These qualitative remarks point out the complexity of the system when gelation and aggregation phenomena accompany the coacervation process. These complications will be dealt with in more detail in later papers in this series. For the present, however, we will focus our attention on $C_{C,\epsilon,\rho}$ and θ where these refer to the average or total values for all of the coacervate layers considered as one phase. Figures 4, 5 and 6 show plots of C_C,ρ and θ isotherms, respectively, at 35, 30, 25.5, 19, 15 and 10°. In the θ isotherms one can see the progressive increase in the intensity of coacervation as T decreases and a decided change in the character of the θ–C_T relationship. The latter change coincides with the presence of multi-layer coacervates in the higher C_T region. For example, the 35° coacervate consists of two layers. The higher density layer is turbid, the lower density layer clear at 40°. The turbid layer increases in volume, just as the 40° coacervate does, until $C_T \backsimeq 6-7 \times 10^{-3}$ g./cc. and then decreases sharply as C_T is increased further. The clear layer becomes visible at $C_T \backsimeq 5 \times 10^{-3}$ g./cc. and increases in volume as C_T is increased.

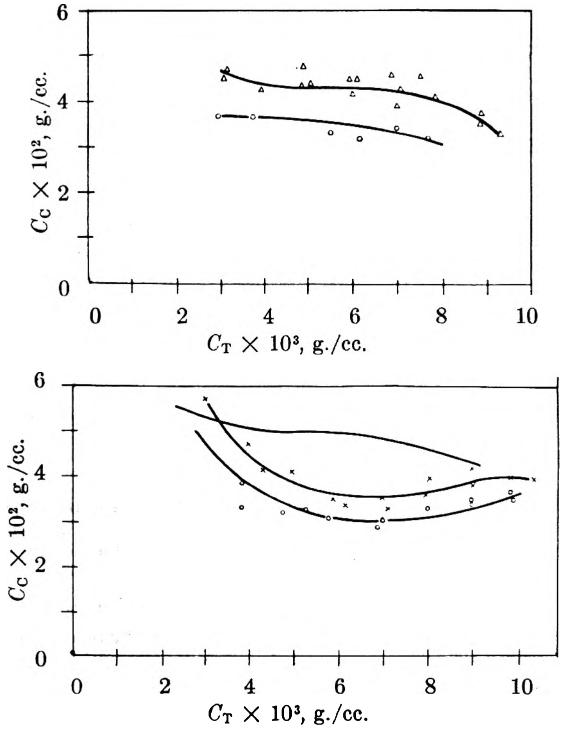

Fig. 4a and b.—Coacervate concentration as a function of initial concentration at temperatures below the critical gelation temperature: (A) △, 35°; ○, 30°; (B) ○, 10°; ×, 15°, the smooth curve represents the data at 25.5° computed from the equation

$$C_C = 0.07283 - 11.52C_T + 1.978 \times 10^3C_T^2 - 1.185 \times 10^5C_T^3$$

The standard deviation σ was 4.49×10^{-3}. The equation was computed by the same techniques given in the legend of Fig. 2.

Discussion

I. The Applicability of the Voorn–Overbeek Model for Coacervation.—The Voorn–Overbeek treatment of the complex coacervation phase equilibria predicts, through equation 5 (and eq. 42 ref. 2b), the equilibrium concentrations of the supernatant and coacervate layers in terms of the parameters σ and r which represent the charge density and polyion size. For any given r and σ, above the critical value for C_T, the mixture of oppositely charged polyions should separate spontaneously into two layers of fixed composition, C_L and C_C, and only the amounts of the two phases should vary as the total concentration progresses from C_L to C_C. It is obvious from the data presented in the preceding section that these direct requirements of the phase rule are not satisfied although the systems come reproducibly to an apparent equilibrium. At every temperature, the equilibrium concentrations depend on the total polyion concentration at the initial mixing. This behavior can be explained in terms of the existence in the real case of more than the two components of the idealized model.

A. The Effect of Molecular Weight Heterogeneity.—Since gelatins are known to be heterogeneous with respect to molecular weight, it is pertinent to consider first the effect of this type of heterogeneity on the phase diagrams, assuming that the Voorn–Overbeek model applies to each of the homologous series of polyions.

Consider a system composed of polycations P_1^+, P_2^+, P_3^+ and a single polyanion Q^- in equivalent amount. Further, let the ratios of amounts of P_1^+, P_2^+ and P_3^+ be some fixed values (a constant mixture of P's) and assume that the critical concentrations of P's for coacervation with Q are C_1', C_2' and C_3' such that $C_1' < C_2' < C_3'$. As C_T is increased from zero, a coacervate P_1Q will begin to form when $C_1 > C_1'$ in an amount proportional to $(C_1 - C_1')$. Only P_1Q will form a separate layer until C_2 exceeds C_2' when a new coacervate P_2Q will form along with P_1Q in an amount proportional to $(C_2 - C_2')$. Similarly, coacervate P_3Q will only form after $C_3 > C_3'$. A plot of ρ *vs.* C_T for this case, *e.g.*, Fig. 7, would consist, starting from the critical value of C_1', of three linear segments of increasing slope. On the other hand, a plot of the average C_C *vs.* C_T would show a negative slope since the Voorn–Overbeek treatment predicts that the

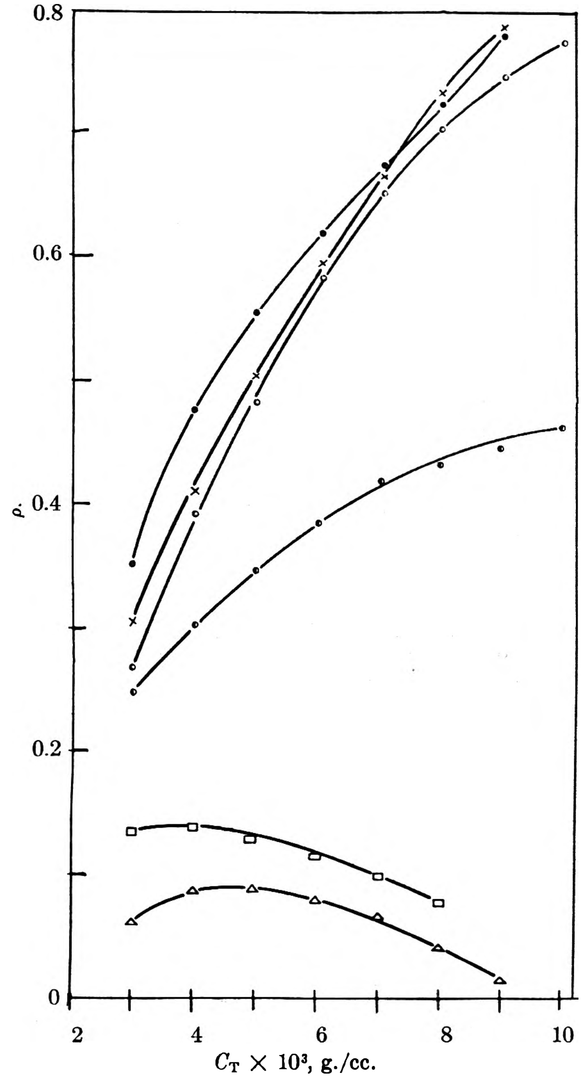

Fig. 5.—The fraction of gelatin in the coacervate phase as a function of initial concentration at temperatures below the critical gelation temperature: △, 35°; □, 30°; ◐, 25.5°; ●, 19°; ×, 15°; ○, 10°.

lower the critical concentration for coacervation, the higher the coacervate concentration will be. The best data against which to test these considerations are those of Figs. 1 and 2, representing the coacervation at 40°, in the non-gelation region. The ρ *vs.* C_T plot is exactly the opposite of that described above and, although C_C decreases with increasing C_T, the slope of the C_C *vs.* C_T plot is not monotonically negative. At lower temperatures (25 to 10°) where gelation-type aggregation does occur, the ρ–C_T plots begin to approximate the shape of the curve for the heterodisperse system but the C_C–C_T curves are still different in character (Figs. 4b and 5). Thus, heterodispersity in molecular weight cannot give rise to the observed behavior, within the framework of the Voorn–Overbeek treatment.

B. Self-suppression of Coacervation.—The shapes of the ρ–C_T and C_C–C_T plots are similar to the three-component case of self-suppression of coacervation noted in mixtures of polymer salts P^+A^-, B^+Q^- where the diffusible microions B^+ and A^- increase the ionic strength as the total polyion concentration is increased. In this case, however, the critical requirement is that the microions must be distributed in nearly equal concentration in both phases. In our system of isoionic polyampholytes, the only microions are H^+ and OH^- and H^+ is at a concentration less than 10^{-6} eq./l. in each phase. It is possible to consider the excess balanced, fixed charge on each polyampholyte as contributing to the total ionic strength but these charges cannot be distributed over the entire solution and hence cannot be used to explain the concentration dependence of C_C and C_L. We are, therefore, obliged to consider other sources for the apparent deviation of the coacervation of polyampholytes from the phase rule and from the Voorn–Overbeek model.

C. The Behavior of Isoionic Gelatin Solutions.—The behavior of salt-free isoionic solutions of randomly coiled polyampholytes has been described by Ehrlich and Doty[10] and applied to gelatin solutions by Boedtker and Doty[9] and by Veis and Cohen.[5] According to these works two effects are evident. First, because of the attraction of oppositely charged segments of the same molecule the extension of that molecule in space is decreased from that of the unperturbed random coil configuration. Second, because of the intermolecular attractive force resulting from charge fluctuations[11] large intermolecular aggregates may be formed under conditions where gelation–aggregation phenomena are absent. The electrostatic aggregates in isoionic solutions may be quite large.

Thus, even at 40° the behavior of the isoionic gelatin solutions before mixing cannot be represented in terms of non-interacting random coils as required by the Voorn–Overbeek treatment. Furthermore, the electrical charge cannot be considered as being uniformly distributed throughout the solution.

When mixtures of isoionic gelatins of different *p*I are made, a net charge is induced on each type of molecule and strong intermolecular electrostatic interactions cause new aggregates to form. These aggregates are governed in size by the initial concentration of the mixture but, once formed, are stable and can be diluted (at zero ionic strength) without dissociation. According to Boedtker and Doty[9] the electrostatic aggregates are more dense, compact structures than the gel-type gelatin aggregates. Clearly, it should not be assumed that the component polyions of any mixture of oppositely charged polyions at low ionic strength can ever exist as independent molecules. Thus, the coacervation equilibrium must be established between dilute solutions of aggregates, of near zero net charge, and the concentrated coacervate phase.

Since reaching this conclusion, we have begun a series of experiments on the state of aggregation in the equilibrium phase. These studies are not ready to be described in detail but the preliminary results confirm that aggregates are present in the dilute equilibrium phase. For example, a mixture of gelatins A and B at 40° and at $C_T = 7 \times 10^{-3}$

---

(10) G. Ehrlich and P. Doty, *J. Am. Chem. Soc.*, **76**, 3704 (1954).

(11) J. G. Kirkwood and J. B. Shumaker, *Proc. Natl. Acad. Sci.*, **38**, 863 (1952).

g./cc. was made in an analytical ultracentrifuge cell. The cell was spun at 20,000 × g for a few minutes to bring down the coacervate phase. The cell speed then was increased and the sedimentation of the equilibrium liquid observed. The S_{40} value computed from these observations was 71.3 S and this should be compared with the S_{40} values of 5.0 for each gelatin alone, shown in Table I. Light scattering measurements[4] also indicated the presence of aggregates in the equilibrium liquid.

D. Gelatin and the Critical Conditions for Coacervation.—Returning to the Voorn–Overbeek model, equation 4 places a minimum value of about 0.4 for the critical product $\sigma^3 r$. For either gelatin (from titration curves and the data of Table I) considered as independent molecules, r is approximately 10^4 sites and σ_{net} at pH 6.5 is $\sim 3 \times 10^{-3}$ charges/site so that $\sigma^3 r$ becomes $\sim 0.3 \times 10^{-3}$. This is far below the critical value for coacervation. If, alternatively, one uses the total charge on a gelatin molecule at pH 6.5 as Overbeek[1] suggests, $\sigma_{\text{Total}} \backsimeq 4 \times 10^{-2}$ and $\sigma_{\text{Total}}{}^3 r \backsimeq 0.6$. This latter value probably is appropriate for use when discussing the freely distributable charge in the concentrated coacervate phase but certainly cannot apply to the dilute equilibrium phase nor to the initial gelatin mixtures at low C_{T}.

Thus, independent gelatin molecules of the size studied and at the pH of our experiments, should not have formed coacervates. Assuming that σ is relatively independent of the environment, r would have to be on the order of 10^7 to surpass the critical value. From this point of view we are again led to conclude that the independent molecule-uniform charge distribution model cannot be valid for the dilute phase.

E. The Temperature Dependence of the Coacervation Process.—From equation 3 and the approximation of equation 5, it would appear that C_{C} should depend on the temperature only through the electrostatic interaction coefficient α in the non-gelation range. In turn, α is a function of $(DT)^{-3/2}$. It is difficult to evaluate the dielectric constant exactly for both phases and for such complicated solutes but it seems reasonable to take the change in D with T to be the same as that of water. Values of D, $(DT)^{3/2}$, α and α^2 are listed in Table II.

TABLE II

THE VARIATION OF THE ELECTROSTATIC INTERACTION COEFFICIENT WITH TEMPERATURE

t, °C.	D (pure water)	$(DT)^{3/2}$ × 10^{-6}	α	α^2
10	84.11	3.67	4.007	16.05
20	80.36	3.61	4.073	16.59
30	76.75	3.55	4.148	17.78
40	73.78	3.48	4.236	17.94
50	69.94	3.40	4.334	18.78

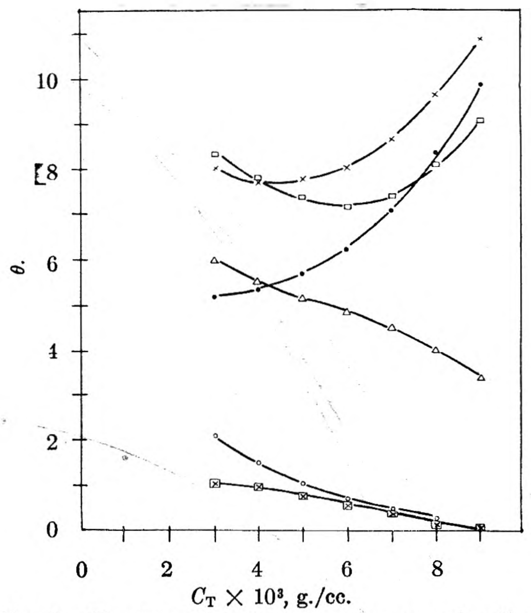

Fig. 6.—The intensity of coacervation as a function of initial concentration at various temperatures: ☒, 35°; ○, 30°; △, 25.5°; □, 19°; ×, 15°; ●, 10°.

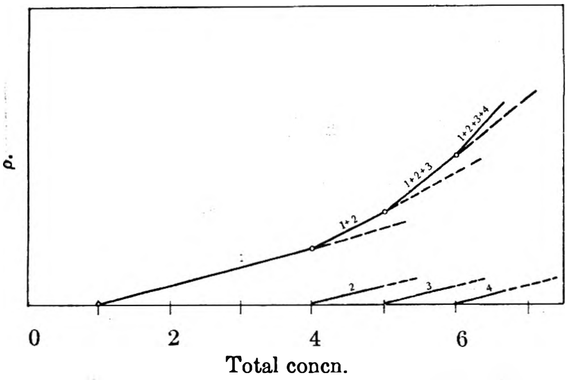

Fig. 7.—An example of the expected effect of molecular weight heterogeneity on the fraction of gelatin in the coacervate phase. If the system contains four components whose relative amounts and critical concentrations for coacervation for each of these components are fixed values as given below, the fraction of material in the coacervate phase will follow the course shown in the diagram. The numbers in the various parts of the diagram represent the component species that make up the coacervate phase at each stage of the process. See the text for the detailed explanation.

	Relative amt. of each component, %	Critical concn. for coacervation for each component	Total concn. at which the components reach their critical concn.	Concn. of each component when coacervation can occur
1	0.25	$C_1' = 0.25$	$C_{\text{T}_1} = 1.00$	$C_1 \geqq 0.25$
2	0.25	$C_2' = 1.00$	$C_{\text{T}_2} = 4.00$	$C_2 \geqq 1.00$
3	0.25	$C_3' = 1.25$	$C_{\text{T}_3} = 5.00$	$C_3 \geqq 1.25$
4	0.25	$C_4' = 1.50$	$C_{\text{T}_4} = 6.00$	$C_4 \geqq 1.50$

Accordingly, equation 5 predicts that C_{C} should increase about 4% for each 10° rise in the temperature. A change in C_{C} of that order of magnitude is within the range of the experimental error at 40 and 50° and the C_{C} data cannot verify this difference. However, ρ decreases significantly between 40 and 50°. Because of the relatively large volume of equilibrium liquid ρ is most sensitive to changes in C_{L} and indicates that, at constant C_{T}, C_{L} should increase with increasing temperature. This is verified by the direct C_{L} measurements.

A plot of C_{C} and C_{L} as a function of temperature at constant C_{T} (C_{T} chosen close to the inflection point of each C_{C} *vs.* C_{T} isotherm), Fig. 8, shows that the coacervation process clearly follows two different mechanisms. The discontinuity in C_{C}

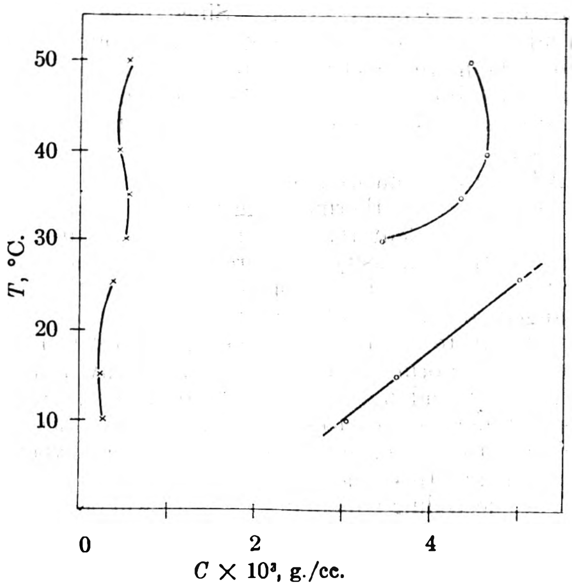

Fig. 8.—The equilibrium liquid and coacervate polyion concentrations as a function of temperature at constant initial concentration $C_T = 6 \times 10^{-3}$ g./cc., × = C_L; ○, C_C.

as a function of T probably matches the significant onset of thermal (non-ionic) gelation at the lower temperatures. However, the decrease in C_C between 40 and 30° is greater than that predicted by the variation in α, so that, again, the Voorn–Overbeek model does not appear to apply in detail to the real coacervation process.

II. The Concentration Dependence of Coacervation.—The reaction considered by the thermodynamic analysis outlined in the introduction may be written schematically as

$$\text{(A)}\quad [P^+ + Q^-]_{C_T,\ \underset{\text{random coils}}{\text{independent}}} \rightleftarrows [P^+ + Q^-]_{C_L,\ \underset{\text{random coils}}{\text{independent}}} + [P^+ + Q^-]_{C_C,\ \underset{\text{random coils}}{\text{independent}}}$$

According to the preceding discussion, however, the real system could be better represented by a series of reactions

$$\text{(B-1)}\quad [P^+]_{C_T,\ \underset{\text{aggregates}}{\text{isoionic}}} + [Q^-]_{C_T,\ \underset{\text{aggregates}}{\text{isoionic}}} \longrightarrow [PQ]_{C_T,\ \text{aggregates}}$$

$$\text{(B-2)}\quad [PQ]_{C_T,\ \text{aggregates}} \rightleftarrows [PQ]_{C_L,\ \text{aggregates}} + [P^+ + Q^-]_{C_C,\ \underset{\text{random coils}}{\text{independent}}}$$

or

$$\text{(B-2}')\quad [PQ]_{C_T,\ \text{aggregates}} \rightleftarrows [PQ]_{C_L,\ \text{aggregates}} + [PQ]_{C_C,\ \text{aggregates}}$$

Since the equilibrium concentrations of the two phases are dependent on the initial mixture concentration, C_T reaction B-1 must itself be the concentration-dependent step. We assume that it is both rapid and, in a practical sense, irreversible at very low ionic strength. The aggregation appears to be irreversible because of the high activation energy required to separate the densely entangled oppositely charged polyion chains. At 40° the average aggregate size at any given value of C_T is some fixed value, not dependent on the length of time the mixtures stand, since the amount of coacervate and the equilibrium concentrations of each phase were the same whether determined immediately or after the mixtures had stood for several hours. This is not true at lower temperatures where thermal gelation interactions proceed for many hours. However, even in these cases, the rates of gelation and hence the coacervate phase distributions are reproducibly governed by the mixing conditions and elapsed time.

One can draw some interesting conclusions on the behavior of gelatin mixtures from the fact that C_C is highest at low C_T (at 40°) and that C_C and, especially, ρ drops precipitously at $C_T \sim 0.7 \times 10^{-3}$ g./cc. Since general thermodynamic considerations of phase separations in polymer solutions show that the concentrated phase is more concentrated the larger the polymer size, the aggregate must, on the average, be larger in the more dilute solutions. This can be rationalized in the following way.

In the individual solutions at high dilution, the isoionic gelatin molecules attract each other by charge fluctuations to form large isoionic clusters. The individual molecules in these clusters have nearly the unperturbed random coil extension.[10] Because of their large effective volume, the gelatin molecules rapidly fill the solutions at successively higher concentrations until the entire system is like a vast network of entangled chains. Under these conditions, individual isoionic clusters become smaller, and ultimately unnecessary, because the charge fluctuations leading to the specific intermolecular associations are now diffused throughout the solution. Upon mixing the two isoionic solutions the isoionic clusters coalesce to dense, nearly neutral aggregates. As in the individual solutions, the average number of chains participating in the initial aggregate becomes smaller as C_T becomes larger because of the greater chance of intermolecular contact and because the original molecular clusters were smaller. At sufficiently high concentrations, the difference between the state of the gelatin in randomly entangled dilute solutions and in more concentrated solutions becomes so slight, energetically speaking, that coacervation drops abruptly as predicted by equation 5.

From the data of Table I, the gelatins we studied have a weight-average molecular weight of $\sim 3 \times 10^5$ and a z-average mean-square end-to-end extension of ~400 Å. From these parameters, a gelatin solution would be effectively filled (all unperturbed molecules in contact with the extremities of other molecules) at a concentration of about 3.0×10^{-3} g./cc. This is the correct magnitude to satisfy the above picture.

This way of looking at the gelatin system dictates the choice of reaction B-2 rather than B-2′. Specific aggregates should not be favored in the concentrated phase. It also shows that a reinterpretation of the relative roles of the electrostatic and entropy terms in bringing about coacervation is required.

In spite of the change in the model, equation 2 still expresses the general case in which F_M and F_e can be treated separately. According to reaction A, the electrostatic attractive forces drive the system to the phase separation because F_e is reduced in the concentrated phase. F_M, which increases on phase separation, works against coacervation. However, from the point of view of B-2, F_e is already minimized in the dilute solution by specific charge neutralization so that there is no, or relatively little, gain to be made on phase separation. However, the gelatin goes from ordered aggregates in dilute solution to the more disordered coacervate phase, giving rise to an increase in entropy on phase separation. Thus, the entropy change drives the phase separation with little contribution from the electrostatic interactions (except through the initial electrostatic establishment of the PQ aggregates, B-1).

Conclusions

We commented earlier that the concentration data could be explained only in terms of having more than two components in the P^+Q^-, H_2O system. However, the model drawn in the preceding section allows a different interpretation of that statement. We now conclude that each coacervation equilibrium system can be treated as a two-component system but that the size and charge density of the PQ aggregate, the real "solute," is different in every case and depends on the mixing concentrations. The equilibrium measured is therefore a different one at every mixing concentration.

In qualitative terms, the coacervation of neutral aggregates rather than randomly coiled linear polyions reverses the roles ascribed by Voorn and Overbeek to the electrostatic free energy change and the entropy change in driving the system toward phase separation. The control that diffusible microions exert is phenomenologically identical for either system. In the Voorn–Overbeek model, an increase in ionic strength lowers F_e and reduces both the tendency toward coacervation and the coacervate concentration. In our model the addition of salt should, through reaction B-1, reduce the aggregate size and hence reduce the coacervate concentration. Since the salt would, in addition, reduce F_e in both phases, our model should be more sensitive to salt. This is in accord with our observations that the dilute mixtures of gelatins are extremely sensitive to salt contamination.

All of the remarks above are restricted to the situation where thermal aggregation is absent. It is quite evident that when gelation occurs the coacervation intensity is increased and the concentration dependence of the coacervation is changed so that C_C ultimately increases as C_T increases (10 to 20° range). The aggregates formed are not uniform. The systems are truly multicomponent and may separate into three or more distinct phases. Coacervation in the presence of gelation thus requires a separate analysis, experimentally and theoretically.

The succeeding papers in this series will deal with the complex coacervation phase separation in terms of the coacervation and properties of aggregates rather than independent molecules and with the coacervation of gelatin gels, two separate types of protein–protein interaction.

DISCUSSION

J. TH. G. OVERBEEK (University of Utrecht).—I agree completely with Dr. Veis that the Voorn–Overbeek theory is not applicable to these salt-free gelatin complex coacervates. At higher salt content the aggregates in solution would be expected to break down and then perhaps the conditions for application of Voorn's line of thought might be more favorable.

ARTHUR VEIS.—I believe that at higher salt concentrations the independent random coil model would apply. In fact, the decrease in C_C (Fig. 1) at $C_T = 0.6 \times 10^{-3}$ g./cc. probably indicates this same type of change in the interacting system. In this case, the balanced fixed charges on the gelatin provide the atmosphere of high ionic strength. The way in which the coacervate concentration decreases with the total concentration from that point on is typical of the way Bungenberg de Jong's data show the effect of increasing salt concentration. However, the aggregation effects at very low ionic strength are not restricted to the case of polyampholytes. Hence, Voorn's treatment will not, in general, be applicable to the very low ionic strength regions where the coacervation intensity is greatest.

COMPARISON OF TRYPSIN X-IRRADIATED IN SOLUTION AND IN AGAR GELS[1]

BY E. S. AUGENSTINE, L. G. AUGENSTINE[2] AND E. R. LIPPINCOTT

Contribution from the Department of Chemistry, University of Maryland, College Park, Maryland, and the Biology Department, Brookhaven National Laboratory, Upton, New York

Received March 7, 1960

A method was developed to measure the enzymatic activity of trypsin recovered from agar gels. From unirradiated gels this activity was always less than that from a corresponding solution containing no agar. The amount of trypsin inactivated in gels by a given dose of radiation was much less than that in trypsin solutions where there was no agar. This was contrary to expectations based on previous studies of gels containing dyes. This inhibition of inactivation in agar is presumed to result from an interaction between agar and trypsin. For example, a complex may form such that susceptible sites of the trypsin are shielded from reaction with radiation-produced radicals. Alternatively, the micellular structure of agar may hinder the trypsin from unfolding once it reacts with a radical.

Introduction

Many cells are seriously affected by an absorbed radiation dose of 10^3 rads (r.); in fact, most mammals are killed by this dose delivered to the whole body. Yet it may require as much as 10^6 r. before an appreciable fraction of individual biochemicals are inactivated[3] when irradiated outside of the cell.

There are a number of potential explanations for this thousand-fold disparity. One of these is that the mechanisms of energy absorption and movement within biological structures is such that absorbed energy is "funnelled" to critical sites within the cell.[4,5] The research reported here was designed to provide an evaluation of this possibility.

It is generally recognized that energy absorbed from ionizing radiation can inactivate biological material in at least two ways. A *direct effect* presumably occurs when the radiation produces a primary event, such as an ionization, within the molecule itself; this can occur either in the dry state or in solution. *Indirect effects* result from reactions between solute molecules and products resulting from the action of radiation on water. The latter presumably are produced by the reactions

$$HOH^0 \rightsquigarrow HOH^+ + e^- \qquad (1a)$$
$$HOH^+ \longrightarrow H^+ + OH^0 \qquad (1b)$$
$$e^- + HOH^0 \longrightarrow HOH^- \qquad (1c)$$
$$HOH^- \longrightarrow OH^- + H^0 \qquad (1d)$$

in which the ejected electron travels a considerable distance before being captured. Thus, a spatial separation of the radical and ion species occurs. As the products diffuse, they can undergo numerous reactions: they may recombine to form HOH again, react with solutes and dissolved gases or they can combine with other radiation products to form H_2^0, $H_2O_2^0$, HO_2^0, etc.[6]

Much work has been done on the irradiation of biochemicals in the dry state or in solution. Dale[7] was the first to show that enzymes in very dilute solutions containing only pure enzyme could be inactivated by doses of the order of 10^4 instead of the 10^6 r. or greater necessary for direct inactivation of dry preparations[8] or impure solutions.[9] Potentially both direct and indirect effects should occur when living cells are irradiated since they may contain as much as 90% water. However, the amount of indirect inactivation of a particular component should be relatively small because of the many competing solutes normally present in a cell.

In attempting to assess the importance of various mechanisms in promoting radiobiological damage it is necessary to recognize that the dry state and solutions containing only one highly purified solute are not representative of cellular conditions. Rather a cell has a gel-like composition with a corresponding semi-ordered structure. Experiments, by Gevantman, *et al.*,[10] discussed below, suggested this "structuredness" might act as a framework which would promote efficient migration of energy in one form or another to critical structures or molecules. Thus, the energy absorbed could be more efficient in inactivating individual biological components within the cell.

An agar gel can be made very similar in consistency and atomic number to tissue.[11] Therefore, it was felt that a study of the effects of radiation on an enzyme in agar[12] should be worthwhile. Since the gels we used were 98–100% water, the same primary reactions that are produced in aque-

---

(1) In part from a thesis by Elizabeth S. Augenstine submitted to the University of Maryland in partial fulfillment of the requirements for the M.A. degree in Science Education.

(2) Division of Biology and Medicine, U. S. Atomic Energy Commission. On leave-of-absence until July 1960 from the Biology Department, Brookhaven National Laboratory, Upton, New York.

(3) In this paper the term *inactivation* is used to designate any solute changes which fall into the particular category being measured experimentally

(4) L. Augenstine, "Joint Committee on Atomic Energy Hearings on Fallout," 1958, p. 123.

(5) E. Augenstine, master's thesis, University of Maryland, 1959.

(6) A. O. Allen, THIS JOURNAL, 52, 479 (1948).

(7) W. Dale, *Biochem. J.*, **34**, 1367 (1940); **36**, 80 (1942).

(8) E. Pollard, *Advances in Biol. Med. Phys.*, **3**, 153 (1953).

(9) (a) R. Havard, *Brit. J. Radiol.*, **8**, 787 (1935); (b) C. Scott, *Med. Research Council (Brit.) Spec. Rept. Ser.*, No. 223 (1937).

(10) (a) L. Gevantman, R. Chandler and J. Pestaner, Technical Report USNRDL-TR-163, MS 081-001, U. S. Naval Radiological Defense Laboratory, San Francisco 24, Calif., May 29, 1957; (b) L. Gevantman, *Rad. Res.*, Suppl. 2 (1960).

(11) M. Day and G. Stein, *Nucleonics*, **8**, 34 (1951).

(12) Some of the reasons which led Gevantman, *et al.*,[10] to choose agar from eleven different compounds considered, also recommended it for the present research: (i) the substance should be adequately soluble in water and yet in low concentration produce a firm gel; (ii) it should be relatively inert to the dose of radiation employed; (iii) it should be inert to the reactants and products formed in the gel as a result of the irradiation; (iv) it should go into solution at the lowest possible temperature in order to minimize the thermal inactivation of added trypsin. Other gel materials including pectin, silica, Kelgin and Kelgin XL were tried, but gelation was not achieved under our experimental requirements. Gelatin would have been undesirable for these studies because trypsin could digest it.

ous solutions should predominate. Further, the diffusion constants for mono and divalent cations were found to be nearly the same in gels as in solution.[13] Radicals would be expected to behave similarly to the cations. Thus the subsequent reactions of the radiation-produced radicals in agar gels should be comparable to those in solution, with the exception that effects of convection and mixing are eliminated.[11] These properties were exploited by other workers to obtain the three-dimensional dosage distributions produced by high-energy electrons in agar blocks containing dyes.[10,11,14]

Besides the usual indirect effects, we expected additional inactivation might result from the "funneling" mechanisms postulated above. This expectation was based on the results of the studies conducted by Gevantman and co-workers. They reported an increase in the amount of "inactivation" per unit of radiation as the gel concentration was increased. For instance, as agar concentration was increased from 0 to 1% there was a linear increase of almost a factor of three in the irradiation yield for a trichloroethylene–brom cresol purple system. A lesser increase of only 60% was observed in the production of free I from KI as the agar concentration was raised from 0.3 to 1.0%.[11]

In the research reported here the enzyme, trypsin, was X-irradiated: in solution alone; in solution with methylene blue as a competing solute for the radiation-produced radicals; and alone in agar concentrations from 0 to 2%. The expected increase in trypsin inactivation with an increase in gel concentration was not observed. In fact, quite the opposite was found—agar exerted a strong inhibitory effect on the amount of inactivation produced. Investigations of the reasons for this marked difference in behavior from the dye systems have led to a number of conclusions concerning the nature of the trypsin–agar interactions which may be important to an understanding of radiobiological effects at the macromolecular and cellular levels.

Experimental Procedures

It was necessary to have experimental materials as free of "contaminants" as possible since radiation-produced radicals will react with other solutes in addition to trypsin.[7,15] Thus, special procedures, as well as "conductivity water" having a specific resistance of 5 × 10⁷ ohms were employed in making up solutions or in cleaning equipment to be used before or during the irradiation.[5]

Preparation of Solutions. 1. Trypsin.—A stock 25 μM solution was made up in sodium phosphate buffer. It was found that the trypsin (2 × crystallized, Worthington Biochemical Co.) did not completely dissolve in the buffer. Therefore, 50 mg. was put in 90 ml. of 6×10^{-4} M HCl in an open beaker and carefully pulverized and agitated with a stirring rod. When all granules had disappeared, 10 ml. of 0.1 M NaH_2PO_4 was added to adjust the pH to 4.5. During preparation and storage, precautions were taken to minimize trypsin deactivation by either heat or "surface denaturation."[16]

2. Agar.—Appropriate amounts of Difco Bacto-Agar in 100 ml. of 0.01 M NaH_2PO_4 were heated with continuous stirring until a clear solution was obtained (at about 90°). Upon cooling to 50° the required aliquots were immediately pipetted (using warmed pipets) into mixtures of trypsin and 0.01 M NaH_2PO_4 to give the desired final agar concentrations (0 to 2%). The 100 ml. of agar solution was freshly prepared for each experiment to avoid excessive hydration changes upon standing.

The Difco Bacto-Agar had been purified during its manufacture by removing extraneous matter and pigmented portions and reducing salts to a minimum. An indication of its relative purity can be ascertained from the fact that a 0.2% solution had very little absorption between 200 and 800 mμ.

Irradiation.—Two different irradiation arrangements were used.

	KVP	mA	Filtration, mm. Al	Dose rate, r./min.	Max. dose delivered, r.	Temp., °C.
A[17]	100	5	1/4	28	10,000	20–25
B	250	30	1/4	285	171,000	4 or 25

Since trypsin will absorb onto glass,[16] all solutions were irradiated (and assayed) in polystyrene vials. Polystyrene was chosen because it was known to contain only a minimal amount of material which would act as competing contaminants.[15] The vials were placed in a circular lucite–brass rack designed (1) to permit temperature control and (2) to achieve more uniform dosage distribution within the vials by providing a "constant-scattering environment."[5] Dosages were calibrated with a Fricke dosimeter[18] in which the Fe^{+2} is oxidized to Fe^{+3} by radiation-produced radicals. Aliquots of the Fe_2SO_4 solution having the same volume as the trypsin samples were irradiated under identical conditions in the lucite–brass rack.

Hemoglobin Assay. 1. In Solution.—Following irradiation the enzymatic activity remaining was measured by a modification of the assay method of Anson.[19] Digestion of the stock solution of hemoglobin (Hb) was carried out for various lengths of time depending upon the trypsin concentration. Digestion was stopped by adding 5% trichloroacetic acid and the mixture was allowed to stand for at least one-half hour before filtering through Whatman #3 paper. Finally the optical density (OD) of the filtrate was measured at 280 mμ. The OD was found to be directly proportional to trypsin concentration when unirradiated samples containing different trypsin concentrations were assayed for a fixed length of time.

2. In Agar.—If Hb solution was added to unirradiated trypsin gels no digestion occurred. To recover active enzyme it was necessary to freeze the gels before assaying.[20] After standing at Dry Ice temperature for at least 1 hour and preferably overnight, the samples were placed in a water-bath at room temperature for one-half hour. At that time they were assayed according to the Hb procedure outlined above. The OD was directly proportional to the trypsin concentration in unirradiated samples containing as much as 2% agar. However, in all experiments more activity was recovered from those unirradiated samples having no agar than from those containing appreciable amounts. The data from three experiments shown in Fig. 1 are typical and show the reproducibility to be expected from this assay method in agar. Using appropriate controls it was determined that the loss in trypsin activity did not result solely from the 50° temperature at which the agar and trypsin were mixed.

More activity was recovered when the frozen samples were pulverized before assaying. However, there was the danger that material would be lost in the transfer from the mortar back to the vial for assaying and it was difficult to be certain that all samples were pulverized equally. Since the addition of a pulverization step made for an unduly cumbersome procedure for a large number of samples, it was ordinarily not used since adequate activity could be recovered without it.

---

[13] A. Thomas, "Colloid Chemistry," McGraw-Hill Book Co., New York, N. Y., 1934, p. 479.

[14] S. Goldblith, B. Proctor and O. Hammerle, *Ind. Eng. Chem.*, **44**, 310 (1952).

[15] L. Augenstine, *Rad. Res.*, **10**, 89 (1959).

[16] R. Ray and L. Augenstine, This Journal, **60**, 1193 (1956).

[17] We are indebted to Prof. D. T. Morgan, Jr., Botany Dept., University of Maryland for the use of setup A and to the Biology and Medical Departments at Brookhaven National Laboratory for setup B.

[18] J. Weiss, A. Allen and H. Schwartz, "Proc. Intern. Conf. Peaceful Uses Atomic Energy," Geneva, Vol. **14**, 1956, p. 179.

[19] M. Anson, *J. Gen. Physiol.*, **22**, 79 (1938).

[20] This procedure was adopted following the suggestion of Dr. C. Markert, Biology Department, Johns Hopkins University that freezing should break up the internal gel structure.

Other procedures to recover enzymatic activity from the gels were tried without success. To liquefy the agar–trypsin gel required a temperature of at least 72°. Trypsin is rapidly inactivated at that temperature. Nevertheless, it was thought that a quick burst of heat might liquefy the gel before the trypsin was appreciably inactivated. However, no success was obtained with an infrared lamp even though only two minutes of heating were required and the Hb solution was added immediately upon liquefaction.

Results and Discussion

Trypsin in Solution (No Agar).—The reliability of the data obtained with the present procedures and facilities was tested by using a recently developed method of analysis.[15] According to that method, in the range of solute concentrations where *indirect* radiation effects predominate, a plot of the reciprocal, $1/Y_{\text{tr}}$, of the inactivation yield (in molecules/unit dose) *versus* the reciprocal, $1/N_{\text{tr}}$, of the concentration of trypsin should give a straight line: (a) whose intercept is the probability that a trypsin molecule will be inactivated in a collision which results in the elimination of a radiation-produced radical; and (b) whose slope is a measure of the reactivity of any "competing solutes"—either those added in the form of a second solute or those present as contaminants in the water. In the presence of added solutes the slope should increase, but the intercept remain unchanged.

A straight line having negative slope was obtained when samples from a particular trypsin concentration were irradiated and the log OD (*i.e.*, log activity remaining) was plotted against the dose, D (*e.g.*, see the data in Fig. 2A). This indicated that inactivation was first order so that the yield could be described by

$$Y_{\text{tr}} \equiv -\frac{\mathrm{d}N_{\text{tr}}}{\mathrm{d}D} = \frac{N_{\text{tr}}}{D_{37}} \qquad (2)$$

where D_{37} is the dose necessary to reduce activity to $1/e$ its initial value.

For trypsin (without the addition of other solutes) irradiated in solution at pH 4.5 with concentrations between 0.5 and 5.0 μM, the slopes and intercepts of plots of $1/Y_{\text{tr}}$ *versus* $1/N_{\text{tr}}$ were consistent with values determined previously.[15] In addition, the intercept did not change significantly when methylene blue (either 2 or 4 μM) was added as a competing solute and the increases in slope were comparable to those reported previously. In general, the deviation of individual points from the expected straight lines was ±10% or less and the reproducibility (between daily runs) of the values for the slope and intercept was also about ±10%.

Trypsin in Agar Gels.—In one set of experiments 2.5 μM trypsin in pH 4.5 NaH_2PO_4 buffer containing 0, 0.2, 0.4,......., or 2.0% of agar was irradiated (using setup A) with doses up to 10,000 r. Inactivation could be demonstrated definitely only in those samples containing no agar. Inasmuch as the D_{37} for 2.5 μM trypsin irradiated in solution alone is about 7500 r. these results were quite unexpected. The findings of Gevantman, *et al.*,[10] showed that trichloroethylene and potassium iodide are inactivated to a greater extent in agar than in "pure" solution. This established that the agar does not compete effectively for the radicals responsible for inactivating these two compounds and, further, that the gel may lead to a more efficient utilization of the absorbed energy. The work of Day and Stein[11] showed that agar also does not compete for the radicals responsible for the methylene blue inactivation. Since trypsin and methylene blue are co-competitors for radiation-produced radicals, the same radical species must be involved in inactivating both. Thus, it is concluded that the agar is not competing for the radicals which inactivate trypsin. It has also been pointed out previously that the migration of radicals should not be seriously affected by the gel structure. This conclusion is consistent with the results of Gevantman and Day and of Stein. From the above considerations as well as those to follow, it appears very likely that trypsin inactivation in the gels is depressed because of an interaction between agar and trypsin.

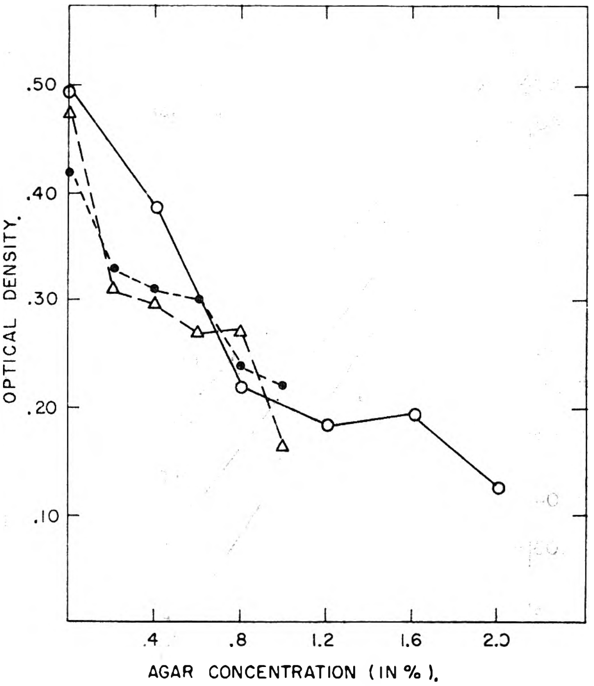

Fig. 1.—The effect of agar concentration on the amount of enzymatic activity which can be recovered from unirradiated gels containing 2.5 μM trypsin at pH 4.5 (three separate experiments).

For example, agar–trypsin complexes would be expected inasmuch as agar has a negative charge and trypsin a positive charge at pH 4.5.[21] If so, susceptible trypsin sites may be shielded. Direct reaction between the agar and critical surface groups could either chemically alter or mask them so that they are unavailable to attack—it has been estimated that in solution about 2.5% (100 Å.^{2}) of the surface of the trypsin molecule is involved in inactivation by radicals.[22] However, even if the critical site is not directly involved in bonding with the agar, reaction with a radiation-produced radical could still be sterically hindered. This

[21] (a) H. Terayama, *C. A.*, **45**, 2989g (1951), original in Japanese; (b) an interaction is known to occur between agar and catalase. Terayama found that agar caused a striking inhibition of catalase activity when the catalase had a positive charge. He attributed this to a colloid-ionic combination.

[22] L. Augenstine, "Proceedings 1st National Biophysics Conference," eds. H. Quastler and H. Morowitz, Yale Univ. Press, New Haven, Conn., 1957, p. 154.

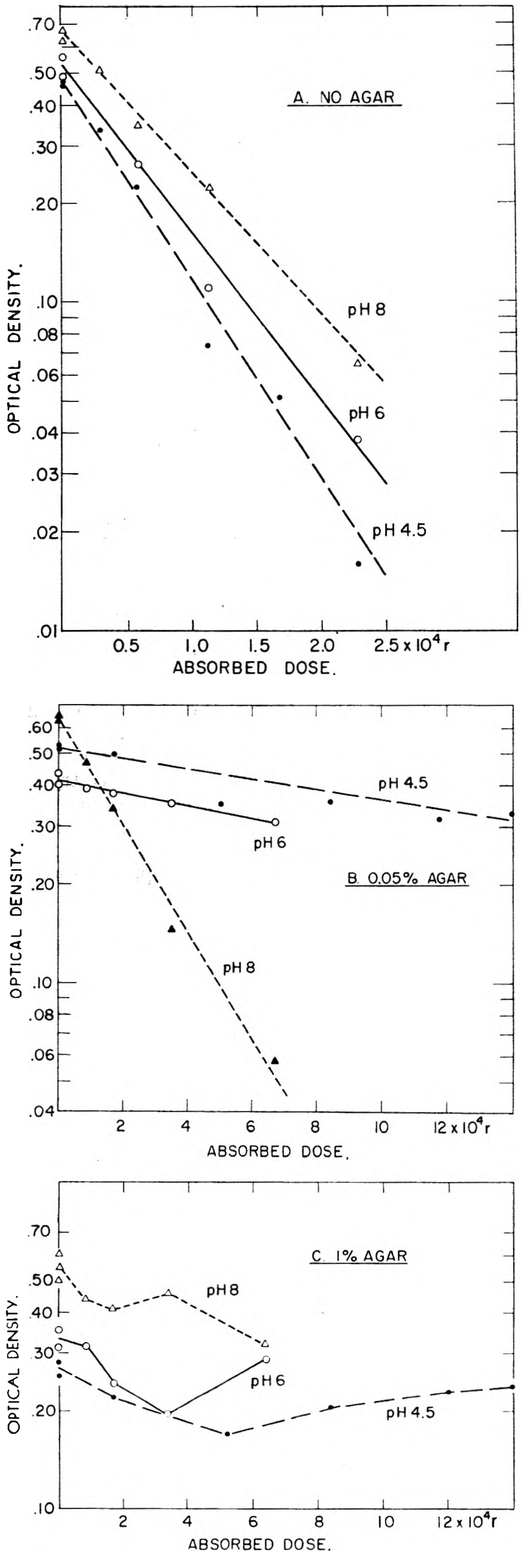

Fig. 2.—The enzymatic activity which can be recovered following the irradiation (with various doses) of 2.5 μM trypsin in 0, 0.05 and 1% agar made up in phosphate buffer at *p*H 4.5, 6 or 8. These results were obtained from irradiations carried out at 0°. Limited data obtained at 25° were not significantly different.

could result from bonding at a nearby site or even a change in molecular conformation induced by the formation of the complex.

Alternatively, the known micellular structure of the agar[23] may provide a "cage effect." It has been postulated by L. Augenstine that the inactivation of an enzyme requires a considerable rearrangement in its structure.[24] If trypsin is rigidly held within an agar micelle, it could be prevented from undergoing large structural rearrangements. In this manner incipient inactivation initiated by a radical could be prevented from proceeding to completion. Thus, inactivation depending upon an unfolding of a trypsin molecule should only occur after the gel structure surrounding that molecule has been sufficiently disrupted.

Six studies employing dosages as high as 170,000 r. and three different *p*H's indicated that both the formation of a complex and a cage effect may contribute to the depression of the inactivation yield of trypsin in agar. The selected data shown in Fig. 2 present the main features observed. Those in 2A show that in the absence of agar there is no significant difference in the inactivation rates at *p*H's 4.5, 6 or 8. As agar is added in low concentration the inactivation rate decreases. The data in Fig. 2B demonstrate that the magnitude of the decrease depends upon the *p*H. This *p*H effect is such as would be expected if the formation of a complex between trypsin and agar was involved; that is, the increase in *p*H should tend to neutralize the positive charge on the trypsin. Even though the amount of inactivation for a given dosage is decreased by a factor of 30, the inactivation still follows first-order kinetics. However, for larger agar concentrations, at which a firm gel is formed, the inactivation yield apparently can no longer be completely described by equation 2. Although the reliability of the data is less at the higher agar concentrations and longer irradiation times (up to 10 hours), results such as those in Fig. 2C suggest that there is an initial drop in *recoverable* activity followed by a return to approximately the initial value, with increasing dose. With sufficient irradiation the activity would eventually all be destroyed. The dosages necessary to produce the two suggested inflection points appear to increase as *p*H decreases for the three *p*H's tested.

An initial decrease in activity followed by an apparent increase with larger doses would be consistent with the notion that not only can radiation inactivate the trypsin but it can also disrupt the micellular structure responsible for maintaining a cage effect. Some observations on the assay method are also in accord with a cage effect. That the amount of activity which can be recovered

---

(23) T. Takahashi and S. Miyake, *C. A.*, **47**, 9523b (1953). Original in Japanese.

(24) (a) L. Augenstine and R. Ray, THIS JOURNAL, **61**, 1385 (1957); (b) L. Augenstine, *Rad. Res.*, Suppl. 2, in press (1960).

utilizing the freezing technique declines with increasing agar concentration is shown by the data in Fig. 1. However, the amount of activity recovered can be increased if the Hb solution is added before the gel solidifies or if the gel is more thoroughly broken up (*e.g.*, by pulverizing) before the assay is performed.[25] In some of the 1% gels and in all of the 2% gels, rings of agar were seen on the filter paper following digestion. Therefore, some of the trypsin was likely not released from the agar structure which remained. With the highest doses the rings remaining after digestion contained less material and appeared to be more "porous."

A more definitive evaluation of the relative contributions of the two types of interactions to the decreased trypsin inactivation in agar will probably require detailed studies of at least two types: (a) measurements of the physico-chemical changes produced by radiation in agar gels and in agar–trypsin mixtures; and (b) determinations of the extent and nature of the protection from radiation damage afforded to trypsin by very low levels of agar. If the masking of solute sites susceptible to attack by radicals is an important factor in radiation-inactivation in gels, then the ratio of the size of the solute to the size of the individual micelles may be an important consideration. Thus an evaluation of the effect of the size of the solute on the enhancement or depression of its inactivation in agar seems worthwhile.

Acknowledgments.—The authors gratefully acknowledge helpful suggestions made by C. Markert, L. Gevantman and R. Feinstein. One of us (ESA) wishes to especially thank Professor Orval L. Ulry, Education Department, University of Maryland, for arranging that the thesis based upon this chemical research could partially fulfill the requirements for a master of arts degree in the education department.

DISCUSSION

L. K. JAMES.—May not an alternative explanation for the inhibition of trypsin inactivation in the agar gel lie in a consideration of ordered water within the gel structure and surrounding the enzyme?

L. G. AUGENSTINE.—Intuitively I would doubt that this alone could account for the large inhibitions we observe, except, of course, as disarrangement of ordered water may be a crucial step in the formation of an agar–trypsin complex or in the induction of a conformation change. However, this is one of many possible explanations which cannot be ruled out by our present data.

The reasons for initially choosing the trypsin–agar system are discussed in the text. We now know, however, that some of the features of this system are quite undesirable for investigating the current problems of interest. I still feel that the idea that absorbed energy may be "funnelled" to critical sites within the cell as a result of the semi-ordered structure of biological material is a reasonable one and should be evaluated more critically. Accordingly, we would welcome suggestions of other more desirable systems.

L. H. REYERSON.—Although you pointed out the reasons for initially rejecting gelatin, you might want to reconsider it because of the ease with which it can be liquefied and thus the trypsin recovered. Silica gels would also seem to offer many advantages.

J. TH. G. OVERBEEK.—It might be worth while to try polymethacrylic acid cross-linked by divinylbenzene or polyvinyl alcohol as described by A. Katchalsky as the gel basis because the degree of cross-linking and the degree of swelling can be changed at will.

---

[25] R. Feinstein, *Arch. Biochem. Biophys.*, **79**, 399 (1959), reported increased catalase recovery from mouse liver homogenates when 1% of a non-ionic detergent, Triton X-100, was added.

COAGULATION OF LYOPHOBIC COLLOIDS IN MIXED SOLVENTS. INFLUENCE OF THE DIELECTRIC CONSTANT

By J. P. Kratohvil, M. Orhanović and E. Matijević[1]

Laboratory of Physical Chemistry, Faculty of Science, University of Zagreb; Department of Physical Chemistry, Institute "Rudjer Bošković," Zagreb, Croatia, Yugoslavia, and Clarkson College of Technology, Potsdam, New York

Received March 7, 1960

Negative silver bromide sols *in statu nascendi* were coagulated by potassium, barium and lanthanum nitrate in isodielectric mixtures of water with methanol, *n*-propanol and isopropyl alcohol, respectively. Dielectric constants varied from 80 to 29. The results are compared with those for water–ethanol mixtures published previously. Coagulation concentrations decreased with a lowering of the dielectric constant and with an increase in the concentration of stabilizing ions (Br^-). Coagulation concentrations of individual counterions were approximately the same for a given concentration of the stabilizing ion and mixtures of different solvents having the same dielectric constant. The results are discussed in the light of the current theories of stability and coagulation of lyophobic colloids.

Introduction

In a series of previous papers[2–6] numerous results of the influence of ethanol, acetone, dioxane and glycine in aqueous solutions on the electrolytic coagulation of negative silver halide sols *in statu nascendi* were described and compared. The change of the dielectric constant (DC) of medium in these investigations covered the range from 126 (2 *M* glycine solutions) to 30 (87 wt. % of ethanol). These results have shown several regularities in the behavior of silver halide sols in mixed solvents, the main one being a direct relationship between the coagulation values of a given counterion and the DC of the medium. Compared with the values for water, the coagulation values of KNO_3, $Ba(NO_3)_2$ and $La(NO_3)_3$ have generally decreased in media of lower DC and increased in glycine solutions.

However, a comparison of coagulation values of the same counterion in mixtures of different solvents with water (water–ethanol, water–acetone or water–dioxane) having the same DC, showed appreciable differences indicating specific influences of the solvent used. In case of isodielectric mixtures, coagulation values of mono-, di- and trivalent counterions were the highest in dioxane mixtures, intermediate in acetone, and the lowest in ethanol solutions.[6] The differences were particularly significant at greater concentrations of stabilizing ions in solution and with sols of higher charge.

In view of this specific influence of solvents of various chemical composition we decided to undertake some additional investigations of the coagulation of negative silver bromide sol *in statu nascendi*, using a series of homologous solvents of similar chemical properties and structure. The solvent mixtures, used were water–methanol, water–1-propanol and water–isopropyl alcohol in the range of DC from 80 to 29. The results are compared with those for water–ethanol media obtained previously.

Since current theories of the stability and coagulation of lyophobic colloids include also the influence of DC of medium, the experiments described in this communication may serve as a test of these theories.

Experimental

Negative silver bromide sols *in statu nascendi* were used. They were prepared by mixing a silver nitrate solution with a solution containing KBr (or HBr) and the coagulating electrolyte. Every run consisted of several systems having constant concentrations of $AgNO_3$ and halide component but various concentrations of the coagulation electrolyte. The concentration range of the latter was determined according to its coagulation ability under the given experimental conditions. In all measurements the concentration of bromide ions was kept higher than the concentration of silver ions; however, the constant excess concentration was changed from run to run in order to investigate the influence of the charge density of sol particles. All reaction solutions were prepared in mixed solvents of desired composition.

The coagulation process was followed by changes in light scattering intensities ($\theta = 45°$) in a Pulfrich–Zeiss photometer with an attachment for turbidity measurements. The temperature was kept constant at 20°. The details of the experimental technique and the method for analyzing the turbidity data for the determination of coagulation concentrations have been described previously.[7,6]

In order to obtain the isodielectric mixtures of desired dielectric constants, the required compositions were calculated from the data of Akerlöf[8] and are listed in Table I. The corresponding water–ethanol mixtures used in previous investigations[3,6] and utilized in this paper for comparison purposes were of slightly different dielectric constants. However, these differences were very small and could not affect the coagulation concentration by more than the experimental error in coagulation measurements themselves.

The data on ethanol–water mixtures are also included in Table I.

Table I

Composition of Water–Alcohol Mixtures and Corresponding Dielectric Constants (DC) at 20°

	Concn. of organic solvent, wt. %			Ethanol	
DC	Methanol	1-Propanol	Isopropyl alc.	Wt. %	DC
80.4	0	0	0	0	80.4
62.5	37.5	25.0	24.0	29.6	62.7
50.5	62.0	42.0	40.5	49.0	51.0
39.5	85.5	57.5	56.0	68.0	40.0
29.0		75.0	71.0	86.8	30.5

All chemicals were of reagent grade purity. Solvents were distilled several times over silver nitrate. Their refractive index and density was checked before use. The concentrations of all components are given for the final volume (10.0 ml.) of the reaction mixtures.

---

(1) Clarkson College of Technology, Potsdam, New York.

(2) B. Težak and J. Kratohvil, *Arhiv kem.*, **24**, 1 (1952).

(3) B. Težak, *et al.*, This Journal, **57**, 301 (1953).

(4) B. Težak, E. Matijević, K. Schulz, J. Kratohvil, R. Wolf and B. Černicki, *J. Colloid Sci.*, Supplement **1**, 118 (1954).

(5) B. Težak, E. Matijević, K. F. Schulz, J. Kratohvil, M. Mirnik and V. B. Vouk, *Disc. Faraday Soc.*, **18**, 63 (1954).

(6) J. Kratohvil and B. Težak, *Arhiv kem.*, **27**, 73 (1955).

(7) B. Težak, E. Matijević and K. Schulz, This Journal, **55**, 1557 (1951)

(8) G. Akerlöf, *J. Am. Chem. Soc.*, **54**, 4125 (1932).

Results

A graphical analysis of the kinetics of coagulation[7] showed that the critical time for coagulation of negative silver bromide sol in all solvent mixtures used was approximately ten minutes after mixing the reaction components. Thus, the 10-minute coagulation curves were used for graphical determination of the coagulation values.

Because of the large number of experimental results, the graphical presentation was preferred to tabulation. In Figs. 1 to 4 results are plotted as logarithms of coagulation concentrations of coagulating electrolyte (expressed in normalities) for various media *vs.* the logarithm of the total concentrations of stabilizing bromide ions. The results for water and water–ethanol mixtures from previous papers[3,6] are also included. It should be mentioned here that the great dependence of the coagulation concentration on the excess concentration of stabilizing ion requires experiments in a range of Br^- concentrations. Furthermore, the data must be compared only at equal Br^- concentrations. Otherwise erroneous conclusions could easily be drawn.

In the determination of coagulation concentration of potassium ion, the sum of concentrations of both KNO_3 and KBr was utilized. In the case of coagulation with $Ba(NO_3)_2$ and $La(NO_3)_3$ we did not take into account the concentration of K^+ introduced by KBr (or H^+ from HBr). The concentration of KBr (or HBr) was in most cases appreciably smaller than the critical coagulation concentration of the potassium as counterion. Therefore, no significant effect of ion pair coagulation should be expected.[9]

Figure 1 represents the results for a monovalent coagulation ion (K^+). The coagulation values for all solvent mixtures and at all concentrations of stabilizing ion decrease as the DC of the medium decreases. In addition, the coagulation values decrease with increase of the concentration of Br^-, whereas in pure aqueous solutions the coagulation concentration of monovalent ions usually *increases* with increasing concentration of stabilizing ions.[10] Although the values for various isodielectric mixtures are somewhat scattered, this scatter is random and all values for a particular DC tend to crowd around a mean value. Only coagulation values in isopropyl alcohol–water mixtures were always somewhat greater than for 1-propanol solutions.

Similar results were obtained with $Ba(NO_3)_2$ as the coagulating electrolyte (Fig. 2). The decrease of coagulation values with increasing concentration of stabilizing ions was even more pronounced than with KNO_3.

Additional experiments were carried out using hydrobromic acid instead of potassium bromide but no influence of the acidity of the medium could be detected (Figs. 1 and 2). This is in agreement with our previous results for acetone and dioxane solutions.[6]

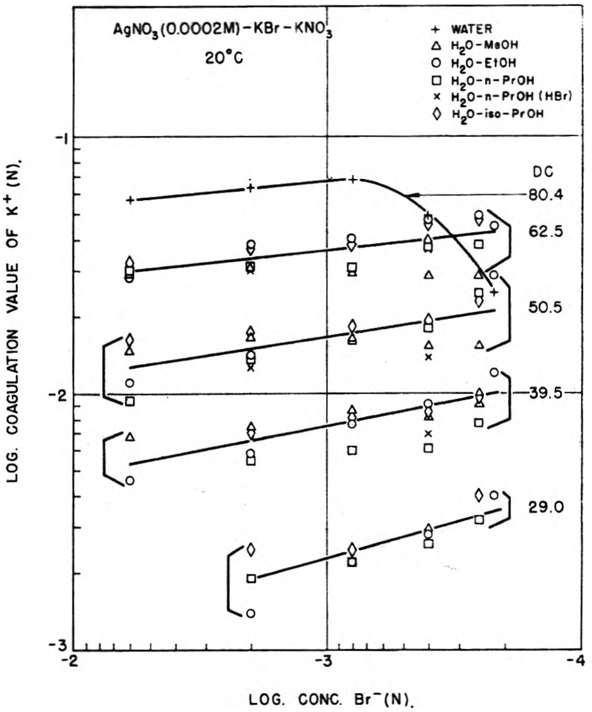

Fig. 1.—Critical coagulation concentrations of K^+ (from KNO_3 and KBr) *vs.* log concentration of Br^-. In water–ethanol mixtures (circles) HBr was used instead of KBr as stabilizing electrolyte.

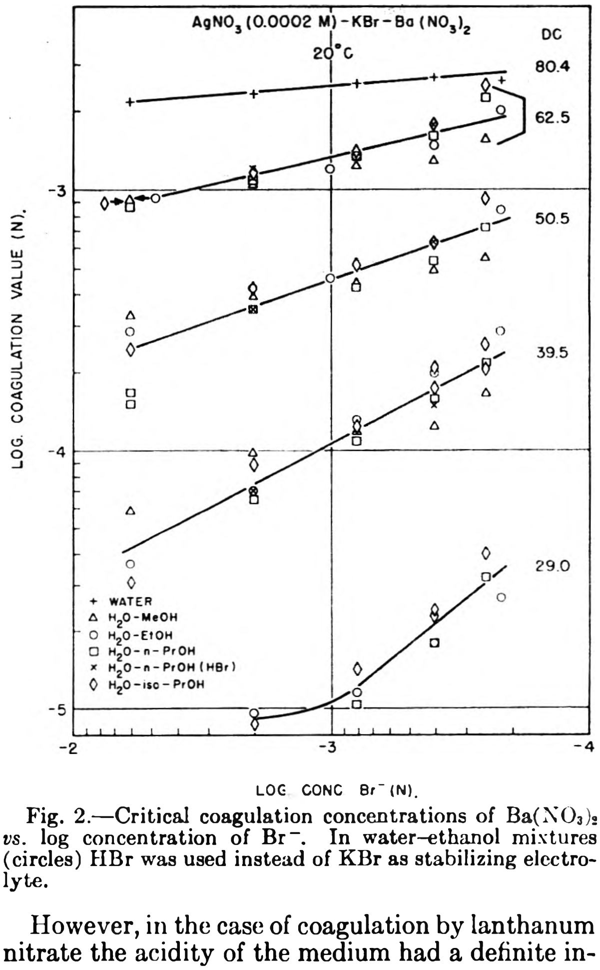

Fig. 2.—Critical coagulation concentrations of $Ba(NO_3)_2$ *vs.* log concentration of Br^-. In water–ethanol mixtures (circles) HBr was used instead of KBr as stabilizing electrolyte.

However, in the case of coagulation by lanthanum nitrate the acidity of the medium had a definite in-

---

[9] B. Težak, E. Matijević, K. F. Schulz, R. Halassy and I. Kostinčer, *Proc. Int. Conf. Surface Activity*, **3**, 607 (1957).

[10] E. Matijević, K. F. Schulz and B. Težak, *Croat. Chem. Acta*, **28**, 81 (1956).

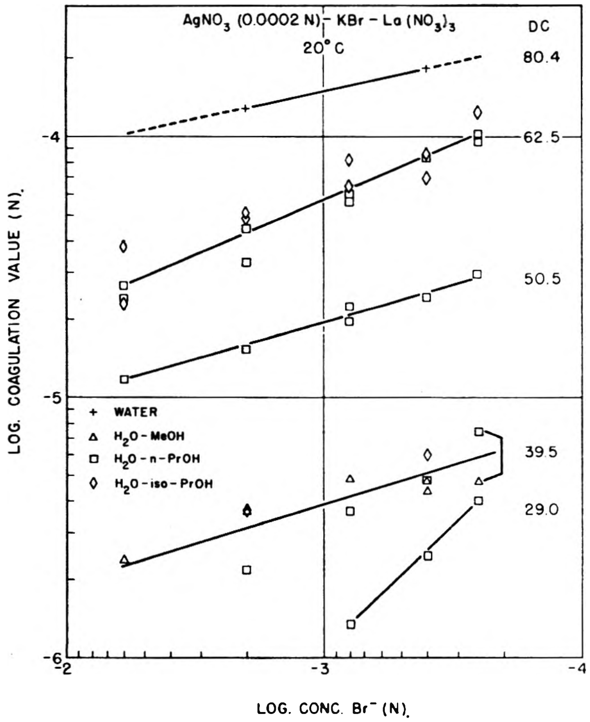

Fig. 3.—Critical coagulation concentrations of $La(NO_3)_3$ *vs.* log concentration of Br^- (from KBr.)

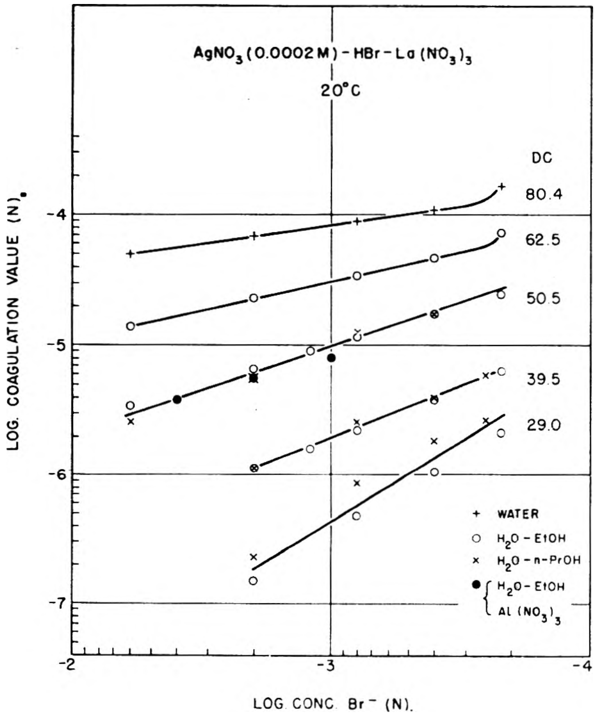

Fig. 4.—Critical coagulation concentrations of $La(NO_3)_3$ *vs.* log concentration of Br^- (from HBr). Full circles denote the values for $Al(NO_3)_3$.

fluence as can be seen when Figs. 3 and 4 are compared. Coagulation values were always smaller for acid solutions irrespective of the DC of the medium. Since lanthanum is a polyvalent ion susceptible to hydrolysis, the coagulation values obtained in acidic solutions should be accepted as representative for the unhydrolyzed ion. In solutions of higher *p*H the hydrolytic products have a smaller charge and hence a lower coagulation ability. It has been shown recently that coagulation effects can be utilized successfully in detecting such hydrolysis processes.[11] Otherwise, the effects of lanthanum nitrate on coagulation in mixed solvents resemble those of KNO_3 and $Ba(NO_3)_2$.

Some measurements with $Al(NO_3)_3$ in water-ethanol mixture (DC 50.5) in acid solutions were performed and the results included in Fig. 4. It can be seen that there is no difference in coagulation values as compared to $La(NO_3)_3$.

Discussion

Although many papers have been published dealing with the influence of solvents on coagulation of lyophobic colloids (see *e.g.*, literature surveys given by Ostwald, *et al.*,[12] and Kratohvil[13]), the situation in this field leaves much to be desired. This is partly due to the lack of systematic investigations using media of a wide range of dielectric constants. In addition, the sols used were frequently not too well defined and were poorly reproducible, and the experimental techniques used in observing the coagulation process were very crude.

It also should be emphasized that the results from the literature indicate the need for distinguishing between the coagulation in the presence of relatively large amounts of organic solvents, where DC is changed considerably and coagulation in the presence of small quantities of added organic compounds (non-electrolytes), especially if the latter have pronounced properties as surface-active agents. This distinction is not always realized leading sometimes to rather obscure conclusions (see *e.g.*, Kruyt,[14] p. 332). In addition, very little emphasis is given to hydrolysis and complexing effects of counterions in various mixed solvents.[11,15]

Our results reported here combined with those published previously should give a clearer picture of the phenomena involved when coagulation of lyophobic sols is performed in mixed solvents. We wish to emphasize some characteristics of our experimental investigations: (a) use of well-defined sols (at least in regard to stoichiometric composition, exactness, ease and reproducibility of their preparation); (b) suitable and reliable method for following coagulation processes; (c) unambiguous criteria in determination of coagulation values, based on the analysis of kinetics of coagulation; (d) very wide range of composition and properties of solvent.

Data from the literature, dealing with additives which cause considerable change of DC, all indicate the same general correlation between coagulation value and DC as predicted by coagulation theories.[3,5,12,16–19] Present results are also in quali-

---

[11] E. Matijević, M. B. Abramson, K. F. Schulz and M. Kerker, This Journal, **64**, 1157 (1960).

[12] Wo. Ostwald, H. Kokkoros and K. Hoffmann, *Kolloid-Z.*, **81**, 48 (1937).

[13] J. Kratohvil, Ph.D. Thesis, University of Zagreb, 1954.

[14] H. R. Kruyt, "Colloid Science," Vol. I, Amsterdam, 1952.

[15] B. Težak, E. Matijević, J. Kratohvil and H. Füredi, *Proc. Symp. Co-ordination Chem.*, Copenhagen, 1953, p. 92.

[16] B. Derjaguin and L. Landau, *Acta Physicochim.*, *U.S.S.R.*, **14**, 633 (1941).

[17] E. J. Verwey and J. Th. G. Overbeek, "Theory of the Stability of Lyophobic Colloids," New York, N. Y., 1948.

[18] E. L. Mackor, *Rec. trav. chim.*, **70**, 841 (1951).

[19] B. Težak, *Arhiv kem.*, **22**, 26 (1950).

tative agreement with such theoretical predictions. The quantitative comparison of various theoretical requirements with our experimental results in different solvents was extensively treated in previous papers.[5,6]

It has been shown[6] that Ostwald's theory of constant activity coefficients[12] could not be successfully applied to our results. Since the main postulate of Ostwald's theory may be directly derived from the Derjaguin–Landau–Verwey–Overbeek theory (D-L-V-O),[16,20] one could infer also the inapplicability of the latter theory. In fact, neither exact nor approximate check of D-L-V-O theory is possible. The coagulation values should be proportional to the third power of the DC of medium. However, the expression which defines the coagulation value contains besides the DC two other quantities which should change when the composition and properties of the solvent is changed. These are the attraction constant A of long-range van der Waals–London forces and the Stern potential of the double layer, ψ_δ. Nothing is known about the values of constant A when medium is changing (the values for vacuum or air as medium, measured or calculated, may differ as much as four orders of magnitude[21–24]), while the Stern potential is not measurable by a direct experimental method.[25] The evaluation of this potential by indirect methods, is not a very reliable procedure,[18,26] and to carry this out for a large number of solvent mixtures would be a formidable task, if possible at all.

However, it should be emphasized that the decrease of coagulation values with the increase of the concentration of stabilizing ions in solution, observed in our experiments for all counterions and all solvent mixtures used, is completely inconsistent with the D-L-V-O theory. In fact, the contrary was to be expected (*cf.* ref. 17, Fig. 31, p. 120).

We have shown previously,[2–6] following the reasoning by Težak,[5,19] that there exists a good linear correlation between the logarithms of coagulation values and the critical distance for the formation of ionic pairs (Bjerrum's distance) as given by the expression ${}_cd = z_1z_2e^2/2DkT$, where z_1 and z_2 denote the ionic charge of the coagulating and stabilizing ions, respectively, e is the elementary electric charge, D is the dielectric constant of the medium, k Boltzmann constant and T absolute temperature. Since DC is widely varied in our experiments, the calculated Bjerrum's distances change considerably (from 3.7 to 28 Å.). A typical plot is represented in Fig. 5, where the coagulation values at one concentration of Br⁻ (0.0004 N) are used. The linear trend is obvious for all three counterions over the whole range of DC, except at DC lower than 39.5 for lanthanum ion as coagulant. Coagulation ability of polyvalent ions in media of lower DC was discussed in a previous paper.[15] The linear correlation between the logarithm of coagulation value and Bjerrum's distance was even better for systems with higher concentrations of bromide ions.

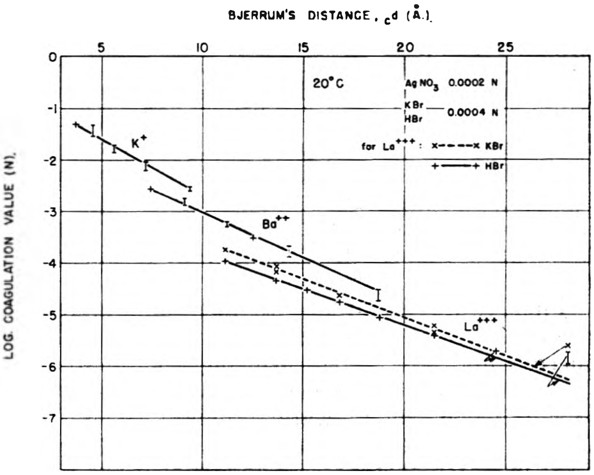

Fig. 5.—Critical coagulation concentrations *vs.* Bjerrum's distance for various values of the dielectric constant. The data for various isodielectric mixtures fall within short vertical lines.

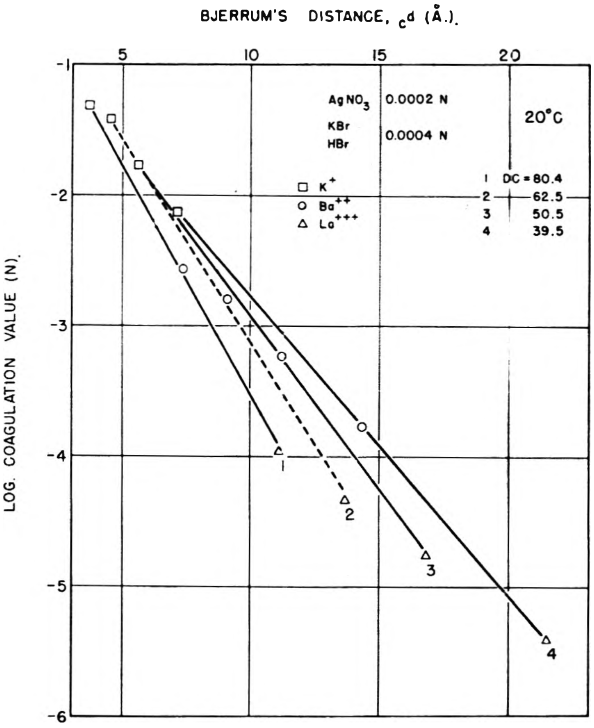

Fig. 6.—Critical coagulation concentrations *vs.* Bjerrum's distance as they change with the valency of counterions for several dielectric constants. The points denote the mean values of coagulation concentrations for various isodielectric mixtures.

Težak's conception may be tested in another way, *i.e.*, by plotting the logarithm of coagulation value *versus* Bjerrum's distance as it changes with the charge of counterions at constant value of DC. This is illustrated in Fig. 6, using the same data as in Fig. 5. Again the linearity is obtained as required. It was shown, previously, that the same linear relationship was also obtained using other solvents (water–glycine, water, water–acetone, water–dioxane) and the same silver halide sol.[5] However, when solvents of basically different

---

(20) V. B. Vouk, *Nature*, **170**, 762 (1952).

(21) J. Th. G. Overbeek and M. J. Sparnaay, *Disc. Faraday Soc.*, **18**, 12 (1954).

(22) B. V. Derjaguin and I. I. Abricossova, *ibid.*, **18**, 24 (1954).

(23) B. V. Derjaguin, I. I. Abricossova and E. M. Lifshitz, *Quart. Revs. (London)*, **10**, 295 (1956).

(24) A. P. Prosser and J. A. Kitchener, *Nature*, **178**, 1339 (1956).

(25) M. Mirnik, *Disc. Faraday Soc.*, **18**, 204, 207 (1954).

(26) H. Reerink and J. Th. G. Overbeek, *ibid.*, **18**, 74 (1954).

chemical constitution were employed (such as alcohols, ketones, etc.) the straight lines obtained in "Bjerrum's distance–coagulation concentration" plots for the same DC did not coincide, clearly indicating specific effects in addition to the major effect of the DC. In our present paper all data for a series of solvents of homologous chemical composition (all alcohols) gave one single straight line. Therefore, the DC should be considered as the dominating factor when the solvent is changed if the specific factors are eliminated.

Finally, we would like to mention that results of other investigators using different sols could be successfully interpreted utilizing the ion-pairing concept. This was shown for results of Ostwald, *et al.*[12] (As_2S_3 sol in water–ethanol), Weiser and Mack[27] (HgS sol in water–propanol) and Mackor[18] (AgI in water–acetone). The fact that the results for several different sols over a wide range of dielectric constant (from 126 to 29) and through a concentration range of counterions from about 10^{-1} to nearly 10^{-7} N could be interpreted in the same way is quite striking.

Acknowledgment.—We wish to record our thanks to Professor Božo Težak for his interest in this work.

DISCUSSION

VICTOR K. LA MER (Columbia University).—Between what ions is the Bjerrum distance calculated? What is the meaning? Does it not amount to plotting against $1/D$?

J. P. KRATOHVIL (National Research Council).—The Bjerrum distance was calculated for the stabilizing ion (Br^-)–counter ion (K^+, Ba^{++}, La^{+++}) pair. The diagram corresponds to a $1/D$ plot.

J. TH. G. OVERBEEK (University of Utrecht).—The fact that the slope of the lines representing the relation between log of the coagulating concentration and valency is not identical to the slope between log C and $1/D$ shows that the Bjerrum distance is not the only determining factor in these cases.

E. MATIJEVIĆ.—We certainly agree that the Bjerrum plot is the first approximation. This also follows from the fact that isodielectric mixtures of water with solvents of different chemical composition give different coagulation values for the same sols and same counter ions. However, it is obvious that this plot fits experimental data quite well.

J. TH. G. OVERBEEK.—The increase in coagulation value with decrease of Br^- concentration may be related to the reduced supersaturation of AgBr which leads to fewer and larger particles. Larger particles would have a higher energy barrier and the smaller number would lead to slower coagulation kinetics, both factors leading to higher concentration for coagulation.

E. MATIJEVIĆ.—We firmly believe that the decrease of the coagulation concentration with increase of the concentration of stabilizing ion is a general effect. We have found it with all silver halide sols. In addition, under comparable experimental conditions, the coagulation values for trivalent ions are the lowest for the AgI sol and the highest for AgCl sol. As is well known, the AgI is the least soluble silver halide.

---

[27] H. B. Weiser and G. L. Mack, THIS JOURNAL, 34, 101 (1930).

NON-IONIC SURFACE-ACTIVE COMPOUNDS. III. EFFECT OF STRUCTURE ON MICELLE FORMATION IN BENZENE SOLUTION

BY PAUL BECHER

Chemical Research Department, Atlas Powder Co., Wilmington, Del.

Received March 7, 1960

Light scattering measurements have been used to determine micellar properties of several pure non-ionic compounds, including the four isomeric isohexide monostearates and polyoxyethylene glycol ethers of dodecanol and tridecanol. In the case of the stearate esters the presence of an endo-ester group appears to be necessary for micelle formation; data on the alcohol derivatives seem to indicate that the geometry of the groups which make up the interior of the micelle is more significant structurally than that of the lipophilic heads.

One of the problems associated with the study of the surface properties of non-ionic compounds is the fact that many of these materials, as prepared commercially, are heterogeneous mixtures of homologous compounds. Nonetheless, as shown in previous papers in this series,[1] and as will be demonstrated in subsequent papers, a great deal of useful information may be obtained from the study of such compounds. On the other hand, it is necessary to check conclusions drawn from such data by reference to measurements on reasonably pure, well-characterized compounds.

The present study concerns itself with the behavior of the four isomeric monostearate esters of the dianhydro-hexitols, and with that of polyethylene glycol ethers of dodecanol and tridecanol. The ether-alcohols studied were the pure hexaethylene glycol ether of *n*-tridecanol, the hexaethylene glycol ether of tridecyl (Oxo-process) alcohol, the monoethylene glycol ether of *n*-dodecanol, and the diethylene glycol of *n*-dodecanol. In addition, the corresponding commercial compounds, *i.e.*, polyoxyethylene (6) tridecyl alcohol, polyoxyethylene (1) lauryl alcohol, and polyoxyethylene (2) lauryl alcohol also were studied.[2] Micelle formation was observed by means of light scattering measurements in benzene solution.

Experimental

Materials.—The preparation of the pure compounds will be described elsewhere. The isohexide esters were of not less than 98% purity (based on saponification equivalent), except that the isosorbide mono(endo)stearate may have contained up to 10% of the exo-ester, as indicated by the infrared spectrum. The purity of the ethers of *n*-tridecanol and *n*-dodecanol was better than 96% (based on hydroxyl number); that of the hexaethylene glycol ether of tridecyl alcohol was about 92%. The commercial materials were used as received.

All solutions were made up volumetrically in freshly-distilled reagent grade benzene, and reagent grade iodine was used in the determination of the critical micelle concentrations by the method of Ross and Olivier.[3]

Methods.—The light scattering measurements were carried out in a conventional Brice–Phoenix Light Scattering Photometer[4] using the standard 40 × 40 × 120 mm. semioctagonal cell. Measurements were carried out at 435 mμ. All solutions were clarified by pressure filtration under dry nitrogen through a Corning UF (ultrafine) sintered glass disc. The usual precautions to exclude dust and other extraneous matter were taken.

Refractive index increments were measured with a Phoenix Automatic Recording Differential Refractometer.[4] The values found are listed in the last column of Table I.

TABLE I

MICELLAR PROPERTIES IN BENZENE SOLUTION

Compound	c_0 (g./dl.)	M_m	n	dn/dc (ml./g.)
Isosorbide mono(exo)stearate	None	....	..	−0.0503
Isosorbide mono(endo)stearate	0.51	14,300	35	− .0344
Isomannide monostearate	0.35	9,000	22	− .0433
Isoidide monostearate	None	....	..	− .0414
Monoethylene glycol *n*-dodecanol ether	None	....	..	− .0975
Diethylene glycol *n*-dodecanol ether	0.22	9,800	34	− .0595
Polyoxyethylene (1) lauryl alcohol	None	....	..	− .0862
Polyoxyethylene (2) lauryl alcohol	0.10	20,900	73	− .0745
Hexaethylene glycol *n*-tridecanol ether	0.12	45,500	99	− .0531
Hexaethylene glycol tridecyl alcohol ether	0.13	45,100	98	− .0542
Polyoxyethylene (6) tridecyl alcohol	0.27	12,000	26	− .0566

In this connection, it should be noted that the measurements reported herein cannot be considered to be of the highest precision, both because of the low solute turbidity and the low refractive index increment. However, it is probable that the values are correct to within ±10%.

Results

In agreement with the data of previous workers on monoglyceride esters,[5] the monoesters form only relatively small micelles, when, indeed, any micelles are formed at all. However, when micelles are formed they tend to be somewhat bigger than those of the monoglycerides, for reasons which will be apparent from the subsequent discussion.

The critical micelle concentrations (c_0), micellar molecular weights (M_m), aggregation numbers (n), and refractive index increments (dn/dc) for the various compounds studied are given in Table I. As can be seen, no evidence for micelle formation is found for the isosorbide mono(exo)stearate and the isoidide monostearate esters, as well as for the comparable monoethylene glycol ether of *n*-dodecanol and the polyoxyethylene (1) lauryl alcohol, at least up to the maximum concentration studied, *i.e.*, 1.20 g./dl.[6]

---

(1) (a) P. Becher, THIS JOURNAL, 63, 1675 (1959); (b) P. Becher and N. K. Clifton, *J. Colloid Sci.*, 14, 519 (1959).

(2) Although the implication of our nomenclature should be clear, it is perhaps well to define it exactly. The term "hexaethylene glycol ether-" implies the derivative of a polyoxyethylene chain containing *exactly* six units, while the term "polyoxyethylene (6)-" implies a polyoxyethylene chain containing an average of six units. Similarly, the use of the terms "*n*-dodecanol, *n*-tridecanol" implies the straight 12- or 13- carbon alcohol in the highest purity obtainable, while "lauryl, tridecyl" implies the commercial material obtainable under that designation.

(3) S. Ross and J. P. Olivier, THIS JOURNAL, 63, 1671 (1959).

(4) Phoenix Precision Instrument Co., Philadelphia, Pa.

(5) P. Debye and W. Prins, *J. Colloid Sci.*, 13, 86 (1958).

(6) There is some indication, based on rough iodine solubilization observations, that some micelle formation may occur with at least the esters at very high concentrations, *e.g.*, about 10 g./dl.

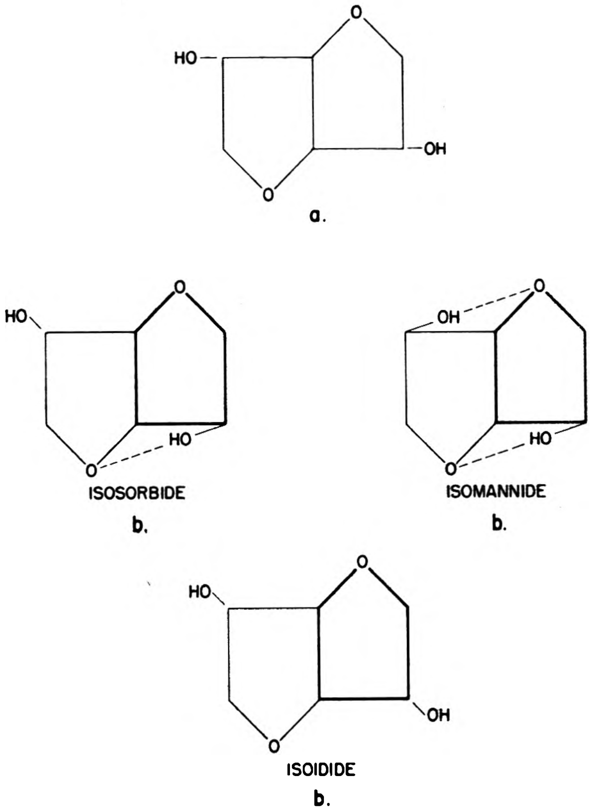

Fig. 1.—(a) Fischer projection formula of 1,4:3,6-dianhydrohexitol. (b) The three possible types of orientation of the hydroxyls in dianhydrohexitols. The ring drawn with the light lines is to be thought of as being in the plane of the paper; the ring drawn with heavy lines is tilted slightly out of the plane of the paper. Only the endo-hydroxyls can form hydrogen bonds (indicated by dashed lines).

The light scattering data show no appreciable dissymmetry, and the slope of the Hc/τ *vs.* c plot is in all cases zero, corresponding to a second virial coefficient of zero. This is consistent with the small size of the micelles.

Discussion

The 1,4:3,6-dianhydrides of the isomeric hexitols, D-glucitol (sorbitol), D-mannitol and L-iditol have the general structure indicated by the projection formula of Fig. 1a. However, the structure so portrayed is insufficient to indicate the difference in symmetry exhibited by these compounds. The fused tetrahydrofuran rings are *cis*-oriented, *i.e.*, they are not coplanar but folded toward each other. A representation of this is attempted in Fig. 1b, where the ring drawn with the lighter lines (the 1,4-ring) is to be thought of as in the plane of the paper, while the ring drawn with heavy lines (the 3,6-ring) is to be imagined as tilting slightly up out of the paper plane.

It follows that the hydroxyl groups may be oriented into the fold between the two rings (endo-hydroxyl) or out of the fold (exo-hydroxyl). It thus turns out that in the case of isosorbide (1,4:3,6-dianhydro-D-glucitol) there exists one exo-hydroxyl (the 2-hydroxyl of the hexitol), and one endo-hydroxyl. Isomannide (1,4:3,6-dianhydro-D-mannitol) has both hydroxyls endo-oriented; while isoidide (1,4:3,6-dianhydro-L-iditol) has two exo-hydroxyls.

It should be noted that the endo-hydroxyl may form a hydrogen bond to the ether ring-oxygen of the opposite ring, which is sterically impossible for the exo-hydroxyl. The possibility of hydrogen-bond formation is indicated by the presence of dashed lines in the structures of Fig. 1b.

From these considerations, it appears that four isomeric monoesters of the three isohexides can be prepared, *i.e.*, two isomeric isosorbide esters, and one each for the other isohexides. It is thus possible to investigate the effect of the endo- or exo-nature of the free hydroxyl, and, by the same token, the effect of the position of the ester linkage, on the micellar properties of these compounds.

If we consider that the presence of c.m.c. and the consequent formation of micelles is evidence of surface activity, we can attempt to correlate the presence or absence of surface activity with the various structural factors. This is done in Table II, where a plus sign indicates the presence of the property and a minus sign the absence.

TABLE II

RELATION BETWEEN STRUCTURAL FACTORS AND MICELLAR ACTIVITY

Compound	Micelle former	Hydroxyl Exo	Hydroxyl Endo	Ester Exo	Ester Endo	Free OH H-bonded
Isosorbide mono(exo)-stearate	−	−	+	+	−	+
Isosorbide mono(endo)-stearate	+	+	−	−	+	−
Isomannide monostearate	+	−	+	−	+	+
Isoidide monostearate	−	+	−	+	−	−

We might suppose that an exo-hydroxyl would confer a slightly more hydrophilic character to the hydrophilic moiety of the molecule, than the endo-hydroxyl, since the latter is inside the fold of the rings, and is hydrogen-bonded in addition. Whether or not this is correct, the *a priori* assumption that this might be the controlling factor in determining surface activity is shown to be false by the data of Table II. In fact, examination of these data leads to the somewhat surprising conclusion that it is only the presence of the ester linkage at an endo-hydroxyl that leads to surface activity.

It might be pointed out that if the free exo-hydroxyl does in fact make a small contribution to the hydrophilic character of the molecule, the isosorbide mono(endo)stearate should be slightly more surface active than the isomannide ester. This would appear to be the case, but the data are probably insufficiently precise to be certain.

The fact that a hydroxyl group apparently is less hydrophilic than an ether-oxygen would perhaps serve to explain the smaller micelles formed by monoglyceride stearates[5] where the total hydrophilic contribution comes from the presence of these groups.

The data for the *n*-dodecanol derivatives offer little in the way of interpretative difficulty. Obviously, the addition of one mole of ethylene oxide contributes so little in the nature of hydrophilic properties that solubility in benzene remains unaffected and no micelle formation occurs. On the other hand, the addition of the second ethylene oxide group, to form the diethylene glycol ether, produces a molecule in which the hydrophile-lipophile nature is such that micelle formation is necessary in order to maintain solubility.

The same general observations apply to the commercial, heterogeneous, lauryl alcohol derivatives. However, there is a considerable difference between the c.m.c. and micellar molecular weight of the diethylene glycol ether of *n*-dodecanol and of the polyoxyethylene (2) lauryl alcohol.

From these data, it would appear as though the polyoxyethylene (2) lauryl alcohol behaves as though it were less lipophilic than the corresponding pure compound. Evidently, the effect of the molecules on the high side of the distribution on micellar behavior is less than those on the low side.

The data on the tridecanol derivatives cast some light on the effect of structure also. For example, virtually identical results are obtained with the hexaethylene glycol ethers of the *n*-tridecanol and of the Oxo-process tridecyl alcohol. This occurs in spite of the fact that the Oxo-process material is highly branched, and thus has an effective chain-length much lower than the straight-chain material, an effect which shows up, for example, in the critical micelle concentrations of the water-soluble derivatives.[1a] It would thus appear that, all other things being equal, the size of the micelle is largely dictated by the properties of the solvophobic portion of the molecule, which makes up the micelle interior.

If we now compare the data on the hexaethylene glycol ethers with that on the polyoxyethylene (6) tridecyl alcohol, however, significant difference arises, not only among the homologs, but with respect to the dodecanol derivatives.

As opposed to the dodecanol derivatives, the polyoxyethylene (6) tridecyl alcohol appears to be *more* lipophilic than the corresponding homogeneous compounds. Consequently, it may be concluded that here the compounds of *lower* ethylene oxide content have the controlling effect on micelle formation.

In fact, it is this sort of effect, rather than the opposite effect found with the lauryl alcohol derivatives, that would be expected. If we assume, with Flory,[7] that the distribution of ethylene oxide chain lengths is represented by the Poisson law, the curve is skewed so that more than half of the product (in terms of mole fraction) is at a chain length lower than the nominal one.

Thus, for example, more than 60 mole % of the product has a chain-length of six or lower in a polyoxyethylene (6)-compound. On the other hand, it should be pointed out that 75 mole % of the polyoxyethylene (2)-compound is in this condition.

The difference, however, is that more than half of this 75 mole % is composed of polyoxyethylene (0)- and polyoxyethylene (1)-compounds which have little or no contribution to make to the surface activity in this solvent. Hence, they act as mere diluents, and the *effective* chain length is thus much higher. In the case of polyoxyethylene (6)-compounds, this diluent is no more than one or two per cent.

At much higher polyoxyethylene chain lengths, from the nature of the Poisson distribution, very little difference in behavior between the compounds of exact composition and average composition would be expected.

Acknowledgments.—The author gratefully acknowledges the work done in the preparation of the pure compounds by Dr. L. W. Wright, and Messrs. L. Hartmann, R. H. Hunter, R. H. Varland and M. J. Megraw of the Atlas Powder Company, and Dr. W. A. Mosher of the University of Delaware. The light scattering measurements were carried out by Mrs. Nancy Clifton Soistmann.

DISCUSSION

DAVID B. FORDYCE (Rohm and Haas Co.).—How were the hexaethylene glycol derivatives prepared?

PAUL BECHER.—Pure tetraethylene glycol was converted to hexaethylene glycol by a Williamson ether synthesis, and the glycol coupled to the alcohol in precisely the same way.

DONALD G. DOBAY (B. F. Goodrich Company).—Can you comment on any work you may have done on the relation between the size of micelles in different solvents?

PAUL BECHER.—At the moment we have no such data. Compounds in this marginal solubility range are quite difficult to work with. I don't think there is any reason to expect a simple correlation.

G. M. GANTZ (General Aniline and Film Corporation).—Was there much lauryl alcohol in the 2 mol commercial product?

PAUL BECHER.—The commercial product contained about 75% of alcohol plus 1 mol product.

---

[7] P. J. Flory, "Principles of Polymer Chemistry," Cornell University Press, Ithaca, N. Y., 1953, pp. 336–339.

EQUILIBRIUM CONSTANTS FOR THE FORMATION OF POLYNUCLEAR TRIDENTATE 1:1 CHELATES IN URANYL–MALATE, –CITRATE AND –TARTRATE SYSTEMS[1]

By Isaac Feldman, Carol A. North and Hugh B. Hunter

Division of Radiation Chemistry and Toxicology, Department of Radiation Biology, School of Medicine and Dentistry, University of Rochester, Rochester, N. Y.

Received October 22, 1959

*p*H titrations have been analyzed to determine the over-all dimerization constants K_{III} and the trimerization constants K_{Tr} for the tridentate 1:1 chelates in the uranyl–malate, –citrate and –*d*-tartrate systems at 25°. For these three systems, respectively, log K_{III} was found to be 7.76, 7.68 and 5.54 (±0.04 in each case) at $\mu = 0.136$ and 9.08, 9.04 and 6.76 (±*ca.* 0.05) at infinite dilution. At $\mu = 0.20$, pK_{Tr} was 10.56 ± 0.05 for the uranyl–malate system and 9.7 ± 0.12 for the uranyl–*d*-tartrate system. The unexpected increase in the tendency of uranium to polymerize after tridentate chelation is explained on the basis of decreased 5f orbital participation in the uranium to oxygen bonds of the uranyl entity as a result of deformation of the normally-collinear uranyl entity. The fact that relative to the uranyl–malate system the uranyl–*d*-tartrate system has a lower K_{III} but higher K_{Tr} is believed due to more hydrogen bonding plus greater inductive effect in the tartrate ion than in malate ion. In accord with these hypotheses, the equimolar uranyl–*meso*-tartrate system seems to contain a mixture of unhydrolyzed mononuclear bidentate chelate and olated binuclear tridentate chelate.

In previous studies[2] on the reaction of uranyl nitrate with *l*-malic, *d*-tartaric and citric acids the following conclusions were reached: (i) in equimolar systems, and also in excess carboxylic acid, each of these α-hydroxy polycarboxylic acids reacts with uranyl ion in the *p*H range 2–4 to form predominantly binuclear 1:1 tridentate chelates. The chelation involves two carboxylate groups and one alcoholic OH. (ii) At about *p*H 4 these dimers begin to react further until at about *p*H 7 the chelates, although still tridentate, are entirely in the trinuclear state. The trinuclear system is a mixture of *3:3* and *2:3* chelates.[3] The trimers lose their alcoholic hydrogen atoms by *p*H 7.

In the present paper *p*H titrations have been analyzed to determine the equilibrium constants for the formation of the three binuclear tridentate chelates and for the reaction of two, the uranyl–malate and the uranyl–*d*-tartrate dimers, to form the *3:3* trimers.

Experimental

Materials.—The chemicals used were: Mallinckrodt AR citric acid, *d*-tartaric acid, potassium nitrate and uranyl nitrate; Eastman white label *l*-malic acid, and Aldrich Chemical Company *l*- and *meso*-tartaric acids, and *d*-malic acid. The uranyl nitrate stock solution was standardized gravimetrically by ignition to U_3O_8. All carboxylic acids were standardized by titration. All solutions were prepared under nitrogen with boiled deionized water.

Methods.—The experimental technique involved pointwise titrations. Standardized CO_2-free sodium hydroxide was added dropwise slowly from a buret to mixtures of uranyl nitrate and carboxylic acids in volumetric flasks, each flask being shaken constantly by hand during this addition of base. Necessary amounts of potassium nitrate solution were added to furnish the desired ionic strength and solutions were brought to final volume with boiled deionized water. Aliquots of these original mixtures were diluted with potassium nitrate solutions of the proper concentration to give solutions of various total uranium concentrations. Solutions were shaken and then stored two to four days in the dark at 25 ± 0.5° in a constant-temperature room, after which *p*H readings were taken in the same room using a Beckman Model G *p*H meter. The storing time was sufficient to ensure equilibrium.

The electrode system was calibrated in terms of *p*cH (= −log hydrogen ion concentration) with standard $HClO_4$ solutions below *p*H 4 and with acetate buffers above *p*H 4. These calibrations were performed at the various ionic strengths of interest, using potassium nitrate as an inert salt. Solutions were kept under a nitrogen atmosphere at all times, including during *p*H measurement.

Results

Dissociation Constants of Carboxylic Acids.—Determination of equilibrium constants for the uranyl nitrate–carboxylic acid systems required knowledge of the dissociation constants of the carboxylic acids in terms of concentration units at ionic strengths prevailing in this study. Application of the Debye–Hückel equation to the apparent constants of Bates, *et al.*,[5,6] using their values for the ion-size parameter gives concentration constants pK_1 and pK_2, respectively, of 2.85 and 4.32 for citric acid and 2.82 and 3.94 for *d*-tartaric acid at an ionic strength of 0.136.

The concentration constants for malic acid and *meso*-tartaric acid at μ of 0.136 ± 0.003 were determined by the method described by Edsall and Wyman.[7] In this method *p*cH values were measured for a series of buffer solutions prepared by adding varying amounts of CO_2-free sodium hydroxide to a constant concentration of carboxylic acid, the ionic strength being kept approximately constant by addition of potassium nitrate. The applicable equation is[7]

---

[1] This paper is based on work performed under contract with the United States Atomic Energy Commission at the University of Rochester Atomic Energy Project, Rochester, New York.

[2] (a) I. Feldman and W. F. Neuman, *J. Am. Chem. Soc.*, **73**, 2312 (1951); (b) W. F. Neuman, J. R. Havill and I. Feldman, *ibid.*, **73**, 3593 (1951); (c) I. Feldman and J. R. Havill, *ibid.*, **76**, 2114 (1954); (d) I. Feldman, J. R. Havill and W. F. Neuman, *ibid.*, **76**, 4726 (1954).

[3] In this paper, ligand/uranium ratios are employed in accord with the well-accepted suggestions of Fernelius, *et al.*[4] In our previous papers[2] the reciprocals (U/ligand) were used. However, as in the preceding paper,[2d] a ratio in arabic numerals has *no significance* with regard to the polymeric state of a complex. The polymeric state is indicated by ratios in italics. Furthermore, for the sake of simplicity the polynuclear chelates will be referred to by the common uranyl-ligand name, such as "uranyl-citrate" dimer, despite the fact that they are all anionic. Conformity to rigidly-correct nomenclature[4] would require very frequent use of lengthy names such as: bis-(monohydrogencitrate)-μ-diol-dioxouranium(VI) ion.

[4] W. C. Fernelius, E. M. Larsen, L. E. Marchi and C. L. Rollinson, *Chem. Eng. News*, **26**, 520 (1948).

[5] R. G. Bates and G. D. Pinching, *J. Am. Chem. Soc.*, **71**, 1274 (1949).

[6] R. G. Bates and R. G. Canham, *J. Research Natl. Bur. Standards*, **47**, 343 (1951).

[7] J. T. Edsall and J. Wyman, "Biophysical Chemistry," Vol. 1, Academic Press, Inc., New York N. Y., 1958, pp. 479–482.

$$\bar{h} = \frac{(\mathrm{H}^+) + B}{T} = \left[\frac{K_1}{(\mathrm{H}^+)} + \frac{2K_1K_2}{(\mathrm{H}^+)^2}\right] \div \left[1 + \frac{K_1}{(\mathrm{H}^+)} + \frac{K_1K_2}{(\mathrm{H}^+)^2}\right]$$

where $(\mathrm{H}^+) = 10^{-p\mathrm{cH}}$, B = concentration which added base would have if there were no reaction, and T = total concentration of carboxylic acid.

Table I represents the titration of *meso*-tartaric acid, from which pK_1 and pK_2 were calculated to be 2.99 ± 0.02 and 4.44 ± 0.03, respectively, at $\mu = 0.133 \pm 0.003$. The same procedure yielded pK_1 and pK_2 values of 3.15 ± 0.04 and 4.68 ± 0.02 for *l*-malic acid and 2.81 ± 0.04 and 3.95 ± 0.02 for *d*-tartaric acid. As expected, identical titration curves were obtained for *d*- and *l*-malic acid and for *d* and *l*-tartaric acid. As an indication of the reliability of these constants, the *d*-tartaric acid pK's may be compared with those of Bates, *et al.*, cited above. No literature values seem to exist with which the *meso*-tartaric acid and malic acid values can be compared at $\mu = 0.136$.

TABLE I

DISSOCIATION CONSTANTS OF *meso*-TARTARIC ACID

$T = 0.04275M$; temp. = 25 ± 0.5°; $\mu = 0.133 \pm 0.003$

$B \times 10^3$	pcH	$\bar{h}$	$pK_1{}^a$	$pK_2{}^b$
1.022	2.70	0.3528	3.001	4.27[d]
2.043	2.81	.4201	2.976	4.24[d]
4.086	3.06	.5798	2.963	4.33[d]
6.129	3.36	.7679	3.007	4.477
8.172	3.68	.9802	3.011	4.430
10.215	4.02	1.2058	2.997	4.416
12.462	4.40	1.4622	3.131[c]	4.415
14.301	4.74	1.6747	...	4.404
16.344	5.49	1.9119	...	4.472
		Av.	2.99 ± 0.02	4.44 ± 0.03

[a] pK_1 values calculated from successive $\bar{h}$ pairs. [b] pK_2 values calculated from each $\bar{h}$ using average pK_1. [c] This value ignored since $(\mathrm{H_2X})$ = only 2% of T. [d] These values ignored since $(\mathrm{X}^-) \leq$ only 2% of T.

Cannan and Kibrick[8] determined apparent dissociation constants at $\mu = 0.2$ for malic and *dl*-tartaric acids. By subtracting from each apparent constant their value for the negative logarithm of the hydrogen ion activity coefficient, *i.e.*, 0.1, one obtains concentration pK values at $\mu = 0.2$ of 3.16 and 4.58 for malic acid and 2.78 and 3.84 for *dl*-tartaric acid. The latter values were used for *d*-tartaric acid at $\mu = 0.2$.

Dimerization of Tridentate Chelates.—In titration curves, presented in the preceding paper,[2d] for equimolar mixtures of uranyl nitrate with each of the tridentate acids (malic, citric, *d*-tartaric), the first inflection point occurred near pH 3.5 when B/T (ratio of moles of added sodium hydroxide to total number of gram atoms of uranium) was three. This point was believed to represent completion of the formation of the diolated (or oxolated) binuclear chelate.

To investigate the dimerization, eleven solutions were prepared equimolar, 0.01069 M, in uranyl nitrate and carboxylic acid, 0.10 M in potassium nitrate, and containing sodium hydroxide in varying amounts to give B/T from zero to *ca.* 2.6. Aliquots of each of these solutions were then diluted with 0.136 M potassium nitrate to give three more series of solutions having total uranium concentrations of 0.005345, 0.002138 and 0.001069 M. Calculations showed that the ionic strength in each series remained within 0.135 ± 0.002 for each solution. pcH measurements were made after two days.

The concentration equilibrium constant was calculated for each of the 44 solutions for each of three cases

Case I: $\mathrm{UO_2^{++} + X^- \rightleftharpoons UO_2X}$

Case II: $\mathrm{UO_2^{++} + X^- + H_2O \rightleftharpoons UO_2X(OH)^- + H^+}$

Case III: $\mathrm{2UO_2^{++} + 2X^- + 2H_2O \rightleftharpoons Dimer^= + 2H^+}$

Case I.—All parenthetical quantities below represent molar concentrations at equilibrium.

$$(\mathrm{UO_2X}) = \frac{1}{2}\left[(\mathrm{H}^+) + B - (\mathrm{HX}^-) - 2(\mathrm{X}^=)\right] \qquad (1)$$

Ignoring the virtually-negligible hydrolysis of uncomplexed uranyl ion in these solutions,[9] gives

$$(\mathrm{UO_2X}) = T - (\mathrm{UO_2^{++}}) \qquad (2)$$

Since the uranyl ion and the carboxylic acids studied react 1:1 in equimolar solutions at the first inflection point[2a,c]

$$(\mathrm{UO_2^{++}}) = \text{uncomplexed } [(\mathrm{H_2X}) + (\mathrm{HX}^-) + (\mathrm{X}^=)] \qquad (3)$$

Substituting this sum into the term f defined by

$$f = (\mathrm{H_2X})/(\mathrm{UO_2^{++}}) \qquad (4)$$

gives

$$f = \left[1 + \frac{K_1}{(\mathrm{H}^+)} + \frac{K_1K_2}{(\mathrm{H}^+)^2}\right]^{-1} \qquad (5)$$

where K_1 and K_2 are the first and second dissociation constants of the carboxylic acid in molar concentration units.

Combining (1) to (5) gives

$$(\mathrm{UO_2^{++}}) = \frac{2T - (\mathrm{H}^+) - B}{1 + g} \qquad (6)$$

where

$$g = \frac{(\mathrm{H}^+)^2 - K_1K_2}{(\mathrm{H}^+)^2 + K_1(\mathrm{H}^+) + K_1K_2}$$

From (4) and $K_1K_2 = (\mathrm{H}^+)^2(\mathrm{X}^=)/(\mathrm{H_2X})$, one obtains

$$\frac{1}{(\mathrm{X}^=)} = \frac{(\mathrm{H}^+)^2}{K_1K_2f(\mathrm{UO_2^{++}})} \qquad (7)$$

From equations 2 and 7 one can then obtain the equilibrium constant

$$K_{\mathrm{I}} = \frac{(\mathrm{UO_2X})}{(\mathrm{UO_2^{++}})(\mathrm{X}^=)} = \frac{(\mathrm{H}^+)^2(T - (\mathrm{UO_2^{++}}))}{K_1K_2f(\mathrm{UO_2^{++}})^2}$$

Case II.—The calculations for case II differ from those of case I only in that the factor two in the denominator of equation 1 is replaced by the factor three, resulting in (8)

$$(\mathrm{UO_2^{++}}) = \frac{3T - (\mathrm{H}^+) - B}{2 + g} \qquad (8)$$

---

(8) R. K. Cannan and A. Kibrick, *J. Am. Chem. Soc.*, **60**, 2319 (1938).

(9) J. Sutton, *J. Chem. Soc.*, *Suppl. No.* **2**, s275 (1949), gives constant of 1.14×10^{-6} for hydrolysis of $\mathrm{UO_2^{++}}$ to $\mathrm{U_2O_5^{++}}$ at $\mu \cong 0.15$. In each solution less than 0.5% of uncomplexed uranium hydrolyzed, the calculation being made by treating this hydrolysis as a secondary correction to $(\mathrm{UO_2^{++}})$ obtained by equations 6 and 8 below.

Hence

$$K_{\mathrm{II}} = \frac{(\mathrm{H}^+)(\mathrm{UO_2XOH}^-)}{(\mathrm{UO_2}^{++})(\mathrm{X}^=)} = \frac{(\mathrm{H}^+)^3(T - (\mathrm{UO_2}^{++}))}{K_1K_2f(\mathrm{UO_2}^{++})^2}$$

Case III.—For case III

$$2(\mathrm{Dimer}^=) = \frac{1}{3}\,[(\mathrm{H}^+) + B - (\mathrm{HX}^-) - 2(\mathrm{X}^=)] = T - (\mathrm{UO_2}^{++})$$

resulting in equation 8 again. The equilibrium constant K_{III} is then given by

$$K_{\mathrm{III}}{}^{1/2} = \frac{(\mathrm{H}^+)(\mathrm{Dimer}^=)^{1/2}}{(\mathrm{UO_2}^{++})(\mathrm{X}^=)} = \frac{(\mathrm{H}^+)^3(T - (\mathrm{UO_2}^{++}))^{1/2}}{2^{1/2}K_1K_2f(\mathrm{UO_2}^{++})^2}$$

In Table II are presented the titration results obtained for the equimolar uranyl nitrate–citric acid system for the highest and lowest T values studied, 0.01069 and 0.001069 M. It is immediately evident that only the log $K_{\mathrm{III}}{}^{1/2}$ column shows unquestionable constancy independent of concentration. The same constant, 3.84 ± 0.03, also was obtained at T = 0.00534 and at 0.002138 M.

TABLE II

TITRATION OF EQUIMOLAR URANYL NITRATE–CITRIC ACID SYSTEM AT 25° AND μ = 0.136

pcH	B/T	log K_{I}	log K_{II}	log $K_{\mathrm{III}}{}^{1/2}$
		T = 0.01069 M		
2.02	0	5.24	2.70	3.82
2.05	0.1892	5.37	2.73	3.82
2.07	.3822	5.53	2.81	3.86
2.11	.5733	5.64	2.79	3.83
2.15	.8600	5.97	2.88	3.87
2.22	1.147	6.32	2.83	3.81
2.29	1.433	6.28	2.84	3.78
2.36	1.703	..	2.88	3.79
2.45	2.005	..	2.90	3.79
2.57	2.294	..	2.92	3.80
2.76	2.580	..	2.92	3.78
		Av.	2.84 ± 0.06	3.81 ± 0.03
		T = 0.001069 M		
2.73	0	6.65	2.39	3.87
2.76	0.1892	..	2.35	3.82
2.79	.3822	..	2.37	3.83
2.82	.5733	..	2.39	3.84
2.87	.8600	..	2.43	3.84
2.91	1.147	..	2.54	3.95
2.99	1.433	..	2.47	3.87
3.08	1.703	..	2.41	3.80
3.17	2.005	..	2.53	3.89
3.32	2.294	..	2.46	3.81
3.53	2.580	..	2.51	3.85
		Av.	2.44 ± 0.06	3.85 ± 0.03

There is no hint of constancy at any concentration in the log K_{I} column even for the early part of the titration. There appears to be a positive trend of 0.22 log unit in the log K_{II} column for the higher concentration. Similar trends occurred for the titrations at T = 0.00534 and 0.002138 M. However, it is seen that at the lowest concentration K_{II} might possibly be considered constant. In a given titration an increase of 0.22 log unit in log K_{II}, as for T = 0.01069 M, might possibly be experimental error due to a cumulative pH error of only 0.05 unit. However, the regular negative trend shown in Table III in the average log K_{II} values with decreasing concentration, amounting to 0.40 unit for a tenfold change in concentration, unquestionably is real.

TABLE III

AVERAGE LOG K VALUES AT 25° AND μ = 0.136

Ligand	$T \times 10^3$, M	pcH Range	log K_{II}	log $K_{\mathrm{III}}{}^{1/2}$
Malate⁼	1.069	2.83–3.59	2.44 (±0.10)	3.89 (±0.05)
(*d* or *l*)	2.138	2.62–3.37	2.58 (± .07)	3.90 (± .03)
	5.345	2.36–3.08	2.74 (± .08)	3.88 (± .03)
	10.69	2.14–2.90	2.84 (± .09)	3.85 (± .04)
Citrate⁼	1.069	2.73–3.53	2.44 (± .05)	3.85 (± .03)
	2.138	2.51–3.27	2.60 (± .04)	3.88 (± .04)
	5.345	2.21–2.97	2.70 (± .06)	3.81 (± .03)
	10.69	2.02–2.76	2.84 (± .05)	3.81 (±. 02)
Tartrate⁼	1.069	2.84–3.64	1.37 ±(.04)	2.81 (± .04)
(*d* or *l*)	2.138	2.62–3.40	1.49 (± .04)	2.79 (± .04)
	5.345	2.36–3.12	1.60 (± .06)	2.73 (± .04)
	10.69	2.15–2.92	1.76 (± .06)	2.73 (± .04)

Very similar results were obtained for the uranyl nitrate–malic acid system. In fact, virtually the same value, 3.88 ± 0.03, was obtained for log $K_{\mathrm{III}}{}^{1/2}$ as for the uranyl–citrate system. Needless to say, *d*-malic acid reacted exactly as did the *l*-malic acid.

For the uranyl-*d*-tartrate system the results were only slightly less conclusive. The same results were obtained for both *l*- and *d*-tartrate systems. For each titration log K_{I} showed a large trend and there was a positive trend of 0.14 and 0.26 in the log K_{II} column, but there was also a negative trend of 0.05 to 0.12 in log $K_{\mathrm{III}}{}^{1/2}$ at each of the four concentrations studied. However, as is shown in Table III, the average value of log $K_{\mathrm{III}}{}^{1/2}$, 2.77 ± 0.04, was independent of concentration, whereas the average log K_{II} decreased 0.39 unit with tenfold decrease in concentration. The trend obtained for log $K_{\mathrm{III}}{}^{1/2}$ for each titration could be produced by a cumulative pH error of only 0.01 and 0.03 unit and is believed to be insignificant[10] in view of the constancy in the average log $K_{\mathrm{III}}{}^{1/2}$ values. Furthermore, the variation with T in average log K_{II} is practically the same as for the uranyl–citrate and uranyl–malate systems, as expected if all three systems consist principally of dimers formed according to Case III.

The constants K_{IIIa} in terms of activities were estimated by extrapolation to infinite dilution of plots of log $K_{\mathrm{III}}{}^{1/2}$ *vs.* $\mu^{1/2}$ determined at seven ionic strengths for equimolar solutions over a μ range of 0.0030 to 0.058. For each solution T was 8.550 × 10^{-4} M. Except for the solution of lowest μ, varying amounts of potassium nitrate were present. At each μ, three B/T ratios were studied: namely, 0.72, 1.44 and 2.15. For each system, the plots conformed to the Debye–Hückel equation,[11] which for the dimer system gives

$$\log K_{\mathrm{III}}{}^{1/2} = \log K_{\mathrm{IIIa}}{}^{1/2} - \log \frac{\gamma_{\mathrm{D}^=}{}^{1/2}\gamma_{\mathrm{H}^+}}{\gamma_{\mathrm{UO_2}^{++}}\gamma_{\mathrm{X}^=}} = \log K_{\mathrm{IIIa}}{}^{1/2} - \frac{5A\mu^{1/2}}{1 + Ba\mu^{1/2}}$$

---

[10] Though considered insignificant this slight trend may be due to a remnant of CO_2, the effect of which might be noticed on the tartrate chelate without being detected for the stronger malate and citrate chelates. In pointwise titrations performed with *no precautions* being taken to exclude CO_2, log $K_{\mathrm{III}}{}^{1/2}$ trends of 0.4 occurred for the tartrate systems, but only 0.1 unit trends were obtained for the malate and citrate systems.

where K_a is activity constant, and a and A are the Debye–Hückel constants. A value of 5 was used for a. All points fell within 0.05 log unit of the Debye–Hückel curve. The extrapolated activity constants, log $K_{\mathrm{IIIa}}{}^{1/2}$, were 4.54, 4.52 and 3.38 for the uranyl-malate, -citrate and-*d*-tartrate systems, respectively, with uncertainties estimated to be about ± 0.05 unit.

Trimerization of Tridentate Chelates.—The second inflection point in the titration curves of equimolar mixtures of uranyl nitrate with each of the acids, malic, citric and *d*-tartaric, occurs in slightly alkaline solution when B/T equals $1^2/_3$ plus the number of carboxyl groups in the original carboxylic acid.[2d] The $^2/_3$rds factor was interpreted as an indication of completion of a trimerization, represented as: $^3/_2$ dimer$^=$ + $2OH^- \rightarrow$ trimer^{-5}, for the uranyl-malate and -tartrate systems and $^3/_2$ dimer$^=$ $+5OH^- \rightarrow$ trimer^{-8}, for the uranyl-citrate system.

The trimer state was shown[2d] to consist of a mixture of two trinuclear chelates, having *3:3* and *2:3* ligand/uranium ratios,[3] except in solutions having large excess of carboxylic acid, in which case only the *3:3* form was present.

Continuous-variations curves showed that in the equimolar uranyl-malate system (T = 0.005 M, $\mu \cong 0.11$) at pH 7.5 about 10% of the uranium is bound in a *2:3* complex, the rest being in the *3:3* state, but in twofold excess malate practically all the uranium is in the *3:3* state. For the other two systems, uranyl-tartrate and uranyl-citrate, even 2:1 ligand/uranium mixtures contain a small amount of *2:3* chelate.

To determine the trimerization constant for the *3:3* uranyl-malate chelate, five 100-ml. solutions were prepared containing 0.01069 M uranyl nitrate and 0.02138 M malic acid (*i.e.*, 2:1 ligand/U ratio), various NaOH concentrations (26.50, 27.00, 27.50, 28.00 and 28.50 ml. of 0.2043 M NaOH), and sufficient KNO_3 to give an ionic strength of 0.20. Five, 10.0 and 25.0-ml. aliquots of each solution were diluted to 50 ml. with 0.20 M KNO_3. pH readings were taken after the solutions had been stored four days.

The trimerization constant is $K_{\mathrm{Tr}} = (\mathrm{Tr}^{-5})\cdot(\mathrm{H}^+)^2/(\mathrm{D}^=)^{3/2}$, where $(\mathrm{D}^=)$ and (Tr^{-5}) represent *2:2* dimer and *3:3* trimer concentrations, respectively.

Since these solutions had pH values between the first and second inflection points, they should contain only *2:2* dimers and *3:3* trimers, no uranium remaining uncomplexed. Hence

$$T = (\mathrm{D}^=) + 3(\mathrm{Tr}^{-5}) \qquad (9)$$

Since the first and second inflection points for titration of an equimolar mixture occur at B/T ratios of 3 and $3^2/_3$, respectively

$$B + (\mathrm{H})^+ - (\mathrm{OH}^-) - (\mathrm{HX}^-) - (2\mathrm{X}^-) = 6(\mathrm{D}^=) + 11(\mathrm{Tr}^{-5}) \qquad (10)$$

Solving these two equations simultaneously gives (Tr^{-5}).

$$(\mathrm{Tr}^{-5}) = \frac{1}{2}\,[B + (\mathrm{H}^+) - (\mathrm{OH}^-) - (\mathrm{HX}^-) - (2\mathrm{X}^-) - 3T] \qquad (11)$$

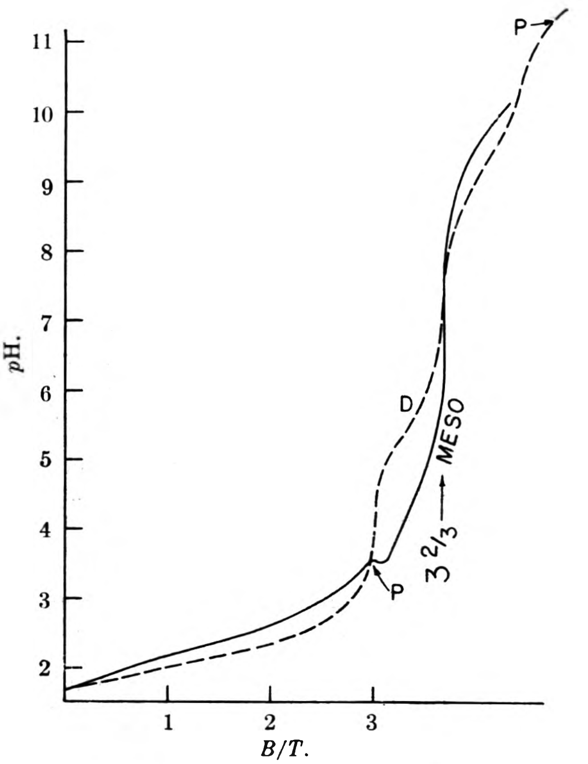

Fig. 1.—Titration curves of equimolar uranyl-*meso*-tartrate and uranyl-*d*-tartrate systems at 25°; T = 0.05 M.

and

$$(\mathrm{D}^=) = \frac{1}{2}\,[T - 3(\mathrm{Tr}^{-5})] \qquad (12)$$

Good constants were obtained for each total uranium concentration. They are summarized in Table IV. The average pK_{Tr} was 10.56 ± 0.05. The very slight apparent trend in pK_{Tr} may be due to our assumption that the Lewis ionic strength principle is valid in these solutions even though the trimer is pentavalent. An error in this assumption would affect mainly the solution of highest T.

TABLE IV

TRIMERIZATION CONSTANT FOR *3:3* URANYL-MALATE CHELATE IN 2:1 MALATE/URANIUM SYSTEM AT μ = 0.2 AND 25°[a]

$T \times 10^3$, M	p_cH Range	pK_{Tr}
10.69	5.57–6.14	10.63 ± 0.04
5.345	5.63–6.19	10.58 ± .01
2.138	5.65–6.23	10.49 ± .02
1.069	5.72–6.30	10.53 ± .03
	Av.	10.56 ± 0.05

[a] % U as trimer ranged from 20 to 70% at each T.

For 2:1 tartrate/uranium systems, a trend of 0.10 to 0.15 in the calculated pK_{Tr} was obtained at each total uranium concentration. The average pK_{Tr} values calculated were 9.96 ± 0.03 (for the highest T), 9.68 ± 0.07, 9.56 ± 0.08, and 9.64 ± 0.03 (for the highest T), 9.68 ± 0.07, 9.56 ± 0.08, and 9.64 ± 0.03 (for the lowest T). The over-all average pK_{Tr}, 9.7 ± 0.12, may be considered as an approximate value for the *3:3* uranyl-tartrate chelate, even though there obviously is a small amount of *2:3* chelate even in a 2:1 mixture.

---

(11) R. G. Bates, "Electrometric pH Determinations," John Wiley and Sons, Inc., New York, N. Y., 1954, p. 51.

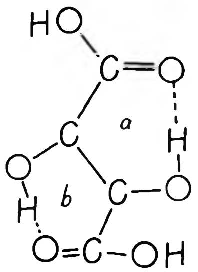

Fig. 2.—Hydrogen bonding in tartaric acid.

No attempt was made to obtain even an approximate trimerization constant for the uranyl–citrate system. There are two reasons. First, the ratio of *2:3* chelate concentration to the *3:3* concentration is even greater for this system than for the tartrate system.[2d] Second, ionization of the third carboxyl group occurs during the trimerization step. The pK for this ionization should not be the same as for uncomplexed citric acid and, hence, is unknown.

Uranyl–*meso*-Tartrate System.—Titrations of equimolar uranyl nitrate–*meso*-tartaric acid solutions were performed. A conventional (continuous) titration curve for this system is given in Fig. 1. It is immediately obvious that *meso*-tartaric acid and *d*-tartaric acid react differently with the uranyl ion. Whereas no precipitate forms in the uranyl–*d*-tartrate system until *p*H 11, for the uranyl–*meso*-tartrate system a precipitate is visible at about *p*H 3 (point P) when B/T equals three.

Despite this precipitation the continuous titration curve shows a very sharp rise at B/T equal to exactly $3^2/_3$. Since this ratio is that of the second inflection point characteristic of the uranyl–*d*-tartrate and uranyl–malate systems, trimer formation is indicated for the uranyl–*meso*-tartrate system also. However, trimerization seems to reach completion at a slightly lower *p*H than for the *d*-tartrate and malate systems.

In a pointwise titration (*i.e.*, a number of separate solutions with varying B/T) slight precipitation was noticed after four days for mixtures having B/T equal to two and T as low as 0.00534 M. Analysis of the pointwise titration curves was therefore attempted only for those solutions in which no precipitation occurred, *i.e.*, up to $B/T \cong 2$. Equimolar solutions having total uranium concentrations of 0.001069, 0.002138, 0.003207, 0.005345 and 0.01069 M were studied. At each value of T, there was a large positive trend of about 3 log units in log $K_{\rm I}$, and negative trends in log $K_{\rm III}{}^{1/2}$ increasing from 0.2 unit at the lowest value of T to 0.6 unit at the higher T value. For log $K_{\rm II}$, apparently constant values of 1.34 ± 0.02 and 1.47 ± 0.01, were obtained at total uranium concentrations of 0.001069 and 0.002138 M, respectively. At the three higher concentrations, log $K_{\rm II}$ also showed trends, increasing with T, as shown in Table V.

It seems obvious that before precipitation no single species can be considered as the principal ion in the uranyl–*meso*-tartrate system. Rather, there is indicated a mixture of species for which the average number of hydroxyl ions reacting for uranium lies between 2 and 3.

Table V

$K_{\rm II}$ for Uranyl–*meso*-Tartrate System at 25° and μ = 0.136

$T \times 10^3$, M	log $K_{\rm II}$
1.069	1.34 ± 0.02
2.138	1.47 ± 0.01
3.207	1.70 → 1.58
5.345	1.70 → 1.61
10.69	2.01 → 1.73

Discussion

The uranyl–malate and uranyl–citrate dimers have the same formation constants, log $K_{\rm IIIa}$ = 2 × 4.53 = 9.06. Hence, the third carboxyl group of citrate must remain completely undissociated up to the first inflection point and has no role either in the initial chelation or in the dimerization.

These two dimers are more stable than the uranyl–*d*-tartrate dimer, for which log $K_{\rm IIIa}$ = 2 × 3.38 = 6.76. Doubtless, some portion of this stability difference is attributable to the smaller basicity of the tartrate ion which results from (i) the inductive effect of its non-chelating alcoholic OH group and (ii) the fairly strong hydrogen bond between this alcohol group and the carboxyl group beta to it (see Fig. 2), since the chelation strongly enhances the dimerization. However, a large part of this stability difference probably is due also to the relative strength of the internuclear bonds in each dimer, since some dimer bridges must be broken in the formation of the trimer. A coördination number of nine would be required if both tridentate chelation and diol bridging were present in the trimer.

The titration results (*i.e.*, B/T = 3 at first inflection point and constancy of $K_{\rm III}$) do not prove the nature of the internuclear bridges, although it is our belief[2d] that they are olation or (oxolation) bridges, as in

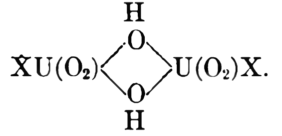

$$\mathrm{XU(O_2)}\begin{matrix}\mathrm{H}\\ \mathrm{O}\\ \diamond\\ \mathrm{O}\\ \mathrm{H}\end{matrix}\mathrm{U(O_2)X}$$

It has been suggested by a referee, however, that equally-plausible dimer structures are the non-olated structures

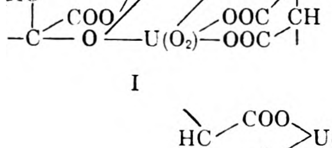

I

or

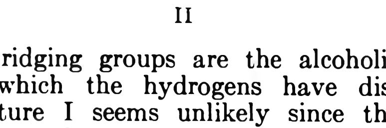

II

in which the bridging groups are the alcoholic oxygens from which the hydrogens have dissociated. Structure I seems unlikely since the uranyl–glycolate[12] and uranyl–salicylate[13] systems contain only mononuclear complexes below about *p*H 3.5 even though the complexing is strong in both

---

(12) S. Ahrland, *Acta Chem. Scand.*, **7**, 489 (1953).

(13) B. Hok-Bernstrom, *ibid.*, **10**, 163 (1956).

systems. Polymerization in these systems begins above *p*H 3.5, but it almost certainly involves olation since it also starts near this *p*H in virtually all uranyl systems containing monodentate or bidentate ligands. The failure of the uranyl–*meso*-tartrate chelate to dimerize completely seems to eliminate Structure II.

The olated structure postulated by us is also contrary to normal expectation[12–14] for it indicates that the tendency of uranium to hydrolyze and dimerize by olation is *increased*[15] by tridentate chelation despite the fact that the chelating oxygen atoms should lower the positive charge density about the uranium atom. In this case, however, it is possible to offer (below) a plausible explanation on the basis of deformation of the normally-collinear uranyl entity, because of mutual repulsion of the uranyl oxygen atoms and the chelating oxygens of the tridentate ligands, with subsequent rehybridization of the bonds in the uranyl entity.

Uranyl Ion Structure.—The uranyl ion is considered to be "a linear ion disturbed to a certain extent by strong local fields."[16] The collinearity persists in a number of solid uranyl compounds and in UO_3[17] and in aqueous uranyl perchlorate solution.[18] The special stability of the uranyl entity has been attributed by Connick and Hugus[19] and by Eisenstein[20] to strong participation of 5f orbitals in σ and π-bonds. The latter showed that linear df hybrid orbitals (for two bonds) are exceptionally strong and that strong π-bonds can also be formed by overlap of the two remaining stable 5f uranium orbitals with 2p orbitals of the oxygen atoms. One would expect, therefore, that the waters in a hydrated uranyl ion are connected to the uranium by bonds which are chiefly electrostatic with possibly a slight f-covalent contribution.

ADDED June 28, 1960.—Since this paper was submitted there has appeared a paper by Li, *et al.*,[21] in which they claim that in the *p*H region 1.9 to 2.5 the 1:1 uranyl–citrate complex is a monomer with log $K_{MA} = 8.5$, the Cit^{-3} ion being assumed as the ligand. Their conclusions seem in error for several reasons.

First, it has been shown previously[2d] that the third carboxyl hydrogen of citric acid is not removed in the uranyl–citrate system until above the first inflection point, which occurs at $B/T = 3$ (near *p*H 3.5) not only for this system but also for the uranyl-malate and uranyl-tartrate systems. The latter two ligands have only two carboxyl groups. In addition, the second buffer region in the titration of the uranyl–citrate system begins near *p*H 4 and ends near *p*H 7 at $B/T' = 4^{2}/_{3}$, exactly one unit higher than the B/T value of $3^{2}/_{3}$ obtained for the uranyl–malate and uranyl–tartrate systems. Further, in the present paper we obtained almost exactly the same stability constant for dimer formation in the uranyl-citrate and uranyl-malate systems.

Second, Li, *et al.*, have erroneously attributed to us the postulation of the dimer formula, $(UO_2Cit)_2^{-2}$. The formula put forth by us is the diolated structure, $(HCitUO_2OH)_2^{-2}$. Accordingly, their linear equation (16) has incorrect slope and intercept and should be

$$\bar{n}/(1 - \bar{n})(A^{-3}) = K_{(HA)M(OH)}/K_3] + [K_{\text{dimer}} \times 2T_M(1 - \bar{n}n)(A^{-3})/K_3^2]$$

However, the use of this equation alone easily can lead to an erroneous conclusion since a small, but real, trend in the $\bar{n}/(1 - \bar{n})(A^{-3})$ values might be ignored. This is evident from the table below, in which are presented the results of the first titration of Li, *et al.*, *i.e.*, titration of 50 ml. of solution containing (0.01 *M* $UO_2(NO_3)_2$, 0.01 *M* citric acid, 0.01 *M* HCl, 0.11 *M* NaCl) with 0.2986 *M* NaOH.

NaOH, ml.	*p*H	log K_{monomer} Li, *et al.*	log K_{monomer} Feldman[a]	log $K^{1/2}_{\text{dimer}}$ Feldman[b]
1.0	1.98	8.50	8.49	4.08
2.0	2.10	8.50	8.49	3.97
3.0	2.21	8.57	8.55	3.95
4.0	2.33	8.63	8.64	3.98
4.5	2.40	8.56	8.68	3.99

[a] Calculated from data of Li, *et al.*, using their formula for K_{monomer}. [b] Using data of Li, *et al.*, but our formula for K_{dimer}. $K^{1/2}_{\text{dimer}}$ values are compared with K_{monomer} since both contain $(H^+)^3$ and, therefore, are affected to the same extent by any *p*H error.

It is obvious that the first titration of Li, *et al.*, shows a better constancy for $K^{1/2}_{\text{dimer}}$ than for K_{mon}. On the other hand, more constant values for log K_{mon} are calculated for their second and third titrations, the values being 8.45 for titration of (0.01 *M* $UO_2(NO_3)_2$, 0.02 *M* citric acid) and 8.60 for titration of (0.04 *M* $UO_2(NO_3)_2$, 0.05 *M* citric acid). However, this difference, 0.15 log unit, cannot be ignored, for the trends in the log $K^{1/2}_{\text{dimer}}$ values for their second and third titrations amount to only 0.26 and 0.18 log unit.

The inconsistent results of Li, *et al.*, probably derive from non-attainment of equilibrium in their continuous titrations, a phenomenon we encountered in our own preliminary work. Our finding that the time required for constant *p*H to be attained was even greater than 24 hours for some solutions led us to resort to pointwise titrations, *p*H's being measured at least 48 hours after preparation of solutions.

Effect of Deformation on Electronic Structure of Uranyl Entity.—Although two σ(df) and two πf-bonds appear to be also possible for a non-linear uranyl-entity,[20] their strengths should be less than in the collinear arrangement. Hence, resonance between this configuration and other possible configurations involving some f-covalent contribution to the secondary (non-uranyl) bonds in a uranyl chelate could be significantly large *if* the uranyl entity is deformed sufficiently in the chelate. From a semi-quantitative calculation[22] it appears that in the formation of the tridentate chelate a deformation of roughly 20 degrees from collinearity should occur in the uranyl entity.

Any increase in the covalent nature of the bonds to waters of hydration (which occupy coördination sites not occupied by the tridentate ligand) should increase the acidity of these water molecules, resulting in increased tendency of the uranium to hydrolyze and dimerize.

Effect of Deformation on Relative Strengths of the Dimers.—The extent of non-linearity produced in the uranyl group should be an inverse function of the chelate bond distances, which in turn should vary inversely with the magnitudes of the negative charges on the chelating oxygen atoms. Further,

---

[14] S. Chaberek and A. E. Martell, "Sequestering Agents," John Wiley and Sons, Inc., New York, N. Y., 1959, pp. 24 and 75.

[15] One can calculate from Sutton's constant[9] that only 1% of the uranium in 0.01 *M* uranium perchlorate is hydrolyzed at *p*H 3 and $\mu = 0.15$, whereas it appears that for each of the tridentate systems about 90% of the uranium is hydrolyzed in equimolar solution of the same *p*H, μ, and total uranium concentration.

[16] J. J. Katz and G. T. Seaborg, "The Chemistry of the Actinide Elements," John Wiley and Sons, Inc., New York, N. Y., 1957, p. 177.

[17] W. H. Zachariasen, *Acta Cryst.*, **7**, 795 (1954).

[18] L. H. Jones and R. A. Penneman, *J. Chem. Phys.*, **21**, 542 (1953).

[19] R. E. Connick and Z. Z. Hugus, Jr., *J. Am. Chem. Soc.*, **74**, 6012 (1952).

[20] J. C. Eisenstein, *J. Chem. Phys.*, **25**, 142 (1956).

[21] N. C. Li, A. Lindenbaum and J. M. White, *J. Inorg. Nucl. Chem.*, **12**, 122 (1959).

[22] I. Feldman, THIS JOURNAL, **64**, 1332 (1960).

the decrease in 5f orbital participation in the uranyl entity when its linearity is destroyed should be least for minimum bending.

Thus, in the uranyl–*d*-tartrate dimer the inductive effect of the non-chelating OH group and the hydrogen bond effect combine to cause a smaller uranyl-entity deformation than in the uranyl–malate dimer. Consequently, the OH bridges should be weakest in the uranyl–tartrate dimer, because of the greater residual 5f orbital participation in the uranyl entity and the consequent greater reluctance of the uranium to form additional bonds having some 5f character.

Since some of these bridges must be broken during trimerization, the uranyl–tartrate dimers should, as they do, trimerize more easily than the uranyl–malate dimers. This may even explain the observation noted previously[2d] that in uranyl–malate systems having large excess of malate (ligand/U = 5) trimerization is considerably slower than in similar uranyl–*d*-tartrate or uranyl–citrate systems.

Monodentate and Bidentate Ligands.—Since monodentate and bidentate ligands can arrange themselves about the equator of the uranyl entity, so that their chelating oxygens are about 2.9 Å. from the uranyl oxygens, they should have little tendency to distort the uranyl entity. Hence, the above discussion requires that there be no increase in the tendency of uranyl ion to hydrolyze after complexing by monodentate or bidentate ligands. This condition appears to be satisfied. Stability constants for a number of uranyl complexes containing monodentate ligands have been tabulated by Katz and Seaborg.[16] A number of uranyl–monodentate ligand salts have been crystallized and all are normal salts or double salts containing no hydrolysis constituent.[16]

Bidentate ligands also show little, if any, tendency to increase uranyl ion hydrolysis. Titrations of equimolar solutions of uranyl ion and the dicarboxylic acids, oxalic and malonic, show a first inflection point near *p*H 3 when $B/T = 2$ and a visible precipitate very soon thereafter, indicating formation of the unhydrolyzed complex. The normal salt $UO_2C_2O_4 \cdot 3H_2O$ has been prepared.[16] Glycolate ion also chelates uranyl ion strongly but does not increase its tendency to hydrolyze.[12]

On the other hand, bidentate chelation will not prevent hydrolysis of the uranyl ion at higher *p*H's where uncomplexed uranyl ion normally hydrolyzes. In the uranyl–salicylate system[13] the initial chelate UO_2X^+ begins to hydrolyze to the hydroxo monomer at *ca.* *p*H 3 for 0.3 *M* solution, this reaction nearing completion at *ca.* *p*H 5. The uranyl–lactate chelate was shown[2d] to be completely in the trinuclear form by *p*H 5.5 for 0.05 *M* equimolar solution, at least one log unit lower than the *p*H where the tridentate chelates are completely trimeric. This latter phenomenon is in agreement with the observation, discussed above, that the weaker uranyl–*d*-tartrate dimer trimerizes more readily than the stronger uranyl–malate dimer.

The Uranyl–*meso*-Tartrate System.—It follows from the above discussion that at low *p*H (below P in Fig. 1) an equimolar uranyl–*meso*-tartrate system should contain a mixture of the binuclear tridentate chelate (as in uranyl–*d*-tartrate system) and unhydrolyzed bidentate 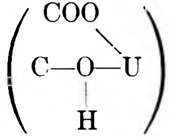 mononuclear chelates. Depending on the *p*H the mononuclear chelates may be UO_2X and/or UO_2HX^+. The titration results agree with this expectation; *i.e.*, below point P between two and three hydroxyl ions react per uranium.

This prediction resulted from a consideration of the steric arrangements and hydrogen bonding in the tartaric acids. Atom models indicate that two strong hydrogen bonds can exist simultaneously in *d*-tartaric acid, both bonds closing six-membered rings, represented by a and b in Fig. 2. On the other hand, *meso*-tartaric acid can have only one strong and one weak hydrogen bond, or two bonds of intermediate strength. Accordingly, *d*-tartaric acid has lower pK_1 and pK_2 (2.82 and 3.94 at $\mu = 0.136$) values than does *meso*-tartaric acid (2.99 and 4.44). The latter in turn has lower *pK* values than malic acid (3.15 and 4.68), which obviously can have only one hydrogen bond.

Atom models also show that in malate and *d*-tartrate ions the three oxygen atoms which are responsible for tridentate chelation can form a roughly equilateral triangle without any weakening of hydrogen bonds. When the tridentate chelate is formed, the hydrogen bond present in this triangle undoubtedly is ruptured completely because of repulsion of the hydrogen by the positive uranium atom, but, for steric reasons, tridentate chelation by the *meso*-tartrate ion requires rupture of both hydrogen bonds. However, bidentate chelation by one carboxyl group and one alcohol group of the *meso*-tartrate ion would allow both hydrogen bonds to exist.

Hydrogen bonding would thus stabilize the bidentate chelate by about 10 kcal. per uranium relative to the energy of the tridentate chelate. On the other hand, the tridentate chelate would benefit by a chelate effect of about 2 kcal.[22] per uranium. Even more important, there is surely a favorable enthalpy effect for the binuclear tridentate chelate, but the magnitude is not excessively large since ΔF^0 for the formation of the uranyl–*d*-tartrate dimer is only 4.9 kcal. per uranium. The mononuclear bidentate and binuclear tridentate chelates should therefore exist in equilibrium, as it appears is the case.

---

[22] C. G. Spike and R. W. Parry, *J. Am. Chem. Soc.*, **75**, 2726 (1953).

REFLECTIVITY OF FATTY ACID MONOLAYERS ON WATER

BY D. T. F. MARPLE AND T. A. VANDERSLICE

General Electric Research Laboratory, Schenectady, New York

Received November 7, 1959

Changes in reflectance caused by a monolayer film of fatty acid on a water surface have been measured. Measurements were made at near normal incidence and 4000 Å. wave length with several fatty acids. Measurements were also made on stearic and palmitic acid at 2537 Å. wave length and at 4000 A. with polarized light and a high angle of incidence. The fatty acid monolayers were compressed with oleic acid to about 30 dynes/cm. pressure for all the measurements. The reflectance change is caused by interference between light reflected at the air–film and film–water interfaces. For stearic and palmitic acid, if the index of refraction of the monolayer is assumed to be the same as that for solid acid, the observed reflectance changes at 4000 Å. agree with the calculations, provided the film thickness is taken to be about 3 Å. less than the molecular chain length of the solid. Reduced film thickness may be due to immersion into the water of the hydrophilic group at the end of each chain, or to tilt of each chain away from an axis perpendicular to the water surface. Measurements on monolayers of other fatty acids at 4000 Å. showed that the reflectance changes varied as the square of the number of carbon atoms in the molecular chain, and thus approximately as the square of the film thickness, as expected theoretically. The effects of change in wave length and angle of incidence are consistent with the interference theory. The reflectance change is sensitive to the purity of the water used as the film substrate, probably because impurities in the water change the film thickness.

Theory

When a smooth surface is coated with a thin film of a transparent substance, the reflectivity of the surface is changed due to interference between the radiation reflected at the air–film and film–substrate interfaces. Expressions for the reflectivity of such a system have been derived and summarized by Heavens.[1] The film is assumed to be homogeneous, isotropic and transparent. The reflectivity R at any angle of incidence is given in Heavens' notation as

$$R = \frac{r_1^2 + 2r_1r_2 \cos 2\delta_1 + r_2^2}{1 - 2r_1r_2 \cos 2\delta_1 + r_1^2r_2^2} \quad \text{(Heavens eq. 4 (48))} \tag{1}$$

where r_1 and r_2 are the Fresnel coefficients. A subscript s or p is added to R, r_1 and r_2 to denote the polarization of the incident radiation. The thickness parameter δ_1 is given by

$$\delta_1 = \frac{2\pi n_1 d_1}{\lambda} \cos \phi_1 \tag{2}$$

where d_1 is the film thickness, and λ is the wave length of the radiation.

At normal incidence $R_s = R_p$, and in the special case of very thin films ($\delta_1 < 0.1$) simplification of the expressions results if the $\cos 2\delta_1$ term is expanded in a power series. Only the first two terms are retained in the numerator, and only the first term is retained in the denominator. If R^* is the reflectivity at $d_1 = 0$, then with these approximations

$$\frac{R - R^*}{R^*} = \frac{\Delta R}{R} = \frac{-4r_1 4_2 \delta_1^2}{r_1^2 + 2r_1r_2 + r_2^2} \tag{3}$$

Apparatus and Procedure.—The changes in reflectance due to the monolayer films were expected to be a few per cent. or less. Therefore a bridge circuit was used for the reflectivity measurements. Two beams of radiation from an incandescent lamp were directed by mirrors toward two trays of water and the reflected beams from the trays were picked up by the photocells.

To reduce vibration of the water surfaces the trays were mounted on a weighted base (about 50 lb.) hung by springs from a supporting framework. The weighted base was magnetically damped in three perpendicular planes.

For measurements at 4000 Å. radiation was obtained from a 500 watt projection lamp in a water-cooled housing and Corning number 5850 filters were placed over each photocell. With the lamp operating at about 2950°K., these filters gave a spectral band width of about 800 Å. centered at 4000 ± 100 Å. For the measurements at 59° angle of incidence the optics were rearranged and a Polaroid was placed over each phototube, passing the s component of the radiation.

For the measurements at 2537 Å. the filters were removed and a 4 watt Germicidal lamp was substituted for the 500 watt incandescent lamp. Tests with filters showed that less than 5% of the radiation of this lamp was at wave lengths longer than 3100 Å.

The bridge was designed so that the balance would not be sensitive to slight changes in battery voltage or radiation intensity. The electrical drift in the balance of the bridge was less than two parts in 10^6 in one minute. Vibration of the water in the trays caused unsteadiness in the balance of the bridge of about two parts in 10^4 under average conditions. After agitation of the trays, three to five minutes were required for the waves to die out to this residual valve of noise.

Eastman Kodak (E.K.) and Armour "research grade" (Arm.) stearic acids were used. All the acids used were analyzed chemically to find the acid number, and all appeared to be quite pure on this basis. Tap water, distilled water and quartz distilled water stored in polyethylene tanks were tried in different experiments. Monolayers were prepared by the usual method of dropping a benzene solution of the fatty acid on the cleaned water. They were compressed to a fixed surface pressure of 30 dynes/cm. by oleic acid.[2] Under this compression the films were of the solid type. All measurements were made at room temperature without special temperature control.

After reading the unbalance of the bridge, a monolayer of the same acid under identical pressure was placed on the second tray and a reading taken to determine whether the original balance point with two clean surfaces was reached. In practice the original balance point usually was closely approached, indicating that the two films were the same.

Results

In about a third of all the trials a film was produced which had visible flaw in the field of view of the photocells. Flaws included crumpled films, paraffin spots from the edge of a tray carried onto the water surface by the benzene, or dust. Only data from films that were free of visible flaws are included in Table I and Table II. In these tables measurements on a given acid are in the same vertical column and measurements on different days are grouped together horizontally. The weighted mean value of the reflectivity change for each acid is given at the bottom of each vertical column. Weight factors were assigned by a systematic procedure.[3] Probable errors were estimated from

---

(1) O. S. Heavens, "Optical Properties of Thin Solid Films," Academic Press, New York, N. Y., 1955, pp. 49–58.

(2) N. K. Adam, "Physics and Chemistry of Surfaces," 3rd Edition, Oxford Press, New York, N. Y.

TABLE I

SUMMARY OF THE REFLECTANCE CHANGES OBSERVED AT 4000 Å. WAVE LENGTH AND 16° ANGLE OF INCIDENCE

	Name of acid and carbons in chain											
	Myristic 13		Palmitic 15		Stearic[a] 17		Arachidic 19		Behenic 21		Cerotic 25	
	Mean $\Delta R/R$, %	Σw[b]	Mean $\Delta R/R$, %	Σw	Mean $\Delta R/R$, %	Σw	Mean $\Delta R/R$, %	Σw	Mean $\Delta R/R$, %	Σ2	Mean $\Delta R/R$, %	Σw
Run												
A	0.36 ± 0.03	11	0.55 ± 0.04	9	0.71 ± 0.92	7					1.36	5
B	.39 ± .03	8	.57	4	.77 ± .03	6	1.08	6				
C					.68 ± .03	6			1.03	17		
D					.76	2	.9	13	1.08	4		
Grand mean	.375 ± .03	19	.55 ± .03	13	72 ± .03	21	1.02 ± 0.05	19	1.04 ± 0.04	21	1.36 ± 0.08	5

[a] Eastman Kodak Co. stearic acid. [b] Σw is the sum of the weights for data used to obtain a mean.

TABLE IIA

SUMMARY OF THE REFLECTANCE CHANGES OBSERVED AT 2537 Å. WITH DISTILLED WATER AND WITH TAP WATER

	Stearic acid				Palmitic acid		
Water	$\Delta R/R$, %	Σw	λ, Å.	Type	$\Delta R/R$, %	Σw	λ, Å.
a	1.85 ± .07	17	2537	E.K.			
a	2.05	13	2537	Arm.			
c	3.19	8	2537	Arm.	3.46	8	2537
b	1.90	6		Arm.			

TABLE IIB

SUMMARY OF REFLECTANCE CHANGES OBSERVED AT 59° INCIDENCE ANGLE

	Stearic acid				Palmitic acid		
Water	$\Delta R/R$, %	Σw	λ, Å.	Type	$\Delta R/R$, %	Σw	λ, Å.
b					1.89 ± 0.05	23	4000

[a] Res. lab. distilled water. [b] Quartz distilled water. [c] Tap water.

the scatter and total weight for the observations on a given acid, and are given in Table I.

Discussion

The scatter between repeated observations on one acid in a given run, given in Table I, is uncomfortably small compared to the differences between average values for different runs. It is possible that the chemical composition of the films was different in different runs. Distilled water was always used in the trays in the experiments included in Table I. The water was changed several times and the pans were washed with detergent and rewaxed in the course of all the observations. Termination of the hydrophilic ends of the molecules in the film by metal ions, such as Zn, Ca, Ba, etc., might modify the film thickness. Owing to the lack of definite knowledge on this point however, the results for each acid in different runs may have been averaged together and further discussion will be concerned with the average values of the reflectivity changes.

Solid stearic acid is a monoclinic crystal. The chain length of the molecule in the crystalline solid as measured by X-ray diffraction is 24.4 Å. and the index of refraction $n_z = 1.53$.[4] When laid down as a compressed monolayer on water, the chain is nearly perpendicular to the water surface. Equation 3 may be used with the observed values $\Delta R/R = 0.72$, $\lambda = 4000$ Å. and $n = 1.53$ to deduce the film thickness. The result, 21.5 Å., is about 3 Å. less than the molecular chain length of the crystalline solid.[5]

A similar calculation for palmitic acid, with $\Delta R/R = 0.55$, $n = 1.53$, $\lambda = 400$ Å. gives $d = 18.8$ Å., about 4 Å. less than the X-ray diffraction chain length of 22.9 Å.[5]

These differences may be due to the fact that the hydrophilic, (COOH), ends of the molecules in the film are immersed in the water to some depth, thus reducing the thickness of that part of the film having a refractive index markedly different from water. Another possibility is that even when compressed by oleic acid the molecules on the surface are tilted, which reduces the average film thickness. Lyons and Rideal[6] have suggested that the molecules in compressed fatty acid monolayers are all tilted to an angle of 26$^1/_2$° to the surface normal. It is interesting that this tilt angle accounts very well for the thickness difference noted above. A third possibility is that the index of refraction of the film differs significantly from that of the solid: for example, calcium stearate films on glass have refractive index 1.47.[7]

To a first approximation the numbers of carbon atoms in the molecules N are proportional to the film thickness d_1 and hence by eq. 3 if all the acids have the same index of refraction, it is expected that $\Delta R/R$ is proportional to N^2. Figure 1 shows this relation is satisfied by the observed values to within the accuracy of observations, except for arachidic acid. The reason for the discrepancy in this case is not known.

Langmuir has deduced the thickness of several compressed fatty acid monolayers from measurements of the weight and film area.[8,9] If from these film thickness values 3 Å. is subtracted to account for immersion of the hydrophilic groups in the water, an effective thickness of the film of each acid

---

(3) Unit weight was assigned to an observation on a film in one pan only. Weight two was assigned to the average of two observations made in succession (first on one pan and then on the other) if the initial and final balance readings differed by more than 10% of the change of balance. Weight four was assigned if the initial and final balance readings differed by less than 10% because this indicated that probably the films were free of flaws, the water was adequately cleaned before either film was laid down, and that little dust fell into the field.

(4) A. N. Winchell, "Optical Properties of Organic Compounds," Academic Press, New York, N. Y., 1954, pp. 23–24.

(5) In the present case, with angle of incidence of 16°, the difference between R_s or R_p and R as given by eq. 4 (48) for normal incidence is less than the experimental error. For example, exact calculation with $d = 21.5$ Å. and $n = 1.52$ gives $(\Delta R/R)_s = 0.68\%$ $(\Delta R/R)_p = 0.72\%$. Eq. 4 (48) for $\phi = 0$ gives $(\Delta R/R)_s = (\Delta R/R)_p = 0.72\%$.

(6) C. G. Lyons and E. K. Rideal, *Proc. Roy. Soc. (London)*, **A124**, 333 (1929).

(7) K. B. Blodgett, *J. Am. Chem. Soc.*, **57**, 1007 (1935).

(8) I. Langmuir, *ibid.*, **39**, 1848 (1917).

(9) N. K. Adam, "The Physics and Chemistry of Surfaces," Oxford Press, New York, N. Y., p. 25, points out that these results may be in error because of unknown changes in the density of the film from the bulk density.

is obtained. Figure 2 shows a plot of the square of this effective thickness against observed values of $\Delta R/R$. These points lie on a straight line that does not pass through the origin. Assuming that the thickness calculation is correct, then two alternate assumptions, or a combination of them, will account for this result. The first assumption is that the index of refraction of acids shorter than $N = 13$ increases with decreasing N. The line on Fig. 2 then curves to pass through the origin. The alternate assumption is that the index of refraction of all the acids is the same and greater than about 1.53, and also that the hydrophilic ends of the chains are immersed to about 10 Å. in the water. The line in Fig. 2 then is straight, but displaced to the left and passes through the origin, while the increased index accounts for the observed reflectance change from the thinner films. It appears unlikely that the films of fatty acids are immersed as much as 10 Å. in the water.

Comparison of the results in Table IIA for the Eastman Kodak stearic acid and the Armour research grade stearic acid on either kind of distilled water shows that they are the same, within the experimental error. On the other hand, the results with either stearic or palmitic acid show that the reflectivity change measured on tap water is significantly greater than for distilled water. This may result from a change of either the thickness or the refractive index of the film. In the case of stearic acid, if the refractive index is assumed unchanged, the thickness must increase from 21.5 to 27.5 Å. to account for the results; or, if the thickness is assumed unchanged, the refractive index must increase from 1.53 to 1.64. Of course, a combination of both is possible.

It has been suggested that the hydrophilic end of the stearic acid molecules may be immersed about 3 Å. in the water. If, on tap water, the hydrophilic end is terminated in a metal ion, the thickness of the film may be increased. If one assumes that the metal ion (monovalent Ca for example) rests with its center in the plane of the water surface, and with the stearic acid joined to the calcium, then a thickness increase of 4 or 5 Å. may result, somewhat less than the 6 Å. needed if the refractive index is unchanged.

For stearic acid on distilled water at normal incidence, the ratio of the reflectivity change at 2537 to that at 4000 Å. is 2.71. The inverse square of the wave length ratio is 2.5. If the refractive index of the acid were the same at both wave lengths, these ratios should be the same. An increase of refractive index from 1.53 at 4000 to 1.538 at 2537 Å. would account for this difference and is a reasonable possibility. However, if the absorption coefficient of stearic acid at 2537 Å. is greater than 10^5 cm.$^{-1}$, the theoretical ratio, calculated above assuming negligible absorption, is in error.

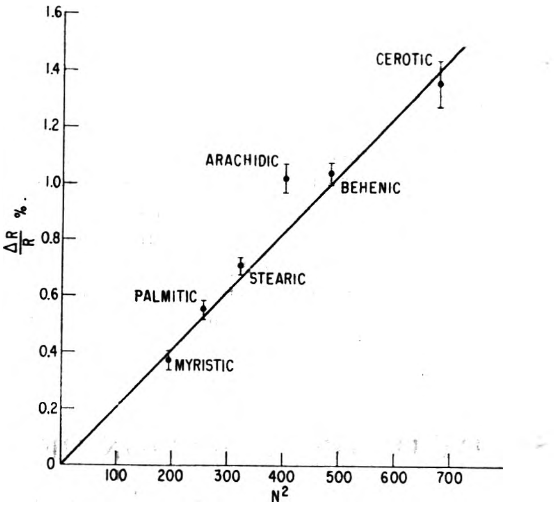

Fig 1.—Per cent. change in reflectivity, $\Delta R/R$, for several fatty acid monolayers on water, as a function of the square of the number of carbon atoms in the molecule N.

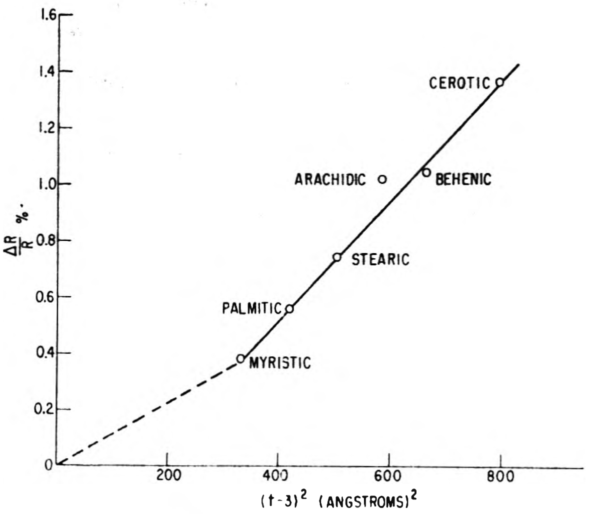

Fig. 2.—Per cent. change in reflectivity, $\Delta R/R$, for several fatty acid monolayers as a function of the square of the effective thickness.

The reflectance change for 59° incidence and s polarization was calculated for palmitic acid, (d = 18.8 Å., n = 1.53), as +0.202%. This result is in good agreement with the observed value, Table IIB, and provides additional proof of the correctness of the idea that the reflectance changes are due to interference. The reflected intensity obtained with the polarizers set to pass the p component of radiation was smaller than the s component by about a factor of 30 (as also expected from calculation). This intensity was too small to obtain satisfactory operation of the photocell bridge. Not even the sign of the reflectivity change for the p component could be measured. Calculation shows it is negative and about 65% as large as for the s component.

Summary and Conclusion

Changes in the reflectance of water produced by addition of monolayer films of fatty acids on the water surface have been measured. The reflectance change is caused by interference between light reflected at the air–film and film–water interfaces. Measurements on monolayers of fatty acids ranging from about 21 to 31 Å. thickness showed that the reflectance changes varied as the square of the number of carbon atoms in the chain.

For stearic and palmitic acid, if the index of refraction of the monolayer is assumed to be the same as that for solid acid, the observed reflectance changes agree with the calculations, provided the film thickness is taken to be about 3 Å. less than the molecular chain length of the solid. Reduced film thickness may be due to immersion into the water of the hydrophilic group at the end of each chain, or to tilt each chain away from an axis perpendicular to the water surface. The reflectivity change caused by a stearic or palmitic acid monolayer is sensitive to the purity of the water. This probably is due to a change in film thickness and possibly to a change in refractive index. Interference theory accounts satisfactorily for the reflectivity change increase with decreasing wave length and for the reflectivity change at high angles of incidence.

Acknowledgments.—We are greatly indebted to Dr. Katherine Blodgett for her helpful advice on the preparation and properties of fatty acid monolayers, and for critical reading of this report. We also wish to thank C. P. Goody for his assistance in construction and operation of the equipment and in calculation of the results.

STUDY OF DEHYDRATION OF MONTMORILLONITE AND VERMICULITE BY INFRARED SPECTROSCOPY

BY J. J. FRIPIAT,* J. CHAUSSIDON** AND R. TOUILLAUX*

**Laboratoire des colloïdes des sols tropicaux, I.N.E.A.C., Institut Agronomique de l'Université de Louvain (Belgique), and **Centre National de la Recherche Agronomique, Versailles (France)*

Received January 18, 1960

Dehydration processes for homoionic montmorillonites and vermiculites have been investigated by studying variations of $d00l$ spacings (by X-ray diffraction), intensity of angular vibration band of water (at 6.1 μ) and intensity and composition of OH vibration band (2.7 to 3.5 μ), in relation to dehydration temperature. Experimental results show that: 1. Water molecules remain up to a final stage of dehydration, and even after the collapse of the interlayer space. 2. Lattice dehydroxylation starts before dehydration is achieved. It has been proved that, as dehydration progresses, the stretching vibration frequency of water hydroxyls unexpectedly increases progressively, since the collapse of layers should decrease OH. . .O distance and strengthen hydrogen bond. A theoretical interpretation is proposed, which consists in introducing in Schrödinger's equation, an additional potential energy originating from the application of fields existing inside the interlayer space, to the OH dipoles. It is assumed that molecules remain in this internal space after the apparent collapse of layers and indirect proofs of this are given.

The dehydration of montmorillonite and vermiculite has been investigated by means of infrared spectroscopy using two absorption bands: the first one corresponds to the angular vibration of the water molecule at 6μ, the second to the O–H stretching vibration of H_2O between 2.7 and 3.5μ.

This band covers a wide frequency range since various hydrogen bonds may be formed between the hydroxyl group and neighboring oxygen atoms.

Lattice hydroxyls are characterized by vibration frequencies depending upon the crystal structure. For vermiculite, one vibration band only occurs at 3704 cm.$^{-1}$, whereas for montmorillonite two bands may be observed, at 3745 and 3650 cm.$^{-1}$, respectively.

The study by infrared spectroscopy of the dehydration of silica gels and glass powders has already been the subject of many papers. Kiselev,[1] Benesi and Jones,[2] Young[3] have shown that as the coverage by water and the surface density of silanol groups decrease, the maximum of the absorption band shifts toward higher frequencies. This fact is easily interpreted by the increase of the average OH . . . . O distance.

It is interesting to study dehydration processes for expanding lattice clay minerals, where the space occupied by water molecules can be defined by basal spacings ($d00l$) measurements.

Moreover, the structures as they are now known show the absence of surface hydroxyl groups, as far as the interlayer space is concerned. This fact greatly simplifies the interpretation.

Therefore the purpose of this study is to investigate the relations between characteristic features of the OH vibration band of hydration water molecules and the basal spacing. In order to point out the influence of cations, several homoionic clays have been studied.

I. Experimental Methods

A. Samples.—The fraction smaller than 2μ of the Camp Berteau Montmorillonite and of a Transvaal Vermiculite was separated by centrifuging and saturated by chlorides of Sr, Li, Na and K.

The main properties of these clays are summarized in Table I.

TABLE I

CATION EXCHANGE CAPACITY (B.E.C.), SPECIFIC SURFACE (S_0) AND CHARGE DENSITY (σ) OF THE CLAYS STUDIED

	B.E.C., meq./100 g.	S_0, m.^{2}/g.	σ (electrons/ mμ^2)
Montmorillonite	95	725	0.8
Vermiculite	130	600	1.3

The base exchange capacity is determined by desorbing ammonium from clays saturated with this cation at pH 7.

The specific surface, S_0, is measured by ethylene glycol retention according to a variant of the Hendricks and Dyal method.[4]

The chemical compositions of the clays are

---

(1) A. V. Kiselev and V. I. Lygin, Second Intern. Congress of Surface Activity. II. Solid-gas interface, Butterworths, London, 1957, p. 204.

(2) H. A. Benesi and A. C. Jones, THIS JOURNAL, **63**, 179 (1959).

(3) G. J. Young, *J. Colloid Sci.*, **13**, 67 (1958).

(4) S. B. Hendricks and L. A. Dyal, *Soil. Sci.*, **69**, 421 (1950).

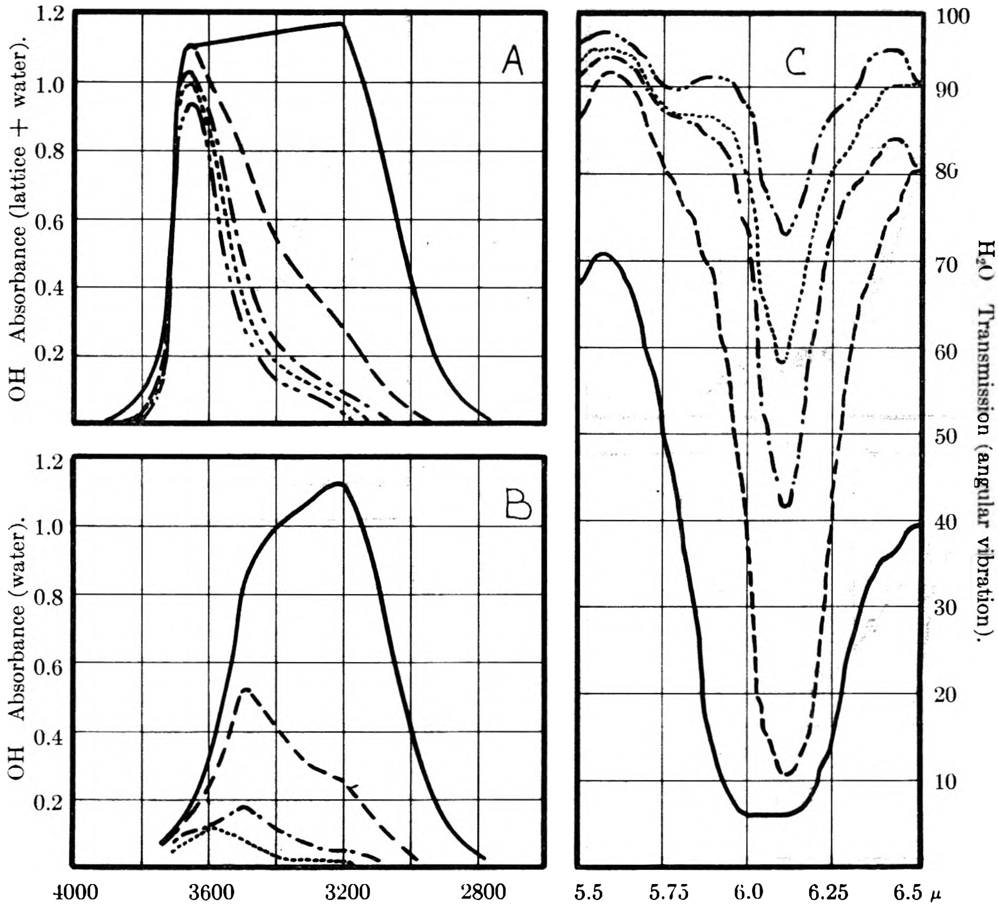

Fig. 1.—Typical spectra obtained for Li-montmorillonite: A, absorbance of the OH stretching vibration (lattice + water) band, as recorded *versus* the wave number for several dehydration temperatures; B, absorbance of the OH (water) stretching vibration *versus* the wave number for several dehydration temperatures; C, angular vibration band of water. Transmission (%) *versus* wave length (μ) for several dehydration temperatures. Temperatures: —, 20°; - -, 95°; -·-, 175°; ...., 250°; -··-··-··, 390°.

Montmorillonite:

$$[\mathrm{Si}_8{}^{4+}]^{\mathrm{IV}}[\mathrm{Al}_{2.92}{}^{3+},\mathrm{Fe}_{0.41}{}^{3+},\mathrm{Fe}_{0.03}{}^{2+},\mathrm{Mg}_{0.64}{}^{2+}]^{\mathrm{VI}}\mathrm{O}_{20}(\mathrm{OH})_4$$

Vermiculite:

$$\mathrm{Si}_{6.44}{}^{4+}\ (\mathrm{Al}^{3+},\mathrm{Fe}^{3+})_{1.56}]^{\mathrm{IV}}\ [(\mathrm{Al}^{3+},\mathrm{Fe}^{3+})_{0.28}(\mathrm{Mg}^{2+},\mathrm{Fe}^{2+})_{5.72}]^{\mathrm{VI}}\mathrm{O}_{20}(\mathrm{OH})_4$$

The samples have been used as films, the surface weight of which was about 30 mg./cm.². These films are obtained by slow evaporation of the suspensions under vacuum.

B. Apparatus.—The film is placed on a 2 × 1 cm. platinum screen and pressed between two copper plates. The bottom plate holds a heating wire and a thermocouple. It is thus possible to heat screen and film up to 400°, measure the temperature and keep it almost constant.

The sample holder may be introduced in one of the beams of the IR4 Beckman spectrograph, fitted with calcium fluoride optics, while an empty screen is introduced in the reference beam.

The same holder can be used in the goniometer of an X-ray Philips diffractometer (Cu tube).

Settings of both instruments were as follows: *IR4*: speed, 0.25 μ/min., gain 3%; period 2″, slit, 2 × standard slit. *Philips diffractometer*: slit 1°; rate meter × 4 or × 8; period 16″ or 8″; multiplier × 1; speed ¼°/min.

C. Procedure.—Two similar films are used in each experiment; one for infrared and the other for X-ray study. The first recording is obtained with the film just taken out of the desiccator. For the following observations the temperature is increased up to about 70–90°. 45 minutes are allowed to reach equilibrium.

Other measurements are done at about 150–170°, 220–230°, 290–300° and 350–370°.

The location of the 001 reflection is noted and a correction is made in order to take account of the slightly lowered position of the clay film in the diffractometer.

From infrared spectra, transmittances are converted into absorbances and the curve obtained between 2.5 and 4μ in this new scale is drawn. For vermiculite, it can be seen that the curve is dissymmetric in respect to the wave length axis; the absorbance at 2.5μ is always stronger than the absorbance observed at 4.0μ; this probably is due to diffusion initiated by the distribution of particle sizes.[5] A straight line is drawn between points representing absorbances at the limits of the band, and measurements of absorbance at intermediate wave lengths are taken as the differences between the curve and the straight line. For montmorillonite the curve is distinctly more symmetric; the same method of calculation, however, is used.

Figure 1 gives a example of calculation for typical spectra. In the case of the angular vibration band at 6μ, it is impossible to operate in a similar way. Clay minerals containing magnesium give a band of variable intensity, centered approximately at 6.8μ; both bands overlap partially. For this reason the measurement of absorbance for the water band was taken as the difference between absorbance at 5.6μ and absorbance at the minimum of transmittance curve, that is to say at about 6.1μ.

The difficulty in getting "good" films of vermiculite must be emphasized particularly as compared with the ease of obtaining them for montmorillonite. For example, it was practically impossible to make Na-vermiculite films suitable for infrared study.

All experiments were repeated two or three times.

---

(5) G. Duykaerts, *The Analyst*, **84**, 201 (1959).

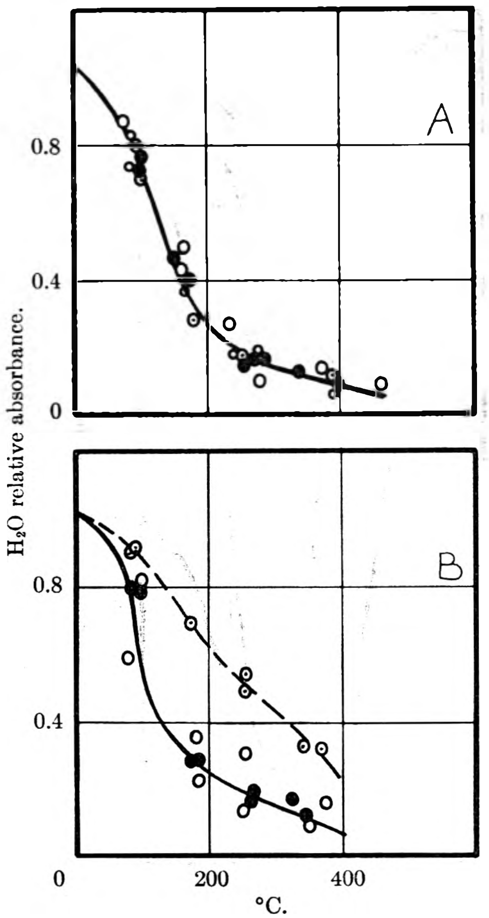

Fig. 2.—Variation of relative absorbance of the angular vibration band of water with the dehydration temperature. A, montmorillonites: ⊙, lithium; o, sodium: O potassium; ●, strontium. B: vermiculites: ⊙, lithium; O, potassium; ●, strontium.

II. Experimental Results

Figure 2 shows the variation of relative absorbance at 6.1 μ, plotted against dehydration temperature. By "relative absorbance" is meant the ratio of absorbance measured at a given temperature to the absorbance before heating. This ratio is calculated in order to make the results comparable.

The study of these data shows a very important fact: at temperatures up to 400°, *free water* still exists in all the samples.

For montmorillonites, experimental points referring to different homoionic clays fall on one smooth curve, while for vermiculites, the variability is greater; moreover, for the lithium sample, relative absorbance follows a distinctly different curve.

Figure 3 shows the change of *d*00*l* spacing during dehydration; the average curves are given.

Weak values for vermiculites are observed; they are accounted for by the fact that, before the first recording, films were dried under vacuum at room temperature. It is well known that vermiculite is particularly sensitive to dehydration.

Glaeser and Pezerat[6] studied for us vermiculites which had been dried under various conditions and in suspension.

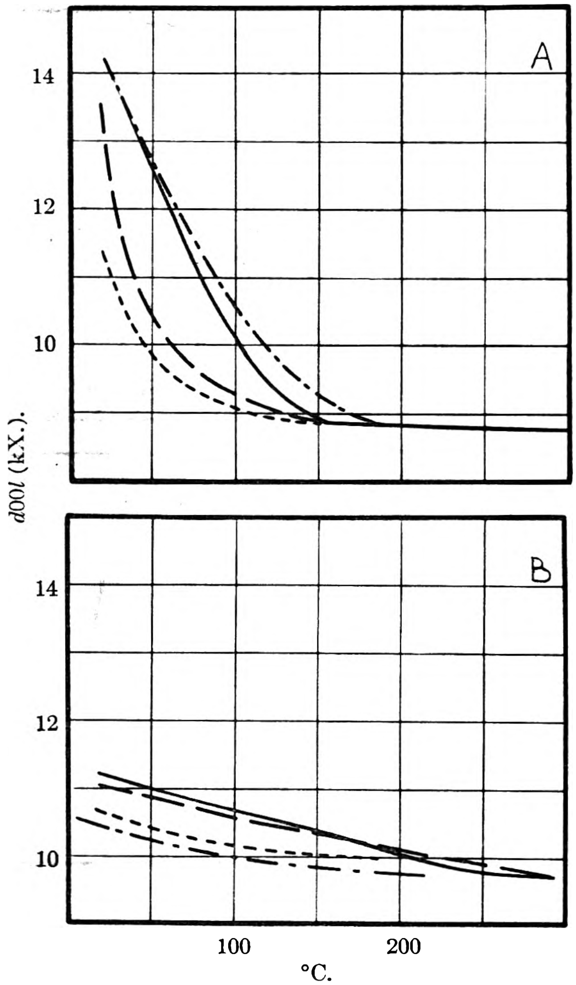

Fig. 3.—Average change of *d*00*l* distance with the dehydration temperature. A from above: -·-, Li-montmorillonite; — —, Sr-montmorillonite, — — Na-montmorillonite; —, K-montmorillonite. B from above: —, Sr-vermiculite; — —, Na-vermiculite; —, K-vermiculite, -·-, Li-vermiculite.

We summarize their results in Table II.

Table II

Vermiculites: High Order Spacings in kX., (Temperature ≃ 20°)

Exchangeable cation	Air dried		Hydrated at $P/P_0 = 0.59$		Suspension	
Li	11.95	11.2	12.7	11.4	15.0	12.4
Na	14.4	12.2	14.8	12.8	14.8	12.4
K	10.1	..	..	..	..	..
Sr	14.4	12.3	14.9	12.5	15.0	12.8

For all samples, except the potassium vermiculite, the presence of two peaks may be observed, the second one being generally broader than the first. As soon as dehydration proceeds, the first peak disappears. The variation of location of this reflection is given in Fig. 3.

It should be pointed out that, in all spectra, the presence of a peak at 7.2 kX. subsists after heating half an hour at 550°, and even after three hours at 600°, inasmuch as no reflection occurs at 14.4 kX.

---

(6) We thank Dr. J. Mering and his co-workers, R. Glaeser and J. Pezerat for help and numerous suggestions.

From this, the presence of kaolinite may be ruled out, according to prevailing ideas.[7]

On the other hand, when studying crystals by electron microscopy, numerous curled flakes are seen besides thin micaceous plates. As a matter of fact, the question could be raised whether the two high order reflections quoted in Table II, are not due to the existence of both morphologic features, the tubular form being less expanding than the flat one.

During dehydration one reflection only, characteristic of interstratification, can be observed.

Comparison between results obtained from montmorillonites and vermiculites shows the different behavior of the clays according to the nature of the base saturation. The order in which collapsing of the layers is observed is for montmorillonites K, Na, Sr, Li; for vermiculites Li, K, Na, Sr.

If Figs. 2 and 3 are compared, it must be concluded that after the apparently complete collapse of the interlayer space, at about 150°, a noticeable amount of water remains in the samples.

The problem of locating these residual molecules is difficult because there are two localization possibilities, either on the external surface or in the interlayer space.

In order to collect additional information the same experiments were repeated on a Na-kaolinite film.

The relative absorbance of the vibration band of hydration water decreases for this clay much more rapidly with temperature than was the case for montmorillonite and vermiculite.

The absorbance of the residual band after heating at 90° is 15% only of the band from the original material, whereas for montmorillonite and vermiculite, the corresponding value is about 80%.

The external surfaces of kaolinite and montmorillonite are very much comparable structurally; further, surface charge densities are about the same.

For substances without any electrical superficial charge, as silica gel, for instance, De Boer and Vleeskens[8] have shown that beyond 120°, there is no more free water upon the surface, but only hydroxyl groups.

Our conclusion is that the most likely localization of molecules remaining after dehydration at 150°, is the internal space, but that assumption does not exclude that some molecules are retained by external surfaces.

The internal space is, however, too thin to locate residual molecules anywhere else than in the hexagonal holes. The number of these holes probably is greater than the number of molecules to be accommodated, but, unfortunately, measurements of electronic density are not precise enough to give a positive evidence for this assumption.[9]

As far as the OH stretching vibration band is concerned, we subtracted ordinates of the absorbance curve after heating at 350° (approximately) from ordinates of the other curves in order to separate the contribution of the water hydroxyls from the contribution of the lattice hydroxyls (see Fig. 1).

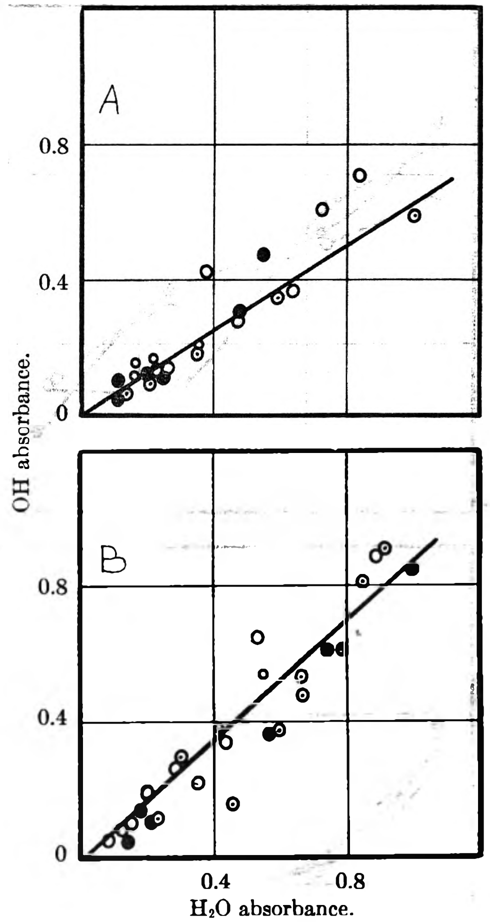

Fig. 4.—Variation of the absorbance of the OH (H_2O) stretching vibration band with the absorbance of H_2O angular vibration band. A: ⊙, Li-montmorillonite; o, Na-montmorillonite; O, K-montmorillonite; ●, Sr-montmorillonite. B: ⊙, Li-vermiculite; (o), Na-vermiculite; O, K-vermiculite; ●, Sr-vermiculite.

According to this calculation, we consider as negligible the amount of water remaining after the experiment at the highest temperature.

Absorption bands due to water hydroxyls are obtained, the intensity of which decreases as dehydration progresses, while the frequency shifts toward higher values. The fact that these bands actually must be attributed to water, is proved by the satisfying linear relationship between their absorbance at the maxima and *absolute* absorbances recorded for corresponding bands at 6.1 μ, as is shown by Fig. 4.

Figure 5 shows the frequency shift of OH stretching vibration of hydration water molecules, plotted against dehydration temperature for homoionic vermiculites and montmorillonites. We have represented the difference of frequency ($\Delta\nu = \nu_0 - \nu_x$), where ν_0 is the unperturbed OH stretching vibration frequency at 3.750 cm.$^{-1}$, and ν_x the frequency corresponding to the absorbance maximum.

Average experimental results only are reproduced.

It can be seen that the general shape of $\Delta\nu$ variation with temperature depends upon the ex-

---

(7) G. W. Brindley, "X-Ray Identification and Structures of Clay Minerals," The Mineralogical Society, London, 1951.

(8) J. H. De Boer and J. M. Vleeskens, *Proc. B, Koninkl. Nederl. Akad. Wetenschap. (Amsterdam)*, **60**, 165, 234, 45 (1957); **61**, 2 (1958).

(9) Dr. Pezerat, personal communication.

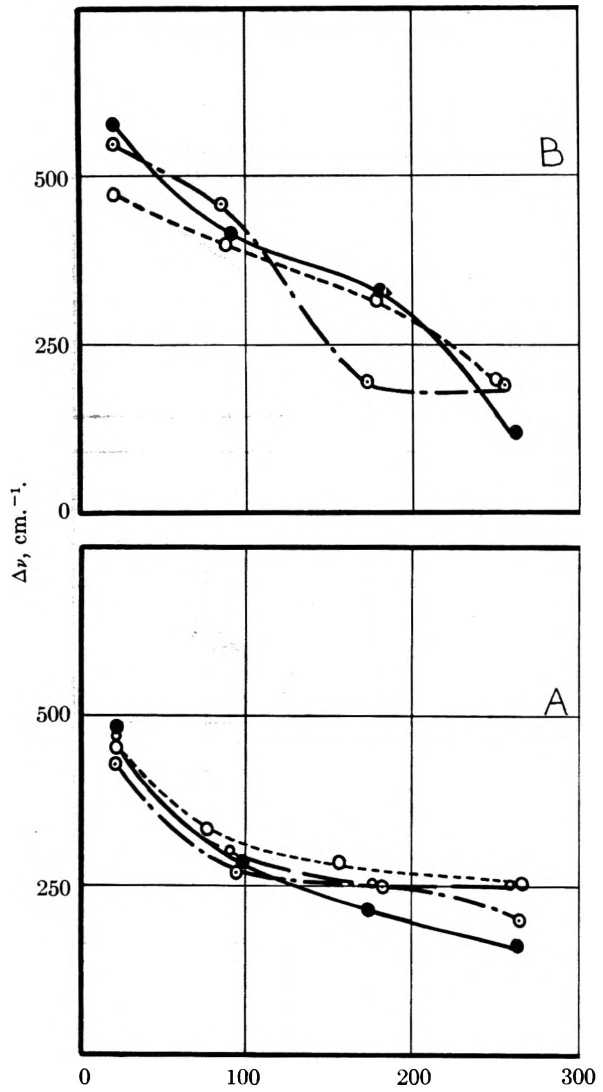

Fig. 5.—Frequency shift of OH (H_2O) stretching vibration as a function of dehydration temperature. A: ⊙, Li-montmorillonite; o, Na-montmorillonite; O, K-montmorillonite, ●, Sr-montmorillonite. B: ⊙, Li-vermiculite; O, K-vermiculite; ●, Sr-vermiculite.

changeable cation and the type of clay mineral. The plots have a common feature, however: Δν decreases as the dehydration proceeds.

We also have studied the change of the intensity of the band due to lattice hydroxyls with the heating temperature.

For montmorillonite, Mering[10] has compared the dehydration process to the dehydroxylation, that is to say to the change in the amount of constitution water contained in the unit cell of the lattice. The thermal treatment of our samples involves the first of the four stages in which he divided the whole process. It corresponds to hydration water desorption, without important loss of lattice hydroxyls. The upper limit of temperature is in agreement with the range covered by Mering's experiments (0–350°).

In fact, a comparative study of the change of intensities of both lattice hydroxyls band and water angular vibration band shows that dehydroxylation starts before dehydration is complete.

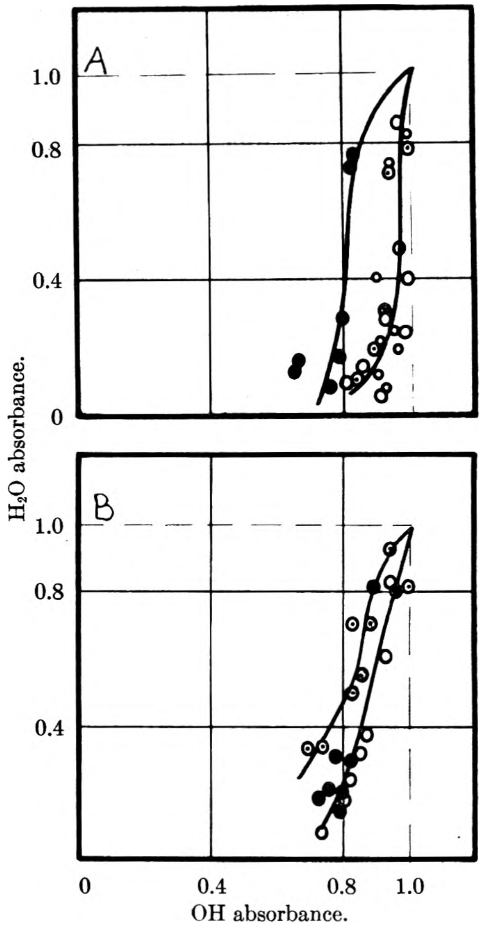

Fig. 6.—Change of the relative absorbance of H_2O angular vibration band with the relative absorbance of lattice hydroxyls stretching vibration band. A: ⊙, Li-montmorillonite; o, Na-montmorillonite; O, K-montmorillonite; ●, Sr-montmorillonite. B: ⊙, Li-vermiculite; O, K-vermiculite; ●, Sr-vermiculite.

Figure 6 gives such a picture of the phenomenon and shows that the behaviors of vermiculite and montmorillonite are very similar.

The relation between dehydration and dehydroxylation may be interpreted by the extreme affinity of cations for water; when thermal effect tends to reduce the cations hydration number, losses are partly replaced by an intervention of constitution water, which means that lattice hydroxyls specialize as water.

III. Discussion

Among experimental facts previously described, these items need to be discussed: (1) localization of hydration water molecules. References for discussion are taken from Figs. 2 and 3 and from the comparison with the Na-kaolinite behavior. (2) Frequency shift of the OH stretching vibration of hydration water, shown by Fig. 5. (3) Relation between dehydroxylation and dehydration, shown by Fig. 6.

1. Localization of Hydration Water Molecules.—It is generally admitted that interlayer water forms a discrete series of layers, the thickness of which is measured by basal reflection. It is

---

(10) J. Mering, *Trans. Faraday Soc.*, **42B**, 205 (1946).

also known that dehydration progresses stepwise, following the removal of one or several layers.

The apparently continuous variation of *d00l* parameter originates from the fact that interstratification of sheets with 0, 1, 2 or more water layers gives a complex reflection resulting from the conjunction of fundamental reflections of lattices with 0, 1, 2 or more water layers.

Unfortunately, nowadays, there is no adequate theoretical treatment for predicting the right interstratification orders from the position of the complex reflection. Nevertheless, from Fig. 3, it can be stated that the following mixing of layers obtains:

Montmorillonite.—12 kX. < *d00l* < 15 kX.: interstratification of lattices with 1 and 2 water layers; 10 kX.< *d00l* <12 kX.: interstratification of lattices with 0 and 1 layer

Vermiculite.—10 kX. < *d00l* < 11.5 kX.: interstratification of lattices with 0 and 1 water layer.

The change of *d00l* spacing with temperature corresponds to the complex reflection and depends, as already shown, upon the nature of exchangeable cation whereas the change of *relative* absorbance of the angular vibration band of water does not show this relationship. One exception has been noted, concerning Li-vermiculite.

This means that the dehydration rate process is independent of the ionic species saturating the clay.

As soon as *d00l* distance becomes smaller than 10 kX., it is impossible to locate in the interlayer space a coherent water monolayer.

We have given previously indirect arguments in favor of the localization of part of the residual molecules in hexagonal holes, the other ones being possibly adsorbed on external surfaces.

Walker[11] points out the difficulty in removing hydration water completely from a vermiculite and suggests the existence of inclusions. He mentioned the possibility for cations to be included in the lattice at the end of the dehydration process.

We have determined for K-montmorillonite the total amount of water in the sample dried at 105°; from Fig. 2, this temperature is high enough for the almost complete collapse of the interlayer space. We have found 10.9% when taking as reference the calcined sample. Allowing 5% for constitution water, there is about 6% of hydration water, that is to say 3.3 mmoles/g. If these molecules were spread on the external surface (80 m.^{2}/g.) in hexagonal packing (11.7 Å.^{2}/molecule), this would require a sheet three layers thick.

This seems very unlikely, and we will conclude accordingly that an important part of the hydration water is localized in the interlayer space after its apparent collapse.

2. **Frequency Shift of the OH Stretching Vibration of Hydration Water.**—It is known that the formation of a hydrogen bond decreases the OH stretching frequency. Regarding the nature of this type of bond, two different hypotheses have been proposed; they were reviewed recently by S. Diner.[12] Let A–H. . .B be the bond. The lone pair of atom B repulses electrons of bond A–H toward A, allowing an extension of the lone pair toward H. Thus, a strong polarity of bond OH and a strong negativity of B constitute two conditions to get a hydrogen bond. From the viewpoint of quantum theory the A–H. . .B system is considered as a four electrons system, three following structures being possible: A–H---B, A$^-$-H$^+$B and A$^-$HB$^+$

This theory underlines the role played by delocalization of the lone pair of B in the establishment of an hydrogen bond. Within the limits of our problem, three distinct effects on the hydroxyl group of interlayer water may be considered: mutual interaction of molecules, interaction between molecules and oxygen atoms of the lattice, influence of the electrical field created by superficial charges.

These three effects would act upon molecules bound to external surfaces in the same way, but differences may be expected when, at further stages of dehydration, molecules will be "trapped" between collapsing sheets.

Lippincott and Schroeder[13] have given a theoretical approach to the calculation of OH. . .O interaction and a function giving the hydroxyl frequency shift with O–O distance. It may be approximated by a rectangular hyperbola and shows particularly that as soon as the O–O distance reaches 3 Å., the frequency shift is smaller than 100 cm.$^{-1}$.

Elementary considerations based on hexagonal packing predict that a distance of 3 Å. is realized in "*horizontal*" interaction (between molecules belonging to the same layer) for a completed monomolecular coverage.

Figure 5 shows that the measured frequency shifts are always greater than 100 cm.$^{-1}$; this means that O–O distances are always smaller than 3 Å. When conditions are such that either external or internal surfaces are covered by a bi- or plurimolecular layer, O–O distance in vertical interaction (between molecules belonging to two adjacent layers), possibly decreases down to 2.75–2.8 Å.

From Lippincott and Schroeder's function it requires a frequency shift of 500–400 cm.$^{-1}$, in agreement with the observed one at the early stage of dehydration.

The first difficulty in interpreting the experimental data from Fig. 5 consists in that, in the initial hydrated state, this frequency shift is reached as well for montmorillonites as for vermiculites, whereas only Li, Sr and Na montmorillonites can form a two-layers complex in these conditions. The question may be eluded, however, since no information allows us to state that the plurimolecular complex does not exist on the external surface.

On the other hand, when dehydration temperature is increased, it is difficult to suppose the existence of a bimolecular film on the external surfaces,

---

(11) G. F. Walker, "Clays and Clay Minerals," Proc. of the Fourth Intern. Conference on Clays and Clay Minerals, Washington Nat. Acad. of Sc., 1956, p. 96.

(12) S. Diner, *Bull. soc. chim. France*, 1021 (1959).

(13) E. Lippincott and R. Schroeder, *J. Chem. Phys.*, **23**, 1099 (1955).

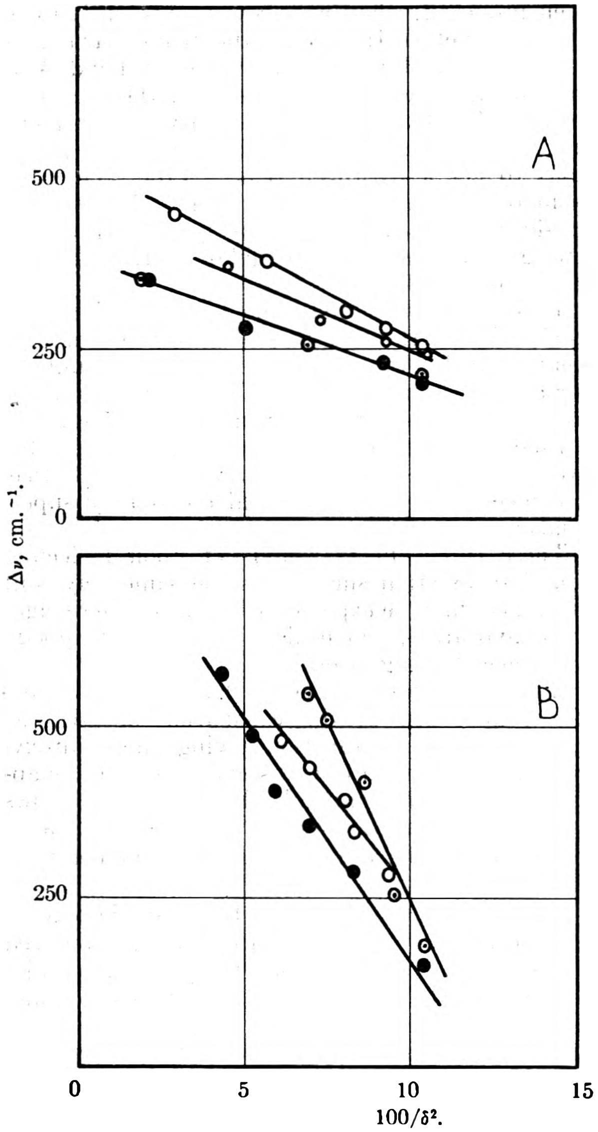

Fig. 7.—Frequency shift as a function of $1/\delta^2 \times 10^2$. A: o, Na-montmorillonite; O, K-montmorillonite; ●, Sr-montmorillonite; ⊙, Li-montmorillonite. B: ⊙, Li-vermiculite; O, K-vermiculite; ●, Sr-vermiculite.

while *d*00*l* values demonstrate that the interlayer space contains no more than one monomolecular layer. At this time, *horizontal interaction* could produce only a frequency shift of approximately 100 cm.$^{-1}$ when, experimentally, values greater than 250 cm.$^{-1}$ are found. At this stage, the most important effect is the *vertical interaction* set up between one water hydroxyl and one oxygen belonging to the lattice. Since an undetermined but noticeable part of hydration water remains between the internal surfaces, it might be expected that the collapse would increase the strength of the hydrogen bond and increase frequency shift.

Accordingly, one should observe a *minimum* in the plot of $\Delta\nu$ against temperature. In fact it is not observed and, on the contrary, the $\Delta\nu$ values decrease continuously. In order to realize the significance of the experimental results, we must try to define the origin of the perturbations acting on the hydroxyl group of the water molecule. One may suggest that OH dipole is in fact acted upon by two different electrical fields: the first one, negative, issuing from surface oxygen atoms, the second one positive, resulting from cations bound to this surface.

Coggeshall[14] investigated such a type of perturbation. Let F be the field component along the dipole direction and q the unbalanced charge of the hydroxyl group; the potential energy qFz, where z is the internuclear displacement from equilibrium position, must be introduced in the Schrödinger equation, applied to the vibrator.

When taking the Morse's function for the unperturbated potential energy, it is found that

$$\Delta\nu = -\frac{3qF}{4\mu C(2\mu)^{1/2}D^{1/2}}$$

where D is the O–H dissociation energy (110.2 kcal.mole^{-1}), C the light velocity, and μ the reduced mass of the vibrator.

Consider the total field F at a point in the interlayer space at a constant distance from the nearest wall "1." This field is the sum of three components, F_1 the field arising from the nearest wall "1," F_2 the field arising from the opposite wall, and F_3 the field due to cations, *i.e.*, $\bar{F} = -\bar{F}_1 + \bar{F}_2 + \bar{F}_3$, the fields originating from the lattice being essentially negative and the cationic field F_3, positive.

As wall "2" is moved up to wall "1," $(\bar{F}_2 - \bar{F}_1)$ gradually decreases and the relative contribution of $\bar{F}_3$ to the total field increases.

If the *d*00*l* variation could be connected to the true modifications which occur in interstratification, we should try to compute F, but it is unfortunately impossible.

However, it is interesting to study the empirical variation of $\Delta\nu$ with $1/\delta^2$ where δ is the distance between the centers of oxygen atoms forming the boundary of the interlayer space. This function will be considered as representing F.

The δ distance will be calculated by subtracting, from *d*00*l* values, the lattice sheet thickness, 6.6 kX.

We acknowledge making two rough approximations in so doing since on the one hand, *d*00*l* does not correspond to a simple and real reflection, and on the other hand, the collapse of the internal space does not occur continuously.

Figure 7 demonstrates that $\Delta\nu$ changes roughly linearly with $1/\delta^2$, that the variation depends on the cationic species and is more pronounced for vermiculites than for montmorillonites.

In account of previous approximations, this result tends to show that the positive cationic field is stronger for vermiculites than for montmorillonites. This last conclusion is in good agreement with the fact that surface charge density is higher for vermiculite than for montmorillonite (Table I).

3. Relationship between Dehydration and Dehydroxylation.—Experimental results shown in Fig. 6 indicate that dehydroxylation begins before dehydration is completed. We have suggested that this phenomenon could be ascribed to the great affinity of cations for water.

Sr-montmorillonite exhibits the most rapid

---

(14) N. D. Coggeshall, *J. Chem. Phys.*, **18**, 978 (1950).

decrease, whereas for vermiculites, it is the Li sample which can be distinguished from the others.

The classification order of hydration energies is known to be: Sr^{++}, 350 kcal./ion; Li^+, 125 kcal./ion; Na^+, 100 kcal./ion; K^+, 79 kcal./ion.

It is not necessarily the same one which can be applied to exchangeable ions since the penetration in the lattice is variable as well as the degree of charge neutralization.

Experimental data allow us to conclude that Sr ion shows the greatest affinity for water in montmorillonites, whereas the same role is displayed by Li for vermiculites.

From previous considerations, it seems that neither the value of absolute hydration energy nor the ionic radius explains the particular behavior of these two cations.

Moreover, since dehydroxylation progresses together with dehydration the first phenomenon may create lattice defects in which residual water molecules could be localized.

THERMODYNAMIC FUNCTIONS FOR MIXING AT "CONSTANT VOLUME"[1]

BY ROBERT L. SCOTT

Department of Chemistry, University of California, Los Angeles 24, California

Received February 11, 1960

In interpreting the thermodynamic functions for mixing non-electrolyte liquids, experimentally determined at constant pressure (Process I), it is frequently useful to correct these to "constant volume." However there are several different constant volume processes. Two of these, a "constant volume–equal initial pressure process" (II) and a "constant molecular concentration process" (III) are examined carefully; the appropriate functions may be calculated from those of Process I and properties of the pure components only. Constant volume functions for both II and III are calculated for seven binary systems of various kinds including two hydrocarbon + fluorocarbon mixtures. Process III is that suggested by lattice theories of solutions. However, whenever the difference between the molar volumes of the pure liquids is significant, the numbers computed are not susceptible to simple interpretation. Both this process and the lattice model appear to be rather artificial. Process II, while not completely justified by any theoretical treatment, appears to be the more interesting. For many simple systems the entropy of mixing for Process II is approximately ideal (within $0.1R$ per mole). For these systems the excess entropy in the constant pressure process appears to be largely a result of the volume expansion or contraction on mixing.

Introduction

It is obvious that experimental measurements on the mixing of liquids to form solutions normally are carried out under conditions of constant pressure (usually one atmosphere) and that the appropriate thermodynamic quantities to be reported are the Gibbs free energy of mixing $\Delta\bar{G}^M$, the heat of mixing $\Delta\bar{H}^M$, the volume change on mixing $\Delta\bar{V}^M$, etc., or the corresponding excess functions per mole of mixture $\bar{G}^E = \Delta\bar{G}^M - RT(x_1 \ln x_1 + x_2 \ln x_2)$, $\bar{H}^E = \Delta\bar{H}^M$, $\bar{V}^E = \Delta V^M$, etc.

However, theoretical treatments of solutions, particularly those based upon lattice models, usually yield more directly the thermodynamic functions for a constant volume process; so it has become fashionable recently to report constant volume functions computed from the experimental measurements of constant pressure. Thermodynamic equations relating these have been extensively discussed[2,3] but it has not been realized generally that the constant volume process so calculated is not that to which the lattice theories would seem to be most nearly applicable. Consequently, conclusions based upon these conversions are likely to be ambiguous and misleading.

There are in fact at least two kinds of "constant volume" processes, one in which the two separate initial components are at the same pressure before mixing and one in which they are at different pressures, but have equal molar volumes.[4] We therefore distinguish three processes of interest: a constant pressure process (I), a "constant volume—(equal initial pressure)" process (II), and a "constant molecular concentration" process (III). Table I outlines the specification of initial and final states. For convenience of evaluation, the same final state is taken for all three processes, so we label these special cases IIA and IIIA. This is not necessary; there is another useful process II (which we shall call IIB) in which the initial state is the same as that of I and the final (solution) state is expanded or compressed to the appropriate volume. The differences between the thermodynamic functions for variants of process II (*e.g.*, IIA and IIB) are small compared with the differences between II and III. The general equations (and specific equations for process IIB) will be found in the appendix. Here and throughout the paper all volumes $\bar{V}$ are molar volumes.

Process II (either IIA or IIB) is that computed in most experimental papers, even those using equations derived from lattice models; however process III would seem to be that to which lattice theories should be more nearly applicable.

The pressure P'' and the volumes V_1'' and V_2'' needed for the specification of process IIA are defined by the relations

---

(1) Presented at the 135th National Meeting of the American Chemical Society, Boston, Mass., April 9, 1959.

(2) (a) G. Scatchard, *Trans. Faraday Soc.*, **33**, 160 (1937); (b) J. H. Hildebrand and R. L. Scott, "Solubility of Nonelectrolytes," 3d edition, Reinhold Publ. Corp., New York, N. Y., 1950, pp. 136–143.

(3) R. L. Scott, *Disc. Faraday Soc.*, **15**, 44 (1953).

(4) R. L. Scott, *J. Chem. Phys.*, **25**, 193 (1956).

TABLE I

MIXING AT CONSTANT TEMPERATURE

(x_1 moles of 1) + (x_2 moles of 2) → (1 mole of mixture)

I.	Constant pressure	$P', \tilde{V}_1'$	$P', \tilde{V}_2'$	$P', \tilde{V}_m'$
IIA	Constant volume (equal initial pressure)	$P'', \tilde{V}_1''$	$P'', \tilde{V}_2''$	$P', \tilde{V}_m' = x_1V_1'' + x_2V_2''$
IIIA	Constant molecular concn.	$P_1''', \tilde{V}_1''' = \tilde{V}_m'$	$P_2''', \tilde{V}_2''' = \tilde{V}_m'$	$P', \tilde{V}_m'$

$$P'' - P' = \int_{x_1\tilde{V}_1'+x_2\tilde{V}_2'}^{\tilde{V}_m'} \left[x_1 \left(\frac{\partial P}{\partial V}\right)_{T,1} + x_2 \left(\frac{\partial P}{\partial V}\right)_{T,2}\right] \mathrm{d}\tilde{V}_m = \int_{\tilde{V}'}^{\tilde{V}_1''} \left(\frac{\partial P}{\partial V}\right)_{T,1} \mathrm{d}\tilde{V}_1 = \int_{\tilde{V}_2'}^{\tilde{V}_2''} \left(\frac{\partial P}{\partial V}\right)_{T,2} \mathrm{d}\tilde{V}_2 \quad (1)$$

where of course

$$x_1(\tilde{V}_1'' - \tilde{V}_1') + x_2(\tilde{V}_2'' - \tilde{V}_2') = \tilde{V}_1'x_1 - x_2\tilde{V}_2' = \tilde{V}^{\mathrm{E}} \quad (2)$$

If the derivatives $(\partial P/\partial \tilde{V})_{\mathrm{T}}$ are expanded as power series in $(\tilde{V} - \tilde{V}')$, we may solve equations 1 and 2 for $\tilde{V}_1'' - \tilde{V}_1'$ and $\tilde{V}_2'' - \tilde{V}_2'$ as a function of $\tilde{V}^{\mathrm{E}}$, obtaining

$$\tilde{V}_1'' - \tilde{V}_1^0 = \frac{(V_{\mathrm{P}}^0)_1}{\langle V_{\mathrm{P}}^0\rangle} \tilde{V}^{\mathrm{E}} + \frac{x_2[(V_{\mathrm{PP}}^0)_1(V_{\mathrm{P}}^0)_2 - (V_{\mathrm{PP}}^0)_2(V_{\mathrm{P}}^0)_1]}{2\langle V_{\mathrm{P}}^0\rangle^3} (\tilde{V}^{\mathrm{E}})^2 + \ldots \quad (3a)$$

$$\tilde{V}_2'' - \tilde{V}_2^0 = \frac{(V_{\mathrm{P}}^0)_2}{\langle V_{\mathrm{P}}^0\rangle} \tilde{V}^{\mathrm{E}} + \frac{x_1[(V_{\mathrm{PP}}^0)_1(V_{\mathrm{P}}^0)_2 - (V_{\mathrm{PP}}^0)_2(V_{\mathrm{P}}^0)_1]}{2\langle V_{\mathrm{P}}^0\rangle^3} (\tilde{V}^{\mathrm{E}})^2 + \ldots \quad (3b)$$

Here the symbols V_{P} and V_{PP} are shorthand for the derivatives $(\partial\tilde{V}/\partial P)_{\mathrm{T}}$ and $(\partial^2\tilde{V}/\partial P^2)_{\mathrm{T}}$, respectively, the superscript 0 represents the standard state of the pure substance (*i.e.*, at one atmosphere pressure), and the average symbol $\langle V_{\mathrm{P}}^0\rangle$ is shorthand for $(x_1(V_{\mathrm{P}}^0)_1 + x_2(V_{\mathrm{P}}^0)_2)$. This symbolism will be used consistently throughout the paper.

The initial pressure P'' for the constant total volume process is then

$$P'' - P^0 = \frac{1}{\langle V_{\mathrm{P}}^0\rangle} \tilde{V}^{\mathrm{E}} + \frac{\langle V_{\mathrm{PP}}^0\rangle}{2\langle V_{\mathrm{P}}^0\rangle^3} (\tilde{V}^{\mathrm{E}})^2 + \ldots \quad (4)$$

Similar equations yield the pressures necessary for Process III

$$P_1' - P^0 = \frac{1}{(V_{\mathrm{P}}^0)_2} (\tilde{V}_m^0 - \tilde{V}_1^0) + \frac{(V_{\mathrm{PP}}^0)_1}{2(V_{\mathrm{P}}^0)_1^3} (\tilde{V}_m - \tilde{V}_1^0)^2 + \ldots \quad (5a)$$

$$P_2'' - P^0 = \frac{1}{(V_{\mathrm{P}}^0)_2} (\tilde{V}_m - \tilde{V}_2^0) + \frac{(V_{\mathrm{PP}}^0)_2}{2(V_{\mathrm{P}}^0)_2^3} (\tilde{V}_m^0 - \tilde{V}_2^0) + \ldots \quad (5b)$$

The magnitude of the changes involved can be seen easily if we select as an example an equimolar mixture ($x = 1/2$) for which $\tilde{V}_1 = 95.0$ cm.^{3}, $\tilde{V}_2^0 = 105.0$ cm.^{3} and $\tilde{V}_m^0 = 101.0$ cm.^{3}; so $\tilde{V}^{\mathrm{E}} = 1.0$ cm.^{3}. Furthermore we assume that $V_{\mathrm{P}} = (\partial V/\partial P)_{\mathrm{T}}$ is 1.0×10^{-2} cm.^{3} atm.$^{-1}$ and $V_{\mathrm{PP}} = (\partial^2 V/\partial P^2)_{\mathrm{T}}$ is 1.2×10^{-5} cm.^{3} atm.$^{-2}$, each the same for both species.

Then the initial pressure P'' in the constant volume process IIA is about -93 atm., while for the constant molecular concentration process IIIA, the initial pressures are approximately $P_1''' = -383$ atm. and $P_2''' = 497$ atm. The introduction of negative pressure is not in fact necessary; appropriate volumes can be chosen which make all pressures positive. This is physically most meaningful, but the alternative equations, although sometimes simple (see the Appendix) involve properties of the mixture which are frequently not available; in most cases the differences are small.

The Thermodynamic Functions

The thermodynamic functions for these various processes are interrelated by standard thermodynamic integrals, but in general the necessary thermodynamic data exist (if they exist at all) only at a pressure of one atmosphere. We therefore expand all these integrals into Taylor series as powers of $(V - V^0)$ and evaluate successive derivatives at the standard state of atmospheric pressure symbolized by the superscript 0. These series may in fact fail to converge at large volumes (which correspond to large negative pressures), but since this feature can be avoided by changing the reference final pressure and final volume, this need not concern us here.

II. Constant Volume–Equal Initial Pressures.—For constant volume processes, of course, the appropriate free energy is the Helmholtz free energy A. Since the usual "excess functions" are all defined relative to the constant pressure process, we cannot use the symbols $\bar{A}^{\mathrm{E}}$, $\bar{S}^{\mathrm{E}}$, etc., for these other processes. Consequently we define new functions $\bar{A}^{\mathrm{VE}}$, $\tilde{S}^{\mathrm{VE}}$, etc., for this commonly used constant volume process II (recognizing that process III, for which we must use a different superscript is also "constant volume").

$$\Delta\bar{A}_{\mathrm{IIA}} = \bar{A}_m(T,\tilde{V}_m^0) = x_1\bar{A}_1(T,\tilde{V}_1'') - x_2\bar{A}_2(T,\tilde{V}_2) = RT(x_1 \ln x_1 + x_2 \ln x_2) + \tilde{A}^{\mathrm{VE}} = \Delta\bar{A}_{\mathrm{I}} + x_1 \int_{\tilde{V}_1^0}^{\tilde{V}_1''} P\,\mathrm{d}\tilde{V}_1 + x_2 \int_{\tilde{V}_2^0}^{\tilde{V}_2''} P\,\mathrm{d}_2\tilde{V} \quad (6)$$

$$\tilde{A}^{\mathrm{VE}}(T,\tilde{V}_m^0) = \tilde{A}^{\mathrm{E}}(T,P^0) + P\tilde{V}^{\mathrm{E}} + \frac{x_1}{2(V_{\mathrm{P}}^0)_1} (\tilde{V}_1'' - \tilde{V}_1^0)^2 + \frac{x_2}{2(V_{\mathrm{P}}^0)_2} (\tilde{V}_2'' - \tilde{V}_2^0)^2 + \ldots \quad (7)$$

Using the relation $\bar{G}^{\mathrm{E}} = \bar{A}^{\mathrm{E}} + P\tilde{V}^{\mathrm{E}}$ and eq. 3ab for $\tilde{V}_1'' - \tilde{V}_1^0$ and $\tilde{V}_2'' - \tilde{V}_2^0$, we obtain

$$\bar{A}^{\mathrm{VE}}(T,V_m^0) - \bar{G}^{\mathrm{E}}(T,P^0) = \frac{(\tilde{V}^{\mathrm{E}})^2}{2\langle V_{\mathrm{P}}^0\rangle} + \ldots \quad (8)$$

Since $\langle V_{\mathrm{P}}^0\rangle$ is necessarily negative, $\bar{A}^{\mathrm{VE}} < \bar{G}^{\mathrm{E}}$.

$$\Delta_{\mathrm{IIA}} = \bar{S}_m(T,\tilde{V}_m^0) - x_1\bar{S}_1(T,\tilde{V}_1'') - x_2\tilde{S}_2(T,\tilde{V}_2'') = -R(x_1 \ln x_1 + x_2 \ln x_2) + \bar{S}^{\mathrm{VE}} = \Delta\bar{S}_{\mathrm{I}} - x_1 \int_{\tilde{V}_1^0}^{\tilde{V}_1''} \left(\frac{\partial S}{\partial V}\right)_{T,1} d\tilde{V}_1 - x_2 \int_{\tilde{V}_2^0}^{\tilde{V}_2''} \left(\frac{\partial S}{\partial V}\right) \mathrm{d}\tilde{V}_2 \quad (9)$$

$$\tilde{S}^{\mathrm{VE}}(T,\tilde{V}_{\mathrm{m}}{}^{0}) = S^{\mathrm{E}}(T,P^{0}) - x_1\left(\frac{\partial S}{\partial V}\right)_1^0 (V_1'' - V_1{}^0) - x_2\left(\frac{\partial S}{\partial V}\right)_2^0 (\tilde{V}_2'' - \tilde{V}_2{}^0) - \frac{x_1}{2}\left(\frac{\partial^2 S}{\partial V^2}\right)_2^0 (V_1'' - V_1{}^0)^2 - \frac{x_2}{2}\left(\frac{\partial^2 S}{\partial V^2}\right)_2^0 (V_2'' - V_2{}^0)^2 \ldots \quad (10)$$

The derivatives $(\partial S/\partial V)_{\mathrm{T}}$ and $(\partial S/\partial V^2)$ may be expressed in terms of the coefficients V_{P}, V_{PP} and two additional ones, $V_{\mathrm{T}} = (\partial\tilde{V}/\partial T)_{\mathrm{P}}$ and $V_{\mathrm{PT}} = (\partial^2\tilde{V}/\partial P\partial T)$

$$\left(\frac{\partial S}{\partial V}\right)_{\mathrm{T}} = \left(\frac{\partial P}{\partial T}\right)_{\mathrm{V}} = -\frac{(\partial V/\partial T)_{\mathrm{P}}}{(\partial V/\partial P)_{\mathrm{T}}} = -\frac{V_{\mathrm{T}}}{V_{\mathrm{P}}} \quad (11)$$

$$\left(\frac{\partial^2 S}{\partial V^2}\right)_{\mathrm{T}} = \left(\frac{\partial^2 P}{\partial T\partial V}\right) = -\frac{[(\partial P/\partial T)_{\mathrm{V}}/(\partial^2 V/\partial P^2)_{\mathrm{T}} + (\partial^2 V/\partial P\partial T)]}{(\partial V/\partial P)_{\mathrm{T}}{}^2} = \frac{V_{\mathrm{PP}}V_{\mathrm{T}} - V_{\mathrm{PT}}V_{\mathrm{P}}}{V_{\mathrm{P}}{}^3} \quad (12)$$

With these relations and eq. 3ab, we obtain for $\tilde{S}^{\mathrm{VE}}$

$$\tilde{S}^{\mathrm{VE}}(T,\tilde{V}_{\mathrm{m}}{}^0) - \tilde{S}^{\mathrm{E}}(T,P^0) = \frac{\langle V_{\mathrm{T}}{}^0\rangle}{\langle V_{\mathrm{P}}{}^0\rangle}\tilde{V}^{\mathrm{E}} + \frac{1}{2}\left[\frac{\langle V_{\mathrm{PT}}\rangle\langle V_{\mathrm{P}}\rangle - \langle V_{\mathrm{PP}}\rangle\langle V_{\mathrm{T}}\rangle}{\langle V_{\mathrm{P}}\rangle^3}\right](\tilde{V}^{\mathrm{E}})^2 \quad (13)$$

III. Constant Molecular Concentration.—In Greek mythology, the inn-keeper Procrustes made his guests fit his bed by stretching their legs if too short or cutting them off if too long. To calculate the thermodynamic functions for Process IIIA we must do much the same thing, compress the component of larger molar volume and expand that of smaller molar volume until both have the same molar volume, *i.e.*, have the same molecular concentration as does the system after mixing. It is convenient to define a third set of excess functions $\tilde{A}^{\mathrm{CE}}$, $\tilde{S}^{\mathrm{CE}}$, etc.

$$\Delta\tilde{A}_{\mathrm{IIIA}} = \tilde{A}_{\mathrm{m}}(T,\tilde{V}_{\mathrm{m}}{}^0) - x_1\tilde{A}_1(T,\tilde{V}_1 = \tilde{V}_{\mathrm{m}}{}^0) - x_2\tilde{A}_2(T,\tilde{V}_2 = \tilde{V}_{\mathrm{m}}{}^0) = RT(x_1 \ln x_1 + x_2 \ln x_2) + \tilde{A}^{\mathrm{CE}} = \Delta\tilde{A}_{\mathrm{I}} + x_1\int_{\tilde{V}_1{}^0}^{\tilde{V}_{\mathrm{m}}{}^0} P_1\,\mathrm{d}\tilde{V}_1 + x_2\int_{\tilde{V}_1{}^0}^{\tilde{V}_{\mathrm{m}}{}^0} P_2\,\mathrm{d}\tilde{V}_2 \quad (14)$$

$$\tilde{A}^{\mathrm{CE}}(T,\tilde{V}_{\mathrm{m}}{}^0) = \tilde{A}^{\mathrm{E}}(T,\tilde{P}^0) + P^0\tilde{V}^{\mathrm{E}} - \frac{x_1}{(V_{\mathrm{P}})_1}(\tilde{V}_{\mathrm{m}}{}^0 - \tilde{V}_1{}^0)^2 - \frac{x_2}{(V_{\mathrm{P}})_2}(\tilde{V}_{\mathrm{m}}{}^0 - \tilde{V}_2{}^0)^2 + \ldots \quad (15)$$

$$\Delta\tilde{S}_{\mathrm{IIIA}} = \tilde{S}_{\mathrm{m}}(T,\tilde{V}_{\mathrm{m}}{}^0) - x_1S_1(T,\tilde{V}_1 = \tilde{V}_{\mathrm{m}}{}^0) - x_2S_2(T,\tilde{V}_2 = \tilde{V}_{\mathrm{m}}{}^0) = -R(x_1 \ln x_1 + x_2 \ln x_2) + \tilde{S}^{\mathrm{CE}} = \Delta S_{\mathrm{I}} - x_1\int_{\tilde{V}_1{}^0}^{\tilde{V}_{\mathrm{m}}{}^0}\left(\frac{\partial S}{\partial V}\right)_{\mathrm{T},1}\mathrm{d}\tilde{V}_1 - x_2\int_{\tilde{V}_2{}^0}^{\tilde{V}_{\mathrm{m}}{}^0}\left(\frac{\partial S}{\partial V}\right)_{\mathrm{T},2}\mathrm{d}\tilde{V}_2 \quad (16)$$

$$\tilde{S}^{\mathrm{CE}}(T,\tilde{V}_{\mathrm{m}}{}^0) = \tilde{S}^{\mathrm{E}}(T,P^0) - x_1\left(\frac{\partial S}{\partial V}\right)_1^0(\tilde{V}_{\mathrm{m}}{}^0 - \tilde{V}_1{}^0) - x_2\left(\frac{\partial S}{\partial V}\right)_2^0(\tilde{V}_{\mathrm{m}}{}^0 - \tilde{V}_2{}^0) - \frac{x_1}{2}\left(\frac{\partial^2 S}{\partial V^2}\right)_1^0(\tilde{V}_{\mathrm{m}}{}^0 - \tilde{V}_1{}^0)^2 - \frac{x_2}{2}\left(\frac{\partial^2 S}{\partial V^2}\right)_1^0(\tilde{V}_{\mathrm{m}}{}^0 - \tilde{V}_2{}^0)^2 - \ldots \quad (17)$$

To compare equations 15 and 17 and 7 and 13, it is convenient to use the relations $\tilde{V}_{\mathrm{m}} - \tilde{V}_1{}^0 = \tilde{V}^{\mathrm{E}} - x_2(\tilde{V}_1{}^0 - \tilde{V}_2{}^0)$ and $\tilde{V}_{\mathrm{m}}{}^0 - \tilde{V}_2{}^0 = V^{\mathrm{E}} + x_1(\tilde{V}_1{}^0 - \tilde{V}_2{}^0)$. Making these substitutions and those of eq. 11 and 12 we obtain

$$\tilde{A}^{\mathrm{CE}} - \tilde{G}^{\mathrm{E}} = \frac{1}{2}\left\langle\frac{1}{V_{\mathrm{P}}}\right\rangle(\tilde{V}^{\mathrm{E}})^2 - x_1x_2\left[\frac{1}{(V_{\mathrm{P}})_1} - \frac{1}{(V_{\mathrm{P}})_2}\right](\tilde{V}_1{}^0 - \tilde{V}_2{}^0)V^{\mathrm{E}} + \frac{x_1x_2}{2}\left[\frac{x_2}{(V_{\mathrm{P}})_1} + \frac{x_1}{(V_{\mathrm{P}})_2}\right](\tilde{V}_1{}^0 - \tilde{V}_2{}^0)^2 \quad (18)$$

$$\tilde{S}^{\mathrm{CE}} - \tilde{S}^{\mathrm{E}} = \left\langle\frac{V_{\mathrm{T}}}{V_{\mathrm{P}}}\right\rangle\tilde{V}^{\mathrm{E}} + \frac{1}{2}\left\langle\frac{V_{\mathrm{PT}}V_{\mathrm{P}} - V_{\mathrm{PP}}V_{\mathrm{T}}}{V_{\mathrm{P}}{}^3}\right\rangle(\tilde{V}^{\mathrm{E}})^2 - x_1x_2\left[\left(\frac{V_{\mathrm{PT}}V_{\mathrm{P}} - V_{\mathrm{PP}}V_{\mathrm{T}}}{V_{\mathrm{P}}{}^3}\right)_1 - \left(\frac{V_{\mathrm{PT}}V_{\mathrm{P}} - V_{\mathrm{PP}}V_{\mathrm{T}}}{V_{\mathrm{P}}{}^3}\right)_2\right](\tilde{V}_2{}^0 - \tilde{V}_1{}^0)\tilde{V}^{\mathrm{E}} - \frac{x_1x_2}{2}\left[x_2\left(\frac{V_{\mathrm{PT}}V_{\mathrm{P}} - V_{\mathrm{PP}}V_{\mathrm{T}}}{V_{\mathrm{P}}{}^3}\right)_1 + x_1\left(\frac{V_{\mathrm{PT}}V_{\mathrm{P}} - V_{\mathrm{PP}}V_{\mathrm{T}}}{V_{\mathrm{P}}{}^3}\right)_2\right](\tilde{V}_2{}^0 - \tilde{V}_1{}^0)^2 \quad (19)$$

The terms proportional to $(\tilde{V}^{\mathrm{E}})^2$ are invariably small, but the others may be sizable. This derivation does not involve any assumption that the pressure P^0 for process I is small; in fact, one way of avoiding negative pressures in the other processes is to start with a high pressure process I. (Needless to say, the coefficients must then be evaluated at this high pressure "standard state," not at one atmosphere.) By retaining the same final state for the mixture in all three processes, the coefficients in these power series involve properties of the pure components only and not those of the mixture.

It is interesting to note that the free energy $\tilde{A}^{\mathrm{CE}}$ is necessarily smaller algebraically than $\tilde{A}^{\mathrm{VE}}$. This can be demonstrated by a careful comparison of eq. 18 with 8, but is more easily seen by the following argument: The initial states of Process IIA and IIIA have the same total volume, but the two substances in III are at different pressures (*e.g.*, with a piston between); if the inhibition upon IIIA is removed, it proceeds spontaneously to IIA with a decrease in free energy A. To summarize for the same final pressure and volume

$$\tilde{A}^{\mathrm{CE}} < \tilde{A}^{\mathrm{VE}} < \tilde{G}^{\mathrm{E}} \quad (20)$$

No such inequalities are required for the different entropies.

Evaluation of the Parameters

By retaining the same final state for the mixture in all three processes, the coefficients in these power series involve properties of the pure components only and not those of the mixture.

All the coefficients V_{P}, V_{T}, V_{PP} and V_{PT} may be evaluated from the isothermal compressibility $\kappa = -(\partial \ln V/\partial P)_{\mathrm{T}}$, the coefficient of thermal expansion $\alpha = (\partial \ln V/\partial T)_P$, and their temperatures and pressure derivatives

$$V_P = \left(\frac{\partial \tilde{V}}{\partial P}\right)_T = -\tilde{V}\kappa \tag{21}$$

$$V_T = \left(\frac{\partial \tilde{V}}{\partial T}\right)_P = \tilde{V}\alpha \tag{22}$$

$$V_{PP} = \left(\frac{\partial^2 \tilde{V}}{\partial P^2}\right)_T = \tilde{V}\left[\kappa^2 - \left(\frac{\partial \kappa}{\partial P}\right)_T\right] \tag{23}$$

$$V_{PT} = \frac{\partial^2 \tilde{V}}{\partial P \partial T} = -\tilde{V}\left[\alpha\kappa + \left(\frac{\partial \kappa}{\partial T}\right)_P\right] = -\tilde{V}\left[\alpha\kappa - \left(\frac{\partial \alpha}{\partial P}\right)_T\right] \tag{24}$$

Unfortunately precision measurements of $(\partial\kappa/\partial P)_T$ in the low pressure region are virtually nonexistent, so this quantity must be evaluated indirectly. If we utilize the observation[5] that within experimental error $(\partial^2 P/\partial T^2)_V$ is zero, in agreement with most theories of liquids, we can write

$$\left(\frac{\partial^2 P}{\partial T^2}\right)_V \frac{1}{\kappa}\left(\frac{\partial \alpha}{\partial T}\right)_P - \frac{\partial \alpha}{\kappa^2}\left(\frac{\partial \kappa}{\partial T}\right)_P - \frac{\alpha^2}{\kappa^3}\left(\frac{\partial \kappa}{\partial P}\right)_T \cong 0$$

Then

$$V_{PP} \cong \tilde{V}\kappa^2\left[1 - \frac{1}{\alpha^2}\left(\frac{\partial \alpha}{\partial T}\right)_P + \frac{2}{\alpha\kappa}\left(\frac{\partial \kappa}{\partial T}\right)_P\right] \tag{25}$$

For most purposes it suffices to evaluate $(\partial^2 S/\partial V^2)_T$, which, to the above approximation, is given by

$$\frac{\partial^2 \bar{S}}{\partial \bar{V}^2} = \frac{V_{PP}V_T - V_{PT}V_P}{V_P{}^3} \cong \frac{1}{\tilde{V}\kappa}\left[\frac{1}{\alpha}\left(\frac{\partial \alpha}{\partial T}\right) - \frac{1}{\kappa}\left(\frac{\partial \kappa}{\partial T}\right)\right] \tag{26}$$

Actually, one of the best ways of determining the compressibility is from the thermal pressure coefficient $\gamma = (\partial P/\partial T)_V = \alpha/\kappa$. If $(\partial^2 P/\partial T^2)_V = 0$, $(\partial^2 S/\partial V^2)$ is directly related to the temperature variation of $(\partial P/\partial T)_V$ at constant *pressure*.

$$\left(\frac{\partial^2 \bar{S}}{\partial \bar{V}^2}\right)_T \cong \frac{1}{\tilde{V}\alpha}\left(\frac{\partial \gamma}{\partial T}\right)_P = \frac{1}{(\partial \bar{V}/\partial T)_P}\left[\frac{\partial}{\partial T}\left(\frac{\partial P}{\partial T}\right)_V\right]_P \tag{27}$$

Experimental Systems

Seven binary non-electrolyte mixtures for which there are fairly complete thermodynamic measurements are benzene + ethylene chloride, benzene + carbon tetrachloride, acetone + chloroform, acetone + carbon disulfide, carbon tetrachloride + neopentane (2,2-dimethylpropane), isooctane (2,2,4-trimethylpentane) + perfluoroheptane, and n-hexane + perfluorohexane. These cover a wide range of situations and will serve for comparing the constant volume processes with the constant pressure process.

The relevant data for the pure components are summarized in Table II. From these data and the excess functions (at constant pressure) for equimolar mixtures, the constant volume functions for processes IIA and IIIA have been computed[12] (Tables III–IX).

The term $P^0\bar{V}^E$ is always negligible (for P^0 = 1 atmosphere), so for process I, the values for $\bar{G}^E$ and $\bar{H}^E$ are equally well those for $\tilde{A}^E$ and $\tilde{E}^E$.

Values in parentheses for the constant molecular concentration are probably unreliable; $\bar{V}_1{}^0 - \bar{V}_2{}^0$ is so large that the $(\bar{V}_1{}^0 - \bar{V}_2{}^0)^2$ terms in eqs. 18 and 19 are very large and the series cannot safely be terminated with the square terms. No attempt was made to calculate functions for Process III for the system hexane + perfluorohexane (Table VIII).

TABLE II[a]

	t, °C.	$\bar{V}$, cm.³	$-V_P$, 10^{-3} cm.³ atm.	V_T, 10^{-2} cm.³ deg.⁻¹	$-\left(\frac{\partial^2 \bar{S}}{\partial \bar{V}^2}\right)_T$ atm. deg.⁻¹ cm.⁻³	Ref.
Benzene	25	89.4	8.98	11.02	0.65	6, 7
Ethylene chloride	25	79.5	6.55	9.11	.74	7
Carbon tetrachloride	25	97.1	10.59	11.90	.60	7, 8
	0	94.2	8.49	11.10	.75	8, 9
Acetone	35	75.1	10.71	11.18	.54	7
Chloroform	35	81.7	9.52	10.78	.58	7
Carbon disulfide	35	61.4	6.35	7.52	.87	7
Neopentane	0	117.5	30	21.3	(.30)	6, 9
n-Hexane	25	131.6	23.1	18.5	.302	6, 10
Isoöctane	25	166.1	(20)	18.8	(.30)	6
Perfluorohexane	25	202.2	59.0	36.5	.145	10, 11
Perfluoroheptane	25	225.8	53.3	36.3	(.15)	5

[a] Numbers in parentheses are estimates.

TABLE III

Benzene + ethylene chloride, 25°, $x = 1/2$ (ref. 13–15), $\bar{V}^E = 0.24$ cm.³, $\bar{V}_1{}^0 - \bar{V}_2{}^0 = 9.9$ cm.³

Process	I	IIA	IIIA
$\bar{G}^E$, $\tilde{A}^{VE}$, $\tilde{A}^{CE}$/cal.	6.2	6.1	−32
$T\bar{S}^E$, $T\bar{S}^{VE}$, $T\bar{S}^{CE}$/cal.	8.3	−13.9	18
$\bar{H}^E$, $\tilde{E}^{VE}$, $\tilde{E}^{CE}$/cal.	14.5	− 7.8	−14

TABLE IV

Benzene + carbon tetrachloride, 25°, $x = 1/2$ (ref. 14, 16, 17), $\bar{V}^E = 0.01$ cm.³, $\bar{V}_1{}^0 - \bar{V}_2{}^0 = 7.7$ cm.²

Process	I	IIA	IIIA
$\bar{G}^E$, $\tilde{A}^{VE}$, $\tilde{A}^{CE}$/cal.	19.5	19.5	1.2
$T\bar{S}^E$, $T\bar{S}^{VE}$, $T\bar{S}^{CE}$/cal.	6.6	5.8	25
$\bar{H}^E$, $\tilde{E}^{VE}$, $\tilde{E}^{CE}$/cal.	26.1	25.3	26

TABLE V

Acetone + chloroform, 35.2°, $x = 1/2$ (ref. 18–21), $\bar{V}^E = -0.19$ cm.³, $\bar{V}_1{}^0 - \bar{V}_2{}^0 = 6.6$ cm.³

Process	I	IIA	IIIA
$\bar{G}^E$, $\tilde{A}^{VE}$, $\tilde{A}^{CE}$/cal.	−133	−133	−120
$T\bar{S}^E$, $T\bar{S}^{VE}$, $T\bar{S}^{CE}$/cal.	−304	−289	−269
$\bar{H}^E$, $\tilde{E}^{VE}$, $\tilde{E}^{CE}$/cal.	−437	−422	−389

---

(5) B. J. Alder, E. W. Haycock, J. H. Hildebrand and H. Watts, *J. Chem. Phys.*, **22**, 1060 (1954).

(6) "Selected Values of Physical and Thermodynamic Properties of Hydrocarbons and Related Compounds," American Petroleum Institute Research Project 44, Carnegie Press, 1953.

(7) L. A. K. Staveley, W. I. Tupman and K. R. Hart, *Disc. Faraday Soc.*, **15**, 130 (1953); *Trans. Faraday Soc.*, **51**, 321 (1955).

(8) H. Benninga and R. L. Scott, *J. Chem. Phys.*, **23**, 1911 (1955).

(9) H. Benninga and R. L. Scott, unpublished data.

(10) R. D. Dunlap and R. L. Scott, to be published.

(11) R. D. Dunlap, C. J. Murphy, Jr., and R. G. Bedford, *J. Am. Chem. Soc.*, **80**, 83 (1958).

(12) The constant total volume functions for the first four systems were computed by Staveley and co-workers[7] using the unmixed components as the reference and adjusting the volume of the mixture accordingly.

(13) L. Sieg, J. L. Crutzen and W. Jost, *Z. physik. Chem.*, **A198**, 263 (1951).

(14) G. H. Cheesman and A. M. B. Whitaker, *Proc. Roy. Soc. (London)*, **A212**, 406 (1952).

(15) E. A. Coulson, J. L. Hales and E. F. G. Herington, *Trans. Faraday Soc.*, **44**, 636 (1948).

(16) G. Scatchard, S. E. Wood and J. M. Mochel, *J. Am. Chem. Soc.*, **62**, 712 (1940).

(17) S. E. Wood and J. P. Brusie, *ibid.*, **65**, 1891 (1943).

(18) J. v. Zawidski, *Z. physik. Chem.*, **35**, 129 (1900).

(19) J. C. Hubbard, *Phys. Rev.*, **30**, 740 (1910).

(20) H. Hirobe, *J. Faculty Science, Imperial University of Tokyo*, **1**, 155 (1926).

(21) C. R. Mueller and E. R. Kearns, THIS JOURNAL, **62**, 1441 (1958).

TABLE VI

Acetone + carbon disulfide, 35.2°, $x = {}^1/_2$ (ref. 11, 18, 22), $\tilde{V}^E = 1.07$ cm.^{3}, $\tilde{V}_1^0 - \tilde{V}_2^0 = 13.7$ cm.^{3}

Process	I	IIA	IIA
$\tilde{G}^E$, $\tilde{A}^{VE}$, $\tilde{A}^{CE}$/cal.	250	248	170
$T\tilde{S}^E$, $T\tilde{S}^{VE}$, $T\tilde{S}^{CE}$/cal.	99	19	115
$\tilde{H}^E$, $\tilde{E}^{VE}$, $\tilde{E}^{CE}$/cal.	349	267	285

TABLE VII

Carbon tetrachloride + neopentane, 0°, $x = {}^1/_2$ (ref. 23, 24) $\tilde{V}^E = 0.5$ cm.^{3}, $\tilde{V}_1^0 - \tilde{V}_2^0 = -20.4$ cm.^{3}

Process	I	IIA	IIIA
$\tilde{G}^E$, $\tilde{A}^{VE}$, $\tilde{A}^{CE}$/cal.	76	76	− 25
$T\tilde{S}^E$, $T\tilde{S}^{VE}$, $T\tilde{S}^{CE}$/cal.	−1	26	(−318)
$\tilde{H}^E$, $\tilde{E}^{VE}$, $\tilde{E}^{CE}$/cal.	75	102	(−343)

TABLE VIII

Isoöctane + perfluoroheptane, 30°, $x = {}^1/_2$ (ref. 25–27), $\tilde{V}^E = 4.8$ cm.^{3}, $\tilde{V}_1^0 - \tilde{V}_2^0 = -59.7$ cm.^{3}

Process	I	IIA	IIA
$\tilde{G}^E$, $\tilde{A}^{VE}$, $\tilde{A}^{CE}$/cal.	326	318	(−117)
$T\tilde{S}^E$, $T\tilde{S}^{VE}$, $T\tilde{S}^{CE}$/cal.	182	−60	(−683)
$\tilde{H}^E$, $\tilde{E}^{VE}$, $\tilde{E}^{CE}$/cal.	508	258	(−800)

TABLE IX

n-Hexane + *n*-perfluorohexane, 25°, $x = {}^1/_2$ (ref. 26–28), $\tilde{V}^E = 4.84$ cm.^{3}, $\tilde{V}_1^0 - \tilde{V}_2^0 = -70.6$ cm.^{3}

Process	I	IIA	IIIA
$\tilde{G}^E$, $\tilde{A}^{VE}$, $\tilde{A}^{CE}$/cal.	323	316	...
$T\tilde{S}^E$, $T\tilde{S}^{VE}$, $T\tilde{S}^{CE}$/cal.	193	−59	...
$\tilde{H}^E$, $\tilde{E}^{VE}$, $\tilde{E}^{CE}$/cal.	516	257	...

Discussion

In statistical mechanics it is usually more convenient to specify the volume of a system than to specify its pressure, so most theories of solutions start by calculating ΔA for a constant volume mixing process. While the distinction is not always made explicitly clear, it is evident that a formulation which calculates the properties of N molecules in volume V will yield directly our Process III, that at constant molecular concentration. It is obvious that, in any simple lattice theory of solutions, the lattice dimensions are conserved and that only Process III is of direct significance. Yet, in experimental papers, the functions for the constant total volume Process II are computed and compared with lattice predictions which appear to apply only to Process III.

It is evident from the calculations of the previous section that the differences in free energy and entropy between the two "constant volume" processes II and III are frequently greater than between I and II, so conclusions can be drawn from the "constant volume" functions only with great caution.[29] Indeed one might suggest that "constant volume" quantities are of significance only if compared with a theory which can distinguish between the two kinds of "constant volume" and predict a difference between them, or when $V_1^0 - V_2^0$ is so small that the differences are negligible.

A careful examination of Tables III to VIII suggests that this negative conclusion may be too severe.

We first exclude the system acetone + chloroform (Table V) where hydrogen-bonding produces a large negative excess entropy compared with which volume effects are unimportant. In the other six systems the constant volume functions IIA seem better than I or IIIA (or at least as good—in benzene + ethylene chloride and benzene + carbon tetrachloride, the differences are trivial, and the $TS^{VE} = 26$ cal. for carbon tetrachloride + neopentane, while larger than TS^E, is still small). Large constant pressure excess entropies for three systems (Tables VI, VIII and IX) are reduced to S^{VE}'s for process IIA which are small fractions of S^E. It should not be surprising that no excess entropy is exactly zero, but small values of TS^{VE} (*e.g.*, less than ± 30 cal. or 10% of RT) are in rough agreement with Hildebrand's picture of a regular solution[30] and Scatchard's similar model,[31,2a] and also with the predictions of a simple lattice model (*e.g.*, the "strictly regular solution" of Guggenheim[32]) if we can avoid the conclusion that it is TS^{CE} which is appropriate to this last.

The large values of the excess functions for mixing at constant molecular concentration are probably without any simple physical significance, but rather a measure of the artificiality of applying a lattice model to mixtures of molecules of different size. The process of compressing one component and expanding the other to fit the same lattice is required by the rigidity of the lattice model, which also requires the mixture to arrange its various molecules on the same lattice. In the actual solution, the molecules can accommodate themselves to size differences; no one really expects A–A, A–B and B–B nearest neighbor distances to be identical.

It appears that the constant volume (equal initial pressure) process II is much more meaningful than the constant molecular concentration process III, and somewhat more meaningful than the constant pressure process I, and that for simple non-electrolyte systems the major contribution to large excess entropies is the entropy of expansion or contraction resulting from the volume change on mixing.

Support for this conclusion is offered by the fact that the excess entropy of dilute solutes is almost entirely eliminated when one corrects from $\bar{S}_1^E$ to $\bar{S}_1^{VE}$. Hildebrand and Scott[33] have shown that the partial molar excess entropy of solution of iodine in solvents such as carbon tetrachloride and perfluoroheptane is very large (as much as 8 cal. deg.$^{-1}$ mole^{-1}) for the constant pressure process but much smaller for the constant total volume

---

(22) G. C. Schmidt, *Z. physik. Chem.*, **121**, 221 (1926).

(23) V. Mathot and A. Desmyter, *J. Chem. Phys.*, **21**, 782 (1953).

(24) A. Englert-Chwoles, *ibid.*, **23**, 1168 (1955).

(25) C. R. Mueller and J. E. Lewis, *ibid.*, **26**, 287 (1957).

(26) A. G. Williamson and R. L. Scott, *J. Phys. Chem.*, accepted for publication.

(27) C. Booth and R. L. Scott, to be published.

(28) R. D. Dunlap, R. G. Bedford, J. G. Woodbury and S. D. Furrow, *J. Am. Chem. Soc.*

(29) To this situation there is one exception. If, as we have assumed, $(\partial^2P/\partial T^2)_V = 0$, then $(\partial C_V/\partial V)_T$ is also zero; in that case ΔC_V will be the same for all three processes, although of course very different from ΔC_P.

(30) Reference 2, especially Chapters VI and VIII.

(31) G. Scatchard, *Chem. Revs.*, **8**, 321 (1931); *Kemisk Maanedsblad, (Copenhagen)*, **13**, 77 (1932).

(32) E. A. Guggenheim, "Mixtures," Oxford University Press, 1952.

(33) J. H. Hildebrand and R. L. Scott, *J. Chem. Phys.*, **20**, 1520 (1952).

process II. (Here $\tilde{V}_1^0 - \tilde{V}_2^0$ is so large that the third process would be physically meaningless.)

A completely satisfying theoretical justification of these conclusions remains to be found; the simple corresponding states approach is a notable failure in this regard.[4]

Still other "constant volume" processes can be envisioned, for example:

1. A process in which the two pure components are adjusted so that they have the same degree of expansion over the close-packed volumes (*i.e.*, the volume of the hypothetical supercooled liquid at 0°K.). This might be a better constant volume process than the simple constant total volume process II, but extensive density–temperature data are required for extrapolation to 0°K.

2. Mixtures of chain molecules can be treated by an extension of the lattice theory to molecules occupying multiple sites.[29] A constant segment concentration model analogous to Process III for molecules occupying single sites would then be appropriate. Since the number of segments is approximately proportional to the molar volume, this is unlikely to give results significantly different from those for the simple constant total volume process II. However, for such kinds of molecules, this more carefully defined model offers an explanation for the satisfactory numbers obtained for process II. Unfortunately it does not seem possible to extend this argument to all systems (*e.g.* to hydrocarbon–fluorocarbon systems where the length of a CF_2 and a CH_2 segment may be the same, but the cross-sectional area is so different as to make the placement of different kinds of segments on regular lattice sites an absurdity.)

3. Another "constant volume process" would be obtained by taking as the initial states the pure components at molar volumes equal to their partial molar volumes in the solution. For solutions whose compositions are near $x = {}^1/_2$, the thermodynamic functions so calculated would not differ greatly from those for the simple constant total volume process II. In dilute solutions, however, this model will give very peculiar results. For example, the partial molar volume $\bar{V}_2$ of iodine in perfluoroheptane at 25° is 100 cm.^{3}, far greater than the $V_2 = 59$ cm.^{3} for hypothetical liquid iodine at 25°. The entropy of expanding liquid iodine by 70% is hard to estimate, but it is surely far more than that needed to account for $\bar{S}_2^E$.

In conclusion, it appears that the usual practice of converting thermodynamic functions for mixing at constant pressure to the corresponding functions for mixing at constant total volume has considerable empirical justification and probably yields more meaningful numbers than any other procedure.

Acknowledgments.—The research here reported was started in 1955 while the author was a John Simon Guggenheim Fellow at the University of Cambridge and completed with the support of the U. S. Atomic Energy Commission under Project 13 of Contract AT(11-1)-34 with the University of California. The author wishes to thank Dr. M. L. McGlashan of the University of Reading, Professor R. D. Dunlap of the University of Maine, and Dr. A. G. Williamson of the University of Otago for helpful and stimulating discussions of these problems.

Appendix

Some of the processes outlined above involve initial or final states which are under a negative pressure. Such states are at least thermodynamically metastable, and possibly completely unstable (negative compressibility κ) and thus non-existent. If any are in fact unstable, a power series in $(\tilde{V} - \tilde{V}^0)$ of the kind we terminated at the square terms might not converge. Under such conditions, which occur when $\tilde{V}_1^0 - \tilde{V}_2^0$ is large, it is questionable whether any constant molecular concentration process is physically meaningful. However, the negative pressures can be avoided by choosing reference volumes such that all pressures are positive.

We define processes II and III more generally

		(x_1 moles of 1) +	(x_2 moles of 2) $\longrightarrow$	(1 mole of mixture)
II	Constant volume equal initial pressures	P_i'', $\tilde{V}_1''$	P_i'', V_2''	P_m'', $\tilde{V}_m'' = x_1\tilde{V}_1'' + x_2\tilde{V}_2''$
III	Constant molecular concn.	P_1''', $\tilde{V}'''$	P_2''', $\tilde{V}''$	P_m''',$\tilde{V}'''$

None of these pressures (P_i'', P_m'', P_1''', P_2''' or P_m''') are necessarily the pressure $P' = P^0$ of the constant pressure process, nor are any of the volumes necessarily equal to any of the volumes $\tilde{V}_1^0$, $\tilde{V}_2^0$ or $\tilde{V}_m^0$ of the constant pressure process.

By integrations and power series expressions similar to those utilized in obtaining eq. 1–19, one can obtain the relations

Process II

$$\tilde{A}^{VE}(T,V_m'') - G^E(T,P^0) = -\frac{1}{2(V_P{}^0)_m}(\tilde{V}_m'' - \tilde{V}_m{}^0)^2 + \frac{1}{2\langle V_P{}^0\rangle}(\tilde{V}_m'' - \tilde{V}_m{}^0 + \tilde{V}^E)^2 + \ldots \quad (28)$$

$$\tilde{S}^{VE}(T,V_m'') - \tilde{S}^{VE}(T_1P^0) = -\left(\frac{V_T{}^0}{V_P{}^0}\right)(\tilde{V}_m'' - \tilde{V}_m{}^0) + \frac{\langle V_T{}^0\rangle}{\langle V_P{}^0\rangle}(\tilde{V}_m'' - \tilde{V}_m{}^0 + \tilde{V}^E) - \frac{1}{2}\left(\frac{V_{PT}{}^0V_P{}^0 - V_{PP}{}^0V_T{}^0}{(V_P{}^0)^3}\right)_m(\tilde{V}_m'' - \tilde{V}_m{}^0) + \frac{\langle V_{PT}{}^0\rangle\langle V_P{}^0\rangle - \langle V_{PP}{}^0\rangle\langle V_T{}^0\rangle}{2\langle V_P{}^0\rangle^3}(\tilde{V}_m'' - \tilde{V}_m{}^0 + \tilde{V}^E)^2 + \ldots \quad (29)$$

When $\tilde{V}_m''$ is set equal to $\tilde{V}_m{}^0$, the volume of the solution after mixing at constant pressure, we convert eq. 28 and 29 into eq. 8 and 10 for process IIA. If, on the other hand, we set $\tilde{V}_m''$ equal to $\tilde{V}_u{}^0 = x_1\tilde{V}_1{}^0 + x_2\tilde{V}_2{}^0$, the volume of the unmixed components, we obtain a different constant volume–equal initial pressure process which we designate as Process IIB. In this variant, the original "constant volume" process first studied by Scatchard,[2a] we perform the necessary expansion or compression on the solution rather than on the unmixed components. If we substituted $\tilde{V}_m'' = \tilde{V}_u^0 = \tilde{V}_m^0 - \tilde{V}^E$ into eq. 28 and 29 we obtain

Process IIB

$$\tilde{A}^{VE}(T,\tilde{V}_u^0) - G^E(T,P^0) = -\frac{1}{2(V_P^0)_m}(\tilde{V}^E)^2 + \ldots \tag{30}$$

$$\tilde{S}^{VE}(T,\tilde{V}_u^0) - S^E(T_1P^0) = -\left(\frac{V_T^0}{V_P^0}\right)\tilde{V}^E - \frac{1}{2}\left[\frac{V_{PT}^0V_P^0 - V_{PP}^0V_T^0}{(V_P^0)^3}\right]_m (V^E)^2 + \ldots \tag{31}$$

Equations 30 and 31 are actually even simpler than eq. 8 and 10, but the necessary data are generally less available for the solution than for the pure components.

The differences between the IIB and IIA functions usually are trivial because of the small size of $\tilde{V}^E$, so that the distinction between the two usually can be ignored. Thus, for benzene + ethylene chloride (Table III), $\tilde{A}_{IIB}{}^{VE} - \tilde{A}_{IIA}{}^{VE} = 0.2$ cal., while $T(\tilde{S}_{IIB}{}^{VE} - \tilde{S}_{IIA}{}^{VE}) = -0.03$ cal. In the worst of our seven cases, *n*-hexane + *n*-perfluorohexane (Table IX), $\tilde{A}_{IIB}{}^{VE} - \tilde{A}_{IIA}{}^{VE} = 12$ cal., while $T(\tilde{S}_{IIB}{}^{VE} - \tilde{S}_{IIA}{}^{VE}) = 42$ cal.; this last correction is small compared with the differences between Processes I and II, and is of uncertain significance. $T\tilde{S}_{IIB}{}^{VE}$ becomes -17 cal., closer to zero than the value for process II. This improvement may result from the fact that when the volume change is positive, process IIB takes place in a smaller volume, at higher density, where the intuitive notion that S^{VE} should be zero is possibly more nearly valid.

We now turn to the general process III

Process III

$$\tilde{A}^{CE}(T,\tilde{V}''') - A^E(T,P^0) = -\frac{1}{2(V_P^0)_m}(\tilde{V}''' - \tilde{V}_m^0)^2 + \frac{x_1}{2(V_P^0)_1}(\tilde{V}''' - \tilde{V}_1^0)^2 + \frac{x_2}{2(V_P^0)_2}(\tilde{V}''' - \tilde{V}_2^0)^2 + \ldots \tag{30}$$

$$\tilde{S}^{CE}(T,\tilde{V}''') - \tilde{S}^E(T,P^0) = \left(\frac{V_T^0}{V_P^0}\right)_m(\tilde{V}''' - \tilde{V}_m^0) - x_1\left(\frac{V_T^0}{V_P^0}\right)_1(\tilde{V}''' - \tilde{V}_1^0) - x_2\left(\frac{V_T^0}{V_P^0}\right)_2(\tilde{V}''' - \tilde{V}_2^0) - \frac{1}{2}\left(\frac{\partial^2 S}{\partial V^2}\right)_m(\tilde{V}''' - \tilde{V}_m^0)^2 + \frac{x_1}{2}\left(\frac{\partial^2 S}{\partial V^2}\right)_1(\tilde{V}''' - \tilde{V}_1^0)^2 + \frac{x_2}{2}\left(\frac{\partial^2 S}{\partial V^2}\right)_2(\tilde{V}''' - \tilde{V}_2^0)^2 + \ldots \tag{31}$$

Presumably we should select $\tilde{V}'''$ as the smallest of the set $\tilde{V}_1^0$, $\tilde{V}_2^0$, $\tilde{V}_m^0$, in which case negative pressures are avoided. This we designate as process IIIB.

The differences between the IIIB and IIIA functions are more important because $\tilde{V}_m^0 - \tilde{V}'''$ is sizable in most cases. For example, for benzene + ethylene chloride, if we choose $\tilde{V}''' = \tilde{V}_2^0 = 79.5$ ml., we obtain $\tilde{A}_{IIIB}{}^{CE} - \tilde{A}_{IIIA}{}^{CE} = 17$ cal. and $T(\tilde{S}_{IIIB}{}^{CE} - \tilde{S}_{IIIA}{}^{CE}) = -7$ cal.; this makes $\tilde{A}_{IIIB}{}^{CE} = -15$ cal. and $T\tilde{S}_{IIIB}{}^{CE} = 11$ cal. These are still significantly different from those for process II, but their difference from the values for process IIIA is a measure of the unreality of the constant molecular density process for large $\tilde{V}_1^0 - \tilde{V}_2^0$.

THE REACTION OF HYDROGEN ATOMS WITH SOLID PROPENE AT LOW TEMPERATURES[1]

BY RALPH KLEIN,[2a] MILTON D. SCHEER AND JOHN G. WALLER[2b]

National Bureau of Standards, Washington, D. C.

Received February 15, 1960

The reaction of hydrogen atoms with solid films of propene has been studied below 100°K. The hydrogen atoms diffuse through and react with the propene films to form propane and 2,3-dimethylbutane. A one dimensional diffusion equation containing a chemical reaction term is used to describe the kinetics of this process. A value of 5×10^7 cc./mole sec. is obtained for the specific rate constant at 77°K. for the reaction $H + CH_3\text{-}CH{=}CH_2 \rightarrow CH_3\text{-}CH\text{-}CH_3$. The ratio of propane to 2,3-dimethylbutane is about 9 and does not change as the concentration of propene is varied over two orders of magnitude. The propane as well as the 2,3-dimethylbutane must therefore be formed by a process which is second order with respect to the isopropyl radical concentration.

Introduction

The observation that hydrogen atoms react with solid olefins at low temperatures, and the technique used for following these reactions, provide a quantitative approach to kinetic studies in the low temperature region. Simplification occurs through the absence of high activation energy reactions, but diffusion processes could in some instances be rate controlling.

In the approach described previously,[3] the reaction between hydrogen atoms and solid olefins deposited on a −195° wall was followed by noting the pressure decrease in the reaction vessel containing the hydrogen gas. The atoms were generated thermally on a tungsten ribbon. Observations also have been made using an electrodeless discharge as the atom source with similar results. Direct information on the course of the reaction may be obtained by examining the olefin film during reaction by spectroscopic methods. Spin resonance measurements are used to establish

---

(1) This research was performed under the National Bureau of Standards Free Radicals Research Program, supported by the Department of the Army.

(2) (a) Guest Scientist, Melpar, Inc.; (b) Guest Scientist, British Oxygen Research and Development, Ltd.

(3) R. Klein and M. D. Scheer, THIS JOURNAL, **62**, 1011 (1958).

an upper limit on the number of free spins in the solid. Certain features of a reaction system in which gas phase species impringe on, diffuse into, and react with a solid can be described in a general way. The propene–hydrogen atom system has been chosen for study.

Experimental Results

The reaction was studied in a system described previously.[3] Products were analyzed after warm-up with gas–liquid chromatography and mass spectroscopy. In the hydrogen atom addition to solid propene, only propane and a six carbon alkane are formed. Methane, a product of atomic cracking reactions, never has been observed. The hexane products for the gas phase reaction have been shown to be predominantly 2,3-dimethylbutane,[4a,b] with a small amount of 2-methylpentane. The hydrogen atom addition to *solid* propene also results in 2,3-dimethylbutane, the dimer of isopropyl. At most about 8% of the C_6 fraction is 2-methylpentane. This is indicated in Table I where pertinent mass spectral peaks are compared with those for standard samples of 2-methylpentane and 2,3-dimethylbutane.

The ratio of propane to 2,3-dimethylbutane in the products is of considerable importance for establishing the mechanism of the hydrogen atom addition reaction to solid propene. Analysis was made with gas chromatography on a two meter dimethylsulfolane on Chromosorb column at 50°. Table II gives the propane–C_6 ratios for various film thicknesses, temperatures, propene concentrations, conversions, and gas phase concentration of hydrogen atoms. The concentration of propene was controlled by admixture with butane and the H atom concentration was fixed by the tungsten ribbon temperature. The results given in Table II show that the propane–C_6 ratio is remarkably constant, but considerably higher than the value of about 0.5 found for the gas phase reaction in the pressure region where atomic cracking is minimized.[4b]

TABLE I

RELATIVE MASS SPECTRAL PEAKS FOR THE C-6 FRACTION FROM THE PRODUCTS OF THE REACTION OF H WITH SOLID C_3H_6 AT 77°K.

Standard samples shown for comparison.

m/e	2-Methylpentane	2,3-Dimethylbutane	C-6 fraction from H atom addition to solid propene
86	7.7	16.0	16.0
71	100.0	100.0	100.0
70	23.4	3.9	5.0
57	42.5	3.1	6.2
56	16.9	4.2	5.2
55	21.0	33.4	32.0

TABLE II

PROPANE/C_6 RATIO UNDER VARIED EXPERIMENTAL CONDITIONS

Relative film thickness	Film temp., °K.	Mole fraction of propene	Fractional conversion	Tugsten ribbon temp., °K.	$\frac{\text{Propane}}{C_6}$
1	77	1.0	0.45	1600	8.3
3	77	0.3	.45	1600	9.2
10	77	.1	.45	1600	9.8
60	77	.01	.20	1600	9.2
1	90	1.0	.40	1600	9.1
10	90	0.1	.50	1600	9.7
1	77	1.0	.20	1100	7.9
1	77	1.0	.05	2000	9.2

The distribution of deuterium in the products of the deuterium atom addition to solid propene is of interest. The isotope experiments, reported briefly in reference 1, have been extended to include the analysis of both propene and propane. These were separated on a two meter silica gel column, and each fraction was analyzed separately with a mass spectrometer. The isotope distribution is shown in Table III. A sample of the deuterium remaining in the reaction vessel at the end of the deuteration reaction showed no HD.

The possibility of stabilizing alkyl radicals in the matrix by hydrogen atom addition to solid olefins has been previously implied. This has now been investigated with electron spin resonance spectroscopy. A cylindrical x-band microwave cavity (H_{111} mode) was designed to serve as a reaction vessel. The hydrogen atom source was a hot tungsten ribbon mounted in the cavity. The latter could be immersed in liquid nitrogen during operation. Free spins were not observed, even when the propene was diluted to 1% in propane. The maximum steady-state radical concentration was less than 10^{15} per cc.

TABLE III

THE ADDITION OF D ATOMS TO PROPENE AT 77°K.

$T_{\text{ribbon}} = 2000$°K; $(P_{D_2})_{\text{initial}} = 150\ \mu$; 80 μmoles of propene initially.

	Product analysis, μ moles
Propene-d_0	41
Propene-d_1	7
Propene-d_2	1
Propene-d_3	0.2
Propene-d_4	0.1
Propane-d_1	19
Propane-d_2	6
Propane-d_3	1
Propane-d_4	0.2
Propane-d_5	0.06

The question of effect of film thickness on the rate of reaction has been re-investigated. Ten to one butane to propene mixtures were condensed in films whose thickness was varied from 6×10^{-6} to 3×10^{-4} cm. Figure 1 shows the change in the initial rate of hydrogen pickup with film thickness. It is clear that for films above a certain thickness (in this case about 2×10^{-4} cm.), the rate is independent of thickness. Below this value a linear relationship holds. For films of pure propene a similar behavior must apply but the linear region would occur at much smaller film thicknesses. The observations reported previously[3] were made only in the thick film region.

Diffusion in the Solid.—Hydrogen atoms produced in the gas phase impinge on the deposited olefin film and diffuse through and react with it. The layer of propene is taken as a slab of uni-

---

(4) (a) W. J. Moore and L. A. Wall, *J. Chem. Phys.*, **17**, 1325 (1949); (b) P. J. Boddy and J. C. Robb, *Proc. Roy. Soc.* (*London*), **249**, 518 (1959).

form thickness, l (Fig. 2). At $X = l$ the hydrogen atom concentration is designated as H_0. The appropriate one dimensional steady-state diffusion equation with chemical reaction is

$$D\,\frac{\partial^2 H}{\partial X^2} = KH \qquad (1)$$

where D is the diffusion coefficient and $K = k_1(\mathrm{Pr})$, k_1 being the specific rate constant for the hydrogen atom addition to propene, Pr. The boundary conditions are

$$H = H_0 \text{ at } X = 0$$

$$\frac{\partial H}{\partial X} = 0 \text{ at } X = l$$

The latter arises because the surface on which the olefin is deposited is assumed neither to adsorb nor cause recombination of hydrogen atoms. The solution of (1) is

$$H = H_0\left[\cosh\sqrt{\frac{K}{D}}\,X - \tanh\sqrt{\frac{K}{D}}\,l\,\sinh\sqrt{\frac{K}{D}}\,X\right] \qquad (2)$$

In terms of the observed rate

$$-\frac{2}{A}\left(\frac{\mathrm{d}H_2}{\mathrm{d}t}\right)_{\text{initial}} = \int_0^l KH\,\mathrm{d}x = \sqrt{DK}\,H_0\tanh\sqrt{\frac{K}{D}}\,l \qquad (3)$$

where A is the area of the film. Two limiting cases for the rate are those in which (a) the hyperbolic tangent is approximately equal to its argument and (b) the hyperbolic tangent is approximately equal to one. Case (a) is equivalent to a film in which the hydrogen atom concentration is constant throughout and equal to H_0.

$$-\frac{2}{A}\left(\frac{\mathrm{d}H_2}{\mathrm{d}t}\right)_{\text{initial}} = KH_0l \qquad (4)$$

It is evident that the rate should be directly proportional to the film thickness and the propene concentration in this region. If the boundary condition $H = 0$ at $X = l$ obtained, the hydrogen atom concentration profile for thin films and low propene concentrations would be linear in X. This requires a dependence of rate proportional to the second power of the film thickness. The experimental results clearly show a linear relationship, and hence the boundary condition $\partial H/\partial X = 0$ at $X = l$ is most probably correct. For case (b)

$$-\frac{2}{A}\left(\frac{\mathrm{d}H_2}{\mathrm{d}t}\right)_{\text{initial}} = \sqrt{DK}\,H_0 \qquad (5)$$

Here the rate is independent of film thickness but proportional to the square root of propene concentration. As the film thickness is increased, the expected departure from linearity occurs as seen in Fig. 1. The entire curve closely approximates that of a hyperbolic tangent as required by the model. This indicates that the assumptions made are reasonably correct.

Calculation of the pertinent constants can now be made. It is assumed that the concentration of H atoms on either side of $X = 0$ is approximately the same. The value of H_0, the concentration of hydrogen atoms at the surface of the film, is computed from the tungsten ribbon temperature, 2000°K. in these experiments, and the hydrogen pressure in the vessel, 30 μ. The assumption is made that atom recombination does not occur in the gas and the rate of dissociation at the filament is rapid compared to recombination at the wall. This leads to a value of H_0 equal to 5×10^{-10} moles/cc. The slope of the linear region of Fig. 1 gives a value for KH_0 of 25×10^{-6} mole/cc. sec. With $(\mathrm{Pr}) = 1 \times 10^{-3}$ mole/cc., the reaction rate constant for the addition of hydrogen atoms to propene at 77°K. is calculated to be $k = 5 \times 10^7$ cc./moles sec. This is a lower limit for k since the hydrogen atom concentration used in the calculation represents an upper limit value. It is interesting to note that, without taking account of the change from solid to gas, a value of 1.5 kcal. for the activation energy of this reaction leads to a value of $k = 10^{11}$ at 300°K. the same as that determined by Melville and Robb.[5] The diffusion coefficient D for H atoms in butane at 77°K. may be derived from the data of Fig. 1 and equation 6.

$$\sqrt{DK}\,H_0 = 2.5 \times 10^{-9}$$

$$D = 5 \times 10^{-4}\ \text{cm.}^2/\text{sec.} \qquad (6)$$

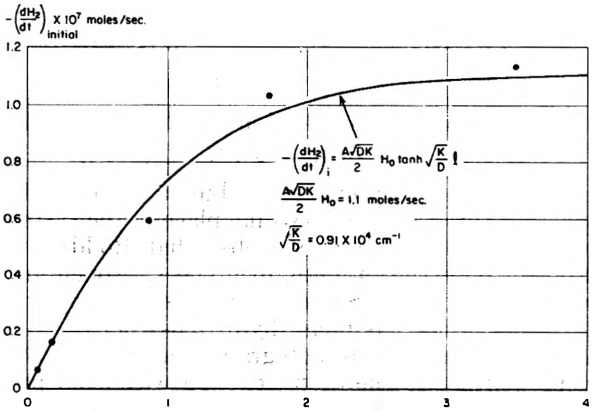

Fig. 1.—The variation of the initial rate of hydrogen pickup with film thickness.

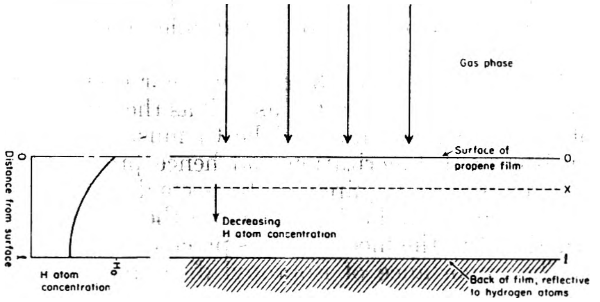

Fig. 2.—Schematic model for the interaction of hydrogen atoms with propene films.

Chemical Mechanism.—Chemical evidence shows that reactions (1), (2) and (3) occur in the hydrogen-atom–solid propene system at low temperatures

$$\mathrm{H} + \mathrm{CH_3{-}CH{=}CH_2} \longrightarrow \mathrm{CH_3{-}\dot{C}H{-}CH_3} \qquad [1]$$

$$\mathrm{CH_3{-}\dot{C}H{-}CH_3} + \mathrm{CH_3{-}\dot{C}H{-}CH_3} \longrightarrow \mathrm{CH_3{-}CH_2{-}CH_3} + \mathrm{CH_3{-}CH{=}CH_2} \qquad [2]$$

---

(5) H. W. Melville and J. C. Robb, *ibid.*, **A196**, 494 (1949).

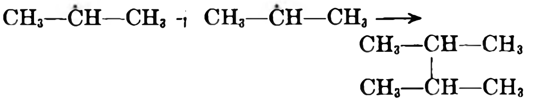
$$CH_3—\dot{C}H—CH_3 + CH_3—\dot{C}H—CH_3 \longrightarrow \begin{matrix} CH_3—CH—CH_3 \\ | \\ CH_3—CH—CH_3 \end{matrix}$$ [3]

The hydrogen atom addition to the radical has

$$H + CH_3—\dot{C}H—CH_3 \longrightarrow CH_3—CH_2—CH_3 \quad [4]$$

been postulated previously,[3] but it is doubtful whether this reaction does take place in the system under study. It may be noted that Boddy and Robb[4b] observed 4-methylpentene-1, isopentane, and eight other fractions upon subjecting the products of the gas phase hydrogen-atom reaction with propene to chromatographic analysis. This is in contrast to the atom reaction with solid propene at −195° where only propane and a C_6 are ever observed. The latter, as previously noted, consists of at least 92% 2,3-dimethylbutane. Further, methane never has been detected either mass spectrometrically or with g.l.c. There is no doubt that reactions referred to as "atomic cracking" do not occur.

Equations 1, 2 and 3, if they occur exclusively, explain product formation as well as the invariance of the propane-C_6 ratio. The C_6 must be formed by isopropyl dimerization and hence propane formation is also required to be second order with respect to the radical. Therefore the inclusion of reaction 4 in the mechanism is precluded.

The importance of isopropyl disproportionation is further demonstrated by the deuterium distribution in the products of $D + CH_3—CH═CH_2$ shown in Table III. The extensive deuteration of the propene and the formation of deuterated propanes other than propane-d_2 is most readily accounted for by the occurrence of reaction 2 rather than 4.

The high propane to 2,3-dimethylbutane ratio might be interpreted to support the hypothesis of persistence of excess energy in the radical since the addition of a hydrogen atom to propene is exothermic to the extent of 43 kcal./mole. In the gas phase, in the region of 300°K., a ratio of 0.5 is obtained under conditions where the radicals are thermalized.[4b,6] It has been observed that this ratio increases at lower pressures, an indication that disproportionation is favored over dimerization for "hot" radicals.[4b,7] It must be pointed out, however, that the high value of the propane to C_6 ratio obtained in this work at 77°K. in comparison with the ratio for temperatures in the vicinity of 300°K. obtained by other investigators[4b,8] may well be explained by an activation energy difference of only 0.3 kcal. between the disproportionation and recombination reactions.

[6] M. H. J. Wijnen and E. W. R. Steacie, *Can. J. Chem.*, **29**, 1092 (1951).

[7] R. A. Back, *ibid.*, **37**, 1834 (1959).

[8] R. W. Dunham and E. W. R. Steacie, *ibid.*, **31**, 377 (1953).

SOME ASPECTS OF THE ROTATING SECTOR DETERMINATION OF THE ABSOLUTE RATE CONSTANTS IN RADICAL POLYMERIZATION REACTIONS[1]

By HAROLD KWART[2]

Converse Memorial Laboratory of Harvard University and the Department of Chemistry of the University of Delaware, Newark, Del.

Received February 18, 1960

Some of the possible sources of error in the rotating sector determination are examined. A method of computing the absolute rate constants in radical photopolymerization reaction has been devised which takes account of dark reaction rates in both the dark and light periods of the measurement. A basis is presented for estimating the magnitudes of dark reaction rates which can be neglected in such calculations. Consideration also is given to the effect of a non-uniform distribution of radical centers due to such factors as non-uniform absorption of the incident beam.

The average lifetime of radicals in a chain reaction is most readily determined by means of the rotating section method. The theory of this experiment was delineated originally by Briars, Chapman and Walters[3] and subsequently discussed by Dickinson,[4] Swain and Bartlett[5] and by Burnett and Melville.[6] All these authors[4–6] have developed somewhat different approaches to computing radical lifetimes in homopolymerization reactions from data obtained by rotating sector measurements in photoinitiated reactions. Similar developments have been published with certain extensions to take consideration of a steady dark rate accompanying the intermittent photoreaction. Gee and Bateman[7] have presented a method of computation in cases of radical chain oxidation processes where the thermal dark rate is very appreciable. Matheson, Auer, Bevilacqua and Hart[8] have shown that this situation also occurs in many photopolymeri-

---

[1] This work was supported by the Office of Naval Research, Project No. NR-056-095; Principal Investigator, Professor P. D. Bartlett. Part of the material in this article was presented in a technical report to the O.N.R., No. N5-ori-76, June 1, 1949.

[2] Department of Chemistry, University of Delaware, Newark, Delaware.

[3] F. Briars, D. L. Chapman and E. Walters, *J. Chem. Soc.*, 562 (1926).

[4] See W. A. Noyes, Jr., and P. A. Leighton, "The Photochemistry of Gases," Reinhold Publ. Corp., New York, N. Y., 1941, p. 202, *et seq.*

[5] C. G. Swain and P. D. Bartlett, *J. Am. Chem. Soc.*, **68**, 2381 (1946).

[6] G. M. Burnett and H. W. Melville, *Proc. Roy. Soc. (London)*, **A189**, 456 (1947).

[7] G. Gee and L. Bateman, *Proc. Roy. Soc. (London)*, **A195**, 376 (1948).

[8] M. S. Matheson, E. E. Auer, E. B. Bevilacqua and E. J. Hart, *J. Am. Chem. Soc.*, **71**, 497 (1949).

zation reactions and particularly where photosensitizers have been used as secondary initiators. However, the treatment of these authors, essentially an extension of the Dickinson treatment,[4] deals only with cases where the thermally induced and other dark reaction rates are accounted in the dark periods and are neglected in the light periods of a full cycle of sector alternation.

Several assumptions have been made tacitly in all these analyses. One of the most important is the fact that the distribution of radicals throughout the reaction system has been taken to be perfectly uniform. In using photoinitiation it is implied that the absorption of the incident radiation is quite weak. This is also to say that the entire entrance face of the reaction cell must be uniformly illuminated and must transmit an entirely homogeneous incident beam with uniform intensity to each element of volume. Some difference of view[5,6] has occurred as to what extent this idealization of the experimental method must be approached. Kwart, Broadbent and Bartlett[9] have attempted to minimize the possibility of a significant effect due to such non-uniformity in illumination. Burnett, Valentine and Melville[10] have taken some steps in the effort to demonstrate whether or not radical polymerization is localized in a given experiment. An evaluation of the extent of non-uniformity of this nature which could or could not be neglected in the rotating sector measurements has not been presented previously.

In this article we have undertaken to examine the open questions posed above, namely, development of a form of the rotating sector procedures in calculating the rate parameters, taking into account dark reaction rates in the light period as well as the dark. Furthermore, we are presenting here an estimate of the extent of thermal and other kinds of dark reaction initiation, as well as the extent of non-uniformity in illumination and consequently radical formation, that can be neglected in ordinary calculations of these parameters.

Rotating Sector Measurements with Significant Dark Reaction Throughout a Cycle.—The mechanism of polymerization under these circumstances is given by the equations

$$\text{Heat and/or light} \xrightarrow[\text{sensitizer}]{via} 2\text{R}\cdot$$

$$\text{R}\cdot + \text{M} \xrightarrow{k_p} \text{R}\cdot$$

$$2\text{R}\cdot \xrightarrow{k_t} \text{Inert products either through disproportionation or bimolecular combination}$$

Denoting the light intensity by I and the rate of chain initiation *via* light as fI, we shall assume in the first case that the absorption of light by sensitizer (and therefore chain initiation) occurs uniformly throughout the body of polymerizable liquid. In addition we have a dark rate denoted by ρ due to thermal dissociation of the sensitizer into chain initiating radicals of the same nature as those resulting from photodissociation. Thus, during a period of illumination

$$\frac{dR}{dt} = (fI + \rho) - 2k_tR^2 \qquad (1)$$

This readily is integrated to

$$R = R_s + \tanh(B_1t)$$

where

$$R_s = \sqrt{\frac{fI + \rho}{2k_t}} \text{ and } B_1 = \sqrt{(fI + \rho)2k_t}$$

Let $\tau = B_1t$ and $Y = R/R_s$; hence

$$Y = \tanh(\tau) \qquad (2)$$

During a period of darkness

$$\frac{dR}{dt} = \rho - 2k_tR^2 \qquad (3)$$

which may be integrated

$$R = R_s' \coth(B_2t) \qquad (4)$$

By comparing coefficients it will be seen that $R_s' = \sqrt{\rho/2k_t}$, $B_2 = 2k_tR_s'$; and on proper substitution in (4) we get

$$R = R_s' \coth\left(\frac{B_2}{B_1}\tau\right) \qquad (5)$$

and finally

$$Y = R_s'/R_s \coth\left(\frac{B_2}{B_1}\tau\right) = \gamma \coth(\gamma\tau) \qquad (6)$$

since

$$R_s'/R_s = \frac{B_2}{B_1} = \gamma = \sqrt{\rho/fI + \rho}$$

During rhythmic alternation of steady light and darkness Y, a measure of the degree of polymerization, rises in accordance with eq. 2 from a minimum value Y_1 to a maximum value Y_2 and declines according to eq. 6 exactly to Y_1 again. In combining these two equations to determine the limits and average value of Y during each interval we do not start the time scale of eq. 2 at $\tau = 0$ but use the positive lower and upper limits of τ defined, respectively, by $Y_1 = \tanh \tau_1$ and $Y_2 = \tanh \tau_2$. Since the value of Y at the end of the light period must be identical with the value at the beginning of the dark period, a factor π is introduced such that

$$Y = \gamma \coth \gamma(\tau + \pi) \text{ and} \qquad (7)$$

$$Y_2 = \gamma \coth \gamma(\tau_2 + \pi) = \tanh \tau_2 \qquad (8)$$

at the beginning of the dark period. The value of π will be evaluated easily in terms of the other parameters since from eq. 8 it is seen that $\tanh(\gamma\pi) = \gamma \coth \tau_2$.

The average value for Y, $(\bar{Y})$, for any frequency of alternation[11] is given, therefore, by the equation

$$\frac{1}{(q + 1)(\tau_2 - \tau_1)} \int_{\tau_1}^{\tau_3} Y d\tau = \bar{Y} = \frac{1}{(q + 1)(\tau_2 - \tau_1)} \ln\left[\frac{\cosh \tau_2}{\cosh \tau_1} \cdot \frac{\sinh \gamma\, q(\tau_2 - \tau_1) + \pi}{\sinh \gamma T}\right] \qquad (9)$$

This may be simplified to eliminate the necessity of evaluating π by applying the addition theorem, whereby

---

(9) H. Kwart, H. S. Broadbent and P. D. Bartlett, *ibid.*, **72**, 1060 (1950).

(10) G. M. Burnett, H. W. Melville and L. Valentine, *Trans. Faraday Soc.*, **45**, 960 (1949).

(11) This amounts to illuminating from $T_1 \rightarrow T_2$ and darkening from $T_2 \rightarrow T_3$, so that, since the length of the dark period is q times the length of the light period, $T_3 - T_2 = q(T_2 - T_1)$, the total length of a cycle, $T_3 - T_1 = (q + 1)(T_2 - T_1)$.

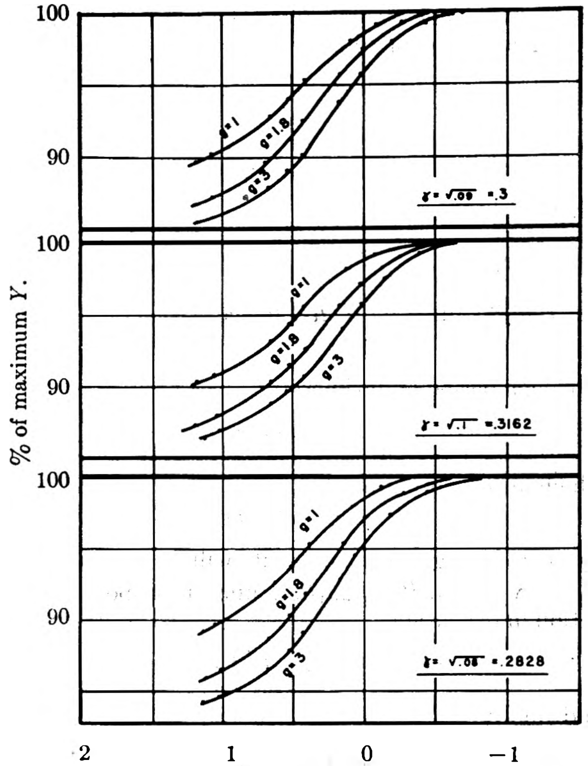

Fig. 1.

$$\sinh[q\gamma(\tau_2 - \tau_1) + \gamma\pi] = \sinh q\gamma[\tau_2 - \tau_1]\cdot\cosh \gamma\pi + \cosh[q\gamma(\tau_2 - \tau_1)\cdot\sinh \gamma\pi]$$

and thus

$$\frac{\sinh (\gamma q(\tau_2 - \tau_1) + \pi)}{\sinh \gamma \pi} = \sinh q\gamma(\tau_2 - \tau_1)\cdot\coth \gamma\pi + \cosh q\gamma(\tau_2 - \tau_1)$$

On substitution of this result and eq. 8 into 9 we obtain

$$\bar{Y} = \frac{1}{(q+1)(\tau_2 - \tau_1)} \text{ in } \left\{\frac{\cosh \tau_2}{\cosh \tau_1} \cdot \frac{Y_2 \sinh q\gamma(\tau_2 - \tau_1)}{\gamma} + \cosh q\gamma(\tau_2 - \tau_1)\right\} \quad (10)$$

It can be shown that this equation reduces to the Briars, Chapman and Walters[3] relation in the limiting case where the dark rate is zero or negligible. Thus, in the limit

$$\gamma \rightarrow 0 \; \frac{\sinh q\gamma(\tau_2 - \tau_1)}{\gamma} = q(\tau_2 - \tau_1)$$

and $\cosh 2\gamma(\tau_2 - \tau_1) = 1$, which on substitution into (10) results in the B.C.W. eq.

$$\bar{Y} = \frac{1}{(q+1)(\tau_2 - \tau_1)} \ln \left\{\frac{\cosh \tau_2}{\cosh \tau_1} \cdot [q(\tau_2 - \tau_1)Y_2 + 1]\right\} \quad (11)$$

Solutions for eq. 10 from experimental data can be accomplished graphically in a manner entirely analogous to that applied by Swain and Bartlett to eq. 11. Cases for a variety of sector cutouts are discussed in an appendix to this article.

The Maximum Dark Rate Which Can Be Neglected.—It is apparent that equations 10 and 11 differ by the terms within the brackets: let C = this term in eq. 10, A = the term in eq. 11, ϕ = $\cosh \tau_2/\cosh \tau_1$, and $\Delta = C - A$. If we set $\tilde{Y}$ = the value of $\bar{Y}$ when the dark rate is not neglected and $\sigma = \tilde{Y} - \bar{Y}$, then

$$\tilde{Y} = \frac{1}{(q+1)(\tau_2 - \tau_1)} \ln (C\phi) \quad (12)$$

$$\bar{Y} = \frac{1}{(q+1)(\tau_2 - \tau_1)} \ln(A\phi) \text{ and} \quad (13)$$

$$\sigma = \frac{1}{(q+1)(\tau_2 - \tau_1)} \ln \frac{C}{A} = \frac{1}{(q+1)(\tau_2 - \tau_1)} \ln \left(1 + \frac{C - A}{A}\right) \quad (14)$$

For a given case, say $q = 2$, it readily can be demonstrated that in the significant portion of our curve in the (graphical solution) plot $\bar{Y}$ *vs.* $\log (\tau_2 - \tau_1)$, namely, when the value of $\bar{Y}$ is most sensitive to flashing frequency, the value of $2\gamma(\tau_2 - \tau_1) < 1$. We are thus permitted to undertake a Taylor's series expansion of the term C in process of $2\gamma\cdot(\tau_2 - \tau_1)$, which, on discarding terms of higher order than the third, results in

$$C = \left\{\frac{2\gamma(\tau_2 - \tau_1)}{\gamma} + \frac{8\gamma^2}{6} (\tau_2 - \tau_1)^3\right\} Y_2 + 1 + 2\gamma^2(T_2 - T_1)^2 \quad (15)$$

Consequently

$$\Delta = C - A = \gamma^2(\tau_2 - \tau_1)^2 \left(\frac{4}{3} Y_2 (\tau_2 - \tau_1) + 2\right) \quad (16)$$

which is transformable to

$$\Delta = \gamma_2(\tau_2 - \tau_1)^2\cdot \left[2 + 4Y_2(\tau_2 - \tau_1) - \frac{8}{3} Y_2(\tau_2 - \tau_1)\right] \quad (17)$$

Substituting the value of the term A into (17) produces

$$\Delta = 2/3\gamma^2\cdot(\tau_2 - \tau_1)^2\cdot(A + 2) \text{ and, therefore} \quad (18)$$

$$\frac{C - A}{A} = 2/3\gamma^2(\tau_2 - \tau_1)^2\left(1 + \frac{2}{A}\right) \leqq (\tau_2 - \tau_1)^2 \ll 1$$

Apparently, then, the error resulting from neglecting a steady rate of dark initiation, ρ, is a little less than

$$\sigma = \frac{\gamma^2(\tau_2 - \tau_1)}{3} \quad (19)$$

and the maximum relative error is

$$\frac{\sigma}{Y} = \frac{\gamma^2}{3Y} (\tau_2 - \tau_1) \quad (20)$$

a function of both the dark rate and the flashing frequency.

The Effect of Non-uniformity in the Distribution of Reaction Centers.—The approach we have taken in the analysis of this effect is to assume that variation in the uniformity of the incident light beam is a circumstance that could occur readily and would result in a non-uniform distribution of radicals through the body of the polymerizing liquid. For this purpose we assume a square area for the entrance face of the reaction vessel with varying intensity of illumination over its surface. The assumption of a square rather than a circular area will introduce very little error in the argument since it involves only a difference in a numerical factor of very nearly "one" and makes no difference in the principle of our approximation.

We introduce a system of coördinates X, Z with the center of the square as origin. Let L be half the side length of the square. We then choose an element of area $d\psi = dXdZ$ over which the illumination $I(X,Z)$ is considered constant. According to the general theory[3-6] (which is also the basis for the derivations above) we have

$$\bar{Y} = F_1(t\sqrt{2k_t \cdot fI}) = F_1(\tau) \qquad (21)$$

where F_1 is an empirical function closely related to the one used in experimental plotting (see *e*, Fig. 3, ref. 5). Here $F_1(\tau) = F_2(\log \tau)$ and F_2 is plotted *vs.* log τ.

We now compute at the element of area the value of $R_s = \sqrt{fI/k_t}$ and $\bar{R}(X,Z) = \bar{Y}(X,Z)\bar{R}_s$. It can be deduced readily that the total amount of radical over the entire area, $\bar{r}$, as compared to the same quantity in steady state illumination, $\bar{r}_s$, is given by

$$\frac{\bar{r}}{\bar{r}_s} = \frac{\int\int F_1(t\sqrt{k_t fI(X,Z)})\sqrt{I(X,Z)}\,dX\,dZ}{\int\int\sqrt{I(X,Z)}\,dX\,dZ} \qquad (22)$$

This equation demonstrates that the ratio $\bar{r}/r_s$ is an average of the function $F_1(\tau)$ with the weighing function $\sqrt{I(X,Z)}$. If we had assumed a completely uniform illumination intensity, I_0, we would have obtained our theoretical ratio

$$\bar{Y}_{th} = \frac{\bar{r}}{\bar{r}_s} = F_1(t\sqrt{k_t I_0}) \qquad (23)$$

Consequently, the error committed (by assuming uniform distribution of reaction centers) in the determination of $\bar{r}/\bar{r}_s$ is given by $(\bar{r}/r_s) - \bar{Y}_{th}$. In order to determine the possible error we consider the following special case. Let $\sqrt{I} = \sqrt{I_0} + \alpha X + \beta Z$. This may be considered as the first term of a Taylor's series development, where the power terms higher than the first have been neglected. This would be consistent with an assumption that the largest variation in illumination intensity incident upon the entire area of the cell is no greater that 10% of I_0. On substituting this value of I into equation 22 we obtain

$$\frac{\bar{r}}{\bar{r}_i} = \frac{\int\int F_1(N[\sqrt{I_0} + \alpha X + \beta Z])\cdot(\sqrt{I_0} + \alpha X\ \beta Z)dX\,dZ}{\int\int(\sqrt{I_0} + \alpha X + \beta Z)\,dX\,dZ} \qquad (24)$$

where $N = t\sqrt{f2k_t}$. To integrate here we replace the empirical function $F_1(\tau)$ by a linear function which again involves a Taylor's series. The net result of this integration between limits and rearrangement of terms is the equation

$$\frac{\bar{r}}{\bar{r}_i} = F_1(\tau_0) + 1/3\left(\frac{(\alpha^2 + \beta^2)}{I_0}\right)L^2[\tau_0 F_1'(T_0)] \qquad (25)$$

where $[\tau_0\ F_1'(T_0)]$ is the slope of the experimental curve at the point T_0.

It remains to discuss the significance of the term $(\alpha^2 + \beta^2/I_0)L^2$. It may be pointed out that if a quantity has the form $\alpha X/\sqrt{I_0} + \beta Z/\sqrt{I_0}$ and X and Z vary independently over the range $-L$ to $+L$, the average value of this quantity is $L(\alpha^2 + \beta^2/I_0)$. This demonstrates, therefore, that this term in equation 25 is the square of the deviation of the relative light intensity. Now, since

$$\sqrt{I} = \sqrt{I_0} + \alpha X + \beta Z = \sqrt{I_0}\left(1 + \frac{\alpha X}{\sqrt{I_0}} + \frac{\beta Z}{\sqrt{I_0}}\right)$$

where the largest value of the term in the brackets occurs for $X = L$ and $Z = L$ and is actually $1 + L(\alpha + \beta)/I_0$, then $(2(\alpha^2 + \beta^2)/I_0)L^2$ is an upper limit for the square of the maximum relative deviation of light intensity.[12]

To illustrate the significance of this result, let us suppose that the slope of the curve at the point τ_0 is 30. Thereupon, the error in $\bar{r}/\bar{r}_s$ produced by a 10% maximum relative deviation of light intensity from I_0, *viz.*, $\bar{r}/\bar{r}_s - F_1(\tau_0)$, becomes by substitution in equation 25, $30(^1/_3)(^1/_2)^2(0.1)^2 = 0.025$ or 2.5% error.

The question still remains: how does an error, as expressed in the equation

$$\delta\bar{Y} = 1/3\left[\left(\frac{\alpha^2 + \beta^2}{I_0}\right)L^2\right][\tau_0 F_1'(\tau_0)] \qquad (26)$$

affect the value of k_t computed from our experimental determination of $\bar{Y}$? On differentiating (21) with respect to k_t and suitable transformation of terms we get

$$\frac{d\bar{Y}}{d(k_t)} = [F_1'(\tau)]\left[\frac{\tau}{k_t}\right] \qquad (27)$$

Hence

$$\frac{d(k_t)}{k_t} = \delta k_t = \frac{2\delta\bar{Y}}{F_1'(\tau)\tau} \text{ and finally} \qquad (28)$$

$$k_t = 2/3\left(\frac{\alpha^2 + \beta^2}{I_0}\right)L^2 \qquad (29)$$

This means, apparently, that the per cent. error in k_t is independent of the part of the experimental curve utilized for the computation and, furthermore, that the error is no greater than $^1/_6$ the square of the maximum relative deviation of light intensity from I_0.

Appendix

Computations of the absolute rate constant of radical chain reactions applying eq. 10 may be carried out by a method similar to the graphical procedure used by Swain and Bartlett.[5] The calculations undertaken in the interests of plotting the theoretical curves required for this procedure were made on a Bendix G-15D Computer using the intercom 1000 Double Precision Programming System. The actual computing program used was devised by Miss Mary Mintzer[13] under the supervision of Dr. Robert Jackson.

Series of calculations were made for sector cutouts of $q = 1.0$, 1.81 and 3.0. Within each set the effect of varying the fraction of the total initiation rate due to dark reactions from 0.01 to 0.1 at intervals of 0.01 also was calculated, *i.e.*, for values of $\gamma = 0.1000$ to $\gamma = 0.3162$. A total of thirty theoretical curves were plotted from the data thus obtained.

Each curve was begun by picking the Y_2 value as close to 1 as the computer permitted, $1-10^{-12}$. The corresponding value of τ_2 was computed from eq. 8. The parameter π was calculated by means of the equivalent form of eq. 8, *viz.*, $\pi = 1/2\gamma$

---

[12] This is clear from the following: $\sqrt{I}/\sqrt{I_0} = 1 + L(\alpha + \beta)/I_0$: where Δ is denoted as the maximum relative error, $\Delta = L(\alpha + \beta)/I_0$ and therefore $\Delta^2 = L^2(\alpha + \beta)^2/I_0$; clearly, $(\alpha + \beta)^2 < 2(\alpha^2 + \beta^2)$ and thus $\Delta^2 < 2L^2(\alpha^2 + \beta^2)/I_0$.

[13] Miss Mintzer carried out these computations in partial fulfillment of the requirements for the B.S. degree with honors in Chemistry at the University of Delaware, June, 1959.

$\ln [(Y_2 + \gamma)/(Y_2 - \gamma)] - \tau_2$. Computation of the value of τ_1 was performed by an iterative procedure using Newton's method

$$\tau_1 = \tau_1' + \frac{f(\tau_1')}{(f'(\tau_1')} \qquad (30)$$

$$= \tau_1' - \frac{\gamma \coth \{\gamma[(q+1)\tau_2 - q\tau_1' + 1]\} - \tanh \tau_1'}{Y^2 q \operatorname{csch}^2 \{\gamma[(q+1)\tau_2 - q\tau_1' + 1]\} - \operatorname{sech}^2 \tau_1'}$$

The criterion for accuracy of τ_1 was $|\tau_1 - \tau_1'| < 10^{-4}$. Finally the values of $\bar{Y}$ used for the theoretical curves were computed by means of the basic eq. 10.[14]

Some idea of the magnitude of the error resulting from neglect of the thermal rate of initiation associated with a typical sensitizer may be gleaned from the following case. Given a sensitizer with a dark rate which is 8% of the measured rate in steady state illumination. (See the appropriate theoretical curve in the accompanying figure.) Given also a sector cut-out providing equal light and dark periods. The value of λ_s, the average lifetime of growing chains at the steady state, was determined by the above procedures to be 1.12 seconds. By neglecting the dark rate and computing by the method of Swain and Bartlett[5] we obtained a value of λ_s = 1.30 seconds. Thus, by neglecting an 8% dark rate, an error of about 16% was experienced.

Acknowledgment.—We are indebted to the Office of Naval Research for financial support during the course of this work, to Prof. P. D. Bartlett of Harvard for much encouragement and to Miss M. Mintzer and Prof. R. D. Jackson at the University of Delaware for very valuable assistance in bringing the latter phases of this work to conclusion.

[14] The tables of associated data and the thirty theoretical curves plotted therefrom, as referred to in this paper, have been deposited as Document number 6274 with the ADI Auxiliary Publication Project, Photoduplication Service, Library of Congress, Washington 25 D. C. A copy may be secured by citing the Document number and by remitting in advance $2.50 for photoprints or $1.75 for 35 mm. microfilm payable to: Chief, Photoduplication Service, Library of Congress.

ON THE PAPER ADSORPTION CHROMATOGRAPHIC PHENOMENA

BY DALE F. RUDD

Department of Chemical and Metallurgical Engineering, University of Michigan, Ann Arbor, Michigan

Received February 22, 1960

A mathematical analysis of an equilibrium adsorption paper chromatography system is presented. This analysis shows the gross features of the chromatographic phenomena such as the movement of the solvent front and the separation of the solute bands. The diffusion model for solvent penetration yields an experimentally obtained correlation.

Introduction

The analysis of the phenomena of paper chromatography is by no means complete. The relative motion of the solute bands during the travel of the solvent through the paper is caused by a combination of solute adsorption, ion exchange, and solvent partition. The chromatographic phenomena have been analyzed in detail by Consden, Gordon and Martin[1] when solvent partition is the controlling mechanism as in the separation of carbohydrates.

This paper gives an analysis of the phenomena when equilibrium solute adsorption on the paper fibers predominates as in the separation of dyestuffs. Also an analysis of the diffusion model for solvent penetration shows that an experimentally obtained correlation between the height of solvent rise and the time of rise follows directly from the assumption that the solvent is transferred according to Fick's law.

Solvent Penetration.—The detailed experimental work of Müller and Clegg[2] indicates that, over the range of interest, the relationship between the visual height of rise, X_v, of a solvent in a strip of paper and time of rise, t, is quadratic in X_v. An analysis of the diffusion model for solvent penetration shows that this empirical correlation follows directly from the assumption that the solvent is transferred according to Fick's law.

Fick's law states that the mass rate of solvent transfer through the paper in the direction x is $-DA(\partial c/\partial x)$, where D is the diffusion transfer coefficient, A is the cross-sectional area of the paper, and c is the solvent concentration in mass per unit volume of the paper.

Consider a long strip of chromatographic paper initially dry. One end of the paper is placed in a solvent reservoir and a solvent front then progresses through the paper. The motion of this solvent front is obtained from the solution of the partial differential equation form of the transient conservation of mass law.

Consider now a transient mass balance on the interval of paper $(x, x + \delta x)$. The net rate of solvent influx into the interval by diffusion equals the rate of change of the solvent mass. Hence

$$-DA \left.\frac{\partial c}{\partial x}\right)_x + DA \left.\frac{\partial c}{\partial x}\right)_{x+\delta x} = A\,\delta x\,\frac{\partial c}{\partial t}$$

which becomes as $\delta x \rightarrow 0$

$$D\frac{\partial^2 c}{\partial x^2} = \frac{\partial c}{\partial t} \qquad (1)$$

The boundary conditions on the partial differential equation 1 are

$c(x,0) = 0$ paper is initially dry
$c(0,t) = c_0$ paper end is always saturated
$\lim_{x\to\infty} c(x,t) = 0$ paper is dry far ahead of the solvent front

The solution of equation 1 subject to the boundary conditions is, by Laplace transform theory

---

[1] R. Consden, A. H. Gordon and A. J. Martin, *Biochem. J.*, **38**, 224 (1944).

[2] R. Müller and D. L. Clegg, *Anal. Chem.*, **23**, 396 (1951).

$$c(x,t) = c_0 \operatorname{erfc}\left[\frac{x}{2\sqrt{Dt}}\right] \qquad (2)$$

The motion of the solvent front can be represented by the constant solvent concentration contours in the x,t plane. The ratio c/c_0 is constant when the group $x/2\sqrt{Dt}$ is constant. The visually observed solvent frontal motion corresponds to the motion of a constant solvent concentration front. Hence if c_v/c_0 is the solvent concentration ratio of the visually observed front and E is the constant whose complementary error function is c_v/c_0 then, by equation 2, the relationship between the height of solvent rise, X_v, and the time of rise, t, is

$$X_v^2 = 4EDt \qquad (3)$$

Equation 3 is of the same form as the empirical relationship obtained by Müller and Clegg. Thus, over the range of interest, the diffusion model adequately represents the solvent penetration phenomenon.

It should be noted that Washburn's analysis[3] of flow through horizontal capillaries yields an equation of the same form as equation 3. This indicates that the penetration of solvent through the chromatographic paper may be thought of as either a diffusion or capillary phenomenon. The diffusion model is used in the further discussion.

Solute Penetration.—The solute materials are carried along with the advancing solvent and are adsorbed on the fibers of the chromatographic paper. The solute adsorption causes the solute frontal velocities to differ, allowing the chromatographic separation of the solutes. The solute adsorption phenomenon has been analyzed mathematically for chromatographic columns by Amundson and Lapidus.[4] The diffusion model for solvent penetration and the ideas of equilibrium solute adsorption on the fibers are now combined to give a model for paper chromatography.

Consider the chromatographic separation of m solutes. Each of these solutes is transferred through the paper along with the advancing solvent and is in equilibrium adsorption with the paper fibers. The equilibrium relationship is

$$y_i = \phi(z_i) \qquad i = 1,2,\ldots,m \qquad (4)$$

where y_i is the mass of solute adsorbed on the paper fibers per unit volume of paper and z_i is the mass of solute in the solvent phase per unit mass of solvent. Equation 4 is a general form of the equilibrium adsorption isotherm but does not allow solute interference.

A transient mass balance on the ith kind of solute in the solvent phase over the interval of paper $(x, x + \delta x)$ yields

$$-DAz_i \left.\frac{\partial c}{\partial x}\right)_x + DAz_i \left.\frac{\partial c}{\partial x}\right)_{x+\delta x} - \delta x A \frac{\partial y_i}{\partial t} = \delta x A \frac{\partial(z_i c)}{\partial t}$$

The first two terms on the left are the rates of solute influx into the interval along with the advancing solvent. The third term is the rate of loss of solute from the solvent phase by adsorption on the paper fibers. These terms equal the mass rate of change of solute in the solvent phase. This mass balance becomes as $\delta x \to 0$ and by use of equations 1 and 4

$$\frac{\partial z_i}{\partial x}\left[D\frac{\partial c}{\partial x}\right] - \frac{\partial z_i}{\partial t}\left[c + \frac{\partial \phi(z_i)}{\partial z_i}\right] = 0 \qquad (5)$$

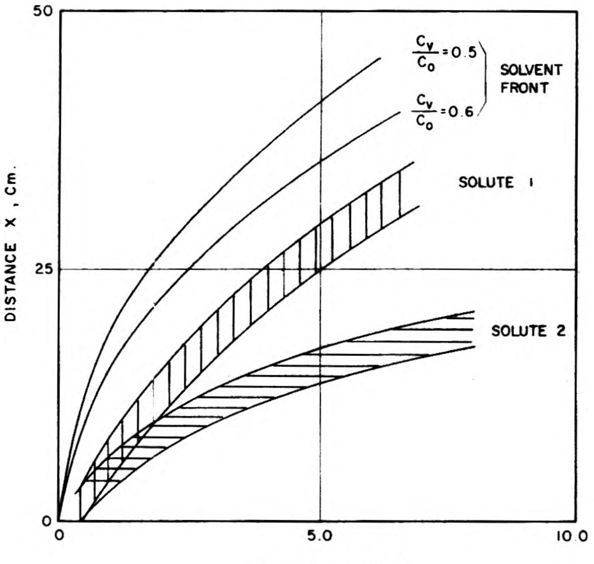

Fig. 1.—Chromatographic separation: $D = 178$ cm.²/sec.; $C_0 = 0.8$ g./cm.³; $\alpha_1 = 0.1$; $\alpha_2 = 1.0$.

The movement of the solute bands through the paper can be represented by the constant solute concentration contours in the x,t plane. These contours can be obtained immediately from equation 5. Quasi-linear partial differential equations of the first order such as equation 5 possess characteristics in the x,t plane. In this case these characteristics correspond physically to the constant solute concentration contours. From the theory of characteristics[5] the constant concentration contours are given by the solution of the ordinary differential equation

$$\frac{dx}{dt} = \frac{-D\dfrac{\partial c}{\partial x}}{c + \dfrac{\partial \phi}{\partial z_i}} \qquad (6)$$

In general the solution of equation 6 can be achieved numerically.[5]

To illustrate these methods consider the chromatographic separation of two solutes with linear equilibrium adsorption isotherms.

$$y_i = z_i\alpha_i + \beta_i \qquad i = 1,2$$

At $t = 0$ the end of the dry paper is placed in the solvent reservoir. At $t = 18$ min. a sample of the solute mixture is placed on the paper in the interval (0,3.0 cm). The solvent penetration is characterized by equation 2 or 3. The chromatographic separation of the two solutes is characterized by their constant concentration contours obtained from the solution of equation 6, which is, in this case

---

(3) E. W. Washburn, *Phys. Rev.*, **17**, 276 (1921).

(4) N. R. Amundson and L. Lapidus, THIS JOURNAL, **54**, 821 (1950).

(5) A. Acrivos, *Ind. Eng. Chem.*, **48**, 703 (1956).

$$\frac{dx}{dt} = \frac{\sqrt{D}\,c_0}{\sqrt{\pi t}}\;\frac{\exp -\left[\dfrac{x}{2\sqrt{Dt}}\right]^2}{\operatorname{erfc}\left[\dfrac{x}{2\sqrt{Dt}}\right] + \alpha_i} \qquad i = 1,2$$

The solution was obtained using the Euler method of numerical integration. Figure 1 shows this chromatographic separation. The solvent front precedes the solute bands. The movement of the solute bands is characterized by the characteristics (constant concentration contours) emanating from the front and back of the initial solute pulse. The chromatographic separation is caused by the difference in the adsorption isotherm constants α_i for the two solutes.

Discussion

The analysis presented shows that the diffusion model for solvent penetration does represent the physical phenomena and that the paper chromatographic effect can be explained when equilibrium solute adsorption predominates. The secondary effect of solute diffusion has been neglected. Attempts to include this led to equations which preclude the use of the simple method of characteristics. Solvent evaporation from the paper surface also has been neglected since in practice chromatography is accomplished in a saturated atmosphere. This simple analysis gives further insight into the fundamental mechanism of adsorption paper chromatography.

A NEW PROCEDURE FOR CALCULATING THE FOUR DIFFUSION COEFFICIENTS OF THREE-COMPONENT SYSTEMS FROM GOUY DIFFUSIOMETER DATA[1]

BY HIROSHI FUJITA[2] AND LOUIS J. GOSTING

Contribution from the Department of Chemistry and the Enzyme Institute, University of Wisconsin, Madison 6, Wisconsin

Received February 22, 1960

An exact procedure is developed which permits calculation of the four diffusion coefficients at a given composition of a ternary system from suitable free-diffusion experiments performed with the Gouy diffusiometer. This new procedure can be applied regardless of the relative magnitudes of the diffusion coefficients and should yield somewhat more accurate results than do previous methods. The data required are the reduced height–area ratios of the refractive index gradient curves and the areas of graphs of Gouy fringe deviations which summarize deviations of the refractive index gradient curves from Gaussian shape. Data for the system NaCl–KCl–H₂O at 25° which were reported previously from this Laboratory are reanalyzed to illustrate the use of this proceure. It is found that the new values so obtained for the diffusion coefficients satisfy Onsager's reciprocal relation somewhat better than did the values which were calculated by a former method.

The thermodynamics of irreversible processes requires four diffusion coefficients for complete description of isothermal diffusion in a ternary system. During the past few years several procedures have been published for calculating four such diffusion coefficients, D_{ij}, from experimental data. We review briefly those methods here to show their relation to the new method which is presented in this paper.

Baldwin, *et al.*,[3] presented a method which uses data for the reduced second and fourth moments, $\mathfrak{D}_{2m}$ and $\mathfrak{D}^2_{4m}$, of the refractive index gradient curves obtained from suitable free-diffusion experiments; for given mean concentrations of both solutes, 1 and 2, at least two experiments are required with different values of α_1, the fractional refractive index increment of solute 1 across the sharp initial boundary. Subsequently a procedure was developed by Fujita and Gosting[4] who used data for the $\mathfrak{D}_{2m}$ and the reduced height–area ratios, $\mathfrak{D}_A$, of the refractive index gradient curves for these experiments. The second procedure yields more accurate results than the first because experimental determinations of $\mathfrak{D}^2_{4m}$ are quite inaccurate compared to those of $\mathfrak{D}_A$. However, results from the second procedure may still contain appreciable errors because the $\mathfrak{D}_{2m}$ are somewhat less accurate than the $\mathfrak{D}_A$ (which can be measured to 0.1% or better with interferometric instruments such as the Gouy diffusiometer). Both of these methods are general, being applicable regardless of the values of the diffusion coefficients. A modification by Dunlop[5] of the second procedure achieves improved accuracy for some systems by determining experimentally the two values of α_1 for which the refractive index gradient curves become Gaussian. These values of α_1, when combined with the data for $\mathfrak{D}_A$, permit calculation of $\mathfrak{D}_{2m}$ for any value of α_1. Unfortunately the applicability of this method is limited in practice because inverted density gradients may be encountered for some systems in determining the required values of α_1. A different method[4] developed by Fujita and Gosting uses data for the $\mathfrak{D}_A$ and for reduced Gouy fringe deviations,[6] $\Omega(\zeta)$, corresponding to a particular value of the reduced fringe number, $f(\zeta)$ $(= f(\sqrt{2}) = 0.73854)$; experiments for at least two values of α_1 are required. When applicable this method can give more accurate results than the first two methods; however it depends on a series expansion which converges satisfactorily only for suitable

---

[1] Presented at the 136th meeting of the American Chemical Society, Atlantic City, New Jersey, September, 1959.

[2] On leave from the Physical Chemistry Laboratory, Department of Fisheries, University of Kyoto, Maizuru, Japan.

[3] R. L. Baldwin, P. J. Dunlop and L. J. Gosting, *J. Am. Chem. Soc.*, **77**, 5235 (1955).

[4] H. Fujita and L. J. Gosting, *ibid.*, **78**, 1099 (1956).

[5] P. J. Dunlop, THIS JOURNAL, **61**, 994 (1957).

[6] D. F. Akeley and L. J. Gosting, *J. Am. Chem. Soc.*, **75**, 5685 (1953).

ratios of the diffusion coefficients (for values of σ_-/σ_+ not greatly different from unity). Thus it complements Dunlop's procedure[5] because these two methods are applicable to systems with different ratios of diffusion coefficients. In the present paper we develop an exact procedure which is applicable regardless of the relative magnitudes of the diffusion coefficients. The data required are the $\mathfrak{D}_A$ and the *areas* of the Gouy fringe deviation graphs measured from suitable free-diffusion experiments. Because data from all parts of the refractive index curve are used in obtaining each area, this method should yield more accurate values for the diffusion coefficients than does the corresponding previous method[4] which uses only one point (*i.e.*, $\Omega(\sqrt{2})$) from each fringe deviation graph.

A method which uses data from studies of restricted diffusion has been developed by Fujita.[7] His procedure is applicable to all systems which may be studied with Harned's conductance method.[8] A procedure for using the diaphragm cell to determine some of the diffusion coefficients for a ternary system has been announced recently by Stokes.[9]

The main diffusion coefficients, D_{11} and D_{22}, and the cross-term diffusion coefficients, D_{12} and D_{21}, considered in the present paper are defined, as before,[3,10] by flow equations for one-dimensional isothermal diffusion of the form

$$J_1 = -D_{11}\frac{\partial c_1}{\partial x} - D_{12}\frac{\partial c_2}{\partial x} \qquad (1)$$

$$J_2 = -D_{21}\frac{\partial c_1}{\partial x} - D_{22}\frac{\partial c_2}{\partial x} \qquad (2)$$

Here $\partial c_1/\partial x$ and $\partial c_2/\partial x$ are the concentration gradients of solutes 1 and 2, respectively, with the concentrations c_1 and c_2 expressed as amounts (grams or moles) per unit volume of solution. The solute flows J_1 and J_2 denote the amount of each solute crossing a unit area per second for a volume-fixed frame of reference, and therefore the diffusion coefficients, D_{ij}, should be identified with this reference frame. These coefficients are identical with one set of diffusion coefficients considered by Hooyman[11]; they differ from, but are related to, diffusion coefficients defined by Lamm[12] and by Onsager.[13] We restrict our considerations to the customary experimental condition that concentration differences between the two initial solutions in the cell are sufficiently small that the partial specific volume of each component may be considered independent of the concentrations. When every partial specific volume is constant the mean volume velocity is everywhere zero relative to the cell,[14] and J_1 and J_2 in equations 1 and 2 can be identified with the flows of solutes 1 and 2 relative to the cell-fixed frame of reference.

Theory

In the following development frequent use will be made of symbols and equations appearing in an article by Fujita and Gosting.[4] To save space we will refer directly to equation numbers in that article and distinguish such numbers from those in this article by adding the letter F.

First we will derive an expression for the area, Q, of Gouy fringe deviation graphs as a function of α_1 for experiments with the same value of $\bar{c}_1$ and also of $\bar{c}_2$, the mean solute concentrations defined by equation 7F; α_1 (and also α_2) has been defined by equations 45F-48F. It is then shown that $Q/\sqrt{\mathfrak{D}_A}$ is a quadratic function of α_1; this may be compared with equation 56F which indicates $1/\sqrt{\mathfrak{D}_A}$ to be a linear function of α_1. Exact equations then are derived for the four diffusion coefficients, D_{ij}, in terms of the coefficients relating $Q/\sqrt{\mathfrak{D}_A}$ and $1/\sqrt{\mathfrak{D}_A}$ to α_1.

An Expression for the Area, Q, of Each Fringe Deviation Graph.—Starting equations for this derivation can be obtained from a paper by Gosting and Onsager[15] who gave a general theory of Gouy interference patterns. In the Appendix of this article their theory has been specialized to the case of isothermal free diffusion in ternary systems by using equation 49F for the refractive index distribution. Equations in the Appendix are identified by a letter A before the equation number. The reduced fringe deviation Ω_j, the reduced cell coördinate y_j and the special variable ζ_j for Gouy fringe number j may be treated as continuous functions, so we omit from these symbols the subscripts j. By defining

$$z = \sqrt{\sigma_+}\,y \qquad (3)$$

and

$$p = \sqrt{\sigma_-/\sigma_+} \qquad (4)$$

and remembering that

$$\Gamma_+ + \Gamma_- = 1 \qquad (5)$$

(see equation 52F) equation A-5 may be written

$$f(z) - f(\zeta) = \Gamma_-[f(z) - f(pz)] \qquad (6)$$

Here the function $f(\xi)$ is defined by[16]

$$f(\xi) = \frac{2}{\sqrt{\pi}}\left[\int_0^{\xi} e^{-q^2}\,dq - \xi e^{-\xi^2}\right] \qquad (7)$$

Also, by combining equations 3, 4, 5, A-6 and A-7 with A-8 we obtain

$$\Omega(\zeta) = e^{-\zeta^2} - \frac{(1-\Gamma_-)e^{-z^2} + \Gamma_- p e^{-p^2z^2}}{1-\Gamma_-(1-p)} \qquad (8)$$

The area Q of a fringe deviation graph is defined as the area enclosed by the curve of $\Omega(\zeta)$ *versus* $f(\zeta)$.

$$Q = \int_0^1 \Omega(\zeta)\,df(\zeta) \qquad (9)$$

---

[7] H. Fujita, THIS JOURNAL, **63**, 242 (1959).

[8] H. S. Harned and D. M. French, *Ann. N. Y. Acad. Sci.*, **46**, 267 (1945); H. S. Harned and R. L. Nuttall, *J. Am. Chem. Soc.*, **69**, 736 (1947).

[9] Work by R. H. Stokes and F. J. Kelly reported at a conference on the Physical Chemistry of Solutions, Perth, Australia; see *Proc. Roy. Australian Chem. Inst.*, **26**, No. 10, 412 (1959).

[10] P. J. Dunlop and L. J. Gosting, *J. Am. Chem. Soc.*, **77**, 5238 (1955).

[11] G. J. Hooyman, *Physica*, **22**, 751 (1956).

[12] O. Lamm, *Arkiv Kemi, Mineral. Geol.*, **18A**, No. 2 (1944); **18B**, No. 5 (1944); THIS JOURNAL, **61**, 948 (1957).

[13] L. Onsager, *Ann. N. Y. Acad. Sci.*, **46**, 241 (1945).

[14] G. J. Hooyman, H. Holtan, Jr., P. Mazur and S. R. de Groot, *Physica*, **19**, 1095 (1953).

[15] L. J. Gosting and L. Onsager, *J. Am. Chem. Soc.*, **74**, 6066 (1952).

[16] See equation 12 of G. Kegeles and L. J. Gosting, *J. Am. Chem. Soc.*, **69**, 2516 (1947).

Because it can be seen from equations 6 and 7 that $\zeta \to 0$ and $z \to 0$ as $f(\zeta) \to 0$, and also that $\zeta \to \infty$ and $z \to \infty$ as $f(\zeta) \to 1$, equation 9 may, after substitution for $\Omega(\zeta)$ from equation 8, be put in the form

$$Q = \int_0^\infty e^{-\zeta^2} \frac{df(\zeta)}{d\zeta} d\zeta - \frac{1}{1 - \Gamma_-(1-p)} \times \left[(1 - \Gamma_-) \int_0^\infty e^{-z^2} \frac{df(\zeta)}{dz} dz + \Gamma_- p \int_0^\infty e^{-p^2z^2} \frac{df(\zeta)}{dz} dz\right] \quad (10)$$

From equation 7 we have

$$\frac{df(\zeta)}{d\zeta} = \frac{4}{\sqrt{\pi}} \zeta^2 e^{-\zeta^2} \quad (11)$$

Differentiation of equation 6 with respect to z, rearrangement, and substitution of equation 7 gives

$$\frac{df(\zeta)}{dz} = \frac{4}{\sqrt{\pi}} [(1 - \Gamma_-)z^2e^{-z^2} + \Gamma_- p^3z^2e^{-p^2z^2}] \quad (12)$$

By introducing equations 11 and 12 into 10, performing the integrations, and using equation 5, we obtain finally the desired expression

$$Q = \frac{1 + p - (2\sqrt{2}p/\sqrt{1 + p^2})}{2\sqrt{2}[1 - \Gamma_-(1 - p)]} \Gamma_+\Gamma_- \quad (13)$$

Expression for the Ratio $E = Q/\sqrt{\mathfrak{D}_A}$.—From equation 74F we have

$$\Gamma_+\Gamma_-(p - 1)^2 = \frac{S_A^2}{S_{2m}\sigma_+} \left[S_{2m}\alpha_1\alpha_2 + \left(\frac{R_1}{R_2}\right) D_{12}\alpha_2 - \left(\frac{R_2}{R_1}\right) D_{21}\alpha_1 \right] \quad (14)$$

and from equations 56F and 55F, after substituting equations 4 and 5

$$1/\sqrt{\mathfrak{D}_A} = I_A - S_A\alpha_1 = \sqrt{\sigma_+}\,[1 - \Gamma_-(1 - p)] \quad (15)$$

Use of the relation

$$\alpha_1 + \alpha_2 = 1 \quad (16)$$

and definition of the quantities

$$E_0 = \frac{PS_A^2}{S_{2m}\sqrt{\sigma_+}} \left(\frac{R_1}{R_2}\right) D_{12} \quad (17)$$

$$E_1 = \frac{PS_A^2}{S_{2m}\sqrt{\sigma_+}} \left[S_{2m} - \left(\frac{R_1}{R_2}\right) D_{12} - \left(\frac{R_2}{R_1}\right) D_{21}\right] \quad (18)$$

$$E_2 = \frac{PS_A^2}{\sqrt{\sigma_+}} \quad (19)$$

in which

$$P = \frac{1 + p - (2\sqrt{2}p/\sqrt{1 + p^2})}{2\sqrt{2}(1 - p)^2} \quad (20)$$

permits equations 13–15 to be combined in the form

$$E \equiv Q/\sqrt{\mathfrak{D}_A} = E_0 + E_1\alpha_1 - E_2\alpha_1^2 \quad (21)$$

This relation indicates that when corresponding values of Q and $\mathfrak{D}_A$ are combined in the form $Q/\sqrt{\mathfrak{D}_A}$ the values of this ratio, E, are a quadratic function of α_1. To use equations 15 and 21 in evaluating the four D_{ij}, the quantities Q and $\mathfrak{D}_A$ must be measured for two or more experiments with different values of α_1.

It is important to recognize that the five coefficients I_A, S_A, E_0, E_1 and E_2 in equations 15 and 21 are not independent; each coefficient may be expressed in terms of the four diffusion coefficients by using equations 4, 17–20 and the appropriate relations from ref. 4. Therefore if I_A and S_A are first determined from the linear dependence of $1/\sqrt{\mathfrak{D}_A}$ on α_1, as may be done conveniently by the method of least squares, it is *not* then permissible to adjust all the other coefficients E_0, E_1 and E_2 independently to make equation 21 fit best the experimental data for E *versus* α_1. These three coefficients may be determined by a method of successive approximations. To do this equation 21 is rewritten in the form

$$\hat{E} \equiv [(E/E_2) + \alpha_1^2] = (E_0/E_2) + (E_1/E_2)\alpha_1 \quad (22)$$

An approximate starting value is assumed for E_2 so that a first approximation of the quantity $\hat{E}$ can be calculated for each experiment. Then the ratios E_0/E_2 and E_1/E_2 are determined to describe best the linear dependence of those $\hat{E}$ on α_1. From these values of E_0/E_2 and E_1/E_2, together with the values of I_A and S_A, first approximations for the four diffusion coefficients readily may be obtained by using equations derived in the next section (equations 23–25 and 39–42, or equations 25a–25c and 39a–42a). An improved value of E_2 is then calculated from these approximate diffusion coefficients by using equation 19, together with equations 20, 4, 30F and 31F; this improved E_2 is used as a second approximation in equation 22 to determine second approximations for the $\hat{E}$, the ratios E_0/E_2, and E_1/E_2, and then for the four D_{ij}. This process is repeated systematically until no further changes occur, indicating that the best values of the D_{ij} corresponding to the given data have been obtained. To facilitate calculations the quantity P, equation 20, has been computed for the entire range of values of p which may be encountered, and these results are presented in Table I.

Equations for the Four Diffusion Coefficients.—We now derive expressions which readily permit calculation of the four D_{ij} from values for the four quantities I_A, S_A, E_0/E_2 and E_1/E_2. The derivation may be facilitated by defining the parameters

$$r = \frac{1}{(E_1/E_2) - 1} \quad (23)$$

$$s = -\frac{(E_0/E_2)}{(E_0/E_2) + (E_1/E_2) - 1} \quad (24)$$

$$u = \frac{S_A}{I_A} \quad (25)$$

Then we obtain from equations 18 and 19

$$S_{2m} = -r[(R_1/R_2)D_{12} + (R_2/R_1)D_{21}] \quad (26)$$

and from equations 17–19

$$(R_1/R_2)D_{12} = s(R_2/R_1)D_{21} \quad (27)$$

To simplify the next few equations we denote certain ratios of the diffusion coefficients by the symbols

$$q_1 = \frac{D_{22}}{D_{11}} \quad (28)$$

$$q_2 = \left(\frac{R_1}{R_2}\right) \frac{D_{12}}{D_{11}} \quad (29)$$

$$q_3 = \left(\frac{R_2}{R_1}\right) \frac{D_{21}}{D_{11}} \quad (30)$$

Equation 27 then becomes

$$q_2 = sq_3 \quad (31)$$

TABLE I[a]

VALUES OF P (EQUATION 20) AS A FUNCTION OF p

p	P	Diff.	p	P	Diff.	p	P	Diff
0.00	0.353553	−584	0.34	0.348620	817	0.68	0.309176	1372
.01	.354137	−537	.35	.347803	847	.69	.307804	1377
.02	.354674	−490	.36	.346956	876	.70	.306427	1381
.03	.355164	−443	.37	.346080	903	.71	.305046	1384
.04	.355607	−397	.38	.345177	931	.72	.303662	1387
.05	.356004	−350	.39	.344246	957	.73	.302275	1389
.06	.356354	−303	.40	.343289	982	.74	.300886	1391
.07	.356657	−258	.41	.342307	1007	.75	.299495	1393
.08	.356915	−210	.42	.341300	1030	.76	.298102	1393
.09	.357125	−165	.43	.340270	1054	.77	.296709	1394
.10	.357290	−119	.44	.339216	1075	.78	.295315	1394
.11	.357409	− 74	.45	.338141	1096	.79	.293921	1395
.12	.357483	− 28	.46	.337045	1116	.80	.292526	1393
.13	.357511	16	.47	.335929	1136	.81	.291133	1393
.14	.357495	61	.48	.334793	1155	.82	.289740	1391
.15	.357434	105	.49	.333638	1172	.83	.288349	1390
.16	.357329	148	.50	.332466	1189	.84	.286959	1388
.17	.357181	191	.51	.331277	1205	.85	.285571	1385
.18	.356990	234	.52	.330071	1221	.86	.284186	1383
.19	.356756	275	.53	.328850	1235	.87	.282803	1381
.20	.356481	316	.54	.327615	1250	.88	.281422	1377
.21	.356165	357	.55	.326365	1262	.89	.280045	1374
.22	.355808	397	.56	.325103	1275	.90	.287671	1370
.23	.355411	437	.57	.323828	1287	.91	.277301	1367
.24	.354974	474	.58	.322541	1298	.92	.275934	1362
.25	.354500	513	.59	.321243	1308	.93	.274572	1358
.26	.353987	549	.60	.319935	1317	.94	.273214	1354
.27	.353438	586	.61	.318618	1327	.95	.271860	1349
.28	.352852	621	.62	.317291	1335	.96	.270511	1344
.29	.352231	656	.63	.315956	1343	.97	.269167	1339
.30	.351575	690	.64	.314613	1350	.98	.267828	1334
.31	.350885	723	.65	.313263	1356	.99	.266494	1329
.32	.350162	756	.66	.311907	1363	1.00	.265165	
.33	.349406	786	.67	.310544	1368			

[a] It may be seen from equations 30F and 31F that $\sigma_+ > \sigma_-$; hence we have tabulated values of P only for the range $0 \leqslant p \leqslant 1$. The differences between successive values of P are included to facilitate interpolation. To calculate values of P near $p = 1$ equation 20 was written in the series form

$$P = \frac{1}{2\sqrt{2}}\left[\frac{3}{4} + \frac{3}{8}(1-p) + \frac{5}{64}(1-p)^2 - \frac{9}{128}(1-p)^3 - \frac{49}{512}(1-p)^4 - \frac{61}{1024}(1-p)^5 - \ldots\right],$$

and by substitution of equation 26 into 61F we obtain

$$1 - q_1 + (1 + r)q_3 + (r - 1)q_2 = 0 \qquad (32)$$

Equations 25, 17F, 20F–23F, 57F, 58F and 64F may be combined to give

$$1 + u - q_1 - (1 + u)q_2 + q_3 = -u\sqrt{q_1 - q_2q_3} \qquad (33)$$

and equations 17F, 20F–23F, 57F and 65F yield

$$D_{11} = \frac{(1 - q_1 - q_2 + q_3)^2}{S_A{}^2(q_1 - q_2q_3)(1 + q_1 + 2\sqrt{q_1 - q_2q_3})} \qquad (34)$$

Expressions for the four diffusion coefficients may be obtained by solving equations 28–34 as follows. By using equations 31 and 32 it is possible to write equation 34 in the form

$$D_{11} = \frac{r^2q_3{}^2(1 + s)^2}{S_A{}^2(q_1 - q_2q_3)[(1 + \sqrt{q_1 - q_2q_3})^2 + sq_3{}^2]} \qquad (35)$$

From equations 31 and 32 it is found that

$$q_1 = 1 + [r(1 + s) + (1 - s)]q_3 \qquad (36)$$

and from equations 31, 32, 33 and 36 we obtain, after some manipulations

$$q_3 = \frac{u[2 + u + (u/r)]}{r\{1 + s[1 + (u/r)]^2\}} \qquad (37)$$

Combination of equations 31, 32, 33 and 37 leads to

$$\sqrt{q_1 - q_2q_3} = \frac{(1 + u)\{1 + s[1 + (u/r)]\} + (u/r)}{1 + s[1 + (u/r)]^2} \qquad (38)$$

An expression for D_{11} in terms of the parameters r, s and u then is found by substitution of equations 37 and 38 into 35. Corresponding equations for the three other diffusion coefficients are obtained from equations 28–30 by using this relation for D_{11} and substituting equations 31, 36 and 37. The final results of these manipulations are[17]

---

(17) Although equations 39–42 (with equations 23–25) permit straight-forward calculations of the D_{ij} from values of S_A, I_A, E_0/E_2 and E_1/E_2, we also express those equations in terms of another set of parameters so that they may be somewhat more convenient for use with calculating machines. Thus if we define

$$u = S_A/I_A \qquad (25a)$$

$$v = -(E_0/E_2)u \qquad (25b)$$

$$w = (E_1/E_2)u \qquad (25c)$$

equations 39–42 may be written in the form

$$D_{11} = \frac{\left[1 + \left(\frac{s}{1+s}\right)\left(\frac{u}{r}\right)\left(2 + \frac{u}{r}\right)\right]}{I_A{}^2\left[1 + u + \frac{u}{r} + u\left(\frac{s}{1+s}\right)\left(\frac{u}{r}\right)\right]^2} \tag{39}$$

$$\left(\frac{R_1}{R_2}\right) D_{12} = \frac{1}{I_A{}^2}\left(\frac{s}{1+s}\right)\left(\frac{u}{r}\right) \times \frac{[2 + u + (u/r)]}{\left[1 + u + \frac{u}{r} + u\left(\frac{s}{1+s}\right)\left(\frac{u}{r}\right)\right]^2} \tag{40}$$

$$\left(\frac{R_2}{R_1}\right) D_{21} = \frac{1}{I_A{}^2}\left(\frac{1}{1+s}\right)\left(\frac{u}{r}\right) \times \frac{[2 + u + (u/r)]}{\left[1 + u + \frac{u}{r} + u\left(\frac{s}{1+s}\right)\left(\frac{u}{r}\right)\right]^2} \tag{41}$$

$$D_{22} = \frac{\left[\left(\frac{1}{1+s}\right)\left(1 + u + \frac{u}{r}\right)^2 + \left(\frac{s}{1+s}\right)(1+u)^2\right]}{I_A{}^2\left[1 + u + \frac{u}{r} + u\left(\frac{s}{1+s}\right)\left(\frac{u}{r}\right)\right]^2} \tag{42}$$

The constants R_1 and R_2 are coefficients in the equation relating refractive index to the solute concentrations (equation 45F); they may be determined[18] from the Gouy experiments which are used to obtain Q and $\mathfrak{D}_A$.

Series Expressions for Limiting Cases of Small Cross-Term Diffusion Coefficients.—In many cases the cross-term diffusion coefficients are expected to be quite small in comparison with the main diffusion coefficients. Therefore it is of interest to derive series equations for the D_{ij} which are relevant to such cases. Three cases may be considered; *i.e.*, $D_{12} \to 0$ (but $D_{21} \neq 0$), $D_{21} \to 0$ (but $D_{12} \neq 0$), and both $D_{12} \to 0$ and $D_{21} \to 0$. The desired equations may be obtained by expanding equations 39–42 in powers of the appropriate parameter which tends to zero in each of these limiting cases.

For the case $D_{12} \to 0$ but D_{21} remains non-zero it is seen from equation 27 that $s \to 0$. By expanding equations 39–42 in powers of s we obtain the series

$$D_{11} = \frac{1}{I_A{}^2[1 + u + (u/r)]^2}\left\{1 + \left(\frac{u}{r}\right)\left[\left(\frac{u}{r}\right) + \frac{2[1 + (u/r)]}{[1 + u + (u/r)]}\right] s + 0(s^2)\right\} \tag{43}$$

$$\left(\frac{R_1}{R_2}\right) D_{12} = \frac{(u/r)[2 + u + (u/r)]}{I_A{}^2[1 + u + (u/r)]^2}\, s\{(1 + 0(s)\} \tag{44}$$

$$\left(\frac{R_2}{R_1}\right) D_{21} = \frac{(u/r)[2 + u + (u/r)]}{I_A{}^2[1 + u + (u/r)]^2}\left\{1 - \left[1 + \frac{2u(u/r)}{[1 + u + (u/r)]}\right] s + 0(s)^2)\right\} \tag{45}$$

$$D_{22} = \frac{1}{I_A{}^2}\left\{1 - \frac{(u/r)}{[1 + u + (u/r)]}\left[2u + \frac{[2 + 2u + (u/r)]}{[1 + u + (u/r)]}\right] s + 0(s^2)\right\} \tag{46}$$

When $D_{21} \to 0$ but D_{12} remains non-zero equation 27 shows that $|s| \to \infty$. For this case we may expand equations 39–42 in powers of $1/s$ to give

$$D_{11} = \frac{1}{L_A{}^2}\left\{1 - \left(\frac{u}{r}\right)\left[\frac{2 + (u/r) - u(u/r)}{[1 + (u/r)]^2(1 + u)}\right]\left(\frac{1}{s}\right) + 0\left(\frac{1}{s^2}\right)\right\} \tag{47}$$

$$\left(\frac{R_1}{R_2}\right) D_{12} = \frac{(u/r)[2 + u + (u/r)]}{L_A{}^2[1 + (u/r)]^2}\left\{1 - \left[\frac{1 + u + (u/r) - u(u/r)}{[1 + (u/r)](1 + u)}\right]\left(\frac{1}{s}\right) + 0\left(\frac{1}{s^2}\right)\right\} \tag{48}$$

$$\left(\frac{R_2}{R_1}\right) D_{21} = \frac{(u/r)[2 + u + (u/r)]}{L_A{}^2[1 + (u/r)]^2}\left(\frac{1}{s}\right)\left\{1 - 0\left(\frac{1}{s}\right)\right\} \tag{49}$$

$$D_{22} = \frac{1}{I_A{}^2[1 + (u/r)]^2}\left\{1 + \frac{(u/r)}{(1 + u)} \times \left[2\frac{[1 + u + (u/r)]}{[1 + (u/r)]} + \frac{(u/r)}{(1 + u)}\right]\left(\frac{1}{s}\right) + 0\left(\frac{1}{s^2}\right)\right\} \tag{50}$$

Here $L_A = I_A + S_A$ (see equation 59F).

Finally if both $D_{12} \to 0$ and $D_{21} \to 0$ it is seen from equation 26 that $|r| \to \infty$ because in general $S_{2m} \neq 0$. The series for this case may be obtained by expanding equations 39–42 in terms of $1/r$.

$$D_{11} = \frac{1}{L_A{}^2}\left\{1 - \frac{2u}{(1 + s)(1 + u)}\left(\frac{1}{r}\right) + 0\left(\frac{1}{r^2}\right)\right\} \tag{51}$$

$$\left(\frac{R_1}{R_2}\right) D_{12} = \frac{(2u + u^2)}{L_A{}^2}\left(\frac{s}{1 + s}\right)\left(\frac{1}{r}\right)\left\{1 + 0\left(\frac{1}{r}\right)\right\} \tag{52}$$

$$\left(\frac{R_2}{R_1}\right) D_{21} = \frac{(2u + u^2)}{L_A{}^2(1 + s)}\left(\frac{1}{r}\right)\left\{1 + 0\left(\frac{1}{r}\right)\right\} \tag{53}$$

$$D_{22} = \frac{1}{I_A{}^2}\left\{1 - \frac{2us}{(1 + s)}\left(\frac{1}{r}\right) + 0\left(\frac{1}{r^2}\right)\right\} \tag{54}$$

Application

The procedure developed in the theoretical section of this article has been used to reanalyze the Gouy diffusiometer data reported by O'Donnell and Gosting[18] and by Dunlop[19] for isothermal free diffusion at five compositions of the system NaCl–KCl–H$_2$O. Quantities relevant to this calculation are listed in Table II. First, the mean solute concentrations considered are given in lines 1 and 2. Then in lines 3–6 are shown the required data[18,19] for R_1, R_2, I_A and S_A. The area, Q, of the fringe deviation graph for each experiment is reported in lines 7, 10, 13 and 16. To obtain each of these areas a smooth curve was drawn through a large graph of the average values of Ω (indicated by crosses on the published fringe deviation graphs). Values of Ω which were read from this curve at intervals of 0.1 of the reduced fringe number, $f(\zeta)$, were then used to calculate the area, Q, by using Simpson's $^1/_3$ rule for numerical integration. An independent determination of each area was made at a later time; each value of Q shown in Table II is an average of the two determinations. To obtain $E \equiv Q/\sqrt{\mathfrak{D}_A}$ (equation 21), a smoothed value of $\mathfrak{D}_A$ was calculated for each experiment by substituting the values of I_A and S_A, lines 5 and 6, into equation 15 and then using the data for α_1 reported in the original articles[18,19]; those α_1 were so close to 0.0, 0.2, 0.8 and 1.0 that these rounded values were used for the remainder of the calculations. From

---

$$D_{11} = [1 + v(2 - u + w)]/(\Lambda I_A{}^2) \tag{39a}$$

$$(R_1/R_2)D_{12} = [v(2 + w)]/(\Lambda I_A{}^2) \tag{40a}$$

$$(R_2/R_1)D_{21} = [(w - u - v)(2 + w)]/(\Lambda I_A{}^2) \tag{41a}$$

$$D_{22} = [(1 + w)^2 - v(2 + u + w)]/(\Lambda I_A{}^2) \tag{42a}$$

where

$$\Lambda = (1 + w + uv)^2 \tag{39b}$$

[18] I. J. O'Donnell and L. J. Gosting, in "The Structure of Electrolytic Solutions" (W. J. Hamer, ed.), Chapter 11, John Wiley and Sons, Inc., New York, N. Y., 1959.

[19] P. J. Dunlop, THIS JOURNAL, 63, 612 (1959).

TABLE II[a]

DATA FOR RECALCULATING THE FOUR DIFFUSION COEFFICIENTS OF THE SYSTEM NaCl–KCl–H_2O AT 25°

$\bar{C}_1 \equiv C_{NaCl}$; $\bar{C}_2 \equiv C_{KCl}$

1	$\bar{C}_1$ (moles/l.)	0.2500	0.5000	0.2500	0.5000	1.5000
2	$\bar{C}_2$ (moles/l.)	0.2500	0.2500	0.5000	0.5000	1.5000
3	$\bar{R}_1 \times 10^3$	9.760	9.593	9.534	9.438	8.523
4	$R_2 \times 10^3$	9.663	9.488	9.479	9.321	8.367
5	I_A	234.43	235.05	233.32	233.83	228.54
6	S_A	24.28	23.47	23.29	22.56	15.35
7	$Q \times 10^4$ $(\alpha_1 = 0.0)$	−0.36	0.77	−0.35	−0.28	−5.78
8	E $(\alpha_1 = 0.0)$	−0.008	0.018	−0.008	−0.007	−0.132
9	$E_{calc.}$ $(\alpha_1 = 0.0)$	0.005	0.012	−0.002	0.004	−0.130
10	$Q \times 10^4$ $(\alpha_1 = 0.2)$	7.51	5.42	6.98	6.56	0.50
11	E $(\alpha_1 = 0.2)$	0.180	0.130	0.166	0.156	0.012
12	$E_{calc.}$ $(\alpha_1 = 0.2)$	0.160	0.138	0.163	0.147	0.016
13	$Q \times 10^4$ $(\alpha_1 = 0.8)$	12.22	9.22	15.96	13.30[b]	14.86
14	E $(\alpha_1 = 0.8)$	0.310	0.234	0.402	0.335	0.358
15	$E_{calc.}$ $(\alpha_1 = 0.8)$	0.327	0.236	0.383	0.318	0.334
16	$Q \times 10^4$ $(\alpha_1 = 1.0)$	11.37	6.89	13.64	10.66	15.67
17	E $(\alpha_1 = 1.0)$	0.294	0.178	0.350	0.273	0.382
18	$E_{calc.}$ $(\alpha_1 = 1.0)$	0.284	0.175	0.366	0.289	0.401
19	E_0/E_2	0.0078	0.0200	−0.0028	0.0074	−0.5281
20	E_1/E_2	1.4518	1.2805	1.6471	1.5315	3.1556
21	E_2	0.61840	0.58279	0.56773	0.53595	0.24615
22	r	2.2134	3.5651	1.5454	1.8815	0.46391
23	s	−0.0170	−0.0666	0.0043	−0.0137	0.3245
24	u	0.10357	0.09985	0.09982	0.09648	0.06717
25	v	−0.00081	−0.00200	0.00028	−0.00071	0.03547
26	w	0.15036	0.12786	0.16441	0.14776	0.21196

[a] The values shown in lines 19–26 (and perhaps those for Q) should probably be rounded off by one or more figures; however the extra figures were retained to minimize accumulation of errors during computation. [b] Average value for experiments 10 and 11.

the Q and $\mathfrak{D}_A$ obtained in this way were calculated the values of E given in lines 8, 11, 14 and 17.

For each composition the quantities E_0/E_2, E_1/E_2 and E_2, together with the D_{ij}, were computed by a procedure of successive approximations as described in connection with equation 22. To start these calculations a first approximation for E_2 was obtained (see equation 21) from the slope of a graph of $(E - E_0)/\alpha_1$ *versus* α_1; for this graph the value of E from the experiment with $\alpha_1 = 0$ was used for E_0. Then from the values of $\hat{E}$ *versus* α_1 the ratios E_0/E_2 and E_1/E_2 were determined, both in this and in subsequent approximations, by the method of least squares. Convergence of the calculations (within 0.0001×10^{-5} in all D_{ij}) was obtained with the third or fourth approximation. Final values for E_0/E_2, E_1/E_2 and E_2 are shown in lines 19–21 of Table II. Equations 39a–42a containing the parameters u, v and w were used in making the required successive approximations; identical results could be obtained by using equations 39–42 containing the other set of parameters, r, s and u. Final values of both sets of these quantities are reported in lines 22–26. It will be noted that of these five parameters only u $(= S_A/I_A)$ is obtained directly without successive approximations.

The values of D_{ij} obtained by this new procedure are presented in lines 3, 4, 5 and 6 of Table III. A subscript V is affixed to the D_{ij} to emphasize that these diffusion coefficients are for the volume-fixed frame of reference. Beneath each new value of $(D_{ij})_V$ in Table III is shown in parentheses the value [18,19] which had been obtained from the $\mathfrak{D}_A$ and $\Omega(\sqrt{2})$ by a previous method of calculation.[4] It is seen that for two compositions some of the new values of $(D_{ij})_V$ differ from the previous values by approximately 0.01×10^{-5}.

To check the calculations, and to investigate the self-consistency of the areas, Q, for experiments at each composition, values of E were computed from the values of $(D_{ij})_V$ reported in lines 3, 4, 5 and 6 of Table III. Equations 17–21 were used for these calculations and the resulting values, $E_{calc.}$, are reported in lines 9, 12, 15 and 18 of Table II for comparison with the original values of $E = Q/\sqrt{\mathfrak{D}_A}$.

Tests of the Onsager Reciprocal Relation

Here we show the effect of using the new values of $(D_{ij})_V$ reported in Table III on tests of the Onsager reciprocal relation for isothermal diffusion in this ternary system. These tests differ from those reported previously from this laboratory only in the values used for the $(D_{ij})_V$; the data used here for activity coefficients and for partial molal volumes are the same as given before.[19–21] To avoid repetition, we refer directly to the required data and equations in the articles by Dunlop and Gosting[20] and by Dunlop[19] by adding the letters DG or D, respectively, to the numbers of equations and of tables in those papers.

First the new values of $(D_{ij})_V$ were converted to $(D_{ij})_0$, the corresponding diffusion coefficients for the solvent-fixed frame of reference, by using equa-

---

(20) P. J. Dunlop and L. J. Gosting, *ibid.*, **63**, 86 (1959).

(21) Values for the chemical potential derivatives in ref. 19 were corrected as indicated in footnote *b* of Table III.

TABLE III[a]

DIFFUSION COEFFICIENTS FOR THE SYSTEM NaCl–KCl–H_2O AT 25° AND TESTS OF THE ONSAGER RECIPROCAL RELATION MADE WITH THESE VALUES; $C_1 \equiv C_{NaCl}$; $C_2 \equiv C_{KCl}$

1	C_1 (moles/l.)	0.25	0.5	0.25	0.5	1.5
2	C_2 (moles/l.)	0.25	0.25	0.5	0.5	1.5
3	$(D_{11})_V \times 10^5$	1.3729	1.4176	1.3555	1.3865	1.3971
3a		(1.3723)	(1.4142)	(1.3431)	(1.3893)	(1.3908)
4	$(D_{12})_V \times 10^5$	−0.0024	−0.0060	0.0008	−0.0021	0.1000
4a		(−0.0053)	(−0.0116)	(−0.0010)	(−0.0102)	(0.1015)
5	$(D_{21})_V \times 10^6$	0.1422	0.0919	0.1907	0.1570	0.3198
5a		(0.1429)	(0.0959)	(0.2053)	(0.1536)	(0.3269)
6	$(D_{22})_V \times 10^5$	1.8224	1.8170	1.8360	1.8314	1.8021
6a		(1.8258)	(1.8235)	(1.8381)	(1.8407)	(1.8004)
7	$(D_{11})_0 \times 10^5$	1.380	1.433	1.364	1.403	1.464
8	$(D_{12})_0 \times 10^5$	0.011	0.021	0.015	0.026	0.199
9	$(D_{21})_0 \times 10^5$	0.150	0.099	0.207	0.173	0.387
10	$(D_{22})_0 \times 10^6$	1.836	1.831	1.863	1.859	1.901
11	$(L_{12})_0 \times RT \times 10^9$	−0.750	−1.030	−0.992	−1.515	−3.97
11a		(−0.755)	(−1.040)	(−0.989)	(−1.548)	(−3.93)[b]
12	$(L_{21})_0 \times RT \times 10^9$	−0.729	−1.017	−0.973	−1.452	−3.71
12a		(−0.729)	(−1.006)	(−0.946)	(−1.474)	(−3.63)[b]
13	$\%\Delta_{exp.}$	−2.8	−1.3	−1.9	−4.2	−6.8
13a		(−3.5)	(−3.3)	(−4.4)	(−4.9)	(−7.9)[b]

[a] All diffusion coefficients are expressed in c.g.s. units; values of the cross-term diffusion coefficients correspond to concentrations expressed as moles of solute per unit volume of solution. All numbers in parentheses in this table are values reported in previous articles (refs. 18, 19 and 20); they are included to facilitate comparison of those results with the new values immediately above them which result from using the new calculation procedure described in this article. An extra figure was retained in each value of $(D_{ij})_V$ to facilitate comparisons and because it is desirable if the $(D_{ij})_V$ are used to compute values of $\mathfrak{D}_A$ for comparison with the measured values. Probably the third figure after the decimal should be made a subscript throughout lines 3–12a inclusive. [b] We are indebted to Dr. Peter J. Dunlop (private communication) for these corrected values of the required data from ref. 19 (see list of corrections in the December, 1959, issue of THIS JOURNAL).

tion 2DG; the results are shown in lines 7–10 of Table III. In these calculations data from Tables I-DG and III-D were used for the partial molal volumes, $\bar{V}_i$, and the solvent molarities, C_0. Then the values of $(D_{ij})_0$ and the derivatives of solute chemical potentials with respect to solute molarities (the μ_{ij} given in Tables II-DG and[21] IV-D) were substituted into equations 1e-DG, 1f-DG and 1h-DG to evaluate the Onsager coefficients $(L_{12})_0$ and $(L_{21})_0$ for the solvent-fixed frame of reference. These two coefficients should be equal if Onsager's reciprocal relation is satisfied. The values thus obtained for these coefficients are shown in lines 11 and 12 of Table III; the percentage differences between them, $\%\Delta_{exp.}$, defined by equation 21a-DG, are given in line 13. Previous values[19,20] for these coefficients and for the observed percentage differences are given in lines 11a, 12a and 13a for comparison. Because the new values of $(L_{12})_0$ and $(L_{21})_0$ for each composition are in better agreement than those reported previously, the new values of $(D_{ij})_V$ reported in this article seem to provide an improved test of the Onsager reciprocal relation for this system.

Acknowledgments.—The authors wish to acknowledge the assistance of Miss Sharon Rudd who calculated Table I. The work reported in this paper was supported in part by the National Science Foundation and by the Research Committee of the Graduate School from funds supplied by the Wisconsin Alumni Research Foundation.

Appendix

Equations 6 and 8, which are basic to the developments for ternary systems in this paper, will now be derived from the general theory of the Gouy method which was presented previously[15]; equation numbers in that article will be indicated by adding the letter G.

The interference condition for zeros of intensity in a Gouy fringe pattern arising from any symmetrical refractive index gradient curve is obtained by setting the intensity, $I(Y)$, equal to zero in equation 46G. By substituting equations 42G and 35G, changing the notation for the phase difference function defined by equation 4G from $\Phi(x)$ to $\phi(x)$ (to avoid a conflict in notation), and expanding $\arctan(V_2/W_2)$ in powers of W_2/V_2 we obtain

$$\frac{1}{\pi}\phi(x_2) = \left[j + \frac{3}{4} - \frac{1}{\pi}\left(\frac{W_2}{V_2}\right) + \frac{1}{3\pi}\left(\frac{W_2}{V_2}\right)^3 - \dots\right] \qquad (j = 0, 1, 2, \dots) \qquad \text{(A-1)}$$

Here j is the number of the particular zero of intensity considered ($j = 0$ for the intensity zero which is farthest from the undeviated slit image). The required condition for maxima, $\phi(x_2)$, in the phase function $\phi(x)$ is obtained by setting the derivative of equation 4G with respect to x equal to zero.

$$Y = ab(\mathrm{d}n/\mathrm{d}x) \qquad \text{(A-2)}$$

For use later we note (equation 9G) that the maximum displacement of light predicted by ray optics is

$$C_t = ab(\mathrm{d}n/\mathrm{d}x)_{\max} \qquad \text{(A-3)}$$

Substitution of equation A-2 into equation 4G after changing the symbol n_m to n_c gives

$$\phi(x_2) = (2\pi a/\lambda)[(n - n_c) - x(\mathrm{d}n/\mathrm{d}x)] \qquad \text{(A-4)}$$

The origin of x is taken at the position of the maximum refractive index gradient, where $n = n_m$

$(= n_c)$. Equations 4G and A-4 are applicable to experiments for which the cell dimension, a, and the displacements, Y_j, of all Gouy fringes from the undeviated slit image are small compared to the optical lever arm, b. Introduction of equation A-4 for $\phi(x_2)$ into equation A-1 gives the required interference condition for any refractive index distribution which is an odd function of x.

To obtain the interference condition for isothermal free diffusion in ternary systems, we first replace a/λ in equation A-4 by $J/\Delta n$ (equation 8G), where J is used now to denote the total number of fringes and Δn is the refractive index difference between the solutions across the initially sharp boundary. Next we observe that the refractive index distribution required for equation A-4 is given by equation 49F provided that the concentration increments, Δc_1 and Δc_2, (equation 8F) are sufficiently small. By recalling that $y = x/(2\sqrt{t})$, equation 9F, equations A-1 and A-4 may then be combined to give the required interference condition in the form

$$\Gamma_+ \mathrm{f}(\sqrt{\sigma_+}\; y_j) + \Gamma_- \mathrm{f}(\sqrt{\sigma_-}\; y_j) = \left[j + \frac{3}{4} - \frac{1}{\pi}\left(\frac{W_2}{V_2}\right) + \frac{1}{3\pi}\left(\frac{W_2}{V_2}\right)^3 - \dots\right] \Big/ J \equiv \mathrm{f}(\zeta_j) \simeq \frac{Z_j}{J} \qquad \text{(A-5)}$$

$$(j = 0,1,2, \dots)$$

where the function $\mathrm{f}(\zeta_j)$ is defined by equation 7. The asymptotic series $[j + {}^3/_4 - \dots]$ may be expressed in terms of derivatives, $\phi^m(x_2)$, of the phase function by using equations 40G and 41G. This procedure would be required to obtain the maximum accuracy of equation A-5. In most experiments J is sufficiently large that negligible errors are introduced if this series is approximated by the values Z_j (Table I of ref. 22); these numbers, which are independent of J, were obtained by fitting the phase difference function at $x = 0$ and at its maximum with a cubic of the form $gx + hx^3$. Equation A-5 defines[23] the variable ζ_j corresponding to the jth zero of intensity; y_j is the reduced cell coördinate corresponding to this intensity zero.

The relative displacement from the undeviated slit image of Gouy fringe j for a ternary system is obtained by division of equation A-2 by A-3 and substitution of equation 49F

$$\frac{Y_j}{C_t} = \frac{\Gamma_+\sqrt{\sigma_+}\;\Phi'(\sqrt{\sigma_+}\; y_j) + \Gamma_-\sqrt{\sigma_-}\;\Phi'(\sqrt{\sigma_-}\; y_j)}{(2/\sqrt{\pi})(\Gamma_+\sqrt{\sigma_+} + \Gamma_-\sqrt{\sigma_-})} \qquad \text{(A-6)}$$

where

$$\Phi'(\beta) = (2/\sqrt{\pi})e^{-\beta^2} \qquad \text{(A-7)}$$

The validity of equations A-5 and A-6 for ternary systems is not restricted to any special values of the diffusion coefficients or of Γ_+ and Γ_-. However, it is assumed that Δc_1 and Δc_2 are sufficiently small that over the range of concentration encountered in the cell we may consider the diffusion coefficients to be constant, the refractive index to be a linear function of the solute concentrations, and the partial specific volumes to be constant; furthermore it is assumed that extreme values of Γ_+ and Γ_- are avoided so that there are no unstable density gradients, and hence no convection, in the diffusing boundary.

Finally, as before,[24] the reduced Gouy fringe deviation, Ω_j, corresponding to fringe j is defined by

$$\Omega_j = e^{-\zeta_j^2} - (Y_j/C_t) \qquad \text{(A-8)}$$

Equation 8 is obtained readily by substitution of equation A-6 in A-8 as indicated in the theoretical section. It is seen that equation 8 is not restricted in its validity to a limited range of σ_-/σ_+ as was equation 72F. In practice C_t for each photograph is obtained as the intercept at $Z_j = 0$ of a plot of $Y_j/e^{-\zeta_j^2}$ *versus* $Z_j^{2/3}$. This extrapolation (which should become linear as $Z_j \rightarrow 0$) is believed to be of general validity for obtaining C_t. However it has been proved only for systems with fairly small values of Γ_+ or Γ_-, or with σ_-/σ_+ near unity, for which series expressions for the fringe deviations have been obtained.[25]

---

[22] L. J. Gosting and M. S. Morris, *J. Am. Chem. Soc.*, **71**, 1998 (1949).

[23] Equation 8 of ref. 6.

[24] See equation 9 of ref. 6 or equation 38 of ref. 10.

[25] See footnote 16 of ref. 4 and equations 28–31 of ref. 6.

A NEW REFRACTIVE INDEX GRADIENT RECORDING INTERFEROMETER SUITABLE FOR STUDYING DIFFUSION, ELECTROPHORESIS AND SEDIMENTATION

BY OLOF BRYNGDAHL AND STIG LJUNGGREN

Institute of Optical Research and the Department of Physical Chemistry, Royal Institute of Technology, Stockholm 70, Sweden

Received February 23, 1960

A new simple and versatile interferometer has been developed in which the interference fringes produce a direct plot of the refractive index gradient. The fringe system appears within a *sharp image* of the cell, each fringe representing the refractive index gradient curve for that part of the cell through which the fringe passes. The distance between the fringes can be varied by varying the parameters of the arrangement. The theory of the optical method is given in detail together with an estimate of possible errors. The records of some diffusion experiments are reproduced.

Introduction

There are now a great many methods available for the registration of the concentration of levelled solutions. The preference for any one of these methods often is dictated by habit or other casual circumstances. Since the primary amount of information is unchanged, the methods differ mainly in respect to the form in which the information is conveyed to the observer. This is, indeed, an important item, since the precision of a method is largely determined by the errors introduced in the evaluation of the interferograms. Also, in many instances, it is desirable that the methods should not presuppose any knowledge about the mathematical form of the concentration distribution. If, however, such information is available, it may, of course, be utilized to increase the precision of measurement of a particular property, for example, the diffusion coefficient.[1] As a property suitable for direct registration, the authors have chosen the refractive index gradient, since there seems to exist a need for such methods, for example in sedimentation and electrophoresis. Such a method might also be suitable for diffusion measurements. Although there already exist a few such methods, it seems that an alternative method would fill a need.

There are a few other desirable features which the authors think should be included. First, the method should give a sharp image of the cell on the photographic plate. This permits impurities and other imperfections in the cell to be kept under control and allows an accurate determination of the scale factor. Secondly, the method should be simple, easy to adjust and insensitive to mechanical vibrations. Finally, as has been pointed out elsewhere,[2] the interferences should be produced between rays with only a few wave length differences.

By a suitable combination of birefringent Savart plates, it has proved possible to produce a derivative-recording direct-imaging interferometer which combines all the features mentioned above. Since it is very easy to set up and to adjust, it seems that it could be recommended also for those who have no previous experience in this field.

I. The Optical Method.—The general outline of the method is illustrated by Fig. 1. The entrance slit is illuminated with monochromatic light from a conventional source. From the slit *via* the cell to the lens L_2, inclusively, the arrangement is the one common to most kinds of interferometers and does not require a separate description. The rest of the arrangement from the polarizer to the image plane 2, inclusively, is essentially new and its theory will be the subject of a following section.

The lens L_2 produces an image of the cell on the image plane 1. This plane is then, in turn, imaged on the image plane 2 which means that a *sharp* image of the cell is obtained together with the interference fringes. The core of the method is formed by the two Savart birefringent plates S_1 and S_2 together with the polarizers P_1 and P_2. The method works with interference with polarized light. The exact orientation of S_1 and S_2 will be made clear in what follows.

Figure 2 shows how the Savart plate works in parallel light. A plane-polarized wave front entering the plate is split up into two coherent component wave-fronts with oscillation planes described by the unit vectors ξ and η, respectively, and displaced vertically a distance b with respect to one another and horizontally a distance $b/2$ both in the same direction (*cf.* Fig. 2). The amplitudes of the two component wave-fronts are determined by the polarization direction of the incident wave-front according to the rules of ordinary vector decomposition. For example, if the incident wave-front is polarized in such a way that the oscillation plane bisects the two principal planes of the crystal sub-plates (*i.e.*, x- or y-direction in Fig. 2), then the component wavefronts will be equally strong. In a previous work[1] it is shown how a precision interferometer suitable for diffusion studies can be built, using only one Savart plate.

If, on the other hand, the Savart plate is placed in convergent light, an entering wave-front will be split up into two wave fronts with polarization directions perpendicular to one another (in the directions ξ and η, respectively) and making a small angle with one another, Fig. 3. The optical path difference, Δ, between the two emerging component wave-fronts in the image plane depends on the y-coördinate *via* the corresponding incident angle i and on the thickness of the Savart plate. For further details we refer to the general treatment in ref. 3, 4 and 5.

---

(1) O. Bryngdahl, *Acta Chem. Scand.*, **11**, 1017 (1957).

(2) E. Ingelstam, *Arkiv Fysik*, **9**, 197 (1955).

(3) O. Bryngdahl, Technical Report No. TR 16.4.1957, Institute of Optical Research, Royal Institute of Technology, Stockholm 70.

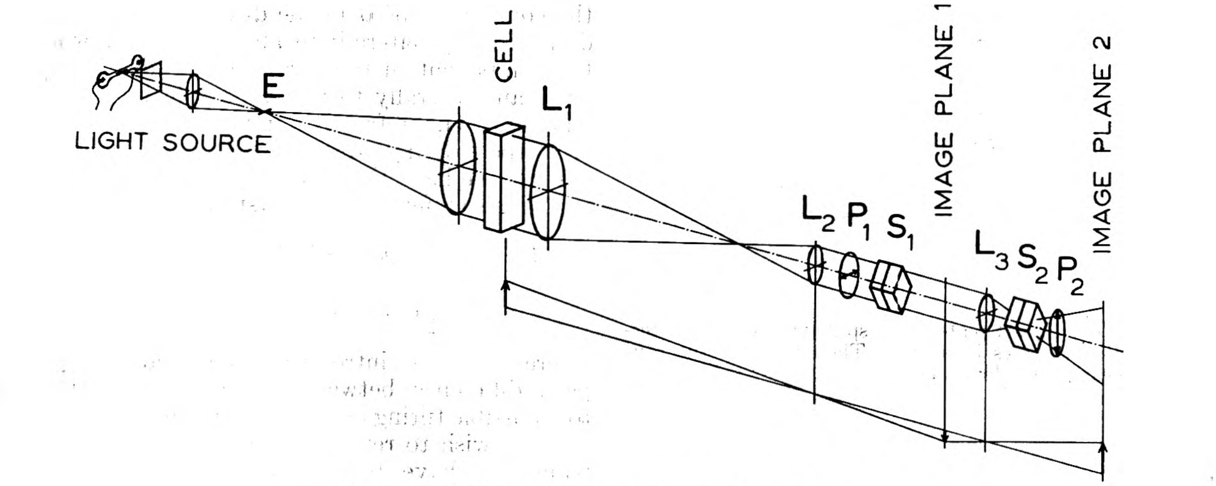

Fig. 1.—Optical arrangement. For notation see text.

$$\Delta = b \sin i \cos \psi \left(1 - \frac{n_0}{n_e \sqrt{n_0^2 + n_e^2}} \sin i \sin \psi\right) \quad (1)$$

where i is the angle between the crystal-surface normal and the entering ray, ψ its azimuthal angle and n_0 and n_e the principal refractive indices.

The first Savart plate, S_1, introduces a vertical displacement between the two wave-fronts polarized in the ξ- and η-directions. The second crystal plate, S_2, in convergent light, is turned through 90° with respect to S_1, which is irrelevant in this connection. The wave-fronts entering S_2 are oscillating in the ξ- and η-directions and are equally strong owing to the setting of the polarizer P_1. The principal planes of S_2 also lie in the ξ- and η-directions and thus each entering wave-front emerges without intensity reduction, polarized in the same direction as before S_2. The second Savart plate only introduces a small angle between the wave-fronts coming from S_1.

The interference fringes become visible in the image plane 2 by means of the analyzer P_2. P_2 ordinarily is used perpendicularly to P_1 and the resulting wave-fronts interfere destructively and constructively according as the path difference between the two wave-fronts is an integral number of wave lengths or a half-integral number of wave lengths, respectively. The interferogram gives us directly the derivative curve as will be clear from the theoretical section.

II. Apparatus

1. **The Lens System.**—The lens system is shown schematically in Fig. 1. E is a horizontal slit illuminated by monochromatic light. It is located in the focal plane of the first lens in the system L_1, so that parallel light traverses the cell. The system L_1 is composed of two equal achromatic lenses corrected for spherical aberration, each having a focal length of 100 cm. By means of the lens L_2, f = 12 cm., an image of the cell plane is obtained in the image plane 1. A strict collimation, necessary in the wave-fronts traversing the crystal plate, is accomplished by the adjustment of L_2. An optical reduction is introduced by L_2 in order to keep down the dimensions of the Savart plates. By means of the lens L_3, an ordinary microscope objective with a magnification factor = 5, the image plane 1 is transformed to the image plane 2.

2. **The Savart Plates.**—The first crystal plate, S_1, which is traversed by strictly parallel light, introduces a displacement between the wave-fronts in the x-direction equal to b_1. If the Savart plate is adjusted so as to be perpendicular to the optical axis, so that no phase shift is introduced between the two wave-fronts, then b is determined by the equation

$$b = e\sqrt{2}\,\frac{n_e^2 - n_0^2}{n_e^2 + n_0^2} \quad (2)$$

where e is the thickness of each part of the double plate and n_e and n_0 are the principal refractive indices. The quartz plates (S_1 and S_2), which are used in our experimental arrangement, have e = 10 mm. and b = 84.2 μ.

The Savart plates were purchased from Bernhard Halle Nachfolger, Hubertusstrasse 11, Berlin-Steglitz.

3. **The Monochromator.**—The horizontal entrance slit is illuminated by a 100 w. fine-capillary, low pressure mercury lamp with a filter that only transmits the green Hg line (5461 Å.). The width of the entrance slit is carefully adjusted as a compromise between light intensity and coherence. In our apparatus, the width of the entrance slit is 75 μ.

4. **The Camera and Photography.**—In the experiments with liquid gradients, where a quick registration of the beginning of the run is desired (an exposure every tenth second), a Robot camera which automatically feeds the film was used. For all photographic recordings, Ilford HPS film was used with Ilford Microphen fine grain developer. HPS film was used to attain a minimum exposure time (about 2 sec.).

5. **Support.**—All of the optical components were mounted on a 3 m. steel beam resting on sheets of sponge rubber on concrete tubes standing on the floor. In this way, vibrations from the floor were effectively damped out.

III. Theory.—In the light entering the cell, we may fasten our attention exclusively on the horizontal oscillation component. This is possible, since we later on introduce a polarizer P_1 in the light path. The oscillation plane of the polarizer can be set horizontally or vertically as desired. In this way, the two sheared wave fronts (ξ and η) will have the same amplitude after the Savart plate S_1. We can therefore describe the horizontal component of the wave entering the cell by a transversal electric field strength amplitude vector referred to the base system of vectors ξ and η and to the cell plane

$$\mathbf{U} = (\xi + \eta)\,\frac{A}{\sqrt{2}}\,\exp(ikz) \quad (3)$$

where $k = 2\,\pi/\lambda$ and A is the scalar amplitude. If, now, we denote the refractive index of the solution in the cell by $n(x)$ and the cell thickness by a,

---

(4) M. Born, "Optik," Springer Verlag, Berlin, 1933, p. 253.

(5) M. Françon, *J. Opt. Soc. Amer.*, **47**, 528 (1957).

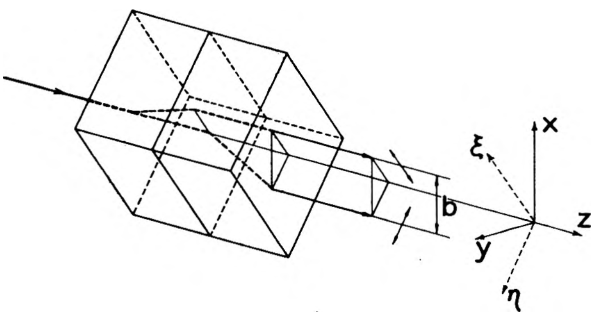

Fig. 2.—The Savart plate: the splitting-up of an entering ray into two rays is shown. The arrows at the rays indicate polarization directions.

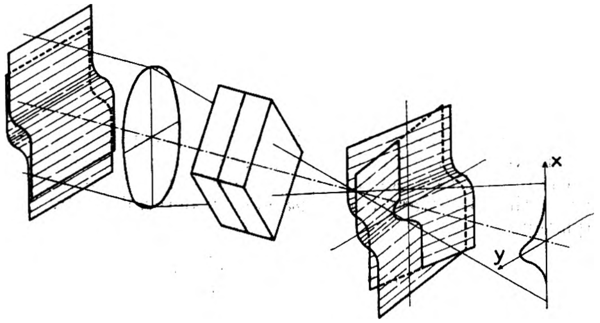

Fig. 3.—(Left) the refractive index as a function of x for the concentration gradient. A doubling of the wave front results from the first Savart plate. (Middle) introduction of a small angle between the wave-fronts due to the second Savart plate. (Right) the appearance of destructive interference in the image plane.

then the optical path of a ray passing through the cell will be

$$W(x) = an(x) \qquad (4)$$

independent of y. The amplitude vector of the light leaving the cell referred to the cell plane will therefore be

$$\mathbf{U} = (\xi + \eta)\frac{A}{\sqrt{2}}\exp\{ik[W(x) + z_0]\} \qquad (5)$$

where z_0 is an arbitrary reference plane in front of the cell. Equation 5 is true apart from certain very small corrections, the theory of which has been studied by Svensson.[6-8] Among these corrections, we note, for example, the Wiener skewness which can be eliminated by focusing on a plane one third of the cell width from the front surface of the cell. These corrections are as a rule very small and usually are neglected.

Next, the light passes through the last lens of the system L_1 and L_2, the purpose of which is to effect a scale reduction. Denoting the reduction factor by r, we have to introduce a new function

$$w(rx) = W(x) \qquad (6)$$

and can then write down the amplitude vector of the wave entering the first Savart plate S_1 in the following way as referred to the first image plane

$$\mathbf{U} = (\xi + \eta)\frac{A}{r\sqrt{2}}\exp\{ik[w(x) + z_1]\} \qquad (7)$$

New constants z_1, z_2, z_3, . . ., are introduced after each transformation. In passing the Savart plate, the component of $\mathbf{U}$ in the direction ξ is displaced downward and laterally by an amount $b_1/2$, whereas the component in the direction η is displaced upward and laterally to the same side by the same amount. The refractive index being a function of x, the sideways displacement is of no concern. After S_1 we have therefore the following amplitude vector, also referred to the first image plane

$$\mathbf{U} = \xi\frac{A}{r\sqrt{2}}\exp\{ik[w(x + b_1/2) + z_2 + \chi/2]\} + \\ + \eta\frac{A}{r\sqrt{2}}\exp\{ik[w(x - b_1/2) + z_2 - \chi/2]\} \qquad (8)$$

where we have introduced the quantity χ, the path difference between the wave-fronts, related to a possible tilting angle of the Savart plate.

If we wish to refer instead to the second image plane, we have to introduce the magnification factor m and a new function

$$V(mx) = w(x) \qquad (9)$$

Referred to this plane, the light entering the second Savart plate S_2 is described by the vector

$$\mathbf{U} = \xi\frac{A}{rm\sqrt{2}}\exp\{ik[V(x + mb_1/2) + z_3 + \chi/2]\} + \\ + \eta\frac{A}{rm\sqrt{2}}\exp\{ik[V(x - mb_1/2) + z_3 - \chi/2]\} \qquad (10)$$

On passing the second Savart plate, there is introduced firstly a vertical displacement, which is of no concern, and secondly an optical path displacement of different sign for the polarization directions ξ and η and of magnitude

$$\Delta/2 = \frac{1}{2}b_2 \sin i \cos \psi(1 - c \sin i \sin \psi) \qquad (11)$$

where i is the angle between the surface normal and the entering ray, ψ its azimuthal and

$$c = \frac{1}{n_e^2}\left(\frac{1}{n_e^2} + \frac{1}{n_0^2}\right)^{-1/2} \qquad (12)$$

If we now introduce the coördinates in the image plane (denoting by h the distance between the focal plane of L_3 and the final image plane 2)

$$x = h \operatorname{tg} i \sin \psi$$
$$y = h \operatorname{tg} i \cos \psi$$

we can rewrite (11) in the following way

$$\Delta = b_2 \frac{y}{h} \cos i \left(1 - c\frac{x}{h}\cos i\right) \qquad (13)$$

The expression for the emergent wave, referred to the second image plane, then can be written as

$$\mathbf{U} = \xi\frac{A}{rm\sqrt{2}}\exp\{ik[V(x + mb_1/2) + \Delta/2 + \\ z_4 + \chi'/2]\} + \eta\frac{A}{rm\sqrt{2}}\exp\{ik[V(x - mb_1/2) - \\ \Delta/2 + z_4 - \chi'/2]\} \qquad (14)$$

where, for simplicity, we have neglected explicitly to write out the obvious transition $x \rightarrow x + b_2/2$ resulting from the vertical displacement. After passing the second polarizer, we can write the resulting amplitude as

$$U = \mathbf{U}\cdot(\xi + \eta)/\sqrt{2} = \frac{A}{2rm}[\exp\{ik[V(x + mb_1/2) + \\ \Delta/2 + z_5 + \chi'/2]\} + \exp\{ik[V(x - mb_1/2) - \\ \Delta/2 + z_5 - \chi'/2]\}] \qquad (15)$$

---

(6) H. Svensson, *Optica Acta*, **1**, 25 (1954).
(7) H. Svensson, *ibid.*, **3**, 164 (1956).
(8) R. Forsberg and H. Svensson, *ibid.*, **1**, 90 (1954).

Using the Lagrange mean value theorem we have

$$V(x + mb_1/2) - V(x - mb_1/2) = mb_1V'(x - mb_1/2 + \theta mb_1)$$

where $0 < \theta < 1$ which also can be written

$$V(x + mb_1/2) - V(x - mb_1/2) = mb_1V'(x + \theta_1 mb_1/2)$$

where, now, $-1 < \theta_1 < 1$. We therefore can write

$$U = \frac{A}{2rm} \exp \{ik[V(x - mb_1/2) - \Delta/2 + z_6 - \chi'/2]\} \times [[\exp \{ik[V'(x + \theta_1 mb_1/2)mb_1 + \Delta + \chi']\} + 1] \quad (16)$$

where $-1 < \theta_1 < 1$. Hence, the image intensity becomes

$$I = |U|^2 = (A/2rm)^2 |\exp \{ik[mb_1V'(x + \theta_1 mb_1/2) + \Delta + \chi']\} + 1|^2 \quad (17)$$

If we denote

$$\varphi = k[mb_1V'(x + \theta_1 mb_1/2) + \Delta + \chi'] \quad (18)$$

we obtain the illustration of the intensity function given in Fig. 4. We have

$$I = (A/2rm)^2 |e^{i\varphi} + 1|^2 = (A/rm)^2 \cos^2 \frac{\varphi}{2} \quad (19)$$

Before introducing the expression for (13), we rewrite it, utilizing the fact that

$$\cos i = 1 - \theta_2 i^2/2$$

where $0 < \theta_2 < 1$ and tg $i = (x^2 + y^2)^{1/2}/h$. Thus

$$\Delta = b_2 \frac{y}{h} (1 - \theta_2 i^2/2) \left\{1 - c \frac{x}{h} (1 - \theta_2 i^2/2)\right\} = b_2 \frac{y}{h} \left(1 - c \frac{x}{h}\right) - (b_2 y/h)O(i^2) \quad (20)$$

The expression for φ then becomes

$$\varphi/k = mb_1V'(x + \theta_1 mb_1/2) + b_2 \frac{y}{h} \left(1 - c \frac{x}{h}\right) - \frac{b_2 y}{h} O(i^2) + \chi' \quad (21)$$

Destructive interference is obtained for $\varphi = 2n\pi$, $(n = 0, 1, 2, \ldots)$ with crossed polarizers. The equations of the curves of constant intensity (constant φ) can thus be written

$$y = \frac{hmb_1}{b_2} \cdot \frac{-V'(x) + (\varphi/k - \chi')/mb_1}{1 - cx/h} - \frac{\theta_1 hm^2 b_1^2}{2b_2} \cdot \frac{V''(x + \theta_1\theta_3 mb_1/2)}{1 - cx/h} + yO(i^2) \quad (22)$$

where $-1 < \theta_1 < 1$, $0 < \theta_3 < 1$. By suitable dimensioning, the denominator easily can be made to deviate by less than 1% from unity. However, the deviation is a systematic one depending on x and, in accurate measurements, the height of the curve at a certain value of x is always measured with reference to the fringe distance at that point, a procedure which takes account of the variation of the denominator. Thus, from (22) it is seen that increasing φ by 2π, which means passing from one dark fringe to the next, changes y by the same amount as a change in $V'(x)$ amounting to λ/mb_1. Now

$$V(x) = w(x/m) = W(x/mr)$$

whence

$$V'(x) = \frac{1}{mr} W'(x/mr); \quad = V''(x) = \frac{1}{m^2r^2} W''(x/mr)$$

On introduction of this expression in (22), we obtain our final equation

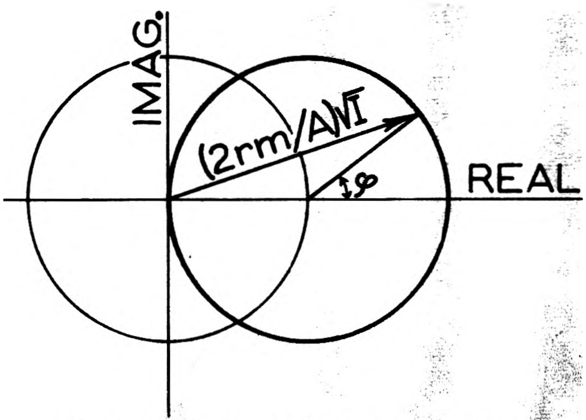

Fig. 4.—Illustration of the intensity function.

$$y = \frac{hb_1}{b_2 r} \cdot \frac{-W'(x/mr) + (\varphi/k - \chi')r/b_1}{1 - cx/h} - \theta_1 \frac{hb_1^2}{2b_2 r^2} \cdot \frac{W''(x/mr + \theta_1\theta_3 b_1/2r)}{1 - cx/h} + y \cdot O(i^2) \quad (23)$$

$(-1 < \theta_1 < 1;\ 0 < \theta_3 < 1)$

$$y = \frac{ahb_1}{rb_2} \cdot \frac{-n'(x/mr) + (\varphi/k - \chi')r/ab_1}{1 - cx/h} - \theta_1 \frac{ahb_1^2}{2r^2 b_2} \cdot \frac{n''(x/mr + \theta_1\theta_3 b_1/2r)}{1 - cx/h} + y \cdot O(i^2) \quad (24)$$

or

$$y \approx \frac{An'(x/mr) + B}{1 - cx/h} = An'(x/mr) + B + O(x/h) \quad (25)$$

where

$$A = -\frac{ahb_1}{rb_2}; \; B = \frac{h}{b_2}(\varphi/k - \chi')$$

Another convenient and more exact expression reads

$$y(1 - cx/h) = C \frac{\Delta n}{\Delta x'} + B + yO(i^2) \quad (26)$$

where $C = -ah/b_2$ and $\Delta x' = b_1/r$. $x' = x/mr$ is the height coördinate in the cell whereas x still refers to the image plane 2.

IV. Applicability and Results.—As was pointed out above, the method described is particularly recommendable in all cases where the form of the refractive index gradient curve is not known in advance. In the cases of electrophoresis and ultracentrifugation, a direct record of the refractive index gradient curve is often the kind of information that is wanted and, in such cases, this new method would mean a saving of time. Also in diffusion, it is very often desirable to obtain a check on the curve form.[9] The records reproduced in this paper refer to diffusion experiments.

Figure 5 shows a record obtained with a glass plate of varying thickness. The form of the corresponding optical path gradient appears in good detail although the peak value of the gradient amounts to no more than 0.58 wave length (of the light used) per mm., which should give an indication of the sensitivity of the method.

Figure 6 shows a record of an ordinary free diffusion experiment, started by levelling pure water above a 0.5% solution of NaCl. The record was

---

(9) For the study of boundary-formation in diffusion, previously undertaken,[10] the new method seems particularly convenient.

(10) O. Bryngdahl, *Acta Chem. Scand.*, **12**, 684 (1958).

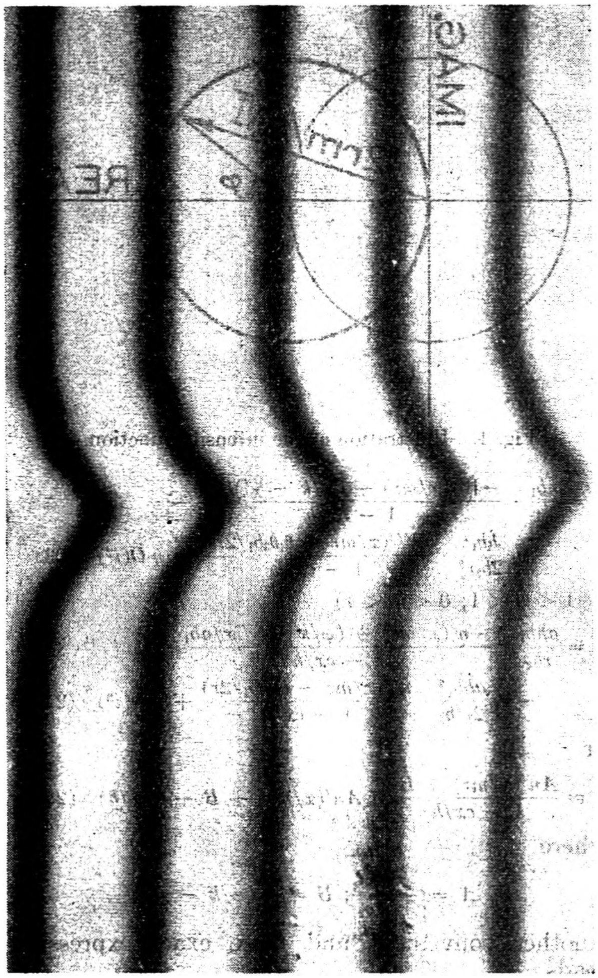

Fig. 5.—Record of glass gradient.

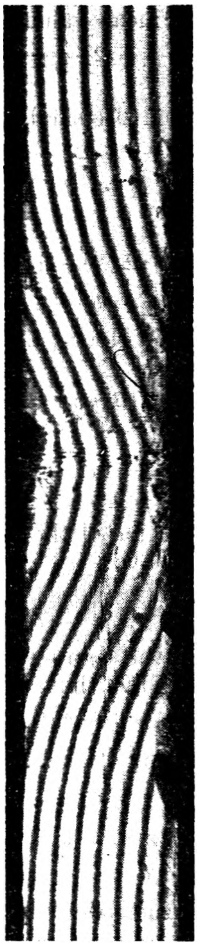

Fig. 6.—Record of ordinary diffusion experiment with 3% NaCl in water.

taken 1 hour after the levelling. The initial condition is illustrated in Fig. 7a. The total refractive index increment corresponds to an optical path difference of 100 wave lengths. The ideal curve is in this case of the Gaussian type, and the ideality of a diffusion experiment can be checked by comparison of the experimental curve with the ideal one. For the evaluation of the diffusion coefficient, any of the methods proposed by Lamm in connection with the scale method can be used.[11]

To demonstrate the capability of the method, some experiments with bottom layer diffusion were performed. In this type of diffusion,[12] the experiment is started by injecting a thin layer of rather concentrated solution at the bottom of the cell by means of a syringe. The initial condition is shown schematically in Fig. 7b. With this type of initial condition, the gradient curves are asymmetrical and, for a monodisperse substance, can be described as the derivative of a Gaussian curve. Figures 8 and 9 are records of this type. Figure 8 is a record of an experiment where 0.5 ml. of 3% NaCl has been levelled below pure water whereas in the experiment recorded in Fig. 9 the 3% NaCl solution has been replaced by a solution of 2.9% NaCl and 0.1% Macrodex (a commercial dextran solution purchased from the Pharmacia AB, Uppsala, Sweden). There are two peaks in the curve, one resulting from the sodium chloride and one from the dextran. The records were taken 2 and 3 hours after the levelling, respectively.

It may be of interest to give some figures on the sensitivity of the method in concentration units. If we have chosen $b_1/r = 1$ mm. which is a rather normal value and a cell width of 5 cm., we find that a gradient in KCl dissolved in water of 10^{-2} $M/$cm. gives a deviation (y-value) equal to the fringe distance. In the Lamm scale method,[11] for example, the same gradient and cell, with a scale distance of 20 cm., would give a scale line displacement of 100 μ.

V. Discussion.—As appears from the theoretical section above, the method is basically a difference quotient registering method. To be precise, however, the difference quotient is not plotted in the Cartesian coördinate system, x, y, of the plate but in the curvilinear coördinate system x, u, where $u = y(1 - cx/h)$. Actually, the curves u = const. form one branch of a bundle of like-sided hyperbolas[4] but the distance from their origin is so large that the deviation from a Cartesian coördinate system is not disturbing, especially as the term cx/h can be made negligibly small by proper dimensioning of the system. Since the interferogram consists of a large number of curves at a

---

[11] O. Lamm, *Nova Acta Regiae Soc. Sci. Upsaliensis*, **10**, No. 6 (1937).

[12] S. Ljunggren and O. Lamm, *Acta Chem. Scand.*, **11**, 340 (1957).

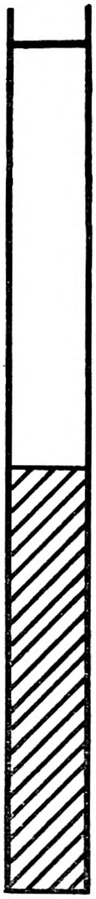

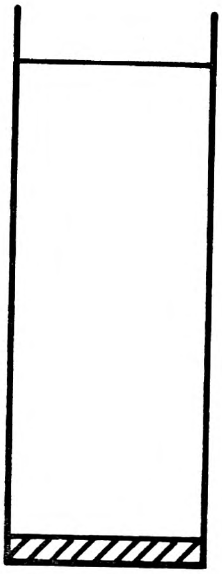

Fig. 7a.—Initial condition of ordinary free diffusion.
Fig. 7b.—Initial condition of bottom layer diffusion.

mutual distance corresponding to one wave length difference, the deviation from linearity is automatically compensated for and the height of the curves is automatically obtained in the corresponding number of wave length differences without the introduction of scale factors if the height at each value of x is given in terms of the fringe displacement at that level.

It is apparent from the theory given above that there are two main sources of systematic error. One is the term in eq. 24

$$\theta_1 ahb_1{}^2n''(x'\theta_1\theta_3b_1/2r)/r^2b_2(1 - cx/h)$$

which is the difference between the difference quotient $\Delta n/\Delta x'$ actually registered by the method and the corresponding differential quotient $\mathrm{d}n/\mathrm{d}x'$ which one wishes to obtain. The magnitude of this error can be reduced at will by making $\Delta x' = b_1/r$ sufficiently small. In ordinary circumstances it is quite negligible. There are, however, cases—for example in electrophoresis—where the gradient may reach very high values and where the second derivative becomes correspondingly high. On the other hand, $\Delta n/\Delta x'$ can never exceed the value $(\Delta n)_{\max}/(b_1/r)$.

If one wishes the corresponding fringe deviation not to exceed the width of the cell image in the y-direction, the dimensioning of the system will cause no trouble. Mathematically, this condition would be

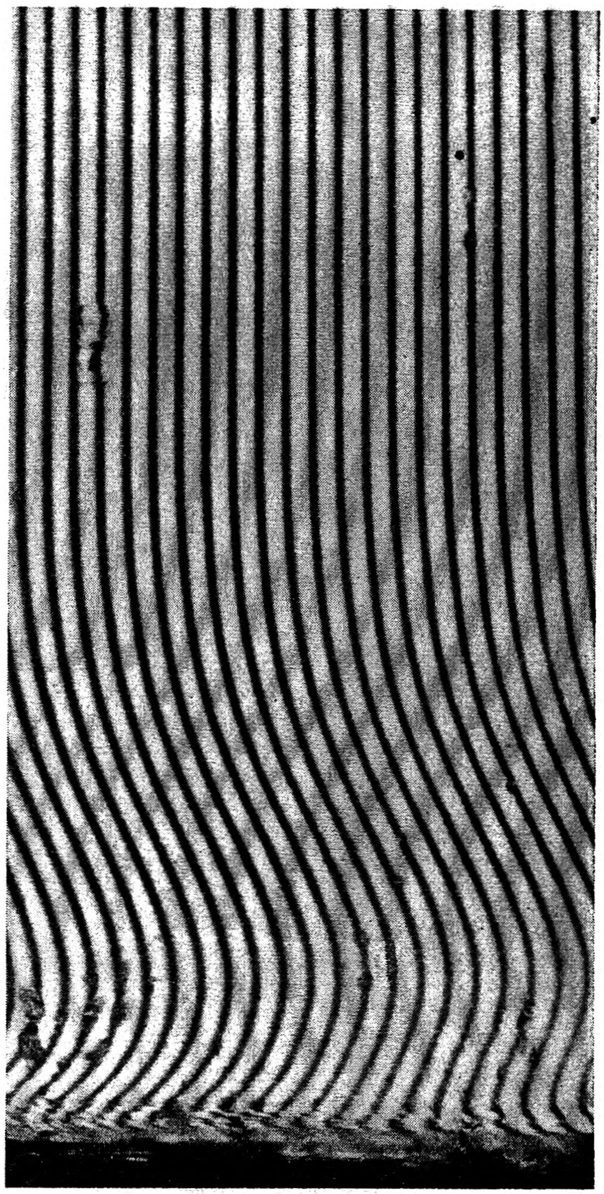

Fig. 8.—Record of bottom layer diffusion experiment with 3% NaCl injected below pure water.

$$d > ah(\Delta n)_{\max}/mb_1b_2$$

where d is the width of the cell in the y-direction. One further property of the interferograms calls for some comment. If we integrate our curves from $x' = \alpha$ to $x' = \beta$, we obtain

$$\int_\alpha^\beta (\Delta n/\Delta x')\,\mathrm{d}x' = \int_\alpha^\beta [n(x' + b_1/2r) - n(x' - b_1/2r)]\frac{r}{b_1}\,\mathrm{d}x' =$$

$$\int_{\alpha+b_1/2r}^{\beta+b_1/2r} (r/b_1)n(x')\,\mathrm{d}x' - \int_{\alpha-b_1/2r}^{\beta-b_1/2r} (r/b_1)\,n(x')\,\mathrm{d}x' =$$

$$\int_{\beta-b_1/2r}^{\beta+b_1/2r} (r/b_1)n(x')\,\mathrm{d}x' - \int_{\alpha-b_1/2r}^{\alpha+b_1/2r} (r/b_1)\,n(x')\,\mathrm{d}x' =$$

$$n(\beta + \gamma_2b_1/2r) - n(\alpha + \gamma_1b_1/2r) \quad (27)$$

where $-1 \leq \gamma_1, \gamma_2 \leq +1$. Thus, even if the gradient is very high at some point in the interval (α,β), an almost correct value for $n(\beta) - n(\alpha)$ is obtained by integration of the curves, provided only that the gradient $n'(x')$ has a moderate value

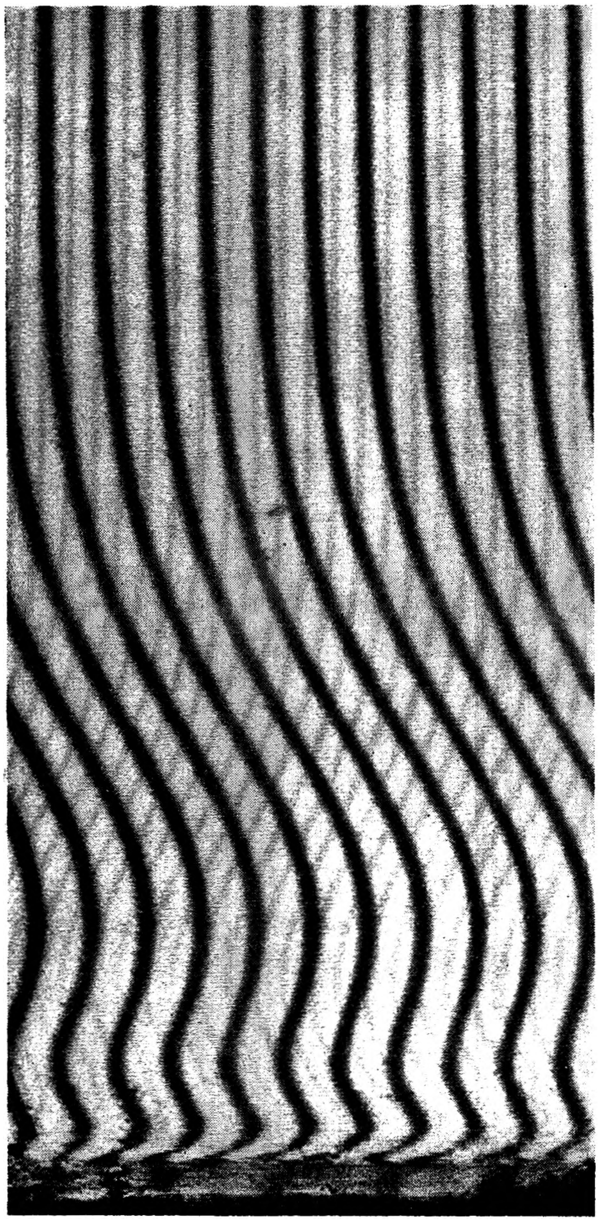

Fig. 9.—Record of bottom layer diffusion experiment with 2.9% NaCl and 0.1% dextran.

at the end-points of the integration interval. A rather trivial difficulty common to all interferometers, which may arise with very high gradients, is the appearance of schlieren effects due to part of the light falling outside the aperture of the lens L_3. The suppression of very high gradients combined with a corresponding broadening (this broadening never exceeds the value $2\Delta x' = 2b_1/r$, referred to the cell coördinate) of the peaks should be regarded rather as an advantage which allows a better utilization of the sensitivity available.

The second source of error, inherent in the term $O(i^2)$ in eq. 24, is very small in ordinary circumstances. Even in the most unfavorable cases, i is less than 1/10, *i.e.*, $i^2 < 10^{-2}$. With suitable dimensioning, $i < 10^{-2}$ and the relative error in y then will be below 10^{-4}.

Regarding the aberrations in the cell, reference is again made to the work of Svensson where also higher order aberrations are calculated.[6-8] It is shown how the aberrations can be almost totally eliminated in a simple way.

One important feature of these types of interferometers is that, on the logarithmic scale, due to photography the dark fringes are inherently sharper than the light ones. As a consequence of this, it is advantageous to work with as high light intensity as possible. The dark fringes will then appear very thin on the photographic plate. In any case, the apparent width (to the eye) of the fringes should not be taken as a measure of the sensitivity of the method since the position of the intensity minima can be determined with a much higher precision. In this connection it is appropriate to refer to the theories of Wolter on the subject of "Minimistrahlkennzeichnung."[13] Another interesting procedure is the "Äquidensitenverfahren" of Lau and Krug[14] who use a kind of relief technique to obtain very thin curves. The technique has been developed into a standard procedure.

A very recent, automatic method for redrawing oscillograms[15] might perhaps prove useful for our purpose in routine work. However, there is still lacking a method that can utilize the increased precision due to the large number of "identical" curves obtained in one experiment (which mainly differ only by accidential errors to be eliminated).

The cell image obtained together with the interferogram is a double image both in the horizontal and in the vertical direction. The displacement is, however, rather small and provides no inconvenience, *cf.* Figs. 5, 6, 8 and 9.

The present form of the method is intended for the registration of one-dimensional refractive index gradients. However, it does not seem altogether impossible to combine two similar apparatuses for simultaneous registration in two dimensions.

Acknowledgment.—S. Lj. gratefully acknowledges economic support from the "Swedish Technical Research Council."

(13) "Handbuch der Physik," Bd. XXIV, Springer Verlag, Berlin, 1956, pp. 577–588.

(14) E. Lau and W. Krug, "Die Äquidensitometrie," Akademie Verlag, Berlin, 1957.

(15) R. K. Swank and E. A. Mroz, *Rev. Sci. Instr.*, **10**, 880 (1959).

BASE-INITIATED DEHYDROHALOGENATION AND REARRANGEMENT OF 1-HALO-2,2-DIPHENYLETHYLENES IN *t*-BUTYL ALCOHOL. THE EFFECT OF DEUTERATED SOLVENT

BY J. G. PRITCHARD AND A. A. BOTHNER-BY

Mellon Institute, Pittsburgh, Penna.

Received March 1, 1960

The reactions of 1-chloro-, 1-bromo- and 1-iodo-2,2-diphenylethylene with excess potassium *t*-butoxide in *t*-butyl alcohol (BH) solution at 95°, yielding diphenylacetylene, have been followed quantitatively *via* the ultraviolet spectra of the reactants and product. For concentrations of the halodiphenylethylenes (C_{EH}) *ca.* 10^{-3} *M*, and of potassium *t*-butoxide (C_{KB}) in the range 0.01 to 1.0 *M*, the kinetic results are fitted well by an equation of the form: $\mathrm{d}C_{EH}/\mathrm{d}t = k_{obs}C_{EH} = kC_{EH}C_{KB}^{3/2}/C_{BH}$. The values of the coefficients k are 2×10^{-6}, 1.5×10^{-3} and 9×10^{-4} $\mathrm{l.}^{1/2}$ $\mathrm{mole}^{-1/2}$ $\mathrm{sec.}^{-1}$ for the Cl-, Br- and I-substituents, respectively. An investigation of the kinetics of the concomitant but much more rapid exchange of the 1-hydrogen substituent on 1-bromo-2,2-diphenylethylene in potassium *t*-butoxide solution, shows that this reaction is also first order in substrate and three-halves order in base. In the solvent *t*-butanol-*d* (2-methyl-2-deuteroxypropane) rates of rearrangement are higher: $k^D/k^H = 1.9 \pm 0.3$. These observations indicate that the reaction proceeds in two stages: a rapid pre-equilibrium, in which a configurationally stable vinyl carbanion is formed, and a subsequent slow step, in which rearrangement occurs as halide ion is liberated. The three-halves-order dependence of reaction rates on the formal potassium *t*-butoxide concentration can be explained by invoking complexing of this substance and its ions in *t*-butyl alcohol solution.

Introduction

The dehydrohalogenation and rearrangement of 1-halo-2,2-diarylethylenes yielding diarylacetylenes (tolans) may be brought about by a variety of strongly basic reagents (eq. 1). The reaction was first reported by Fritsch and his co-workers,[1] who used ethanolic solutions of sodium ethoxide at temperatures above 150° as reaction media. More recently such reagents as potassium amide in liquid ammonia,[2,3] and butyl- and phenyllithium[4,5] in ether solution, have been shown to be very effective.

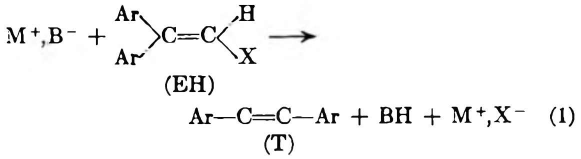

$$M^+,B^- + (Ar)_2C{=}C(H)(X)\ (EH) \longrightarrow Ar{-}C{\equiv}C{-}Ar\ (T) + BH + M^+,X^- \quad (1)$$

Previous studies of the mechanism of this reaction have established that the rearrangement is stereospecific. In the potassium *t*-butoxide initiated[6] reaction of both *cis*- and *trans*-1-bromo-2-(*p*-bromophenyl)-2-phenylethylene it has been shown that the group *trans* to the leaving halogen migrates predominantly.[7] Curtin, Flynn, and Nystrom[8] have demonstrated a similar stereospecificity in the butyllithium-initiated reaction of *cis*- and *trans*-2-bromo-1-(*p*-chlorophenyl)-1-phenylethylene. These findings suggest that a configurationally stable vinyl carbanion is produced as an intermediate in the reaction.[7] The investigations reported in this paper were undertaken for the purpose of establishing more firmly whether such an anion is an intermediate and, if so, to cast some light on its role in a detailed reaction mechanism.

Several studies appeared promising and were undertaken: (1) a study of the form of the rate-law governing the potassium *t*-butoxide-initiated reaction of 1-bromo-2,2-diphenylethylene; (2) a comparison of the rate constants for the elimination–rearrangement reaction of variously substituted 1-halo-2,2-diarylethylenes; (3) an investigation of the possible occurrence of a base-catalyzed deuterium exchange between solvent and olefinic substrate, and a study of the effect of deuterated solvent on the rate of reaction.

The rates of elimination–rearrangement of three 1-halo-2,2-diphenylethylenes were followed quantitatively *via* the ultraviolet spectra of the reactants and product. The potassium *t*-butoxide concentration was varied from 0.01 to 1.0 *M*. The halodiphenylethylene concentration was kept very low (*ca.* 10^{-3} *M*) so that the interpretation of the reaction-rate data should be as simple as possible. This measure also minimized the effect of the substrate concentration on the nature of the reaction medium. Kinetics in *t*-butanol-*d* (2-methyl-2-deuteroxypropane) were followed by the same techniques. Exchange of the deuterium into the olefinic substrate was detected and the kinetics thereof followed *via* the infrared spectrum of the unreacted substrate.

The system potassium *t*-butoxide–*t*-butyl alcohol was chosen for the reaction medium as one lending itself well to quantitative kinetic work. Also, the substitution reaction through the alkoxide ion, which may compete with elimination, appeared to be less important for *t*-butyl alcohol than for the more common primary alcohols. Thus, Fritsch and co-workers[1] reported that in the case of 1-chloro-2,2-diphenylethylene, reaction with sodium ethoxide in ethanol produced about 50% elimination–rearrangement and about 50% substitution yielding 1-ethoxy-2,2-diphenylethylene. However, they reported no substitution in the case

---

[1] P. Fritsch, W. P. Buttenberg and H. Wiechel, *Ann.*, **279**, 319 (1894).

[2] G. H. Coleman and R. D. Maxwell, *J. Am. Chem. Soc.*, **56**, 132 (1934).

[3] G. H. Coleman, W. H. Holst and R. D. Maxwell, *ibid.*, **58**, 2310 (1936).

[4] D. Y. Curtin and J. W. Crump, *ibid.*, **80**, 1922 (1958).

[5] D. Y. Curtin and E. W. Flynn, *ibid.*, **81**, 4714 (1959).

[6] Since base is consumed in the reaction, the rearrangement may not be termed "base-catalyzed," even though an anionic intermediate appears to be in equilibrium with substrate and base. The reaction mechanism to be suggested is classified by Ingold as unimolecular elimination through conjugate base, E1cB (*cf.* C. K. Ingold, "Structure and Mechanism in Organic Chemistry," Cornell University Press, Ithaca, N. Y., 1953, p. 423).

[7] A. A. Bothner-By, *J. Am. Chem. Soc.*, **77**, 3293 (1955).

[8] D. Y. Curtin, E. W. Flynn and R. F. Nystrom, *ibid.*, **80**, 4599 (1958).

of 1-bromo-2,2-diphenylethylene which rearranged much faster than the chloro derivative. We therefore have checked our reaction product particularly from 1-chloro-2,2-diphenylethylene.

Experimental

Materials.[9]—*t*-**Butyl alcohol and** *t*-**Butanol-*d*** were prepared as described elsewhere.[10] Pure potassium was provided by the MSA Research Corporation, Callery, Pa.

1-Chloro-2,2-diphenylethylene.—Fifteen g. of benzene was condensed with 20 g. of dichloroacetal by stirring for one hour at 0° with 60 ml. of sulfuric acid plus 15 ml. of acetic acid. The product was precipitated in ice-water as a dark viscous fluid. Chromatography on neutral alumina with *n*-hexane yielded white, crystalline 1,1-dichloro-2,2-diphenylethylene, m.p. *ca.* 80°. This product was boiled with excess sodium hydroxide in methanol solution for six hours and the organic material precipitated and washed with water. The yellow oil resulting was crystallized from methanol yielding 4 g. of 1-chloro-2,2-diphenylethylene as white, crystalline flakes, m.p. 42°.

Anal. Calcd. for $C_{14}H_{11}Cl$: C, 78.3; H, 5.1. Found: C, 78.1; H, 5.2.

1-Bromo-2,2-diphenylethylene.—To a solution containing 10 g. of 1,1-diphenylethylene and 4.8 g. of sodium acetate in 300 ml. of acetic acid was added an equal volume of acetic acid containing 18.5 g. of pyridinium bromide perbromide. The bromine was decolorized very rapidly. The solvent was removed by vacuum distillation and the solid residue extracted with water. The organic product was crystallized slowly from 95% ethanol yielding 7.7 g. of 1-bromo-2,2-diphenylethylene as pale green blocks, m.p. 47°. Repeated recrystallization gave an almost colorless product, m.p. 48–49°.

Anal. Calcd. for $C_{14}H_{11}Br$: C, 64.85; H, 4.2. Found: C, 64.9; H, 4.4.

1-Bromo-2,2-diphenylethylene-1-*d*.—Ordinary 1-bromo-2,2-diphenylethylene was allowed to exchange in a solution containing 0.3 *M* potassium *t*-butoxide in *t*-butanol-*d* for 36 hours at 35°. The product was precipitated in dilute hydrochloric acid solution, washed and dried, m.p. 49–50°. The infrared spectrum of this material showed significant differences from ordinary 1-bromo-2,2-diphenylethylene in the expected regions for the three degrees of freedom of the olefinic CH group (*cf.* Table II).

1-Iodo-2,2-diphenylethylene.—Thirty ml. of dry ether, 0.4 g. of magnesium turnings and 3.6 g. of 1-bromo-2,2-diphenylethylene were placed in the usual apparatus for Grignard reactions. The reaction was started by heating and by the addition of traces of iodine and methyl iodide, and needed only slight heating to sustain it. After one-half hour a further 40 ml. of dry ether and excess iodine were added and the whole stirred. The mixture then was treated with sodium hydroxide solution to destroy iodine and the organic constituents were removed in pentane. Evaporation of the pentane gave a purple solid which was filtered off and a brownish oil which was chromatographed on neutral alumina with pentane. Recrystallization of the chromatography fractions from 95% ethanol gave needles, m.p. 42–43°. Careful recrystallization from 95% methanol–water gave 200 mg. of pure 1-iodo-2,2-diphenylethylene as fine, pale green needles, m.p. 44.5° (sharp).

Anal. Calcd. for $C_{14}H_{11}I$: C, 54.9; H, 3.6. Found: C, 54.8; H, 3.6.

The purple solid on recrystallization from ethanol gave white needles, m.p. 196–197°. This product accounted for the bulk of the starting material and was tentatively identified as 1,1,4,4-tetraphenyl-1,3-butadiene (lit. m.p. 195–196°,[11] 196–196.5°[12]).

Anal. Calcd. for $C_{28}H_{22}$: C, 93.85; H, 6.15. Found: C, 93.4; H, 6.2.

Spectra.—The infrared spectra of the 1-halo-2,2-diphenylethylenes were run on a Beckman IR4 instrument equipped with sodium chloride and cesium bromide optics, for *ca.* 0.1 mm. capillary films of the melts. Accuracy is estimated as ± 10 cm.$^{-1}$ for the 4000 to 2000 cm.$^{-1}$ region and ± 2 cm.$^{-1}$ for the remainder.

The ultraviolet spectra were run in 95% ethanol as solvent on a Carey # 14 instrument. The extinction coefficients for the broad maximum of each of the 1-halo-2,2-diphenylethylenes are: chloro- 1.26×10^4 (255 mμ); bromo- 1.31×10^4 (259 mμ); iodo- 1.4×10^4 (263 mμ). The spectrum of *sym*-diphenylacetylene has five sharp maxima, the highest two of which (*cf.* Fig. 1) have extinction coefficients 3.20×10^4 (279 mμ) and 2.81×10^4 (296 mμ).

Reaction of 1-Chloro-2,2-diphenylethylene with Potassium *t*-Butoxide.—One-half g. of 1-chloro-2,2-diphenylethylene was dissolved in a solution of potassium *t*-butoxide prepared from 0.34 g. of potassium and 25 ml. of *t*-butyl alcohol. The resulting solution was heated in a sealed tube at 105–110° for 30 days. The precipitated product was filtered off, dissolved in hexane and chromatographed on neutral alumina from which it was eluted with benzene–carbon tetrachloride. On recrystallization from ethanol–water, 0.29 g. of pure *sym*-diphenylacetylene was obtained as white flakes, m.p. 61° (lit.[5] 60–61°) the identity of which was checked by comparison of infrared spectra with an authentic sample. A similar experiment was carried out using 1 g. of 1-chloro-2,2-diphenylethylene, 1.4 g. of potassium and a temperature of 95° for 7 days, resulting in the recovery of 0.60 g. of pure *sym*-diphenylacetylene.

Kinetic Methods. A.—The reactions at 95° to give diphenylacetylene were carried out as follows. A solution of potassium *t*-butoxide in *t*-butyl alcohol was prepared in a vessel protected from atmospheric moisture and to this was added a small quantity of a solution of one of the diphenylhaloethylenes in *t*-butyl alcohol, sufficient to give a concentration *ca.* 10^{-3} *M*. The mixture was homogenized at room temperature and quickly transferred to a series of glass tubes. These were sealed with the contents frozen, preheated in a bath at *ca.* 95° for 15 seconds and then transferred rapidly to a thermostated bath at 95 ± 0.05° at a recorded time ($t = 0$). Tubes were withdrawn at intervals and quenched by freezing. After homogenization, the contents of the tubes were accurately diluted with 95% ethanol to a standard volume at room temperature (26°). The ultraviolet spectra of these solutions were run *versus* an equivalent solvent as blank.

A plot of tolan peak heights at 296.5 mμ (*cf.* Fig. 1) against time gave a smooth representation of a first-order reaction (as tested by the Guggenheim procedure[13]) in all cases in which the reaction was fast enough to follow to completion in a reasonable time. Infinity peak values corresponded to at least 90% reaction to give tolan, as far as could be discerned from the spectra.[14] Hence the reaction may reasonably be described by: $dC_T/dt = -dC_{EH}/dt = k_{obs}\,C_{EH}$, where C_T and C_{EH} are molar concentrations of tolan and ethylene derivatives, respectively. Values of k_{obs} were calculated from Guggenheim plots taken from the smoothed rate data. For the very slow reactions at low concentrations of potassium the above differentiated form of the first-order rate equation was used directly to calculate initial rates: $(dC_T/dt)_{t=0} = k_{obs}(C_T)_{t=\infty}$, assum-

---

(9) Melting points are uncorrected. Microanalyses are by the Alfred Bernhardt Microanalytisches Laboratorium, Max Planck Institute, Kaiser Wilhelm Platz 1, Mulheim (Ruhr), Germany.

The halodiphenylethylenes employed in this study have been reported, while this manuscript was in preparation, by Curtin and Flynn (ref. 5). They gave the following corrected melting points: 1-chloro-2,2-diphenylethylene, 42–43°; 1-bromo-2,2-diphenylethylene-*d*, 42–43°; 1-iodo-2,2-diphenylethylene, 40–41°. They also included references to previous preparations and melting points, where available. Our methods of preparation differed in many important details and are therefore reported fully. Particularly our melting points for the bromo derivatives agree with those given in two of the previous references (49–50°).

(10) J. G. Pritchard and H. M. Nelson, This Journal, **64**, 795 (1960).

(11) H. A. Bruson and J. W. Kroeger, *J. Am. Chem. Soc.*, **62**, 36 (1940).

(12) H. M. Walborsky and F. M. Hornyak, *ibid.*, **77**, 6396 (1955).

(13) E. A. Guggenheim, *Phil. Mag.*, [7] **2**, 538 (1926).

(14) A side reaction leading to a species absorbing very strongly at ~260 mμ could be detected from the changes in the ultraviolet spectra. This reaction may well be the competing substitution reaction: $Ar_2C{=}CHX + RO^- \rightarrow Ar_2C{=}CHOR + X^-$, as reported by Fritsch and coworkers (ref. 1). It could conceivably be due to the addition of alcohol to the acetylenic product: ArHC═CORAr, *cf.* S. I. Miller and G. Shkapenko, *J. Am. Chem. Soc.*, **77**, 5038 (1955). In our case side reactions must account for less than 10% of the total reaction.

ing the theoretical value of C_T at t = infinity. Stoichiometric concentrations of base in samples of the reaction solutions were determined by dilution of aliquots with water at 26° and potentiometric titration against standard acid solutions. Lists of k_{obs} for various concentrations of base are given in Table I.

Reaction-solution densities at 26 and 95° were measured using a sealable dilatometer under conditions similar to those obtaining in the reaction tubes. The densities (D) varied linearly with the stoichiometric potassium concentration according to the equations

$$D^{26°} = 0.7795(1 + 0.0548C_{KB})$$
$$D^{95°} = 0.6998(1 + 0.0712C_{KB})$$

where C_{KB} is the concentration of dissolved potassium t-butoxide at 26° in molar units. From these data concentrations of t-butyl alcohol and potassium t-butoxide in the reaction solutions at 95° were calculated for use in determining the series of k values in Table I.

B.—The exchange reaction was examined as follows. (i) A solution containing *ca.* 1 g. of 1-bromo-2,2-diphenylethylene in 10.0 ml. of t-butanol-d was added quickly to a solution containing 0.3877 g. of dissolved potassium in 15.0 ml. of t-butanol-d at a recorded time at 35.0°. (ii) A second experiment employing 0.0398 g. of potassium bu otherwise identical with the first was carried out beside it. Quantities of *ca.* 5.00 ml. were removed at suitable times and quenched in cold dilute hydrochloric acid solution. The precipitated samples of partly exchanged 1-bromo-2,2-diphenylethylene were thoroughly washed and dried. The infrared spectra of the samples then were run quantitatively as melts in a 0.1 mm. spaced sodium chloride cell on a Beckman IR4 recording spectrophotometer, repeatedly for the region containing the 863 cm.$^{-1}$ band. This band showed maximum change during the exchange and a fairly constant base line. The observed absorbancies at various times were as follows: (i) O(abs.), O(sec.); 0.1015, 986; 0.161, 1765; 0.2145, 2625; 0.2995, 4130; 0.4285, 10170; and (ii) O, O; 0.0105, 3630; 0.023, 9570; 0.036, 14900; 0.0565, 22700; 0.16f, 87800.

Results

Product Analysis.—From two small-scale experiments in which 1-chloro-2,2-diphenylethylene reacted in t-butyl alcohol with *ca.* 0.3 and *ca.* 1.3 M potassium t-butoxide, respectively, yields of 82 and 72% of pure *sym*-diphenylacetylene were obtained, after crystallization. This indicates that probably at least 85% of the reaction of 1-chloro-2,2-diphenylethylene goes *via* the desired path of elimination–rearrangement when relatively high concentrations of t-butoxide are employed. The spectroscopic analysis for the kinetic experiments confirmed that at least 90% of the reaction went by the desired path for all three substrates.

Rate Law.—The reaction mechanism which we shall attempt to substantiate may be written as

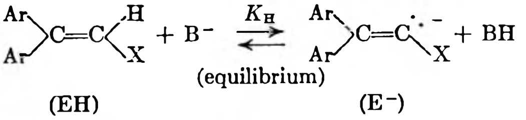

$$\mathrm{Ar_2C{=}C(H)X} + \mathrm{B^-} \underset{\text{(equilibrium)}}{\overset{K_H}{\rightleftharpoons}} \mathrm{Ar_2C{=}\ddot{C}^-X} + \mathrm{BH} \qquad (2)$$

(EH) (E⁻)

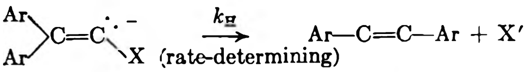

$$\mathrm{Ar_2C{=}\ddot{C}^-X} \underset{\text{(rate-determining)}}{\xrightarrow{k_H}} \mathrm{Ar{-}C{\equiv}C{-}Ar} + \mathrm{X'} \qquad (3)$$

Table I lists the main kinetic results and we shall consider in this section the first part (i) dealing with the reaction of 1-bromo-2,2-diphenylethylene. The first two columns show broadly that the set of pseudo-first-order rate coefficients (k_{obs}) changes by three powers of ten for a variation of two powers of ten in concentration of potassium t-butoxide (C_{KB}). Assuming that the reaction occurs through a mechanism similar to that shown in equations 2 and 3, except that the basic species (B$^-$) is not necessarily t-butoxide ion but is instead some base, the concentration of which varies as the three-halves power of the formal potassium t-butoxide concentration, the appropriate rate law for low concentrations of reagents and $K_H << 1$ is

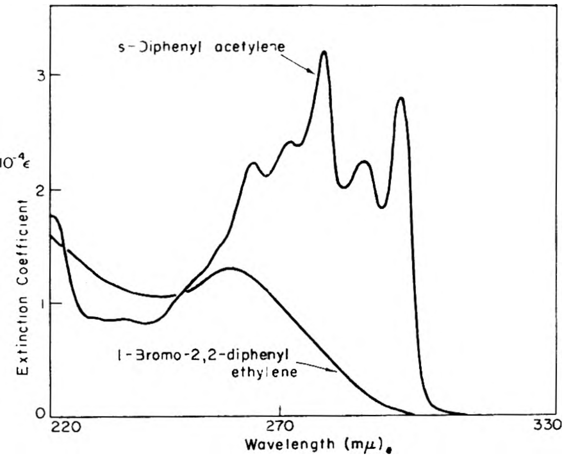

Fig. 1.—Ultraviolet spectra of 1-bromo-2,2-diphenylethylene and *sym*-diphenylacetylene.

$$-dC_{EH}/dt = kC_{EH}C_{KB}^{3/2}/C_{BH} \qquad (4)$$

where

$$\log k = \log k_{obs} + \log C_{BH}^{95°} - (3/2)\log C_{KB}^{95°} \qquad (5)$$

The rate coefficients (k) calculated from this expression (listed in Table I) show fair consistency considering that a 100-fold variation of base concentration is involved; there is also very reasonable continuity between the coefficients derived from initial rates and those derived from observation of the most part of the reaction for the higher concentrations of base. The contribution due to variation of solvent concentration with the potassium t-butoxide concentration at 95° is small but in the direction consistent with the equilibrium mechanism. Since the solvent probably is strongly complexed with the active base, the effect of the free solvent in equation 2 may be greater than that calculated in Table I, although in any event the effect is not large. In this type of reaction medium, which contains a high ratio of reagent to solvent on a molar basis, we would expect some medium effect on reaction rates and equilibria; however, it is most unlikely that there should occur a kinetic salt effect having the activity coefficient term directly proportional to a one-half or a three-halves power in the base (salt) concentration. Hence, we conclude that the present results indicate a rate law of the form in equation 4.

Deterium Exchange.—A base-catalyzed exchange reaction occurs when the olefinic substrate is dissolved in t-butanol-d containing potassium t-butoxide; it may be formulated as

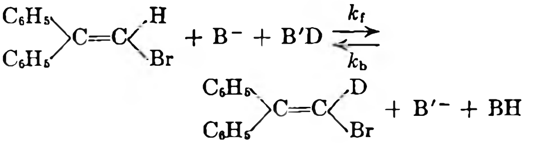

$$\mathrm{(C_6H_5)_2C{=}C(H)Br} + \mathrm{B^-} + \mathrm{B'D} \underset{k_b}{\overset{k_f}{\rightleftharpoons}} \mathrm{(C_6H_5)_2C{=}C(D)Br} + \mathrm{B'^-} + \mathrm{BH} \qquad (6)$$

Application of the Guggenheim procedure[13] to a smooth plot of the data shows that the forward

TABLE I

RATE DATA AT 95° FOR DEHYDROHALOGENATION OF 1-HALO-2,2-DIPHENYLETHYLENE IN SOLUTIONS OF POTASSIUM *t*-BUTOXIDE IN *t*-BUTYL ALCOHOL

$C_{KB}^{25°}$, M	$10^7 \times k_{obs}$, sec.$^{-1}$	$C_{BH}^{95°}$, M	$10^3 \times k$, l.$^{1/2}$ mole$^{-1/2}$ sec.$^{-1}$
(i) 1-Bromo-2,2-diphenylethylene			
0.939	2040	8.78	2.3
.867	1700	8.83	2.1
.666	820	8.97	1.6
.531	530	9.06	1.4
.363	267	9.18	1.3
.275	180	9.24	1.4
.215	121	9.29	1.3
.135	65.5	9.34	1.4
.118	48.5	9.35	1.3
.060	20.6[a]	9.39	1.6
.055	18.5[a]	9.40	1.6
.0345	8.94[a]	9.41	1.6
.0205	3.83[a]	9.42	1.4
.0165	3.60[a]	9.43	1.9
.011	2.14[a]	9.43	2.0
.0074	0.93[a]	9.43	1.6
(ii) 1-Bromo-2,2-diphenylethylene-*d* (in *t*-butanol-*d*)			
0.860	3000	8.84	3.8
.338	516	9.20	2.8
.238	222	9.27	2.1
.114	107	9.36	3.1
(iii) 1-Iodo-2,2-diphenylethylene			
0.940	735	8.78	0.96
.568	333	9.04	0.82
.323	125	9.21	0.74
.213	75	9.29	0.96
.079	20.7	9.38	1.01
(iv) 1-Chloro-2,2-diphenylethylene			
0.607	10.2	9.01	0.023
.469	6.15	9.11	.021
.335	2.85[a]	9.20	.016
.217	1.39[a]	9.29	.015

[a] Initial rate.

reaction is reasonably first order in concentration of 1-bromo-2,2-diphenylethylene. The ratio of initial rates for the two experiments is forty. Hence, a value for the reaction order with respect to potassium *t*-butoxide concentration is given by log (40)/log (0.3877/0.0398) = 1.6 ≈ 3/2. Therefore the concentration of the active base (B^-) in this exchange also varies as the three-halves power of C_{KB}. The pseudo-first-order rate constant for the exchange at 35° in the presence of 0.3877 M potassium *t*-butoxide is 2.4×10^{-4} sec.$^{-1}$. Assuming reasonable energies of activation, this means that the exchange is at least a hundred times faster than the conversion to diphenylacetylene at the same temperature.

Observed Isotope Effect on Rate.—Because of the rapid exchange reaction, the determination of the kinetics of the elimination–rearrangement reaction in *t*-butanol-*d* actually is made on the system which is reacting according to the scheme

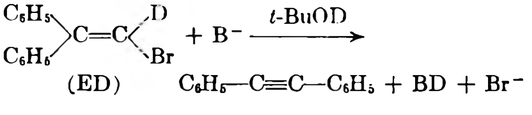

$$(C_6H_5)_2C{=}CDBr\ (\mathrm{ED}) + B^- \xrightarrow{t\text{-BuOD}} C_6H_5{-}C{\equiv}C{-}C_6H_5 + BD + Br^- \quad (7)$$

Table I (ii) gives observed rates for the reaction in *t*-butanol-*d*. A series of rate constants may be calculated assuming the rate law in equation 5 and that the molar volumes of *t*-butyl alcohol and *t*-butanol-*d* are the same. A comparison of rates at equivalent base concentration shows that the rates are consistently faster in the deuterated medium. There is a marked experimental variation, but the k^D/k^H ratios lie in the range 1.9 ± 0.3 and there is no consistent change of k^D/k^H over the considerable range of base concentrations employed.

Effect of Different Halogen.—The rate coefficients k for 1-iodo-2,2-diphenylethylene show reasonable constancy for the variation of more than one power of ten in potassium *t*-butoxide concentration (Table I (iii)). This result is an additional valid demonstration of the rather unexpected three-halves-order dependence of rate on C_{KB}. The reaction of 1-chloro-2,2-diphenylethylene was observed to be much slower than that of the other two haloethylenes and the study was not continued over a wide range of base concentration since increasing salt effects at high concentrations might complicate the interpretation of rates (Table I (iv)). A modest discrepancy between the k values derived from initial rates and those derived from observation of most of the reaction also was noted. The results, nevertheless, serve as a measure of the reactivity of the chloroethylene. Mean k values for the three ethylenes thus may be compared: 2×10^{-5}, 1.5×10^{-3} and 9×10^{-4} l.$^{1/2}$ mole$^{-1/2}$ sec.$^{-1}$ for the chloro, bromo and iodo substituted compounds, respectively.[15]

Discussion

The kinetic results show that there occurs a prelimary equilibrium between the 1-halo-2,2-diphenylethylene and base to give some form of anionic intermediate and that the formation of such an intermediate depends on the three-halves power of the formal potassium *t*-butoxide concentration. It is then highly plausible that the elimination–rearrangement reaction should be completed through unimolecular decomposition of the intermediate and hence that the reaction mechanism is in fact basically of the form shown in equations 2 and 3.

It is significant that the relative rates for the three 1-halo-2,2-diphenylethylenes studied are not in the order of electronegativities of the halogen substituents. This in itself strongly suggests a two-stage mechanism in which the halogen is not liberated in the first stage. A similar situation has been noted previously[16] and probably has a parallel explanation. Thus, if the two-stage mechanism is operative, changing the halogen from chlorine through bromine to iodine may have effects in opposite directions on stabilizing the carbanion in the first stage and facilitating its rearrangement to tolan in the second. Under such circumstances a

---

(15) Reported in a preliminary presentation: J. G. Pritchard and A. A. Bothner-By, Abstracts, 135th Am. Chem. Soc. Nat. Meeting, Boston, Mass., April 1959, sect. 35-R.

(16) J. D. Roberts, D. A. Semenow, H. W. Simmons, Jr., and L. A. Carlsmith, *J. Am. Chem. Soc.*, **78**, 601 (1956). These authors discuss the rate order PhBr > PhI > PhCl >> PhF observed for the amination of halobenzenes by potassium amide in liquid ammonia.

maximum in the over-all rate for the bromine substituent easily may occur.

There remain two important questions, which will be pursued in detail below. What is the form of the active base "B^-"? What is the significance of the solvent deuterium isotope effect and does the observed value of *ca.* 2 for $k^{\mathrm{D}}/k^{\mathrm{H}}$ help to confirm the proposed reaction mechanism?

Nature of the Active Base.—Little is generally known about the association–dissociation phenomena for solutions of metal alkoxides in alcohols. It appears very reasonable, however, to assume that in solutions of potassium *t*-butoxide in *t*-butyl alcohol some form of potassium *t*-butoxide ion-pairs are in equilibrium with small quantities of dissociated ion fragments, as indicated in the simple equation

$$\underset{(\mathrm{KB})}{t\text{-BuO}^-,\ \mathrm{K}^+} \overset{K_d}{\rightleftharpoons} \underset{(\mathrm{K}^+)}{\mathrm{K}^+} + \underset{(\mathrm{B}^-)}{t\text{-BuO}^-} \qquad (8)$$

The equilibrium constant K_d and the degree of dissociation d are then related by the usual equation

$$K_d = C_{\mathrm{K}^+}C_{\mathrm{B}^-}/C_{\mathrm{KB}} = d^2/(1 - d) \qquad (9)$$

In the known case of solutions of potassium ethoxide in ethanol, the K_d has the value 0.019 at 25°; and so for 1 *M* potassium ethoxide, for example, the degree of dissociation would be *ca.* 0.13.[17] The dielectric constant of ethanol at 25° is *ca.* 24, but that for *t*-butyl alcohol at 95° is far less and may be estimated by an extrapolation of data for lower temperatures[18] as *ca.* 5. The degree of dissociation for 1 *M* solutions of potassium *t*-butoxide should then be <<0.13 under our reaction conditions for the Fritsch rearrangement, probably < 0.01. It should then be legitimate to approximate K_d by $C_{\mathrm{B}^-}{}^2/C_{\mathrm{KB}}$. Hence, if dissociated *t*-butoxide ion is kinetically important, the reaction rate should be proportional to $C_{\mathrm{B}^-} = K_d{}^{1/2}C_{\mathrm{KB}}{}^{1/2}$; *i.e.*, it should contribute to the rate-expression a one-half-order dependence on C_{KB}. The experimental order with respect to C_{KB} is clearly 3/2 so that the *t*-butoxide ion cannot alone be responsible for bringing about the Fritsch rearrangement even though it may exist in very small concentration in the basic solution.

Given that the dielectric constant of *t*-butyl alcohol is low and therefore that the degree of dissociation of ion-pairs is low, the probability of formation of triple ions[19,20] or other multiple ions is high.

$$\underset{(\mathrm{KB})}{3\mathrm{K}^+,\mathrm{B}^-} \overset{K_c}{\rightleftharpoons} \mathrm{K_2B}^+ + \underset{(\mathrm{BKB}^-)}{\mathrm{KB_2}^-} \qquad (10)$$

If ionization according to equation 10 were most important for potassium *t*-butoxide in the concentration range 0.01 to 1 *M*, with $K_c << 1$ the reaction rate would be proportional to $C_{\mathrm{BKB}^-} = K_c{}^{1/2}C_{\mathrm{KB}}{}^{3/2}$. It therefore appears very plausible that the active base for the Fritsch rearrangement may be the negatively charged triple ion. In this case the rate expression for the over-all reaction would be as observed (eq. 4) with $k = k_{\mathrm{H}}K_{\mathrm{H}}K_c{}^{1/2}$.

The Isotope Effect.—Let the rate expression for the Fritsch reaction in pure *t*-butanol-*d* as solvent be formulated, by analogy with equation 4, as

$$-\mathrm{d}C_{\mathrm{ED}}/\mathrm{d}t = k^{\mathrm{D}}C_{\mathrm{ED}}C_{\mathrm{KB}}{}^{3/2}/C_{\mathrm{BD}},\ \text{where } k^{\mathrm{D}} = k_{\mathrm{D}}K_{\mathrm{D}}(K_c{}^{\mathrm{D}})^{1/2} \qquad (11)$$

The effect of the isotopic solvent on the individual reaction steps, *i.e.*, the magnitudes of $(K_c{}^{\mathrm{D}}/K_c{}^{\mathrm{H}})^{1/2}$, $K_{\mathrm{D}}/K_{\mathrm{H}}$ and $k_{\mathrm{D}}/k_{\mathrm{H}}$, will now be considered in general terms. The term in K_c will differ from unity only if the degree of solvation of the species in equation 10 is significantly different for the two sides of the equation. It appears reasonable to assume that the effect here would be small since the distribution of charge on the ion-pairs and triple ions on either side of the equation is probably fairly well balanced—if, indeed, equation 10 is precisely significant in the mechanism. For equilibria of the type in equation 2, at least as far as reactions with base in deuterium oxide and water solutions are concerned (to quote known examples), values of $K_{\mathrm{D}}/K_{\mathrm{H}}$ of about 1.4 are indicated.[21–23] The isotopic medium effect on k_{H} should be quite small since the rate-determining decomposition of the anionic intermediate does not involve breaking of any bonds to hydrogen. For similar rate steps in various aqueous systems, there have been observed values of $k_{\mathrm{D}}/k_{\mathrm{H}}$ ranging from *ca.* 1.2 to 0.7, representing pure medium effects.[21,22,24–26]

It is then plausible from the above observations to predict that if the reaction mechanism involves reversible carbanion formation and slow unimolecular decomposition thereof, it should proceed at about the same rate or more rapidly in deuterated solvent. On the other hand if the formation of carbanion were irreversible, so that its formation became the rate-determining step (the exchange reaction would then have to be a side reaction), previous experience suggests that the reaction of deuterated substrate would proceed more slowly. Values of 0.1 to 0.5 are commonly measured for $k^{\mathrm{D}}/k^{\mathrm{H}}$ ratios in reactions of this type,[21,27–29] in which a C–H bond is broken in the rate-determining step. In particular, Shiner has shown that the bimolecular elimination (class E-2)[6] of hydrogen bromide from isopropyl bromide by sodium ethoxide in ethanol is about 6.7 times faster than the same elimination from isopropyl bromide containing deuterium in the methyl groups.[28] The mechanism of this concerted reaction is illustrated in equation 12 and a similar concerted mechanism

---

[17] A. G. Ogston, *Trans. Faraday Soc.*, **32**, 1684 (1936).

[18] N. Koizumi and T. Hanai, *Bull. Inst. Chem. Research, Kyoto Univ.*, **33**, 14 (1955).

[19] R. M. Fuoss and C. A. Kraus, *J. Am. Chem. Soc.*, **55**, 2387 (1933).

[20] *Cf.* R. A. Robinson and R. H. Stokes, "Electrolyte Solutions," Butterworths Scientific Publications, London, 1955, Chap. 14, particularly pp. 390–393. (We are indebted to a referee for suggesting this reference material.)

[21] *Cf.* K. Wiberg, *Chem. Revs.*, **55**, 713 (1955).

[22] P. Ballinger and F. A. Long, *J. Am. Chem. Soc.*, **81**, 2347 (1959).

[23] C. G. Swain, A. D. Ketley and R. F. W. Bader, *ibid.*, **81**, 2353 (1959).

[24] P. M. Laughton and R. E. Robertson, *Can. J. Chem.*, **34**, 1714 (1956).

[25] F. A. Long and D. Watson, *J. Chem. Soc.*, 2019 (1958).

[26] J. G. Pritchard and F. A. Long, *J. Am. Chem. Soc.*, **78**, 6008 (1956).

[27] H. Eyring and F. W. Cagle, THIS JOURNAL, **56**, 889 (1952).

[28] V. J. Shiner, *J. Am. Chem. Soc.*, **74**, 5285 (1952).

[29] V. J. Shiner, *ibid.*, **75**, 2925 (1953).

may, of course, be written for the Fritsch elimination–rearrangement reaction. In our case, an expected value of k^D/k^H for E-2 reaction in the Fritsch rearrangement may be estimated by the reciprocal of the zero-point-energy term in Table II for ν_{CH} and ν_{CD}: 1/4.37 or *ca.* 0.2 (see Appendix).

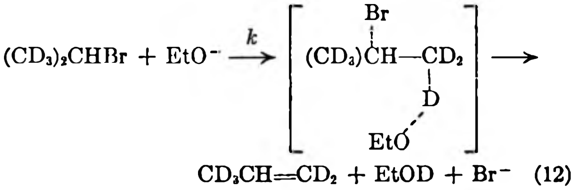

(12)

In this connection, it is of considerable interest that the recent results of Curtin and Flynn[5] imply that when butyllithium is the basic reagent, elimination–rearrangement to form *sym*-diphenylacetylene is at least twice as fast for 1-bromo-2,2-diphenylethylene as it is for 1-bromo-2,2-diphenylethylene-1-*d*. The mechanism of this reaction is most probably of the type in which the C–H bond is broken in a rate-determining step, as in equations 13 and 14. In this case, the first stage (13) is almost certainly not reversible.

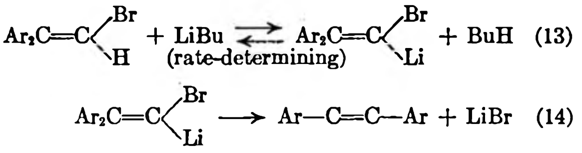

(13)
(14)

It may therefore be concluded that our observed value of k^D/k^H for the Fritsch rearrangement provides strong support for the proposed mechanism in the sense that the observed isotope effect *is greater than unity*. Additional support may be derived from a statistical calculation of the constant (K_E) for the liquid-phase equilibrium of equation 18 since it may be shown that $K_E \approx K_D/K_H$ in good approximation, provided certain medium effects are excluded (see Appendix). The value of K_D/K_H so calculated is *ca.* 1.2, which confirms our general supposition that the equilibrium of equation 2 should introduce a factor somewhat greater than unity into the value of k^D/k^H, and supplies semi-quantitative support for the proposed reaction mechanism.

The experimental value of k^D/k^H is *ca.* 2 and differs by a factor of perhaps 1.7 from the calculated K_E value. It is interesting to speculate as to how a medium effect amounting to *ca.* 1.7 might arise in *t*-butyl alcohol. The calculation quoted above ignores (*inter alia*) differences in solvation between the active base and the intermediate organic ion. Such difference may be considerable since the active base probably consists of a partly inorganic polyion (*cf.* eq. 10) involving a high degree of charge localization whereas the aromatic nature of the organic intermediate probably allows the dispersal of its formal negative charge to a considerable degree. The greatest contribution to the total partition function for the *t*-butyl alcohol and *t*-butanol-*d* is due to the difference in zero-point-energies of the OD and OH stretching vibrations (Appendix). Also, it is known that *powerful* hydrogen-bonding results in a shift of the normal OH (and OD) stretching frequency[30–32] to lower frequencies ranging from 2500 to 1000 cm.$^{-1}$. This would be equivalent to a change in the zero-point-energy contribution to the partition function per mole of the *t*-butyl alcohol species of from *ca.* 5.55 to the range 3.5 to 1.7 (*cf.* Table II). Thus, the difference in solvation proposed for equation 2 should reflect a difference in hydrogen-bonding which easily could give rise to a factor of 1.7 in the isotope effect (in the right direction). Hence the observed isotope effect appears consistent with the proposed mechanism.

Appendix

A statistical method is available for the calculation of a quantity equivalent to K_D/K_H, provided certain assumptions are made, as follows. For small concentrations of potassium *t*-butoxide and olefinic substrate, the equilibria in the isotopic solvents may be described as in equations 15 and 16, where C signifies concentration. For the situation in which the equilibria in the two isotopic solvents involve equal concentrations of B^- and of E^- in the two solvents, one may write formally

$$K_H = C_{E^-}C_{BH}/C_{EH}C_{B^-} \qquad (15)$$
$$K_D = C_{E^-}C_{BD}/C_{ED}C_{B^-} \qquad (16)$$

$$K_D/K_H = C_{EH}C_{BD}/C_{ED}C_{BH} \qquad (17)$$

If it is assumed that *t*-butyl alcohol and *t*-butanol-*d* behave as identical solvents for each other and for the isotopic forms of the olefinic substrate, then the expression for K_D/K_H (eq. 17) becomes equal to K_E, the equilibrium constant for the reversible reaction in equation 18.

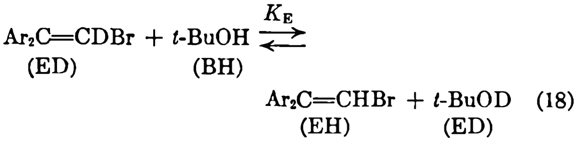

$$\underset{(ED)}{Ar_2C{=}CDBr} + \underset{(BH)}{t\text{-}BuOH} \overset{K_E}{\rightleftharpoons} \underset{(EH)}{Ar_2C{=}CHBr} + \underset{(ED)}{t\text{-}BuOD} \qquad (18)$$

A theoretical value of K_E for the hypothetical case of infinite separation of the reactants may be calculated[23,33] from ratios of the partition functions for the translational, rotational and vibrational motions for the pure liquid state of each molecular species in equation 18. It is now assumed that identical changes in the environment of the EH and ED molecules occur when small quantities of these are dissolved in *t*-butyl alcohol. Subject to all the above assumptions, a statistical value of K_E(eq. 19) calculated from the spectral characteristics of the pure liquid species (EH, ED, BH and BD) may be equated with the ratio K_D/K_H as it pertains to the separate equilibria (eq. 2) in the isotopic solvents.

$$K_E = (Q_{BD}/Q_{BH})/(Q_{ED}/Q_{EH}) \qquad (19)$$

The total partition function Q for each of the four substances involved is the product of the partition functions for the translational, rotational and vibrational motions of the molecules, Q^t, Q^r and Q^v. The contribution to the expression for K_E made by the Q^t and Q^r terms is given by the

---

[30] M. Davies and W. J. O. Thomas, *J. Chem. Soc.*, 2858 (1951).

[31] W. Klemperer and G. C. Pimentel, *J. Chem. Phys.*, **22**, 1399 (1954).

[32] N. Albert and R. M. Badger, *ibid.*, **29**, 1193 (1958).

[33] J. Bigeleisen and M. G. M. Mayer, *ibid.*, **15**, 261 (1947).

ratio of the molecular weight (M) and moment of inertia (I) terms quoted in the Redlich formula (eq. 20) for each molecular type, the terms for the EH–ED species being *divided* by those for BH–BD. The total value of these terms for 1-bromo-2,2-diphenylethylene may be estimated as 0.99 from the molecular weight ratio 259/260, using a simplified molecular model; and that for *t*-butyl alcohol has been calculated previously[10] as 0.927. There will therefore be a contribution of the factor 1.07 to the isotope effect from the Q^t and Q^r terms.

$$\pi_i\omega_i^{\mathrm{H}}\omega_i^{\mathrm{D}} \leqq (m^{\mathrm{D}}/m^{\mathrm{H}})^{3/2} (M^{\mathrm{H}}/M^{\mathrm{D}})^{3/2} \times (I_x^{\mathrm{H}}I_y^{\mathrm{H}}I_z^{\mathrm{H}}/I_x^{\mathrm{D}}I_y^{\mathrm{D}}I_z^{\mathrm{D}})^{1/2} \quad (20)$$

The vibrational partition function for a harmonic oscillator of frequency ω_i(cm.$^{-1}$) is given by

$$Q_i^{\mathrm{v}} = \sum_{n=0}^{\infty} e^{-(n+1/2)\alpha_i} \text{ for } n = 0,1,2, \ldots, \infty \quad (21)$$

or

$$Q_i^{\mathrm{v}} = e^{-\alpha_i/2}\,(1 - e^{-\alpha_i})^{-1} \quad (22)$$

where $\alpha_i = hc\omega_i/\kappa T$ and h is Planck's constant, c is the velocity of light, κ is the Boltzmann constant and T is the temperature for which the isotope effect is required: 368.2° Kelvin in our case. The frequency conversion formula is then $\alpha_i = 3.907 \times 10^{-3}\omega_i$.

The partition function terms for the vibrational degrees of freedom are given for each species contributing to K_E by $Q^{\mathrm{v}} = \pi_i Q_i^{\mathrm{v}}$, the calculations for which are summarized in Table II. The observed frequencies for the appropriate degrees of freedom of the H and D atoms are listed and are in agreement with the Redlich product formula.[34] The values $\pi_i{}^{\mathrm{D}}Q_i^{\mathrm{v}}/\pi_i{}^{\mathrm{H}}Q_i^{\mathrm{v}}$ for the alcohol and olefin are, respectively, 15.9 and 14.4 so that the contribution to the isotope effect from the Q^{v} terms is a factor of 1.10. The total calculated isotope effect is therefore 1.10 × 1.07 = 1.18. It is interesting to note that the main contributions to this calculated effect come from the differences in zero-point-energy between the OH, OD, CH and CD stretching vibrations (*cf.* Table II, third column), and from the difference in molecular weight of the two reactants which also reflects difference in inertia. These two effects are counteracted to a considerable extent by the zero-point-energy effect for the out-of-plane bending motions of the H and D substituents (frequencies 490 to 808 cm.$^{-1}$ in Table II). The effects of quantum level distribution are very small (Table II, last column) and the contributions due to the in-plane bending motions cancel.

TABLE II

DATA ON CALCULATION OF VIBRATIONAL PARTITION FUNCTIONS FOR EQUILIBRIUM BETWEEN 1-BROMO-2,2-DIPHENYLETHYLENE AND *t*-BUTANOL-*d*

Mode	ω_i^{H} (cm.$^{-1}$)	Mode	ω_i^{D} (cm.$^{-1}$)	$\dfrac{e^{-\alpha_i^{\mathrm{D}}/2}}{e^{-\alpha_i^{\mathrm{H}}/2}}$	$\dfrac{(1 - e^{-\alpha_i^{\mathrm{D}}})}{(1 - e^{-\alpha_i^{\mathrm{D}}})}$
		(i) *t*-Butyl alcohol[10]			
ν_{OH}	3362	ν_{OD}	2485	5.55	1.000
δ_{COH}	1380	$\rho_{\mathrm{CH_3}}$	1276	1.23	1.002
$\rho_{\mathrm{CH_3}}$	1189	δ_{COD}	952	1.59	1.015
τ_{OH}	640	τ_{OD}	490	1.34	1.077
		(ii) 1-Bromo-2,2-diphenylethylene			
ν_{CH}	3040	ν_{CD}	2285	4.37	1.000
$\delta_{\mathrm{C:CH}}$	1324[35]	$\delta_{\mathrm{C:CD}}$	983	1.95	1.016
δ_{CH}	808[35]	δ_{CD}	581	1.56	1.068

Acknowledgments.—The authors wish to express their appreciation of the experimental work carried out by Miss J. S. Hartman, Dr. H. M. Nelson and Mr. Lynn Thomas in connection with various stages of this investigation.

[34] G. Hertzberg, "Infrared and Raman Spectra of Polyatomic Molecules," D. Van Nostrand Co., Inc., New York, N. Y., 1945, p. 232.

[35] *Cf.* L. J. Bellamy, "Infrared Spectra of Complex Molecules," John Wiley and Sons, Inc., New York, N. Y., 1958, Chap. 3.

γ-RAY INDUCED OXIDATION OF STANNOUS CHLORIDE IN AQUEOUS HYDROCHLORIC ACID SOLUTIONS

BY ALEXANDER R. AMELL

Department of Chemistry, University of New Hampshire, Durham, New Hampshire

Received March 1, 1960

γ-Ray induced oxidation of Sn(II) in aqueous hydrochloric acid solutions is independent of the concentration of Sn(II), concentration of Sn(IV) and irradiation time. The "G"-values found in 3 N HCl are 1.50 ions Sn(II)/100 e.v. This value is independent of acid concentration above 1.5 M but decreases at lower acid concentrations. There is a slight dependence of G upon concentration of chloride. This is postulated as being related to changes in activity and oxidation potentials. The mechanism of the reaction is postulated using previously reported reactions.

Introduction

Aqueous hydrochloric acid solutions of the strong reducing agent Sn(II), exposed to the γ-radiation of cobalt-60, yield Sn(IV) and hydrogen gas as the products. This system is of particular interest because of the nature of the reducing agent, a two electron transfer being involved in the oxidation to Sn(IV). Determination of the "G"-values for the system will help elucidate the mechanism by which Sn(II) acts as a reducing agent as well as add to the general field of knowledge of radiation chemistry of aqueous solutions. Since Sn(II) is such a strong reducing agent in aqueous solutions it might also offer possibilities as a scavenger for some radicals produced in irradiation of aqueous systems.

Boyle, Weiner and Hochanadel[1] have studied the irradiation of Sn(II) in aqueous sulfuric acid solutions and mixtures of Sn(II) and Fe(II) or Sn(II)

[1] J. W. Boyle, S. Weiner and C. J. Hochanadel, THIS JOURNAL, 63, 892 (1959).

and Fe(III). All of their work was in 0.4 *M* sulfuric acid.

Experimental

Stock solutions of stannous chloride were prepared by dissolving solid stannous chloride in concentrated hydrochloric acid and diluting with distilled water to the final desired concentration of both stannous ion and acid. These solutions were stored under an atmosphere of carbon dioxide or nitrogen to minimize the air oxidation of the Sn(II). The Sn(II) concentration was determined by titration with a standard iodine solution which had been standardized against arsenious oxide. The acid concentration of the solutions was determined by titration against primary standard sodium carbonate.

During the first two days following preparation of the solutions, the Sn(II) concentration decreased, but then remained constant. This probably is due to reaction with dissolved oxygen. Brubaker and Court have noted[2] that saturation of Sn(II) solutions with air just prior to the reaction between Sn(II) and Ce(IV) had no effect upon this reaction. Thus the oxidation of Sn(II) by dissolved oxygen is a slow reaction agreeing with the slow change we have found here.

The acid concentration of the solutions remained constant from the start.

All transfers and titrations of solutions were carried out under carbon dioxide or nitrogen to prevent air oxidation. Results of duplicate titrations were reproducible to better than 1%.

Irradiations were carried out in all-glass vessels placed in a position which was reproducible with respect to a 150 curie cobalt-60 source. The dose rate, determined by use of the Fricke ferrous sulfate dosimeter,[3] was 1.43×10^{17} e.v./g./min. at the start of the irradiations. The dose rate was corrected for decay. All irradiations were carried out at ambient temperature which varied from 15 to 25°. This temperature variation appeared to have no effect upon the reaction as determined by duplicate samples run at different temperatures.

Analyses generally were made within half an hour after removal of the sample from the source. A few samples were titrated both within half an hour and upon standing overnight without any difference greater than the experimental error found in the other samples.

Results

In all experiments the reducing titer of the solution decreased indicating an oxidation of Sn(II) to Sn(IV). While Sn(II) and Sn(IV) interact in solution[4] so that determination of concentration of each by light absorption is not practical, it is possible to determine qualitative changes. Spectra of irradiated solutions taken on a Perkin–Elmer Spectracord 4000 showed a decrease of Sn(II) and increase of Sn(IV) upon irradiation.

Hydrogen gas also was identified as a product of irradiation, both by the "pop" obtained upon igniting the gas released when the irradiation cells were opened, and by passing a sample through a gas chromatographic column. No other gaseous products (a slight air peak was present for calibration) were found.

The effects of the following variables upon the yield were studied: (1) total dose; (2) Sn^{+2} concentration; (3) Cl^- concentration; (4) Sn^{+4} concentration; (5) H^+ concentration.

Exposure Time.—Figure 1 is a plot of the moles of Sn(II) oxidized as a function of the total dose. The extent of oxidation in various experiments is from about 25% of the Sn(II) present to slightly over 95% with no change in the *G*-value not within the possible experimental error. The linearity of this plot would also confirm that dissolved oxygen is not involved in the oxidation. If it were, we would expect a change in the slope at the point where all the dissolved oxygen is used up, as found in the oxidation of air saturated ferrous sulfate.[5] From the observation that the Sn(II) concentration decreased for a time following preparation of the stannous chloride solutions it can be concluded that the dissolved oxygen reacts with the Sn(II) in solution and is thus removed.

Effect of Initial Sn(II) Concentration.—To determine the effect of the initial concentration of Sn(II) upon the oxidation, two solutions were prepared for irradiation. These solutions differed only in Sn(II) concentration, the concentration of one being one-half the concentration of the other. The results of both of these are included in Fig. 1. Within these concentration limits there is no effect of concentration Sn(II) upon the oxidation.

From Fig. 1 it is determined that the $G(-\text{Sn(II)})$ is 1.50 ions/100 e.v. in a 3 *N* HCl solution with an initial Sn(II) concentration 10^{-2} *M*.

Effect of Added Sn(IV).—While the constant *G*-values obtained for the oxidation of Sn(II) as the total dose is changed would indicate that there is no effect of Sn(IV) upon the oxidation, the effect of added (Sn(IV)) upon the reaction was studied. $SnCl_4$ was added to some solutions so that the initial Sn(II) and Sn(IV) concentrations were the same. These solutions were irradiated and analyzed as before. The data are included in Fig. 1. The average "*G*"-value for these solutions was 1.45. The value agrees within the possible experimental error with the solutions without added Sn(IV).

Effect of Hydrogen Ion.—The concentration of hydrochloric acid used in the solution was varied to determine hydrogen ion effect. The concentration of chloride was kept constant by the addition of NaCl to the solutions. All other conditions were unchanged. In Fig. 2 a graph of the "*G*"-value as a function of (HCl) is given. Each point represents an average of a number of runs made on a given solution.

Boyle, Weiner and Hochanadel determined *G* (SnIV) in 0.8 *N* H_2SO_4 to be 0.49, as compared to $G(-\text{Sn(II)})$ we have determined in 0.8 *M* HCl of 1.25 (from Fig. 2). In addition to the difference in anion present, there is a difference in (SnII), Boyle, *et al.*, using $(\text{Sn(II)}) = 10^{-3}M$. We have prepared two solutions of Sn(II) in 0.8 *N* H_2SO_4 with $(\text{Sn(II)}) = 10^{-2}$ *M* and determined the $G(-\text{Sn(II)})$ for these solutions. These points are included in Fig. 2. The "*G*"-values found were 0.52 and 0.79, in satisfactory agreement with the value of 0.49. These solutions in H_2SO_4 are much less stable than those in HCl, a precipitate (presumably of hydrated stannic oxide) forming both upon irradiation of the solutions and upon long standing. The end-point of the titration was not sharp with this precipitate present. The same effect was found in HCl when the acid concentration was decreased below about 0.5 *M*, the lower

---

(2) C. H. Brubaker and A. J. Court, *J. Am. Chem. Soc.*, **78**, 55 (1956).

(3) (a) C. J. Hoehanadel and J. A. Ghormley, *J. Chem. Phys.*, **21**, 880 (1953); (b) R. H. Schuler and A. O. Allen, *ibid.*, **24**, 56 (1956).

(4) C. L. Browne, R. P. Craig and N. Davidson, *J. Am. Chem. Soc.*, **73**, 1946 (1951).

(5) N. F. Barr and C. G. King, *ibid.*, **76**, 5565 (1954).

limit of HCl concentration studied because of this precipitate.

Effect of Added Cl^-.—The results of the above experiments would indicate that the anion has an effect upon the reactions occurring. A series of solutions of constant (H^+) with (Cl^-) varied by the addition of NaCl was prepared, all other conditions the same, and $G(-Sn(II))$ determined. Data are given in Fig. 3. At both acid concentrations studied there appears to be a dependence of $G(-Sn(II))$ upon the (Cl^-). The dependence is slight but still appears real.

It is felt that this dependence might be due to changes in the oxidation potential of the solutions as the (Cl^-) is changed. Measurements of the oxidation potential of a series of such solutions is being made to confirm this hypothesis.

Conclusions

Sn(II) forms many different complex ions with Cl^-[6]. Thus there will be changes in the reacting species as the Cl^- is changed, with simultaneous changes in both the oxidation potential and the rates of reaction. Schwarz[7] has found a (Cl^-) effect upon the radiation induced oxidation of ferrous chloride similar to the effect found here for stannous chloride. However, he found initial G-values for the ferrous oxidation to be essentially the same in hydrochloric acid as in sulfuric acid, in contrast to the large difference found in this work with the change in anion.

This reaction can be explained by steps previously proposed for other radiation induced reactions.[8]

$$H_2O \rightsquigarrow H, OH, H_2O_2, H_2 \quad (1)$$

$$Sn^{++} + nCl^- \longrightarrow SnCl_n^{2-n} \quad (2)$$

$$SnCl_n^{2-n} + OH \longrightarrow SnCl_n^{3-n} + OH^- \quad (3)$$

$$SnCl_n^{3-n} + OH \longrightarrow SnCl_n^{4-n} + OH^- \quad (4)$$

$$SnCl_n^{2-n} + H_2O \rightleftharpoons SnCl_{n-1}OH_n^{2-n} + H^+ + Cl^- \quad (5)$$

These reactions explain the effect of both H^+ and Cl^- upon the oxidation. If the rates of reaction between the Sn(II) complex and OH increases with increasing number of Cl^- in the complex the "G"-value might be expected to increase with increasing Cl^-. The effect of H^+ may be explained through its effect on the equilibrium 5.

While the reaction between Sn(II) and H_2O_2 apparently is slow,[1] $2G(Sn(IV))$ should be equal to $G(OH) + 2G(H_2O_2)$ if no other reactions were occurring. The reactions proposed by Boyle, *et al.*,[1] will explain the lower $G(Sn(IV))$ determined. In these reactions Sn^{++} will be used to indicate all possible forms of Sn(II) in solution.

$$Sn^{++} + H \longrightarrow Sn^{+} + H^{+} \quad (6)$$

$$Sn^{+} + OH \longrightarrow Sn^{++} + OH^{-} \quad (7)$$

$$Sn^{+3} + H \longrightarrow Sn^{+2} + H^{+} \quad (8)$$

$$Sn^{+} + Sn^{+3} \longrightarrow 2Sn^{++} \quad (9)$$

In addition to these reactions, similar reactions can be written involving H_2O_2 instead of OH.

We have not included any reactions involving Sn(IV) as a reactant because of the lack of effect of Sn(IV) upon the oxidation.

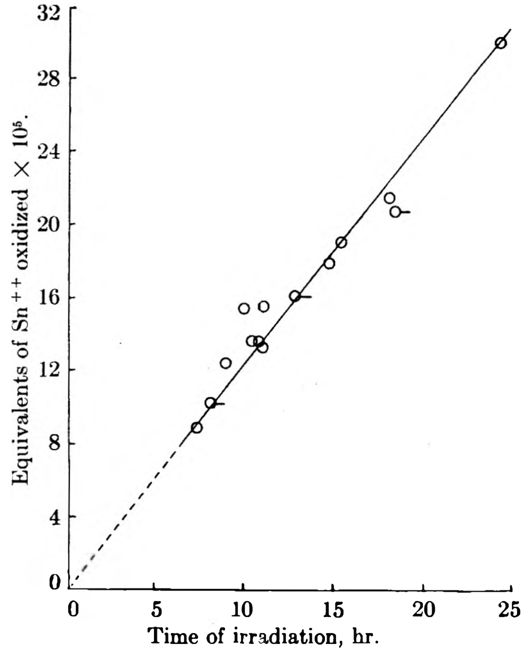

Fig. 1.—Oxidation of Sn(II) as a function of irradiation time: (Sn(II)) = 10^{-2} M; (HCl) = 3 M; ○- (Sn(IV)) = 10^{-2} M; dose rate, 1.4 × 10^{17} e.v./g./min.

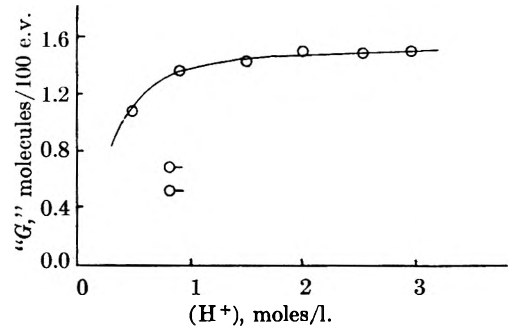

Fig. 2.—Dependence of "G" upon (H^+): ○, (Cl^-) = 3.0 M; ○- (SO_4^{--}) = 0.4 M.

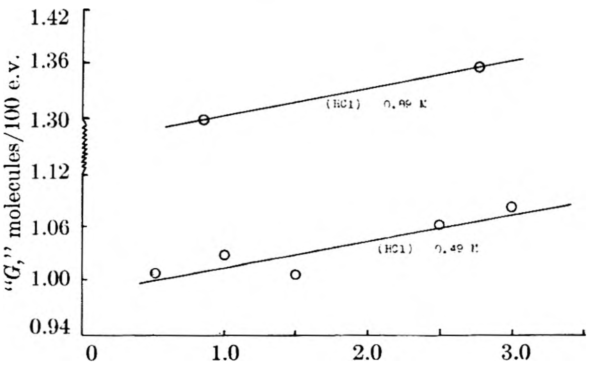

Fig. 3.—Dependence of "G" upon (Cl^-) at constant (HCl).

Acknowledgment.—The cobalt irradiator used in these experiments was purchased under contract AT(30-1)-1911 with the Atomic Energy Commission and the Perkin-Elmer Spectracord 4000 by a grant to the Chemistry Department of the University of New Hampshire from the National Science Foundation. The author expresses his appreciation for both.

---

(6) C. E. Vanderzee and D. E. Rhodes, *ibid.*, **74**, 3552 (1952).

(7) H. A. Schwarz, *ibid.*, **79**, 534 (1957).

(8) (a) F. S. Dainton, *Radiation Research*, Supplement 1, 1 (1959); (b) E. J. Hart, *J. Chem. Educ.*, **34**, 586 (1957).

THE FLASH PHOTOLYSIS OF HALATE AND OTHER IONS IN SOLUTION[1]

By N. K. Bridge and M. S. Matheson

Argonne National Laboratory, Argonne, Illinois

Received March 4, 1960

The photochemistry of aqueous bromate solutions has been examined by the technique of flash photolysis. Two transients were observed and tentatively identified; a short-lived transient (~10 μsec.) absorbing at 350–390 mμ was assigned to $BrO_3\cdot$ radical (disappearance probably first order), and a longer lived transient (~1 msec.) absorbing at 460 mμ to $BrO\cdot$ radical (disappearance second order). Some experimental evidence in support of these assignments is presented. For example the "$BrO\cdot$" transient is observed in BrO^- solutions. The flash photolysis results are correlated with the steady-state photochemical work of Farkas and Klein.

The spectra and photochemistry of simple ions in solution have been investigated in some detail,[2–5] especially since Rabinowitch[6] suggested that illumination of ion pair complexes in their electron transfer absorption bands might lead to photochemical reactivity. Farkas and Klein,[7] using the well established techniques of conventional photochemistry, studied the ultraviolet decomposition of halate (XO_3^-) ions in air saturated aqueous solution and found that the main reaction was the formation of hypohalite (XO^-) and oxygen. Furthermore, the irradiation of the XO^- caused the formation of halide (X^-) and halate ions and the evolution of oxygen. In all these cases it was assumed that the primary process of light absorption was the transfer of an electron to the hydration layer.

For the halate ion, the detailed reactions postulated for neutral solutions are

$$(XO_3^-H_2O) + \text{light} \longrightarrow (XO_3\cdot H_2O\cdot)^-\text{: electron transfer} \quad (1)$$

$$(XO_3\cdot H_2O\cdot)^- \longrightarrow (XO_3^-H_2O)^* \quad (2)$$

This excited complex, because of the known exothermicity of the thermal decomposition of the halates to O_2 and hypohalite, (5 and 10 kcal., for ClO_3^- and BrO_3^-, respectively)[7] is then presumed to decompose as

$$(XO_3^-H_2O)^* \longrightarrow XO^- + O_2 + H_2O \quad (3)$$

This explained the observed relatively high XO^- quantum yield of 0.19 (<260 mμ). In more acid solutions (*p*H 6–8), some hydrogen also was evolved, and this was explained as being due to an increased probability of the photoexcited electron jumping from the solvating water molecule to a neighboring proton, the reactions being

$$(XO_3^-H_2O) + \text{light} \longrightarrow (XO_3\cdot H_2O\cdot)^-$$
$$(XO_3\cdot H_2O\cdot)^- + H^+ \longrightarrow XO_3\cdot + H\cdot + H_2O \quad (4)$$

accompanying reactions giving for bromate the observed Br^-, O_2, BrO^- and H_2. For the hypohalite ion, a similar "self"-decomposition is postulated

$$(XO^-H_2O) + \text{light} \longrightarrow (XO\cdot H_2O\cdot)^- \longrightarrow (XO^-H_2O)^* \quad (5)$$

$$(XO^-H_2O)^* \longrightarrow X^- + H_2O + O \quad (6)$$

the oxygen atoms being responsible for the subsequent formation of bromate. These results were obtained mainly for the BrO_3^- ion, but it was found that chlorate and iodate behaved similarly. However, chlorate, because of its very low ultraviolet absorption, gave a low experimental yield, and iodate, being unstable, liberated iodine which absorbed the active light and once again led to decreased decomposition.

The technique of flash photolysis already has been used with some success to study photochemical processes in solution,[8,9] and in the latter study the intermediate $X_2\cdot^-$ was detected. Consequently, it was considered that the method might prove useful in elucidating some of the processes postulated by Farkas and Klein.[7]

Experimental

The flash photolysis apparatus already has been described,[9] but the reaction vessel was slightly different. This had an additional outer fused silica jacket so that a 1 cm. thickness of liquid filter could be used when necessary to modify the flash wave length; also the two fused silica windows were carefully sealed to the vessel so as to minimize scattered light. For most experiments the photolysis flash was nominally 1520 joules, (37.5 μFd. at 9 Kv.) duration approximately 25 μsec., and useful light absorbed approximately 10^{19} quanta/flash. Most spectra are plotted as ΔR *vs.* wave length: ΔR equals $R_0 - R$ where R_0 is the microdensitometer reading of the photographic plate for the spectroflash exposure through the solution before the photolysis flash, and R is the corresponding reading for the spectroflash exposure through the solution at time t after the photolysis flash. ΔR equals $\gamma(D - D_0)$ where γ refers to the plate γ and D_0 and D are the optical densities of the solution before and at time t after the photolyzing flash. This assumes negligible scattered light from the photolysis flash.

The inorganic chemicals were all of reagent grade either from Matheson Company or Mallinckrodt Chemical Works, while the organic chemicals were the highest quality available from Eastman. All were used without further purification. The water was triply distilled.[10] For flash experiments, solution concentrations usually were chosen to give optimum light absorption and, unless otherwise stated, the solutions were not degassed. Reaction temperature was about 25°.

Results

A. Preliminary Observations.—Before the preliminary observations are considered, the spectra of the various species should be noted—see Fig. 1.[5,6,11]

It was found that a 10^{-1} *M* $KBrO_3$ solution in water gave a strong, short lived (approx. 100 μsec.) transient absorption in the region 300–500

---

[1] Based on work performed under the auspices of the U. S. Atomic Energy Commission.

[2] J. Franck and G. Scheibe, *Z. physik. Chem.*, **A139**, 22 (1929).

[3] A. Farkas and L. Farkas, *Trans. Faraday Soc.*, **34**, 1113 (1938).

[4] K. W. Young and A. J. Allmand, *Can. J. Research*, **27B**, 318 (1949).

[5] M. G. Evans and N. Uri, *Nature*, **164**, 404 (1949).

[6] E. Rabinowitch, *Revs. Modern Phys.*, **14**, 112 (1942).

[7] L. Farkas and F. S. Klein, *J. Chem. Phys.*, **16**, 886 (1948).

[8] N. K. Bridge and G. Porter, *Proc. Roy. Soc.* (*London*), **A244**, 259 (1958).

[9] L. I. Grossweiner and M. S. Matheson, This Journal, **61**, 1089 (1957).

[10] E. J. Hart, *J. Am. Chem. Soc.*, **73**, 68 (1951).

[11] M. Anbar and I. Dostrovsky, *J. Chem. Soc.*, 1105 (1954).

mμ (see Fig. 2a) and a permanent absorption increase with a maximum at 340 mμ (see Fig. 2b). In addition gas was liberated. Similar solutions of KIO_3, $KClO_3$ and KNO_3 gave much weaker, short lived (<90 μsec.) transient absorptions: the first in the region 450–500 mμ, the second at wave lengths below 250 mμ and the KNO_3 transient absorption overlapped the KNO_3 300 mμ peak.

As the $KBrO_3$ concentration decreased from 10^{-1} to 10^{-3} *M* the transient absorption also decreased. $NaBrO_3$ gave the same spectrum as $KBrO_3$. Degassing the $KBrO_3$ solution before flashing had no detectable effect on the transient or on the permanent change.

B. Identification of the $KBrO_3$ Transients and Permanent Change. (I).—The permanent increase in absorption around 340 mμ fits well the known BrO^- absorption (see Fig. 1) and corresponds to approximately 2×10^{-4} *M* BrO^- after 3 flashes. Also, the very strong absorption at lower wave lengths due to the BrO_3^- decreases slightly. However, changes were observed in the solution even at relatively long times after flashing, which were thought possibly to involve an hydrolysis reaction. For this reason, further experiments were carried out in buffered solutions. The buffer usually used was phosphate at a total concentration of 2×10^{-2} *M*. Phosphate buffer at this concentration is known not to interfere appreciably with the normal thermal aqueous reactions,[12] and further this buffer was shown to have no absorption permanent or transient in the region of interest. The dotted curves in Figs. 2a and 2b show the effect of the buffer. Figure 2a also shows that there are in fact *two* transients, one with a double peak in the region 350–390 mμ and a longer lived one with a peak at approximately 460 mμ. Neither of these can be the halogen transient, $Br_2\cdot^-$, previously detected in solution,[9] as this radical has a longer life time and its absorption is narrower and occurs at a different wave length (365 mμ).

It is proposed to explain the behavior of the two transient absorptions in terms of the 350–390 mμ band being due to the $BrO_3\cdot$ [or $(BrO_3 \cdot H_2O\cdot)^-$] radical formed initially as shown in equation 1 and the other at 460 mμ as due to the $BrO\cdot$[or $(BrO \cdot H_2O\cdot)^-$] radical formed subsequently from BrO^- as in equation 5.

(II) Effect of *p*H.—If this postulate is correct, then at low *p*H's "$BrO_3\cdot$" would still be formed but the BrO^- should be reduced (compare equations 3 and 4) so that less $BrO\cdot$ transient would be present, while at high *p*H's relatively more $BrO\cdot$ than $BrO_3\cdot$ should be observed. Figure 2c gives some of the results showing the absorption of solutions at 10 μsec. after the photolysis flash (minimum delay) where it is seen that at low *p*H's, as expected, there is less of the $BrO\cdot$ (460 mμ) absorption. However, if the competition of reactions in (3) and (4) explains this *p*H effect, then the H atoms produced in (4) disappear largely by reaction other than H–H recombination since the quantum yield for H_2 formation in the *p*H range 6–8 is <0.001.[7] Another possible explanation of the *p*H effect is that the BrO^- is converted rapidly to HBrO at low *p*H's and as this species absorbs less light (Fig. 1) it is decomposed less by the photolysis flash. Difficulties were experienced at low *p*H's due to the formation of Br_2 by the thermal decomposition of BrO_3^-. In alkaline solution the permanent change was mainly to BrO^- which disappeared over a period of hours probably by the reaction $3BrO^- \rightarrow BrO_3^- + 2Br^-$ (see ref. 7). In acid, the permanent change was to HBrO which disappeared in

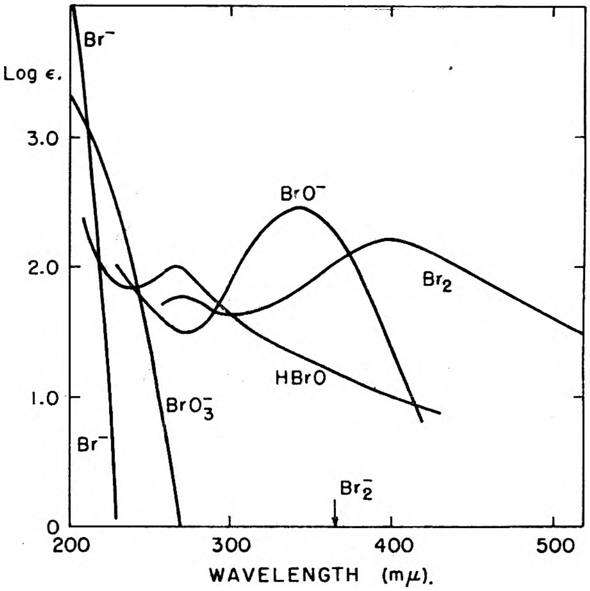

Fig. 1.—Spectra of some bromine species in water (ref. 5, 6 and 11).

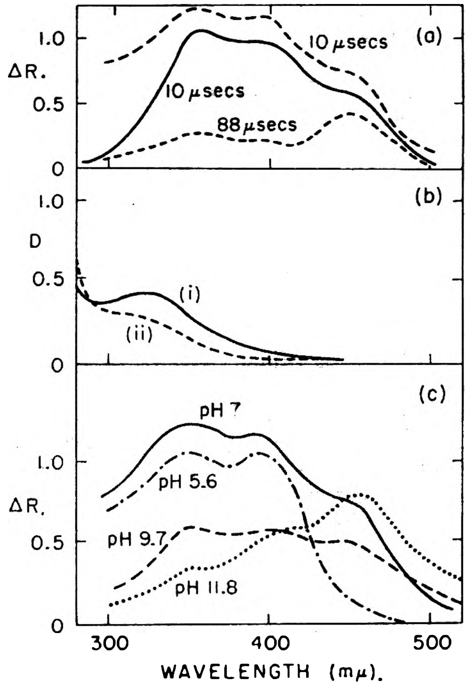

Fig. 2.—Spectra of 10^{-1} *M* $KBrO_3$ solutions after flashing: (a) full line, in water; dashed line, phosphate buffer *p*H 7. (b) (i) Permanent change in water after three flashes (measured in 10 cm. cell in Beckman). (ii) Same in phosphate buffer *p*H 7. (c) 10 μsec. after first flash; *p*H 5.6 and 7, phosphate buffer; *p*H 9.7 and 11.8, carbonate buffer.

---

(12) R. M. Chapin, *J. Am. Chem. Soc.*, **56**, 2211 (1934).

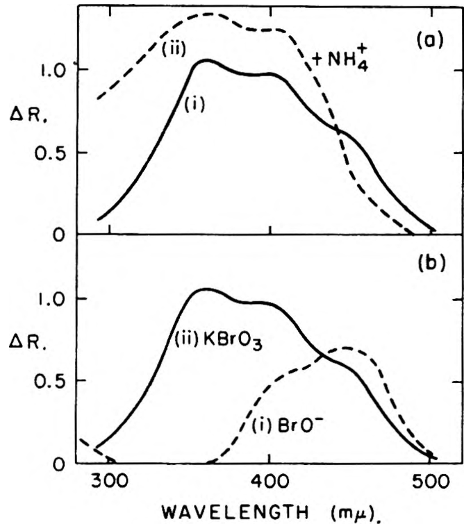

Fig. 3.—Miscellaneous transient spectra: (a) (i) 10^{-1} M KBrO$_3$ in water, transient at 10 μsec. delay. (ii) Same plus 5 × 10^{-2} M $(NH_4)_2SO_4$. (b) Transients at 10 μsec. delay. (i) 5 × 10^{-4} M BrO$^-$ in N KOH; (ii) 10^{-1} M KBrO$_3$ in water.

minutes probably by reactions such as $BrO^- + 2HBrO \rightarrow BrO_3^- + 2H^+ + 2Br^-$ (see ref. 13 and 14).

(III) Effect of Added NH$_4^+$.—Farkas and Klein found that this ion, by reacting with the BrO$^-$ to produce the much less light absorbing Br$^-$ (+N$_2$), enhanced the BrO$_3^-$ photolysis. If this is the case, then there should be relatively less BrO· absorption at 460 mμ in the presence of NH$_4^+$ than in its absence. Figure 3a shows this to be the case, the BrO$_3$· absorption having increased as expected. In addition there was considerably greater permanent change.

(IV) Effect of Flash Wave Length.—If the photolyzing light could be confined to the BrO$_3^-$ region of absorption and not to that of the BrO$^-$ then no BrO· should appear. Several different filter combinations were tried, but it proved impossible to get sufficient intensity into the BrO$_3^-$ band (below 300 mμ) without also allowing appreciable amounts to fall on the BrO$^-$ 340 mμ band (see Fig. 1).

(V) Photolysis of BrO$^-$ Alone.—Photolyzing BrO$^-$ alone proved to be more successful. The BrO$^-$ was prepared[12,13] by the addition of Br$_2$ to ice-cold N KOH and was checked spectrophotometrically. Figure 3b shows that on flashing this solution the BrO$_3$· 390 mμ band is not present at minimum delay leaving only the BrO· absorption with main peak at 450 mμ.

(VI) Effect of Solvent.—Insufficient BrO$_3^-$ would dissolve in glycerol, dioxane or ethanol to give an absorption exceeding that of the absorption of the solvent itself. It is interesting to note that in ethanol a sharp maximum appeared at 215 mμ ($d_{1cm.}$ = 0.3 in saturated solution), which may correspond to the electron transfer peak of BrO$_3^-$ in water shifted to higher wave lengths in the different solvent. Attempts to solubilize the ion in non-aqueous solvents were made using tetramethylammonium and tetra-n-propylammonium[15] ion. Silver bromate, freshly precipitated from a silver nitrate–potassium bromate solution in water, was washed and then added to an aqueous solution of either tetramethyl- or tetra-n-propylammonium hydroxide, and the product was crystallized from ethanol. However the methyl compound still was not sufficiently soluble and the n-propyl compound, though it did dissolve, gave no detectable transient absorptions in ethanol, a very faint one in hexane, and the normal ones in water. This shows clearly the over-riding importance of solvent in this reaction.

(VII) Quantum Yield of BrO$^-$ Production.—It is of interest to see whether the quantum yield for BrO$^-$ formation differs appreciably from the steady illumination value of Farkas and Klein of 0.2. Light output was determined using the ferrioxalate actinometer, (which Hatchard and Parker[16] have shown to give reliable results in this intensity range) first for the whole flash, then for all wave lengths greater than 280 mμ (using Corning Glass Filter 9700), and hence by simple subtraction for wave lengths less than 280 mμ where the BrO$_3^-$ absorbs. The figure obtained was 3.8 × 10^{-6} $Nh\nu$/flash One flash exposure of 10^{-1} M KBrO$_3$ in phosphate buffer, pH 7, gave 1.2 × 10^{-4} M BrO$^-$ as determined after flashing by the use of 10 cm. cells in the Beckman spectrophotometer. If the fraction of light absorbed by the solution is estimated as approximately 0.8 (a figure open to many uncertainties), the quantum yield of BrO$^-$ production is approximately 0.4 in fair agreement with the figure of Farkas and Klein (0.19). This calculation neglects the loss of BrO$^-$ by further photolysis during the flash.

C. Rate Determinations (Flash Spectrophotometry).—When the photomultiplier arrangement was used (see ref. 9), cathode ray oscilloscope deflections were found to be proportional to percentage light transmitted by the reaction cell at various wave lengths from 313 to 546 mμ. Observations were made at 450 mμ for BrO·, and 365 mμ for BrO$_3$·.

(I) 10^{-1} M KBrO$_3$ in Water or Phosphate Buffer.—At 365 mμ, a relatively strong, short lived transient absorption was found (half-life approximately 10 μsec.). This is shown in Fig. 4, the lower trace. At 450 mμ, the weaker transient absorption had a half-life of approximately 1 millisecond. As flashing continued, the latter transient absorption increased and the former decreased as expected, since more BrO$^-$ is formed at the expense of BrO$_3^-$.

(II) 5 × 10^{-4} M BrO$^-$ in N KOH.—Only the longer lived (BrO·) transient was observed but its absorption was stronger than in the above BrO$_3^-$ solution. The concentration observed, of course, cannot be compared directly with the previous

---

(13) M. C. Sneed, J. L. Maynard and R. C. Brasted, "Comprehensive Inorganic Chemistry," Vol. III, D. Van Nostrand Co., Inc., New York, N. Y., 1954, p. 168.

(14) F. Ephraim, "Inorganic Compounds," 4th English Ed. Gurney and Jackson, London, "Oxygen Compounds of the Halogens," 1943, p. 358.

(15) L. F. Fieser and M. Fieser, "Organic Chemistry," 3rd Ed., Reinhold Publ. Corp., New York, N. Y., 1956, p. 228.

(16) C. G. Hatchard and C. A. Parker, *Proc. Roy. Soc.* (*London*), **A235**, 518 (1956).

TABLE I

DECAY CONSTANTS FOR $BrO_3\cdot$ AND $BrO\cdot$

(d_m = maximum optical density)

	KBrO₃ in phosphate buffer, pH 7			KBrO₃ in water			BrO⁻ in N KOH		
	d_m	$k \times 10^{-5}$ sec.$^{-1}$	$t_{1/2}$	d_m	$k \times 10^{-5}$, sec.$^{-1}$	$t_{1/2}$	d_m	k	$t_{1/2}$
$BrO_3\cdot$ (365 mμ)	0.79	1.25	5.2 μsec. (1st order)	0.73	1.17	5.9 μsec. (1st order)	Nil	..	......
$BrO\cdot$ (450 mμ)	0.11	?	1.5 msec. (2nd order?)	0.17	?	1.0 msec. (2nd order?)	0.25	?	0.26 msec. (2nd order?)

results, since this experiment involved "pure" BrO^- to produce on photolysis $BrO\cdot$, whereas in the above BrO_3^- solution only a small amount of BrO^- was being flashed in the presence of presumably a large excess of BrO_3^-.

(III) **Order of Radical Reactions.**—The weaker, longer lived $BrO\cdot$ radical, absorbing at 460 mμ, in most cases followed a second-order decay process rather than a first order (see Fig. 5a). However since the maximum optical density was so low (usually <0.2), too much reliance could not be placed on the determination of the order of the reaction, but the estimated lifetimes (ranging from 0.3–1.5 millisec., see Table I below) are probably in error by only 0.1 millisec.

In the case of the stronger, short lived $BrO_3\cdot$ absorption at 350–390 mμ, the trace of the flash itself (upper curve in Fig. 4) shows that the flash lasts nearly as long as the $BrO_3\cdot$ radical and obviously proper allowance should be made for the nature of the flash intensity distribution with time, in order to obtain the correct rate of decay of the radical. (The middle curve in Fig. 4 shows the small contribution due to scattered light.) If a simple first-order decay is assumed, the $BrO_3\cdot$ variation with time will be given by

$$d(BrO_3\cdot)/dt = I(t) - k(BrO_3\cdot)$$

where $I(t)$ is flash intensity at time t. Integration and rearrangement give

$$\frac{1}{(BrO_3\cdot)}\int_0^t (BrO_3\cdot)dt = \frac{1}{k(BrO_3\cdot)}\int_0^t I(t)dt - \frac{1}{k}$$

Consequently a plot of $(1/D)\int_0^t D\ dt$ against $(1/D)\int_0^t I(t)dt$ (where D = change in optical density of the solution at 365 mμ and this change is attributed to $BrO_3\cdot$ absorption since the permanent change in D is negligibly small) should be linear with intercept $(-1/k)$ on the former axis. Figure 5b shows this to be the case, the very small negative intercept giving a value of $k = 1.17 \times 10^5$ sec.$^{-1}$ and half-life, $t_{1/2} = 6$ μsec. To test the validity of this analysis, two additional computations were made. First, for the longer lived, first-order decay of the triplet state of duroquinone in liquid paraffin[8] for which $t_{1/2}$ is known to be 33.5 μsec. the above method gave a correspondingly larger negative intercept, and the decay constant calculated from this intercept agreed with that determined from that portion of the triplet decay curve beyond the end of the flash. This observation provides good support for the method, but the second check, which concerns the sensitivity of the plot to the order of the reaction was not as satisfactory. It was found that the plot, if the order was assumed to be second and not first was only slightly curved, indicating poor sensitivity to the order of the reaction. It is concluded that the $BrO_3\cdot$ radical probably disappears by a first-order process with half-life of 6 μsec. in water and a rate constant of 1.17×10^5 sec.$^{-1}$.

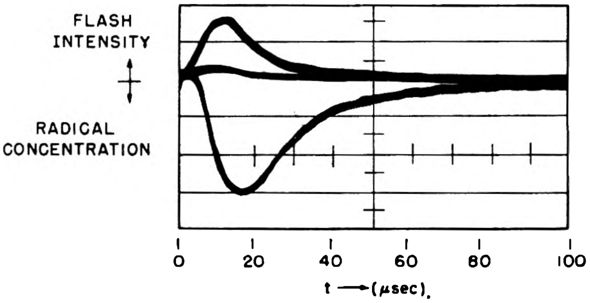

Fig. 4.—Photomultiplier record of BrO_3^- (lower trace) and of the flash (upper trace). (10^{-1} M $KBrO_3$ in water at 365 mμ).

(IV) **Disappearance of BrO_3^- and Buildup of BrO^-.**—Because the transient absorption is considerably greater than that of BrO^- and BrO_3^- and overlaps these other absorptions in the region available for photometric study, it was not possible to detect and correlate quantitatively the disappearance of BrO_3^- and appearance of BrO^- with the buildup and decay of the radicals. However, at 335 mμ, for example (the maximum of BrO^- absorption), a composite curve was obtained corresponding to the build up and decay of the $BrO_3\cdot$ radical superimposed on the buildup of BrO^-. The absorption was approximately constant (and not increasing) beyond approximately 50 μsec., which indicates that the BrO^- is formed in about the same time as the $BrO_3\cdot$ radical forms and decays. In principle it is possible to analyze this curve quantitatively, but because of the low densities and the known sensitivity of such analyses to the precise shape of the curve, this was not attempted.

(V) **Quantum Yield.**—Figures were obtained for the $BrO_3\cdot$ radical yield in terms of its extinction coefficient $\epsilon^{365}_{BrO_3\cdot}$ by noting its maximum optical density (d_m). The light absorbed was determined as before from an estimate of the output per flash below approximately 300 mμ; to this same order of accuracy the value was obtained

$$Q.Y.(BrO_3\cdot) = 2 \times 10^3/\epsilon^{365}_{BrO_3\cdot}\cdot(10^{-1}\ M\ K\ BrO_3 \text{ in phosphate buffer } pH\ 7)$$

$$(\text{Note } \epsilon^{365}_{BrO_3\cdot} > \epsilon^{365}_{BrO^-} = 100)$$

If a Q. Y. of the order of unity is assumed, $\epsilon^{365}_{BrO_3\cdot}$ would be 2×10^3.

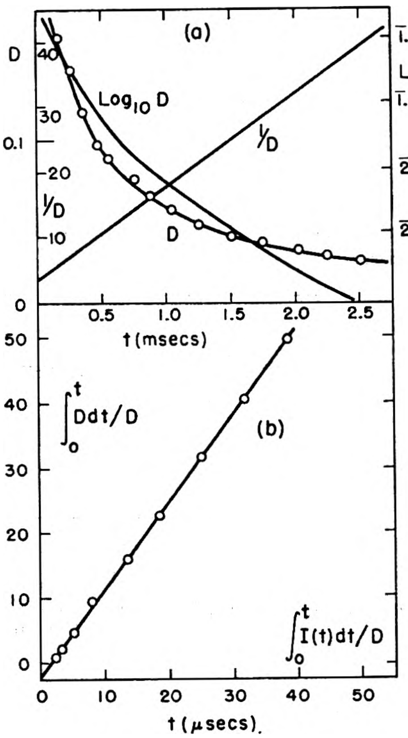

Fig. 5.—Transient decays: (a) second-order decay of $BrO\cdot$ at 460 mμ; (5×10^{-4} *M* BrO^- in *N* KOH). (b) $BrO_3\cdot$ decay plot at 365 mμ; (10^{-1} *M* $KBrO_3$ in phosphate buffer, *p*H 7.) *D* = optical density of solution and is proportional to transient concentration.

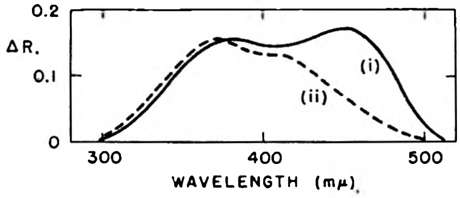

Fig. 6.—Transient spectra in $CH_2BrCOOH$ solutions. (i) 10^{-2} *M* in water, 10 μsec. delay, oxygenated. (ii) Same, degassed.

Discussion

The above results appear to confirm the analysis of the system by Farkas and Klein. It can be seen that if one assumes that the two transients are in fact $BrO_3\cdot$ and $BrO\cdot$ or the corresponding hydrated radicals, a plausible explanation for the observations can be given. However, there are two difficulties which must be discussed and for which some additional work was carried out. This work is reported in the final section. These difficulties concern the so-called $BrO\cdot$ radical which apparently decays *via* a second-order process (with the limitations noted). On the simple scheme of Farkas and Klein a first-order reaction is expected, but since a much greater initial radical concentration is produced in flash experiments, it seems reasonable to find such a bimolecular radical process occurring, presumably to give Br_2 and O_2. (A peak at approximately 400 mμ—the Br_2 solution peak—did appear in all the experiments in which $BrO\cdot$ was detected.) However, a greater difficulty is the position of the $BrO\cdot$ absorption band at 460 mμ.

Zeelenberg[17] recently detected the $BrO\cdot$ radical by flash photolysis of mixtures of the vapors of bromo substituted methanes and oxygen. It absorbed in the region 300–350 mμ in agreement with work of Ramsey[18] and had a half-life of approximately 0.5.–1 millisec. Lipscomb, Norrish and Porter[19] have studied the $ClO\cdot$ radical in detail in the gas phase. It absorbs from 260–300 mμ and has a half-life of a few milliseconds, disappearing *via* a bimolecular process similar to that postulated above for $BrO\cdot$ in solution (however in the case of $ClO\cdot$, Cl_2O_2 is probably an intermediate). Hence, though the general behavior of this so-called $BrO\cdot$ radical is in accord with previous observations, its absorption spectrum in solution does not agree with that in the gas phase, being shifted to the red by approximately 100–150 mμ—an unusually large shift.

It was in an attempt to resolve this difficulty that the following further experiments were carried out.

Additional Observations

Zeelenberg argued that the $BrO\cdot$ radical is difficult to form from Br_2 and O_2 directly, because the weakness of the Br–O· bond makes the process energetically unlikely. In his method, more is formed because a radical such as $CCl_3O{-}O\cdot$ produced by the photolysis of, *e.g.*, CCl_3Br plus O_2, probably has a much weaker RO–O· bond and so the $Br\cdot$ atoms can pull off an O atom with much greater probability. For this reason, bromoacetic and dibromoacetic acids and dibromoethane all of which are soluble in water were flashed, in the hope that the $BrO\cdot$ absorption in solution could be detected in the presence of oxygen.

(I) **Bromoacetic Acid in Water. (Absorbs below 260 mμ).**—Figure 6 shows the transient absorptions obtained 10 μsec. after flashing oxygenated or degassed aqueous solutions of bromoacetic acid. The oxygenated solution was prepared by bubbling oxygen through the water for 40 minutes before adding the acid. The peak at 450 mμ is seen to disappear when the oxygen is removed as would be expected if this peak is due to $BrO\cdot$. The peak at 370–410 mμ does not change, consequently it is unlikely to be the $\cdot OOCH_2COOH$ radical. If $\cdot CH_2COOH$ reacts somewhat slowly and therefore only partially with O_2, then the 370–410 mμ band possibly could be due to $\cdot CH_2COOH$. Alternatively, it could be due to the $Br_2\cdot^-$ ion which absorbs in this region[9] (365 mμ uncorrected), although it is not easy to explain $Br\cdot^-$ formation here unless there was an appreciable concentration of Br^- ions before flashing. Further, the band envelope is not identical with that given for $Br_2\cdot^-$ in ref. 9.

(II) **Dibromoacetic Acid in Water.**—This compound gave the same species as bromoacetic acid but in smaller amounts.

(III) **1,2-Dibromoethane (Absorbs below 240 mμ).**—1,2-Dibromoethane in water when flashed gave a strong peak at 370 mμ with lifetime > 100

---

(17) A. P. Zeelenberg, *Nature*, **181**, 42 (1958).

(18) D. A. Ramsay, *Ann. N. Y. Acad. Sci.*, **67**, 485 (1957), and unpublished work.

(19) F. J. Lipscomb, R. G. W. Norrish and G. Porter, *Nature*, **174**, 785 (1954) and earlier papers.

μsec. There was little permanent change and oxygen increased this change by approximately 15%. In hexane (not degassed) with a similar concentration of approximately 10^{-2} M a very intense transient was obtained at entirely different wave lengths, that is continuous absorption was found below 300 mμ. There was also a large permanent change, probably to HBr and Br_2. Since Br^- was produced in the aqueous experiments by flashing (as checked by precipitation of AgBr), it seems very probable that the transient in water with absorption at 370 mμ is $Br_2\cdot^-$ (see ref. 9). As regards the transient in hexane, perhaps this is the same as that produced on flashing Br_2 itself in hexane (see below).

(IV) **CCl_3Br (Absorbs below 300 mμ).**—CCl_3Br was the most effective substance used by Zeelenberg.[17] In oxygenated hexane and CCl_4 no transient absorption could be detected with this compound.

(V) **NaClO.**—It was thought that ClO^- might produce a transient spectrum analogous to that obtained from BrO^-. However, despite its high photochemical reactivity,[4] and the use of concentrations of it varying from 10^{-2} to 10^{-5} M both in water and 0.1 N sodium hydroxide, ClO^- showed only a permanent disappearance at 300 mμ and a slight transient decrease at higher wave lengths.

(VI) Further experiments were done with solutions of the halogens in water, acid, CCl_4 and hexane both oxygenated and degassed. No absorption attributable to BrO· was detected but some very interesting observations were made which are reported elsewhere.[20]

(VII) **Conclusions.**—Apart from the 450 mμ absorption detected in oxygenated bromoacetic and dibromoacetic acids, no further confirmatory evidence could be found for the assignment of this band to the BrO· radical. In view of this, despite the fact that the transient behaves in all respects as expected, it is considered that further evidence should be sought before a final assignment can be made.

One of us (N.K.B.) is indebted to the British Rayon Research Association, Manchester, England for leave of absence. We are also indebted to Mr. W. A. Mulac for technical assistance.

(20) N. K. Bridge, *J. Chem. Phys.*, **32**, 945 (1960).

THE HEAT OF ADSORPTION OF ARGON AND KRYPTON ON MOLYBDENUM DISULFIDE—SEPARATION OF ENTHALPIES INTO RATIONAL COMPONENTS

BY PETER CANNON

General Electric Research Laboratory, Schenectady, N. Y.

Received March 16, 1960

The molar integral heats of adsorption of two rare gases on oxide-free MoS_2 are presented as functions of coverage. The data are analyzed in terms of both sorbate–solid and sorbate-sorbate interactions. The values of each separate interaction are calculable from the fundamental physical properties of the components of the system. The calculation of the dispersion forces for the gas–solid pair is most successful using London's form for the dispersion constant. The data cover the ranges $4 \times 10^{-7} < p/p_0 < 2 \times 10^{-3}$(Ar) and $4 \times 10^{-4} < p/p_0 < 4 \times 10^{-1}$(Kr). The argon film exhibits a gas–liquid transition and the krypton film shows a maximum self interaction energy equal to one half the heat of liquefaction.

Introduction

When we consider the changes in state of a monatomic film of an adsorbate on a uniform substrate with various degrees of coverage, it is apparent that the anticipated behavior should be equivalent (in two dimensions) to that of a regular bulk fluid compressed isothermally from very small to quite high densities. In addition, if the temperature of the experiment is appropriate, phase transitions analogous to those which would occur in the bulk should appear. Such interpretations have been applied in a phenomenological manner to the behavior of films of insoluble long chain polar molecules on the surface of water[1] and various aqueous systems, and have been invoked to rationalize the behavior of adsorbed films on, *e.g.*, graphite.[2] In the former case, objections recently have been advanced[3] to the concept of actual phase changes involving discontinuous changes in molecular coarea. Only a few quantitative treatments of the behavior of adsorbed films have been attempted, and here the emphasis has perhaps been on forecasting the pressures at which two dimensional condensation will occur, and accounting for these values in terms of mutual interaction potentials between the atoms of gas and the solid.[4] The evaluation and use of total equations of state for adfilms has not received a great deal of attention, perhaps due to the fact that the van der Waals equation

$$pv = kT\left(1 + \frac{\beta}{v}\right)$$

has a considerable range of applicability and the virial coefficient β becomes rapidly more intractable as we attempt to use more than a very simple picture of the molecular events occurring in the system.

It is therefore of considerable interest to attempt the interpretation of energies of adsorption in terms of the degree of coverage, the adsorbent–adsorbate interaction, the adsorbate–adsorbate

---

(1) I. Langmuir, *Coll. Symp. Monog.*, **3**, 48 (1925).

(2) G. Jura and D. Criddle, THIS JOURNAL, **55**, 163 (1951).

(3) R. Aranow and L. Witten, *J. Chem. Phys.*, **28**, 405 (1958).

(4) B. B. Fisher and W. G. McMillan, *ibid.*, **28**, 562 (1958).

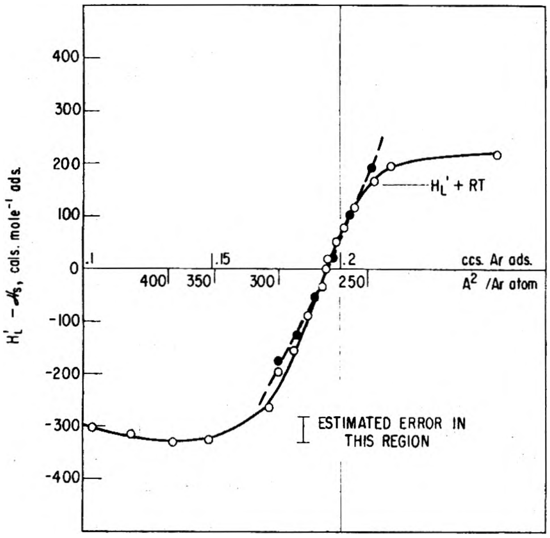

Fig. 1.—The molar integral heat of adsorption of argon on MoS_2 in the co-area range 460–180Å.^{2}/Ar: open circles, experimental points; closed circles, points calculated for the compression of two dimensional argon gas from a co-area of 310 Å.^{2}, according to a 6:12 force law; $\bar{T}$ = 83.8°K.

interactions and the temperature of the experiment, thus: $\Delta H_s = f(\theta, \epsilon_\perp, \epsilon_\parallel, T)$. The major experimental problem is to find systems in which the variables can be separated, and this has been achieved partially by working with graphite,[5a] metal films[5b] and by using preadsorbed layers of various materials.[5c] The importance of $\epsilon_\parallel$, which in the above cases is frequently small compared with $\epsilon_\perp$, lies in its significance to the theory of the liquid state: adsorption experiments have been recognized for some time[6] to be one of the few available approaches to the assessment of such self-interaction potentials. A complete description of adsorption energies in the above terms would be cognate with the theory of regular solutions as expounded by Hildebrand, and would be valuable for direct comparison of various systems in terms of a given set of parameters. The question of whether these parameters could in turn be assessed from first principles is a vexed one: such a development is unlikely in view of the fact that it would constitute a solution to a many-bodied problem involving dissimilar species. But the situation is not as gloomy as this might suggest. Provided the adsorption involves no electron transfer, and the energy associated with it is comparable with the heat of liquefaction of the bulk adsorbate (*i.e.*, "physical" adsorption), it should be possible to assess from fundamental considerations the energy of a film of say a monatomic sorbate on a solid which could be treated as a semi-infinite continuum. These restrictions limit the experimentally available systems primarily to inert gases on single crystal metals and on highly anisotropic solids. In the latter case, the solids of choice should be covalently bound, since Gaines[7] has demonstrated the marked effect of ionic substitution on the mica basal plane upon the adsorption of the inert gases. Thus, graphite has been of interest in this respect, but a molecular crystal might be expected to be even better behaved.

In the present work, an account[8] already has been given of the behavior of the adsorption of inert gases on molybdenum disulfide, in which a phenomenonological comparison with similar results on graphite was made. A number of striking similarities were evident. In this paper, therefore, I propose to examine the data presented earlier to see whether it is possible to separate the enthalpies calculated from the isotherm data into parts cognate with the parallel and perpendicular force fields in the adfilm, as functions of coverage and, if possible, to account for them from first principles, within the above restrictions.

Results

Molar integral enthalpies of adsorption were computed from the isotherm data using the procedures described by Hill, Emmett and Joyner.[9] Plots of these quantities as functions of coverage are shown on Figs. 1 and 3. In the evaluation of the spreading pressure plots for argon, it was found that the curves for spreading pressure *vs.* log relative pressure crossed, showing a reversal in sign of enthalpy with respect to a three dimensional liquid standard state. For the purposes of choice of limits for theoretical computation it was then necessary to determine whether this change was associated with a change of phase in the adfilm: therefore, a plot of film compressibility *vs.* log gas pressure was prepared,[10] and it is shown on Fig. 2. It shows clear evidence of a discontinuous change in the adfilm compressibility, with a deviation from ideal behavior commencing at the position corresponding to the crossing of the ϕ-plots (spreading pressure, $\phi = KkT\int_0^{p/p_0} v \, d\ln p/p_0 = KT\cdot(\partial/\partial s)\log F(T)$ where $F(T)$ is the grand partition function of the adfilm and the other symbols are as defined by Hill, Emmett and Joyner[9]). The deviation becomes large very rapidly with increasing pressure, up to a pressure of 251 μ, where the compressibility of the film finally drops to a very low value.

Molar quantities are used throughout, since this type of quantity is interpreted easily, and most of statistical thermodynamic reasoning is recorded in this form.

The conditions under which the surface was prepared were such that oxide contamination is unlikely.[11] Heats based on the results obtained from 350° outgassed, oxide-contaminated samples were calculated and found to be not very different from those from the 950° material suggesting perhaps that oxide contamination has not too important an influence on physisorption in the systems Ar–MoS_2 and Kr–MoS_2. The heat plots yield

---

(5) (a) J. G. Aston and Q. Stottlemeyer, Symposium Proc., "The Chemistry of Solid Surfaces," Duke Univ., March, 1958, pp. 11-14; (b) G. D. Halsey, Jr., and J. H. Singleton, *Can. J. Chem.*, **33**, 184 (1954); (c) P. Cannon, THIS JOURNAL, **63**, 1292 (1959).

(6) J. E. Lennard-Jones and A. F. Devonshire, *Proc. Roy. Soc.* (*London*), **163A**, 53 (1937).

(7) G. L. Gaines, Jr., THIS JOURNAL, **62**, 1526 (1958).

(8) P. Cannon, *ibid.*, **64**, 858 (1960).

(9) T. L. Hill, P. H. Emmett and L. G. Joyner, *J. Am. Chem. Soc.*, **73**, 5102 (1951).

(10) S. J. Gregg and F. P. Maggs, *Trans. Faraday Soc.*, **44**, 123 (1948).

(11) P. Cannon, *Nature*, **183**, 1612 (1959).

values of 2000 cal./mole for the Kr–MoS_2 interaction at $\theta = 0$, and 1370 cal./mole for the Ar–MoS_2 interaction at the coverage corresponding with a gas-like Ar film. These are near enough to the heats of vaporization in each case that we should be able to synthesize a calculated heat of adsorption from this quantity and the self-interaction enthalpies of the adfilms, by direct addition. A problem which occurs in such analyses is whether they are of any real meaning, since the technique of calculation demands not only the necessary condition of a flat heat plot, implying surface homogeneity, but certain sufficient conditions also. The shape of the heat plot in itself is not sufficient to establish the homogeneity of the surface and the validity of the calculation, since one can easily imagine various site populations of different energies giving compensating effects and consequent flat isosteric heat plots and linear molar heat plots. A condition which is sufficient, however, is that one should be able to follow an enthalpy change at low coverages corresponding to the compression of a gas-like film, and its collapse into liquid-like regions. This process should commence at the area per molecule corresponding with the normal cross section of the gas at the same temperature, follow the well-known laws for total energy of a fluid under compression, and, when this energy exceeds by approximately kT the value at which another phase is stable, one should observe the collapse of the film and the phase transition. Let us examine the results for evidence of processes of this kind.

Theoretical Considerations and Discussion of Results

London[12] derived an expression for the interaction energy, φ_D, between a single gas atom and a semi-infinite solid, based on pure dispersion forces without permanent dipole formation

$$\varphi_D = -\frac{N\pi C}{6r^3}$$

where N is the number of substrate atoms/cc., r is the perpendicular distance between the mass center of the sorbate atom and the uppermost plane of mass centers of the substrate, and C is the so-called dispersion constant, In the absence of a single characteristic energy, $h\nu_0$, by which to represent the gas and solid atoms in C, London[13] used the fair approximation $h\nu_0$ equal to ionization potential. Thus the expression for φ_D becomes

$$\varphi_D = -\frac{N\pi}{4} \times \frac{\alpha\alpha'}{r^3} \times \frac{JJ'}{J + J'}$$

where α, α' are the polarizabilities of the gas and the solid and J, J' are the respective ionization potentials. The numerical values for interaction energies given by this approximation are generally lower than those found using other popular formulas for C.[14] Using this approximation, the values calculated for MoS_2 are Ar/MoS_2, $\varphi_D < 1350$ cal./mole, K/MoS_2, $\varphi_D < 2000$ cal./mole. The quoted values are the upper estimates due to the use of an $r^2 \ln r$ denominator in place of r^3, as suggested by Prosen and Sachs[16] for substrates containing conduction electrons. By comparison of the crystal structure of MoS_2 and graphite, it was considered that the minimum separation for Ar of Kr and MoS_2 was 4 Å. (Barrer[17] chose 3.7 Å. as the equilibrium separation distance for Ar on graphite.) The values of α' and J' for MoS_2 were estimated by direct experiment: α' is not very different from the value for graphite, but J' is rather larger, being made up of 1.76 e.v. (valence-conduction gap)[18] and about 6 e.v. (conduction-first vacuum state).[19] The calculated values agree well with those observed at the lowest coverages.

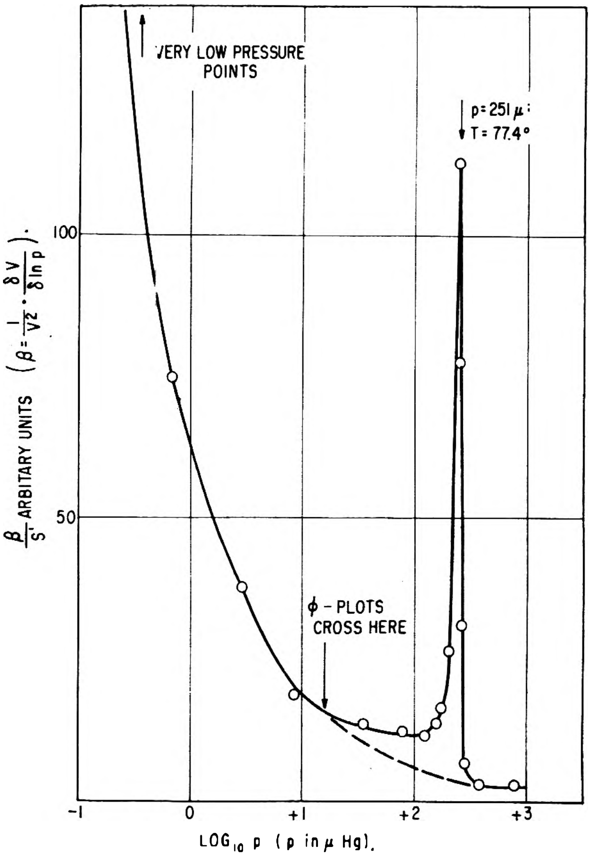

Fig. 2.—Compressibility of the argon film *vs.* log pressure, showing departure from ideality and lambda-point transition; $T = 77.4$°K.

Having evaluated the gas–solid interaction energies, the heat content of the film must be added to this quantity as the coverage increases. For a monatomic gas-like adsorbate, this self enthalpy will increase from zero at zero coverage linearly to the enthalpy of the gas at a coverage corresponding

---

(12) F. London, *Z. physik. Chem.*, **B11**, 222 (1930).

(13) F. London, *Trans. Faraday Soc.*, **33**, 8 (1937).

(14) R. A. Pierotti and G. D. Halsey, Jr., THIS JOURNAL, **63**, 680 (1959), give a table showing numerical values for several systems involving conducting substrates using seven different modes of computation. The London calculation gives the lowest results in all but a few cases, where the Margenau-Pollard[15] formulas, involving free, non-ideally polarizable electrons, gives lower values because of the negative polarizability included in their analysis. It perhaps should be mentioned that MoS_2 is indeed a semiconductor and hence may be considered as having free electrons.

(15) H. Margenau and W. G. Pollard, *Phys. Rev.*, **60**, 128 (1941).

(16) E. J. Prosen and R. G. Sachs, cited in Brunauer "Physical Adsorption," Princeton Press, Princeton, N. J., 1940, p. 214.

(17) R. M. Barrer, *Proc. Roy. Soc.* (*London*), **161A**, 476 (1937).

(18) P. Cannon, presented to the 1960 Graphite Conference of the Société de Chimie Physique, Paris.

(19) H. Phillip, private communication.

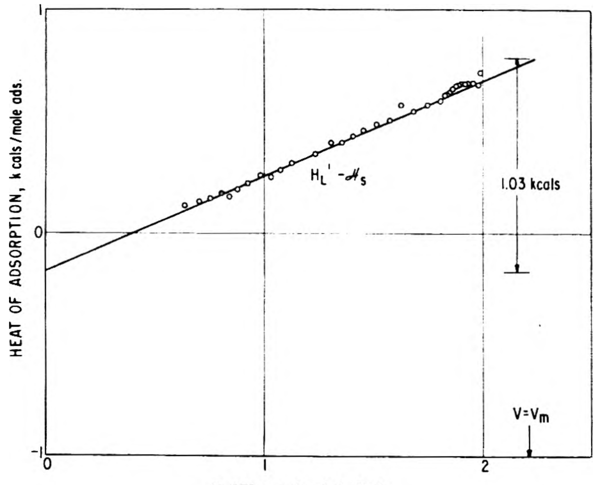

Fig. 3.—The molar integral heat of Kr on MoS_2: open circles, experimental points; solid lines, best fit and extrapolation to $v = 0$ and $v = v_m$ $(\theta = 1)$; $T = 83.8$°K.

to the film density equal the bulk gas density, at the experimental temperature (for Ar, this corresponds to a co-area of approximately 410 Å.^{2} per Ar atom at 83°K., based on extrapolated p–v data). Thereafter, the increase in film enthalpy (assuming there are no substantial entropy changes) will be approximated by an equation of the type derived by Devonshire[20] for dense fluids, employing a 6:12 force law, *viz.*

$$\Delta H_{ads} \sim F_{ads} = -kT\left(k_1 + k_2\left\{1.06\left(\frac{r_0}{r}\right)^6 - 0.5\left(\frac{r_0}{r}\right)^{12}\right\}\right)$$

In the present work, the constant k_1 was taken as the gas–solid interaction energy per mole at the coverage corresponding to a co-area of 410 Å.^{2}, that is (H_s exp. $- H_g$ calcd.). This quantity was experimentally indistinguishable from that found at co-areas down to 310 A.^{2}/Ar. The constant k_2 was taken as $H_g$calcd. $= 5/2RT$, the enthalpy of ideal gas at T°K. r_0/r was evaluated from the co-area per atom, which in turn was based on a BET surface area determination using the value 19.5 A.^{2} for the co-area of Kr at $v = v_m$. The result of this calculation is shown as a dashed line in Fig. 1, starting from the co-area value 310 A.^{2}/Ar. When ΔH_{ads} calculated in this way exceeds ΔH^V, the normal heat of liquefaction of the sorbate, by RT cal./mole, a transition to a liquid-like film would be expected, and indeed the calculated and observed values agree well until this value is reached. The subsequent enthalpy of the Ar film is that expected for self-interactions in liquid Ar at any particular degree of coverage, although the observed coverage range is really too small to be certain of this, compared with the krypton case. The coverage at which the deviation between the calculated and observed enthalpy curves begins to be appreciable corresponds with the transition seen in the compressibility plot, implying again that the film is collapsing at this point. The choice of 310 Å.^{2}/Ar as a starting point for the enthalpy calculation is somewhat arbitrary, but may be defended on the basis that it corresponds with the last value of enthalpy after the minimum which is not significantly different from the minimum in terms of experimental error (±25 cal./mole). In other words, the starting point used in Fig. 1 is statistically the same as the minimum. It happens to be a convenient basis for graphical purposes.

Self-interaction in the Kr Film.—In a sense, the two gases give a continuous set of data for the energetics of a rare gas–MoS_2 system from $4 \times 10^{-7} < p/p_0 < 0.002$(Ar) through $0.0004 < p/p_0 < 0.4$ (Kr), and hence a description of the total process over the equivalent coverage range. The data for the first 20% of coverage with Kr yield spreading pressure curves that can be extrapolated linearly to the origin. Since this coverage range corresponds with the experimentally difficult partial pressure range below 4×10^{-4}, it is not possible to compare these results directly with the argon data. However, it is customary to regard the analytic integration under the straight line as a satisfactory approximation to reality.[9]

Examining the higher coverage data from the krypton experiments (Fig. 3), the molar integral heat of adsorption is found to follow a linear, rising plot with respect to amount adsorbed in the range $0.2 < \theta < 0.9$. Attempts to extend these observations to higher coverage results in apparent multilayer formation at relative pressures of approximately 0.4. However, the linearity of the plot over the fairly large range described is encouraging, and we proceed to extrapolate this line to determine the total change in enthalpy in the system from $\theta = 0$ to $\theta = 1$. The value of this change is -1.03 kcal./mole of Kr adsorbed. The position of this line (starting from a value slightly negative with respect to the enthalpy of bulk liquid krypton) suggests that the increase in enthalpy is due to self-interaction forces between adsorbate particles, and that under the influence of the substrate wall the krypton atom ensemble has been restrained into an array of potential energy higher than that which ordinarily would be reached by the bulk liquid (in equilibrium with krypton vapor of pressure such as was present in this experiment). It seems likely that this array is one of monatomically thick, densely packed Kr atoms, thus: the amount of energy required to remove one Kr atom from its (approximately) twelve nearest neighbors in bulk liquid Kr, is $\Delta H^v/N$ where ΔH^v is the molar latent heat of vaporization and N the Avogadro number. ΔH^v for Kr is 2.15 kcal./mole,[21] and we would expect the corresponding number in a monatomic liquid layer to be approximately half this, since in a monofilm each atom may be thought of as having six nearest neighbors. The agreement on this model between that calculated (1.08 kcal.) and that found (1.03 kcal.) is excellent.

General Discussion.—It seems to be possible to separate the sorbate–solid and sorbate–sorbate dispersion energies in these systems, and to ac-

---

(20) A. F. Devonshire, *Proc. Roy. Soc.* (*London*), **163A**, 137 (1937).

(21) NBS Circular 500, "Selected Values of Chemical Thermodynamic Properties," Washington, D. C. 1952, p. 545.

count for their magnitudes in a realistic way. The systems involved are unusual in that the fundamental sorbate–solid interactions are small, and comparable with the heats of liquefaction of the gases involved. This being the case, it is reasonable to expect that the linear analysis of enthalpies employed in this work would be unusually successful, even more so than in the case of graphite, where the gas–solid interactions tend to be higher. Having arrived at these conclusions, it would seem possible to be able to calculate the enthalpy-coverage plots, and hence the isotherms, for a number of similar systems, provided some weighting factor can be introduced for topographical heterogeneities and that the gas–solid dispersion constant is accessible.

Acknowledgments.—I wish to thank Miss A. D. Warner for assistance with the calculations, and Dr. A. M. Bueche for critical comments on several occasions during this work.

THE CHEMISTRY OF THE SOLVATED METAL CHELATES. III. THE BIS-(ACETYLACETONATO)-URANIUM(VI) SOLVATES[1]

By Wesley W. Wendlandt, John L. Bear and G. Robert Horton

Department of Chemistry, Texas Technological College, Lubbock, Texas

Received March 19, 1960

The bis-(acetylacetonato)-uranium(VI) solvates with water, *n*-propyl alcohol, *n*-butyl alcohol, ethyl alcohol, acetone, acetophenone, acetylacetone, dioxane, ammonia and pyridine were studied by calorimetric and thermogravimetric methods and by differential thermal analysis (DTA). The heats of solvation, ΔH_4, for the reaction (where AA is acetylacetone) $UO_2(AA)_2(s) + \text{solvate}(l) = UO_2(AA)_2\cdot\text{solvate}(s)$ were found to be from −3.22 to −20.7 kcal. mole^{-1}. All of the complexes with oxygen-containing solvate molecules were much less stable thermally than those containing nitrogen. In the case of the former, the desolvation was generally a one-step process, followed by the decomposition of the anhydrous complex. With the latter, total disruption of the anhydrous complex immediately followed the desolvation reaction. The DTA thermograms showed that in many of the desolvation reactions, two or more endothermic energy changes took place.

Introduction

Bis-(acetylacetonato)-uranium(VI) readily forms solvates with compounds such as water, ammonia, acetylacetone, pyridine, the alcohols, acetone and others.[2,3] In an effort to elucidate the structure of these solvates, particularly in reference to the coördination number of uranium(VI), Sacconi and co-workers[4–6] and Comyns and co-workers[7] studied the complexes by ultraviolet and infrared spectroscopy, magnetic susceptibility and conductivity measurements. It was concluded that the O–U–O group in the complex was coördinatively unsaturated and that the solvate molecules were attached directly by U–O or U–N bonds, giving uranium a coördination number greater than six.

In an effort to elucidate further the nature of the interaction between the solvate molecule and the metal complexes, the solvated complexes were prepared and subjected to thermal decomposition on the thermobalance and by differential thermal analysis (DTA). Further information on this interaction was obtained by measuring the heats of solvation using an indirect calorimetric procedure.

Experimental

Reagents.—The uranium(VI) nitrate 6-hydrate was obtained from Merck and Co., Rahway, N.J. The acetylacetone was obtained from Eastman Organic Chemicals, Rochester, N. Y. It was distilled just prior to use; the fraction used had a boiling point of 133–135°. All other chemicals used were of C.P. quality.

Preparation of Solvated Complexes.—The bis-(acetylacetonato)-uranium(VI) and its solvates were prepared as previously described.[6,7] The compounds were analyzed by ignition to U_3O_8 in porcelain crucibles at 800°. The metal oxide contents were within 0.5% of that required by theory.

Calorimeter.—The calorimeter used has been previously described.[8]

The finely powdered complexes or the liquid solvate compounds were allowed to react with 250 ml. of 11.7 *N* hydrochloric acid contained in the Dewar calorimeter flask. Duplicate and in some cases triplicate runs were made on each compound.

Thermobalance.—The automatic recording thermobalance and its modification previously have been described.[9,10]

Sample sizes ranged in weight from 50 to 90 mg. and were run in duplicate or triplicate. The furnace heating rate was linear with time at 6.6° per min. A slow stream of air was permitted to flow through the furnace during the pyrolyses.

DTA Apparatus.—The DTA apparatus has been described previously.[11] The platinum–platinum–10% rhodium alloy thermocouples were replaced by thermocouples made of chromel and alumel alloys to achieve greater sensitivity. Samples ranged in weight from 0.10 to 0.18 g. and were run in duplicate or triplicate. The furnace heating rate was 6.5° per min. with a recorder chart speed of 6 in. per hr.

Experimental Results

Heat of Solvation Studies.—The heats of solvation were calculated indirectly by measuring the heats of solution of the anhydrous bis-(acetylacetonato)-uranium(VI) complex, the solvated metal complex, and the solvate compound in 11.7 *N* hydrochloric acid at 25.0°. These heats of solution reactions can be illustrated by the example of $UO_2(C_5H_7O_2)_2\cdot H_2O$; it is assumed that the complexes are completely dissociated in the acid.

---

[1] Presented at the 15th Southwest Regional Meeting of the American Chemical Society, Baton Rouge, Louisiana, December 3–5, 1959.

[2] W. Biltz and J. A. Clinch, *Z. anorg. allgem. Chem.*, **40**, 221 (1904).

[3] K. Hager, *ibid.*, **162**, 85 (1927).

[4] L. Sacconi and G. Giannoni, *J. Chem. Soc.*, 2368 (1954).

[5] L. Sacconi and G. Giannoni, *ibid.*, 2751 (1954).

[6] L. Sacconi, G. Caroti and P. Paoletti, *ibid.*, 4257 (1958).

[7] A. E. Comyns, B. M. Gatehouse and E. Wait, *ibid.*, 4655 (1958).

[8] J. H. Van Tassel and W. W. Wendlandt, *J. Am. Chem. Soc.*, **81**, 813 (1959); (b) **82**, 4821 (1960).

[9] W. W. Wendlandt, *Anal. Chem.*, **30**, 56 (1958).

[10] W. W. Wendlandt, *ibid.*, **32**, 848 (1960)

[11] W. W. Wendlandt, *J. Chem. Educ.*, **37**, 94 (1960).

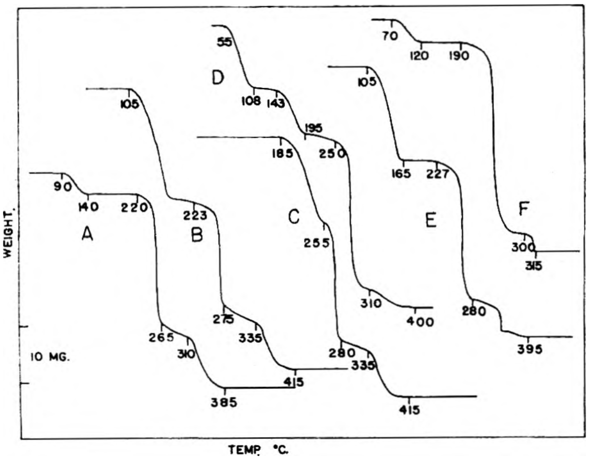

Fig. 1.—Thermogravimetric curves for the bis-(acetylacetonato)-uranium(VI) solvates: A, $UO_2(AA)_2$·water; B, $UO_2(AA)_2$·acetophenone; C, $UO_2(AA)_2$·pyridine; D, $UO_2(AA)_2$·1.25-dioxane; E, $UO_2(AA)_2$·acetylacetone; F, $UO_2(AA)_2$·n-butyl alcohol.

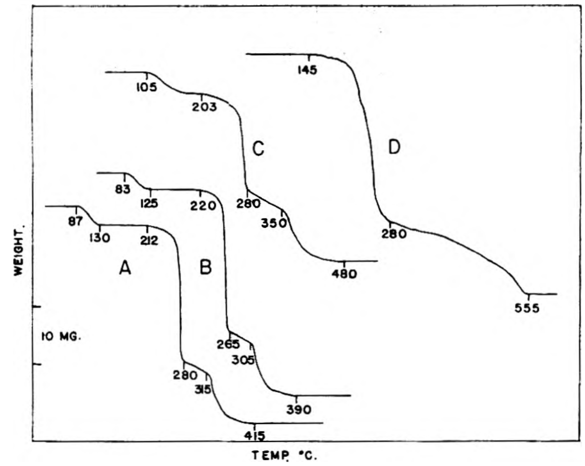

Fig. 2.—Thermogravimetric curves for the bis-(acetylacetonato)-uranium(VI) solvates: A, $UO_2(AA)_2$·n-propyl alcohol; B, $UO_2(AA)_2$·acetone; C, $UO_2(AA)_2$·ethyl alcohol; D, $UO_2(AA)_2$·ammonia.

$$UO_2(C_5H_7O_2)_2(s) + 2H^+(aq) + 2Cl^-(aq) = UO_2^{++}(aq) + 2C_5H_8O_2(aq) + 2Cl^-(aq) \qquad \Delta H_1 \quad (1)$$

$$UO_2(C_5H_7O_2)_2 \cdot H_2O(s) + 2H^+(aq) + 2Cl^-(aq) = UO_2^{++}(aq) + 2C_5H_8O_2(aq) + H_2O(aq) + 2Cl^-(aq) \qquad \Delta H_2 \quad (2)$$

$$H_2O(l) = H_2O(aq) \qquad \Delta H_3 \quad (3)$$

The heat of solvation, ΔH_4, is represented by

$$UO_2(C_5H_7O_2)_2(s) + H_2O(l) = UO_2(C_5H_7O_2)_2 \cdot H_2O(s) \qquad \Delta H_4 \quad (4)$$

and is equal to

$$\Delta H_4 = \Delta H_1 + \Delta H_3 - \Delta H_2$$

The heats of solution of all of the compounds studied are given in Table I; the average heats of solvation are given in Table II. Since the heats of solution values were independent of sample size, they were considered to be equal to the values at infinite dilution.

The interaction between water and the alcohols with bis-(acetylacetonato)-uranium(VI) had the smallest heat of solvation, followed by the ketones and then the ether type compounds. This increase in the heats of solvation is in accord with the increased electron donor ability of the oxygen in the solvate molecule. Since nitrogen has a greater electron donor ability than oxygen, it is to be expected that the heats of solvation would be greater than those found for solvate molecules containing oxygen atoms. This was indeed found to be the case.

From ultraviolet and infrared spectroscopy data, it was found that the solvated uranium complexes contained U–O and U–N bonds.[5,6] If the heats of solvation can be construed as the "binding en-

TABLE I

HEATS OF SOLUTION OF THE BIS-(ACETYLACETONATO)-URANIUM(VI) COMPLEXES IN 11.7 N HYDROCHLORIC ACID AT 25.0°

Compounds	Sample wt., g.	ΔH, kcal. mole^{-1}	Av. $-\Delta H$, kcal. mole^{-1}
$UO_2(AA)_2$·water(s)	1.2922	2.31	2.40
	0.9095	2.50	
$UO_2(AA)_2$·ammonia(s)	0.4477	4.74	4.64
	1.0044	4.54	
$UO_2(AA)_2$·pyridine(s)	0.3847	10.20	10.36
	0.4744	10.53	
$UO_2(AA)_2$·acetophenone(s)	1.3799	0.89	0.80
	1.1946	.71	
$UO_2(AA)_2$·acetylacetone(s)	0.9343	.01	0.00
	1.1065	.00	
$UO_2(AA)_2$·acetone(s)	1.0422	3.38	3.37
	0.9945	3.36	
$UO_2(AA)_2$·1.25-dioxane(s)	.5352	0.87	0.90
	.3458	0.93	
$UO_2(AA)_2$·n-butyl alcohol(s)	.7378	2.35	2.35
	.5663	2.36	
$UO_2(AA)_2$·n-propyl alcohol(s)	.4239	2.49	2.57
	.5150	2.64	
$UO_2(AA)_2$·ethyl alcohol(s)	.9380	2.49	2.46
	1.0100	2.44	
$UO_2(AA)_2$(s)	1.4177	4.72	4.66
	0.9865	4.61	
Water(l)	.4204	0.95	0.96
	.2433	0.97	
Pyridine(l)	.0946	14.33	14.36
	.1552	14.39	
Acetylacetone(l)	.6114	2.07	2.09
	.6015	2.11	
Acetophenone(l)	.9046	0.73	0.75
	.8045	0.76	
Acetone(l)	.5618	3.10	3.20
		3.30	
Dioxane(l)	.3485	3.76	3.60
	.2929	3.43	
n-Propyl alcohol(l)	.6882	1.49	1.42
	.6094	1.35	
n-Butyl alcohol(l)	.9976	1.33	1.27
	.6490	1.20	
Ammonia(g)			20.70[a]
Ethyl alcohol(l)	.2748	1.70	1.79
	.4893	1.88	

[a] Calculated from selected values taken from the National Bureau of Standards, Circular 500, 1952.

TABLE II

HEATS OF SOLVATION OF THE BIS-(ACETYLACETONATO)-URANIUM(VI) COMPLEX AT 25.0°

Solvate molecule	Av. $-\Delta H$, kcal. mole^{-1}
Water	3.22
n-Propyl alcohol	3.51
n-Butyl alcohol	3.58
Ethyl alcohol	3.99
Acetone	4.49
Acetophenone	4.61
Acetylacetone	6.75
Dioxane	7.36[a]
Pyridine	8.66
Ammonia	20.7

[a] For $UO_2(AA)_2 \cdot 1.25$ dioxane.

ergy" of the solvate molecule, it would follow that the U–N bonding is stronger than U–O bond.

Thermal Stability Studies.—The thermobalance pyrolysis curves are given in Figs. 1 and 2.

In all of the solvated complexes except the dioxane complex, the solvate molecule was evolved by a one-step process. With dioxane, however, a two-step decomposition curve was observed. The dioxane complex is also somewhat different from the others in that the ratio of dioxane to anhydrous chelate was 1.25 to 1, rather than 1:1. The mechanism of the two step desolvation reaction for the dioxane solvate is not known since the composition of the curve at 108° did not correspond to a stoichiometric compound.

In the complexes where the solvate molecule contained an oxygen atom, the solvate molecule began to come off in the 83 to 107° temperature range. This was followed by the decomposition of the anhydrous complex in the 190 to 227° temperature range. The thermal stability of the solvated complexes, listed in order of decreasing stability, is: dioxane < n-butyl alcohol < acetone < n-propyl alcohol < water < acetylacetone = acetophenone < ethyl alcohol.

For complexes with solvate molecules containing nitrogen atoms, the minimum decomposition temperatures were much higher. In fact, because of this higher decomposition temperature, the decomposition of the anhydrous complex was rather obscured, indicating perhaps that the solvate molecule cannot be removed without destruction of the entire complex. A break in the curve was observed in the pyridine complex at 225° which could be due to the decomposition of the anhydrous complex; however, it was not present in the ammonia complex.

The DTA thermal decomposition curves are given in Figs. 3 and 4. Two peaks generally were observed in the DTA curves: one corresponding to the evolution of the solvate molecule, the other for the decomposition of the anhydrous complex. However, in several cases, two peaks were observed for the loss of the solvate molecule. This occurred with the acetone and the n-butyl alcohol solvates, with curve shoulders being present on the water and n-propyl alcohol solvates. The dioxane solvated complex gave, as was expected, two well defined peaks for the loss of the dioxane. A rather complex set of peaks was obtained for the acetophenone solvate. If the 190° peak is due to the desolvation of the original complex, then the others must be due to the decomposition of the anhydrous complex or some intermediate compounds formed by the loss of part of the acetophenone.

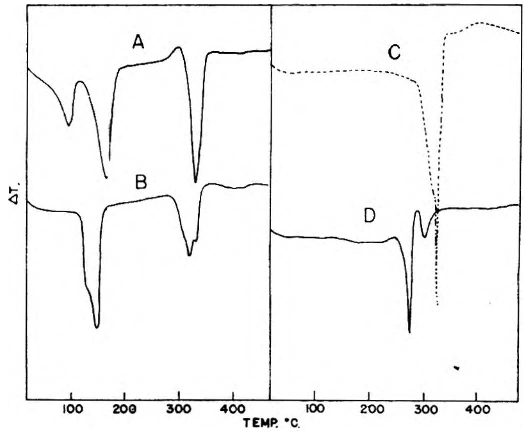

Fig. 3.—DTA curves for the bis-(acetylacetonato)-uranium(VI) solvates: A, $UO_2(AA)_2 \cdot$acetone; B, $UO_2(AA)_2 \cdot n$-propyl alcohol; C, $UO_2(AA)_2 \cdot$pyridine; D, $UO_2(AA)_2 \cdot$ammonia.

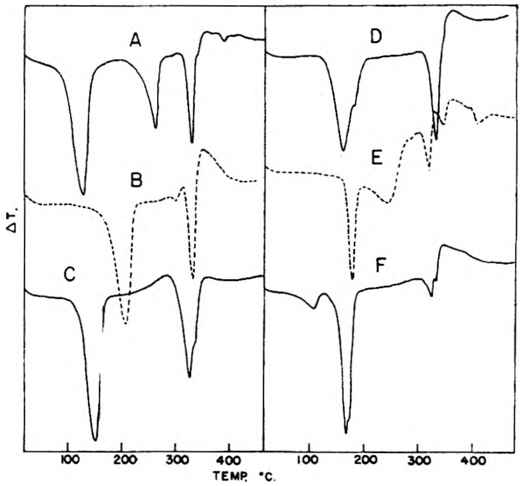

Fig. 4.—DTA curves for the bis-(acetylacetonato)-uranium(VI) solvates: A, $UO_2(AA)_2 \cdot 1.25$-dioxane; B, $UO_2(AA)_2 \cdot$acetylacetone; C, $UO_2(AA)_2 \cdot$ethyl alcohol; D, $UO_2(AA)_2 \cdot$water; E, $UO_2(AA)_2 \cdot$acetophenone; F, $UO_2(AA)_2 \cdot n$-butyl alcohol.

The pyridine and the ammonia solvates gave very sharp decomposition peaks which, in the case of the latter, was followed by a second, smaller peak. From the curve for the pyridine solvate, it is evident that the complex decomposes in one step; the ammonia solvate is similar although an explanation for the second peak is not known. From the qualitative shape of the DTA curves, it can be concluded that the sharp peaks of the pyridine and ammonia solvates indicates a lower order of reaction or a higher activation energy for the thermal decomposition than for those solvates containing oxygen in the solvate molecule.[12]

Acknowledgment.—The helpful assistance of Dr. James H. Van Tassel is gratefully acknowledged.

---

(12) Y. Tsuzuki and K. Nagasawa, *Nendokagaku no Shimpo*, **1**, 144 (1959).

WETTING PROPERTIES OF TETRAFLUOROETHYLENE AND HEXAFLUOROPROPYLENE COPOLYMERS[1]

BY MARIANNE K. BERNETT AND W. A. ZISMAN

U. S. Naval Research Laboratory, Washington 25, D. C.

Received March 25, 1960

It has been shown that the determining factors in the wetting of low-energy solid surfaces are the nature of the atoms in the surface and their physical packing. Of all solid organic polymers polytetrafluoroethylene is known to have the lowest surface energy and thus the lowest critical surface tension of wetting (γ_c). In this study the wettability of a series of copolymers of tetrafluoroethylene with hexafluoropropylene by a variety of organic and inorganic liquids was examined; the results show that these solid plastics have critical surface tensions which are even lower than that of solid polytetrafluoroethylene. As anticipated, the progressive increase in the proportion of perfluoromethyl side chains in the polymer introduces a higher concentration of exposed $-CF_3$ groups in the surface which in turn progressively reduces γ_c. By extrapolation γ_c of a polyhexafluoropropylene has been calculated to give the value of 15 dynes/cm.

Introduction

A series of investigations[2-8] on the effect of constitution on the spreading of liquids on solids has formulated the factors determining the wetting of low-energy solid smooth surfaces or of high-energy surfaces modified by adsorbed films. It was demonstrated that wettability is a function of the nature and physical packing of the atoms in the surface, and that it is essentially independent of the nature and arrangement of the underlying atoms and molecules.

Polytetrafluoroethylene (poly TFE) has the lowest surface energy of all polymeric solids studied to date. Thus, its critical surface tension of wetting (γ_c) of 18.5 dynes/cm.[2] is characteristic of a surface consisting essentially of close-packed perfluoromethylene $-CF_2-$ groups. The surface of lowest energy encountered to date is that of smooth glass or platinum coated with an oriented close-packed monolayer of perfluorododecanoic acid[7]; therefore, its value of γ_c, 6–8 dynes/cm., characterizes the resulting properties of a surface of close-packed perfluoromethyl $-CF_3$ groups. Perfluoroalkanoic acids of lower molecular weight, when adsorbed on high-energy surfaces, do not pack quite as closely due to the lesser contribution of the intermolecular cohesive forces; a close-packed monolayer of perfluorobutyric acid, for instance, has a γ_c of 9.2 dynes/cm.

This investigation reports on the wettability of the solid copolymers prepared from tetrafluoroethylene and hexafluoropropylene. It was undertaken to observe the effect on wetting of the progressive replacement of $-CF_2-$ by $-CF_3$ groups in the surface of the bulk polymer.

Materials and Experimental Procedures

The polymers used were molded experimental samples of fluorocarbon resins in the form of sheets 1/16 inch thick which were furnished through the coöperation of the Polychemicals Department of the du Pont Co. The materials are copolymers of tetrafluoroethylene (TFE) and hexafluoropropylene (HFP) containing HFP in the following concentrations: 6, 8, 11.5, 14, 16 and 23 mole %. This general group of polymers is known as the FEP (fluorinated ethylene propylene) resins. The specimen containing 23% HFP is a low molecular weight wax, which represents the highest concentration of hexafluoropropylene that could then be furnished.[9] The surfaces of these specimens were smooth and specular, and selected areas were sufficiently flat to be used for the wettability studies without further preparation, other than cleaning with concentrated aqueous solutions of the commercial detergent Tide.[5]

All liquids used were highly purified compounds described elsewhere[2,4] and each was percolated just before use through columns of appropriate adsorbents to remove polar impurities. The advancing contact angle (θ) of each of these liquids was measured on a number of glossy areas of each specimen of the copolymer using the drop buildup method[10] and an improved goniometer telescope.[2] Variation of θ was never more than ±2° from the mean; frequently the maximum deviation was ±1°. All data were observed at 25 ± 1° and 50 ± 2% R. H.

Experimental Results and Discussion

The wetting curves obtained for each solid copolymer by plotting cos θ of each liquid *n*-alkane against the liquid surface tension γ_{LV} are shown in Fig. 1. For purposes of comparison, the wetting behavior of clean smooth polytetrafluoroethylene[2] also is given. It can be seen that the data for each solid surface conform to the now well-established rectilinear relationship between cos θ and γ_{LV}. As anticipated, the values of γ_c obtained by the intercepts of the curves with the line $\cos \theta = 1$ become smaller as perfluoromethylene groups in each surface are replaced by perfluoromethyl groups. An exception is provided by the copolymer containing 6% HFP which exhibits a value of γ_c higher than that of the homopolymer. Contact angles of all compounds are consistently lower on this surface than on pure poly TFE; this anomalous behavior in the family of copolymers may be an indication of either decomposition or contamination of the surface, giving rise to a higher-energy surface than poly TFE. Although the individual increments in γ_c from resin to resin are rather small, the regularity of the results with all but one member of the series of copolymers makes it evident that the value of γ_c of the 23% HFP–TFE copolymer is nearly 1 dyne/cm. lower than that of poly TFE.

If the respective γ_c for each surface is plotted against the per cent. substitution of hexafluoropropylene a straight line results, as shown in Fig. 2.

---

(1) Presented before the Division of Colloid Chemistry, American Chemical Society, at the 137th National Meeting in Cleveland, Ohio, April 11–14, 1960.

(2) H. W. Fox and W. A. Zisman, *J. Colloid Sci.*, **5**, 514 (1950).

(3) H. W. Fox and W. A. Zisman, *ibid.*, **7**, 109 (1952).

(4) H. W. Fox and W. A. Zisman, *ibid.*, **7**, 428 (1952).

(5) M. K. Bernett and W. A. Zisman, THIS JOURNAL, **63**, 1241 (1959).

(6) M. K. Bernett and W. A. Zisman, *ibid.*, **63**, 1911 (1959).

(7) E. F. Hare, E. G. Shafrin and W. A. Zisman, *ibid.*, **58**, 236 (1954).

(8) E. G. Shafrin and W. A. Zisman, *ibid.*, **64**, 519 (1960).

(9) C. A. Sperati, private communication.

(10) E. G. Shafrin and W. A. Zisman, *J. Colloid Sci.*, **7**, 166 (1952).

By extrapolation an estimated value of γ_c of 15.6 dynes/cm. is obtained for a hypothetical 100% HFP polymer.

Values of γ_c for each copolymer can be calculated from the surface constitution by assuming that the critical surface tensions, like the surface free energies, are additive quantities and may thus be computed to a first approximation. For this purpose the previously established values of 18.5 dynes/cm. for close-packed $-CF_2-$ groups[2] and of 8 dynes/cm. for close-packed $-CF_3$ groups[7] were used. Assuming that the copolymerization results in a regular repetitive molecular arrangement of the monomers along the principal chain of each molecule and that this same arrangement occurs in the free surface of the solid, an 8% HFP-TFE copolymer would contain one perfluoromethyl group per 24 perfluoromethylene groups. Applying the above values of γ_c to weight the additive contribution of each $-CF_2-$ and $-CF_3$ group, a theoretical value of 18.1 dynes/cm. is obtained for that particular copolymer surface. Employing these same additive assumptions, calculated values for the surfaces of all the copolymers available as well as for the 100% HFP polymer were obtained, and the results are shown in the lower rectilinear plot of Fig. 2. This results in a theoretical value of 13.3 dynes/cm. for the hypothetical 100% HFP polymer.

A linear 100% HFP polymer never has been reported. However, Stuart Briegleb molecular ball models of these copolymers have been constructed and have indicated that chains may consist of no more than three hexafluoropropylene monomers on account of accumulated steric hindrances resulting from the large diameter of the perfluoromethyl group. Whereas a ball model of the 50% copolymer could be made readily, the 75% HFP-TFE copolymer was difficult to assemble because it was nearly a rigid structure.

In Fig. 3 are shown graphs of cos θ *vs.* γ_{LV} for the wetting of a variety of organic and inorganic liquids on the copolymer containing 23% HFP. The intercept with cos $\theta = 1$ results in a critical surface tension of 17.5 dynes/cm., in good agreement with the value of 17.8 dynes/cm. obtained for the *n*-alkane liquids (Fig. 1). The concavity of the lower portion of the curve in Fig. 3 illustrates the increase in wetting arising from weak hydrogen-bonding of such hydrogen-donating liquids as water, glycol and formamide with fluorine-containing surfaces.[11] Contact angles of these same miscellaneous liquids on the other HFE-TFE copolymers resulted in similar cos θ *vs.* γ_{LV} curves for each surface with slight progressive displacements to the right as would be predicted from consideration of the HFP mole % substitution.

If the contact angles exhibited by any one liquid on the various copolymer surfaces are plotted against the HFP content, a linear relationship is obtained as shown in Fig. 4. Thus the contact angle of hexadecane becomes larger for each progressive perfluoromethyl side chain substitution; *i.e.*, it is smallest for 0% substitution (poly TFE) and increases in small increments to its largest value when the HFP content reaches its highest percentage. In Fig. 4 are plotted the wettability results obtained with some of these liquids. In almost every instance straight lines were obtained (with somewhat different slopes) demonstrating clearly the decreasing wettability with increase in HFP content. It will be noted that the contact angles of water, in contrast to those of all other liquids, do not increase with increasing HFP substitution, but remain essentially of equal magnitude throughout. The same results with water were obtained by Allan and Roberts[12] in their recent study of the hydrophobic behavior of some perfluorocarbon polymer films. They also used the hydrophobic contact angle as a measure of the roughness of films prepared in various ways from "Teflon" TFE resins and the new du Pont FEP resin. The latter

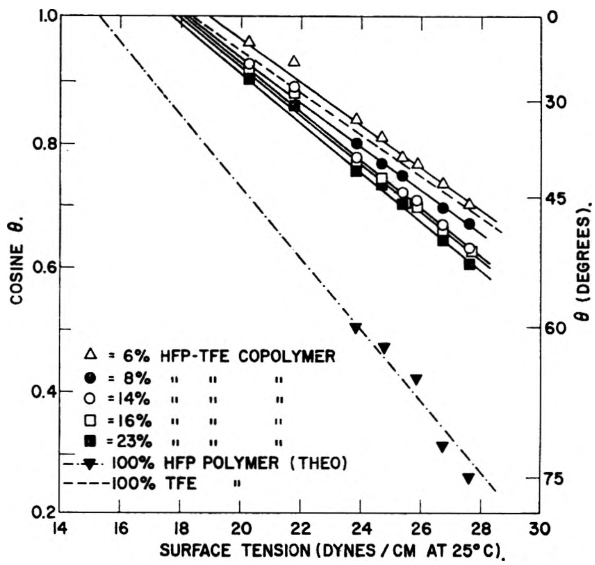

Fig. 1.—Wettability of various HFP-TFE copolymers by *n*-alkanes.

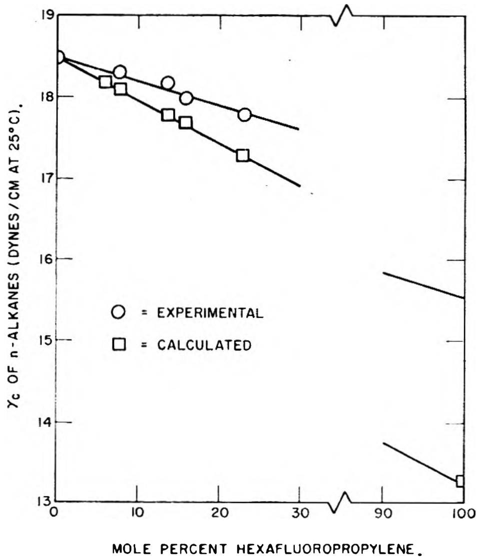

Fig. 2.—Decrease in critical surface tensions of HFP-TFE copolymers with increasing HFP substitution.

---

[11] A. H. Ellison, H. W. Fox and W. A. Zisman, THIS JOURNAL, **57**, 622 (1953).

[12] A. G. J. Allan and R. Roberts, *J. Polymer Sci.*, **39**, 1 (1959).

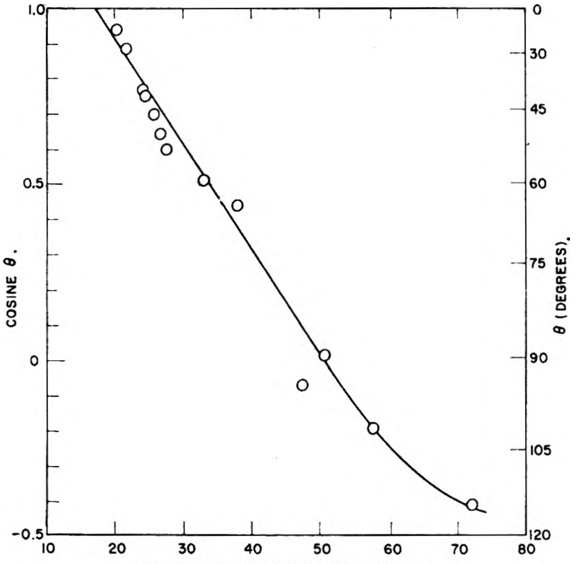

Fig. 3.—Wettability by miscellaneous liquids on a HFP-TFE copolymer containing 23 mole % of HFP.

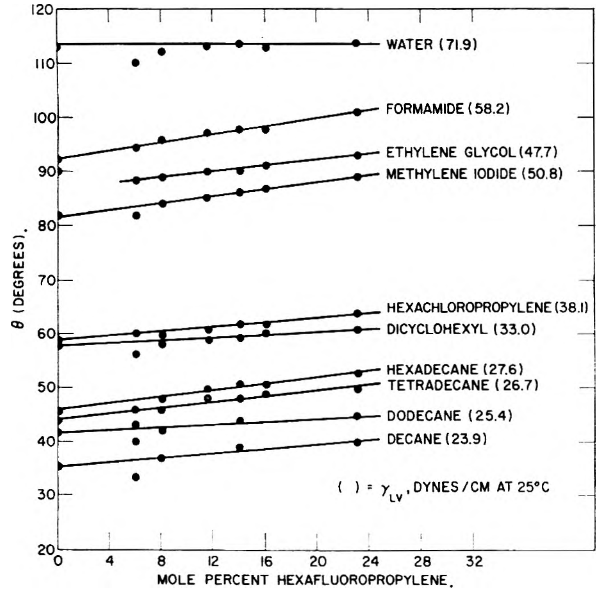

Fig. 4.—Effect of HFP content on the wetting of HFP-TFE copolymers by miscellaneous liquids

resin had been identified earlier as Teflon 100X.[13] They found large differences in the contact angle of water with changes in the surface roughness, but no appreciable difference between smooth surfaces of TFE or of FEP resins. The results obtained with water in the present study corroborate and extend the latter conclusion. However, it also shows that the wetting of the copolymers by liquids of lower surface tension than water does vary appreciably with differences in the chemical constitution of the copolymers. The physico-chemical properties of water are, in many respects, unique. It has a high surface tension, a weak tendency to form hydrogen-bonds with fluorinated surfaces, high permanent dipole moment, and small dimensions; it thus does not exemplify the wetting behavior of most liquids.

Contact angles for the *n*-alkanes on a 100% HFP polymer were estimated by extrapolation of θ *vs.* 0% HFP curves, such as in Fig. 4. By plotting the cosines of these values against the γ_{LV} of the liquids, the wetting curve for a hypothetical 100% HFP polymer can be constructed, along with the attendant value of γ_c. Such a curve is plotted as a dash-dot line on Fig. 1. The critical surface tension in this case is 15.4 dynes/cm., in very good agreement with the value of 15.6 dynes/cm. obtained previously by other means.

Ellison and Zisman in their investigation of halogenated organic solid surfaces,[14] found that a plot of cos θ of various liquids *versus* the atom per cent. fluorine substitution from 0 to 100 in the solid surface will produce curves of several distinct types; these types are determined by the hydrogen-bonding ability of the respective liquid to the underlying surface. Strongly hydrogen-bonding liquids, such as water, glycerol or formamide, present a large curvature, whereas non-polar liquids such as the *n*-alkanes form straight-line graphs. The present study shows rectilinear relationships between cos θ and HFP content for all liquids employed. However, the maximum content is only 23%, and the largest change in θ is only 9°. These limited changes in the magnitudes of the variables produce straight-line plots; however, extrapolation to obtain the respective cosines of the contact angles for a 100% HFP polymer may be only a fair approximation in view of the results of the previous study by Ellison and Zisman.[14]

The value of about 15.5 dynes/cm. for the critical surface tension of wetting for a hypothetical 100% polyhexafluoropropylene polymer was obtained by two methods based on experimental results. The value of 13.3 dynes/cm. was derived by additive relations of the atom groups believed to occupy the surface. The latter value is predicated on a number of assumptions, such as repetitive molecular arrangement, linear chain formation and regular arrangement in the free surface of the solid; because of the steric hindrance of the bulky perfluoromethyl groups and of its increased influence at high molal proportions of the HFP monomer, one or more of these assumptions may not be valid. It is believed, therefore, that the value of 15.5 dynes/cm. for γ_c would be more nearly correct for a 100% polyhexafluoropropylene polymer. The total shift in γ_c from a surface comprised of $-CF_2-$ groups to one comprised of a mixture of $-CF_3$ and $-CF_2-$ groups is at best only 3 or 4 dynes/cm. It therefore can be concluded that no copolymer can be produced from the family of FEP copolymers whose solid smooth surface is as non-wetting as that of a close-packed monolayer of perfluoromethyl groups.

---

(13) R. S. Mallouk and W. B. Thompson, *SPE Journal*, **14**, 42 (1958).

(14) A. H. Ellison and W. A. Zisman, THIS JOURNAL, **58**, 260 (1954).

ASSOCIATION EQUILIBRIA AND COMPOUND FORMATION IN THE PHOSPHORUS TRICHLORIDE–TRIMETHYLAMINE SYSTEM

By Robert R. Holmes

Department of Chemistry, Carnegie Institute of Technology, Schenley Park, Pittsburgh, Pa.

Received March 28, 1960

Examination of the binary system phosphorus trichloride–trimethylamine at −46.5° showed the formation of the solid, $Cl_3P \cdot N(CH_3)_3$. Interpretation of pressure composition data shows that it has an existence in the liquid state and is, hence, not a simple lattice compound. In solution a dissociation equilibrium is established and an interaction energy of 6.4 kcal./mole calculated. In the vapor the complex loses its existence. The heat of dissociation of the solid to the gaseous components was found to be 22.4 kcal./mole. P^{31} magnetic resonance measurements made on the liquid phase support the phase diagram interpretations. The presence of a phosphorus–nitrogen linkage is indicated.

Introduction

Examination of known complexes of trihalides of Group Vb reveals that arsenic, antimony and bismuth trihalides form complexes with donor molecules, whereas phosphorus trihalides do not. For example, donor molecules such as ethers and aldehydes form 1:1 complexes with antimony trihalides,[1] compounds of the type, $C_6H_5NH^+AsX_4^-$, are known with arsenic halides[2] and compounds of the general formula, $R_3N \cdot BiCl_3$, are formed between amines and bismuth trichloride.[1] In view of the above if such a complex involving a phosphorus trihalide molecule is possible, it might be anticipated that the resultant stability would be low. With this in mind a detailed investigation of the interaction of phosphorus trichloride with a typical basic molecule which would show no tendency for side reactions and possess volatility sufficient for convenience in a complete examination of the system using vacuum techniques was undertaken. Trimethylamine was chosen to fulfill these requirements.

Results

Addition of $(CH_3)_3N$ to PCl_3 at −78° where both components are liquid resulted in the formation of a white solid which was easily sublimable and was observed to liquefy on warming to 0°. To establish its composition the system was examined more thoroughly at −46.5°.

The PCl_3–$(CH_3)_3N$ System at −46.5°.—The data for the pressure–composition diagram are shown in Table I and plotted in Fig. 1. The data are represented as pressure of the system *versus* mole fraction of amine, the latter applying to the condensed phase.

The first addition of amine, corresponding to a mole fraction of 0.189, caused the appearance of a solid phase and a resultant drop in the vapor pressure of pure liquid PCl_3 from 2.0 to 1.2 mm. The pressure remained constant on further additions of amine up to a mole fraction of 0.5, the latter plateau corresponding to the vapor pressure of a saturated solution of the solid in liquid PCl_3 (VLC curve). The sharp rise in pressure at 0.5 mole fraction serves to indicate the existence of a 1:1 complex between the components. Further additions of amine caused solution of the complex and the appearance of a second plateau at 54.5 mm., the vapor pressure of the saturated solution of complex in $(CH_3)_3N$ (CLV curve). Solution was complete at a mole fraction of 0.81. One sees that dilution of the solution between the mole fractions of 0.87 to 1.0 gives a linear relationship which closely follows Raoult's law (the dotted line). The light line (V) represents the vapor line and will be discussed after presentation of Table II.

TABLE I

THE PHOSPHORUS TRICHLORIDE–TRIMETHYLAMINE SYSTEM AT −46.5°

Mole fraction[a] $(CH_3)_3N$	Press., mm.	Mole fraction[a] $(CH_3)_3N$	Press., mm.
0	2.0	0.819	57.2
0.189	1.2	.844	61.4
.288	1.3	.869	64.2
.467	1.3	.884	65.6
.499	6.2	.897	66.3
.514	52.8	.910	67.3
.656	54.7	.919	67.8
.710	54.5	.930	68.7
.735	54.5	.938	69.4
.780	54.5	.944	70.5

[a] In this experiment 0.493 mmole of PCl_3 was used.

The Sublimation of Solid $Cl_3P \cdot N(CH_3)_3$.—To obtain the sublimation pressures of $Cl_3P \cdot N(CH_3)_3$ as a function of temperature, the following experimental procedure was employed: The compound was formed at low temperatures using a slight excess of amine and warmed to −46.5°, where small amounts of amine were removed until a pressure minimum was reached. The system had a very small vapor volume (35.8 cc.) to minimize any change in composition in the condensed phase. For example, for the sample size used (2.87 mmoles), if it could be sublimed entirely into the gaseous phase without dissociation to the components a pressure of about 2000 mm. would be exerted. The data reported in Table II show a pressure variation from 0.9 mm. at −46.5° to 8.6 mm. at −21.0°. To ensure pressure independence of the relative amount of vapor, the determination was repeated using a sample size of 1.42 mmoles and a vapor volume of 45.8 ml. The results were the same as those obtained with the smaller vapor volume. Also a small amount of the vapor was removed from the system at the highest temperature, −21.0°, in the two experiments (the measurements being made starting at −46.5° and progressively increasing the temperature). The latter variation did not affect the measurements. To interpret the

---

[1] N. V. Sidgwick, "The Chemical Elements and Their Compounds," Vol. I, Oxford University Press, London, 1950, pp. 798–799.

[2] P. P. Popov, *J. Gen. Chem.* (*U.S.S.R.*), **9**, 1265 (1939).

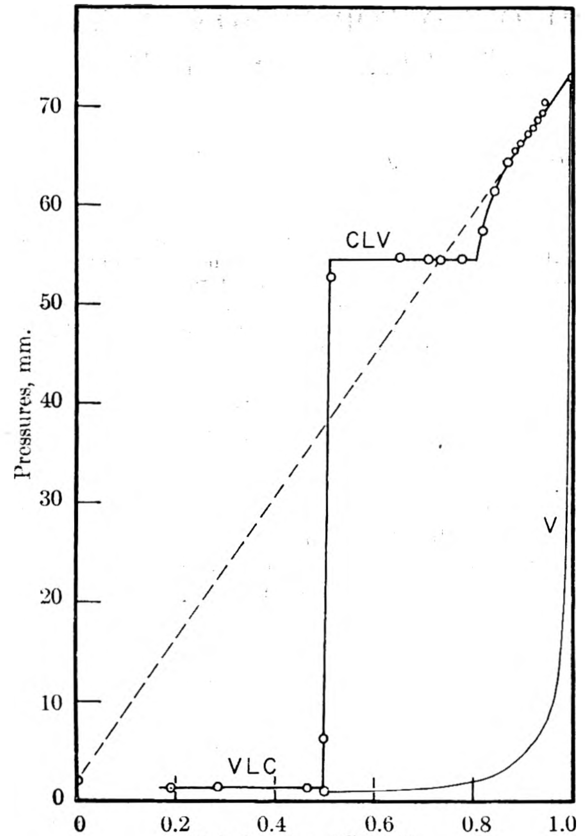

Fig. 1.—The phosphorus trichloride–trimethylamine system at −46.5°.

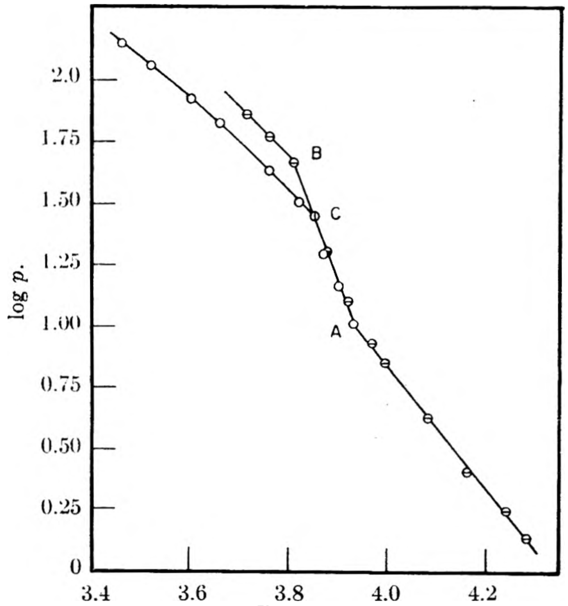

Fig. 2.—Variation with temperature of the vapor pressure of phosphorus trichloride–trimethylamine: ⊖, sample 1; ○, sample 2; ⦶, represents two points, same value for each sample.

TABLE II

SUBLIMATION PRESSURES OF SOLID PHOSPHORUS TRICHLORIDE–TRIMETHYLAMINE

Temp., °C.	−46.5	−39.5	−37.5	−32.7	−28.0	−22.7	−21.0
p, mm.	0.9	1.4	1.8	2.6	4.3	7.2	8.6

sublimation pressures further, studies were made on mixtures of gaseous PCl_3 and $(CH_3)_3N$ at 25°. It was found that the components followed Dalton's law quite closely showing only a slight tendency for association in the gas phase up to a total pressure of 120 mm. Hence, the sublimation pressures of Table II are taken to correspond to the equilibrium $Cl_3P{\cdot}N(CH_3)_3(s) = PCl_3(g) + (CH_3)_3N(g)$. The heat for the above dissociation reaction may be obtained assuming $K = (0.5p)^2$. This is done simply by plotting log p *vs.* $1/T$ and equating twice the slope to $-\Delta H/2.303R$. The resultant heat of dissociation is 22.4 kcal./mole.

The sublimation pressure of 0.9 mm. at −46.5° was used to construct the vapor line in Fig. 1. Of the 0.9 mm., 0.45 mm. corresponds to gaseous PCl_3 at a mole fraction of 0.5. Using the latter value as a maximum for PCl_3 in going to higher amine concentrations the mole fraction of gaseous amine was calculated and the vapor line established.

The measurements on the 2.87-mmole sample (sample 1) described in Table II were continued up to −3.6° and listed in Table III with accompanying information from visual observation.

TABLE III

VAPOR PRESSURE OF THE PHOSPHORUS TRICHLORIDE–TRIMETHYLAMINE SYSTEM

Sample 1			Sample 2	
Temp., °C.	Press.,[a] mm.	Observation, condensed phase	Temp., °C.	Press.,[b] mm.
−18.0	12.8		−20.8	8.9
−15.4	20.5	Solid is moist looking	−19.0	11.5
−13.5	28.1		−17.0	14.8
−10.6	46.8	Looks entirely liquid	−15.3	19.9
− 7.0	59.4	Liquid	−13.6	28.5
− 3.6	72.9	Liquid	−11.8	32.4
			− 7.8	43.4
			0.0	67.7
			4.9	84.4
			11.0	115.2
			15.8	142.6

[a] Vapor volume was 35.8 ml.
[b] Vapor volume was 45.8 ml.

The results combined with those of Table II are plotted in Fig. 2. The log p *vs.* $1/T$ plot shows a sharp increase in slope at −21° and a further slope change at approximately −10°. The slope changes are assumed to be caused by the appearance of a liquid phase at A (previous to this point the equilibrium being C = V and afterwards, LCV) and the disappearance of the solid phase at B(LCV going to L + V) in qualitative agreement with visual observation. Using a smaller sample size, 1.42 mmoles (sample 2 treated in the same manner as that used in obtaining the data of Table II) and a larger vapor volume, 45.8 ml., the measurements were repeated. The results (Table III) plotted in Fig. 2 show the same slope between points A and B but the slope change occurs at point C corresponding to −13.6° instead of −10°. The latter serves to indicate that this point is a function of the ratio of vapor to liquid which is usual for a binary system of this type.[3] The range

---

[3] J. E. Ricci, "The Phase Rule and Heterogeneous Equilibrium," D. Van Nostrand Co., Inc., New York, N. Y., 1951, pp. 158–160.

A to B or A to C then may be called the "melting range under the vapor pressure of the system."

The PCl_3-$(CH_3)_3N$ System at 0°.—To understand more fully what is occurring in the liquid phase (above point B of Fig. 2), the phase diagram was examined in the liquid region.

Additions of $(CH_3)_3N$ to liquid PCl_3 at 0° resulted in the pressure composition diagram shown in Fig. 3; the data are listed in Table IV.

The total pressure curve obtained is of the type expected for a homogeneous, liquid system in which the components are associating to some degree.

In order to establish the type of association taking place in a more quantitative fashion, calculations were carried out using a modified treatment based on Dolezalek's method[4] in which it is assumed that the components, $(CH_3)_3N$, PCl_3 and any complexes present, obey Raoult's law. Using the latter assumption the activities are equated to the calculated mole fractions for each. It is also assumed that the partial pressure of the complex is negligible as measurements of the total vapor pressure of mixtures of gaseous PCl_3 and $(CH_3)_3N$ at 25.0° indicate.

To illustrate, assume an equilibrium in which only a 1:1 adduct is considered to be present and derive an expression for the equilibrium constant for the association

$$PCl_3(l) + N(CH_3)_3(soln.) = Cl_3P{\cdot}N(CH_3)_3(soln.)$$

The definition of symbols to be used are

a_1 and a_2	activities of $(CH_3)_3N$ and PCl_3, resp.
p_1 and p_2	partial vapor pressures of $(CH_3)_3N$ and PCl_3, resp.
$p_1{}^0$ and $p_2{}^0$	vapor pressures of pure $(CH_3)_3N$ and PCl_3, resp.
p_t	total vapor pressure
N_1 and N_2	initial moles of $(CH_3)_3N$ and PCl_3, resp.
N_c	moles of complex formed
a_c	activity of complex
K	equilibrium constant

At equilibrium the activity of $(CH_3)_3N$ is

$$a_1 = p_1/p_1{}^0 = N_1 - N_c/N_1 + N_2 - N_c \qquad (1)$$

A corresponding expression exists for the activity of PCl_3. Solving each of these expressions for the moles of the complex and equating, an expression results for the partial pressure of PCl_3

$$p_2 = \frac{p_2{}^0(p_1{}^0N_2 + p_tN_1 - p_1{}^0N_1)}{p_2{}^0N_1 + p_1{}^0N_2} \qquad (2)$$

Expressions for N_c, a_c and K then follow

$$N_c = \frac{N_2p_2{}^0 - p_2(N_1 + N_2)}{p_2{}^0 - p_2} \qquad (3)$$

$$a_c = \frac{N_c}{N_1 + N_2 - N_c} \qquad (4)$$

$$K = \frac{a_c}{\left(\frac{p_1}{p_1{}^0}\right)\left(\frac{p_2}{p_2{}^0}\right)} \qquad (5)$$

The above expressions may be combined to give

$$K = \frac{(p_2{}^0N_1 + p_1{}^0N_2)[(p_2{}^0N_2 + p_1{}^0N_1) - p_t(N_1 + N_2)]}{p_t{}^2N_1N_2 - p_t(N_2 - N_1)(p_2{}^0N_1 - p_1{}^0N_2) - p_1{}^0p_2{}^0(N_2 - N_1)^2} \qquad (6)$$

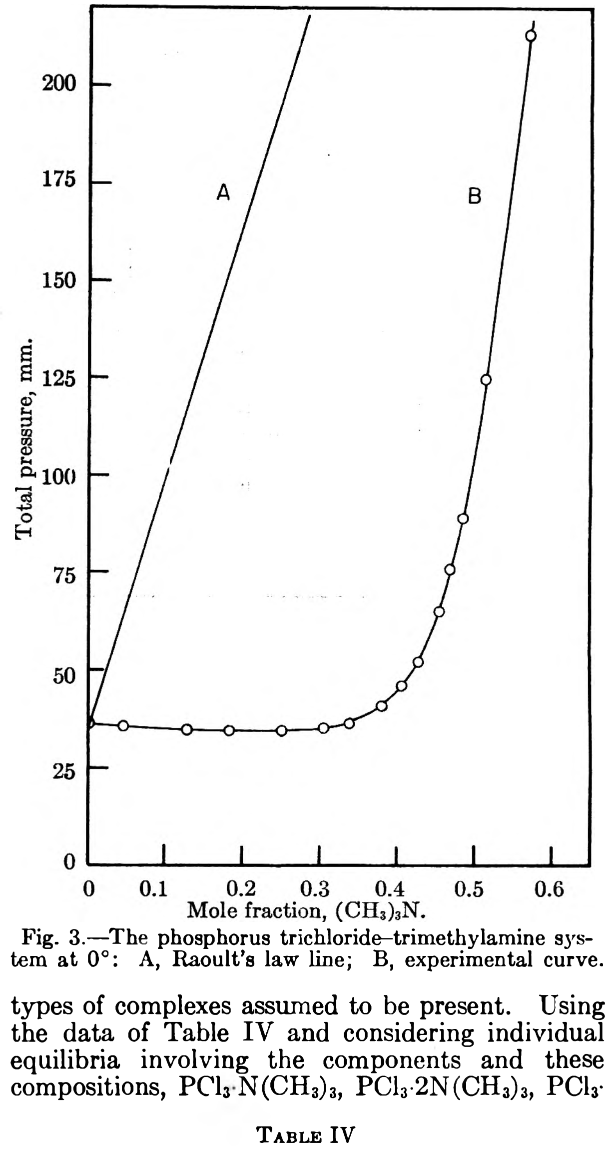

Fig. 3.—The phosphorus trichloride–trimethylamine system at 0°: A, Raoult's law line; B, experimental curve.

Similar expressions may be derived for other types of complexes assumed to be present. Using the data of Table IV and considering individual equilibria involving the components and these compositions, $PCl_3{\cdot}N(CH_3)_3$, $PCl_3{\cdot}2N(CH_3)_3$, $PCl_3{\cdot}$

TABLE IV

EQUILIBRIUM DATA AS A FUNCTION OF CONCENTRATION AT CONSTANT TEMPERATURE (0°)

Mole fraction,[a] $x_{(CH_3)_3N}$	Total press., mm.	$PCl_3{\cdot}N(CH_3)_3$, K	$PCl_3{\cdot}2N(CH_3)_3$, $K \times 10^{-1}$	$PCl_3{\cdot}3N(CH_3)_3$, $K \times 10^{-4}$	$2PCl_3{\cdot}N(CH_3)_3$, K
0.128	34.8	31.7	812	770	28.9
.183	34.4	29.0			
.251	34.4	32.6			
.305	35.2	33.3	203	37.7	240
.339	36.6	34.2			
.381	40.8	35.6			
.408	46.2	35.1	39.8	1.23	26.6
.429	52.2	35.6			
.455	65.2	34.8			
.468	75.8	33.1	9.60	0.0824	0.191
.485	89.1	33.2			
.514	124.8	29.9			
.568	213.0	21.4[b]	0.952	.00182	−2.27

[a] 2.87 mmoles of PCl_3 was used in the experiment. [b] Indications are that this value is low because of decreasing validity of the assumed ideality of the vapor as one goes to higher pressures.[5]

---

[4] J. H. Hildebrand and R. L. Scott. "The Solubility of Nonelectrolytes," 3rd ed., Reinhold Publ. Corp., New York, N. Y., 1950, p. 176.

[5] A current investigation is attempting to correlate in a quantitative manner the phosphorus resonance data with vapor pressure measurements extending to an amine mole fraction of 0.9.

TABLE V

TEMPERATURE VARIANCE OF THE EQUILIBRIUM CONSTANT FOR THE PHOSPHORUS TRICHLORIDE–TRIMETHYLAMINE SYSTEM

Temp., °C.	Mmoles of $(CH_3)_3N$ N_1	Mmoles of PCl_3 N_2	Total press., mm.	$PCl_3 \cdot N(CH_3)_3$ K	$PCl_3 \cdot 2N(CH_3)_3$ $K \times 10^{-2}$	$PCl_3 \cdot 3N(CH_3)_3$ K	$2PCl_3 \cdot N(CH_3)_3$ K
−10.1	4.72	10.52	17.2	59.24	297	-8.46×10^9	501
− 7.4	4.71	10.52	21.2	48.45			
− 5.1	4.71	10.51	24.4	45.07			
− 2.6	4.70	10.51	28.6	40.94	51.5	3.05×10^6	349
0.0	4.70	10.50	34.1	35.96			
+ 2.3	4.70	10.49	39.1	33.21			
5.3	4.69	10.49	47.0	29.58			
7.8	4.68	10.48	55.2	26.33	11.4	1.18×10^5	222
10.0	4.67	10.48	63.2	23.98			
10.4	4.67	10.47	64.6	23.74			
12.6	4.66	10.47	73.6	21.80			
14.8	4.65	10.46	83.8	20.03	5.86	3.05×10^4	157
17.9	4.64	10.44	100.7	17.71			
20.0	4.62	10.43	113.8	16.10			
22.1	4.61	10.42	127.7	15.11			
24.7	4.59	10.40	145.2	14.10	3.94	9.07×10^3	100

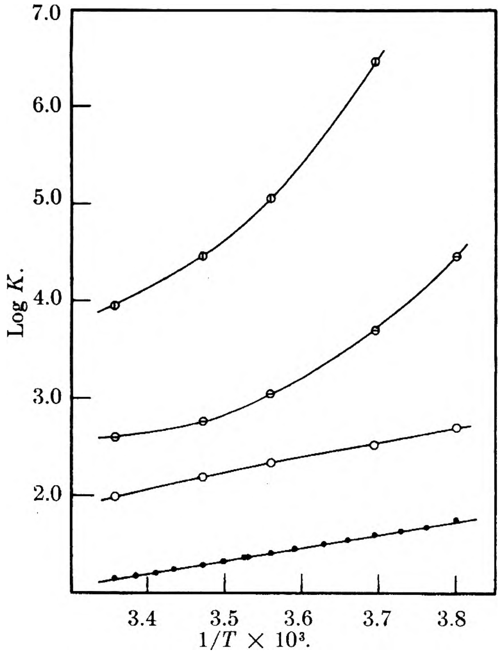

Fig. 4.—Temperature variation of the equilibrium constants calculated for the compositions: ●, $PCl_3 \cdot N(CH_3)_3$; ⊖, $PCl_3 \cdot 2N(CH_3)_3$; ⦶, $PCl_3 \cdot 3N(CH_3)_3$; ○, $2PCl_3 \cdot N(CH_3)_3$.

$3N(CH_3)_3$ and $2PCl_3 \cdot N(CH_3)_3$, values of K were calculated in each case and are listed in Table IV.

It is seen that the best single representation is the 1:1 adduct having a relatively constant value of K. Examination of the trends of the other results with concentration does not seem to favor consideration of the simultaneous presence of a number of complexes in equilibrium with each other.

As a further test, pressure measurements on the PCl_3–$(CH_3)_3N$ system as a function of temperature were made in the liquid range extending from −10 to 25°. From the data so obtained the "equilibrium constants" as a function of temperature were calculated for each of the assumed compositions referred to above. The results are listed in Table V and plotted in Fig. 4; the analytical number of moles of each component present is included.

Treatment of the data was effected entirely analogously to the manner described above for the system at 0°. Values needed for the vapor pressures of pure $(CH_3)_3N$ and PCl_3 at the various temperatures were obtained from the equations $\log p_{mm} = -1342/T + 7.7580$ and $\log p_{mm} = -1710/T + 7.8087$, respectively. The latter equations resulted from a least squares treatment applied to the experimentally determined vapor pressures listed in Tables VI and VII.

Because of the lengthy nature of the calculations in this and the preceding section, the data were programmed on the I.B.M. 650 at Carnegie Tech.

The log K vs. $1/T$ plot in Fig. 4 shows excellent linearity for the 1:1 composition, thus supporting the data at 0° for its presence.[6] While the linearity is also quite good for the assumed equilibrium involving $2PCl_3 \cdot N(CH_3)_3$, its K as a function of concentration (Table IV) was erratic, including negative values (the pressure due to $(CH_3)_3N$, p_1, came out to be greater than the total pressure for calculation resulting in the negative values). The other situations involving $PCl_3 \cdot 2N(CH_3)_3$ and $PCl_3 \cdot 3N(CH_3)_3$, which show trends in K at 0°, show curves for log K as a function of temperature. From the log K vs. $1/T$ plot a value of 6.4 kcal./mole is obtained for the heat of formation of the 1:1 complex in solution.

TABLE VI

VAPOR PRESSURES OF TRIMETHYLAMINE

t, °C.	−67.2	−45.18	−36.25	−23.9	−17.25
p, mm.	17.3	73.9	128.0	238.4	331.2
t, °C.	−10.65	0.0			
p, mm.	445.3	679.9			

TABLE VII

VAPOR PRESSURES OF PHOSPHORUS TRICHLORIDE

t, °C.	0	4.20	8.50	13.40	18.50	24.4
p, mm.	35.3	44.1	54.6	69.7	88.6	115.1

---

[6] Additional data recently obtained as a function of concentration at 20.0° show a constancy of the equilibrium constant for the 1:1 composition similar to that reported here at 0°. Further, conductance measurements rule out the presence of ions in the association process.

P^{31} Magnetic Resonance Measurements.—P^{31} magnetic measurements were made at 26° on mixtures of PCl_3 and $(CH_3)_3N$ having varying mole ratios. One sharp line was observed which was shifted up field with respect to the P^{31} line in pure liquid PCl_3. The shift increased as the concentration of amine was increased in the sample mixture up to an amine mole fraction of 0.6. Table VIII shows the results obtained.

TABLE VIII

P^{31} MEASUREMENTS ON THE SYSTEM PCl_3-$(CH_3)_3N$ AT 26°

Mole fraction $(CH_3)_3N$	δ,[a] p.p.m.
0.144	+5.1[b]
.346	29.1
.502	33.8
.504	33.1[b]
.600	33.1[b]

[a] Relative to the P^{31} line in pure PCl_3. The shift, δ, follows the convention adopted by J. Pople, W. Schneider and H. Berstein.[7] [b] External reference.

The sample mixture containing an amine mole fraction of 0.502 was frozen and allowed to warm up to room temperature. On melting, the line sharpened and began to shift toward that of pure PCl_3 with further warming, *i.e.*, toward lower field values. A sample of pure PCl_3 similarly frozen did not show any noticeable line shift on warming.

Discussion

Both the temperature and concentration dependence of the P^{31} resonance line in the PCl_3-$(CH_3)_3N$ mixtures support the presence of an association equilibrium. The fact that two P^{31} lines were not observed, corresponding to the expected differing chemical environments of free PCl_3 and complexed PCl_3, implies a fast exchange rate such that the observed shift refers to an average, weighted with respect to the relative amounts of the two forms. On warming the line shifts toward that of pure PCl_3 which would be expected for dissociation of a complex of PCl_3.

The change with concentration is also consistent with the presence of a complex, the shift increasing toward the complexed species with increase in amine concentration. The fact that the shift is toward higher fields with increasing amine concentration means little in relation to the electron density at phosphorus in the complex compared to the uncomplexed form since it is well known that little correlation exists between phosphorus shift and electronegativity or inductive effects of substituents attached to phosphorus.

In view of the relative constancy of the equilibrium constant at 0° and the excellent linearity of the log K *vs.* $1/T$ plot in Fig. 4, it is implied that the assumption of ideality of the uncomplexed components in the liquid system is essentially valid. Hence, in the absence of complexing, dilution of PCl_3 with $(CH_3)_3N$ should result in no heat effect and one may take the value of 6.4 kcal./mole obtained for the reaction

$$Cl_3P \cdot N(CH_3)_3(\text{soln.}) = PCl_3(l) + (CH_3)_3N(\text{soln.})$$

to be a measure of the interaction energy.

One might reason that because of the low interaction energy and the known existence of complexes of arsenic and antimony trihalides with donor molecules, a weak phosphorus–nitrogen linkage is present here. Electronically this seems the most favorable process. However, the evidence presented here does not strongly bear on the nature of the interaction; hence, the above conclusion is considered speculatory at this point. The latter topic is the subject of a forthcoming paper. In any event an example is provided of an adduct of a tricoördinated phosphorus compound with a typical donor molecule, heretofore unknown.[8]

Experimental

Materials.—Trimethylamine regenerated from the hydrochloride and dried over Drierite and then phosphorus pentoxide at −78.5° was further purified by fractionation in the vacuum line. The vapor pressure at 0° of the resulting tensiometrically homogeneous sample was 680 mm. Additional vapor pressure data are listed in Table VI.

Mallinckrodt phosphorus trichloride (analytical reagent) was fractionated twice in the line to remove a small amount of hydrogen chloride. The resulting vapor pressure was 35.3 mm. at 0°. Additional vapor pressure data are listed in Table VII.

Apparatus.—A special reaction section was constructed for the pressure–composition measurements and is adequately described elsewhere.[9]

P^{31} Magnetic Resonance Measurements.—A Varian Associates Spectrometer with superstabilizer was used with the R.F. unit at 15.1 mc. Mixtures of PCl_3 and $(CH_3)_3N$ were condensed into 5 mm. tubes attached to a vacuum system. For measurements involving external referencing the sample contained in the 5 mm. tube was placed in a 15 mm. tube containing indentations at the top and bottom to hold the inner tube in a coaxial position. PCl_3 was introduced into the outer tube *via* the vacuum system. The measurements were made employing the side band technique.

Acknowledgment.—The author wishes to express his appreciation to Dr. Audrey Companion for help in programming the data and to Professor Robert Kurland and Mr. Raymond Wagner for assisting with the phosphorus resonance measurements. He also is indebted to the National Science Foundation for a grant which helped this work in part.

---

(7) J. A. Pople, W. G. Schneider and H. J. Bernstein, "High-resolution Nuclear Magnetic Resonance," McGraw-Hill Book Co., Inc., New York. N. Y., 1959. p. 89.

(8) There exists in the literature a report of the complexes $(C_2H_5)_3N \cdot PCl_3$ and $3(C_2H_5)_3N \cdot PCl_5$, W. R. Trost, *Can. J. Chem.*, **32**, 356 (1954), but these could not be verified by later work; see R. R. Holmes and E. F. Bertaut, *J. Am. Chem. Soc.*, **80**, 2980 (1958).

(9) H. C. Brown, L. P. Eddy and R. Wong, *ibid.*, **75**, 6275 (1953).

ADSORPTION STUDIES ON BONE MINERAL AND SYNTHETIC HYDROXYAPATITE[1,2]

BY MARK E. DRY AND RALPH A. BEEBE

Department of Chemistry, Amherst College, Amherst, Massachusetts

Received March 29, 1960

Adsorption isotherms have been determined and calorimetric heats of adsorption have been obtained for the adsorption of both methanol and water vapors on hydroxyapatite dehydrated at 450° both in the form of anorganic bone and in the form of synthetic hydroxyapatite. In the case of the methanol, it was found practicable both on the basis of the isotherms and the differential heat data to separate the total adsorption more or less sharply into "chemisorbed" and physisorbed fractions. In the case of water such a separation was less clearly delineated. The adsorption characteristics differed remarkably little whether the adsorbing hydroxyapatite surface was of synthetic origin or derived from bone. The relatively high heats of adsorption in the first monolayer, for both methanol and water, indicate a high energy of binding on the hydroxyapatite and can probably be attributed to hydrogen bond formation involving the exposed oxygen atoms of the surface. Some experiments have been done with nitrogen adsorption at −195° on the dehydrated hydroxyapatite and on the surface of this material covered by a chemisorbed layer of methanol or of water. It is found that the chemisorbed layers have a rather profound influence on the subsequent physisorption of nitrogen.

Introduction

Because of the importance of the surface chemistry of bone mineral in physiological systems, we have undertaken a series of gas adsorption studies on hydroxyapatite both in the synthetic form and in the form of anorganic bone. The present investigation has been particularly concerned with the adsorption of two polar substances, water and methanol, on dehydrated hydroxyapatite surfaces. Because of the ionic character of the hydroxyapatite, we might expect that the polar adsorbate molecules would be strongly bound to the surface and probably oriented with respect to it. To test this supposition we have determined the adsorption isotherms and have measured the heats of adsorption of these polar adsorbates by means of a calorimeter. The interpretation of the experimental results has enabled us to draw a number of conclusions. In particular we have been able to sort out the "chemisorption"[16] from the physisorption in the total adsorbed film, to compare the states of the adsorbing surfaces of the hydroxyapatites from synthetic and from natural sources and to compare and contrast the characteristics of adsorbed films of water and of methanol on the same hydroxyapatite surface.

Previous calorimetric measurements have been concerned with the adsorption on solid surfaces of polar molecules from the vapor phase.[3-5] Recently several investigators have employed precision liquid immersion calorimetry to study the interaction of water and other polar molecules with silica[6-8] and other[9] surfaces. However we have found no record of such studies on hydroxyapatite.

In order to determine the specific surface areas of the adsorbent materials, we have used the B.E.T. method based on the adsorption of nitrogen at −195°.[10] In this phase of the work we have determined the adsorption of nitrogen not only on the dehydrated surfaces but also on these surfaces when they already are covered with chemisorbed monolayers of water or methanol. We have observed that these chemisorbed layers exert a marked effect on the subsequent physisorption of nitrogen. A similar effect has been noted by other investigators.[11-13]

Experimental

Materials.—The physical chemistry of both bone mineral and synthetic hydroxyapatite has been reviewed in detail by Neuman and Neuman.[14] It is known from electron microscope studies that both bone mineral[15] and synthetic hydroxyapatite have a micro-crystalline structure which leads to high specific surface areas which are of the order of magnitude found by the B.E.T. method. The composition and structure of fluoroapatite has been thoroughly investigated; due to the similarity of the X-ray patterns of hydroxyapatite to that of fluoroapatite, the unit cell of the hydroxyapatite is, by analogy, taken to be $Ca_{10}(PO_4)_6(OH)_2$. Whether hydroxyapatite comes from a natural or a synthetic source, it has a variable composition, which seems in large part to be due to the substitution of variable amounts of H_3O^+ ions for Ca^{++} ions in the crystal surfaces. Thus it is necessary to exercise special care in the control of outgassing procedures in preparation for adsorption runs. We have found that a fairly reproducible adsorbing surface is obtained by overnight degassing at 450°. The loss of weight for the bone mineral with temperature follows a pattern quite similar to that observed by Kunin[14] for synthetic material. Thus, although the per cent. loss of water changes with temperature of outgassing especially in the region from 100 to 400°, the rate of change of loss with temperature is smaller between 400 and 500°. If the

---

(1) Presented in the Symposium on Energetics of Surfaces and Interfaces before the Division of Colloid Chemistry of the American Chemical Society, September 7–12, 1958, in Chicago, Illinois.

(2) This research was supported by Grant NSF-G2765 from the Chemistry Branch of the Division of Physical and Engineering Sciences of the National Science Foundation. The work leading to a previous publication [R. A. Beebe and E. R. Camplin, THIS JOURNAL, **63**, 480 (1959)] also received support from the above grant. Our thanks are due to the Foundation for the support which made these two investigations possible.

(3) A. V. Kiselev, *Kolloidny Zhurn.*, **20**, 339 (1958); A. V. Kiselev, N. V. Kovaleva, V. A. Sinitsyn and E. V. Khrapova, *ibid.*, **20**, 444 (1958).

(4) B. Millard, R. A. Beebe and J. Cynarski, THIS JOURNAL, **58**, 468 (1954).

(5) C. H. Amberg, *J. Am. Chem. Soc.*, **79**, 3980 (1957).

(6) M. M. Egorov, V. F. Kiselev, K. G. Krasil'nikov and V. V. Murina, *Akad. Nauk S.S.S.R.*, (*J. Phys. Chem.*), **33**, No. 1 (1959).

(7) A. C. Makrides and N. Hackerman, THIS JOURNAL, **63**, 594 (1959).

(8) G. J. Young and T. P. Bursh, *J. Colloid Sci.*, in press.

(9) A. C. Zettlemoyer, G. J. Young, J. J. Chessick and F. H. Healey, THIS JOURNAL, **57**, 649 (1953).

(10) (a) E. P. Barrett, L. G. Joyner and P. P. Halenda, *Ind. Eng. Chem.*, **43**, 639 (1951); (b) **44**, 1847 (1952).

(11) F. S. Stone and P. F. Tiley, *Nature*, **167**, 654 (1951).

(12) A. V. Kiselev, N. V. Kovaleva, A. Ya. Korolev and K. D. Shcherbakova, *Compt. rend. Acad. Sci. URSS* (*Doklady Akademii nauk SSSR*), **124**, 617 (1959).

(13) D. S. Melver and H. H. Tobin, THIS JOURNAL, **64**, 683 (1960).

(14) W. F. and M. W. Neuman, "The Chemical Dynamics of Bone Mineral," Univ. of Chicago Press, 1958, p. 39; (ref. to Kunin, p. 43).

(15) R. A. Robinson and D. A. Cameron, *J. Biophys. Biochem. Cytol.*, **2**, 253 (1956).

heating process is extended into the 500 to 800° range, the hydroxyapatite, stable below 500°, is broken down with further loss of water and production of tricalcium phosphate.

The anorganic bone mineral was supplied by the courtesy of the Research Division of Armour and Company, Chicago, Illinois. This material had been freed from collagen and other organic matter by ethylenediamine extraction. The sample used in all the work reported below was the Ossar Bovine Femur Head lot 34. The loss of weight which occurred on evacuation of this material at 500° was made up of 3 to 4% H_2O, 1% CO_2 and 0.3% of gas uncondensable at liquid air temperatures. The amount of water present in the initial samples and hence the amount lost on evacuation at high temperature was dependent upon the humidity of the atmosphere to which the sample had been exposed before degassing. Slight charring of the initially white bone mineral was observed to occur at temperatures above 200°. The material used in the experiments described below was first treated in a stream of oxygen at 500° and in subsequent evacuations the temperature was 450°. The specific surface area of this material after dehydrating at 450° was 100 m.^{2} per g. (For brevity in this paper the adsorbent described above will be designated simply as the bone mineral or Ossar.)

The synthetic hydroxyapatite used in the present work was kindly supplied by Dr. W. F. Neuman of the University of Rochester Medical School. The sample was taken from the apatite preparation batch "31" described in the book by Neuman and Neuman.[14] In this material the Ca/P atomic ratio is given as 1.48. The loss in weight (H_2O) on evacuating at 450° was found to be 5 to 6% (evolved CO_2 and gas uncondensable at −195° constituted less than 0.01% of the total weight of the sample). The dehydrated material had a specific surface area of 67 m.^{2}/g. The outgassing procedure was identical to that described above for the Ossar.

The methanol was de-aerated by bulb-to-bulb distillation in a vacuum system until the vapor pressure reading became constant for a bulb containing liquid methanol (3.07 cm. at 0°). Increments of methanol for adsorption were measured in a gas buret, due consideration being given to the effect of deviation from the perfect gas laws.

Water vapor was drawn off from a weight buret (equipped with a stopcock and the male part of a standard ground glass joint) which contained de-aerated distilled water. In order to measure small increments (1×10^{-4} mole) with reasonable accuracy, water vapor from the weight buret was allowed to expand into a system consisting of two bulbs (one large and the other small) which were connected by a stopcock. In this manner a relatively large amount of water vapor could be drawn from the weight buret and hence the effect of an error in the weighing was minimized. Knowing the volumes of the two bulbs, the distribution ratio of the vapor between the two was obtained readily. The stopcock connecting the bulbs then was closed and the aliquot amount of vapor contained in the smaller bulb was introduced into the adsorption system.

Apparatus.—The gas handling and vacuum systems were standard equipment. The type of calorimeter used in the measurements, and the method of computation of the heats of adsorption were essentially the same as described elsewhere.[5] The only major feature of difference in the construction of the present calorimeter was in the nature of the copper filler. The filler, onto which the heater wire used for calibration purposes was directly wound, was considerably more bulky than those used in previous cases, filling the whole of the inner platinum bucket except for six slots between the filler and the bucket. To ensure as far as possible the even distribution of an increment of adsorbing gas over the entire sample of adsorbent which was embedded in the six lots, the filler had a hole drilled down the center with smaller holes directed outward from it toward the slots. The heat capacity of the adsorbent material was only 3.5% of that of the metal parts of the calorimeter and this arrangement yielded satisfactory time–temperature curves from which the heats of adsorption could be computed with confidence. Due to the high specific surface areas of the adsorbents involved, it was possible to tolerate the loss in sensitivity of the calorimeter caused by the high ratio in the weight of the inert metal of the calorimeter to that of the actual adsorbent.

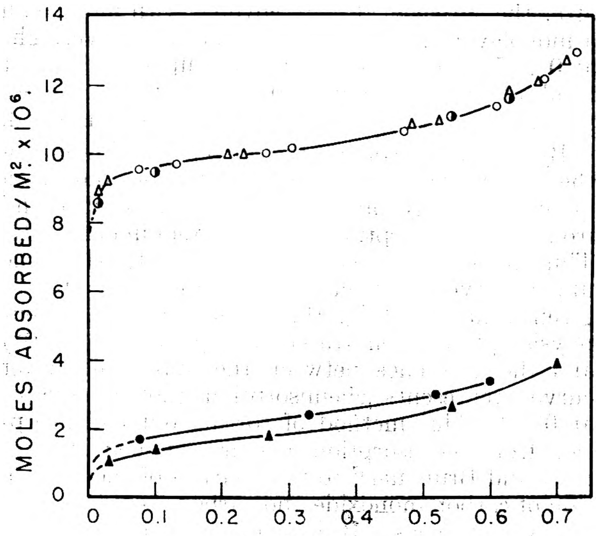

Fig. 1.—Adsorption isotherms for methanol on hydroxyapatite at 0°: ○, ●, ◑, bone mineral; △, ▲, synthetic; upper curve after degassing at 450°; lower curves after degassing methanol covered surface at 0°.

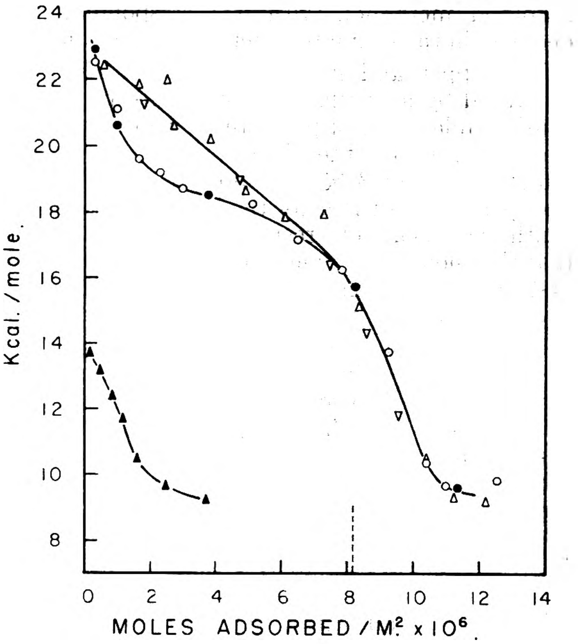

Fig. 2.—Differential heats of adsorption for methanol on hydroxyapatite at 0°: ○, ●, bone mineral; △, ▽, ▲, synthetic; upper curves after degassing at 450°; lower curve after degassing methanol covered surface at 0°.

Results and Discussion

I. The Adsorption of Methanol.—The experimental data for methanol adsorption on the hydroxyapatite samples of both synthetic and natural origin are given in the isotherms of Fig. 1 and the differential heat curves of Fig. 2.

The isotherms, measured at 0°, are plotted on the basis of relative pressure *vs.* moles of methanol adsorbed per m.^{2} of hydroxyapatite surface as determined by the B.E.T. nitrogen adsorption method. The data in the upper curve in Fig. 1 were taken after degassing the sample overnight at 450° and those of the lower curves were obtained after the surfaces, already covered with more than a monolayer of methanol, were degassed overnight at 0°. It is noteworthy that the upper curves for total adsorption per unit area of surface are identical for the synthetic apatite and the bone mineral.

By a comparison of the upper and lower isotherms of Fig. 1, it is possible to sort out, in a qualitative way at least, the "chemisorption" from the physisorption for the system under study. Thus it is reasonable to assume that, while the upper curve represents total adsorption at any given value of P/P_0, the lower curves represent physisorption (removable by pumping at 0°) and the difference between the upper and lower curves represents chemisorption (not removable at 0°).[16] This method of sorting out chemisorption from physisorption was first applied by Emmett and Brunauer[17] to the analysis of the adsorption of carbon monoxide and carbon dioxide on iron catalyst surfaces. It is realized that in the adsorption system being studied this method can hardly be expected to give an entirely clean-cut differentiation between the two types of adsorption. For instance a much longer pumping period might have removed a few per cent. more of the adsorbed methanol, with a corresponding small decrease in the estimated chemisorbed fraction.

The upper and lower isotherms of Fig. 1 are separated by a virtually constant distance over a considerable range of pressure. From this distance we estimate that the chemisorbed layer contains 8.0×10^{-6} and 8.3×10^{-6} mole of adsorbed methanol per m.^{2} of surface for the bone mineral and the synthetic adsorbent, respectively. If we assume that the chemisorbed methanol comprises the whole first monolayer, then we find cross-sections per adsorbed methanol molecule of 20.7 and 20.0 Å.,^{2} respectively, for the above two surfaces. There seems to be no universally applicable value for the cross section of adsorbed methanol molecules in different systems. The value obtained from the liquid density of methanol assuming close-packed spheres is 17.7 Å.^{2}; this would represent physisorption. For methanol in the chemisorbed state, cross sections have been cited which range from 28 Å.^{2}, on a silica gel sample to 15 Å.^{2} on a nickel surface.[18]

The heats of adsorption represented in Fig. 2 are plotted on the basis of kcal. per mole against moles of methanol adsorbed per m.^{2} of surface. In the upper right are given the results of check runs at 0° on each of the two types of hydroxyapatite after outgassing at 450°. In the lower left are the calorimetric data on the synthetic material after outgassing at 0°; this material would presumably retain a chemisorbed monolayer of methanol after outgassing. A dotted vertical line at 8.2×10^{-6} moles/m.^{2} indicates the average value for the completion of the chemisorbed monolayers of the two adsorbents as estimated from the data of Fig. 1.

It is seen in Fig. 2 that the differential heat values are high throughout the estimated chemisorbed layer exceeding the heat of vaporization of methanol (E_L = 9.1 kcal./mole) by about 5 kcal. even at the estimated point of completion of the layer. The heats fall throughout the first layer but the rate of fall is greater near its completion and the values rapidly approach the heat of vaporization as the second layer fills.

Because of the relatively small diameter of the calcium ions, the surface would be largely occupied by oxygen atoms associated either with the phosphate or the hydroxyl ions of the surface. Thus, it seems plausible to postulate the oriented adsorption of methanol on the ionic surface of the hydroxyapatite as the result of dipole attraction plus hydrogen bonding. These hydrogen bonds could involve O—H—O bonds in which the hydrogen might be supplied either by the methanol or in part by the hydroxyl groups of the hydroxyapatite. Such an adsorbed layer of methanol would present a layer of methyl radicals at its surface and would have relatively small attraction for building up a second adsorbed layer of methanol. This model seems consistent with the observed differential heat curve.

II. The Adsorption of Water.—We also have studied the adsorption of water vapor on the hydroxyapatite surfaces. The isotherm for the total adsorption of water at 23° on the bone mineral sample outgassed at 450° is given in Fig. 3. An attempt to split this total adsorption into a physisorption and chemisorption was less successful and more arbitrary than was the case for methanol. Thus, unless the outgassing was very carefully timed, it was difficult to obtain reproducible results for the physisorbed water. For comparison, the isotherm for total adsorption of methanol at 0° is included in Fig. 3. It is immediately obvious that the water isotherm is steeper beyond the estimated monolayer than is the case with methanol.

Some differential heat data for water measured at 23° on bone mineral are shown in Fig. 4. The dotted vertical line represents moles of water adsorbed/m.^{2} at the monolayer as estimated by point B of Fig. 3. It is apparent that the experimental points scatter to some degree. In the first calorimeter which we used for water adsorption this scatter was even more pronounced and it was traced to a non-equilibrium effect previously noticed in earlier work on other adsorption systems.[19,20] Such effects are especially noticeable at low pressures of the ambient adsorbate gases. In the calorimeter used to obtain the data of Fig. 4 the design was altered to eliminate this non-equilibrium effect as far as possible, by bringing the incoming gas increment into contact with a broad annular layer of the adsorbent surrounding a perforated central inlet tube rather than a narrow layer at the top of the calorimeter. However, this device still would not eliminate the possibility of a non-equilibrium state due to slow diffusion of water molecules initially adsorbed on lower energy

---

(16) For convenience we shall refer to the adsorbate not removable by pumping at 0° as being chemisorbed, although the forces of dipole attraction and hydrogen bonding which are probably at play here might not be generally accepted as being chemical in nature.

(17) P. H. Emmett and S. Brunauer, *J. Am. Chem. Soc.*, **59**, 310 (1938).

(18) V. A. Dzisko and V. N. Krasnopol'skaya, *Zhur. Fiz. Khim.*, **26**, 1841 (1952).

(19) R. A. Beebe and D. A. Dowden, *J. Am. Chem. Soc.*, **60**, 2912 (1938).

(20) W. E. Garner and F. J. Veal, *J. Chem. Soc.*, 1483 (1935).

sites, into the body of the crystals where less readily available sites of higher energy might be present. Thus, it is felt that the heat data up to the calculated monolayer may be somewhat erratic depending on the time between admissions of increments. If anything, the experimental points may be too low in this region although we believe that the solid line of Fig. 4 comes close to representing measurements under true equilibrium conditions.

In comparing the heat data for methanol and for water as shown in Figs. 2 and 4 it seems apparent that (1) the heats for water at a given coverage run somewhat lower than those for methanol and (2) the drop in the differential heats is much more gradual for water indicating a less clear-cut separation in binding energy between the first and second adsorbed layers.

We think these observations can be explained on the basis of the hydrogen bonding. Pauling[21] has shown that the energy per hydrogen bond in the pure liquids is stronger in methanol (6.2 kcal./mole) than in water (4.5 kcal./mole). The higher boiling point and heat of vaporization of water as compared to methanol is due to the formation of more hydrogen bonds per mole in the former than in the latter. Methanol presumably would form one hydrogen bond per molecule, binding it to the adsorbing hydroxyapatite surface. It may well be that the water molecules likewise are adsorbed by forming on the average little more than one hydrogen bond per molecule and from analogy with the bonding in the bulk phases the water would then be less strongly bound to the adsorbing surface than would methanol. If the water molecules are singly bonded to the surface then the molecules in the first layer would possess residual capacity for hydrogen bonding to subsequently adsorbed molecules in the second layer. This model would seem to explain the less well-defined separation between the first and second layers as deduced from the heat data as shown in Figs. 2 and 4. This model is also consistent with the observed steeper slope of the water isotherm as compared with that for methanol in Fig. 3.

Neuman and his co-workers[22] have studied the adsorption of water on hydroxyapatite by means of a centrifugation technique. From our present study, we would conclude that the above investigators must have been dealing with water adsorption in the second and subsequent layers, since the first layer probably would be too tightly bound to be removed by centrifugation.

In discussing their results, Neuman, *et al.*, suggest that there may be some direct bonding between the hydroxyapatite crystals and the organic phase (collagen) in live bone, and they cite the electron micrographs of Robinson and Watson[23] as supporting evidence. On the basis of the present research, we suggest that some less direct bonding may be effected through intervening water molecules which are attached by hydrogen bonds to the crystal surface on the one side and to the collagen on the other.

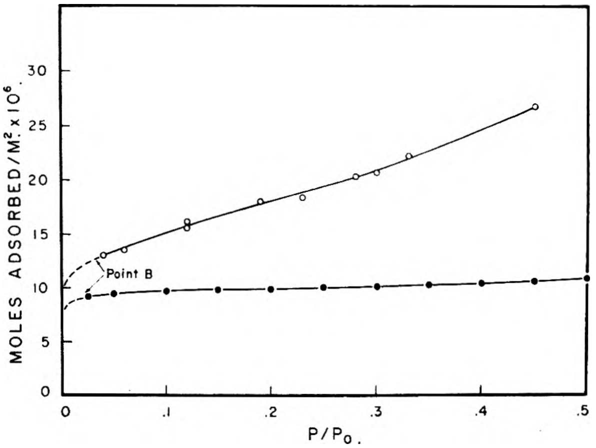

Fig. 3.—Total adsorption isotherms on bone mineral, after degassing at 450°, ○ water at 23°, ● methanol at 0°.

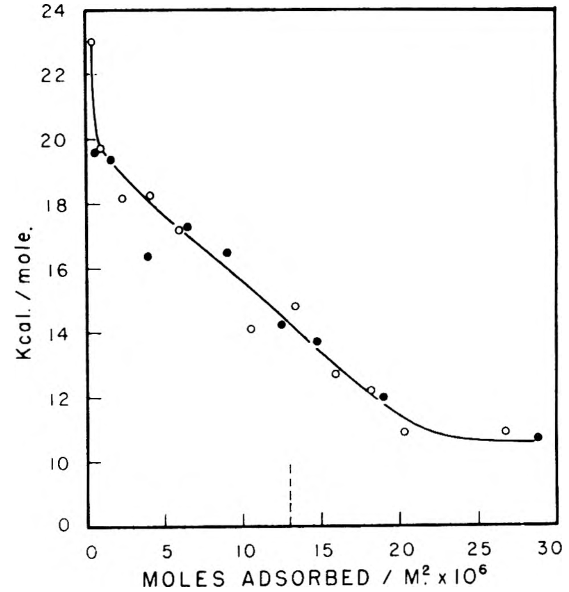

Fig. 4.—Differential heats of adsorption for water on hydroxyapatite at 23°; samples degassed at 450°; ○, bone mineral; ●, synthetic.

III. Experiments with Ethanol.—A limited amount of experimental work was done with ethanol adsorbate on the synthetic hydroxyapatite. The isotherms measured at 30°, (1) after outgassing the adsorbent at 450° and (2) after outgassing the ethanol covered surface at 30°, bore the same relationships as are shown for methanol in Fig. 1. The amount of chemisorption represented 83% of the adsorption at the estimated point B of the upper isotherm. As with methanol it was found impossible to remove the chemisorbed ethanol without some decomposition at high temperatures necessary for degassing. The decomposition products were not identified.

IV. The Adsorption of Nitrogen.—In order to determine the specific surface areas of the hydroxyapatite adsorbents, the adsorption isotherms were determined for nitrogen at −195°. It is of interest that the nature of these nitrogen isotherms was rather profoundly changed by the chemical altera-

---

(21) L. Pauling, "Nature of the Chemical Bond," Cornell Univ. Press, Ithaca, N. Y., Second Edition, 1948, p. 304.

(22) W. F. Neuman, T. Y. Toribara and B. J. Mulryan, *J. Am. Chem. Soc.*, **75**, 4239 (1953).

(23) R. A. Robinson and M. L. Watson, *Anat. Record*, **114**, 383 (1952).

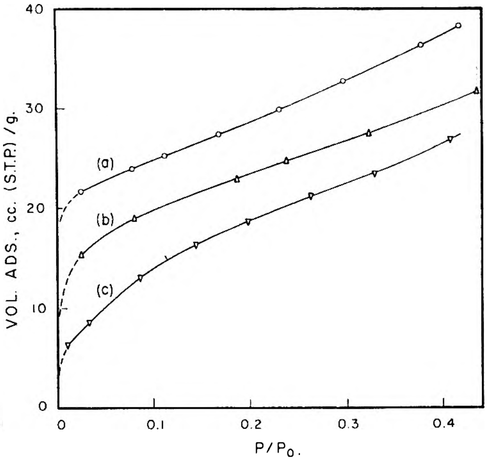

Fig. 5.—Adsorption isotherms for nitrogen on bone mineral at −195°, (a) ○ sample degassed at 450°; (b) △ on water covered surface; (c) ▽ on methanol covered surface.

Table I

Data from Nitrogen Adsorption on Bone Mineral[24]

(1) Treatment (see above)	(2) Spec. surf. m.²/g.	(3) B.E.T. "C" value	(4) Net heat of ads., cal./mole
(a)	100	435	940
(b)	86	142	770
(c)	75	25	500

tion of the adsorbing hydroxyapatite surface. Thus in Fig. 5 are shown the isotherms for the surface of the Ossar after the treatments described: (a) surface degassed overnight at 450°, (b) surface saturated with water vapor at 0° and then degassed overnight at 0°, (c) surface saturated with methanol vapor at 0° and then degassed overnight at 0°. The data of all three isotherms produce the normally encountered straight line B.E.T. plots and the resulting B.E.T. parameters are given in Table I. In column 1 of this table the treatment prior to nitrogen adsorption is indicated as described above. In column 2 are given the specific surface areas as calculated from the B.E.T. "V_m" values, in column 3 are given the B.E.T. "C" values, and in column 4, the net heats of adsorption ($E_1 - E_L$) as calculated from the data of column 3.

The data of columns 3 and 4 as well as the isotherms of Fig. 5 indicate a weakening of the adsorption potential for physisorption by previously chemisorbed material. The observed decrease in the specific surface areas of column 2 from (a) to (c) may be attributed either to, (1) blocking of very fine pores by the chemisorbed water or methanol, or (2) a less condensed packing of the nitrogen molecules on the surfaces of lowered adsorption potential. At the present time, we are unable to decide between these two alternatives.

This alteration of the physisorption potential of a surface by previously chemisorbed material has been observed by other investigators.[11–13] In particular Kiselev and his co-workers[12] have found that the substitution of $\text{-O-Si(CH}_3)_3$ "umbrellas" for the surface hydroxyl groups of silica surfaces has an effect on the nitrogen adsorption very similar to that of adsorbed methanol on a bone mineral surface as shown in Fig. 5 of this publication. The latter authors question the validity of the B.E.T. method for surface area determination in such systems of weakened adsorption potential.

Because of our interest in the above phenomena we have undertaken and partly completed the calorimetric measurement of the differential heats of adsorption of nitrogen on the bone mineral surfaces after treatments (a), (b) and (c) as described above. More detailed adsorption–desorption isotherms at −195° for nitrogen at high relative pressures are being measured in order to obtain information about pore size distribution in the bone mineral. It is hoped to publish the results of this work in the near future.

---

(24) In a set of similar experiments with the synthetic hydroxyapatite, the B.E.T. derived "C" values and net heats of adsorption and the variation of these parameters with treatments (a), (b) and (c) described above were essentially identical with those listed for the bone mineral in Table I, although the specific surface area of the synthetic material was lower.

NUCLEAR MAGNETIC RESONANCE STUDY OF MOLECULAR MOTION IN POLYDIMETHYLSILOXANES[1]

By C. M. Huggins, L. E. St. Pierre and A. M. Bueche

General Electric Research Laboratory, Schenectady, New York

Received April 2, 1960

The proton magnetic resonance (n.m.r.) spectra of a polydimethylsiloxane were determined over the temperature range 77–300°K. The spectra are characterized by an unusually narrow resonance line at room temperature indicating a low microscopic viscosity in the polymer. At 77°K. the line width broadened to 4.9 gauss peak-to-peak, compatible with a rigid lattice and free rotation of the methyl groups. The line narrowing data indicate a chain rotational process with an activation energy of 8 kcal./mole. The combination of the n.m.r. data with X-ray, melting point and dielectric loss data confirms the presence of a "second-order" transition in the crystalline polymer considerably below the crystal melting point. This transition is thought to be primarily the onset of a chain rotation but evidence also is presented for chain translational motion in the crystalline state.

Introduction

The structures and molecular motions of polymers are being subjected to increasing study by nuclear magnetic resonance (n.m.r.) techniques. A comprehensive review of the topic has been given by Slichter.[2] It has been shown that n.m.r. line shape studies provide a measurement of the relative

---

(1) Based on a paper presented at the ACS Meeting, Boston, Mass., April, 1959.

(2) W. P. Slichter, *Advances in Polymer Sci.*, **1**, 35 (1958).

spatial orientations of magnetic nuclei and a description of their relative motions (0–50 kc. range). Of particular interest are the proton-containing polymers for which X-ray studies give only vague descriptions of position and indirect evidence of motion.[3]

The silicones have been studied only superficially by n.m.r. Honnold, McCaffrey and Mrowca[4] discussed the unusually narrow proton resonance line width for silicone oil down to −50° and attributed it to intrachain rotation about the -O-Si-O- axis. They also postulated free methyl-group rotation down to −148°. Rochow and LeClair[5] give line width measurements on hexamethylcyclotrisiloxane (D_3), octamethylcyclotetrasiloxane (D_4), and decamethylcyclopentasiloxane (D_5) in support of their argument for freely-rotating methyl groups. Their measured line width second-moment $(\Delta H_2{}^2)$ down to liquid N_2 temperatures was considered compatible with the theoretical value for randomly-oriented, freely-rotating methyl groups with a reasonable amount of inter-group broadening. The same authors measured a line-width transition from about 5 gauss to less than 1 gauss at about 200°K. in G.E. SE450 silicone rubber. Banas and Mrowca[6] reported a line-width transition in silicone rubber at 125°K.

Silicone rubber (crosslinked polydimethylsiloxane with 17% by volume fine silica filler) was studied by Ohlberg, Alexander and Warrick[7] and Warrick,[8] who measured X-ray, dilatometric and mechanical properties; they found a crystal melting point of −55° and the per cent. crystallinity rising to 60% at −80°.

Experimental

All n.m.r. measurements were made on a Varian Associates V-4300B Dual-Purpose n.m.r. spectrometer operating at a field strength of approximately 9400 gauss and 40 megacycles. Derivative spectra were recorded with v-mode under slow-passage conditions using 40-c.p.s. field modulation and lock-in detection. The field modulation peak-to-peak amplitudes were maintained at less than one-fourth of the true line width (peak-to-peak) to ensure a minimum of modulation broadening. The rf. power input was continually monitored for saturation effects; the level was set so that an increase of 5 db. produced no significant change in the measured n.m.r. line width.

The cryostat was a modification of one used by Rempel, Weaver and Sands.[9] The sample was inserted to a depth of one inch and a copper–constantan thermocouple was buried $^1/_4$ inch in the sample. Temperatures were recorded on a Rubican #2732 Potentiometer to ±1°. Thermal equilibrium rates in the sample were checked in a sample holder containing two thermocouples, one located at the bottom of the holder. This experiment indicated a maximum error of ±10° in the sample temperature at the receiver coil; the probable error is estimated to be less than ±5°.

To avoid effects of supercooling, a special cooling procedure was followed. The sample was cooled slowly over a period of two hours or longer to about 80°K. The line widths then were recorded continuously until no further changes with time were observed. The sample was maintained in this temperature range for at least one hour after maximum line width was attained. The sample temperature was raised in small intervals by decreasing the flow of cold N_2 gas to the cryostat and the sample was at thermal equilibrium during each measurement. Reproducible results could be obtained by this procedure. Severe hysteresis effects were observed with rapid cooling.

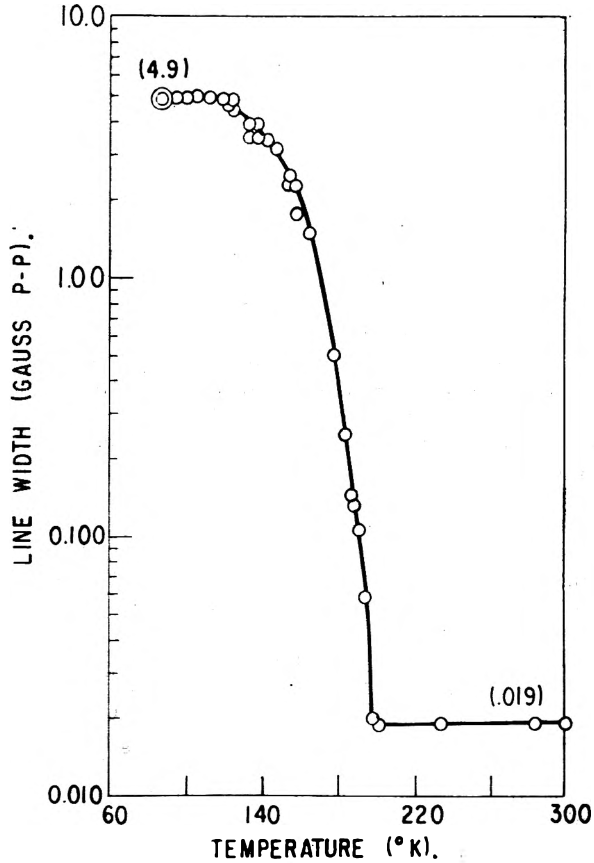

Fig. 1.—Peak-to-peak line widths of polydimethylsiloxane (mol. wt. 75,000).

Materials.—The polydimethylsiloxane was prepared from octamethylcyclotetrasiloxane (D_4) through the agency of 3–15 p.p.m. potassium hydroxide. The molecular weight was fixed by the addition of an appropriate amount of hexamethyldisiloxane. After polymerization was complete the product was neutralized with tris-chloroethyl phosphite and vacuum dried. The sample used for these measurements had a viscosity of $\eta = 2.95 \times 10^4$ cp. at 25° and a weight-average molecular weight of 7.5×10^4.

A source of n.m.r. line-width irreproducibility was found to be the presence of volatiles in the polymer sample. Vacuum treatment of the sample at 10^{-4} mm. and 100° for 24 hours prior to n.m.r. measurements removed this difficulty. The nature of the "impurity" was not determined.

Results and Discussion

Line-width measurements were made over the temperature range 80–300°K. The measured derivative peak-to-peak line widths are recorded on Fig. 1. The sample exhibited a low-temperature line width (ΔH) of 4.9 gauss peak-to-peak; the room temperature plateau line-width is 0.019 gauss peak-to-peak and the root second moment is 0.008 gauss. Both measurements include some residual magnetic field inhomogeneity broadening; it was not considered profitable to attempt to correct for field broadening since calibrations with water

---

(3) (a) W. P. Slichter, *J. Polymer Sci.*, **24**, 173 (1957); (b) C. W. Wilson, III, and G. E. Pake, *J. Chem. Phys.*, **27**, 115 (1957).

(4) V. R. Honnold, F. McCaffrey and B. A. Mrowca, *J. Appl. Phys.*, **25**, 1219 (1954).

(5) E. G. Rochow and H. G. LeClair, *J. Inorg. Nucl. Chem.*, **1**, 92 (1955).

(6) E. M. Banas and B. A. Mrowca, *Phys. Rev.*, **98**, 1548A (1955).

(7) S. M. Ohlberg, S. E. Alexander and E. L. Warrick, *J. Polymer Sci.*, **27**, 1 (1958).

(8) E. L. Warrick, *ibid.*, **27**, 19 (1958).

(9) R. C. Rempel, H. E. Weaver and R. H. Sands, private communication.

varied considerably, depending on magnet cycling. The exact temperature dependence of the line width near room temperature is masked somewhat by field inhomogeneity.

The line-width of 4.9 gauss peak-to-peak at 80°K. is in satisfactory agreement with the line-width measurements of Rochow and LeClair[5] on silicone rubber. Structural correlations require the determination of the second moment, ΔH_2^2, to compare with calculated values. Two spectra were chosen for optimum signal-to-noise, sweep broadening, and rf. saturation and the second moments determined graphically. The value of $\Delta H_2^2 = 7.0 \pm 0.2$ gauss^2 (corrected for modulation broadening) was obtained, which is somewhat lower than the value of 10.0 gauss^2 reported by Rochow and LeClair[5] for silicone rubber. Of course, the experimental determination of second moments is subject to some arbitrariness, but the observed discrepancy is felt to be outside of reasonable experimental error. Furthermore, the possible effects of filler in silicones on n.m.r. parameters are not known, so it is not reasonable to compare these numbers quantitatively.

The lower value for the second moment does, however, require a re-examination of the broadening terms discussed by Rochow and LeClair. It has been shown[5,10,11] that an isolated, rigid methyl group should exhibit a ΔH_2^2 of about 21.5 gauss^2. Free rotation about the C–Si bond would reduce this to about 5.4 gauss^2, depending upon the precise values of the C–H bond distances and the angles. It is presumed then that the second moments for silicone polymers at 80°K. are represented by freely-rotating methyl groups and an inter-group broadening term of 1.6 gauss^2. The temperature independence of the line width over a relatively wide temperature range makes it unlikely that the inter-group broadening includes any significant partially-excited oscillations about the chain axis, but rather is a result of the more or less static intermethyl group fields. Measurements at much lower temperatures will be necessary for confirmation.

A detailed correlation in the VanVleck manner of the intermethyl group interactions with the observed second moments is not warranted in the absence of crystal structure data. A description of this kind of inter-group broadening for methyl groups has been presented in terms of the theoretical spectrum for a rotating methyl group perturbed by a Gaussian broadening term

$$\Delta H_2^2 = \Delta H_2^2\,(\mathrm{Me}) + \beta^2$$

where β is the exponential broadening term as used by Powles and Gutowsky.[10,11] According to Andrew and Bersohn,[12] the absorption curve for a freely-rotating methyl group is characterized by a larger central absorption flanked by a pair of smaller wings. Powles and Gutowsky then plotted the methyl group spectrum (rotating) for values of β^2 through 2.0 gauss^2. According to their analysis, the broadening term of 1.6 gauss^2 for silicones should just permit observation of the outer wings separated by about 8.2 gauss. These outer wings are not visible in the recorded spectra; their apparent absence may be due to poor signal-to-noise ratio or to the inapplicability of the Gaussian broadening function. Powles and Gutowsky also observed the apparent absence of wings on the low-temperature spectrum of 2-chloro-2-nitropropane for which $\beta^2 = 1.5$ gauss^2.

The n.m.r. line width of the sample underwent a transition to a narrow line upon warming. The transition range, as shown in Fig. 1, is rather diffuse, extending over a wide temperature interval. The transition temperature, arbitrarily defined as the point at which the line width has changed by one-half the total change in log ΔH, is 180°K. The temperature-dependence of n.m.r. line narrowing has been treated theoretically by many workers. The two general cases of rapid rotation and translational diffusion are reviewed by Waugh[13]; more specific applications to polymers are reviewed and discussed by Slichter.[2] The n.m.r. narrowing in polymers has been considered to be a result of the onset of intramolecular rotations (*i.e.*, chain-twisting and torsional oscillation) of a frequency greater than several tens of kilocycles per second. The assumptions have been justified to the extent that Arrhenius plots usually give straight lines corresponding to "reasonable" activation energies. The motional correlation time, τ_c, is given by

$$\tau_c = A(\Delta H)^{-1} \tan\,[(\pi/2)(\Delta H^2 - B^2)/C^2]$$

where A is a constant involving the nuclear magnetic constants and some integration limits, ΔH is considered to be the line derivative peak-to-peak spacing, B is the high temperature plateau value of ΔH, and C is the low-temperature plateau value of ΔH. The Arrhenius relation equates the correlation time in the usual way to an activation energy term and a fundamental frequency factor. The above equation then can be rewritten

$$E/RT = \ln\,\{(\Delta H)^{-1} \tan\,[(\pi/2)(\Delta H^2 - B^2)/C^2]\} + \ln A$$

Following these procedures, the plot shown on Fig. 2 is obtained.

The data indicate definite curvature over the temperature range. This non-linearity might be attributed to several possible causes: supercooling effects not removed by the thermal procedures used, temperature measurement errors, a breakdown of the theory, or the presence of two activation energies. The latter effect is not unlikely; data for linear and branched polyethylenes are best fitted by two straight lines.[14,15] The calculated activation energies, including both the best single slope and two slopes are 5.9, 8.7 and 2.6 kcal./mole, respectively.

At least two classes of molecular motion must be considered in connection with the n.m.r. line narrowing and the activation energies. The most obvious physical change giving rise to line width change is the phase change associated with crystal-

---

[10] J. C. Powles and H. S. Gutowsky, *J. Chem. Phys.*, **21**, 1695 (1953).

[11] J. C. Powles and H. S. Gutowsky, *ibid.*, **23**, 1692 (1955).

[12] E. R. Andrew and R. Bersohn, *J. Chem. Phys.*, **18**, 159 (1950).

[13] J. S. Waugh, *Ann. N. Y. Acad. Sci.*, **70**, 900 (1958).

[14] D. W. McCall and W. P. Slichter, *J. Polymer Sci.*, **26**, 171 (1957).

[15] R. C. Rempel, H. E. Weaver, R. H. Sands and R. L. Miller, *J. Appl. Phys.*, **28**, 1082 (1957).

lization or glass formation. In most crystalline compounds, melting is accompanied by a sudden, large decrease in line width. An application of the Arrhenius plot of line widths to such a first-order phase change would yield very large, essentially infinite, activation energies. The theory is, of course, not valid for first-order phase changes. With crystalline materials, the worker generally is protected from making such false assumptions by both the inherent sharpness of the transition and some prior knowledge of the thermodynamics of the system. It should first, then, be ascertained that the polymer line narrowing is not a direct measure of a diffuse, first-order transition. One would expect that the "liquid" line would be considerably narrower than the crystal or glass line; hence, the absence of marked two-phase structure of the n.m.r. absorption line is evidence that the narrowing results from motion in the rigid phase rather than a change of phase.

More conclusive evidence is offered by other studies; preliminary measurements on the X-ray powder pattern of these polymers show no significant change in X-ray line spacings or widths from −195 to about −50°.[16] Work is in progress to extend the X-ray measurements to crystal melting points and the effects of cross-linking on crystal structure, but the present data indicate that the crystal melting point is higher than the temperature for which the n.m.r. line is completely narrowed. The crystalline melting point of silicone polymers has been investigated by a variety of methods. The volumetric behavior of a series of closely-related silicone gums was studied by Weir, Leser and Wood,[17] who found a first-order phase change at about −65° and second-order transition at −123°. Palmanteer and Hunter[18] reported the onset of crystallinity in polydimethylsiloxane gum to occur at about −45.3°. Small differences among these sets of data are expected in view of the diversity of materials in molecular weight and extent of filler interaction.

The crystalline melting point of the dimethylsilicone gum (mol. wt. 75,000) studied here was investigated in a conventional melting point apparatus. The gum was cooled to −100° for several hours and then cooled to −197°; the sample was then thermally isolated and allowed to warm slowly to room temperature while continuously recording the sample temperature. The warming curves so obtained showed clear evidence of crystal melting over a temperature range up to −40°. The melting point obtained in this manner also corresponds with the visual transition from opaque cloudy-white to water clear—a change usually associated with the crystal–liquid transition.

Independent investigations[19] of the X-ray structure of these polymers have shown the fraction crystallinity to be about 50% up to a few degrees below the melting point, −40°. By analogy to other polymers, notably polyethylene,[18] the n.m.r. spectrum might be expected to show two-phase structure in the temperature range −70 to −40°. A concerted effort was made to detect a wide line in addition to the observed narrow line without success. Repeated spectra run under all reasonable conditions of sweep modulation, rf. power, gain and scan rate show only the reported, narrow band. Other workers[4,5,20] observed only a single line for similar materials in this same temperature interval. The conclusion is forced that the narrow line includes contributions from the crystalline phase.

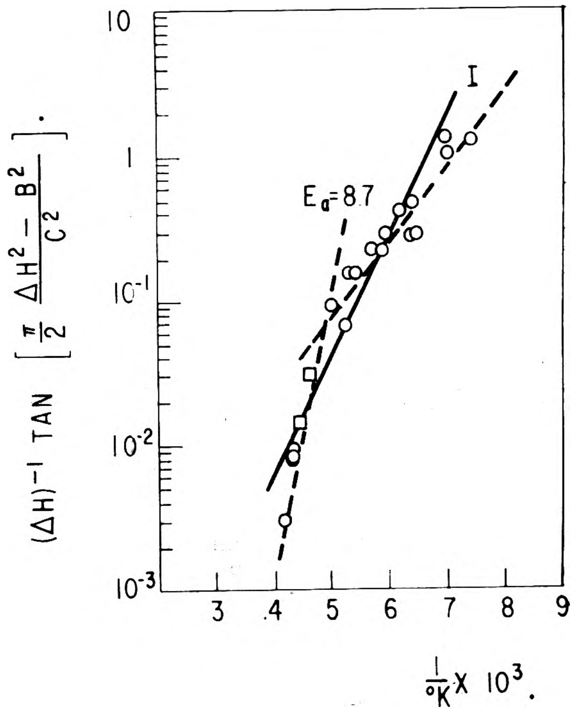

Fig. 2.—Temperature dependence of correlation time.

It seems fairly clear then that the observed n.m.r. transition is not associated with crystal melting, but rather with a motional, presumably second-order, transition in the crystalline phase. The motion effecting the n.m.r. line narrowing is then assumed to be primarily a rotation about the chain axis made particularly favorable by the low, torsional force constant of the Si–O–Si linkage. Rempel, Weaver, Sands and Miller[15] discuss a similar concept of rotational shear waves in polyethylene. It remains to be shown how such a transition can generate the extremely narrow n.m.r. lines without disturbing the X-ray or optical properties of the crystals.

At the low-temperature limit, the major part (5.4 gauss^2) of the second moment is intra-methyl; the remainder (1.6 gauss^2) is due to combinations of interactions among methyls on the same silicon atoms, on the same chain, and on neighboring chains. The intra-methyl contribution can quite reasonably be reduced to zero by a chain rotation as shown by Gutowsky and Pake.[21] The inter-methyl group interactions are more difficult to analyze. The second moment contribution be-

---

[16] C. M. Huggins and L. E. St. Pierre, to be published.

[17] C. E. Weir, W. H. Leser and L. A. Wood, *J. Research Natl. Bur. Standards*, **44**, 367 (1950).

[18] K. E. Palmanteer and M. J. Hunter, *J. Appl. Polymer Sci.*, **1**, 3 (1959).

[19] S. M. Ohlberg, L. E. Alexander and E. I. Warrick, *J. Polymer Sci.*, **27**, 1 (1958).

[20] H. S. Gutowsky, private communication, 1960.

[21] H. S. Gutowsky and G. E. Pake, *J. Chem. Phys.*, **18**, 162 (1950).

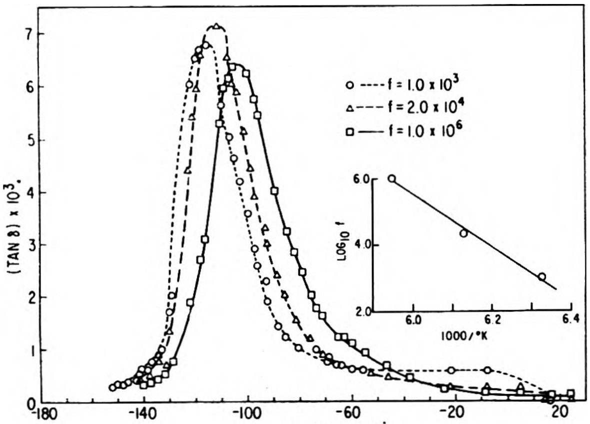

Fig. 3.—Dielectric loss data for polydimethylsiloxane (mol. wt. 75,000); irradiation doses, 6 MR.

tween methyl groups on the same silicon atom was calculated using accepted values of bond distances and tetrahedral angles to be about 0.25 gauss^2. Methyl groups on the same chain, but on different silicon atoms, yield second moments of from about 1.5 gauss^2 to about 0.030 gauss^2, dependent upon the value of the Si–O–Si angle and the degree of staggering. Likewise, the interchain contribution is calculated to be from 1.5 gauss^2 to 0.001 gauss^2. The broadening due to members of the same chain conceivably can be reduced to a very small number by a combination of rotation and wagging; however, it was not possible to construct a model which would permit the total inter-methyl group second moment to be reduced to below 0.001 gauss^2 even with all chains rotating. The only conclusion left is that there must be a considerable amount of interchain translation in the crystal.

This conclusion is supported by further observations[22] on the effect of radiation-induced cross-linking on the line-width parameters. It is shown that small amounts of cross-linking, which would not be expected to influence short-range rotational motion, significantly increase the value of the narrow line width. This broadening is interpreted to be a measure of the hindrance to the translational motion occurring in the uncrosslinked polymer.

The assumption of gross interchain translation in the crystal satisfies the condition of small line width at the transition point and makes more credible the absence of any apparent change in band structure at the higher temperature coincident with crystal melting. The X-ray data make it necessary that the interchain translation take place by a jumping mechanism such that the time-average X-ray structure is not altered. This condition would be satisfied by a series of inversions about the tetrahedral silicon atom or, just as likely, a series of rotations through interstitial holes or defects in the crystal lattice.

Two alternative explanations, both of which are considered unlikely, are still possible. If the crystallinity ratio is very small, say 5–10%, in contradiction to existing X-ray data, then it is not unreasonable that the crystalline wide line is not visible in the spectra. Secondly, if the spin lattice relaxation time, T_1, of the crystalline phase were extremely long then the signal might be missed even at the deliberately low rf. levels used. Either of these possibilities would make it unnecessary to speculate about motions in the crystalline phase, since only the amorphous glass–liquid transition is observed. More direct measurements of T_1 and T_2 should be useful in deciding among these alternatives.

Confirmation of the qualitative conclusions on the n.m.r. transitions was obtained from the results of dielectric loss measurements[23] on a polydimethylsiloxane sample which had been lightly crosslinked for experimental convenience (see note[24]). The material exhibits, Fig. 3, a very small $\tan \delta = 10^{-5}$ at room temperature to compare with the value of about 9×10^{-4} for a silicone liquid gum measured by Baker and Waddington,[25] rising to about $\tan \delta = 7 \times 10^{-5}$ at the loss peak. The temperatures for maximum $\tan \delta$ for audiofrequencies very closely approximate the temperatures of the n.m.r. transition as shown in Fig. 1. No observable change in $\tan \delta$ is detectable in the region of the crystalline melting point. Figure 3 also shows the usual Arrhenius plots of the dielectric data yielding an activation energy of 37 kcal./mole. This energy is about fivefold larger than the corresponding n.m.r. activation energy. Detailed correlations between n.m.r. and dielectric loss activation energies have not been made, but a variety of investigations have shown that, in general, dielectric loss activation energies are several factors larger and that their trends within homologous series are similar to energies derived from n.m.r. line narrowing data.[26] The absence of any noticeable dielectric effect at the crystal melting point also indicates a high degree of motional freedom in the crystalline state.

Conclusions

The data force a conclusion which is new to classical ideas of polymer physics: namely, that translational motion of an appreciable magnitude occurs in polymer crystals below the crystal melting temperature. This motion is in addition to the accepted rotational motions. When this conclusion was first arrived at there seemed to be no other evidence for such a phenomenon. Since that time however strong support for this thesis has arisen from the work of Statton.[27] He has reported that the annealing of single crystals of polyethylene below their melting points results in an increased thickness of the crystal. This observation

---

(22) C. M. Huggins, L. E. St. Pierre and A. M. Bueche, This Journal, **64**, in press (1960).

(23) The dielectric measurements were made by S. I. Reynolds and D. J. Kaswinkel to whom the authors wish to express their gratitude.

(24) It should be observed that the lightly crosslinked sample used in the dielectric measurements is not identical to the sample used for the n.m.r. measurements. The n.m.r. and dielectric effects due to cross-linking have been studied in detail[22] and while changes are observed, they are not considered germane to the arguments in this paper.

(25) W. P. Baker and F. B. Waddington, *J. Sci. Instr.*, **36**, 309 (1959).

(26) (a) J. G. Powles and K. Luczcynski, *Physica*, **25**, 455 (1959); (b) A. Odagima, "Reports on Progress in Polymer Physics."

(27) W. O. Statton, *J. Chem. Phys.*, in press.

can be explained only by assuming translational motion of polymer chains in the crystals.

Acknowledgments.—The authors wish to thank Mr. D. R. Carpenter for performing a large part of the n.m.r. measurements. They are also indebted to Dr. A. C. Martellock for supplying the silicone sample. The helpful discussions with Drs. Bruno Zimm and F. P. Price are appreciated. Miss Ann Warner was most helpful in some of the numerical calculations.

THE EFFECTS OF A CHLORATE IMPURITY ON THE THERMAL STABILITY OF AMMONIUM PERCHLORATE[1]

BY J. C. PETRICCIANI, S. E. WIBERLEY, W. H. BAUER AND T. W. CLAPPER

Department of Chemistry, Rensselaer Polytechnic Institute, Troy, New York, Research Department, American Potash and Chemical Corporation, Henderson, Nevada

Received April 9, 1960

Differential thermal analysis was used to determine the effect of chlorates on the thermal decomposition of ammonium perchlorate. When 0.1% potassium or sodium chlorate was added as an impurity, the decomposition temperature of ammonium perchlorate was lowered approximately 150°. The differential thermal analysis technique is sensitive to 0.001% chlorate impurity in ammonium perchlorate. The amount of chlorate present in the ammonium perchlorate also can be determined colorimetrically with the same degree of accuracy. Chlorate impurities in ammonium perchlorate also can be determined by infrared absorption techniques; but the minimum amount detectable is in the region of 0.8%. A general theory is presented to account for the marked effect that chlorates have upon the thermal decomposition of ammonium perchlorate.

Introduction

Ammonium perchlorate is an extremely strong oxidizing agent and is used as the crystalline inorganic oxidizing agent in the composite propellant type of solid rocket fuels. Since the presence of chlorates was thought to cause a premature decomposition of ammonium perchlorate, the main objective of this investigation was to determine the effect of a chlorate impurity on the thermal stability of ammonium perchlorate.

Materials and Methods

Ammonium perchlorate obtained from the Fisher Scientific Company was analyzed colorimetrically and found to contain less than 0.001% chlorate impurity.[2] The Fisher ammonium perchlorate was used as the starting material without further purification since it contained a negligible amount of chlorate as compared with the amount of chlorate added in preparing the samples. Samples of ammonium perchlorate containing 0.01, 0.05, 0.10, 0.50, 1.00, 5.00 and 10.00% chlorate impurity were prepared from the starting material. The chlorate was designated as weight per cent. potassium chlorate in ammonium perchlorate. The samples were prepared by introducing the chlorate, as a potassium chlorate solution, to a solution of the starting material. The final solution was slowly evaporated to dryness. The final dry weight was approximately 20 g.

It was thought desirable to have a sample of ammonium perchlorate which was free from even a trace of a chlorate impurity to be used as the basis for the comparison with ammonium perchlorate containing chlorates as an impurity. Approximately 40 g. of the Fisher ammonium perchlorate, containing less than 0.001% chlorate, was recrystallized three times from water. The ammonium perchlorate thus obtained was analyzed colorimetrically and found to be free of any trace of a chlorate impurity.[2] Table I lists the percentage of chlorate impurity in each sample as found by colorimetric analysis.[2]

TABLE I

WEIGHT % KClO$_3$ IN SAMPLES

Sample no.	% KClO$_3$ added	% KClO$_3$ analyzed
1	0.000	0.000
2	.002	.001
3	.010	.009
4	.050	.040
5	.100	.082
6	.500	.370
7	1.000	.870
8	5.000	...
9	10.000	...

The apparatus and procedure used were similar to those developed by Gordon and Campbell.[3] Finely divided silica which previously had been heated to 600° and cooled to room temperature was used as the reference substance. A length of thin-walled Pyrex glass tubing drawn out at one end was used as a thermowell. The copper block was nickel-plated in order to prevent oxidation at the high temperatures.[4] The differential temperature was plotted by a Sargent recorder as a function of time. The sample temperature, measured by means of a thermocouple and a potentiometer, was recorded at intervals which corresponded to respective timing marks of the chart on which the differential temperature was recorded. The recorder was set at a total span of 5 millivolts. A chart speed of 0.2 inch per minute was found to be suitable. A constant heating rate of about 7° per minute was attained with this equipment. The limit of error in reading the potentiometer was ±0.1 mv., or ±2°. The graph on the Sargent recorder could be read to the nearest 0.01 mv., an error of ±0.2°.

The infrared spectra of the samples containing chlorates, pure ammonium perchlorate and pure potassium chlorate were determined with a Perkin-Elmer Model 21 Recording Infrared Spectrophotometer using the KBr technique.[5] Several low percentage chlorate samples were measured using as much as 7 mg. in 100 mg. of KBr in an attempt to get the chlorate absorption band to appear, but the perchlorate absorption band merely spread out and covered any increased absorption due to the chlorate ion. The 0.5 mg. per 100 mg. of KBr concentration was used for the subsequent spectra since the resolution of the perchlorate band was very good at that concentration.

---

[1] Based on a thesis by John C. Petricciani submitted to the Department of Chemistry, Rensselaer Polytechnic Institute, in partial fulfillment of the requirements for the degree of Bachelor of Science, May, 1958, and a Research Project at American Potash and Chemical Corporation, August, 1957.

[2] C. Eger, *Anal. Chem.*, **27**, 1199 (1955).

[3] S. Gordon and C. Campbell, *Anal. Chem.*, **27**, 1102 (1955).

[4] R. A. Powers and N. Hackerman, THIS JOURNAL, **56**, 187 (1952).

[5] M. M. Stimson and M. J. O'Donnell, *J. Am. Chem. Soc.*, **74**, 1805 (1952).

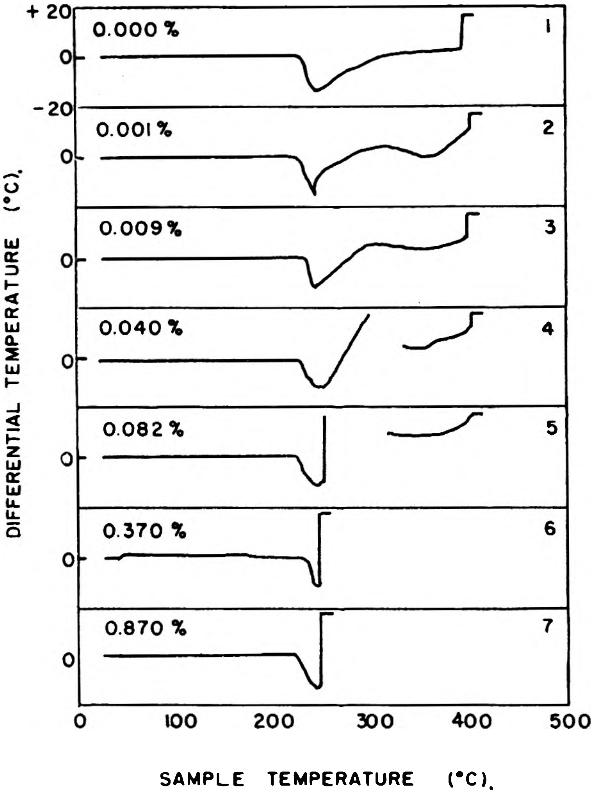

Fig. 1.—Differential thermal analysis curves: the percentage of $KClO_3$ and the sample number are shown at the beginning and end of each curve, respectively. The limit of the ΔT scale for each curve is $+20$ and -20 above and below the baseline, respectively.

Experimental Results

The representative D.T.A. curves presented in Fig. 1 clearly indicate the presence of an increasingly strong exothermal reaction after lattice transition (244°) as the amount of chlorate impurity increases. Detectable decomposition occurs only after the lattice transition in all the samples tested. In the region of 0.1% potassium chlorate impurity, the heat evolved after lattice transition is great enough to initiate complete thermal decomposition of the sample. This is an effective 150° lowering of the thermal decomposition temperature of pure ammonium perchlorate, which decomposes at 400°. A comparison of the D.T.A. curve for pure ammonium perchlorate with that shown by Gordon and Campbell[3] indicates that their sample may have contained chlorate as an impurity. Markowitz[6] also has pointed out that the decomposition of potassium perchlorate proceeds partially through a chlorate intermediate.

Decomposition is indicated by the abrupt change in the differential temperature at the end of each curve in Fig. 1. Curves 4 and 5 of Fig. 1 are discontinuous because the heat evolution after lattice transition was too rapid to follow accurately. Since the furnace was heating at a constant rate of 7° per minute and did not reach the sample temperature for several minutes, the sample cooled somewhat after reaching its peak temperature for those cases. The curve was resumed at the point where the sample temperature began to increase again.

The infrared spectra of ammonium perchlorate, potassium chlorate and a 5% potassium chlorate sample are presented, in Fig. 2. The absorption band due to the chlorate ion (990–960 cm.$^{-1}$) does not interfere with that of the perchlorate ion (1160–1060 cm.$^{-1}$). The 5% potassium chlorate sample shows the chlorate absorption band along with the ammonium perchlorate spectra. However, the appearance of the chlorate absorption band in a sample of ammonium perchlorate containing chlorates did not occur below 0.8% chlorate. This precludes using the infrared method as a rapid analytical technique for the determination of trace amounts of chlorate in ammonium perchlorate.

A comparison of the infrared spectrum obtained for ammonium perchlorate with that presented by Miller and Wilkins shows that the absorption bands are more distinct and sharper using a KBr window than with Nujol.[7] The most distinct difference is the resolution of the perchlorate absorption band of Miller and Wilkins into three components.[7]

Discussion

A discussion of the decomposition of pure ammonium perchlorate is presented by Bircumshaw and Newman, and an electron transfer mechanism for the decomposition is suggested.[8] The region of 0 to 1% potassium chlorate is considered in the following discussion and a solid solution of potassium chlorate in ammonium perchlorate is assumed.

As in the case of the perchlorate ion, an electron transfer from a chlorate ion to an interstitial ammonium ion seems probable as the initial step in decomposition

$$ClO_3^- + NH_4{}^+{}_{\text{interstitial}} \longrightarrow NH_4\cdot + ClO_3\cdot$$
$$NH_4\cdot \longrightarrow NH_3 + H\cdot$$

Although Bircumshaw and Newman suggest that the chlorate radical is stable within the crystal lattice and may function as an electron trap similar to a corresponding perchlorate radical, it seems quite unlikely that a chlorate radical would not decompose in the temperature range of the lattice transition of ammonium perchlorate in view of the fact that ammonium chlorate itself is unstable in the region of 100°. The following steps are tentatively proposed as likely in the decomposition of the chlorate radical, where reaction 1 is about thermally neutral

$$ClO_3\cdot \longrightarrow ClO\cdot + O_2 \qquad (1)$$
$$ClO\cdot + H_2O \longrightarrow H_2ClO_2 \qquad (2)$$
$$H_2ClO_2 + ClO\cdot \longrightarrow HClO_3 + HCl \qquad (3)$$

The H_2O in reaction 2 appears as a decomposition product of perchlorate and ammonium ions in the mechanism of Bircumshaw and Newman. This, then, is a possible route for the formation of both chloric and hydrochloric acids which are listed among the decomposition products.[8] Another possibility is the reaction of two ClO radicals to form

---

(6) M. M. Markowitz, This Journal, **61**, 505 (1957).

(7) F. A. Miller and C. H. Wilkins, *Anal. Chem.*, **24**, 1283 (1952).

(8) L. L. Bircumshaw and B. H. Newman, *Proc. Roy. Soc. (London)*, **A227**, 228 (1955); **A227**, 115 (1954).

chlorine and oxygen, both of which are also listed among the decomposition products.[8]

$$\mathrm{ClO\cdot} + \mathrm{ClO\cdot} \longrightarrow \mathrm{Cl_2} + \mathrm{O_2} \quad 74 \text{ kcal.}$$

Although complete thermal data for all the reactions are not available, a moderate over-all exothermal effect seems probable.

A comparison of the decomposition scheme for pure ammonium perchlorate as presented by Bircumshaw and Newman, and that just described for ammonium perchlorate containing a chlorate impurity results in these conclusions:

1. The production of a chlorate radical requires three steps in pure ammonium perchlorate, while only one step is needed in the cases where chlorates are present.
2. Sublimation competes with decomposition in both the pure and chlorate-contaminated case, but sublimation is reduced in the latter because of the possibility of the potassium ion replacing the ammonium ion, in which case proton transfer is impossible.
3. Decomposition occurs mainly on the surface of the crystal in pure ammonium perchlorate with the elimination of a perchlorate radical. A chlorate radical is not required to be on the surface in order to decompose according to the decomposition scheme just described. More pronounced decomposition within the crystal should be evident in the chlorate containing case, and the heat lost to the outside will be less.

The above considerations suggest that decomposition should be more pronounced in ammonium perchlorate containing a chlorate impurity than in the pure compound.

The decomposition reaction appears to take place only after lattice transition. The transition is from the orthorhombic to the cubic form and subsequently the lattice distances are reduced.[8] During the lattice transition the ammonium ions, especially those which are interstitial, may have a better chance of interacting with both the perchlorate and chlorate ions, which initiates decomposition as previously indicated.

Curve 1 of Fig. 1 shows only a slight tendency toward an exothermic reaction after lattice transition, as indicated by the gentle rise of the differential temperature baseline ($\Delta T/T$ = approximately 0.03). This, however, may be attributed to a change in the specific heat of the ammonium perchlorate after lattice transition. A movement of the differential temperature baseline greater than about 3° over a sample temperature range of 100° was thought to be significant in view of the above.

Curve 2 of Fig. 1 indicates that 0.001% chlorate impurity can be detected by D.T.A. A change in specific heat of the sample after lattice transition would account for an increasing baseline, but the baseline of curve 2 increases more rapidly than would be expected from the specific heat effect which was evident in curve 1. Moreover, a maximum is reached in curve 2 which can be explained only on the basis of an exothermic reaction in the sample, especially in view of the fact that in samples containing increasing concentrations of chlorate impurity a more and more pronounced heat evolution appears in the same region as indicated in curve 2.

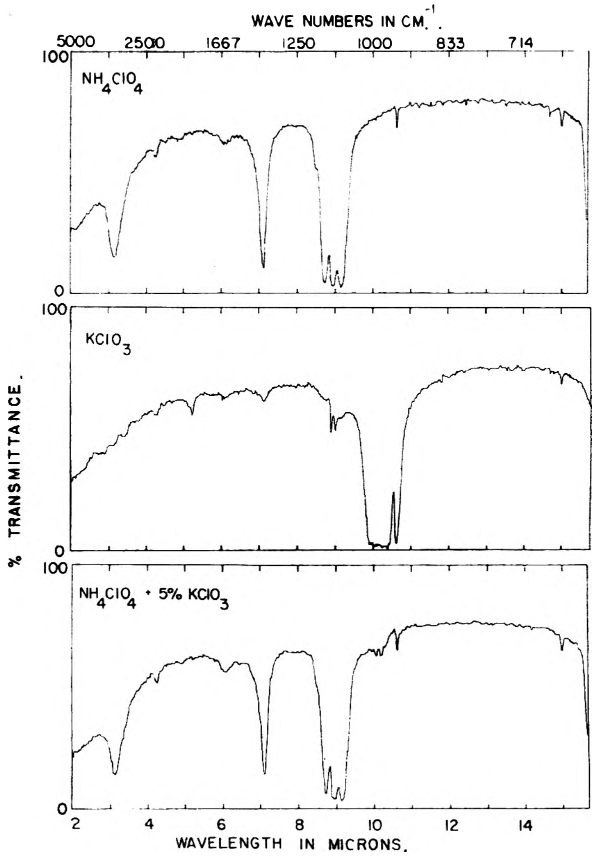

Fig. 2.—Infrared spectra of NH_4ClO_4, $KClO_3$ and NH_4ClO_4 containing 5% $KClO_3$.

It is assumed that decomposition in the 200–300° region occurs largely through elimination of perchlorate radicals produced on the surface of the crystals, and only slightly through the mechanism which would produce a chlorate radical in the interior. Decomposition involving the chlorate radical is suggested for curves 2 through 5 of Fig. 1. The exothermic tendency increases with the amount of chlorate impurity as would be expected according to the scheme presented. Finally, in the region of 0.1% chlorate impurity, the heat evolved due to the combined effects of chlorate and perchlorate decomposition becomes sufficient to induce thermal breakdown of the ammonium and perchlorate ions themselves, and complete decomposition results as is evident in curve 6 of Fig. 1.

No attempt was made to determine any of the thermodynamic properties of any of the decomposition intermediates, but such data would be helpful in a critical analysis and evaluation of the decomposition scheme proposed.

DIAMAGNETIC SUSCEPTIBILITIES OF SIMPLE HYDROCARBONS AND VOLATILE HYDRIDES

By C. Barter, R. G. Meisenheimer and D. P. Stevenson

Shell Development Company, Emeryville, California

Received April 11, 1960

The use of a Pauling Type oxygen meter in the measurement of the diamagnetic susceptibility of gases at subatmospheric pressure and ambient temperature is described. The method has been tested on the rare gases, and applied to measurements on nineteen light ($\leq C_5$) hydrocarbon gases, diborane, ammonia, silane, phosphine, germane, arsine, stibine and methyl fluoride. The results obtained on the various gases are compared with the results of previous measurements and/or values deduced by various extrapolation procedures from measurements on more complex substances in the liquid or solid state.

Introduction

In connection with studies of the relation between the cross sections for ionization by electrons and the constitution and the structure of molecules[1] it became of interest to compare the ionization cross sections with a molecular property directly related to the mean square electronic radius. Such a molecular property is the diamagnetic susceptibility.[2] Fano[3] has suggested that there should exist a proportionality between the diamagnetic susceptibilities of substances and their cross sections for ionization by high energy electrons. A search of the literature[4] revealed the virtual absence of data suitable for comparing the constitutive and structural dependence of diamagnetic susceptibilities and ionization cross sections. Although measurements of the diamagnetic susceptibilities have been reported for an extraordinary number of complex substances, there have not been reported results of measurements on simple, normally gaseous substances of the type particularly suitable for examining the constitution and structural dependence of these molecular properties. The work reported in the present paper eliminates in part this gap in the knowledge of the diamagnetic susceptibilities.

Consideration of the very small magnitude of the effects associated with diamagnetism, quickly reveals why virtually no measurements of the diamagnetic susceptibility of gases have been reported in the past. However, the development of the High Sensitivity (Pauling) Oxygen Meter by the A. O. Beckman Company makes readily available an instrument suitable for the quantitative comparison of the diamagnetic susceptibility of gases even at subatmospheric pressures. In this paper we present the results of measurements of the diamagnetic susceptibilities of nineteen light ($<C_6$) gaseous hydrocarbons, as well as those of diborane, ammonia, silane, phosphine, germane, arsine and stibine made with one of these instruments. The instrument was calibrated and the method tested on the rare gases.

In addition to the results of measurements on the gases indicated above, there are reported for the first time measurements on the liquid cyclanes, cycloheptane, and cyclododecane made by the conventional Gouy technique.[5] There also are reported measurements on several of the light hydrocarbons in the liquid state that were made with the object of providing information on the effect of the state of aggregation on the diamagnetic susceptibilities of substances.[6]

Experimental

As is reasonably well known, Pauling Oxygen Meters, such as the A. O. Beckman Company Model E-2, consist of a small rotor suspended on a quartz fiber in a strong, inhomogeneous magnetic field.[7] A force due to the magnetic field that is proportional to the difference between the magnetic susceptibility of the rotor and that of its surrounding medium (gas) tends to displace the rotor from its equilibrium position. The Model E-2 is constructed with a pair of vanes to which there may be applied a continuously variable electric potential that gives rise to an opposing force by means of which the rotor may be restored to its null position. The position of the rotor is observed by means of a light beam reflected from a small mirror, that is attached to the supporting quartz fiber, on to a graduated scale. The magnitude of the potential necessary to restore the rotor to its null position is directly proportional to the magnetic susceptibility of the medium surrounding the rotor. In the present use, for measurement of diamagnetic gases, it was of course necessary to reverse the polarity of the restoring potential between vanes and rotor from its normal sense that obtains when the instrument is used in the measurement of the concentration of oxygen or other paramagnetic gases.

The instrument was attached to a conventional gas handling vacuum (mercury diffusion pump and "Hyvac" fore pump) bench. That the cell containing the rotor and connections were vacuum tight was established by showing that after evacuation and closing the stopcock leading to the diffusion pump the rotor showed no systematic "paramagnetic drift" during a time comparable with that necessary to make a series of measurements on a sample of a substance. In order to achieve this vacuum-tight condition of the rotor cell it was found necessary to turn off the heater that normally operates to keep the cell above ambient temperature. All measurements were made with the cell at room temperature ranging from 20 to 26°. The procedure of bracketting measurements on a sample of interest between calibrating measurements on a primary or secondary standard substance assures that the lack of thermostating introduces no significant error in the measurements herein reported.

A series of measurements on a sample of a substance consisted of determining the restoring potential (in potentiometer scale division), V, necessary to return the rotor to null at a series of decreasing pressures of the substance in the cell. The series was deemed satisfactory if the plot of V, the restoring potential, *vs.* p, the sample pressure in cm., consisted of a straight line through the origin. The graphically determined slope, V' (scale divisions per cm. pressure), of the restoring potential *vs.* pressure line for such a series of measurements was taken as a direct measure of the relative diamagnetic susceptibility of the substance. The results of

---

[1] J. W. Otvos and D. P. Stevenson, *J. Am. Chem. Soc.*, **78**, 546 (1956).

[2] J. H. Van Vleck, "Electric and Magnetic Susceptibilities," Oxford Press, Oxford, 1932, p. 275.

[3] U. Fano, *Phys. Rev.*, **70**, 44 (1946).

[4] See particularly the comprehensive review, A. Pacault, "Les Systematiques Magnetochemiques," *La Revue Scientifique*, **86**, 38 (1948).

[5] Selwood, "Magnetochemistry," 2nd Ed., Interscience Publishers, New York, N. Y., 1956, p. 3-10.

[6] See ref. 5, p. 90-91.

[7] See ref. 5, p. 248 *et seq.*

TABLE I

MAGNETIC SUSCEPTIBILITIES OF THE RARE GASES

		$-\chi \times 10^6$ c.g.s. emu./mole			
	Helium (8^a)	Neon (5^a)	Argon (7^a)	Krypton (6^a)	Xenon (6^a)
This research[b]	2.02 ± 0.08	6.96 ± 0.14	(19.32)[c]	29.0 ± 0.4	45.5 ± 0.7
Havens[d]	1.91	7.65	19.23	..	..
Mann[e]	..	6.76	19.54	28.02	42.40
Abonnenc[f]	..	..	19.2	29.2	44.1
Wills and Hector[g]	1.88	6.66	(18.13)[h]	..	..

[a] Number of series of measurements on substance in this research. In all cases Linde "Spectroscopically Pure Grade" gases were used. [b] Uncertainties are standard deviations from the arithmetic mean value of the n^a series of measurements. [c] Unweighted arithmetic mean of values[d,e,f] taken in calibrating the instrument. [d] G. G. Havens, *Phys. Rev.*, **43**, 992 (1933). [e] K. E. Mann, *Z. Physik*, 98, 548 (1936). [f] L. Abonnenc, *Compt. rend.*, **208**, 986 (1939). [g] A. P. Wills and L. G. Hector, *Phys. Rev.*, **23**, 209 (1924); **24**, 418 (1924). [h] Not included in average[c] used to calibrate the instrument.

typical series of measurements on n-butane and argon are shown in Fig. 1.

The measurements were carried out over a period of about six months duration. As indicated above, measurements on samples of interest were bracketted by measurements on a secondary standard substance, n-butane. In all, 33 sets of measurements were made on n-butane and there was no evidence of systematic variation in the instrument sensitivity constant, V' (n-butane). The arithmetic mean value of V' (n-butane) for the 33 series of measurements was equal to 24.90 div./cm., with a standard deviation from the mean $\delta = \pm 0.40$ div./cm. On the basis of these results we assign the error of measurements on substances to be ± 0.4 div./cm. or ±1.6%, whichever is the larger.

Argon was chosen as the gaseous substance, readily available in a high state of purity, most suitable as the primary standard for calibration of the instrument. As may be seen by reference to Table I, the three most recent determinations of $-\chi_{\text{molar}}$ (Ar) give $19.32 \pm 0.15 \times 10^{-6}$ c.g.s. emu./mole as the best diamagnetic susceptibility for this substance. Seven series of measurements on argon with the Model E-2 gave $V' = 9.57 \pm 0.07$ div./cm., from which we compute the instrument sensitivity constant to be 1 div./cm. equals $-(2.02 \pm 0.01) \times 10^{-6}$ c.g.s. emu./mole.

As an over-all test of the method, measurements were made on the other four rare gases as summarized in Table I. There is no evidence in these data of systematic error in the method. The "high" value we find for xenon may be attributed to greater purity of our sample of xenon that was shown to be free of any diluent.

It should be noted that efforts to make measurements on gaseous hydrogen were unsuccessful. With hydrogen in the cell it was not found possible to establish a stable null of the rotor. This difficulty is believed to have been caused by a reversible chemisorption of hydrogen by the rhodium plate on the rotor causing the effective magnetic susceptibility of the rotor to change more or less continuously with time of exposure to hydrogen. This difficulty could no doubt be overcome by the substitution of some other inert metal (such as gold) as the necessary conducting surface of the rotor.

As is indicated in the footnotes of Table I, the measurements on rare gases were made on Linde Co. spectroscopically pure grade samples. Previously unopened flasks were employed. After use, the residual contents of the flasks were checked mass spectrometrically for identity and purity. In no case was as much as 0.01% in oxygen or nitrogen found in a flask. The hydrocarbons were in all cases taken from the Spectroscopic Department Bank of pure substances after mass spectrometric test for identity and purity. The samples of diborane, silane, germane and methyl fluoride were prepared and purified by standard methods by Mr. E. R. Bell of the Chemical Physics Department. The phosphine, arsine and stibine were made by acid hydrolysis of calcium phosphide, zinc arsenide and a magnesium–antimony alloy, respectively. These latter three substances were purified by simple trap to trap distillation on the vacuum bench. Ammonia was obtained from a commercial cylinder of the liquid. As with the hydrocarbons, all samples of these latter substances were checked mass spectrometrically for both identity and purity.

The liquids used for these susceptibility measurements were treated to free them of dissolved gases. Each liquid was subjected while in the Gouy tube to repeated freeze–thawing and it was evacuated in each cycle while frozen. The sample tubes finally were sealed under vacuum while the hydrocarbon was frozen. The susceptibility measurements were made at room temperature. A sufficient number of independent measurements was made to reduce the statistical deviations to the values reported in Table II. For calibration purposes there was taken -0.720×10^{-6} c.g.s. emu./gram as the mass susceptibility of water.

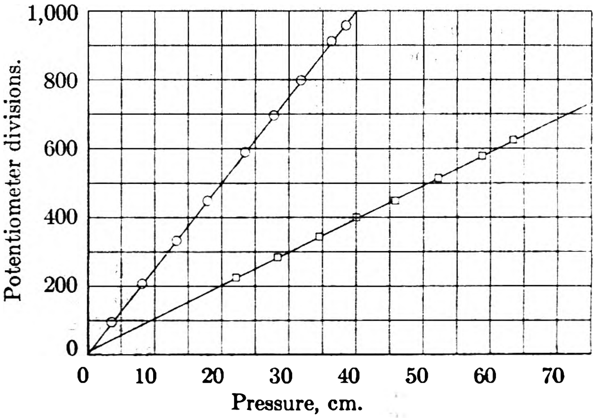

Fig. 1.—The results of typical series of measurements of the Model E-2 oxygen meter response to various pressures of n-butane and argon: ○, n-butane: □, argon.

Results and Discussion[8]

In Table II there are summarized the results of our measurements on saturated hydrocarbons and in Table III there are summarized the results for unsaturated hydrocarbons. In these two tables there are also listed for convenience of reference previously published results of other workers on the substances we examined as well as some pertinent data on homologs of these substances. The only previously reported measurements on gaseous hydrocarbons are those of Bitter.[9] It was the inconsistency of Bitter's results with any kind of extrapolation from data on higher homologs that caused us to include the study of gaseous alkanes and unsaturates in this investigation. Our results on ethane and propane are in reasonable agreement with Bitter's determinations for these two substances, the two results of Bitter that were not inconsistent with the values that had been reported for heavier hydrocarbons. Accepting our values for the susceptibilities of methane, acetylene and ethylene as reasonable, the low values found by Bitter readily can be accounted for by the assumption that his samples of these materials contained the order of 0.5 to 1.0% air, since the paramagnetic

---

(8) Throughout this section of this paper we will for convenience quote in the text values of the molal diamagnetic susceptibilities of substances as multiples of the unit -1×10^{-6} c.g.s. emu/mole.

(9) Table II, footnote *b*.

TABLE II

DIAMAGNETIC SUSCEPTIBILITIES OF SATURATED HYDROCARBONS

Hydrocarbon	Gas		Liquid					Calcd.	
	a	b	a	c	d	e	f	g	h
Methane	17.4 ± 0.8	12.2						16.42	
Ethane	26.8 ± .8	27.3						27.88	26.90
Propane	38.6 ± .8	40.5				39.6		39.34	38.58
n-Butane	50.3 ± .8	57.4	50.0 ± 0.5					50.80	50.26
n-Pentane	61.5 ± 1.0		63.3 ± 1.0	63.05				62.26	61.94
n-Hexane				74.05		75.6[i]	73.63	73.72	73.62
n-Heptane				85.24			85.38	85.18	85.30
n-Octane				96.63	96.47		96.93	96.64	96.98
n-Nonane				108.13	108.00			108.10	108.66
n-Decane				119.51	119.74			119.56	120.34
n-Undecane					131.84			131.02	132.02
n-Hexadecane				187.63				188.32	190.42
Isobutane	50.5 ± 0.8	56.3				51.7			51.15
Isopentane	63.0 ± 1.0			64.40					62.84
Neopentane	63.0 ± 1.0					63.1			63.28
Cyclopropane	39.2 ± 0.8							34.38	35.04
Cyclobutane	40.0 ± .8							44.84	46.72
Cyclopentane	56.2 ± .8			59.2				57.30	58.40
Cyclohexane				65.1		66.9[i]		68.76	70.08
Cycloheptane			73.9 ± 0.1					80.22	81.76
Cycloöctane			85.3 ± .1			91.4[i]		91.68	93.44
Cyclododecane			132.5 ± .2(Xtal)					137.52	140.16

[a] This research. [b] F. Bitter, *Phys. Rev.*, **33**, 389 (1929). [c] S. Broersma, *J. Chem. Phys.*, **17**, 873 (1949). [d] V. C. G. Trew, *Trans. Faraday Soc.*, 49, 604 (1953). [e] J. R. Lacher, *et al.*, *J. Am. Chem. Soc.*, **73**, 2838 (1951). [f] W. R. Angus, G. I. W. Llewelyn and G. Stott, *Trans. Faraday Soc.*, **55**, 887 (1959). [g] Calculated from the least squares equation, $\chi(n - C_mH_{2m} + 2) = 11.46m + 4.96$ based on all data except (b) and (i). Standard deviation, 22 data, $\delta = \pm0.59$, or for liquids only, 17 data, $\delta = \pm0.49$. [h] Calcd. from constant of ref. *f*. Standard deviation of 25 data (excluding b) $\delta = \pm0.86$, or for alkanes including those listed in ref. *f* but not in the table, 51 data in all, $\delta = \pm0.70$. [i] R. C. Pink and A. R. Ubbelohde, *Trans. Faraday Soc.*, **44**, 708 (1948).

TABLE III

DIAMAGNETIC SUSCEPTIBILITIES OF UNSATURATED HYDROCARBON VAPORS

Hydrocarbon	$-\chi \times 10^6$ c.g.s. emu./mole			Pascal and Pacault
	a	b	(Liq.) c	
Acetylene	20.8 ± 0.8	12.5		17.1
Ethylene	18.8 ± .8	12.0; 15.3[d]		18.3
Allene	25.3 ± .8			24.3
Propylene	30.7 ± .8		31.5	30.1
1,2-Butadiene	35.6 ± .8			36.1
1,3-Butadiene	32.1 ± .8			31.0
1-Butene	41.0 ± .8			42.0
Isobutylene	40.8 ± .8		44.4	42.0
trans-2-Butene			43.3	42.0
cis-2-Butene			42.6	42.0

[a] This research. [b] See footnote *b* of Table II. [c] See footnote *c* of Table II. [d] V. I. Vaidhianathan, *Ind. J. Phys.*, **3**, 165 (1928).

susceptibility of oxygen is −3,400 in our present units at room temperature. An even lower air impurity concentration would account for the discrepancy in the case of Vaidhianathan's measurement on ethylene. We can offer no explanation of the origin of the error in Bitter's measurements on the butanes. Our values for these gases are not only reasonable but they are confirmed by the results of measurements on the liquids by different methods.

It has been recognized for many years[4] that the dependence of the magnetic susceptibilities of the alkanes on composition and structure cannot be represented in terms of the classical hypothesis of simple additivity of atomic susceptibilities proposed many years ago by Pascal. Trew[10] proposed that the susceptibilities of the alkanes could be represented in terms of the sum of contributions of the four groups $-CH_3$, $>CH_2$, $-\overset{|}{C}H$ and $-\overset{|}{\underset{|}{C}}-$, of which all alkanes except methane may be thought to be constituted, plus a correction term for positional isomerism and end effects. More recently, on the basis of a larger collection of data, Angus and co-workers[11] have concluded that only terms for the four groups are needed and that there existed no sound basis for assuming either positional isomerism effects or end effects. In column *h* of Table II there are listed the values of the susceptibilities calculated from the values assigned to the four group constants by Angus and co-workers,[11] CH_3 (13.45), CH_2 (11.68), CH (10.80) and C (9.48). The results of our measurements on ethane, propane, *n*-butane, isobutane, *n*-pentane, isopentane and neopentane[12] are seen to be in excellent agreement with the calculated (column *h*) values, and thus appear to substantiate the view that small molecule end effects are indeed negligible in the case of diamagnetic susceptibilities of alkanes.

It is of interest to note that for the normal alkanes alone a two-constant expression of the form

$$\chi(n - C_mH_{2m} + 2) = A_m + B \qquad (1)$$

not only permits the inclusion of methane as a

---

(10) Footnote *a* of Table II.

(11) Footnote *f*, Table II.

(12) Compare also for propane, isobutane and neopentane, Lacher, *et al.*, footnote *e* of Table II.

member of the series,[13] but also gives a statistically better fit of the observations. The results of calculations based on eq. 1 with $A = 11.46$ and $B = 4.96$ are given in column *g* of Table II.[14] Our values of A and B would correspond to changing the group constants for methyl and methylene to 13.94 and 11.46, respectively, from Angus and co-workers[11] values of 13.45 and 11.68. The difference between these constants arises from the fact that Angus and co-workers[11] selected the susceptibilities of particular substances to be used to evaluate the constants, while we obtained a least squares set of constants from all the data on *n*-alkanes, giving all measurements equal weight. The Angus constants appear to give the better fit at low carbon number while our constants give a better fit at the upper end-point, namely, *n*-hexadecane.

In the case of the results for the cycloalkanes shown in Table II there are two unexpected observations. The first of these is that the sign of the difference between the observed susceptibility of cyclopropane from that calculated from an additivity hypothesis is the opposite of that deduced for this structure from measurements on relatively complex derivatives.[15] The second observation, surprising at least to us, is the fact that the difference between the observed diamagnetic susceptibilities of the large ring compounds and the value calculated from the "CH_2-increment" found from alkanes, appears to be independent of ring size. Interestingly enough the molar refractions (electric polarizabilities) and the chemical shift of the proton magnetic resonance frequency of the cycloalkanes show a dependence on ring size that parallels that of magnetic polarizability. This statement is illustrated by the summary of "differences" shown in Table IV. If one were to accept the results of Pink and Ubbelohde[14] on cyclohexane and cyclooctane the preceding statements would become invalid. As indicated in footnote 14 we feel the origin of the discrepancies between the results of Pink and Ubbelohde and those of other workers are the result of systematic error in the results of Pink and Ubbelohde. Mass and infrared spectra in addition to the usual physical properties were employed as criteria for the purity and authenticity of our cycloheptane, cycloöctane and cyclododecane.

As may be seen from a comparison of the numbers in columns 2 and 5 of Table III, the Pascal–Pacault constants for the atoms and structure correction constants provide a good representation of the diamagnetic susceptibilities of the lower olefins, allene and the butadienes, indicating the absence of small molecule end effects for these homologous series. However, acetylene like cyclopropane has a significantly larger diamagnetic susceptibility than that calculated from data on more complex substances containing this particular structural unit.

TABLE IV

COMPARISON OF CYCLOALKANE PROPERTIES WITH *n*-ALKANE PROPERTIES

Cycloalkane	$[(-\chi - 11.68m]$	$[R - 4.64m]^a$	ΔH, c./sec.[c]
Cyclopropane	+4.2 (gas)	+0.08	+50
Cyclobutane	−6.7 (gas)	− .32	−24
Cyclopentane	−2.2 (gas); +0.8 (liq.)	− .06	0
Cyclohexane	−5.0 (liq.)	− .12	0
Cycloheptane	−7.9 (liq.)	− .39	− 8
Cycloöctane	−8.1 (liq.)	− .46	− 7
Cyclononane	....	....	− 6
Cyclodecane	....	− .91	− 6
Cyclododecane	−7.7 (Xtal)	− .63[b]	..

[a] The molar refraction $R = (n_0^2 - 1)/(n_0^2 + 2) \times V$. 4.64 is the average CH_2-increment for R (*n*-alkanes) from N.B.S. circular No. C-461. [b] For this substance, n^{70}_D 1.4536 and D^{70}_4 0.8273 g./ml. were determined in our Analytical Dept. under the direction of W. R. Harp, Jr. [c] The nuclear magnetic resonance proton chemical shift from the corresponding *n*-alkane, measured at 40 Megacycles by Dr. C. A. Reilly of these laboratories. Uncertainty of measurement estimated to be ± 1 to ± 2 c./sec.

No definitive conclusion can be reached with respect to the question of the effect of state of aggregation on the diamagnetic susceptibility from the data in Tables II and III. Considerably greater precision than we have been able to achieve in the measurements on gases would be required to assure that the apparent effect, $|\chi \text{ gas}| < |\chi \text{ liq.}|$, is real. This is in agreement with earlier conclusions of Selwood.[6] Certainly the general quality of the agreement between our measurements for the lower hydrocarbons with the values calculated from the group constants of Angus based on liquids, suggests that there is no real difference between gaseous and liquid values of this molecular quantity.

There are summarized in Table V data on the diamagnetic susceptibilities of gaseous hydrides more or less isoelectronic with rare gases. For comparison with the experimental values shown in columns 2 and 3 of this Table V, there are given in columns 4 and 5 susceptibilities calculated under the hypothesis that the quantity is a constitutive molecular property. In column 4 there are given the sums of the atomic susceptibilities per mole calculated from the Van Vleck equation[2]

$$\chi \text{ atom} = -\frac{6.02 \times 10^{23} e^2}{6mc^2} \sum_i \langle r^2 \rangle \qquad (2)$$

where $\langle r_i^2 \rangle$, is the mean square radius of the ith atomic electron, as evaluated for Slater electronic wave functions for the atoms.[16] In column 6 there are given the sums of the Pascal constants[4] for the atoms. It appears that for elements of any row of the periodic system, the deviation from additivity of the diamagnetic susceptibility increases with the distance of the "central atom" of the molecule from the rare gas atom. Further in the hydrides of any group of the periodic system the

---

(13) Methane becomes a fifth group of one member in the Angus, *et al.*, formulation.

(14) The datum of Pink and Ubbelohde (ref. *i*, Table II) on *n*-hexane was not included because it appears to be greater than the more recent precise work of Broersma and of Angus, *et al.*, by a sufficient amount to conclude that a systematic error occurred in this earlier work.

(15) See pages 42 and 43 of ref. 4.

(16) See for example, J. O. Hirschfelder, C. F. Curtiss and R. B. Bird, "Molecular Theory of Gases and Liquids," John Wiley and Sons, Inc., New York, N. Y., 1954, pp. 951–955. The use of Hartree–Fock electronic wave functions for the atoms, see column 5 of Table V, makes no significant change in the calculated χ's.

TABLE V

DIAMAGNETIC SUSCEPTIBILITIES OF VOLATILE HYDRIDES AND METHYL FLUORIDE

	$-\chi \times 10^6$, c.g.s., emu./mole				
			$<- \Sigma \chi$atom$>$		
	This research	Lit.	Slater	Hartree–Fock[a]	Pascal
H_2	....	4.00	4.76	4.76	5.86
He	2.02 ± 0.08	1.90	1.65	2.06	...
$^1/_2B_2H_6$	10.5 ± .4	...	17.9	19.8	16.0
CH_4	17.4 ± .8	12.2	18.7	20.5	17.7
NH_3	16.3 ± .8	16.5	15.0	17.0	14.3
H_2O	....	13.0 (liq.)	11.7	13.8	10.5
HF	....	8.6	8.68	11.0	9.2
CH_3F	17.8 ± .8	...	24.2	26.7	21.1
Ne	6.96 ± .14	7.02	5.64	8.30	...
SiH_4	20.4 ± .8	...	34.7		24.7
PH_3	26.2 ± .8	...	30.5		18.8
H_2S	....	25.5	26.2		20.9
HCl	....	22.1	22.3		23.0
Ar	(19.32)	19.32	18.5	21.1	...
GeH_4	29.7 ± .8	...	46.9		37.7
AsH_3	35.2 ± .8	...	43.4		29.8
H_2Se	....	...	39.1		28.5
HBr	....	32.9	35.1		33.5
Kr	29.0 ± .4	28.6	31.2	31.9	...
SnH_4	....	...	68.5		...
SbH_3	34.6 ± .8	...	63.1		35.8
H_2Te	....	...	57.4		...
HI	....	47.7	52.1		47.5
Xe	45.5 ± .7	43.2	47.1		...

[a] See J. A. Ibers, *Acta Cryst.*, **11**, 1781 (1958), and B. K. Vainshtein and J. A. Ibers, *Kristallografiya*, **3**, 416 (1958).

deviations from additivity increase rapidly with increasing atomic number of the "central atom." In all cases it will be noted that the sense of the deviation from the sum of the atomic susceptibilities is the same, *i.e.*

$$|\chi_{obs}| < |\chi_{calc}| \qquad (3)$$

Although no previous work has been reported on silane, phosphine and germane, there have been reported diamagnetic susceptibility measurements on disilane,[17] trimethylphosphine[18] and tetramethylgermane.[19] The Gilman and Wu[17] determination of $-\chi(Si_2H_2) = 37.3$ is in quite reasonable agreement with $-2\chi(SiH_4) + 2\chi(H) = 40.8 - 4.0 = 36.8$. However, the values of $-\chi$ reported for trimethylphosphine (36.8)[18] and tetramethylgermane (86.3)[19] are in very poor agreement with the values 60.6 and 75.5, respectively, calculated from our values of the corresponding hydrides by addition of three or four times $-\chi(CH_2) = 11.46$. We can offer no valid opinion on whether these discrepancies are the result of failures of the additivity hypothesis or are the result of experimental inaccuracies, although we are inclined toward the first explanation.

Qualitatively the sense of the inequality, (3), readily can be understood to result from the second, or high frequency paramagnetism, term in the Van Vleck[2] equation for the diamagnetic susceptibility of molecules. The second term, as indicated from its common name, is of opposite sign from the term depending on the mean square electronic radii, and there occur in the denominator of the second term electron excitation energies. The number of low lying electron energy levels of the atoms increases as one moves down in atomic number from a rare gas in a row of the periodic system, and as the atomic number increases in any column (group) of the periodic system.[20]

The difficulties associated with the problem of obtaining a quantitative rationale of the observed diamagnetic susceptibilities of hydrides by means of the Van Vleck equation have been adequately dealt with by Weltner[21] and we have nothing to add to his discussion of the problem.

The correlations that have been found to exist between deviations of both diamagnetic susceptibilities and ionization cross sections from simple additivity laws will be described in papers currently in preparation.

Acknowledgments.—We take great pleasure in acknowledging our indebtedness to the A. O. Beckman Co. for the loan of the Model E-2 Oxygen meter that was used in making the measurements summarized in this paper. Furthermore, we wish to thank Mr. S. E. Steinle of the Instrumentation Department for his assistance in arranging for this loan and for valuable advice in connection with the use of the E-2. As indicated in the text, certain of the hydrides were prepared and purified by Mr. E. R. Bell. The sample of cyclododecane was prepared and purified by Dr. D. E. Winkler.

---

(17) H. Gilman and T. C. Wu, *J. Am. Chem. Soc.*, **75**, 3762 (1953).

(18) P. Pascal, *Compt. rend.*, **218**, 57 (1944).

(19) P. Mazerolles and D. Voight, *ibid.*, **240**, 2144 (1955).

(20) Selwood, ref. 5, p. 85, has noted similar behavior of the magnetic susceptibility of the hexafluorides of the elements of group VIa and VIb.

(21) W. Weltner, *J. Chem. Phys.*, **28**, 477 (1958).

CHEMICAL REACTIONS OF FREE RADICALS AT LOW TEMPERATURE

BY R. A. RUEHRWEIN,[1a] J. S. HASHMAN[1b] AND J. W. EDWARDS[1a]

National Bureau of Standards, Washington, D. C.

Received April 14, 1960

Free radicals generated by subjecting gases to an electrodeless discharge were condensed in a trap cooled to liquid helium temperature. The nature of the radical reactions which had taken place upon condensation and upon warming the solid deposits was indicated by the analyses of the products obtained. The gases discharged (and the principal products) were $O_2(O_3)$, $HO_2(H_2O_2,H_2)$, N_2, $NO_2(N_2,O_3)$, H_2, $NH_3(N_2,H_2)$, $CO(C,CO_2)$, $CO_2(CO,O_3)$, $SO_2(O_2,S)$, and some mixtures therof. Also the reactions of O, OH, H, N and HO_2 radicals with O_2, H_2O, NO, NO_2, CO_2, SO_2, CH_4, C_2H_4, *i*-C_4H_8, CO and CH_3-$COCH_3$ were investigated by blending in the latter downstream from the discharge and ahead of the liquid helium trap. In some of the systems it was apparent that considerable radical reaction occurred before condensation. However most of the experimental results can be interpreted on the basis that at very low temperature the free radicals react by random recombination, by addition to molecules with unpaired electrons, and by addition to carbon–carbon double bonds. It was found that molecular oxygen is loosely bound in several solids such as hydrogen peroxide, water, nitrogen dioxide and probably others. The bound or trapped oxygen is evolved from the solid at temperatures well above the boiling point of oxygen.

Introduction

Within recent years free radicals with an indefinitely long life have been collected and observed in a number of laboratories. It has been shown that free radicals which normally are quite reactive can be stabilized in the solid state by freezing at very low temperatures. Some work has been reported[2-4] on the chemical reactions of free radicals at temperatures below the boiling point of nitrogen, but at the present time it is not very extensive. Therefore, as part of the research program at the National Bureau of Standards, it was of interest to investigate the reactions of highly energetic radicals at temperatures of a few degrees above absolute zero.

The intent of the investigation was to survey a number of systems so with few exceptions no one reaction was studied in detail.

The radicals (or atoms) H, O, OH, N and HO_2 were the principal ones employed since they can be generated readily and have relatively long lifetimes in the gaseous state. This facilitated their handling in the type of apparatus that was employed in these experiments.

Experimental

The design of the Pyrex apparatus (Fig. 1) is the same as that previously employed in a study of ozone formation at low temperature.[5] Briefly, gas was passed through an electrodeless electric discharge at a pressure of approximately 1 mm. The discharge was maintained in a wave-guide resonator by a 2450 mc./sec. power supply (125 watts output). The discharge products then were led into a Pyrex tube, the bottom of which was immersed in liquid helium. This acted as a trap or condenser by freezing out all gases and thus was an effective high speed pump for maintaining the flow of gas. During the course of the work two different cold traps were used, differing in length of the entrance tube from the ring seal at the top to the lower end. The lengths employed were 55 and 70 cm. Furthermore, the distance between the wave-guide and the ring seal, *i.e.*, the length of travel of discharge products in the 13 mm. discharge tube could be varied by adjusting the position of the wave-guide. Four such distances were employed, 2, 5, 10 and 42 cm.

The experimental procedure was similar to that described previously.[5] After termination of flow of the electrically dissociated gas, the cold trap containing the deposit then was warmed slowly by gradually lowering the Dewars. As gas pressure developed on warming, the vapor pressure was determined, the gas then withdrawn by means of a Toepler pump, and the volume of the gas was measured. Products were identified primarily by physical properties, while quantitative analyses were based on weight, gas volume or liquid volume. For the most part, sufficient data were obtained for a check of the material balance within about 2% which is the reliability of the flow meters.

From the identity and quantity of products formed, an attempt then was made to devise reaction mechanisms to explain and correlate the various experimental results.

The intent in these experiments was to generate free radicals in the gas phase, mix them with other reactant gases when desired, and to condense rapidly the reactants so that any reactions would occur primarily at very low temperatures and in the condensed solid phase (or on the surface thereof) either during condensation or upon subsequent warming of the solid. In the work with oxygen[5] it was concluded that virtually all of the low temperature reaction occurred upon condensation of the gas. In the present experiments, the low temperature reactions probably also occurred predominantly upon condensation since other investigators have shown that the concentrations of radicals trapped in the solid are quite small. However, in some of the experiments warm gas phase reactions are suspected to have occurred before deposition. These cases will be noted as they arise in the following discussion.

Results and Discussion

I. Water and the Hydrogen–Oxygen System (Runs 1–10).—The reaction of atomic hydrogen with molecular oxygen has been studied in some detail[6] and additional experiments were also carried out in the present study (Table I). The principal product was hydrogen peroxide (analyzed by decomposition with CrO_3), with very little water being formed. Under the conditions of the present experiments the molecular hydrogen was about 15 to 20% dissociated, judged by the conversion.

Foner and Hudson[7] demonstrated the formation of the hydroperoxyl radical from atomic hydrogen and molecular oxygen in the gas phase. The results of the low temperature reaction experiments can be accounted for on the basis that reactions 1, 2, 3 and 4 were the principal ones

$$H + O_2 = HO_2 \tag{1}$$

$$H + HO_2 = H_2O_2 \tag{2}$$

$$2HO_2 = H_2O_2 + O_2 \tag{3}$$

$$H + H = H_2 \tag{4}$$

and that these reactions took place in or on the

---

[1] (a) Research guest from Monsanto Chemical Co., Dayton, Ohio; (b) Research guest from Callery Chemical Co., Callery, Pennsylvania.

[2] (a) H. P. Broida and J. R. Pellam, *J. Chem. Phys.*, **23**, 409 (1955); (b) E. D. Becker and G. C. Pimentel, *ibid.*, **25**, 224 (1956).

[3] Norman Davidson, Symposium on Formation and Stabilization of Free Radicals, National Bureau of Standards, September 18–20, 1957.

[4] I. L. Mador, *J. Chem. Phys.*, **22**, 1617 (1954).

[5] R. A. Ruehrwein and J. S. Hashman, *ibid.*, **30**, 823 (1959).

[6] J. W. Edwards and J. S. Hashman, Abstr. of Papers of Am. Chem. Soc., 132nd Meeting, New York, N. Y., 1957, p. 42-S.

[7] S. N. Foner and R. L. Hudson, *J. Chem. Phys.*, **23**, 1364 (1955).

TABLE I

PRODUCTS FROM CONDENSATION AT 4.2°K. OF DISCHARGED GASES

Run no.	Time of flow, min.	Discharge to condenser, cm.	Entrance tube surface	Mmoles gas treated		Mmoles	Product	Conversion	
				Discharged	Blended^{a}			From	%
1	23	42 + 70	Clean	21.48 H_2	26.75 O_2(B)	0.54	H_2O_2	H_2	2.5
						0.10	$O_2{}^{b}$		
2	3.5	5 + 70	H_3PO_4	9.64 H_2	5.82 O_2(B)	1.20	H_2O_2	H_2	12.5
						0.43	$O_2{}^{b}$		
3	8.5	10 + 55	Clean	21.21 H_2O^{c}	....	1.67	H_2	H_2O	7.9
						1.70	H_2O_2	H_2O	8.0
						?	O_2		
4	3.5	10 + 70	Clean	7.02 H_2O	....	1.44	H_2	H_2O	20.5
						1.12	H_2O_2	H_2O	17.0
						0.12	$O_2{}^{b}$	H_2O	3.4
5	12.3	2 + 70	Dirty (Iron Oxide)	30.62 H_2O	....	9.62	H_2	H_2O	31.4
						0.11	H_2O_2	H_2O	0.4
						2.06	O_2	H_2O	13.5
						2.77	$O_2{}^{b}$	H_2O	18.1
6	11.5	10 + 70	"Clean"	27.08 H_2O	....	11.97	H_2	H_2O	44.2
						0.88	H_2O_2	H_2O	3.3
						3.11	O_2	H_2O	23.0
						2.28	$O_2{}^{b}$	H_2O	16.8
						Trace	O_3		
7	3.0	10 + 70	H_3PO_4	7.46 H_2O	....	1.30	H_2	H_2O	17.4
						1.26	H_2O_2	H_2O	16.8
						0.08	$O_2{}^{b}$	H_2O	2.1
8	7	2 + 70	H_3PO_4	11.10 H_2O	....	1.94	H_2	H_2O	17.8
						1.90	H_2O_2	H_2O	17.1
						0.21	$O_2{}^{b}$	H_2O	3.8
9	5	10 + 55	Clean	12.39 H_2O^{c}	^{d}	0.37	H_2	H_2O	3.0
				9.42 O_2		1.42	H_2O_2	H_2O	11.5
						1.32	$O_2{}^{b}$	O_2	14.0
						0.60	O_3		
10	5	10 + 55	Clean	15.70 H_2O^{c}	15.43 O_2(T)	1.28	H_2	H_2O	8.1
						1.88	H_2O_2	H_2O	12.0
						1.28	$O_2{}^{b}$	O_2	8.3
11	25	10 + 55	Clean	44.65 N_2	50.96 O_2(T)	0.50	O_3	O_2	1.47
						0.05	NO_2	N_2	0.06
12	6	10 + 55	Clean	9.98 N_2	....	2.67	O_3	O_2	40.0
				9.98 O_2		0.20	NO_2	N_2	1.0
13	5.5	10 + 55	Clean	20.68 N_2	....	5.66	O_3	O_2	41.1
				20.68 O_2		0.34	NO_2	N_2	0.8
14	13	10 + 55	Clean	23.55 N_2	....	7.00	O_3	O_2	39.1
				26.85 O_2		0.77	NO_2	N_2	1.66
15	13	10 + 55	Clean	70.04 N_2	....	1.83	O_3	O_2	58.9
				4.65 O_2		0.27	NO_2	N_2	0.19
						0.19	N_2O	N_2	0.27
16	30	2 + 70	H_3PO_4	29.45 N_2	49.99 NO(B)	(0.20)	N_2O	N_2	(0.34)
17	10.9	5 + 70	Clean	9.65 O_2	22.30 NO(B)	13.90	NO_2	O_2	72.0
						0.74	$O_2{}^{b}$		
18	28	10 + 55	Clean	10.91 NO_2	....	5.14	N_2	NO_2	94.1
						3.53	O_2	NO_2	32.3
						4.67	O_3	NO_2	64.2
						0.51	NO	NO_2	4.7
19	23	10 + 70	Clean	11.60 O_2	34.40 NO_2(T)	3.32	$O_2{}^{b}$		
20	2.2	10 + 55	Clean	47.50 H_2	1.21 N_2(T)	..			
21	3.0	10 + 55	Clean	8.06 H_2	....	0.23	NH_3	H_2	4.3
				3.77 N_2				N_2	3.1
22	2.5	10 + 55	Clean	11.52 H_2	....	0.17	NH_3	H_2	2.2
				3.92 N_2				N_2	2.1
23	7.3	10 + 55	Clean	2.40 H_2	....	0.32	NH_3	H_2	15.0
				14.18 N_2				N_2	1.1
24	5.9	5 + 55	Clean	17.60 NH_3	....	9.95	H_2	NH_3	38.3
						3.09	N_2	NH_3	35.1
25	11.5	5 + 70	H_3PO_4	16.62 O_2	13.0 SO_2(B)	8.55	O_3	O_2	77.8

TABLE I (*Continued*)

Run no.	Time of flow, min.	Discharge to condenser, cm.	Entrance tube surface	Mmoles gas treated		Mmoles	Product	Conversion	
				Discharged	Blended[a]			From	%
26	13	5 + 70	H_3PO_4	17.20 SO_2	....	0.69	O_2		
						0.93	O_2[b]		
						1.18	S	SO_2	6.9
						0.10	SO	SO_2	0.6
27	47	2 + 70	Dirty	27.80 O_2	60.40 CO(B)	3.00	O_3	O_2	16.2
28	47	2 + 70	Dirty	51.90 N_2	59.85 CO(B)	..			
29	8	5 + 70	H_3PO_4	17.29 H_2	27.45 CO(B)	..			
30	3.3	2 + 70	H_3PO_4	6.58 H_2O	(5.03) CO(B)	1.53	H_2	H_2O	23.2
						1.08	H_2O_2	H_2O	16.4
						0.08	O_2[b]	H_2O	2.4
						0.10	O_3	H_2O	4.6
						(0.63)	CO[b]		
31	10	5 + 70	H_3PO_4	12.58 H_2	14.48 R_2CO(B)	..			
32	14	5 + 70	H_3PO_4	H_2	CO_2(B)	..			
33	45	2 + 70	H_3PO_4	27.82 CO	....	0.95	CO_2	CO	3.4
						4.25	$(CO_{.78})$[e]		
34	20	2 + 70	H_3PO_4	18.90 CO_2	....	12.10	CO		
						3.56	O_3	CO_2	56.6
						0.65	O_2		
35	8	2 + 70	H_3PO_4	14.70 N_2	16.59 C_2H_4(B)	..			
36	10	5 + 70	H_3PO_4	20.22 H_2	20.28 C_2H_4(B)	1.47	C_2H_6	H_2	7.9
37	2.2	10 + 70	H_3PO_4	3.84 H_2O	4.52 C_2H_4(B)	0.98	H_2	H_2O	25.5
						.52	H_2O_2	H_2O	13.5
						.24	C_2H_6	H_2O	6.2
						.18	C_2H_5OH		
						.21	CH_3CHO		
						.08	$(CH_3CHO)_3$		
38	8	10 + 70	H_3PO_4	6.43 O_2	16.54 C_2H_4(B)	1.48	$(HCHO)_n$	O_2	44.8
						1.55	(HCOOH)		
						1.00	(C_2H_4O)		
39	8.8	5 + 70	H_3PO_4	9.75 H_2	14.54 O_2 (B)	0.41	O_2[b]		
					11.32 C_2H_4	1.54	H_2O_2	H_2	15.8
						2.34	H_2O		
						0.12	$(C_2H_4O_x)$		
						1.07	(C_4H_6O)		
40	9	5 + 70	H_3PO_4	10.21 H_2	14.74 O_2 (B)	0.94	O_2[b]		
					25.08 *i*-C_4H_8	0.12	H_2O_2	H_2	1.2
						0.70	(H_2O)		
						1.28	(C_4H_8O)		

[a] (T) Gas blended immediately after discharge. (B) Gas blended just prior to condensation. [b] Gas evolved from deposit at temperatures above the boiling point of the gas. [c] Approximately one-half of the water condensed in the entrance tube. [d] Brace denotes that the mixture of gases was discharged. [e] Carbonaceous deposit.

condensed solid deposit, either during condensation or upon subsequent warming.

It was shown[6] that the evolution of molecular oxygen from the solid at a temperature of about 160°K. could be accounted for by the release of oxygen which was loosely bound in the solid and in an amount corresponding to $3H_2O_2{\cdot}O_2$. This "evolved" oxygen also was observed in runs 1 and 2 and it was found to be an irreversible process since oxygen was not absorbed upon recooling the deposit.

A film of phosphoric acid on the entrance tube was effective in preventing hydrogen atom recombination catalyzed by the tube walls (compare runs 1 and 2).

The results of the water-discharge experiments are summarized in Table I, runs 3–8. Hydrogen peroxide and molecular hydrogen were the principal products formed. Accidental contamination of the entrance tube with iron oxide prevented the formation of hydrogen peroxide (run 5) and washing with nitric and hydrofluoric acids did not effectively clean the tube (run 6). In these runs it is apparent that hydrogen atoms recombined and hydroxyl radicals decomposed in the entrance tube. However, coating the entrance tube with a thin film of phosphoric acid resulted in the formation of hydrogen peroxide (runs 7 and 8).

In most respects the results of the water discharge experiments were similar to those reported by other investigators.[8–11] The water apparently was dissociated in the discharge in these experiments into hydrogen atoms and hydroxyl radicals to the extent of up to about 80%. In the clean or coated entrance tube, 90 to 98% of the radicals were preserved with little oxygen being formed. The re-

---

(8) H. P. Broida, *Ann. N. Y. Acad. Sci.*, **67**, 530 (1957).

(9) R. A. Jones and C. A. Winkler, *Can. J. Chem.*, **29**, 1010 (1951).

(10) P. A. Giguère, E. A. Secco and R. S. Eaton, *Disc. Faraday Soc.*, **14**, 104 (1953).

(11) R. Livingston, J. Ghormley and H. Zeldes, *J. Chem. Phys.*, **24**, 483 (1956).

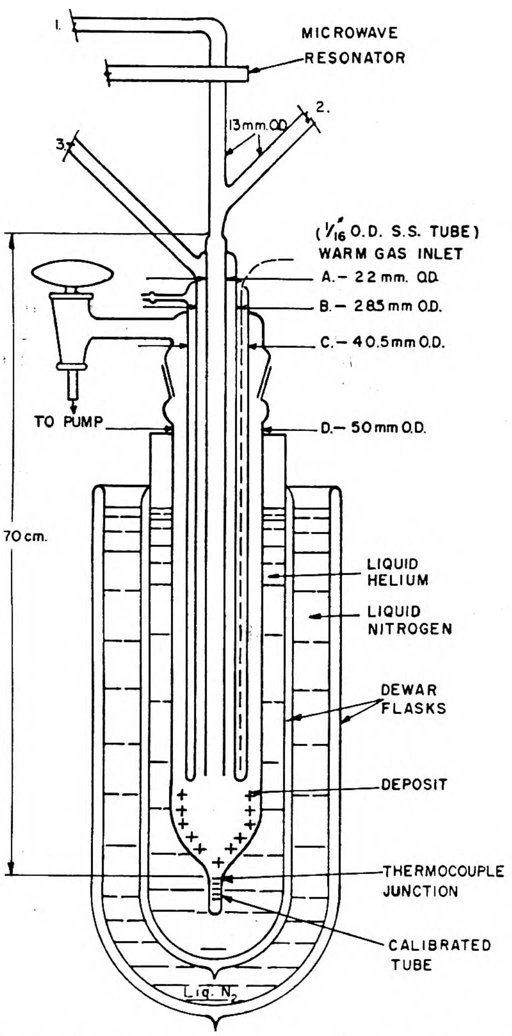

Fig. 1.—Low temperature reaction apparatus (Pyrex).

sults can be interpreted on the basis that upon condensation the radicals randomly recombined in the solid phase (or surface) reactions 4, 5 and 6. Ideally this would lead to conversions

$$OH + OH = H_2O_2 \qquad (5)$$
$$H + OH = H_2O \qquad (6)$$

of 20% (mole) to both hydrogen and hydrogen peroxide from 80% dissociated water vapor, without the formation of any molecular oxygen.

In those runs (5 and 6) in which little peroxide was formed it was observed that oxygen was evolved from the residual deposit over a temperature range of possibly 120 to 200°K. This suggests that solid ice is also capable of trapping molecular oxygen in much the same way as does hydrogen peroxide.[6] Assuming that some of the oxygen is associated with the small amount of peroxide in the proportion corresponding to $3H_2O_2 \cdot O_2$, the ratio of the number of moles of water to the number of moles of remaining trapped oxygen is 7.6 in run 5 and 7.1 in run 6.

The trace of ozone detected in run 6 was formed by reaction 7

$$O + O_2 = O_3 \qquad (7)$$

The increased ratio of hydrogen peroxide to hydrogen formed in run 10 as compared with run 3 is accounted for by the additional reactions 1, 2 and 3 which generate hydrogen peroxide from atomic hydrogen and molecular oxygen. The still greater ratio of hydrogen peroxide to hydrogen, together with a lower total conversion of water, formed in run 9 as compared with run 10 is accounted for by the additional reactions 8 and 9 followed by reactions 3, 5 and 10.

$$H + O = OH \qquad (8)$$
$$OH + O = HO_2 \qquad (9)$$
$$OH + HO_2 = H_2O + O_2 \qquad (10)$$

Since in some of these experiments the hydroperoxyl radical would likely be the most abundant one, its final consumption can be accounted for by reaction 3 which is an abstraction reaction. Using the value of 47 kcal. for the dissociation energy of the $H-O_2$ bond given by Foner and Hudson[7] the activation energy of reaction 3 was estimated to be about 2.6 kcal. using the empirical rule suggested by Hirschfelder.[12] Therefore, it would be expected that reaction 3 would be fairly rapid at a temperature of about 40°K. in a mobile matrix. The similar reactions 10, 11 and 12 would have ac-

$$H + HO_2 = H_2 + O_2 \qquad (11)$$
$$O + HO_2 = OH + O_2 \qquad (12)$$

tivation energies about equal to that of reaction 3 but reactions 11 and 12 are not necessary to account, qualitatively, for the present data.

II. The Nitrogen–Oxygen System (Runs 11–19).—Run 15: ozone and nitrous oxide were separated by allowing the ozone to decompose.

Run 18: nitrogen dioxide and nitric oxide were analyzed by measuring the gas volume before and after treating the mixture with oxygen (and then separating the oxygen) to convert any NO to NO_2. From the change in gas volume and the equilibrium constants for the dissociation of N_2O_4 and N_2O_3 the starting composition was calculated.

That little nitrogen was converted to nitrogen oxides in the present experiments suggests that either the molecular nitrogen was dissociated to a small extent in the discharge or that atomic nitrogen underwent recombination largely to molecular nitrogen during its passage down the entrance tube. The results of run 18 lend support to the latter, possibly by a mechanism[5] involving the fast[13,14] reaction $N + NO = N_2 + O$, since nitrogen dioxide would be expected to be almost completely dissociated in the discharge and yet the nitrogen is found in the product largely as molecular nitrogen. Assuming that the ozone was formed by reactions 13 and 7 in the solid deposit, the amount of ozone

$$O + O = O_2 \qquad (13)$$

found indicates[5] that the oxygen arriving at the condensing surface was dissociated into atomic oxygen to the extent of 20% in runs 12, 13 and 14; 70% in run 15; and nearly 100% in run 18.

If some nitrogen atoms did arrive at the condenser, the formation of some of the products can be accounted for by the solid phase reactions 14, 15, 16 and 17.

(12) J. Hirschfelder, *ibid.*, **9**, 645 (1941).

(13) G. B. Kistiakowsky and G. G. Volpi, *ibid.*, **27**, 1141 (1957).

(14) F. Kaufman and J. R. Kelso, *ibid.*, **27**, 1209 (1957).

$$N + N = N_2 \quad (14)$$
$$N + O = NO \quad (15)$$
$$NO + O = NO_2 \quad (16)$$
$$N + NO = N_2O \quad (17)$$

Run 16 is evidence for reaction 17 since the reactants were mixed just prior to condensation. Run 17 is not good evidence for reaction 16 since the experiment of run 17 was duplicated but without discharging the oxygen stream and the results were identical in all respects to those of run 17. This shows that even in the very short dwell time of the mixture in the gas phase the oxidation of nitric oxide by molecular oxygen was very rapid.

No evidence was found for the reaction of atomic oxygen with molecular nitrogen or for the reaction of atomic nitrogen with molecular oxygen. The small amount of ozone and nitrogen dioxide found in run 11 probably was a result of the diffusion of some oxygen upstream a few centimeters into the discharge.

In run 16, some of the product N_2O was accidentally discarded with the residual nitric oxide so the results are quantitatively unreliable.

Since nothing but the starting materials were found in run 19 (with the exception of a little undetermined nitric oxide), the oxygen atoms were entirely consumed during passage down the entrance tube and before reaching the condenser. This probably can be accounted for by the excess of nitrogen dioxide and the speed[13,15] of the reaction $NO_2 + O = NO + O_2$. As only the starting amount of the molecular oxygen was recovered, the NO must have been reoxidized in the gas phase, possibly by the very rapid[13] reaction $NO + O = NO_2^*$ and even by molecular oxygen as noted above with the net result that NO_2 catalyzed the recombination of atomic oxygen in the gas phase.

Since "evolved" oxygen was observed in runs 17 and 19, run 19 was duplicated but without discharging the oxygen. The deposit looked identical (light yellow color) and evolved the same amount of oxygen, 1 mole of oxygen for 7 moles of NO_2, over a temperature range of about 90 to 160°K. In this system the oxygen evolution was found to be reversible in that oxygen was reabsorbed upon recooling the residual nitrogen dioxide deposit. The vapor pressure was determined to be about 6 mm. at 124°K. and < 1 mm. at 78°K. This is similar to the decomposition pressure of NO_3 reported by Schwarz and Achenback.[16]

Run 19, therefore, does not give conclusive evidence concerning the formation of NO_3 by the addition of atomic oxygen to nitrogen dioxide since the dwell time of the mixture in the gas phase was too long.

III. The Nitrogen–Hydrogen System (Runs 20–24).—Since no products other than molecular nitrogen and hydrogen were found, the results of run 24 indicate that atomic nitrogen nearly completely recombined in the entrance tube.

The results of these experiments with the nitrogen–hydrogen system, like those with the nitrogen–oxygen system, are not conclusive regarding radical reactions in the solid deposit.

IV. The Sulfur–Oxygen System (Runs 25–26).—Run 26: a small amount of free sulfur deposited near the discharge and an opaque orange brown deposit was formed in the liquid helium trap. After removing volatile gases, the residual deposit was heated to 400°K. for about two hours and sulfur dioxide was released leaving a yellow solid which was presumed to be sulfur since it formed sulfur dioxide upon treatment with atomic oxygen.

The large conversion to ozone in run 25 indicates either (1) that the SO_2 solid matrix favored trapping of some oxygen atoms which reacted only with neighboring molecular oxygen, reaction 2, upon warming; or (2) that the ratio of the probabilities of reaction, p_{13}/p_7, of reaction 13 and 7 is about 1.4 instead of 2.6 as suggested in ref. 5.

Absence of ozone as a product of the SO_2 discharge is in sharp contrast to NO_2 and CO_2 (see below) behaviors. This suggests that the recombination reaction 18 was the principal one occurring

$$SO + O = SO_2 \quad (18)$$

This reaction may also be expected in the gas stream since SO has a triplet electronic ground state and may therefore behave as a diradical and have a low activation energy for reaction with oxygen atoms. Too, since the product is a triatomic molecule, intercession of a "third body" would not be required to stabilize the newly formed molecule in the gas phase. Furthermore, any small amount of ozone formed may have reacted with trapped SO radicals ($SO + O_3 = SO_2 + O_2$) upon warming the deposit. It is assumed that the residue found at room temperature contained elemental sulfur and a polymeric form of sulfur monoxide and that the latter disproportionated upon heating to 400°K. giving SO_2 and additional elemental sulfur.

Molecular oxygen was shown to be trapped also by sulfur dioxide, the oxygen being "evolved" over a temperature range of about 100 to 120°K.

V. The Carbon–Oxygen System (Runs 27–34).—Runs 27 and 28: carbon monoxide was used directly from a cylinder and contaminated the entrance tube of the reaction apparatus, presumably by carrying in iron carbonyl. (The results of run 28 may therefore be inconclusive.) In the remainder of the runs the carbon monoxide was treated by condensing and revaporizing it in three successive nitrogen-cooled traps between the supply cylinder and the flow meter.

Run 30: carbon monoxide was apparently trapped in the solid and "evolved" up to a temperature of about 150°K. That CO was part of the evolved gas was deduced from the water material balance and not by analysis of the gas.

Run 33: a dark residue was left in the discharge tube. Some carbon dioxide was formed and from the material balance the residue in the discharge tube was calculated as $CO_{0.78}$ for an empirical composition.

Run 34: the oxygen–carbon monoxide fraction was analyzed by mass spectrometry.

These results indicate that for the radicals employed the activation energies for the addition to carbon monoxide, carbon dioxide and the carbonyl

---

(15) H. W. Ford and N. Endow, *ibid.*, **27**, 1156 (1957).

(16) R. Schwarz and H. Achenback, *Chem. Ber.*, **68**, 343 (1935).

group are large compared with the activation energies for the radical recombination reactions discussed in the preceding sections and suggest that the value of 1.8 kcal. given by Groth[17] for the reaction $O + CO + M = CO_2 + M$ may be too low.

The results of the carbon monoxide experiment suggest that atomic oxygen adds to some extent to excited carbon monoxide. The high yield of ozone from atomic oxygen in the experiment with CO_2 may be accounted for by the same suggestions advanced above (Sulfur–Oxygen System).

VI. Reaction with Olefins (Runs 35–40).—The reactivity of the various radicals with ethylene or isobutylene was tested.

Run 35: no products of reaction of atomic nitrogen with ethylene were detected and the lack of any significant amount of reaction was confirmed by the material balance.

Runs 36 and 37: ethane was analyzed by gas chromatography as the product of reaction and contained in the ethylene fraction. In run 37, ethanol and acetaldehyde were detected, and their relative amounts measured, by mass spectrometry while the total amount was determined by measuring the depression of the freezing point of the water fraction solution. The small amount of white solid product which appeared to be insoluble in the aqueous phase had a melting range from -9 to 6° and a volatility similar to that of ethanol so it was presumed to be paraldehyde. There was no evidence of ethylene glycol as a product of this reaction.

Run 38: the deposit was deeply colored purple, even before beginning to warm it. Upon reaching a temperature of about 48°K., the deposit became completely colorless with the evolution of some heat. The products in the fraction which was volatile in the temperature range of 250 to 300°K. (v.p. of about 60 mm. at 0°) consisted of a single phase of water white liquid. Upon standing for several days in a sealed tube and with occasional warming a precipitate formed in this mixture and was found by infrared analysis to be polyformaldehyde. It was insoluble in acetone, benzene, hot water and hot toluene and melted at about 160°. By analysis it was 41.78% C and 7.37% H. The vehicle from which it polymerized was identified by infrared analysis as possibly formic acid containing some water. The last product of this reaction given in the table as (C_2H_4O) was the residue of the material balance and was presumed to be a nonvolatile product. In fact a small amount of residue was visible in the reaction tube and it was found to be benzene soluble.

Run 39: no ethane was detected by gas chromatographic analysis. A small amount of material of molecular weight about 60 was formed and is labeled $C_2H_4{\cdot}O_x$ in Table I. It was water-soluble, m.p. < 178°K., 9 mm. vap. pres. at 210°K. The last product, a non-volatile and water-soluble residue, was found to have an empirical formula of C_4H_6O from the material balance.

Run 40: the organic product was not identified but the presence of a C–O bond was indicated by infrared absorption. The amounts of water and organic product formed were estimated from the material balance. By gas chromatographic analysis, the unreacted isobutylene contained slight but negligible quantities of C_2's, C_3's and isobutane.

Some of the products of the olefin experiments can be accounted for by the addition of radicals to

$$2H + C_2H_4 = C_2H_6 \qquad (19)$$

$$H + OH + C_2H_4 = C_2H_5OH \qquad (20)$$

the double bond (reactions 19 and 20) as the primary reactions. The results of run 37 suggest, however, that the over-all reaction of ethylene with hydroxyl radical is that given by reaction 21 rather than the formation

$$C_2H_4 + OH = CH_3CHO + {}^1/_2H_2 \qquad (21)$$

of ethylene glycol. Furthermore, it is concluded that the additions of H and OH to ethylene are about equally probable since the amount of acetaldehyde formed was equal to the sum of the amounts of ethane and ethanol formed.

With atomic nitrogen, the relatively stable radical $C_2H_4N\cdot$, postulated by Winkler[18] and co-workers, may have been formed which reacts to regenerate ethylene and molecular nitrogen.

In the three experiments with molecular oxygen added there was no evidence of products resulting from the addition of the original atomic species to the olefin. In run 38 reaction 7 was the primary one, as evidenced by the intense blue color of the deposit, followed by the ozonization of ethylene at about 48°K. According to Harris and Koetschau,[19] the principal products of the decomposition of ethylene ozonide are formaldehyde and formic acid. The last product listed in Table I for run 38, (C_2H_4O), which accounts for the material balance, suggests that some addition of atomic oxygen to ethylene may have occurred resulting in the formation of polyethylene oxide.

In runs 39 and 40 the products found suggest that the HO_2 radical added to the olefin and/or that molecular oxygen added to an alkyl radical. The over-all reaction in the ethylene–oxygen experiment can be expressed by reaction 22. In other words, the oxidation

$$2C_2H_4 + nH + O_2 = C_4H_6O + H_2O + n/2H_2 \qquad (22)$$

of ethylene was promoted by atomic hydrogen. The non-volatile residue, C_4H_6O, may have been a polymerization product.

Molecular oxygen was found to be trapped to some extent by ethylene and isobutylene.

It is concluded from runs 39 and 40 that the addition of a radical to an olefin is less favorable than is the addition of a radical to molecular oxygen.

From the results of these experiments it is concluded that free radicals react at low temperature, in descending order of preference, by (1) random recombination, (2) addition to paramagnetic molecules such as oxygen, and (3) addition to carbon–carbon double bonds. No evidence for abstraction reactions from stable molecules was found.

Acknowledgment.—This research was performed under the National Bureau of Standards Free Radicals Research Program, supported by the Department of the Army. We thank Dr. H. P. Broida for many helpful discussions.

---

[17] W. Groth, *Z. physik. Chem.*, **B37**, 315 (1937).

[18] H. G. Evans, G. R. Freeman and C. A. Winkler, *Can. J. Chem.* **34**, 1271 (1956).

[19] C. Harris and R. Koetschau, *Ber.*, **42**, 3305 (1909).

VAPOR PRESSURES OF PLATINUM METALS. I. PALLADIUM AND PLATINUM

BY LLOYD H. DREGER AND JOHN L. MARGRAVE

Department of Chemistry, University of Wisconsin, Madison, Wisconsin

Received April 22, 1960

Langmuir free-evaporation rates for Pd and Pt samples of high purity establish the equilibrium vapor pressures and the heat of sublimation. For Pt: log $P_{\text{mm}}^{\text{solid}} = 10.362 - 29.100/T$; $\Delta H^0_{298} = 135.2 \pm 0.8$ kcal./mole; estimated b.p. ≈ 4100 ± 100°K. For Pd: log $P_{\text{mm}}^{\text{solid}} = 9.075 - 19{,}425/T$; $\Delta H^0_{298} = 91.0 \pm 0.8$ kcal./mole; estimated b.p. ≈ 3200 ± 100°K.

Among the metallic elements which are available in high purity are ruthenium, rhodium and palladium in the second row of transition elements and osmium, iridium and platinum in the third row of transition elements. Surprisingly enough, quantitative studies of the vapor pressures of these elements have not been reported except for Pt[1] and very recently for Pd.[2] Honig has published a set of recent estimates.[3]

Because of the importance of these elements as resistance elements in furnaces and structural materials in vacuum tubes, gauges, etc., and because of their incomplete d-electron shells which participate extensively in the metal bonding, it is of practical and theoretical interest to examine carefully their vapor pressures and heats of vaporization for trends and to compare the results with data on other transition metals.

Experimental Apparatus and Techniques

Vaporization studies of Pt and Pd were carried out by the Langmuir free-evaporation technique.[4] The rate of evaporation m in g./cm.²-sec., is related to the equilibrium vapor pressure by the equation

$$\alpha_s P_{\text{eq}} = m \sqrt{\frac{2\pi RT}{M}}$$

where α_s is the sublimation coefficient and M is the average molecular weight of the subliming species. For most metals, $\alpha_s = 1$ and monatomic species are predominant in the vapors. During a run, the surface area was assumed to decrease linearly with time and corrections for this changing area were made in the calculation of m. In most cases this change was less than 5% of the original area.

High purity wires or plates were suspended on a microbalance from a tungsten wire in a vacuum system. This balance was constructed by Spinar and has been used for several Knudsen effusion and Langmuir studies at high and low temperatures.[5]

The balance consists of a 17-inch long sample beam supported on two tungsten points which rest in glass cups. To balance the long arm and the sample suspended from it, Spinar arranged an 8-inch long arm extending on the other side of the fulcrum with a permanent magnet enclosed in glass and placed to swing through a soylenoid coil with a known current flowing through it. The balance has a sensitivity of 0.0225 v./mg. making it possible to detect a weight change of ±5 micrograms. A special advantage of the balance design is that samples as large as five grams may be suspended from the long arm which makes it ideal for use with heavy Knudsen cells or samples with high densities.

The samples were heated indirectly by radiation from a hot carbon tube which was itself the susceptor for an induction coil from a GE 450 kilocycle electronic induction heater. Temperatures were observed with an optical pyrometer and by manual control were held constant to ±5°K. during a run. Corrections for windows, emissivities and mirrors were applied to the raw pyrometer data. The calibration vapor pressure study of Pt was carried out to demonstrate the reliability of the balance and pyrometer.

The sample of Pt (commercial, 99.95⁺%) as well as the sample of Pd (99.99⁺%, furnished by the International Nickel Company) were suspended from Al_2O_3 or MgO hooks during the runs. No reaction of the oxides with the metals was observed.

Discussion of Results

The results of the sublimation studies on Pt and Pd are summarized in Tables I and II. Monatomic Pt(g) and Pd(g) were considered the only important gaseous species. Combination of the vapor pressures with free energy functions from Stull and Sinke[6] allow computation of third law heats of vaporization at 298°K. Plots of log P vs. $1/T$ yield the heats of sublimation at the high temperature from the slopes and correction to

TABLE I

VAPOR PRESSURE DATA ON PLATINUM METAL

Run	T, °K.	P, mm.	$\Delta H_{298}{}^0$
1	1771	4.00×10^{-7}	138.0[a]
2	1638	3.01×10^{-8}	136.4
3	1732	3.97×10^{-7}	135.0
4	1743	3.72×10^{-7}	136.4
5	1571	6.76×10^{-9}	135.3
6	1742	3.31×10^{-7}	136.6
7	1742	5.59×10^{-7}	134.7
8	1742	6.76×10^{-7}	134.1
9	1783	1.50×10^{-6}	134.4
10	1783	1.63×10^{-6}	134.1
11	1786	2.56×10^{-6}	132.7[a]

Av. $\Delta H_{298} = 135.2 \pm 0.85$ kcal./mole[b]

From log P vs. $1/T$ slope and $(H_T - H_{298})$ data from Stull and Sinke, one calculates $\Delta H_{298} = 135 \pm 2$ kcal./mole.

[a] Large deviation; given 0 weight. [b] Honig[3] cites $\Delta H^0_{298} = 134.8$ kcal./mole. Stull and Sinke[6] cite $\Delta H^0_{298} = 134.8$ kcal./mole.

---

(1) H. A. Jones, I. Langmuir and G. M. Mackay, *J. Phys. Rev.*, **30**, 201 (1927).

(2) (a) J. F. Haefling and A. H. Daane, *Trans. Met. Soc. AIME*, **212**, 115 (1958); (b) R. F. Walker, J. Efimenko and N. Lofgren, to be published in "Physical Chemistry in Aerodynamics and Space Flight," John Wiley and Sons, Inc., New York, N. Y.

(3) R. E. Honig, "Vapor Pressure Data for the More Common Elements," RCA Laboratories, David Sarnoff Research Center, Princeton, N. J., 1957.

(4) J. L. Margrave, "Physico-Chemical Measurements at High Temperatures," edited by Bockris, White and MacKenzie, Butterworths, 1959, Chapter 10.

(5) (a) L. Spinar, Ph.D. thesis, University of Wisconsin, 1957; (b) F. Greene, G. Leroi, S. Randall, J. Soulen, L. Spinar and J. Margrave, "Proceedings, Conference on Propellant Thermodynamics," American Rocket Society, Columbus, Ohio, July, 1959; (c) W. S. Johnson, V. Bauer, M. Frisch, W. Hubbard, L. Dreger and J. Margrave, *J. Am. Chem. Soc.*, **82**, 1255 (1960).

(6) D. R. Stull and G. C. Sinke, "Thermodynamic Properties of the Elements," Advances in Chemistry Series, No. 18, ACS, 1956.

298°K. can be accomplished by using heat content data from Stull and Sinke.[6]

TABLE II

VAPOR PRESSURE DATA ON PALLADIUM METAL

Run	T, °K.	P, mm.	ΔH_{298} (kcal./mole)
1	1640	9.28×10^{-4}	92.6
2	1640	1.18×10^{-3}	91.8
3	1640	1.62×10^{-3}	90.8
4	1338	3.58×10^{-6}	90.7
5	1340	3.99×10^{-6}	90.6
6	1340	3.54×10^{-6}	90.9
7	1220	1.93×10^{-7}	90.0
8	1363	8.24×10^{-6}	90.2
9	1363	6.49×10^{-6}	90.9
10	1363	7.91×10^{-6}	90.3
11	1501	1.92×10^{-4}	89.7
12	1562	5.14×10^{-4}	90.2
13	1578	6.79×10^{-4}	90.2
14	1484	5.32×10^{-5}	92.3
15	1470	4.95×10^{-5}	91.8
16	1467	3.40×10^{-5}	92.7

Av. $\Delta H^0_{298} = 91.0 \pm 0.8$ kcal./mole

The log P *vs.* $1/T$ plot gives a $\Delta H = 87.9$ at $T_{\text{av.}} = 1468$ which corrected to 298°K. using Stull and Sinke's[6] data gives a heat $\Delta H^0_{298} = 90.0 \pm 2$ kcal./mole.

The high temperature vapor pressure measurements in Table I on Pt confirm the previously reported data summarized by Honig[3] and establish the reliability of the apparatus and technique. The third law heat is slightly higher than reported by Jones, Langmuir and Mackay[1] but is well within their experimental error. Surprisingly, few reports of the vapor pressure of Pt exist in the literature.

The only reports on palladium are in wide disagreement. Daane and Haefling have reported Knudsen effusion measurements on palladium contained in a cell constructed partly of Ta and partly of graphite.[2a] This two-material construction was needed because of the reactivity of Pd(s) with graphite and of Pd(g) with Ta. Walker, Efimenko and Lofgren have reported measurements on Pd done by the Langmuir technique.[2b] Their measured pressures differ by several orders of magnitude from those of Haefling and Daane. The results reported here for Pd fall in between those of Daane, *et al.*,[2a] and of Walker, *et al.*[2b] The heat of sublimation is almost exactly an average. Since both previous investigators are experienced in the vapor pressure field, one can only suggest that perhaps the reactions of Pd with Ta and C which Daane and Haefling were trying to avoid were still significant and that some more volatile impurity was sublimed in addition to the Pd. With graphite crucibles and lids, it is often possible to have cracks or holes through which effusion occurs besides the regular effusion orifice. Elimination of this possibility can only be accomplished by a calibration experiment with the same cell. In the work of Walker, *et al.*,[2b] the use of an emissivity of 0.33 for palladium in the determination of the temperature of the sample may be the source of the error.

Acknowledgment.—The authors are pleased to acknowledge the financial support of the Wisconsin Alumni Research Foundation and of the Atomic Energy Commission. The high purity Pd wire was generously provided by the International Nickel Company through the courtesy of E. M. Wise.

SPECTROPHOTOMETRIC EVIDENCE FOR COMPLEX FORMATION IN THE TRI-*n*-BUTYL PHOSPHATE–WATER–NITRIC ACID SYSTEM

BY T. J. COLLOPY AND J. F. BLUM

Technical Division, National Lead Company of Ohio, Cincinnati, Ohio

Received April 29, 1960

Tri-(normal)-butyl phosphate solutions containing varying concentrations of nitric acid were investigated to determine the stoichiometry and stability of the complexes formed in the reaction between the two. Spectral data in the range 260 to 320 mμ have shown that tri-*n*-butyl phosphate and associated nitric acid react to form a stable equimolar complex. Evidence is presented which indicates that additional stable complexes having different mole ratios are not formed. This work has demonstrated the complex which is present in the tri-*n*-butyl phosphate phase, and has enabled the authors to interpret data that have been obtained for the two phase tri-*n*-butyl phosphate–water–nitric acid system. The significance of this complex can be found in its direct application to metal extraction processes, and an understanding of the fundamental chemistry underlying these processes.

Introduction

Several investigators have determined the equilibrium distribution of nitric acid between tri-*n*-butyl phosphate and water. Three of these investigators[1-3] have indicated, from an interpretation of distribution data, that equimolar complex formation does occur in the tri-*n*-butyl phosphate phase between tri-*n*-butyl phosphate and nitric acid. Other investigators[4] have interpreted their distribution data as indicating the existence of a 1:1 complex and a 1:2 complex between tri-*n*-butyl phosphate and nitric acid in the organic phase.

During an investigation of the chemistry of the tri-*n*-butyl phosphate–uranyl nitrate solvent ex-

---

(1) R. L. Moore, "The Extraction of Uranium in the Tributyl Phosphate Metal Recovery Process," HW-15230, September 1, 1949.

(2) K. Alcock, S. S. Grimley, T. V. Healy, J. Kennedy and H. A. C. McKay, *Trans. Faraday Soc.*, **52**, 39 (1956).

(3) A. T. Gresky, M. R. Bennett, S. S. Brandt, W. T. McDuffie and J. E. Savolianen, Progress Report on Laboratory Development of the Thorex Process, USAEC Report ORNL-1367, January 2, 1953 (Secret).

(4) R. J. Allen and M. A. DeSesa, *Nucleonics*, **15**, (10) 88 (1957).

traction process,[5] it became necessary to determine (1) the mole ratios of tri-*n*-butyl phosphate to nitric acid in the complexes formed, and (2) the stability of the complexes formed. The authors believed that complex formation could be demonstrated most effectively by conducting this investigation in a single phase organic solution containing purified tri-*n*-butyl phosphate and pure nitric acid (100% nitric acid is completely miscible with tri-*n*-butyl phosphate). The data obtained in this investigation could then be used in conjunction with data on the composition of aqueous nitric acid solutions to better explain complex formation in the two-phase tri-*n*-butyl phosphate–water–nitric acid system.

Experimental

Materials.—For the spectral study, commercial-grade tri-*n*-butyl phosphate was purified employing a method of distillation over alkali.[6] The pure associated nitric acid (100% nitric acid was assumed to be completely associated) was prepared by vacuum distillation of the acid from a mixture of concentrated sulfuric acid, 70% nitric acid and solid sodium nitrate. The acid obtained was colorless and gave analysis for greater than 99% nitric acid. The absorption spectrum of the acid was the same as that reported by other investigators for associated nitric acid molecules.[7] The associated acid was frozen except when removing aliquots for experimental purposes, so that discoloration or decomposition of the stock acid did not occur. The solvent used in this work was reagent-grade carbon tetrachloride. The materials used to obtain the distribution curve were reagent-grade nitric acid and commercial-grade tri-*n*-butyl phosphate (produced by Ohio Apex Division of the Food and Machinery Chemical Company).

Apparatus.—The absorption spectra of tri-*n*-butyl phosphate (TBP), associated nitric acid (HNO_3), and the 1:1 $TBP \cdot HNO_3$ complex in the wave length range, 260 to 320 mμ were obtained with a Beckman Model DK-2 spectrophotometer employing matched silica cells of 1-cm. path length. Measurements at fixed wave lengths were made with a Beckman Model DU spectrophotometer using matched 1-cm. silica cells. The apparatus used to determine the distribution curve was a separatory funnel equipped with an interfacial stirrer.

Procedure.—The method of continuous variation[8,9] was employed in determining $TBP \cdot HNO_3$ complex formation in the solvent carbon tetrachloride using individual stock solutions containing 0.125 *M* concentrations of tri-*n*-butyl phosphate and of associated nitric acid. The molar ratio method[10,11] was employed to determine the stability of the 1:1 complex. The concentration of associated acid was held constant (0.0625 *M* in the carbon tetrachloride solvent), and the tri-*n*-butyl phosphate concentrations was varied. The total volume of each solution also was held constant by dilution with carbon tetrachloride to a final volume of 50 ml.

The possible formation of a 1:2 tri-*n*-butyl phosphate–nitric acid complex in carbon tetrachloride also was studied employing the molar ratio method. In this case, the concentration of tri-*n*-butyl phosphate was held constant and the nitric acid concentration was varied until a maximum concentration ratio of 0.16 *M* nitric acid to 0.04 *M* tri-*n*-butyl phosphate was obtained in carbon tetrachloride.

Aqueous nitric acid solutions of varying molarities were prepared for the partition study by adding the required concentration of reagent-grade acid (70%) to distilled water. The molarities of the initial aqueous nitric acid solutions were determined by titration with standard alkali to a phenolphthalein end-point. The nitric acid equilibrium distribution data were obtained by mixing the aqueous nitric acid solutions with tri-*n*-butyl phosphate for a period of three minutes at constant temperature (25°). The mixture was allowed to separate, and the phases were sampled and analyzed. The acidity of both the aqueous and organic phases was determined by titration with standard alkali to a phenolphthalein end-point. The organic aliquot was added to an excess of distilled water and the titration was made directly on this mixture.

Results and Discussion

Aqueous nitric acid solutions have been shown by numerous investigators[12–19] to contain associated nitric acid molecules (HNO_3). The degree of association has been shown to increase rapidly with increasing concentration of the acid.

In a two-phase system of tri-*n*-butyl phosphate and aqueous nitric acid (associated nitric acid and tri-*n*-butyl phosphate being completely miscible), it has been shown that hydrogen ions or nitrate ions do not exist appreciably in the tri-*n*-butyl phosphate phase.[2] If associated nitric acid (HNO_3) were present in the aqueous phase, however, it might be expected that the polar tri-*n*-butyl phosphate would combine with the polar associated nitric acid through hydrogen bonding. The data presented by Redlich and Bigeleisen,[13] illustrating the presence of associated nitric acid in aqueous nitric acid solutions, plus the above considerations, led the authors to believe that any complex formation in the system would be between the associated nitric acid molecules and the tri-*n*-butyl phosphate molecules. A spectrophotometric study was conducted employing tri-*n*-butyl phosphate and associated nitric acid in the organic solvent, carbon tetrachloride, to determine the mole ratio and stability of any significant complexes which are formed. Carbon tetrachloride was chosen as the solvent for this study because of its inertness toward the reactants under investigation.

The spectra of 0.0625 *M* tri-*n*-butyl phosphate, 0.0625 *M* associated nitric acid, and a 1:1 mixture (0.0625 *M* tri-*n*-butyl phosphate–0.0625 *M* associated nitric acid) of the two in the wave length range, 260 to 320 mμ, are presented in Fig. 1. Wave lengths lower than 260 mμ could not be investigated because of the high absorption of the carbon tetrachloride solvent below 260 mμ. The absorbance of the mixture at any wave length should be equal to the sum of the absorbance of each component at the corresponding wave length, if no reaction occurs in the mixture. The sum of the absorbance of A and B in Fig. 1 at any wave length over the range investigated does not equal the absorbance of C at the corresponding wave length. The difference of the observed results of C from the calculated results is attributed to the

---

[5] T. J. Collopy, "The Tributyl Phosphate-Nitric Acid Complex and Its Role in Uranium Extraction," NLCO-749, April 23, 1958.

[6] J. Kennedy and S. S. Grimley, Tri-n-butyl Phosphate Studies, Parts I, II and III, AERE-CE/R-968, October 6, 1952.

[7] R. N. Jones and G. D. Thorn, *Research*, **27B**, 580 (1949).

[8] P. Job, *Compt. rend.*, **184**, 204 (1927).

[9] W. C. Vosburgh and G. R. Cooper, *J. Am. Chem. Soc.*, **63**, 437 (1941).

[10] A. E. Harvey, Jr., and D. L. Manning, *ibid.*, **72**, 4488 (1950).

[11] J. H. Yoe and A. L. Jones, *Ind. Eng. Chem., Anal. Ed.*, **16**, 111 (1944).

[12] O. Redlich, *Chem. Revs.*, **39**, 333 (1946).

[13] O. Redlich and J. Bigeleisen, *J. Am. Chem. Soc.*, **65**, 1883 (1943).

[14] N. R. Rao, *Indian J. Phys.*, **15**, 185 (1941).

[15] W. F. K. Wynne-Jones, *J. Chem. Soc.*, 1064 (1930).

[16] A. Kossiakoff and D. Harker, *J. Am. Chem. Soc.*, **60**, 2047 (1938).

[17] O. Redlich, *Z. physik. Chem.*, **A182**, 42 (1938).

[18] H. von Halban and J. Eisenbrand, *ibid.*, **132**, 401 (1928).

[19] G. C. Hood, O. Redlich and C. A. Reilly, *J. Chem. Phys.*, **22**, 2067 (1954).

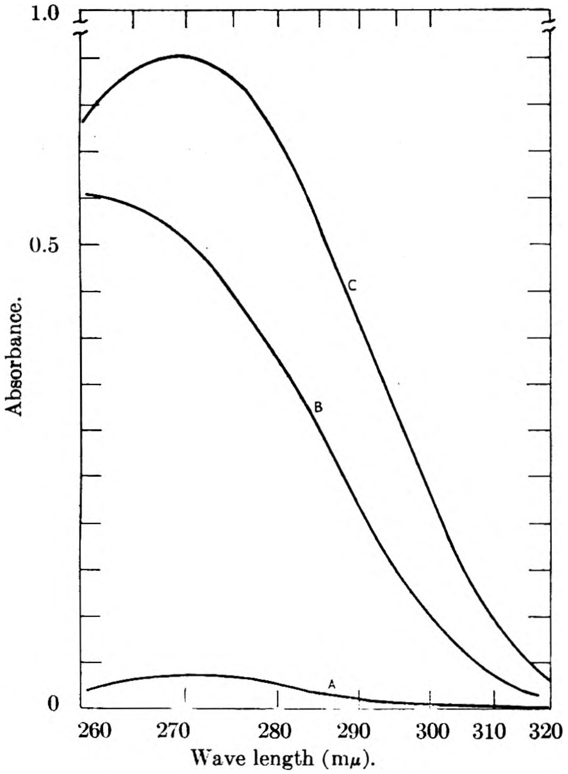

Fig. 1.—Absorption spectra curve A, 0.0625 M TBP in carbon tetrachloride; curve B, 0.0625 M associated nitric acid in carbon tetrachloride; curve C, mixture containing 0.0625 M associated nitric acid and 0.0625 M TBP in carbon tetrachloride.

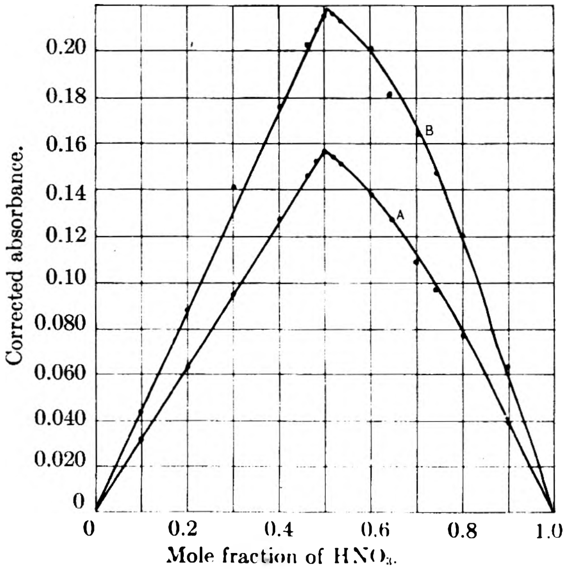

Fig. 2.—Continuous variation plots for the TBP-HNO_3 complex in carbon tetrachloride: curve A, 298 mμ; curve B, 286 mμ.

–NO_2 group band shift, and intensity changes upon reaction of the acid with tri-*n*-butyl phosphate to form the complex.

The Determination of the 1:1 Complex.—The method of continuous variation was employed to examine complex formation in the TBP·HNO_3 system. Continuous variation data for TBP·HNO_3 mixtures show the existence of a 1:1 TBP·HNO_3 complex in carbon tetrachloride (Fig. 2). Data also were obtained which showed a 1:1 TBP·HNO_3 complex in the solvent chloroform and in a mixed solvent, 95% isoöctane by volume and 5% diethyl ether by volume. The fact that the maxima were reproducible at each wave length was attributed to the formation of only one complex in the system[9] at the concentration ranges investigated. The continuous variation curves were slightly unsymmetrical with the absorbance difference being higher on the excess acid side than on the excess TBP side. These data might indicate formation of another complex species in solution. Further study was conducted in excess acid medium, the results are presented in the section on the investigation of higher complexes.

Figure 3 illustrates the method of molar ratios which was employed to show that the 1:1 TBP·HNO_3 complex was very stable. According to theory, for a very stable complex, a plot of absorbance of the complex against the molar ratio of the reagents, which react to form the complex (the concentration of one of the reagents remaining constant), would rise from the origin as a straight line and break sharply to constant absorbance at the molar ratio of the components in the complex. The plot of a complex that dissociates appreciably would not show a sharp break, but would give a continuous curve and approach constant absorbance only at large excesses of the variable component. Curve A (Fig. 3) is a plot of the solution absorbance *versus* molar ratio (TBP/HNO_3 in carbon tetrachloride, associated nitric acid concentration 0.0625 M) at a wave length of 308 mμ. The plot rises from the origin as a straight line (since associated nitric acid absorbs at this wave length, the origin in this case is the absorbance of 0.0625 M associated nitric acid) and breaks sharply at a mole ratio of 1:1, as predicted for a strong complex. With increasing excess tri-*n*-butyl phosphate concentration over that required for complexing, the curve does not achieve constant density but continues to rise linearly. This linear increase of absorbance is due to the absorbance of the excess tri-*n*-butyl phosphate. Line B is the calculated curve obtained by subtracting the excess tri-*n*-butyl phosphate absorbance from the absorbance found experimentally. The actual complex curve then rises from the origin as a straight line and breaks sharply to constant density.

The Investigation of Higher Complex Equilibria.—Figure 4 again illustrates the method of molar ratios used in this case to determine whether any evidence of higher nitric acid complexes [TBP·$(HNO_3)n$, where $n > 1$] is shown in solutions containing excess associated nitric acid. Curves A and B are plots of solution absorbance *versus* associated nitric acid concentration with tri-*n*-butyl phosphate present. The tri-*n*-butyl phosphate concentration was maintained at 0.04 M. Curves C and D are plots of solution absorbance of nitric acid alone. Curves A and B rise from the origin as straight lines and break appreciably at a nitric acid concentration equal to 0.04 M. Once again the break occurred at the point indicating a 1:1 complex. A sharp break would not be expected if higher complex equilibria exist, but rather, a gradual change of slope. Furthermore, if only one complex equilibrium is operating and, as proved earlier, if the complex is extremely stable then the absorbance of the excess acid should be a function of the concentration of the excess acid; that is, absorbance is equal to a constant times the concentration of excess acid ($A = KC$). The constant obtained by plotting A *versus* excess C in the above equation should be equal to the constant obtained by plotting A *versus* associated nitric acid when no tri-*n*-butyl phosphate is present at any wave length investigated. Curves A and B (excess acid) are parallel within experimental accuracy to curves C and D for the absorbance of associated nitric acid at the wave lengths 290 and 295 mμ, respectively. The same results indicative of no second complex also were found to exist at six other wave lengths investigated in the range of 275 to 305 mμ.

Since it has been established that (1) associated nitric acid exists in aqueous nitric acid solution, and (2) that a stable, equimolar complex forms between tri-*n*-butyl phosphate and associated nitric acid, the equilibrium distribution curve for nitric acid between tri-*n*-butyl phosphate and water was interpreted in terms of complex formation between tri-*n*-butyl phosphate and associated nitric acid in the organic phase. Figure 5 presents the equilibrium curve up to an aqueous nitric acid concentration of 12 *M*.

The associated acid values for each aqueous solution (based on data of Redlich and Bigeleisen[13]) are also indicated. Figure 5 shows that as the associated acid increases, the amount of complex formed in the tri-*n*-butyl phosphate phase increases up to the value for the 1:1 complex as would be predicted. The linearity of the equilibrium curve beyond the 1:1 complex and the results of the spectral data indicate that the distribution of associated nitric acid into the organic is a function of its solubility in the 1:1 TBP·HNO$_3$ complex and not of further complex formation. The fact that associated nitric acid distributes very strongly in favor of the organic phase even at low acid concentrations (and low associated acid concentration) was attributed to the associated nitric acid reaction with tri-*n*-butyl phosphate shifting the associated nitric acid equilibrium in the aqueous nitric acid solution.

The results reported herein showed the formation of a stable, equimolar complex between tri-*n*-butyl phosphate and associated nitric acid in the organic phase. It was concluded from these results and from the previously reported data on the presence of associated nitric acid in aqueous nitric acid solutions that the reaction of nitric acid and tri-*n*-butyl phosphate to produce a complex is controlled by the associated nitric acid concentration in the two-phase system under study.

Acknowledgment.—The authors wish to acknowledge assistance by members of the Technical Division, especially Mr. W. C. Manser.

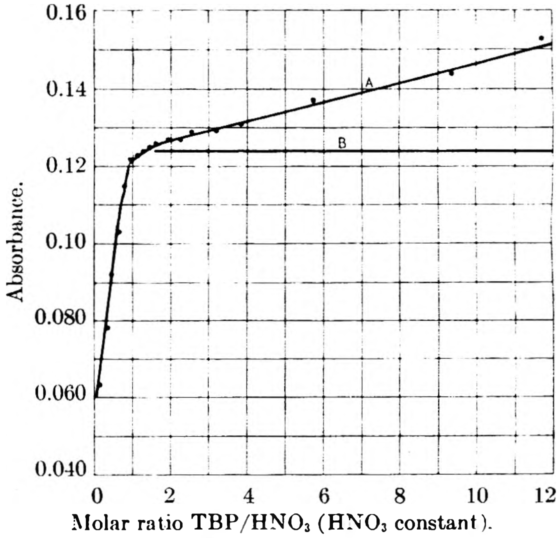

Fig. 3.—The stability of the 1:1 TBP–HNO$_3$ complex in carbon tetrachloride: curve A, experimental curve; line B, experimental curve—correction for TBP absorption 308 mμ.

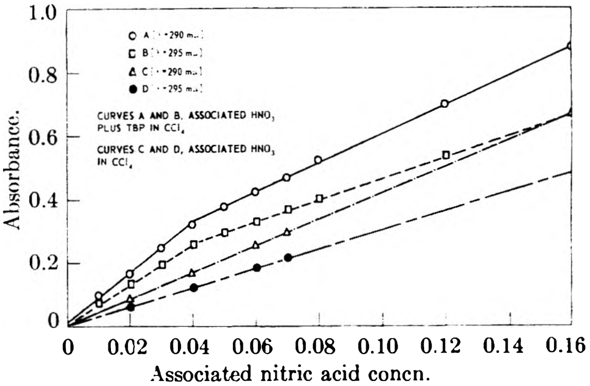

Fig. 4.—The absorbance of the 1:1 complex in the presence of associated nitric acid.

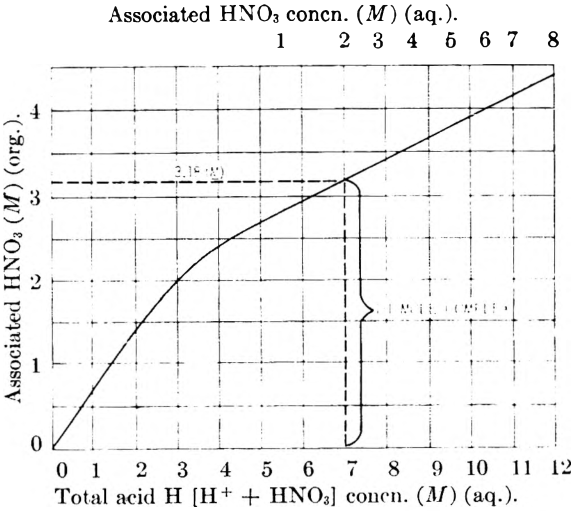

Fig. 5.—Equilibrium distribution of nitric acid between TBP and water at various nitric acid concentrations (25°).

EQUILIBRIUM CONSTANTS FOR THE SYSTEM TRI-*n*-BUTYL PHOSPHATE-WATER-NITRIC ACID

By T. J. Collopy and J. H. Cavendish

Technical Division, National Lead Company of Ohio, Cincinnati, Ohio

Received April 29, 1960

The equilibrium constant for the reaction of tri-*n*-butyl phosphate with associated nitric acid was calculated to be 19.9 ± 0.5. The equilibrium distribution constant for the partition of associated nitric acid into tri-*n*-butyl phosphate was determined as 0.19. The equilibrium constants obtained were used to calculate the concentration of associated nitric acid in dilute aqueous nitric acid solutions. These calculations were made from the equilibrium distribution curve for nitric acid between tri-*n*-butyl phosphate and water at 25° over the concentration range of 0–12 *M* aqueous nitric acid.

Introduction

A previous paper[1] presented data which showed that a stable, equimolar complex was formed by the reaction of associated nitric acid (HNO_3) with tri-*n*-butyl phosphate (TBP). It was concluded from these results that this same reaction takes place between TBP and associated nitric acid in the two-phase system $TBP–H_2O–HNO_3$ since associated nitric acid is present in aqueous nitric acid solutions. This two-phase system then can be represented by (1) an equilibrium reaction in the organic phase

$$TBP_{org} + HNO_{3org} \rightleftharpoons TBP\cdot HNO_{3org} \qquad (I)$$

(2) an equilibrium reaction in the aqueous phase

$$HNO_{3aq} + H_2O_{aq} \rightleftharpoons H_3O^+{}_{aq} + NO_3^-{}_{aq} \qquad (II)$$

and (3) an equilibrium distribution constant (D.C.) for associated nitric acid between phases.

$$\text{D.C.} = HNO_{3org}/HNO_{3aq} \qquad (III)$$

By substituting the value for the associated nitric acid in the organic phase from equation III into equation I and solving for the equilibrium constant (K), for the equilibrium reaction shown by equation I, equation IV is obtained.

$$K_{eq} = [TBP\cdot HNO_3]_{org}/[(\text{D.C.})(HNO_3)_{aq}][TBP]_{org} \qquad (IV)$$

The value for K equilibrium for equation I can be calculated from the data[1,2] which were obtained in constructing the equilibrium distribution curve for nitric acid between TBP and water. Using these experimental data, equation IV would take the form

$$K_{eq} = \frac{[\text{total organic acidity} - (\text{D.C.})(HNO_{3aq})]}{[(\text{D.C.})(HNO_3)_{aq}][TBP]_{org}} \qquad (V)$$

This can be done by (1) obtaining values for the concentration of associated nitric acid in aqueous nitric acid solution from literature data, (2) assuming a value for the equilibrium distribution constant between phases, (3) calculating the concentration of uncombined nitric acid in the TBP phase, (4) calculating the concentration of the $TBP\cdot HNO_3$ complex by subtracting the value above from the total titratable acid in the TBP phase, and (5) calculating the value for uncombined TBP by subtracting the value obtained above from the starting concentration of TBP and compensating for the volume change. These results, when the correct value for the distribution constant was used, would show the value of the equilibrium constant for the reaction of nitric acid and TBP in the TBP phase.

Since purified commercial-grade TBP was used in these studies, the theoretical molarity for the point at which the molarity of TBP would equal the molarity of the nitric acid in the TBP phase can be calculated (*i.e.*, 3.18 *M*). In the two-phase $TBP–H_2O–HNO_3$ system, this condition in the TBP phase is reached at an aqueous nitric acid concentration of 7 *M* (*i.e.*, 2 *M* associated nitric acid).[1] The equilibrium partition data and the spectral data reported previously[1] both showed that beyond this point, the additional nitric acid entering the TBP phase could be attributed to solvent partition rather than further complex formation. This being the case, the region above this point can be separated from the region of complex formation and examined for the value of the equilibrium distribution constant. This can be done by dividing the concentration of associated nitric acid in the TBP phase by the concentration of associated nitric acid in the aqueous phase. This latter value can be obtained from literature data. The value obtained in this way should be close to the assumed value used previously in the calculation of the equilibrium constant using equation V.

Since values for associated nitric acid in aqueous nitric acid solution are unavailable for the range between 0.5 and 4 *M*, the constants which are obtained can be used together with the data from the equilibrium curve to calculate values for the concentration of associated nitric acid in dilute aqueous nitric acid solution. These data would provide an indication of the concentration of associated nitric acid in dilute aqueous nitric acid solutions, which formerly was assumed to be negligible.

Discussion and Results

The equilibrium curve for the distribution of nitric acid between TBP and water at 25° was presented in a previous paper.[1] These results showed that the ratio of the total nitric acid in the TBP phase to the total nitric acid in the aqueous phase decreases with increasing aqueous nitric acid concentration until a constant value is obtained. This behavior was shown by previous papers[1,2] to be attributable to (1) the partition of associated nitric acid between TBP and water plus equimolar complex formation (0 to 7 *M* total H), and (2) partition of associated nitric acid alone between TBP and water at higher aqueous nitric acid concentra-

---

[1] T. J. Collopy and J. F. Blum, This Journal, 64, 1324 (1960).

[2] T. J. Collopy, "The Tributyl Phosphate-Nitric Acid Complex and Its Role in Uranium Extraction," NLCO-749, April 23, 1958.

tions without additional complexes being formed (above 7 *M* total H).

Using assumed values for the equilibrium distribution constant, the value for K_{eq} was calculated using equation V for the region of significant complex formation (*i.e.*, 0–2 *M* associated nitric acid in the aqueous phase). This was done by obtaining the values of associated nitric acid in aqueous nitric acid solution for the various concentrations from the data presented by Redlich and Bigeleisen.[3] The value for associated nitric acid in the TBP phase was obtained by multiplying this value by the assumed value for the distribution constant. The value for the concentration of the $TBP \cdot HNO_3$ complex was obtained by subtracting the value determined above from the total titratable acid. The concentration of free TBP was calculated by subtracting from the starting concentration of TBP the concentration of $TBP \cdot HNO_3$ complex and considering the volume change.

In Table I are presented the values which were calculated for the equilibrium constant using an assumed value for the distribution constant of 0.19. Numerous values ranging from 0.01 to 0.2 were tested; however, Table I presents only the data at an assumed value of 0.19. These calculations were restricted to the region above 4 *M* total aqueous nitric acid because data for the concentration of associated nitric acid in aqueous nitric acid solutions were not available below this point. These results show a value of 19.9 ± 0.5 for the equilibrium constant for the reaction of TBP and nitric acid to yield the equimolar complex.

TABLE I

CALCULATED EQUILIBRIUM CONSTANT FOR THE REACTION OF ASSOCIATED NITRIC ACID WITH TBP

Total acid hydrogen *M*, aq.	Associated nitric acid, *M*, aq.	Associated nitric acid *M* Org [*i.e.*, HNO_3Aq × D.C.	$TBP \cdot HNO_3$ (*M*) total acid in TBP-free HNO_3 in TBP	Free TBP *M*	*K*, l./mole
4	0.60	0.11	2.34	1.06	20.1
4.5	.70	.13	2.45	0.93	20.3
5	.85	.16	2.54	.82	19.4
5.5	1.05	.20	2.63	.67	19.6
6	1.25	.24	2.71	.56	20.2
6.5	1.55	.30	2.78	.46	20.1
7	2.00	.38	2.80	.38	19.4

Utilizing once again the values for associated nitric acid in aqueous nitric acid solution[3] and calculating the value for associated nitric acid in the TBP phase, the equilibrium distribution constant for the partition of associated nitric acid between TBP and water (equation III) was calculated. This was done by assuming that the region above 3.18 *M* associated nitric acid in the TBP phase and 2 *M* associated nitric acid in the aqueous phase was engaged primarily in nitric acid partition with no further complexes being formed and only minor shifts in the concentrations of TBP and $TBP \cdot HNO_3$ which existed in the TBP phase at a concentration of 3.18 *M*.

In Table II are presented the calculated values for the equilibrium distribution constant at several aqueous nitric acid concentrations. These results show a value for the equilibrium distribution constant of 0.19, which corroborates the assumed value which best satisfied the calculation of the equilibrium constant by equation V.

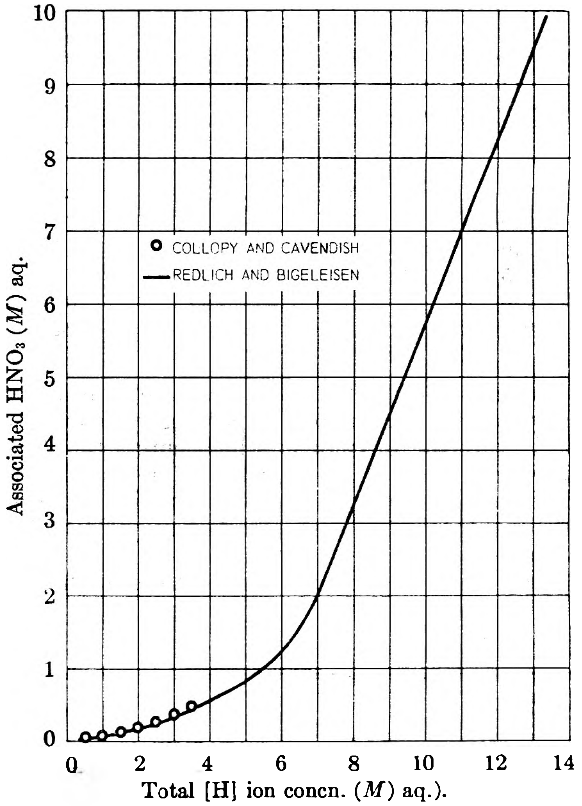

Fig. 1.—Concentration of associated nitric acid in aqueous nitric acid solution.

TABLE II

EQUILIBRIUM DISTRIBUTION CONSTANT FOR THE PARTITION OF ASSOCIATED NITRIC ACID BETWEEN TBP AND WATER

Total acid hydrogen, *M*	Associated nitric acid,[a] *M*, aq.	Associated nitric acid,[b] *M*, org.	D.C. (O/A)
8	1.25	0.24	0.19
9	2.50	.48	.19
10	3.75	.72	.19
11	5	.96	.19
12	6.3	1.21	.19

[a] In excess of 2 *M*. [b] In excess of 3.18 *M*.

Using these values for *K* equilibrium and the distribution constant, the values of associated nitric acid at concentrations below the range used in the determination of *K* equilibrium were calculated from the data obtained when constructing the equilibrium curve. The equation used is

$$(HNO_3)_{aq} = \text{Total organic acidity}/K_{eq}(\text{D.C.})TBP_{org} + (\text{D.C.}) \quad (VI)$$

This calculation showed the amount of associated nitric acid present in aqueous nitric acid solutions below the values reported previously.[3] Table III presents the data for the concentration of associated nitric acid in dilute aqueous nitric acid solution. In Fig. 1 these data are presented together with the data previously reported.[3]

---

[3] O. Redlich and J. Bigeleisen, *J. Am. Chem. Soc.*, **65**, 1883 (1943).

TABLE III

CALCULATED VALUES FOR ASSOCIATED NITRIC ACID IN DILUTE AQUEOUS NITRIC ACID SOLUTIONS

Total acid hydrogen, M	Total organic acidity, M	TBP, M	Associated nitric acid, M, aq.
3.5	2.28	1.24	0.47
3.0	2.04	1.50	.35
2.5	1.77	1.74	.26
2.0	1.42	2.10	.17
1.5	1.07	2.46	.11
1.0	0.75	2.80	.07
0.5	0.48	3.09	.04

The fact that the partition coefficient was a constant is believed to be supporting evidence for considering the nitric acid which enters the TBP phase in excess of a 1:1 ratio as dissolved acid which does not enter into a complexation reaction with the 1:1 TBP·HNO_3 complex to yield higher complexes.

Further data are being collected to show the role which this complex has in metal extraction processes in which metals are extracted from acidic solutions with tri-*n*-butyl phosphate.

Summary

Data are presented which show the values for the equilibrium distribution constant and the equilibrium reaction constant for the partition of associated nitric acid into TBP and the reaction of this acid in TBP to form a complex as 0.19 and 19.9 ± 0.5, respectively. These constants were used to arrive at values for the concentration of associated nitric acid in dilute aqueous nitric acid solutions. These data are offered as indicating that only one complex forms between TBP and nitric acid in a two-phase TBP–H_2O–HNO_3 system.

Acknowledgment.—The authors wish to acknowledge the helpful assistance of Dr. C. E. Crompton of the Division Staff and Dr. D. S. Arnold and W. C. Manser of the Chemical Department.

NOTES

THE SOLUBILITY OF NITROGEN, ARGON, METHANE, ETHYLENE AND ETHANE IN NORMAL PRIMARY ALCOHOLS[1]

BY FRANKLIN L. BOYER[2] AND LOUIS J. BIRCHER

Furman Chemistry Laboratories, Vanderbilt University, Nashville Tennessee

Received February 18, 1960

A study of the solubility of nitrogen, argon, methane, ethylene and ethane in a series of normal primary alcohols at the temperatures of 25 and 35° was made using a modified E. H. Sargent Company manometric Van Slyke–Neill blood gas apparatus. The apparatus was equipped with a chamber similar to a volumetric Van Slyke blood gas apparatus. A manometer was mounted at the waste solvent exit port, which was opened to the solution chamber during the solution process so that the total pressures of gas and vapor in the solution chamber could be adjusted to atmospheric pressure. The procedures given by Van Slyke and Peters[3] for extraction of gases from the solvent, and the measurement of the gas and solvent volume was followed. To avoid the corrections attendant with measuring the extracted gas pressure over the solvent, the solvent was transferred to the bulb below the lower stopcock of the extraction vessel and sealed off. The gas and solvent vapor then was brought to volume over mercury. This also enabled us to make repeated extractions of the solvent to assure complete removal of gas from the solvent. The temperature was controlled at 25° to ±0.01° and at 35° to ±0.05°.

Materials.—All of the alcohols were purified by the removal (if necessary) of the aldehydes and ketones, then dried and distilled. Known procedures for the purification of the alcohols were used.[4,5] We chose middle cuts with

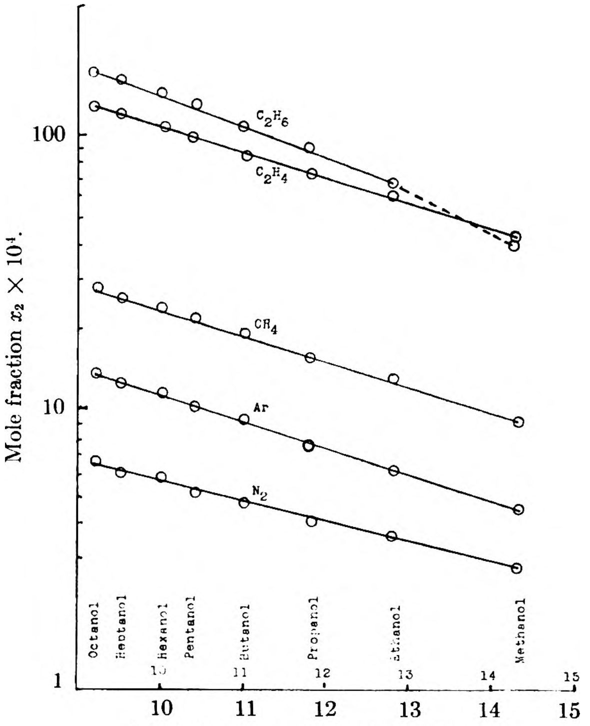

Fig. 1.—Solvent capacity of alcohols for gases and alcohol solubility parameters (25° and 760 mm.).

---

(1) Adapted from Ph.D. thesis of F. L. Boyer, Vanderbilt University, 1959.

(2) E. I. du Pont de Nemours and Co., Inc., Circleville, Ohio.

(3) J. P. Peters and D. D. Van Slyke, "Quantitative Clinical Chemistry," Vol. II, Williams and Wilkins Co., Baltimore, Md., 1932.

TABLE I

OSTWALD COEFFICIENT OF SOLUBILITY AT 25° AND 1 ATM. PRESSURE

Gas →	N_2		Ar		CH_4		C_2H_4		C_2H_6	
Alcohol	Obs.	Lit.	Obs.	Lit.	Obs.	Lit.	Obs.	Lit.	Obs.	Lit.
CH_3OH	0.167	0.164[a]	0.267	0.267[d]	0.552	.....	2.63	....	2.34	2.31[b]
C_2H_5OH	.149	.1489[a]	.258	.258[d]	.539	.....	2.56	....	2.87	2.75[b]
C_3H_7OH	.133	.132[b]	.254	.251[b]	.510	.....	2.41	....	2.98	2.84[b]
C_4H_9OH	.122	.1225[a]	.246	.240[b]	.509	.....	2.26	....	2.93	2.85[b]
$C_5H_{11}OH$	.116	.1225[c]	.229	.224[b]	.483	.....	2.23	....	2.95	2.76[b]
$C_6H_{13}OH$	.114	.....	.224	....	.464	.....	2.08	....	2.84	...
$C_7H_{15}OH$	.105	.....	.218	....	.448	.....	2.05	....	2.76	...
$C_8H_{17}OH$	.102	.....	.213	....	.436	.....	1.91	....	2.66	...

[a] C. B. Kretschmer, J. Nowakowska and R. Wiebe, *Ind. Eng. Chem.*, **38**, 506 (1946). [b] J. C. Gjaldbaek and H. Niemann, *Acta Chem. Scand.*, **5**, 12, 1015 (1958). [c] G. Just, *Z. physik. Chem.*, **37**, 342 (1901). [d] A. Lannung, *J. Am. Chem. Soc.*, **52**, 68 (1930).

TABLE II

MOLE FRACTION SOLUBILITY (×10^4) AT 25°, 1 ATM. PRESSURE, AND GAS FORCE CONSTANT

Gas	ϵ/k^0T	CH_3OH	C_2H_5OH	C_3H_7OH	C_4H_9OH	$C_5H_{11}OH$	$C_6H_{13}OH$	$C_7H_{15}OH$	$C_8H_{17}OH$
N_2	91.5	2.55	3.48	4.18	4.74	5.25	5.64	6.09	6.47
Ar	124	4.15	6.18	7.82	9.23	10.5	11.6	12.6	13.7
CH_4	136.5	8.67	12.8	16.1	19.1	21.5	23.4	26.0	28.0
C_2H_4	205	43.9	59.7	74.6	87.1	98.4	108.4	118.0	126.8
C_2H_6	230	40.5	68.6	90.0	109	126	143	159	173

TABLE III

IDEAL AND CALCULATED ENTROPY OF SOLUTION, GASES IN ALCOHOLS

	N_2		Ar		CH_4		C_2H_4		C_2H_6	
Alcohol	$R \ln x_2$	$\bar{S}_2^0 - S_g$	$R \ln x_2$	$\bar{S}_2^0 - S_g$	$R \ln x_2$	$\bar{S}_2^0 - S_g$	$R \ln x_2$	$\bar{S}_2^0 - S_g$	$R \ln x$	$\bar{S}_2^0 - S_g$
CH_3OH	−16.39	5.73	−15.41	−3.82	−13.97	−8.91	−10.88	−27.68	−10.78	−24.18
C_2H_5OH	−15.77	5.73	−14.63	−1.27	−13.19	−7.64	−10.14	−23.23	− 9.86	−21.64
C_3H_7OH	−15.40	5.73	−14.17	−0.32	−12.73	−7.00	− 9.70	−21.00	− 9.32	−20.05
C_4H_8OH	−15.15	6.04	−13.84	−0.95	−12.41	−6.36	− 9.39	−19.41	− 8.94	−18.77
$C_5H_{11}OH$	−14.96	6.36	−13.59	−2.23	−12.16	−6.04	− 9.15	−18.46	− 8.65	−17.50
$C_6H_{13}OH$	−14.79	6.36	−13.38	−2.86	−11.96	−5.73	− 8.96	−17.50	− 8.41	−16.55
$C_7H_{15}OH$	−14.66	6.36	−13.21	−3.50	−11.79	−5.41	− 8.79	−16.86	− 8.20	−15.91
$C_8H_{17}OH$	−14.54	6.36	−13.06	−4.14	−11.63	−5.73	− 8.64	−15.91	− 8.03	−15.27

constant index of refraction from the distillations. The gases were used without further purification and were: Air Reduction nitrogen 99.7% N_2, Ohio Surgical Company argon 99.6% pure, Phillips Petroleum methane and ethane, each 99.9 mole % pure, and Matheson C.P. ethylene 99.5% pure.

Results and Discussions.—We have reported in Table I the Ostwald coefficients measured at 25° along with those values obtained by other workers whose values have generally been accepted as accurate.

The solubility of the gases in the alcohols increases with decreasing internal pressure of the solvent as shown in Fig. 1 and decreases with decreasing Lennard-Jones force constants of the gases as shown in Table II. The solubility in the normal primary alcohols of the five gases studied was found to follow the equation $\log x_2 = a + b \log C$ where a and b are empirical constants and C is the number of carbon atoms in the alcohol chain. From the equations of this family of curves we were able to calculate the solubility of the gases in the alcohols at 35° using only four measured values in 1-propanol, 1-butanol, 1-pentanol and 1-octanol. We estimated

$$\bar{S}_2^0 - S_g = R\,\frac{d(\ln x_2)}{d(\ln T)}$$

from our solubility measurements, and our results are given in Table III. The results may be subject to error because of the short temperature range over which the measurements were made. They are, however, sufficiently good to warrant some generalizations: (1) as in non-polar solvents the entropy of solution is positive whenever the solubility increases with increasing temperature. (2) The entropy of solution increases with decreasing gas force constant and decreasing solvent internal pressures. These observations are in line with those of Jolley and Hildebrand[6] for solutions of gases in non-polar solvents. (3) The effect of polarity apparently is not as great as would be deduced from the internal pressures alone.

Summary.—The solubilities of N_2, Ar, CH_4, C_2H_4 and C_2H_6 on the series of normal primary alcohols, methanol through octanol, were measured at 25 and 35°. The solubility of the gases in the alcohols has been related to the internal pressure of the solvent and the Lennard-Jones force constant of the gas. The entropy of solution for each system has been estimated.

---

(4) L. F. Fieser, "Experiments in Organic Chemistry," 2nd ed., D. C. Heath and Co., Boston, Mass., 1941, p. 358.

(5) A. Weissberger and E. S. Proskauer, "Organic Solvents," The Clarendon Press, Oxford, 1935.

(6) J. E. Jolley and J. H. Hildebrand, *J. Am. Chem. Soc.*, **80**, 1050 (1958).

HIGH ENERGY γ-IRRADIATION OF VINYL MONOMERS. II. INFRARED SPECTRA OF RADIATION-POLYMERIZED ACRYLONITRILE

By Jett C. Arthur, Jr., and Robert J. Demint

Southern Regional Research Laboratory,[1] New Orleans, Louisiana

Received March 4, 1960

In recent studies to prepare graft polymers of cotton cellulose and acrylonitrile,[2,3] it was noted that when the ratio of acrylonitrile to water was increased, radiation-polymerized acrylonitrile, having decreased solubility in N,N-dimethylformamide, was produced at higher radiation dosages.[4] This decrease in solubility probably was due to radiation-induced crosslinks or to a basic change in the intrinsic structure of the polymer.

In addition to physical-chemical data on Co^{60} γ-radiation polymerized acrylonitrile previously reported,[4] infrared spectra, over the range of 2.5 to 15 μ, were determined for the polymers. Monomer to water ratios were 1:25, 1:12, 1:4 and 29:1; radiation dosages were 5.2, 16, 26, 39, 52, 156, 260 and 520 $\times 10^{21}$ electron volts per liter. Infrared spectra of the twenty-eight samples of polymers in the solid phase were obtained using the KBr disc technique.[5]

The infrared spectra for all of the polymers were practically identical with no apparent correlation between solubility, intrinsic viscosity, or conversion of monomer to polymer and their spectra. On comparing the infrared spectrum of chemically-initiated polymerized acrylonitrile, determined by Liang and Krimm on thin solid films,[6] with the spectra of the radiation polymerized acrylonitrile, it was noted that the sharp bands coincided, as follows: 3.4, 6.8 and 7.4 μ, $-CH_2$; 4.5 μ, $-CN$; 8.0 μ, $-CH$; 9.3 μ, $-C-CN$.

These spectra are consistent with the interpretation of Liang and Krimm[6] that the structure of polyacrylonitrile was based on a head-to-tail arrangement of the $-CH_2CH(CN)-$ monomer units. From the physical-chemical data[4] and these spectra, the change in configuration of the structure of the radiation-polymerized acrylonitrile at the higher radiation dosages was probably that resulting from a dehydrogenation followed by cross-linking between two or more polymeric molecules. Since this would have introduced no new kind of bonds and would have only slightly increased the intensity of existing bonds, the infrared spectra did not indicate any marked change.

Acknowledgment.—The assistance of Elizabeth R. McCall and Donald Mitcham, in obtaining the infrared spectra on which these conclusions are based, is gratefully acknowledged.

---

(1) One of the laboratories of the Southern Utilization Research and Development Division, Agricultural Research Service, United States Department of Agriculture.

(2) J. C. Arthur, Jr., and R. J. Demint. Presented at the 15th Southwest Regional Meeting of the American Chemical Society, Baton Rouge, Louisiana, December 3–5, 1959.

(3) J. C. Arthur, Jr., R. J. Demint, W. F. McSherry and J. F. Jurgens, *Textile Research J.*, **29**, 759 (1959).

(4) J. C. Arthur, Jr., R. J. Demint and R. A. Pittman, This Journal, **63**, 1366 (1959).

(5) R. T. O'Connor, E. F. DuPré and E. R. McCall, *Anal. Chem.*, **29**, 998 (1957).

(6) C. Y. Liang and S. Krimm, *J. Polymer Sci.*, **31**, 513 (1958).

DEFORMATION OF THE URANYL ENTITY IN URANYL-MALATE, -TARTRATE, AND -CITRATE TRIDENTATE CHELATES[1]

By Isaac Feldman

Division of Radiation Chemistry and Toxicology, Department of Radiation Biology, School of Medicine and Dentistry, University of Rochester, Rochester, New York

Received March 8, 1960

It is now well-accepted that the uranyl ion may be considered to be collinear, uranium being the middle atom.[2] Previously, the belief has been expressed[3] that, when the uranyl ion is chelated in a tridentate manner by malate, *d*-tartrate or citrate ions, this collinearity is destroyed because of repulsion between the uranyl oxygen atoms and the chelating oxygens of the tridentate ligand.

It is desirable to establish the reasonableness of this postulate in order to strengthen the interpretation of equilibrium-constant results presented in a separate paper.[4] To do so, we have set up a semi-quantitative potential energy function V for the tridentate chelate relating the mutual repulsion energies of the uranyl oxygen atoms and the ligand atoms with the angle of deformation X of the uranyl entity and have calculated X for $dV/dX = 0$. This energy function is $V = V_1 + V_2 + V_2' + V_3 + V_3' + {}^1/_2kX^2$. V_1 represents repulsion between the uranyl oxygens, O_{Ia} and O_{Ib}; V_2 and V_2' represent repulsion of O_{Ia} and O_{Ib}, respectively, by the tridentate chelating group; V_3 and V_3' represent the sum of the repulsions on O_{Ia} and O_{Ib}, respectively, by the three waters of hydration which still remain[5] attached to uranium after chelation and which tend to prevent the deformation in opposition to the effect of the chelate group. The force constant k equal to 1.28×10^{-11} ergs/radian^2 was calculated from the Raman frequency, 210 cm.$^{-1}$, attributed to the bending vibration of the uranyl ion by Dieke and Duncan.[6]

Each repulsion term consists of an electrostatic term plus a van der Waals repulsion term. Each electrostatic term contains a permanent charge term and an induced dipole term. For the permanent charge term V_p each atom was treated as a point charge, so that $V_p = \Sigma(q_1q_2/r)$, but for the induced dipole term, V_i, each group was treated as an ideal point dipole located at the geometric center of the groups, so that $V_i = \Sigma q_1\mu_i/r^2$. For

---

(1) This paper is based on work performed under contract with the United States Atomic Energy Commission at the University of Rochester Atomic Energy Project, Rochester, New York.

(2) J. J. Katz and G. T. Seaborg, "The Chemistry of the Actinide Elements," Methuen and Co., Ltd., London, 1957.

(3) I. Feldman, J. R. Havill and W. F. Neuman, *J. Am. Chem. Soc.*, **76**, 4726 (1954).

(4) I. Feldman, C. A. North and H. B. Hunter, This Journal, **64**, 1224 (1960).

(5) Our earlier contention[3] that steric considerations should cause the coördination number of uranium to be less than its normal value of 8 is retracted.

(6) G. H. Dieke and A. B. F. Duncan, "Spectroscopic Properties of Uranium Compounds," Chapter 3, Nat. Nuclear Energy Ser. Div. III, 2, 1949.

the carboxylate groups, each oxygen was assigned a permanent charge of $e/2$, where $e = 4.78 \times 10^{-10}$ e.s.u. For the alcoholic group, permanent charges on C, H and O atoms of $+0.80$, $+1.57$, and -2.37×10^{-10} e.s.u., respectively, were estimated from the C–O and H–O permanent bond moments.[7] Also from the latter moment, values of $+1.57$ and -3.14×10^{-10} e.s.u. were assigned as permanent charges for H and O, respectively, in water.

The induced dipole moments of the ligands were estimated only as a first approximation by ignoring the effect of the ligands on each other and setting each induced dipole $\mu_i \cong \alpha q/r^2$, where α is ligand group polarizability, q is effective uranium charge at the location of the ligand group, and r is the distance between ligand group and uranium. A value of $+3e$ was used for q, since Connick and Hugus[8] estimated that "a uranyl ion appears as a $+3$ ion to waters about its equator." A polarizability of 1.28 Å.^{3} was calculated for the COH group from $^4/_3\pi N\alpha = R_{\mathrm{COH}}$, where N is Avogadro's number and R_{COH} is the group refraction,[7] 3.23 cc. Similarly, 3.55 Å.^{3} was calculated for the carboxylate group using an $R_{\mathrm{COO^-}} = {}^1/_2(R_{\mathrm{Ba(OOCH)_2}} - R_{\mathrm{Ba^{++}}}) - R_{\mathrm{H}}$. The value of $R_{\mathrm{Ba(OOCH)_2}}$ was approximated by use of the Lorentz–Lorenz equation, from the mean index of refraction of the biaxial $Ba(OOCH)_2$. A value of 1.48 Å.^{3} was used for the polarizability of water.

A permanent charge of $-1e$ was assigned to the uranyl oxygens in accordance with the entropy calculation of Connick and Hugus.[8] No induced charge was considered.

The van der Waals repulsion terms were estimated[9] by applying Amdur's potential energy function, $V_d = 1.36 \times 10^{-9} d^{-8.33}$ erg/molecule for 2.18 Å.$< d <$2.69 Å., where d is the distance between two atoms.

A reasonable geometry for the chelate had to be assumed. Zachariasen's extrapolated value[10] of 1.60 Å.^{3} was used for the bond lengths in the uranyl entity. A *maximum* value of 2.45 Å. for the secondary U–O bonds, *i.e.*, bonds involving the ligand oxygens, seems quite reasonable whether the bonds are ionic or covalent, for the following reasons. Considering the uranyl entity to behave as a $+3$ ion toward the ligands,[8] Zachariasen's values of 1.03 Å. for the ionic radius[2] of U^{+3} and 1.80 Å. for its covalent radius[11] may be employed to give lengths of 2.43 Å. for an ionic bond or 2.46 Å. for a covalent bond. In fact, 2.45 Å. is the secondary bond length in crystalline $NaUO_2Ac_3$.[9] Since the tridentate chelates are much stronger than the acetate complex,[2,4] the secondary bond length in the tridentate chelates should be shorter than those in the acetate complex.

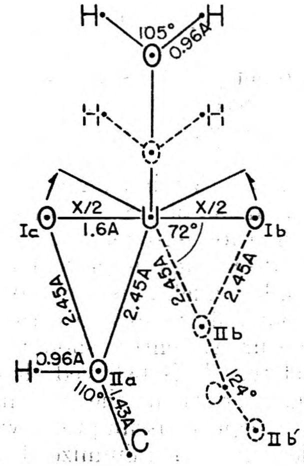

Fig. 1.—Side view of tridentate chelate. Solid-line letters indicate atoms in plane of paper. Dashed-line H_2O and COO groups indicate that groups are not in plane of paper, but in planes at angles shown in Fig. 2, and each has a mirror image.

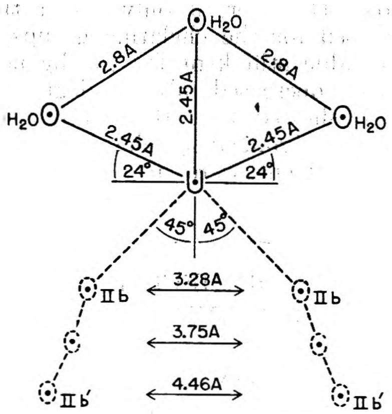

Fig. 2.—End view of tridentate chelate. O atoms of waters are in plane of paper about equator of uranyl entity. COO atoms are not in plane of paper but at angles shown in Fig. 1. COH group not shown in this figure.

Fisher–Hirschfelder–Taylor atom models and a homemade uranium atom model (sphere of radius 1.05 Å.) were employed as an aid in establishing the geometry. However, it was necessary to bear in mind that the van der Waals radius of an F–H–T oxygen atom model is only 1.22 Å., which is decidedly less than oxygen's normal ionic radius of 1.40 Å. and would be valid only if the oxygen atom is under considerable compression. With the scale models, it seems evident that the most favorable arrangement for preserving the linearity of the uranyl entity in the tridentate chelate is represented closely by Figs. 1 and 2 in which O_{IIa} represents alcoholic oxygen, and O_{IIb} and $O_{IIb'}$ represent carboxylate oxygens. For a zero deformation angle each chelating oxygen atom is situated at 2.45 Å. from its nearest uranyl oxygen, and the alcoholic oxygen is also 2.45 Å. from each chelating carboxylate oxygen. When the uranyl deformation is zero, the three waters[5] can be arranged about the equator in such a manner that the nearest water oxygens are 2.80 Å. apart

---

[7] C. P. Smyth, "Dielectric Behavior and Structure," McGraw–Hill Book Co., New York, N. Y., 1955, p. 301.

[8] R. E. Connick and L. Hugus, Jr., *J. Am. Chem. Soc.*, **74**, 6012 (1952).

[9] F. H. Westheimer, Chapter 12 in "Steric Effects in Organic Chemistry," edited by M. S. Newman, John Wiley and Sons, Inc., New York, N. Y., 1956.

[10] W. H. Zachariasen, *Acta Cryst.*, **7**, 795 (1954).

[11] This value may be estimated by subtracting 0.12 Å. from the U^{+3} metallic radius, 1.92 Å., since for U^{+4}, U^{+5} and U^{+6} the covalent radius is 0.12 Å. smaller than the metallic radius.[12]

[12] W. H. Zachariasen, Chapter 18 of "The Actinide Elements," Natl. Nuclear Energy Ser. Div. IV, 14A (1954).

and each water oxygen is 2.93 Å. from each uranyl oxygen.

Applying geometry to Figs. 1 and 2, the distances between each uranyl oxygen and each atom of the ligands was calculated as a function of the uranyl deformation angle X and inserted in the potential energy function V. Minimizing this function gave a deformation angle of 18°, V being (26 kcal./mole U) less than for zero deformation.

This deformation angle is presented, not for its actual magnitude, which must be only a rough approximation, but only as evidence that significant bending of the uranyl entity should occur in the tridentate chelate. It is believed that the actual bending is greater than the calculated angle, since with one exception assumptions were made on the safe side, *i.e.*, to minimize bending. For instance, the O_{IIa}–O_{IIb} distance in Fig. 1 was maintained constant at 2.45 Å., although it should increase if there is any deformation at all.

The exception to our normally-conservative assumptions is the use of $\mu_i \cong \alpha q/r^2$ to obtain μ_i for ligands. However, if only $^1/_2$ of this value had been used for the chelating groups, but the maximum value still kept for the ligand waters, X would have decreased only $1^1/_2$ degrees. Calculations also showed that the deformation angle would not be significantly changed from 20° if the uranyl oxygens were displaced unequal distances.

THE HEATS OF DECOMPOSITION OF ARSINE AND STIBINE[1]

By Stuart R. Gunn, William L. Jolly and LeRoy G. Green

University of California, Lawrence Radiation Laboratory, Livermore, California

Received March 11, 1960

The heats of formation of arsine and stibine are of interest for systematization of the thermodynamics of hydrides and their thermochemical bond energy terms, and for the correlation of the properties with increasing atomic number in group V. The best previous value for $\Delta H_f^0(AsH_3)$ is that of Ariya, Morozova and Tszi-Tai[2] who, by measuring the heats of reaction of zinc arsenide with dilute HCl and with dilute HCl containing Br_2 and of arsenic with dilute HCl containing Br_2, derived a value of +18 ± 1.5 kcal. mole^{-1}. Ogier[3] measured the heat of reaction of arsine with bromine water; from this the NBS compilers[4] derive a value of +41.0 kcal. mole^{-1}. The best value for stibine is that of Stock and Wrede[5] who measured the heat of the explosive decomposition to the elements and obtained +34.0 kcal. mole^{-1} for $\Delta H_f^0(SbH_3)$. Berthelot and Petit[6] measured the heat of reaction of SbH_3 with bromine water; from this Bichowsky and Rossini[7] obtain a value of +79.5 kcal. mole^{-1} for the heat of formation. Stock and Wrede showed this method to be in error, and this would apply also to the same method for arsine.

Stibine, in a closed tube at a pressure greater than about 0.05 atmosphere, decomposes explosively and quantitatively to the elements when any part of the gas is heated sufficiently. In the present work the decomposition was initiated by heating a platinum filament in the tube to its melting point in a few milliseconds. Arsine so treated did not decompose appreciably even at a pressure of 19 atmospheres. Attempts were made to design a calorimetric experiment wherein at least a considerable fraction of an arsine sample would be decomposed by contact with a tungsten filament or passage through a quartz tube at surface temperatures of 500 to 700°. Yields were, however, inadequate to permit accurate measurement of the small reaction heat superimposed on the large filament or furnace heat. It was finally found that ignition of appropriate mixtures of arsine and stibine in a closed tube resulted in complete decomposition of both. In small tubes of about 10-ml. volume and 8-mm. inner diameter, it was found that with a mixture of 0.5 atmosphere stibine and 0.5 atmosphere AsH_3, part of the arsine was decomposed; with 0.75 atmosphere of each, more of the arsine decomposed; and with 1.0 atmosphere stibine and 0.5 atmosphere AsH_3, decomposition was quantitative.

Materials.—The same apparatus was used for preparing both the arsine and the stibine. A solution of 25 ml. of concentrated sulfuric acid in 200 ml. of water was placed in a 500-ml. three-neck round-bottom flask equipped with a magnetic stirrer, a nitrogen inlet tube (dipping beneath the solution), a 100-ml. dropping funnel, and an outlet tube with a Dry Ice cold finger. The flask was immersed in an ice-bath. The outlet tube led, successively, to a Dry Ice trap, two efficient liquid-nitrogen traps, and a stopcock leading to the vacuum pump. During a run, nitrogen was continuously bubbled through the sulfuric acid solution, and the pressure in the system was maintained at approximately 100 mm. by adjustment of the stopcock leading to the vacuum pump.

For the preparation of arsine, 4.0 g. of sodium hydroxide, 8.0 g. of arsenic(III) oxide and 2.0 g. of potassium hydroborate were dissolved, in that order, in 20 ml. of water. (This solution should be prepared immediately before its use, because it decomposes with evolution of arsine and precipitation of arsenic.) The solution was added through the dropping funnel, over a period of 15 minutes, to the sulfuric acid solution. A beautiful orange precipitate of arsenic formed in the flask as a by-product. Another by-product, biarsine (As_2H_4), was recognized by its yellow decomposition product which formed at the entrance to each of the cold traps. The crude arsine that collected in the liquid nitrogen traps was distilled *in vacuo* through a trap containing Ascarite at room temperature and then through traps at −78 and 95°. The arsine that passed through these traps (29.5 mmoles, or 60%, based on hydroborate) had a vapor pressure of 35 mm. at the melting point of carbon disulfide (lit.[8] 35 mm.).

For the preparation of stibine, 12 g. of 85% potassium hydroxide, 15 g. of potassium antimony tartrate and 2.0 g. of potassium hydroborate were dissolved, in that order, in 100 ml. of water. This solution was added through the dropping funnel, over a period of 15 minutes, to the solu-

---

(1) This work was performed under the auspices of the U. S. Atomic Energy Commission.

(2) S. M. Ariya, M. P. Morozova and Khuan Tszi-Tai, *J. Gen. Chem. USSR*, **26**, 2023 (1956); *Zhur. Obhchei Khem.*, **26**, 1813 (1956).

(3) L. Ogier, *Compt. rend.*, **87**, 210 (1878).

(4) F. D. Rossini, *et al.*, Circular 500 of the National Bureau of Standards, 1952.

(5) A. Stock and F. Wrede, *Chem. Ber.*, **41**, 540 (1908).

(6) Berthelot and Petit, *Ann. chim. phys.*, [6], **18**, 55 (1889).

(7) F. R. Bichowsky and F. D. Rossini, "The Thermochemistry of the Chemical Substances," Reinhold Publ. Corp., New York, N. Y., 1936.

(8) W. C. Johnson and A. Pechukas, *J. Am. Chem. Soc.*, **59**, 2065 (1937).

tion of sulfuric acid. A black precipitate of antimony formed in the flask as a by-product. The crude stibine that collected in the liquid nitrogen traps was then distilled *in vacuo* through a series of traps maintained at −78, −95, −130 and −196°. The material that collected in the −78, −95 and −196° traps was discarded. The remaining stibine (25.2 mmoles, or 51%, based on hydroborate) had vapor pressures of 81 and 226 mm. at the melting points of chloroform and chlorobenzene, respectively (lit.[9] 81 and 224 mm.).

Apparatus and Procedure.—Weighed samples of the gases were sealed in Pyrex tubes 2.8 cm. o.d., 20 cm. long, equipped with a break-seal for subsequent withdrawal of the hydrogen. Two tungsten leads also were introduced; across these was welded a short length of 0.002-in. platinum wire. This was fired with a 24-volt storage battery to initiate the reaction. Oscilloscopic power–time measurements indicated that the fuse broke in a few milliseconds and that the energy dissipated was approximately that required to heat the known mass of platinum to the melting point and liquefy it. This correction, about 0.1 cal., has been subtracted from all runs.

The construction of the isothermal calorimeter, laboratory designation XV, has been described in detail,[10] and its application to chemical reactions has been discussed briefly.[11] In these measurements thermal equilibration was complete in about 30 minutes. Several test runs, wherein the internal heater of the calorimeter was operated for a brief period and the bridge output–time curve was integrated, indicated an accuracy of a few tenths of a per cent. under conditions of these measurements.

Following the reaction measurement and calibration of the calorimeter, the hydrogen was transferred through traps at −196° and measured with a Toepler pump-buret system previously described.[12] The traps then were warmed to permit measurement of condensable gases and in some cases the reaction vessel was flamed strongly to liberate hydrogen which might be included in solid hydrides; negligible amounts were found in these operations.

Part of the metal produced in the runs adhered to the tube as a dark-gray blotched mirror and part fell to the bottom as a powder. X-Ray diffraction examination of this powder from tubes that had not been flamed indicated for the Sb runs a normal crystalline pattern, and for the Sb–As mixtures a nearly homogeneous solid solution of the same structure. A certain systematic error must occur in the AsH_3 results because of the heat of formation of this solution from the elements; however, since the two metals have the same crystal structure and are chemically quite similar, it may be expected that this heat is quite small.

Results.—Results of the measurements are given in Table I.

TABLE I

HEATS OF DECOMPOSITION OF AsH_3 AND SbH_3

Run	SbH_3 (millimoles)	AsH_3 (millimoles)	*q*-(SbH_3) (cal.)	*q*-(AsH_3) (cal.)	ΔE-(SbH_3) (kcal. mole^{-1})	ΔE-(AsH_3) (kcal. mole^{-1})	H_2 (% theo.)
1	3.744		130.93		−34.99		99.90
2	4.331		150.70		−34.82		99.85
3	2.674		93.36		−34.91		(99.9)
4	3.123	1.583	(109.02)	25.63		−16.19	99.83
5	3.129	1.582	(109.23)	25.66		−16.22	99.85
6	3.059	1.550	(106.68)	24.97		−16.11	99.94

The defined thermochemical calorie (4.1840 absolute joules) and the 1957 atomic weights are used. The arsine results are calculated assuming $\Delta E(SbH_3) = -34.91$. Converting from ΔE to ΔH and including estimated over-all uncertainties

$$\Delta H_f^0(SbH_3) = +34.61 \pm 0.10$$
$$\Delta H_f^0(AsH_3) = +15.87 \pm 0.25$$

These results are in good agreement with the earlier values. They may be considered more precise and, in the case of arsine, much more direct.

The spectroscopic constants of stibine given by Haynie and Nielsen[13] have been used to calculate the standard entropy and heat capacity. These are given in Table II together with other thermodynamic functions of arsine and stibine; the entropy and heat capacity of arsine are taken from Sherman and Giauque,[14] and auxiliary data from the NBS tables.

TABLE II

THERMODYNAMIC FUNCTIONS OF ARSINE AND STIBINE AT 298.16°K.

	AsH_3	SbH_3
C_p^0 (cal. deg.$^{-1}$ mole^{-1})	9.207	9.887
S^0 (cal. deg.$^{-1}$ mole^{-1})	53.18	55.65
ΔH_f^0 (kcal. mole^{-1})	+15.87	+34.61
ΔS_f^0 (cal. deg.$^{-1}$ mole^{-1})	−35.26	−34.23
ΔF_f^0 (kcal. mole^{-1})	+26.38	+44.82
ΔC_{pf}^0 (cal. deg.$^{-1}$ mole^{-1})	− 6.099	− 5.419

By use of the auxiliary data of Cottrell[15] the thermochemical bond energies may be calculated and compared with his values for the other simple group V hydrides: NH_3, $E(NH) = 93.4$ kcal. mole^{-1}; PH_3, $E(PH) = 77$; AsH_3, $E(AsH) = 66.8$; SbH_3, $E(SbH) = 60.9$.

Acknowledgments.—The X-ray diffraction work was performed by Mr. Vernon G. Silveira and Dr. Allan Zalkin.

---

[9] L. Berka, T. Briggs, M. Millard and W. Jolly, *J. Inorg. Nuclear Chem.*, in press (1960).

[10] S. R. Gunn, University of California Radiation Laboratory Report UCRL-5375, November, 1958.

[11] S. R. Gunn, L. G. Green and A. I. von Egidy, THIS JOURNAL, **63**, 1787 (1959).

[12] S. R. Gunn and L. G. Green, *J. Am. Chem. Soc.*, **80**, 4782 (1958).

[13] W. H. Haynie and H. H. Nielsen, *J. Chem. Phys.*, **21**, 1839 (1953).

[14] R. H. Sherman and W. F. Giauque, *J. Am. Chem. Soc.*, **77**, 2154 (1955).

[15] T. L. Cottrell, "The Strengths of Chemical Bonds," 2nd ed., Butterworth Scientific Publications, London, 1958.

CONDUCTANCE OF ETHANOL-AMMONIUM SALTS IN WATER AT 25°

BY JOSEPH VARIMBI[1] AND RAYMOND M. FUOSS

Contribution No. 1609 from the Sterling Chemistry Laboratory, Yale University, New Haven, Connecticut

Received March 12, 1960

By addition of methyl iodide to ethanolamines, several salts of the pattern $R_{4-n}N(CH_2CH_2OH)_nI$ can be formed. The cation contains at least one external hydroxyl group; it seemed of interest to measure the conductance of these salts in aqueous solution, in order to see whether any interaction between the cation and the hydrogen bond structure of the water could be observed. Briefly summarized, no interaction was detected: the cationic single conductances are determined by the number of heavy atoms in the side chains of the cations, independently of whether these are carbon or oxygen.

Experimental.—Trimethylethylammonium iodide was prepared as a reference compound by addition of ethyl iodide to a 25% methanolic solution of trimethylamine, and recrystallized from ethanol. Analysis by titration with silver nitrate solution: 59.1, 59.2% I *vs.* 59.1% calculated. Trimethyl-2-hydroxyethylammonium iodide was prepared from equimolar quantities of methyl iodide and dimethylethanolamine in

---

[1] Du Pont Postdoctoral Research Fellow, Yale University, 1955–1956.

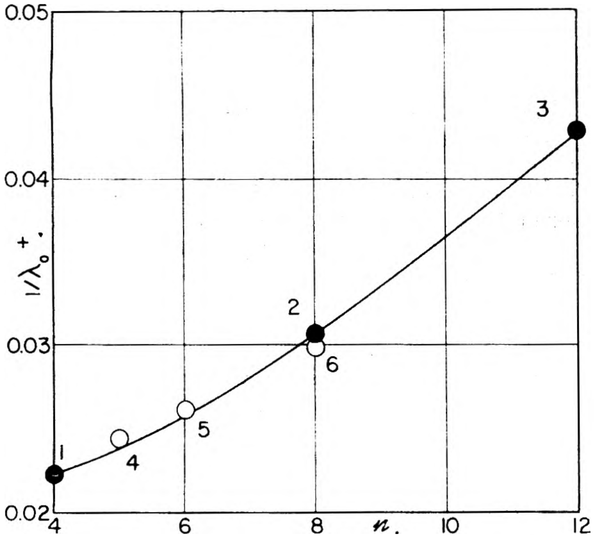

Fig. 1.—Dependence of ionic resistance on number of atoms: 1, Me_4N; 2, Et_4N; 3, Pr_4N; 4, Me_3NEt; 5, $Me_3N(CH_2CH_2OH)$; 6, $Me_2N(CH_2CH_2OH)_2$.

ethanol, and recrystallized from ethanol; m.p. 272–273° with decomposition. Analysis, 54.9, 54.7% I *vs.* 54.9% calculated. Dimethyl-di-(2-hydroxyethyl)-ammonium iodide forms less readily than the preceding compound. It was made by mixing equimolar quantities of methyl iodide and methyl-diethanolamine, and heating at 40° for 12 hours. On chilling in Dry Ice, the mixture crystallized. The hygroscopic product was twice recrystallized from ethanol, dried under vacuum and stored over P_2O_5. The compound melted to a translucent liquid at 90–98°; the liquid became transparent at 98–101°. Recrystallization from 50–50 benzene alcohol gave a product melting at 102–104°. Analysis: 48.7, 48.8% I *vs.* 48.7 calculated.

Addition of methyl iodide to triethanolamine produced only the hydroiodide of triethanolamine (m.p. 168–169°; analysis, 45.7, 45.7, 45.5% I *vs.* 45.8 calculated). Addition of methyl bromide likewise gave the hydrobromide instead of the expected quaternary salt. Possibly the triethanolamine contained some di- or mono-ethanolamine, which would lead to the observed products. Addition of ethylene bromohydrin to triethanolamine gave a good yield of the hydrobromide of triethanolamine instead of the desired quaternary salt with $n = 4$. Lack of time unfortunately prevented further attempts to prepare salts with $n = 3$ or 4.

Conductances were measured at 25.00° in an erlenmeyer cell with a constant of 0.9054, using a modified Shedlovsky bridge.[2] The conductances are summarized in Table I.

The data were analyzed on the IBM 650 computer, using a modified form of Kay's program[3] to determine the constants Λ_0 and a which appear in the conductance equation[4] for unassociated electrolytes

$$\Lambda = \Lambda_0 - Sc^{1/2} + Ec \log c + J(a)c - F\Lambda_0 c + J_2 c^{3/2}$$

The constants are summarized in Table II.

The small value of J obtained for the first salt suggests that a slight association may occur here; analysis of the data using the equation[4] for Λ_K, defined as

$$\Lambda_K = \Lambda + Sc^{1/2} - Ec \log c - Jc + F\Lambda_0 c$$

gave $K_A = 0.8 \pm 0.8$, $\Lambda_0 = 118.06$, when $å = 5.2$ was used to evaluate the coefficient J of the linear term. This is almost negligible association, but probably is real; the example serves to emphasize the fact that the Jc term and the association term in the conductance equation oppose each other and hence a too small $å$-value can always be compensated by the *ad hoc* assumption of slight association. Reliable conclusions concerning association evidently can only be obtained from data covering a range of dielectric constants, through the markedly different sensitivity of J and K_A to this parameter.

TABLE I

EQUIVALENT CONDUCTANCE AT 25°

$10^3 c$	Λ	$10^3 c$	Λ
	$EtNMe_3I$		
14.133	106.08	1.9472	113.98
9.454	108.35	1.3905	114.58
3.2052	112.77	1.1760	114.79
2.2604	113.58	0.9750	115.11
		0.6287	115.61
	$HOCH_2CH_2NMe_3I$		
21.037	102.00	5.491	108.40
11.254	105.59	5.163	108.72
10.760	105.76	3.920	109.56
9.214	106.56	2.1619	111.04
		1.5549	111.76
	$(HOCH_2CH_2)_2NMe_2I$		
19.534	97.78	5.3376	103.84
9.568	101.61	2.7650	105.73
6.430	103.18	1.3723	107.27

TABLE II

DERIVED CONSTANTS

Salt	Λ_0	J	$å$	λ_0^+
Me_3NEtI	118.05 ± 0.05	(193 ± 9)	(3.62 ± 0.16)	41.2
$Me_3N(CH_2CH_2OH)I$	115.22 ± .03	280 ± 3	5.39 ± .07	38.4
$Me_2N(CH_2CH_2OH)_2I$	110.45 ± .04	254 ± 4	5.04 ± .09	33.6

The single ion conductances for the cations were obtained by subtracting λ_0^- (I′) = 76.84 from the observed limiting conductances. Kraus[5] has shown that the equivalent ionic resistance ($1/\lambda_0^+$) of alkyl quaternary ions is a simple function of the number of carbon atoms surrounding the central nitrogen. The solid circles in Fig. 1 are for the ions Me_4N^+, Et_4N^+ and Pr_4N^+, from data obtained at Brown,[6] and the open circles correspond to the three salts of Table II. It will be noted that the points for the two salts containing the external hydroxyl group fall quite near the line through the points for the alkyl salts. If there were any strong interaction between the $-CH_2CH_2OH$ groups of the cations and the solvent molecules, we would expect these ions to move more slowly than purely alkyl ions and the points should then lie above the smooth curve. Since they do not, we conclude that any hydrogen bonding between the ethanol groups and the solvent is completely mobile; the –OH group simply slows the ion by its bulk, much as would a methyl group.

---

[2] H. Eisenberg and R. M. Fuoss, *J. Am. Chem. Soc.*, **75**, 2914 (1953).

[3] R. L. Kay, *ibid.*, **82**, 2099 (1960).

[4] R. M. Fuoss and L. Onsager, THIS JOURNAL, **61**, 668 (1957); R. M. Fuoss, *J. Am. Chem. Soc.*, **81**, 2659 (1959).

[5] C. A. Kraus, *J. Chem. Educ.*, **35**, 324 (1958); M. J. McDowell and C. A. Kraus, *J. Am. Chem. Soc.*, **73**, 3293 (1951).

[6] H. M. Daggett, Jr., E. J. Bair and C. A. Kraus, *ibid.*, **73**, 799 (1951).

THE CRYOSCOPIC AND SPECTROSCOPIC PROPERTIES OF METHYL BORATE AND OF ITS AZEOTROPE WITH METHANOL

BY PHOEBUS M. CHRISTOPHER*

Department of Chemistry, New York University, New York 3, N. Y.

Received March 16, 1960

CH_3OH and $(CH_3O)_3B$ readily form an azeotrope having a lower boiling point than either of the respective components. It is relatively difficult to separate the components of the azeotrope. Too, the tendency for boron to become tetracoördinated and the preparation and characterization of numerous stable salts of the type $M[B(RO)_4]$, where M

---

* Department of Chemistry, Newark College of Engineering, Newark 2, N. J.

may be Li, Na, Ca or other strongly metallic elements, has led to some speculation[1] into the possibility for the existence of a parent tetraalkoxo acid, $(CH_3O)_4BH$. The findings previously reported[1] concerning this speculation, although showing the azeotrope to be essentially a mixture, were inconclusive. The results of the present work, however, make possible the elucidation of definite conclusions.

Experimental

Infrared spectra were taken of CH_3OH, $(CH_3O)_3B$, and of the azeotrope, in an attempt to observe any shifts in the absorption peaks of the separate components after forming the azeotrope. A Baird Infrared Spectrophotometer was used; the cells were of 0.025 mm. thickness and had AgCl windows. The spectra were scanned from 2–16μ at a speed of 1μ/min. with a programmed slit width.

The molecular weight of the azeotrope in the vapor state was previously reported[1] as being slightly higher (69.7 g./mole) than the average value for this property from an equimolar mixture (68.0 g./mole). In the present investigation, a cryoscopic study was made of the azeotrope in solutions of nitrobenzene, benzene and *p*-dioxane. The molecular weight of $(CH_3O)_3B$ in the same solvent media also was determined, after a search of the literature failed to disclose any investigations of this nature for the borate. A simple Beckmann method was used for the cryoscopy, consisting of a 5° thermometer (in hundredths) immersed in an 8 in. test-tube containing the solutions under observation; this was surrounded by a slightly larger glass tube which served to insulate it from the water-ice bath used for all determinations. The solute and solvent were in all cases weighed out directly, and no special attempts were made to correct for the amount of solvent that may have frozen out during the process of supercooling (although this was negligible in most cases, since the cooling bath was maintained so as to keep the amount of supercooling at a minimum). The highest reading at which the temperature remained constant was taken as the freezing point. A manually operated glass-ring stirrer was used for the nitrobenzene solutions, and a steel stirrer for the benzene and *p*-dioxane solutions.

The $(CH_3O)_3B$ and azeotrope (courtesy Callery Chemical Co.) were distilled and assayed for borate content by means of the standard mannitol–phenolphthalein analysis. The borate assayed 100.1% $(CH_3O)_3B$ (the high assay probably is the result of the presence of small amounts of dissolved H_3BO_3, formed by partial hydrolysis). The azeotrope (b.p. 54.5° (758 mm.)) contained 74.83% $(CH_3O)_3B$ (this value being slightly lower than that to be expected for a 1:1 mixture).

Results and Discussion

Spectroscopic.—The infrared spectra of the CH_3OH and $(CH_3O)_3B$ were found to be identical with the spectra already reported for these compounds.[2–4] The spectrum of the azeotrope showed the presence of the B–O stretching peak at 1348 cm.$^{-1}$, the OH stretching peaks (with intermolecular hydrogen bonding) at 3200–3400 cm.$^{-1}$, in addition to the other characteristic assignments found in the separate components.[2–4] Thus the complete additivity of the component spectra indicates the absence of any tendency for compound formation.

Cryoscopic.—Table I presents the results of the cryoscopic study made on the $(CH_3O)_3B$. Six determinations were made in each solvent medium.

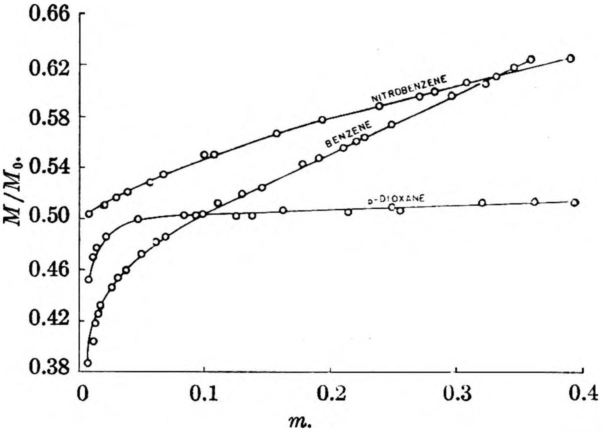

Fig. 1.—Cryoscopic plot of the $CH_3OH–(CH_3O)_3B$ azeotrope.

TABLE I

Solvent	K_f	G. borate/kg. solvent	M (g./mole)
Nitrobenzene	6.852[5]	20.76–40.32	104.3 ± 0.5
Benzene	5.065[6]	26.80–62.27	103.4 ± .4
p-Dioxane	4.63[6]	16.87–60.29	104.0 ± .7

The results reported in Table I show the molecular weight of $(CH_3O)_3B$ (theoretical 103.9) to be normal in the solvents employed.

Figure 1 is the cryoscopic plot for the azeotrope in the same solvent media listed in Table I. The ratio of the apparent to the theoretical molecular weight, M/M_0, where M_0 is 136.0 g./mole, is plotted against the molality, *m*.

Since the azeotrope has been shown to be a true mixture, the curves in Fig. 1 should all be straight lines that approach a limiting value of $M/M_0 = 0.5$ at infinite dilution if the solutions obeyed Henry's law. This relationship is evident for the nitrobenzene plot, which is almost linear, and for solutions in *p*-dioxane greater than 0.1 *m*. The benzene plot, on the other hand, shows no such concordance. Table I shows the molecular weight of the borate to be normal in all three solvents; therefore one must attribute any deviations from linearity and from the limiting value of M/M_0 to the presence of the CH_3OH and to systematic experimental errors. The nitrobenzene and *p*-dioxane plots, however, demonstrate an early view that in the cryoscopic method it is the molecular weight of the solute as vapor which is obtained.[7]

Conclusions

1. A spectroscopic examination in the infrared region (2–16 μ) of the methanol–methyl borate azeotrope gave no evidence for compound formation. 2. Methyl borate exhibits a normal molecular weight in solutions of nitrobenzene, benzene and *p*-dioxane. 3. The azeotrope obtains molecular weights in nitrobenzene and *p*-dioxane that are characteristic for a true mixture in solution, and at infinite dilution gives the same value for this property as the one previously reported for the vapor state.[1] The presence of methanol in the

---

[1] T. J. Tully and P. M. Christopher, THIS JOURNAL, **61**, 1578 (1957).

[2] H. M. Randall, R. G. Fowler, N. Fuson and J. R. Dangl, "Infrared Determination of Organic Structures," D. Van Nostrand Co., Inc., New York, N. Y., 1949, p. 191.

[3] L. J. Bellamy, "The Infra-red Spectra of Complex Molecules," John Wiley and Sons, Inc., New York, N. Y., 1958, p. 348.

[4] R. L. Werner and K. G. O'Brien, *Australian J. Chem.*, **8**, 355 (1955).

[5] W. E. Turner and C. T. Pollard, *J. Chem. Soc.*, 1751 (1914).

[6] C. A. Kraus and R. A. Vingee, *J. Am. Chem. Soc.*, **56**, 511 (1934).

[7] J. M. Peterson and W. H. Rodebush, THIS JOURNAL, **32**, 709 (1928).

azeotrope failed to produce the same concordance in benzene as in the other two solvents.

Acknowledgment.—The author wishes to express his thanks to Mr. Jack Cazes, Department of Chemistry, New York University, for the purification of all reagents and for taking the infrared spectra used in this investigation.

THE EFFICIENCY OF STREAMING POTENTIAL GENERATION[1]

By Armand F. Lewis[2] and Raymond R. Myers

Lehigh University, Bethlehem, Pa.

Received March 19, 1960

Experiments were conducted to determine the efficiency of electric power generation in the electrokinetic streaming process. The electrokinetic streaming efficiency has been defined as the ratio of electrical power, EI (streaming potential times streaming current) to the mechanical power, ΔPQ (pressure difference times volume flow rate through the diaphragm).[3]

Basically, the streaming potential phenomenon can be shown to consist of an interaction between two apparent charge density functions; the *electrokinetic charge density*, $\Delta P/E$, and the *streaming charge density*, I/Q. The electrokinetic charge density has been described in a previous paper[4] where it is defined as the apparent ionic charge concentration, e.s.u./cm.^{3}, within the electrokinetically sensitive portion of the double layer. On the other hand, the streaming charge density represents the ratio of current I (e.s.u. per second) to flow rate Q (cm.^{3} per second); thus from a strict definition of terms, I/Q represents the number of ionic charges moved (or distorted at the double layer) by each cm.^{3} of streaming liquid. The efficiency function therefore can be regarded as a ratio of these two charge density parameters, I/Q divided by $\Delta P/E$.

Experimental

Quartz wool[4] and isocyanate plastic sponge were used in this study. These materials were chosen because of their ease of packing into a diaphragm of reproducible permeability, and because they represent two different types of surface. The isocyanate sponge was similar to that manufactured by the Hudson Cush-N-Foam Corporation. This material was leached with water until free of ionic impurity as determined by the conductivity of the leaching water. The sponge was cut into a cylindrical shape so that it would fit firmly into the sample holder of the apparatus.[4]

The resistance of the plug R was determined using the technique of Neale and Peters. I/Q was calculated from a combination product of the experimental parameters $(E/\Delta P)$ $(\Delta P/Q)(1/R)$. Various plug permeabilities were obtained by compressing the sample into the holder by a thin-walled glass tube retainer. The diaphragm thus was held at a particular compression during the measurement with the minimum possible obstruction.

Results and Discussion

Results of temperature studies on both quartz wool and isocyanate sponge are given in Table I. In general, the streaming efficiency of isocyanate sponge decreased at higher temperature, while with quartz wool, the opposite trend was found. Of greater potential significance is the behavior of the charge density parameters. The streaming charge density I/Q rose with increased temperature for quartz wool, but dropped in the case of isocyanate. The electrokinetic charge density $\Delta P/E$ followed a reverse behavior with the two surfaces. $\Delta P/E$ therefore augmented the temperature dependence of efficiency, since $\Delta P/E$ is inverted in the efficiency computation.

TABLE I

TEMPERATURE DEPENDENCE OF STREAMING EFFICIENCY OF QUARTZ WOOL AND ISOCYANATE SPONGE IN WATER

Material[a]	Temp., °C.	$Q/\Delta P$, cm.^{3}/sec.-cm.	$\Delta P/E$ $\times 10^{-7}$, e.s.u./cm.^{3}	I/Q $\times 10^{-2}$, e.s.u./cm.^{3}	Efficiency $\times 10^5$
Quartz wool	25	0.63	2.10	1.54	0.73
(wt., 0.4 g.)	27	.66	2.06	1.71	.83
	30	.70	1.82	1.71	.94
	40	.88	1.45	2.23	1.54
	49	1.06	1.22	2.58	2.12
	57	1.16	1.07	3.42	3.20
	67	1.37	1.07	3.48	3.25
Isocyanate	25	0.12	1.82	5.46	3.00
sponge	29	.14	1.99	4.54	2.28
(wt., 1.5 g.)	38	.17	2.03	4.56	2.24
	40	.20	2.04	4.62	2.26
	62	.24	2.80	4.93	1.76

[a] Both diaphragms 3.9 cm. long and 1.1 cm. in diameter.

The important variable of conductivity was studied by adding various amounts of KCl to the streaming water. As shown in Table II, the presence of the electrolyte drastically reduces the streaming efficiency of both materials. These data conform to the expected trend wherein the increase in streaming liquid conductance impresses an internal shunt on the voltage produced. Furthermore, the I/Q parameter is shown by this analysis to maintain a remarkable constancy in the face of wide changes in ionic strength. Consequently, all of the efficiency drop with increased conductivity can be attributed to the increase in electrokinetic charge density.

TABLE II

DEPENDENCE OF STREAMING EFFICIENCY ON THE CONDUCTIVITY OF THE STREAMING LIQUID (25°)

Material[a]	KCl $\times 10^6$, moles/l.	Specific conductivity $\times 10^{-6}$ ohm-cm.	$\Delta P/E$ $\times 10^{-7}$, e.s.u./cm.^{3}	I/Q $\times 10^{-2}$, e.s.u./cm.^{3}	Efficiency $\times 10^5$
Quartz wool	0	1.4	2.10	1.54	0.73
$Q/\Delta P$: 0.63	17	2.0	2.84	1.92	.68
cm.^{3}/sec.-	33	5.7	6.89	1.77	.26
cm.	50	8.5	12.46	1.67	.13
	79	12.6	24.88	1.39	.06
	100	17.3	28.46	1.62	.06
Isocyanate	0	1.4	1.82	5.46	3.00
sponge	25	4.6	5.69	5.34	0.94
$Q/\Delta P$: 0.15	42	7.2	8.87	5.86	.66
cm.^{3}/sec. cm.	100	18.0	18.10	6.05	.30

[a] Same diaphragms as used in Table I.

The influence of hydrodynamic permeability of the diaphragm on efficiency was studied by stream-

---

[1] Based in part on the Ph.D. dissertation of Armand F. Lewis, Lehigh University, October, 1958.

[2] American Cyanamid Company, Stamford, Conn.

[3] H. B. Bull and L. S. Moyer, THIS JOURNAL, **40**, 9 (1936).

[4] R. R. Myers and A. F. Lewis, *ibid.*, **64**, 196 (1960).

ing water through quartz wool and isocyanate sponge held at various compressions. In Table III, the permeability changes are represented by two factors, the solids density and the flow rate per unit pressure across the diphragm, $Q/\Delta P$. A wide range of permeability could not be attained with quartz wool plugs; hence the effect of permeability on efficiency was not clearly defined. On the other hand, the permeability of isocyanate sponge was varied in two ways. First, the amount of sample was held constant and then compressed to various lengths; second, the sample was held at constant length (3 cm.) and the permeability was varied by changing the packing. Under both conditions the efficiency increased at decreased permeability. The data presented show that permeability drastically influences the streaming efficiency below a $Q/\Delta P$ of about 0.1 cm.³/sec.-cm. Since this behavior is not predicted by classical theory of streaming potential, much doubt is cast on existing literature which reports streaming data at low permeabilities. A similar conclusion has been made by Biefer and Mason.[5]

TABLE III

EFFECT OF PERMEABILITY ON THE STREAMING EFFICIENCY OF QUARTZ WOOL AND ISOCYANATE SPONGE DIAPHRAGMS

Length,[a] cm.	Solids density, g./cm.³	$Q/\Delta P$, cm.³/sec.-cm.	$\Delta P/E \times 10^{-7}$, e.s.u./cm.³	$I/Q \times 10^{-2}$, e.s.u./cm.³	Efficiency $\times 10^6$
		Quartz wool			
6.3	0.06	0.92	1.21	2.10	1.74
5.5	.07	.82	2.15	1.41	0.65
4.8	.08	.67	2.29	1.30	.57
3.9	.10	.66	2.05	1.74	.85
2.3	.17	.49	2.13	1.62	.76
		Isocyanate sponge			
5.2	.24	.33	1.22	3.55	2.91
4.7	.26	.20	1.35	4.34	3.22
4.6	.27	.19	1.40	3.91	2.80
3.9	.31	.16	1.47	4.47	3.04
3.8	.32	.14	1.51	5.07	3.35
2.6	.47	.04	2.01	13.16	6.55
2.4	.51	.03	2.32	17.04	7.36
2.0	.61	.01	2.46	22.30	9.07
3.0	.05	1.90	1.48	0.38	0.26
3.0	.08	1.60	1.23	.62	0.49
3.0	.09	1.30	1.11	.67	0.60
3.0	.13	0.47	0.95	2.02	2.13
3.0	.38	.19	1.42	3.00	2.12
3.0	.47	.11	1.59	4.95	3.10
3.0	.53	.04	2.21	8.16	3.69
3.0	.61	.01	2.84	20.50	7.23

[a] Diameter of all diaphragms, 1.1 cm.

In general, streaming potential generation is a very inefficient process with efficiency values in the order of 10^{-5}, depending upon experimental conditions. The results presented illustrate that the streaming potential phenomenon can be a useful tool for studying the solid-liquid interface without employing the classical approach. Furthermore, this analysis gives a broad picture of the streaming potential effect which may serve as a basis for future studies in the field.

Acknowledgment.—The authors are pleased to acknowledge the support of the Armstrong Cork Company whose interest in electrokinetics made this work possible. In addition, the authors wish to thank Mr. M. Z. Nammari for obtaining some of the quartz wool data for this study.

(5) G. J. Biefer and S. G. Mason, *Trans. Faraday Soc.*, **55**, 1239 (1959).

THE HEATS OF FUSION OF THE CADMIUM HALIDES, MERCURIC CHLORIDE AND BISMUTH BROMIDE[1]

BY L. E. TOPOL AND L. D. RANSOM

Atomics International, A Division of North American Aviation, Inc. Canoga Park, California

Received March 21, 1960

In the course of investigations of molten metal-metal salt systems in this Laboratory, cryoscopic measurements in $CdCl_2$, $CdBr_2$, CdI_2, $HgCl_2$ and $BiBr_3$ solutions have been carried out. Interpretation of these results required an accurate value for the heat of fusion of the salt solvent. As the literature values for the heats of fusion of the above salts were all based on cryoscopic measurements and thus, as has been shown in recent calorimetric studies with other salts,[2,3] may be of doubtful accuracy, a calorimetric study was made to determine these values.

Experimental

Materials.—$CdCl_2$, $CdBr_2$ and CdI_2 were prepared and purified as described elsewhere.[4]

$BiBr_3$ was synthesized from the elements in a similar manner to $CdBr_2$.

$HgCl_2$, Mallinckrodt analytical reagent grade, was dried overnight at 140° *in vacuo*.

Apparatus and Procedure.—The drop-calorimeter and procedure were identical to those used earlier.[2] A minimum of six drops over a 60 to 100° range both above and below the melting point of each salt was made. The salt samples, 10 to 20 g. in weight, were contained in platinum and were always melted before the measurements were carried out to ensure intimate contact between the salt and container. In the case of $HgCl_2$ the possibility of reaction between the salt and container was checked by X-ray fluorescence techniques. Within the sensitivity of the method (0.5% by weight) no platinum was found in the salt phase.

Results and Discussion

The calorimetric results for $CdCl_2$, $CdBr_2$, CdI_2, $HgCl_2$ and $BiBr_3$ found in this study together with the literature values for the heats of fusion[5,6] are listed in Table I. The heat capacities of the salts were assumed to be constant for the limited temperature ranges of the measurements.

It is interesting to note that the heats of fusion reported in the literature were determined cryoscopically and are lower in every case than the calorimetrically measured values. These lower results might be expected when solute concentrations are not sufficiently dilute to permit accurate use of the Raoult–van't Hoff relation.

(1) This work was supported by the Research Division of the Atomic Energy Commission.

(2) L. E. Topol, S. W. Mayer and L. D. Ransom, THIS JOURNAL, in press.

(3) A. S. Dworkin and M. A. Bredig, THIS JOURNAL, **64**, 269 (1960).

(4) L. E. Topol and A. L. Landis, to be published.

(5) K. K. Kelley, U. S. Bur. Mines Bull. 393, 1936.

(6) L. Brewer *et al.*, "The Chemistry and Metallurgy of Miscellaneous Materials: Thermodynamics," ed. by L. L. Quill, McGraw-Hill Book Co., New York, N. Y., 1950.

TABLE I

HEAT CAPACITIES, HEATS AND ENTROPIES OF FUSION FOR $CdCl_2$, $CdBr_2$, CdI_2, $HgCl_2$ AND $BiBr_3$

Salt	Heat capacity (cal./deg./mole) Solid	Heat capacity (cal./deg./mole) Liquid	M.p., °K.	ΔS_f (e.u.)	ΔH_f (kcal./mole) This work	ΔH_f (kcal./mole) Lit.[6]
$CdCl_2$	28.5 ± 1.5	26.3 ± 2.3	842.1	8.57 ± 0.20	7.22 + 0.17	5.30
$CdBr_2$	22.8 ± 2.0	24.3 ± 1.2	841.2	9.48 ± .09	7.97 ± .08	5.00
CdI_2	21.5 ± 1.6	24.4 ± 2.7	661.2	7.49 ± .20	4.95 ± .13	3.66
$HgCl_2$	19.2 ± 0.6	27.2 ± 1.1	552.7	8.40 ± .09	4.64 ± .05	4.15
$BiBr_3$	26.0 ± 1.0	37.7 ± 1.7	492.2	10.55 ± .40	5.19 ± .20	(4.0)

The entropies of fusion for these salts are of the same magnitude as those for most inorganic substances, *i.e.*, between 2.5 and 3.2 e.u. per gram-atom.[7] However, for the cadmium halides the highest entropy of fusion exhibited by the bromide is interesting. Since $CdCl_2$ and $CdBr_2$ are similar compounds, chemically and structurally, little difference in the entropy of fusion would be expected.

The entropy of fusion of $BiBr_3$, 10.5 e.u., is somewhat lower than that found for $BiCl_3$,[2] 11.2 e.u. As the two salts have similar structures,[8] at least a part of the difference in values may be the result of the solid phase transition which occurs in $BiBr_3$ at 158°.[8] This transition, observed by thermal analysis, does not involve a change in structure. This fact suggests a maximum entropy and heat effect of 0.7 e.u. and about 0.3 kcal./mole, respectively, are associated with the solid phase change. Such a heat effect was not found in the calorimetry studies, possibly as a result of the rapid cooling of the sample during the measurements.[9]

[7] O. Kubaschewski and E. Ll. Evans, "Metallurgical Thermochemistry," Pergamon Press, New York, N. Y., 1958, p. 191.

[8] G. M. Wolten and S. W. Mayer, *Acta Cryst.*, **11**, 739 (1958).

[9] Reference 7, p. 125.

THE AFFINITY OF CERTAIN DISUBSTITUTED AMIDES AND ORGANOPHOSPHORUS COMPOUNDS FOR WATER[1]

By T. H. SIDDALL, III

Savannah River Laboratory, E. I. du Pont de Nemours & Co., Aiken, South Carolina

Received April 11, 1960

Various esters that contain phosphorus have been investigated as extractants for actinide and rare earth elements and for nitric acid. The author also has in process of publication a similar study of extraction by disubstituted amides. However, no extensive study has been reported pertaining to the solubility of water in such compounds. Observations that the volume of samples of dimethyl octylphosphonate increased markedly on being wetted prompted an investigation of water solubility in the octylphosphonate, similar compounds, and in disubstituted amides. Preliminary results of such a study are reported here.

The data in Table I show that those phosphorus compounds and amides with the dipole group (P=O or C=O) exposed have a strong affinity for water. This strong affinity is lost with the diethyl amide but persists even with ethyl groups in the phosphorus compounds. It is also seen that the order of affinity for water is phosphinate > phosphonate > phosphate.

These observations allow two conclusions to be drawn. First, the affinity for water depends greatly on the degree of steric hindrance around the dipole group. Longer alkyl chains seem to prevent the accumulation of water molecules around the dipole group. Second, the affinity for water follows the same trend as the ability to extract actinide elements and nitric acid from aqueous nitrate solutions. The order of extractant strength is also phosphinate > phosphonate > phosphate.

Perhaps the most interesting question that arises from the data in Table I concerns the structure of organic phases that contain so much water. It is obvious that as many as 30 molecules of water cannot be directly fixed to the organic dipole. Instead the effect of the organic dipole must be propagated through a chain or network of water molecules. However, the normal ability of these water molecules to solvate metal ions is little, if any, impaired. Preliminary experiments showed that for tracer concentrations, the extraction coefficients for cesium, strontium and promethium are all about 0.3 with 0.05 *M* nitric acid in the aqueous phase and with dimethyl octylphosphonate. Since cesium, in particular, is not very well extracted by esters that contain phosphorus, the extraction must be due to solvation by water.

TABLE I

WATER SOLUBILITY IN VARIOUS AMIDES AND ORGANOPHOSPHORUS COMPOUNDS

Compound	Weight % H_2O	Temp., °C.	Mole ratio H_2O/organic
N,N-Dimethyloctanamide	26	30	3.3
N,N-Diethyldecanamide	3.0	30	0.34
N,N-Dibutylbutyramide	3.0	30	0.34
Tributyl phosphate	6.4	30	1.0
Dibutyl butylphosphonate	10.4	30	1.7
Dimethyl octylphosphonate	71	0	30
	51	30	13
	35	60	6.6
Diethyl octylphosphonate	43	0	11
	22	30	3.9
	15.4	60	2.5
Octyl diethylphosphinate	59	30	18

Preliminary experiments showed that when nitric acid is extracted, the methyl and ethyl phosphonates lose the ability to extract water. Each molecule of extracted nitric acid removes one phosphonate molecule as a water acceptor.

Further experiments with these compounds are

---

[1] The information contained in this article was developed during the course of work under contract AT(07-2)-1 with the U. S. Atomic Energy Commission.

in progress. Solutions of water in such compounds as dimethyl octylphosphonate should be interesting solvent media and should provoke a number of questions as to the structure and properties of the solutions themselves. Measurements of the solubility of the organic compounds in the aqueous phase also are required. Qualitative indications, so far, are that such solubility is low.

CONDUCTANCE OF TETRABUTYLAMMONIUM TETRAPHENYLBORIDE IN NITRILES[1]

BY ALAN MACKENZIE BROWN AND RAYMOND M. FUOSS

Contribution No. 1616 from the Sterling Chemistry Laboratory, Yale University, New Haven, Connecticut

Received May 2, 1960

Tetrabutylammonium tetraphenylboride ($Bu_4N\cdot BPh_4$) is a useful reference electrolyte for exploring a given solvent system, because both ions have the same volume and therefore half the limiting conductance gives the single ion conductances[2] of Bu_4N^+ and BPh_4^-, whereby the single conductances of other anions and cations can be obtained. Since the ions are large, ion pairs are not very stable until solvents of fairly low dielectric constants are used: at $D = 25$, K_A is about 20, and at a concentration of 3×10^{-3}, for example, the decrease in conductance due to pair formation is only about 4%. In the range $D \geq 25$, the graphical $y - x$ method of determining the association constants from conductance data for this salt fails because it becomes too sensitive to even small experimental error. The purpose of this note is to present a new method of determining small association constants, using as example the conductance of $Bu_4N\cdot BPh_4$ in acetonitrile–isobutyronitrile as solvent.

Experimental

Tetrabutylammonium tetraphenylboride was prepared from recrystallized tetrabutylammonium bromide (20 g. to 100 ml. benzene and 20 ml. of *n*-hexane, m.p. 119.6°) and sodium tetraphenylboride, and recrystallized from 2:1 acetone–water; m.p. 236°. The density of the salt is 1.023 g./ml. **Acetonitrile** was distilled from P_2O_5 twice and then from anhydrous K_2CO_3, using a Todd still; b.p. 81.6°; density 0.7766 g./ml.; conductance, $0.2–0.4 \times 10^{-6}$; viscosity at 25°, 0.003441 poise; dielectric constant at 25°, 36.23. **Isobutyronitrile** was shaken with concentrated hydrochloric acid to remove isonitriles, then with water and with sodium bicarbonate solution. It was dried over P_2O_5 and twice fractionated through the Todd still: b.p. 103.6°; density, 0.7650 g./ml.; conductance, 0.05×10^{-6}; viscosity at 25°, 0.004946 poise; dielectric constant at 25°, 24.90.

Solutions were made up by weight and calculated to volume concentrations from the known densities. Conductances were measured at 25.00°, using cells with constants 0.9021, 0.3478 and 0.08356. The experimental results are summarized in Table I; the mixture was 79.6 wt. % isobutyronitrile, with $D = 27.58$ and $\eta = 0.004414$.

The data were analyzed by a graphical method, using as the starting point the equation[3]

$$\Lambda = \Lambda_0 - S(c\gamma)^{1/2} + Ec\gamma \log c\gamma + Jc\gamma - F\Lambda c - K_A c\gamma f^2 \Lambda \quad (1)$$

Association to ion pairs was very slight; hence the graphical $y - x$ method of evaluating the constants Λ_0, a and K_A could not be used, because the difference $\Delta\Lambda$ which determines y becomes far too sensitive to experimental error.[4] Attempts to process the data by the Kay program[5] for equation 1 on the IBM-650 computer failed, also because association was slight and the computer gave negative K_A-values with an uncertainty of ±100%. When processed by the program for unassociated electrolytes ($\gamma = 1$ and $K_A = 0$ in equation 1), the preliminary values shown in Table II resulted. The small values of a (about 5 Å.) show that some association is taking place, because the J- and K_A-terms in (1) oppose each other and calculating a from the observed coefficient of the net linear term then necessarily will give too low a value to a. Hence another method of analyzing the data was devised which promises to be useful for other cases of slight association.

TABLE I

CONDUCTANCE OF $Bu_4N\cdot NBPh_4$ AT 25°

$10^4 c$	Λ	$10^4 c$	Λ	$10^4 c$	Λ
MeCN		Mixture		Me_2CHCN	
56.732	99.33	38.610	75.88	31.277	66.38
37.179	102.58	30.889	77.28	25.436	67.55
29.077	104.24	23.532	78.86	19.906	68.87
20.575	106.41	20.670	79.53	13.965	70.64
14.839	108.18	14.682	81.33		

TABLE II

DERIVED CONSTANTS

	MeCN	Mixture	Me_2CHCN
Λ_0 (prelim.)	119.90 ± 0.06	92.77 ± 0.06	81.66 ± 0.03
$\mathring{a}$ (prelim.)	5.18 ± .06	5.19 ± .05	5.05 ± .03
Λ_0 (final)	119.85 ± .05	92.70 ± .05	81.61 ± .05
H	1780	2720	3100
K_A	8.2	14.4	18.4

To a close approximation, the quantity Λ'_η, defined as

$$\begin{aligned} \Lambda'_\eta &\equiv \Lambda + Sc^{1/2} - Ec \log c + F\Lambda c \qquad (2) \\ &= \Lambda_0 + Hc \end{aligned}$$

gives a linear plot against concentration when the association constant is small ($\gamma \approx 1$). Using[6] $F = 2.0$ and the preliminary values of Λ_0, Λ'_η was computed and extrapolated to give the final values of Λ_0 (Table II).

The observed slopes H are also given in the table; from (1), we see that

$$H = J - K_A\Lambda_0 \quad (3)$$

Empirically, J is nearly linear in a over small ranges of a-values

$$J = k_1 + k_2 a \quad (4)$$

where k_1 and k_2 are determined easily from a graph of J against a (ref. 4, equation 15.34). Theoretically,[7] if ion–solvent interaction is temporarily neglected

$$K_A = (4\pi N a^3)/3000)e^b = a^3 k_3 e^b \quad (5)$$

whence, for 25°

$$H = k_1 + k_2 a - a^3 k_3 \Lambda_0 \times 10^{243.4/aD} \quad (6)$$

In other words, the slope of the Λ'_η–c plots is a function of a and the dielectric constant (the latter implicitly through k_1 and k_2 and explicitly in the exponential). Rearranging (6) gives

$$\begin{aligned} \alpha \equiv (H - k_1)/k_2 &= a - (a^3 k_3 \Lambda_0/k_2) \times 10^{243.4/aD} \quad (7) \\ &= a - \beta k_3 a^3 10^{\gamma/a} \quad (8) \end{aligned}$$

For each system studied, we have an equation of the form

---

[1] Office of Naval Research Technical Report no. 64. This paper may be reproduced in whole or in part for any purpose of the United States Government.

[2] R. M. Fuoss and E. Hirsch, *J. Am. Chem. Soc.*, **82**, 1013 (1960).

[3] R. M. Fuoss, *ibid.*, **81**, 2659 (1959).

[4] R. M. Fuoss and F. Accascina, "Electrolytic Conductance," Interscience, New York, 1959, Ch. 17. All symbols used are defined here.

[5] Robert L. Kay, *J. Am. Chem. Soc.*, **82**, 2099 (1960).

[6] R. M. Fuoss, J. B. Berkowitz, E. Hirsch and S. Petrucci, *Proc. Natl. Acad. Sci.*, **44**, 27 (1958).

[7] R. M. Fuoss, *J. Am. Chem. Soc.*, **80**, 5059 (1958).

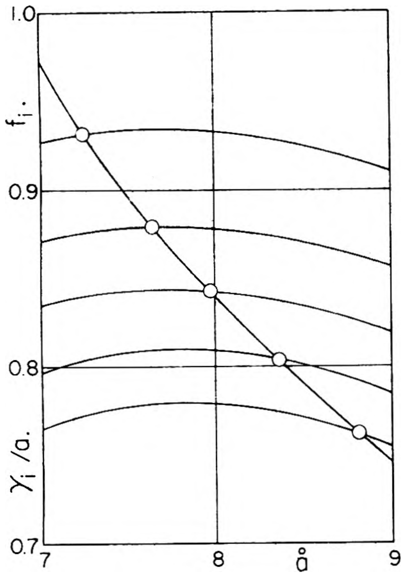

Fig. 1.—Determination of paired (k_3, a) values for $Bu_4N\cdot BPh_4$ in MeCN.

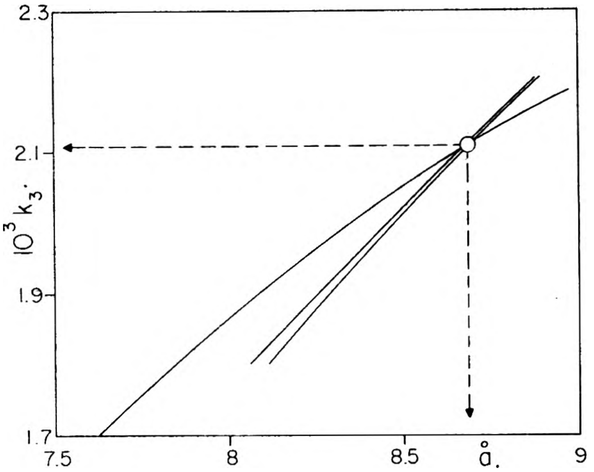

Fig. 2.—Determination of k_3 and a for $Bu_4N\cdot BPh_4$ in three solvents.

(8); the problem is to solve this set of equations for a and k_3. Using subscripts i to denote different systems, (8) rearranges to

$$\gamma_i/a = \log\,[(a - \alpha_i)/\beta_i k_3 a^3] \equiv f_i(a, k_3) \qquad (9)$$

Now γ_i is simply $243.4/D_i$ while f_i depends on k_3 and a. Figure 1 shows a plot of γ_1/a against a range of trial values of a; on the same graph are shown plots of f_1 for $k_3 = 0.00170$, . . ., 0.00215 for the same values of a ($i = 1$ corresponds to acetonitrile as solvent). According to (9), the intersections of the γ_i/a curve with the family of f_i curves gives a set of mutually consistent (k_3, a) pairs. Similar plots were constructed for the other two solvent systems. Then in Fig. 2, these values of k_3 are plotted against their partner a-values. If (5) is correct, *i.e.*, if the functional dependence of K_A on a is as shown in (5), and if a is independent of solvent composition (*i.e.*, characteristic of the solute), the three curves of Fig. 3 should intersect at *one* point, the unique solution of the set of equations. It will be seen that this is indeed the case; from the figure, $k_3 = 2.11 \times 10^{-3}$ and $\mathring{a} = 8.68 \pm 0.05$.

The value of k_3 is somewhat smaller than the theoretical value ($4\pi N \times 10^{-24}/3000$) $= 2.524 \times 10^{-3}$, but if a term is inserted in (5) to allow for solvent–ion interaction,[8] so that

$$K_A = 2.524 \times 10^{-3}\,\mathring{a}^3 \exp(b + E_s/kT) \qquad (10)$$

we find $E_s/kT = -0.185$. Since both ions are large, and the central charge is well shielded in the cation and distributed in the anion, the small value of E_s seems reasonable. The values of K_A in Table II are computed using the constants from Fig. 2: $K_{Ai} = 2.11 \times 10^{-3}\,(8.68)^3\,10^{\gamma_i/8.68}$. Finally, plotting the apparent Stokes radius against reciprocal dielectric constant[9] evaluates the hydrodynamic radius $R_\infty = 3.77$, which is in excellent agreement with Hirsch's value[2] of 3.63 found for this salt in the solvent system nitrobenzene–carbon tetrachloride.

---

[8] W. R. Gilkerson, *J. Chem. Phys.*, **25**, 1199 (1956).

[9] R. M. Fuoss, *Proc. Natl. Acad. Sci.*, **45**, 807 (1959).

THE ULTRAVIOLET ABSORPTION SPECTRA OF A SERIES OF ALKYL-, CYCLOALKYL- AND CHLORO-SUBSTITUTED KETONES[1]

By W. R. Mountcastle, Jr., D. F. Smith and E. L. Grove

School of Chemistry, University of Alabama and the Department of Chemistry, Birmingham-Southern College, Birmingham, Alabama

Received May 6, 1960

The vapor phase absorption spectra of a series of alkyl-, cycloalkyl- and chloro-substituted ketones have been determined in the 220–320 mμ region. The compounds studied included: eight α-methyl-substituted ketones (including 2,2,4,4-tetramethyl-3-pentanone); eight α-chloro-substituted ketones (including 1,1,1,3,3,3-hexachloro-2-propanone); the two α-substituted cyclopropyl ketones; and two cyclo-ketones. The spectra of a number of these compounds were determined in "isoöctane" solution. However, no striking differences were evident for the spectra in the vapor state and in the non-polar solvent.

The compounds studied provided examples of a simple system in which the positive inductive effect of the methyl group can be compared with the negative inductive effect of a chlorine atom. However, this simple effect is overcome by other effects, *i.e.*, steric requirements of the substituent groups, hyperconjugation, etc.

Experimental

The vapor phase ultraviolet spectra were determined by standard methods in a 1-meter fused quartz cell using an Applied Research Laboratories, 1.5 meter, 24,400-lines per inch grating spectrograph. Eastman Kodak No. 103-0 UV 35-mm. film was used. Absorbancy readings were made on a National Spectrographic Laboratories, No. 310-2, Spec-Trol, densitometer, using as a reference an iron arc standard, previously placed on the film as a part of the determination.

All compounds used were commercially available or were prepared by methods described in the literature. All were purified by distillation. The physical properties and λ_{max} of the compounds are summarized in Table I. The spectral data for the thirteen compounds which have not been reported previously have been accepted for publication by the Manufacturing Chemists Association Research Project, Chemical and Petroleum Research Laboratory, Carnegie Institute of Technology, Pittsburgh 13, Pennsylvania.

Discussion of Results

It is evident that the near ultraviolet carbonyl absorption maximum of a ketone undergoes a "red shift" as the α-hydrogens are replaced by methyl

---

[1] This investigation was supported in part by the Atomic Energy Commission. From a dissertation submitted by W. R. Mountcastle, Jr., in partial fulfillment of the requirements for the degree of Doctor of Philosophy, August, 1958. Presented in preliminary form at the Southeastern Regional Meeting, ACS, Gainesville, Florida, December 12, 1958.

TABLE I

PHYSICAL CONSTANTS OF THE COMPOUNDS USED IN THIS RESEARCH

Compounds	λ_{max}, mμ	Refractive index	B.p., °C. (mm.)
2-Propanone	277	n^{20}_{D} 1.3588	56 (755)
2-Butanone	278	n^{20}_{D} 1.3788	79 (748)
3-Pentanone	279	n^{20}_{D} 1.3924	102 (760)
3-Methyl-2-butanone	283	n^{20}_{D} 1.3881	94 (761)
2,4-Dimethyl-3-pentanone	287	n^{20}_{D} 1.3999	125 (762)
3,3-Dimethyl-2-butanone	285	n^{20}_{D} 1.4016	106 (755)
2-Hexanone	279	n^{20}_{D} 1.4003	128 (755)
2,2-Dimethyl-3-pentanone	288	n^{20}_{D} 1.4050	129 (760)
2,2,4-Trimethyl-3-pentanone	290	n^{20}_{D} 1.4060	136 (760)
2,2,4,4-Tetramethyl-3-pentanone	297	n^{20}_{D} 1.4193	153 (760)
1-Chloro-2-propanone	289	n^{25}_{D} 1.4312	67 (110)
1,1-Dichloro-2-propanone	295	n^{26}_{D} 1.4442	121 (760)
1,3-Dichloro-2-propanone	300	....	173 (760) m.p. 43–44°
1,1,1-Trichloro-2-propanone	281	n^{20}_{D} 1.4650	133
1,1,3,3-Tetrachloro-2-propanone	301	n^{18}_{D} 1.5000	47–48 (5.5)
1,1,1,3-Tetrachloro-2-propanone	299	n^{18}_{D} 1.4900	47–48 (6.0)
1,1,1,3,3-Pentachloro-2-propanone	298	n^{26}_{D} 1.4955	189 (750)
1,1,1,3,3,3-Hexachloro-2-propanone	298	n^{25}_{D} 1.5090	201 (750)
Methyl cyclopropyl ketone	276	n^{25}_{D} 1.4222	111 (758)
Dicyclopropyl ketone	276	n^{26}_{D} 1.4657	163 (760)
Ethyl acetoacetate	278	n^{20}_{D} 1.4192	50 (7.0)
Cyclopentanone	300	n^{20}_{D} 1.4335	130 (755)
Cyclohexanone	289	n^{20}_{D} 1.4497	155 (755)

groups.[2] This shift has been ascribed variously to the positive inductive effect of the methyl group, or to hyperconjugation; and it also has been described simply as the "methyl effect." In this investigation it has been observed that the "red shift" is more dependent on the symmetry of substitution than on the number of entering methyl groups.

A possible explanation for this effect is the steric requirements of the entering group and the strain produced by the opposing groups at the carbonyl carbon angle-α.

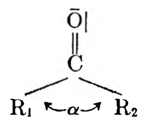

The effect of strain at the carbonyl carbon has been cited to explain the higher λ_{max} of cyclopentanone *vs.* cyclohexanone.[3] The observation that "hexamethylacetone" and "hexachloroacetone" have λ_{max}. values which are almost identical supports the contention that, in this case, the effect is steric.

The following series can be observed for a "red shift" produced by changing the complexity of R

$$\text{methyl} < \text{ethyl} \leq n\text{-butyl} < i\text{-propyl} < t\text{-butyl}$$

The same order is preserved for R_1 *vs.* R_2 and the effect is accentuated by the degree of complexity of R_1 and R_2.[4] The apparently greater effect of an *i*-propyl group when compared with other groups possibly could be the modifying effect of "B" strain in such a group.

Where steric strain is the primary consideration, the case of the chloro-substituted ketones appears to be the same as that observed in the alkyl ketones. However, for the compounds in which the substitution is symmetrical and α-hydrogens are present, simple steric effects do not appear to offer a complete explanation. The resonance extreme shown

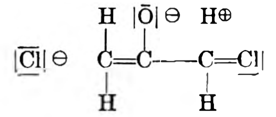

is possible and may be a partial answer; however, this is pure conjecture.

The case for the cyclo-alkyl ketones is perplexing and no simple explanation is offered for the observed spectra. Hart,[5] *et al.*, have reported these same compounds, previously, without any explanation for the spectral data.

---

(2) A. E. Gillam and E. S. Stern, "An Introduction to Electronic Absorption Spectroscopy in Organic Chemistry," Edward Arnold Ltd., London, 1954, pp. 47–51.

(3) M. S. Newman, "Steric Effects in Organic Chemistry," John Wiley and Sons, Inc., New York, N. Y., 1956, pp. 506–507.

(4) R. P. Mariella and R. R. Raube, *J. Am. Chem. Soc.*, **74**, 518 (1952).

(5) H. Hart and O. E. Curtis, *ibid.*, **78**, 112 (1956).

COMMUNICATIONS TO THE EDITOR

COMMENTS ON THE MECHANISM OF THE REACTION OF ACTIVE NITROGEN WITH ETHYLENE AND NITRIC OXIDE

Sir:

It is the purpose of this communication to show that the results of Verbeke and Winkler[1] can be interpreted by assuming that the only constituent of active nitrogen which reacts with nitric oxide is atomic nitrogen in contradistinction to their conclusions. This reaction is quantitative. The results obtained for the reaction between active nitrogen and ethylene then can be explained by a mechanism analogous to Frey's mechanism for the reaction between ethylene and methylene free radicals,[2] *viz.*

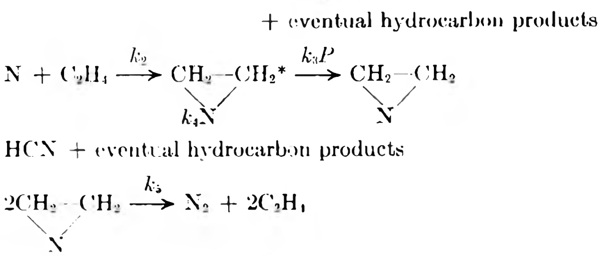

$$N + C_2H_4 \xrightarrow{k_1} (C_2H_4-N) \longrightarrow HCN + \text{eventual hydrocarbon products}$$

$$N + C_2H_4 \xrightarrow{k_2} CH_2-CH_2^*(N) \xrightarrow{k_3P} CH_2-CH_2(N)$$

$$\xrightarrow{k_4N} HCN + \text{eventual hydrocarbon products}$$

$$2CH_2-CH_2(N) \xrightarrow{k_5} N_2 + 2C_2H_4$$

This mechanism predicts that when active ni-

---

(1) G. J. Verbeke and C. A. Winkler, *J. Phys. Chem.*, **64**, 319 (1960).

(2) H. M. Frey, *J. Am. Chem. Soc.*, **79**, 1259 (1957).

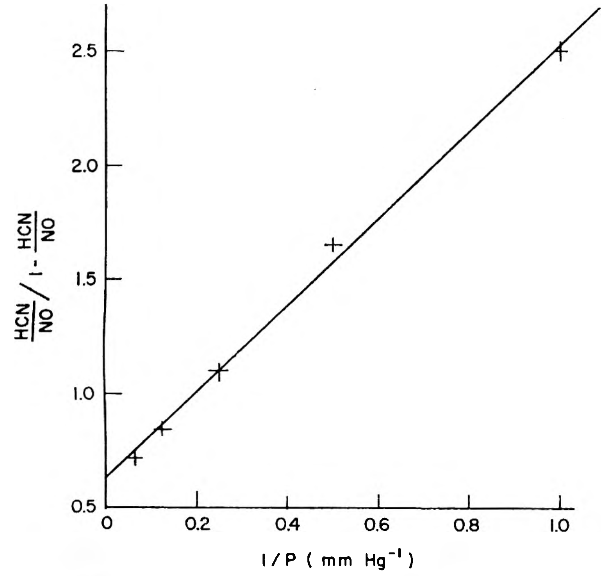

Fig. 1.—Plot of $(HCN_{produced}/NO_{destroyed})(1 - HCN_{produced}/NO_{destroyed})^{-1}$ vs. 1/pressure taken from Verbeke and Winkler (1).

trogen is successively titrated with nitric oxide and ethylene in a given system the variable $(HCN_{produced}/NO_{destroyed}) \times (1 - HCN_{produced}/NO_{destroyed})^{-1}$ will be a linear function of the reciprocal of the total pressure. Figure 1 shows that Verbeke and Winkler's data can be correlated in this way.

The slope of this correlation is 1.9 ± 0.3 mm. (90% confidence limit); the intercept is 0.6 ± 0.6.

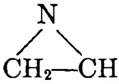

$CH_2—CH_2$ (ring with N) is inherently unstable so that it may be destroyed by other reactions besides the one given above under appropriate experimental conditions. For example, Winkler[3] has found recently that with increasing temperature, the HCN yield from the reaction of ethylene and active nitrogen increases when an unpoisoned vessel is used. This indicated that the wall catalyzed decomposition of 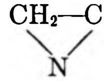 $CH_2—CH_2$ competes with reaction five under these conditions.

MATERIALS DEVELOPMENT LABORATORY
REPUBLIC AVIATION CORPORATION,
FARMINGDALE, LONG ISLAND, N. Y. WALTER G. ZINMAN

RECEIVED JUNE 14, 1960

[3] C. A. Winkler, unpublished communication (1960).

SOLUTIONS OF METALS IN MOLTEN SALTS CERIUM IN CERIUM TRICHLORIDE

Sir:

Investigations of the Ce–$CeCl_3$ system have yielded lately rather surprising results such as a strange dependence of the electrical conductance on metal concentration,[1] a proposal of a novel, monovalent rare earth ion, Ce^+, as the solute species,[2] and the enormous apparent molar volume of 500 cc. per mole of mobile electrons, in dilute solution.[1] The recent discovery[3] of solid halides of divalent neodymium and prasedymium such as $NdCl_2$ and $PrCl_{2.3}$ supports our own view that cerium enters the solution in molten $CeCl_3$ as Ce^{++}, but clarification of the aforementioned findings appeared desirable. A reinvestigation was started in connection with the general study of molten salt–metal systems at this laboratory. The nature of our first results is such as to warrant an early report.

In agreement with available thermodynamic data we have found that refractory oxides such as sintered alumina ("Morganite Triangle RR") or sapphire single crystals are not suited for use with even dilute solutions of Ce in molten $CeCl_3$ as they react readily to form cerium oxychloride according to: $M_xO_y + 2y/3Ce + y/3CeCl_3 = yCeOCl + xM$. For instance, 0.9 g. of cerium metal and 16.3 g. of $CeCl_3$ prepared by dehydration with NH_4Cl and subsequent sublimation were kept molten under argon at 850° in a Morganite crucible for two hours. After leaching with water, 1.62 g. of an insoluble residue consisting mainly of purplish-white crystal platelets of cerium oxychloride were recovered (X-ray identification). The inner wall of the crucible showed severe attack and its weight was reduced by 0.25 g., corresponding to approximately 75% completion of the above reaction. Aluminum metal also was identified. Similar results were obtained with a single crystal of MgO or a slice of high-density ThO_2 ceramic in a molybdenum crucible. (A control experiment with such a crucible, without refractory oxides, yielded only traces of CeOCl.)

On the basis of these findings it is certain that the data obtained in the e.m.f. and conductivity measurements which had been carried out in Morganite crucibles[1,2] *did not pertain to the Ce–$CeCl_3$ system*! Rather, the added cerium must have been largely, if not completely, converted to CeOCl. Although under the circumstances any attempt at interpretation of those measurements must be inadequate, the observed e.m.f.[2] may perhaps be ascribed to a cell such as

$$Mo|MoO_2(solid), CeOCl, CeCl_3||CeCl_3|Cl_2$$

with variable oxygen concentration in the form of CeOCl. We are now in the process of developing methods of investigating the Ce–$CeCl_3$ and similar systems in such a manner as to avoid reaction with unsuitable container materials. Of particular interest is the question whether the simultaneous presence of the two valence states of cerium, Ce^{++} and Ce^{3+}, leads to a high electron mobility.

CHEMISTRY DIVISION, OAK RIDGE NATIONAL LABORATORY
OPERATED FOR THE U. S.
ATOMIC ENERGY COMMISSION H. R. BRONSTEIN
BY UNION CARBIDE CORPORATION A. S. DWORKIN
OAK RIDGE, TENNESSEE M. A. BREDIG

RECEIVED JUNE 17, 1960

---

[1] G. W. Mellors and S. Senderoff, *J. Phys. Chem.*, **64**, 294 (1960).

[2] S. Senderoff and G. W. Mellors, *J. Electrochem. Soc.*, **105**, 224 (1958).

[3] L. F. Druding and J. D. Corbett, *J. Am. Chem. Soc.*, **81**, 5512 (1959); and J. D. Corbett, private communication.

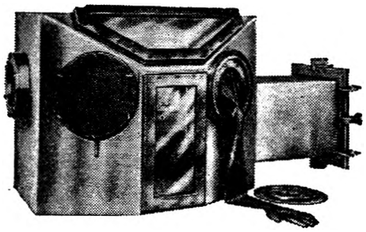

BLICKMAN

VACUUM DRY BOX

Designed for safe handling of radio-isotopes, reactor fuel containing Plutonium or U233 and other hazardous substances. With air-lock, it can be sealed to create a vacuum. Fabricated of stainless steel plate—34" long x 26" high x 24" wide at base. Air-lock measures 18" x 12". Send for Technical Bulletin A-2. S. Blickman Inc. 9009 Gregory Ave., Weehawken, N. J.

BLICKMAN
LABORATORY EQUIPMENT

Look for this symbol of quality Blickman-Built

NONMILITARY DEFENSE

CHEMICAL AND BIOLOGICAL DEFENSES IN PERSPECTIVE

Number 26 in
Advances in Chemistry Series
edited by the Staff of
Industrial and Engineering Chemistry

Complete text of the Symposium which received international attention when presented at the ACS National Meeting in Cleveland, Ohio. The book documents why chemical and biological weapons now must be regarded as nearly on a par with nuclear weapons and stresses what defenses should be in the hands of every citizen for his personal protection and why a protected citizenry will be a major factor in preventing such agents ever being used. The book includes a point by point comparison between chemical, biological, and nuclear weapons; a detailed description of the chemical and biological threat; the medical problems involved in protecting citizens; the individual and collective protection for individuals, companies, institutions, and communities; a detailed discussion of chemical and biological early warning and detection problems; the research still needed to protect individuals from these agents; and detailed, nontechnical discussions of why individuals should be aware of such threats and what they can do about it.

100 pages—paper bound—$2.00 per copy

bulk rates on request

order from:
Special Issues Sales
American Chemical Society
1155 16th Street, N.W.
Washington 6, D. C.

Chemists, Physical Chemists, Chemical Engineers:

SEVERAL POSITIONS OPEN IN ADVANCED PROJECTS OPERATION FOR R&D OF NON-CONVENTIONAL DISPLAY DEVICES

Although details cannot be published here, one of the activities of this new group will concern development of an entire family of unusual information recording, storage and display systems.

Key Posts to be Filled in These Areas:

Gettering
Thermionic Emission
Synthesis and Application of Organic Material to Electronic Components
Ceramic and Glass to Metal Seals

For more information, write informally or forward your resume in confidence to Mr. James F. Leete, Dept. 39-MI. Your inquiry will receive prompt review and an early reply.

CATHODE RAY TUBE DEPARTMENT

GENERAL ELECTRIC

Electronics Park, Syracuse, New York

WILEY — BOOKS —

PROPERTIES and STRUCTURE of POLYMERS

By Arthur V. Tobolsky, *Princeton University.* Describes and explains the mechanical behavior of polymers in terms of the fundamental principles of molecular structure and dynamics. *1960. 331 pages. $14.50.*

CRYSTAL-STRUCTURE ANALYSIS

By Martin J. Buerger, *M.I.T.* Designed for the reader with no background in the subject, this book sets forth the methods—and the theory underlying the methods—for finding the location of atoms in crystal cells. Together with two companion volumes, *X-Ray Crystallography* and *Vector Space,* it will provide lucid and complete coverage of all aspects of crystal-structure investigation. *1960. 668 pages. $18.50.*

TRANSPORT PHENOMENA

By Byron Bird, Warren E. Stewart, *and* Edwin N. Lightfoot, *all of the University of Wisconsin.* A systematic treatment of three analogous transport processes: momentum transport, energy transport, and mass transport. *1960. Approx. 816 pages. $13.75.**

THERMOELECTRICITY

Edited by Paul H. Egli, *U. S. Naval Research Laboratory.* A collection of papers by leading scientists and engineers on thermoelectric methods of energy conversion. Most of the papers were presented at the Conference on Thermoelectricity sponsored by the Naval Research Laboratory in September of 1958. *1960. 407 pages. $10.00.*

X-RAY ABSORPTION and EMISSION in ANALYTICAL CHEMISTRY

By H. A. Liebhafsky, H. G. Pfeiffer, E. H. Winslow, *and* P. D. Zemany, *all of the General Electric Research Laboratory, Schenectady,* N. Y. Offers authoritative coverage of the theory, history, necessary equipment, and techniques of x-ray spectrochemical analysis and describes in detail many important applications of x-ray methods to problems in qualitative and quantitative analysis. *1960. 357 pages. $13.50.*

PHOTOCHEMISTRY in the LIQUID and SOLID STATES

Edited by Lawrence J. Heidt, *M.I.T.;* Robert S. Livingston, *University of Minnesota;* Eugene Rabinowitch, *University of Illinois; and* Farrington Daniels, *University of Wisconsin.* Based on a symposium held at Dedham, Mass., in September 1957. *1960. 174 pages. $6.00.*

PHOTOCONDUCTIVITY OF SOLIDS

By Richard H. Bube, *RCA Laboratories.* A unified presentation and interpretation of photoconductivity phenomena. *1960. 461 pages. $14.75.*

STRUCTURE and PROPERTIES of THIN FILMS

Edited by C. A. Neugebauer, John B. Newkirk, *and* David A. Vermilyea, *all of the General Electric Research Laboratory, Schenectady,* N. Y. The complete proceedings of an international conference held at Lake George, N. Y., in September 1959. *1959. 561 pages. $15.00.*

THERMODYNAMICS

An Introduction to the Physical Theories of Equilibrium Thermostatics and Irreversible Thermodynamics

By Herbert B. Callen, *University of Pennsylvania.* Develops the theory of thermodynamics as a self-contained, simple logical structure. *1960. 376 pages. $8.75.*

DYNAMIC BEHAVIOR of THERMOELECTRIC DEVICES

By Paul E. Gray, *M.I.T.* The first published report on the small signal dynamic behavior of thermoelectric devices. (A Technology Press Research Monograph, M.I.T.) *1960. 136 pages. $3.50.*

COMPARATIVE EFFECTS of RADIATION

Edited by Milton Burton, *University of Notre Dame;* John S. Kirby-Smith, *Oak Ridge National Laboratory; and* John L. Magee, *University of Notre Dame.* Proceedings of a symposium on the comparative effects of infrared, visible, ultraviolet, and high-energy radiations which was held in February 1960. *1960. In Press.*

**Text edition available for college adoption.*

Send for examination copies.

JOHN WILEY & SONS, Inc.

440 Park Avenue South
New York 16, N. Y.